Applications of phytase-mediated phosphate biomineralizaton for the remediation of uranium mine tailings

PhD Thesis

Thomas Mullan

Department of Civil & Environmental Engineering

University of Strathclyde, Glasgow

May 2020

Declaration

This thesis is the result of the author's original research. It has been composed by the author and has not been previously submitted for examination which has led to the award of a degree.

Dedicated to Millie and Margaret Mullan

Acknowledgements

Firstly, I would like to thank my supervisors – Rebecca Lunn and Joanna Renshaw – for their continued support and guidance throughout this PhD.

Secondly, I am grateful to Ian Stalker for funding this PhD through the alumni fund, as well as the useful advice he and Grenvil Dunn provided on the uranium mining industry.

Thirdly, I would not have been able to achieve this without the support – both in a scientific sense, but more importantly, as a community – of the second floor lab users, who are too many in number to name, but are all significant.

Valuable technical support and friendly advice was provided by Tiziana Marrocco, Fiona Sillars (XRD), Pieter Bots (XRD & geochemical modelling), Matt Baker (FTIR), Paul Edwards (SEM), David Miller (TEM), Daniel Dawson (NMR), Alice Macente and James Minto (X-CT), Tatyana Peshkur (ICP-OES and general lab practices), and Mara Knapp (basically everything to do with working in the labs).

A mention is also required for Jan, for providing a stable place to live for the duration of the PhD, and the cats (Lady, Molly, and Timbah).

Finally, I want to thank my family (particularly my parents and Sara) and Shayna for their support and encouragement during this interesting period of my life.

Abstract

The mining of elements such as copper, gold, rare earths, and uranium is an essential part of modern society, providing the raw materials for a wide range of applications in technology, industry, medicine, and energy supply. However, the extraction of these and other resources may cause harm to human and environmental health through the mobilisation of contaminants, including naturally occurring radionuclides.

Phosphate mineral phases have been researched as a method of immobilising contaminants including lead, radium, and uranium as natural analogues demonstrate that these metals can be stably incorporated into phosphate minerals over geological timescales and across varying pH, redox, and chemical conditions. Previous research has indicated that phosphate biominerals (produced *via* the microbial hydrolysis of organic phosphate compounds) may be more sustainable and more efficient at immobilising contaminants than sourcing phosphate minerals from mined phosphate rock.

This PhD has investigated the applications of phytate – a common plant waste product – as a phosphate donor. Experiments have been performed with different microorganisms (*Aspergillus niger* and *Blastobotrys adeninivorans*) and purified phytate-degrading enzymes in batch solution and solid matrices to understand the opportunities and challenges associated with using phytate as a precursor for phosphate minerals.

Both microorganisms tested were able to grow and hydrolyse phytate at environmentally relevant temperatures, an essential property for *in situ* remediation strategies, and both were able to use the low cost carbon source starch for growth. Experiments within solid substrates established that phosphate biomineralization occurs readily in the presence of a sandy matrix, but that challenges related to the interactions between phytic acid and mineral phases such as kaolinite need to be addressed when considering more complex solid media.

Furthermore, it is established that phosphate phases that are insoluble under acidic conditions are suitable targets for phosphate biomineralization – this is demonstrated for lanthanum and lead phosphate, and hypothesised to also be true for uranium – which makes this process a highly promising method for the treatment of acidic, uranium-contaminated mine wastes.

Contents

List of Figures

List of Tables

Acronyms and abbreviations

A_{700}	Absorbance at 700 nm
AMD	Acid mine drainage
ATR	Attenuated Total Reflectance
CD3A	Phosphate-free Czapek-Dox agar
CFU	Colony forming units
CHN	Carbon Hydrogen Nitrogen analysis
Cit	Citrate
COD	Crystallography Open Database
EDX	Energy dispersive X-ray specroscopy
E_h	Redox potential relative to the standard hydrogen electrode
FFT	Fast Fourier Transform
FTIR	Fourier transform infrared spectroscopy
Glu	Gluconate
ICP-OES	Inductively coupled plasma optical emission spectroscopy
ICSD	Inorganic Crystal Structure Database
Ins	*myo*-Inositol
InsP_1	*myo*-Inositol monophosphate
InsP_2	*myo*-Inositol bisphosphate
InsP_3	*myo*-Inositol trisphosphate
InsP_4	*myo*-Inositol tetrakisphosphate
InsP_5	*myo*-Inositol pentakisphosphate
InsP_6	*myo*-Inositol hexakisphosphate
IPA	Isopropyl alcohol
ISL	*In situ* leaching
kPa	kilopascal
Ln	Lanthanide
LOD	Limit of detection
MCE	Mixed cellulose ester
MES	2-(N-morpholino)ethanesulfonic acid
MNX	IR - Minerals & Clays - Bio-Rad Sadtler (FTIR database)
nKat	Nanokatal
NMR	Nuclear magnetic resonance
NORM	Naturally occurring radioactive material
npH_2O	Nanopure water
OD_{425}	Optical density measured at 425 nm
OD_{600}	Optical density measured at 600 nm
ORP	Oxidation-reduction potential
Ox	Oxalate
PBS	Phosphate buffered saline
PDF	Powder Diffraction File™ database

PES	Polyethersulfone
PhyM4A	Phytate minimal agar
PRB	Permeable Reactive Barrier
PTFE	Polytetrafluoroethylene
PZC	Point of zero charge
rcf	Relative centrifugal force
REE	Rare earth elements
rpm	Revolutions per minute
SEM	Scanning electron microscopy
SPE	Solid phase extraction
Tar	Tartrate
TCA	Trichloroacetic acid
TDS	Total dissolved solids
TEM	Transmission electron microscopy
TENORM	Technologically enhanced naturally occurring materials
TES	N-tris(hydroxymethyl)methyl-2-aminoethanesulfonic acid
TRIS	Tris(hydroxymethyl)aminomethane
VPC	Viable plate count
WSAAX	ATR-IR - Sigma-Aldrich Library of ATR-IR Spectra - Wiley (FTIR database)
X-CT	X-ray computed tomography
XRD	X-ray diffraction
YMA	Yeast-mold agar
YMB	Yeast-mold broth
YN	Yeast nitrogen base
YN5B	YN broth with glucose
YN6B	YN broth with galactose
YN9.1B	YN broth with starch and added calcium
YN9B	YN broth with starch

Chapter 1
Introduction and Literature Review

1.0 Background information

The biogeochemical cycling of phosphorus is of interest due to the importance of phosphorus as a key macronutrient, the negative impacts of eutrophication, and the potential applicability of phosphate minerals to the remediation of contaminated environments immobilisation. Up to 80% of phosphorus in soils may be present in an organic form and, of this fraction, as much as 60% may be present as the compound phytate (1–3). Phytate is also abundant in plant matter as a phosphorus reserve and may account for 60–90% of the total phosphorus in seeds (4–9).

As phytate is not bioavailable, it must be hydrolysed to release inorganic phosphate ions for uptake by living organisms; this is achieved through the action of phytate-degrading enzymes known as phytases (10). This transfer of phosphate between inorganic and organic forms (such as phytate) is an important component of the geochemical cycling of phosphorus (2). Recently, interest has emerged in harnessing this naturally occurring process to induce the formation of phosphate minerals; this may occur when inorganic phosphate is released in the presence of sufficient quantities of metals such as calcium or uranium (11).

Phosphates, including apatite group minerals ($Ca_{10}(PO_4)_6(OH,F,Cl)_2$), rare earth element phosphates such as monazite ($(Ce,La,Nd,Th)PO_4$), uranium phosphates such as autunite ($Ca(UO_2)_2(PO_4)_2.10–12H_2O$), and phosphate glasses, have a widely recognised potential for the remediation of radioactive and non-radioactive contaminants. Natural analogues of these materials are known to be stable over geological timescales (12–15). Phosphates, including apatites, are also able to buffer acidic solutions, which is a desirable property for waters impacted by acid mine drainage (AMD) (13). Therefore, this research is focused on the use of phytate as a precursor for the biologically induced formation of phosphate minerals and the application of this process to the remediation of waters and solids contaminated by naturally occurring radioactive material (NORM).

Naturally occurring radioactivity is ubiquitous in the environment in the form of terrestrial and cosmogenic radionuclides. Cosmogenic radionuclides are those produced by the interaction of stable isotopes with cosmic radiation, while terrestrial radionuclides are those which naturally form a part of the Earth's geological environment and include primordial radionuclides (i.e. those that have been part of the Earth since its formation), and any of their radioactive decay products (16).

Where human activities create the potential for these naturally occurring radionuclides to cause harm to human or environmental health by being disturbed or mobilised they are classified as NORM (17). Where human activities lead to the concentration of NORM being artificially increased they are then classified as technologically enhanced naturally occurring materials (TENORM) (16,18). In general, NORM and TENORM is terrestrial in origin and is associated with uranium-238 (~99.3% of natural uranium), thorium-232 (~99.98% of natural thorium), and the isotopes of their respective decay chains (16). Other radionuclides such as uranium-235 (~0.7% of natural uranium), members of its decay chain, and potassium-40 (~0.01% of natural potassium) may be relevant under certain circumstances (19). Cosmogenic radionuclides are usually not significant within the context of NORM, nor are the various other terrestrial radionuclides that exist (18,19).

There are many different industrial activities that may lead to environmental contamination by NORM and TENORM, but the most significant and wide ranging are related to the mining and processing of metal and mineral resources (16,17,20–22). Thorium and uranium are widespread in geological environments (with average crustal concentrations of 6 mg/kg and 1.8 mg/kg respectively) (23) and often co-occur alongside many resources essential for human society. Uranium, and to a lesser extent thorium, are also themselves resources. The invasive techniques used in mining have the potential to mobilise radionuclides, processing operations may lead to enhanced concentrations within waste streams, while in some cases, radionuclides may also remain with the final processed product.

The radioactivity of NORMs is typically low in comparison to the wastes associated with, for example, nuclear power generation and weapons usage but may be large in volume and spread over wide geographic areas (16). The type of contamination and how it moves through the environment will be related to the nature of the geological deposit being mined, the mining and processing operations used, and the level of care taken in managing wastes.

Contaminated media may include waste storage/disposal sites (including tailings ponds and waste rock piles), surface and subsurface soils and rocks, the critical (unsaturated) zone, and surface- and groundwaters (21). The physical form of contaminants may be solid, colloidal, liquid, or gaseous, while the hazards posed include radioactivity, chemical toxicity, extreme (low) pH values, and physical hazards (e.g. landslides and flooding). The contamination of water is a particularly important issue: water is an essential resource for all living organisms and plays a critical role in the mobility of contaminants by acting as a physical transport medium, as a solvent, and as a medium within which other chemical reactions may take place (17,24).

A wide range of treatment technologies exist, the choice of which in any particular context depends on a range of factors, such as: type of contamination, nature of contaminated media, extent of contamination, type of site and industry, potential for recovering valuable materials, cost and available funds, regulatory requirements, government and/or industry policy, and public acceptability (22). Remediation technologies usually rely on isolating a contaminant from the environment by either containing or removing the source term (21,22,25). Removal techniques may be cost, energy, and time-intensive, and there is a growing interest in the development of low cost, passive, *in situ* containment techniques.

This chapter begins by summarising the range of resource extraction industries that may produce NORM wastes or contamination. This is followed by an outline of typical mining operations, the types of wastes produced, and the main potential sources of contamination. Common strategies for treating (or preventing) contamination are then reviewed, with a focus the use of phosphate-based materials. Finally, the principles of phosphate biomineralization are introduced, and the potential advantages and challenges of using phytic acid as a phosphate donor are highlighted.

1.1 Outline of industries that may produce NORM

1.1.1 Uranium

Past and present uranium mining operations exist on every inhabited continent, with the majority of current production supplied by Kazakhstan, Canada, and Australia (17,20,26,27). As of 2013, the world's total inventory of uranium mine tailings was estimated to be over 2

million tonnes, and is distributed across Africa (46%), Europe (21%), North America (19%), Asia (11%), Australia (3%), and South America (0.1%) (27,28).

Issues of contamination may be particularly prominent at legacy sites where little consideration was given to waste management and environmental impacts and the mine operator no longer exists (22). Major legacies exist in regions such as Saxony, Germany (21,22,29,30), Ontario and Saskatchewan in Canada (12,20,26,31–33), Australia (20,30,34,35), regions (particularly Arizona, Colorado, New Mexico, Utah, and Wyoming) across the USA (21,26,30,36–40), Minas Gerais in Brazil (41,42), the Central Asian countries of Kazakhstan, Kyrgyzstan, Tajikistan, and Uzbekistan (43), and the African countries of the Democratic Republic of the Congo, Malawi, Namibia, Niger (20,27,44–46).

As uranium separation and recovery processes will usually not be selective for other co-occurring radionuclides such as thorium and radium, uranium mine tailings will still contain radioactivity (21,22). Additionally, early mining technologies had poor extraction and separation efficiencies which meant that relatively high concentrations of uranium remained in waste tailings (21).

1.1.2 Radium and thorium

Current practical applications of radium and thorium isotopes are limited to select medical (for radium) and industrial (for thorium) contexts (17,47). However, their use during the early twentieth century was much more widespread (21,30,47,48), with associated lasting legacies (for example, Portugal, the UK, and Olen in Belgium, where around half of the world's supply of radium was handled) (17,21,49–52). These legacy sites are associated with many of the same issues as legacy uranium mining sites, in terms of being poorly characterised sites where there had been a lack of forethought given to waste containment during operations (50–52).

1.1.3 Gold

Gold deposits often contain high levels of uranium (47,53). This has been well researched in the Witwatersrand and Wonderfonteinspruit regions of South Africa, where uranium has sometimes been extracted as a by-product and sometimes been disposed as waste (20,24,53–56). These regions are in close proximity to major population areas (including Johannesburg) and the water- and air-borne spread of radionuclides are considered to pose significant public health challenges (57–60,44,30). The total inventory of South African gold mine tailings has

been estimated to be around 6 billion m^3 in volume (17) or 7 billion tonnes in mass (27,58). The mass of tailings associated with non-uranium producing gold mines in South Africa has been estimated to be an order of magnitude larger than the mass associated with the mines that have extracted uranium (27,28,58). Other regions where NORM contamination may be associated with gold mining include the Jacobina and Carajás regions in Brazil, the Copper Belt of Arizona in the USA, and Cuba (17,53).

1.1.4 Rare Earth Elements

Rare earth elements (REEs) are a group of elements consisting of the lanthanides plus scandium and yttrium and are important for a range of industrial processes (16,61,62). Many of the important REE minerals, such as xenotime (YPO_4), monazite ($(Ce,La,Nd,Th)PO_4$), and bastnäsite ($(Ce,La)(CO_3)F$), contain relatively high concentrations of radionuclides including thorium and uranium which may either be co-extracted or transferred to the waste residues (16,17,19,47,61–64).

While the majority of REE mining takes place in China (61,62), the most notable issues of radiological contamination connected with the mining and/or processing of REE ores have been reported in Malaysia (17,65–70). REE wastes in the USA have also been reported as containing thorium and uranium levels above recommended limits (16), with the cost of waste disposal an important factor limiting further mining/production of REEs (66).

1.1.5 Other resources

A wide range of other resources may also be associated with NORM wastes and contamination. These include aluminium, beryllium, coal, copper, fluorite (CaF_2), geothermal energy production, iron, lead, molybdenum, nickel, niobium, oil and gas production, potassium, phosphorus, silver, sulfuric acid, tantalum, tin, titanium, tungsten, vanadium, zinc, and zirconium (16,17,19–21,38,47,48,53,56,71–78). In general, the level of radioactivity and radionuclides present will be highly dependent on the nature of the geological formation being mined (16,17).

1.1.6 Summary

While the radioactivity of wastes associated with NORM-producing industries is typically low, the volumes can be considerable (17,38,47). Additionally, the processes involved in mining may make the NORM wastes more available to the biosphere (17). Also, many legacy NORM-

producing mines have similar issues including a lack of funds being allocated to clean-up operations at the initiation of the project and relating to the fact that the operating company may no longer exist and therefore the responsibility for clean-up is unclear (17,19,22,30,79).

Data are not always available to judge the scale of the issues (79). For example, Abdelouas (26) provided estimates of the volumes of uranium mine tailings in various parts of the world (ranging from 0.03 million m^3 in China, India, and Japan to over 200 million m^3 in Kazakhstan) but indicated that no data for Argentina, Kyrgyzstan, or any country in Africa were available. The data presented by the WISE Uranium Project (28) appear to be slightly more comprehensive, but a number of countries (particularly in Africa) are marked as not having data available (it is also not clear what primary sources have been used when collecting the data). However, data on NORM wastes generated by uranium mining operations are much more readily available and reliable than for other industries that are not connected to the nuclear fuel cycle (80). For some resources, such as iron, it has been highlighted that not all major producers report data on the levels of radioactivity present in their processes or wastes (17). The lack of data regarding the scale of NORM contamination, particularly in developing countries, is a major research gap (17).

1.2 Outline of mining operations and routes of contamination

Of the resources describe above, the NORM issues in the oil and gas industries and in geothermal energy production are significantly different from the other industries and are beyond the scope of this project. Of the other resources described, the processes and potential routes of contamination are similar enough that they can be grouped together, although due to the greater availability of data (at least with regards to radioactive contamination), the primary focus of the project is uranium mining.

The main methods of resource extraction relevant to the production of NORM wastes and contamination are surface (open pit) mining, underground mining, placer deposit mining, heap leaching, and *in situ* leaching (ISL) (17,20–22,47,61).

“Traditional” open pit and underground mining methods are important for most of the resources listed above, including aluminium, coal, copper, gold, REEs, and uranium (20,61,76,78,81).

In contrast, ISL and placer deposit mining techniques are restricted to more specific resources. ISL is important for elements including uranium (20), REEs (61), and copper (78). Placer deposits, meanwhile, are important for gold, REEs, thorium, tin, titanium, and zirconium (17,53,61,81).

Heap leaching is typically performed in conjunction with open pit or underground mining, where low grade ores are subject to biological or chemical leaching mechanisms to recover the resource of interest. Heap leaching is important for metals such as copper and uranium (20,22,78,82).

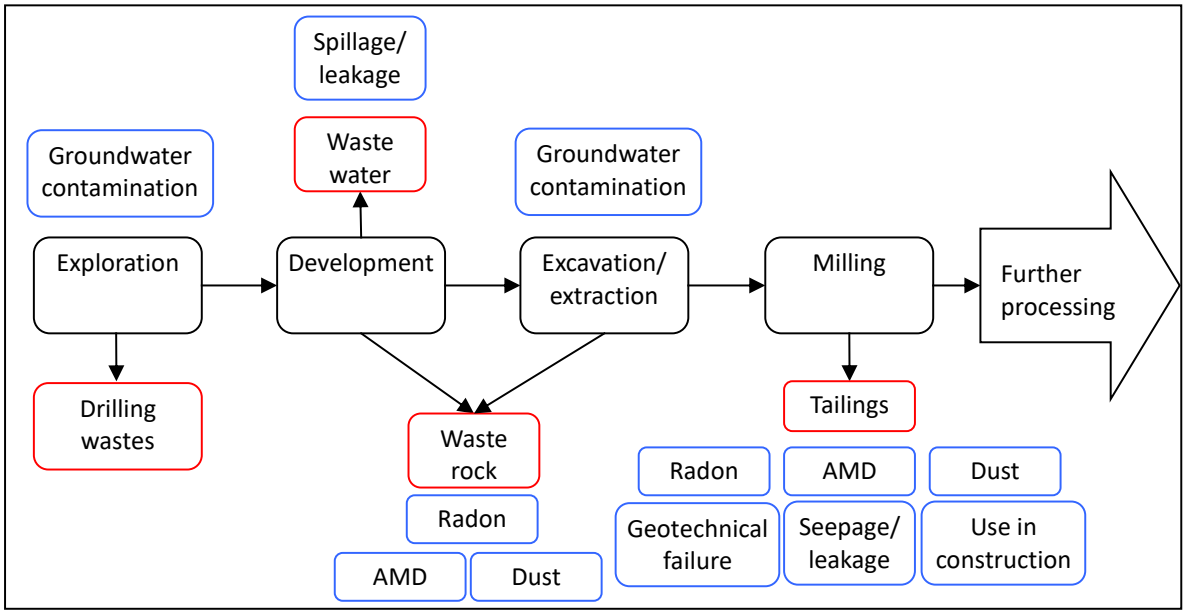

Figure 1.1 Generic overview of operations (black), wastes (red), and potential contamination issues (blue) associated with mining industries. AMD = acid mine drainage.

Figure 1.1 shows a flow chart indicating typical operations, wastes, and contamination streams associated with mining operations, although slight variations will occur depending on the process. The life cycle of mines generally consists of four stages: prospecting and exploration, development of the mine/mine site, exploitation (i.e. extraction, milling, and further processing), and finally site closure (81). Each stage may generate wastes and potential pathways for the spread of contamination, although modern techniques mean that contamination associated with the exploration stage is low (22).

After identifying a mineable deposit, the mine must be developed. For most operations, aside from placer deposit mining, this will include the use of invasive techniques to allow the

orebody to be accessed and exploited. This involves the stripping of overburden for open pit mines (20,81), the excavation of openings for underground mines (81), and the drilling of boreholes for ISL (22). These operations produce waste solids (overburden or excavated rock for open pit and underground mines (22,81) or drilling wastes for ISL (22)) and waste waters (from dewatering of open pit and underground mine areas below the water table (22,81,83) and extracted water for ISL (22)). Potential contamination issues associated with this stage may include the generation of AMD (17,21,22,24,78), spillage/leakage of stored waste water (22), dust generation (21,22), release of radon gas and γ-ray emitting radionuclides (21,22), dispersal of contaminants from waste rock piles into the environment by erosion/rainfall (22), or the creation of hydraulic shortcuts during excavation/drilling (22).

Once developed, exploitation of the mine can begin. For the "traditional" mining operations based upon the extraction of solids, a pre-sorting stage to separate ore from waste gangue material will produce waste solids (22). Contamination issues associated with these waste solids are similar to those associated with waste solids produce during the initial excavation of the mine. For ISL, contamination can be associated with the incomplete recovery of injected leaching solutions and solubilised contaminants (20,22) and plumes of contaminated water extending beyond the boundary of the producing wells (17).

Following extraction of the ore, milling or beneficiation processes are required to separate the resource from the waste; this typically occurs close to the site of extraction (84). Milling processes are generally similar for different mining processes, although ISL does not require the crushing/grinding steps that solid-based mining techniques use to separate the resource of interest from gangue materials (22). The intermediate processing steps performed during milling are typically not important sources of contamination, but the treatment and disposal of wastes produced poses significant challenges (24). Waste waters may either be treated to produce clean water than can be discharged and waste solids that need to be disposed (20,22,85) or stored in evaporation ponds to allow the water to gradually evaporate away, leaving contaminated waste solids behind (17,74). The waste solids generated in milling processes and water treatment are typically stored together as "tailings" in engineered ponds or mined-out pits where they are contained by dams (20,22,85).

In general, the radioactivity of mine or mill tailings will be similar to the ore, particularly where radionuclides have not been co-extracted or in older uranium mining operations where

extraction efficiencies were low (17,21,27,38). These tailings may be significant sources of contamination. AMD, radon exhalation, dust dispersal, seepage/leakage into surface and groundwaters, geotechnical failures, and the unauthorised use of materials in construction are all potentially important pathways for the dispersal of contaminants into the environment (16,17,21,22,82,85–88).

Further processing as indicated in figure 1.1 may include processes such as smelting (e.g. for copper (20,53,78)) or enrichment (for uranium (53,80)). These operations typically occur away from the mining and milling sites and are not explicitly considered in this project.

Once the orebody has been exhausted, mines enter the decommissioning and closure phase. Modern mines are expected to account for decommissioning in the planning stages but for the majority of human history this has not occurred, and this has contributed towards legacies (22,81). For surface and underground mines, decommissioning operations may include backfilling of the mined-out areas (17), flooding of the underground mine areas (22), and taking steps to try and ensure the stability of the waste rock piles and tailings dams (20,22). For ISL mines, the aim is usually to restore groundwater to a baseline established prior to the beginning of operations (17,20). The extraction and injection wells used during operation will be used during the remediation process (20). Once this process is complete, the wells are sealed or capped (20). If these steps are not performed effectively, contamination may arise.

To summarise, mining operations create solid and liquid wastes through a variety of processes that, if not properly handled, may act as sources of contamination. In addition, the disturbance of orebodies during the mining processes may lead to the generation of contamination through AMD or (in ISL) by the incomplete recovery of leaching solutions. Due to the large volumes relative to other wastes, the mine tailings associated with open pit and underground mining operations are the primary focus of the project.

Contaminants may be transported by surface waters, groundwater, or by airborne routes (16,20–22,89). Airborne routes may transport contaminants over large distances (e.g. elevated uranium concentrations, linked to Australian mining operations, have been detected in Antarctica (90)) but are beyond the scope of this project. Factors relating to human intrusion and the inappropriate use of contaminated solids in construction (17,53) are also not considered, as these are sociopolitical challenges rather than

technological/environmental ones. This project is focused on efficient treatment methods for liquid and solid wastes, specifically, chemical immobilisation techniques that can prevent or limit the spreading of contamination through aqueous pathways.

While recent years have seen an increased level of importance placed on the remediation of former mine sites, their long-term successful rehabilitation remains a considerable challenge (30). Additionally, public confidence in *in situ* containment or immobilisation strategies is low compared to strategies that remove the waste and dispose of it elsewhere (17). Developing improved methods of stabilising mining wastes is an important component of addressing this issue.

1.3 Current methods for the stabilisation/remediation of mine tailings

Current methods for the treatment of wastes/contamination can be categorised in several ways: according to the physical state of the contaminated media (solid, liquid, or gaseous/airborne), the level of intervention required (active, semi-passive, passive, or non-intervention), the location of treatment (*ex-situ* or *in-situ*), or the location of disposal (dilute and disperse, removal and disposal in a constructed repository, or containment) (17).

Active, *ex-situ* treatments (e.g. ion exchange or reverse osmosis) are useful for wastes which are relatively well contained, but high costs and low efficiencies associated with recovering the contaminated media (e.g. dig and treat or pump and treat strategies) limit the applicability of these treatments to large scale contaminated areas (17,52,91–93). Non-intervention or dilute and disperse-based strategies are generally not considered appropriate for inorganic or radioactive contaminants (17,22,59,94), and the complete removal of contaminated land is usually only considered in extreme circumstances (e.g. the Moab uranium mine tailings site in Utah, USA where the tailings had to be relocated due to the threat of erosion from the Colorado river (21,22)). In general, however, transport of mine tailings away from the tailings impoundment is considered to be too expensive and a greater source of health, safety, and environmental risks than if the wastes remain *in situ* (19,52).

Therefore, for the large areas covered by mine sites and mine tailings *in situ* containment strategies have received a lot of interest (21,22,79,91,95–98). Containment strategies can attempt to address contamination either at the site where the contamination is generated (i.e. source area treatment) or downstream from where the contamination is generated (e.g.

through the construction of surface or subsurface barriers). Modern mining operations typically require waste management to be considered from the start allowing containment measures to be built into the tailings, but this was not always performed for legacy sites (19,22).

The stabilisation and remediation of mine tailings is a complex and multi-stage process, involving auxiliary tasks such as comprehensive planning, record keeping, and long-term monitoring (19,79,97). The processes directly involved in remediation can be grouped according to three key aspects: the chemical immobilisation of contaminants, physical stabilisation and containment of the tailings, and the longer-term rehabilitation of the site. As with nuclear waste disposal, a multi-barrier approach is considered desirable to minimise the release of any contaminants into the surrounding environment (19).

The engineering strategies involved in the physical stabilisation of the tailings are well researched and established, and are critical to minimising the risks of devastating tailings dams failures (e.g. (99)). These processes may include dewatering of the tailings, and the construction of multi-layered capping, bottom liners, and subsurface barriers (79,98). The longer-term rehabilitation of the site may involve re-vegetation, landscaping, or redeveloping the site for alternative land uses (79,98,100). Clearly, this can only proceed once physical and chemical stabilisation techniques have been shown to be effective.

This project is focused on the chemical immobilisation component, as keeping contaminants in a chemically stable form may be critical for ensuring the long-term performance of remediation strategies. Chemical immobilisation may involve the pre-conditioning of wastes prior to disposal at the tailings site, the direct mixing of treatment materials into contaminated media, or the incorporation of treatment materials into surface or subsurface barriers (17,21,22,38,79,91).

The mechanisms of chemical immobilisation are similar for *ex situ* or *in situ* remediation approaches (17). The fundamental principle is to transform mobile, soluble contaminants into immobile, insoluble, passive forms (19,96). Mechanisms may include sorption, ion exchange, precipitation, redox manipulation, pH manipulation, or vitrification (13,17,21,25). Commonly used materials include aluminium or iron-based materials, activated carbon, cement, clay minerals, gypsum, lime, geopolymers, organic polymers, water glass (sodium silicate), zeolites,

and apatites (13,17,21,38,52,91). Bioremediation strategies involve the use of plants, fungi, or microorganisms to induce chemical changes to make the previously described processes more favourable or to manufacture materials that can then immobilise contaminants through abiotic mechanisms (21,101–104).

Immobilisation of uranium has often focused on the reduction of the more soluble U(VI) to the less soluble U(IV) oxidation state. U(IV) minerals such as uraninite (UO_2) are known to have an extremely low solubility (47,105), and uranium reduction can be readily achieved through chemical or biological mechanisms (21,25,38). However, for the long-term stabilisation of uranium, there is concern that reduced uranium could be re-oxidised to the more mobile U(VI) oxidation state (38). Maintaining reducing conditions under shallow earth conditions, as would be found at most tailings repositories, is likely to be challenging (91). Additionally, while reducing conditions can limit uranium mobility, they may increase the mobility of other elements such as iron, arsenic, radium, and thorium (25,38,52,106,107).

Methods based on increasing pH (e.g. by lime or limestone addition) are widely used due to low costs of the raw materials, their effective ability to neutralise acid mine drainage, and the induced precipitation of hydroxide minerals potentially able to sorb contaminants (21). However, above pH 6.5 and in the presence of carbonate, the formation of highly soluble uranyl carbonate complexes may increase uranium mobility (21,47,105). Lime-precipitated solids may also have undesirable physical properties in terms of having a gel-like consistency and high water contents (108).

For some materials, particularly organic polymers, their long-term stability is unknown (17). This is also true for barium-radium sulfate coprecipitates (52), uranium sorbed to zero-valent iron corrosion products (109), and passive techniques such as constructed wetlands and phytoremediation (52). Also, the usage of some materials may be limited by the volumes of material requiring treatment (particularly for organic polymers) (17).

The suitability of vitrification, particularly for *in situ* remediation strategies, is limited by the potential volatilisation of contaminants such as lead-210, polonium-210 and mercury (17).

Therefore, phosphate-based remediation strategies have become an attractive alternative. While not appropriate at every site, there is considerable evidence that under the right conditions, phosphate can alleviate many of the limitations and concerns highlighted above.

1.4 Phosphate-based remediation strategies

Phosphorus is the tenth most abundant element in the Earth's crust and predominantly exists in the +5 oxidation state as derivatives of the orthophosphate (PO_4^{3-}) anion (110,111). The phosphate ion has a tendency to form low solubility phases with polyvalent cations (111) and phosphate minerals are ubiquitous in geological environments (110). These minerals are known to accumulate high levels of metals including lead, REEs, thorium, and uranium, and phosphate has been suggested to control the solubility of these elements in natural systems (110–114).

In fact, almost every element on the periodic table can be incorporated into phosphate phases – at least in trace amounts (110) – and this has led to phosphate minerals being identified as suitable materials for immobilisation of a wide range of radioactive and non-radioactive contaminants (95,112,114–117). Minerals such as calcium apatite ($Ca_{10}(PO_4)_3(F,Cl,OH)_2$) are particularly promising due to the wide range of possible substitutions (114) including many radionuclides, their low solubility across a wide range of pH values and chemical conditions, their ability to self-anneal radiation damage (116) and their stability against geological weathering (12) across geological timescales (13,14). Similar observations have been made of the rare earth (REE) phosphate minerals (general formula $REEPO_4.xH_2O$, including monazite, xenotime, and rhabdophane) (14,118–120) and the uranyl (U(VI)) phosphate minerals in the autunite group ($M(UO_2)_2(PO_4)_2.8–12H_2O$ where M is a divalent or two monovalent cations) (15).

In addition to the long-term geological stability of phosphates, there is also evidence that uranium immobilised by phosphate minerals such as hydroxyapatite is stable against short-term seasonal fluctuations in saturation and redox conditions (121). It is noteworthy that uranium complexed to phosphate is insoluble in both the U(IV) and U(VI) oxidation states (104).

Phosphate-based strategies have been demonstrated to offer diverse engineering mechanisms, from non-invasive methods to more active technologies (116,122). The phosphate may be supplied directly as a solid or in a liquid, water-soluble form allowing precipitation to take place *in situ* (112,116).

Not every site or waste stream is a suitable target for phosphate-based strategies – particularly if there are high concentrations of arsenic, selenium, or organic carbon-bound thorium (95,123–125), competing cations/high salinity (126–128), high carbonate alkalinity (109,129), or high pH values (130,131). However, at least some of these issues can be addressed through careful choice of the phosphate source used (128,132–135) and the engineering strategy employed (136). Furthermore, for sites characterised by low pH values and/or oxidising conditions, phosphate immobilisation remains a highly promising option (38).

Once a site has been established as a suitable target for phosphate amendments, the principle limitations may include high costs of synthetically prepared phosphate sorbents (133,137) and the variable properties of naturally sourced rock phosphate (91,138–140). Also, phosphate supplied in a soluble form may precipitate too quickly to effectively incorporate contaminants (137), and this may also lead to the clogging of injection wells if using an injection-based strategy (129), while the release of phosphate from rock phosphate may be too slow to capture contaminants (137,141). Furthermore, there are concerns regarding supply, price instability, and contamination associated with the mining of phosphate rock (116,142,143). One option that may be able to address many of these concerns is the use of phosphate biominerals.

1.5 Phosphate biomineralization strategies

Biomineralization is the process by which living organisms induce chemical changes which make the precipitation of mineral phases more favourable (144,145) and the use of phosphate biominerals has emerged as a promising method of sourcing phosphates.

Phosphate biominerals may be acquired from a range of source or produced by a versatile range of mechanisms and are considered to have advantages over abiotically sourced or produced equivalents (i.e. mined directly from geological deposits or chemically synthesised). These advantages include potential cost savings, efficiency improvements, sustainability improvements, and novel engineering mechanisms (11,13,102,103,137).

There are two main options for the sourcing and/or production of phosphate biominerals: the use of waste animal teeth and bones or the induced formation by microorganisms, fungi, and/or plants.

1.5.1 Animal teeth and bones

The most widely researched phosphate biomineral is biogenic hydroxyapatite, a poorly-crystalline, carbonate-substituted form of hydroxyapatite which is synthesised by vertebrate animals as the major inorganic component of their teeth and bones (114). Bone apatite from fish (13,127,129,146–150), mammals (149,151), and non-specific bonemeal (109,137,152) can be sourced as a waste product from animal processing industries and has been applied to various contaminated sites. Most notably, the patented Apatite II™, derived from fish bones, has been commercially applied at mining impacted sites for the sequestration of cadmium, lead, and zinc and at US Department of Energy sites for the immobilisation of uranium and plutonium (13,147).

In some studies, bone apatites have been heat treated to remove organics and alter the structure of the material (109,127,150,151,153), while in others, the presence of organic matter was considered desirable to support contaminant immobilisation (13).

Limitations of animal-sourced biominerals include that their performance may be variable (146) and that engineering options may be limited by these materials only being available in a solid form.

1.5.2 Biologically induced precipitation of phosphate minerals

The use of waste animal bones involves sourcing materials that have been pre-formed. An alternative approach is deliberately using biological processes to induce the formation of phosphate minerals. This may involve the accumulation of inorganic phosphate (154–157), induced pH changes (158–161), induced redox potential changes (104,162), biological cells providing crystal nucleation sites (161–164), degradation of complexing agents such as citric acid (165), the release of phosphate from highly insoluble phosphate minerals (141,166,167), the release of cellular phosphate (163,164,168–173), or the enzymatically-mediated release of phosphate from organic phosphate compounds (11).

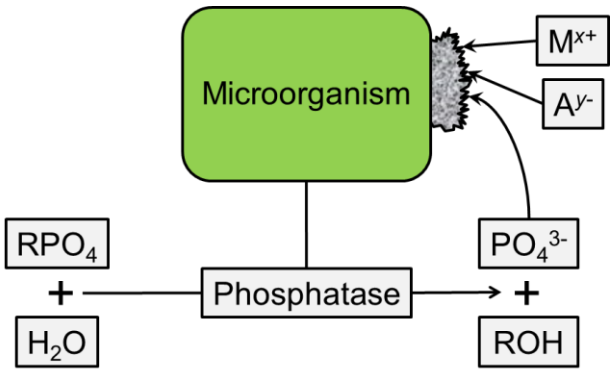

Figure 1.2 Schematic of phosphate biomineral formation (note that the speciation of the hydrolysed phosphate will be pH dependent). M^{x+} and A^{y-} represent cations (e.g. Ca^{2+} or UO_2^{2+}) and anions (e.g. OH^-, Cl^-) that may precipitate with the released phosphate. R represents an organic molecule.

The enzymatically-mediated release of phosphate from organic phosphate compounds is the most widely researched process of induced phosphate biomineralization for the immobilisation of heavy metal and radioactive contaminants. Enzymes known as phosphatases catalyse the hydrolysis of organic phosphate compounds – this releases inorganic phosphate which, under appropriate conditions, may precipitate out of solution with metals such as calcium or uranium (figure 1.2) (11).

The majority of early work on the phosphatase-mediated precipitation of metals *Serratia* sp. N14 (referred to in literature prior to the year 2000 as a strain of *Citrobacter*) and used glycerol 2-phosphate ($C_3H_9O_6P$) as an organic phosphate source (174–180). Further work has demonstrated that a range of bacteria (11,181–183), fungi (181,184,185), plants (186), stimulated mixed microbial consortia (104,187,188), and purified enzymes (189) are capable of carrying out this process. A wide range of phosphate donor molecules have also been considered, including glycerol phosphates (104,177,181,183–185,187,190–199), phytate (182,185,188,200–203), other sugar phosphates (177,204), *p*-nitrophenyl phosphate (177,205,206,189), RNA (207–210), and trialkyl phosphates (177).

Using the phosphatase-mediated process, many different contaminant phosphate phases or potential host phases/sorbent materials have been produced. To date, researchers have demonstrated the precipitation of phosphate with cadmium (189,206), calcium (apatites) (103,128,201,211–216), chromium (189,206), cobalt (189,206), copper (205,217), lanthanum (218–220), lead (202,203), manganese (189), nickel (189,206,217), uranium

(104,180,181,183–185,187,188,190–195,198,199,218–226), zinc (189,217), and zirconium (197,226,227).

Therefore, the induced precipitation of phosphate minerals *via* the phosphatase catalysed hydrolysis of organic phosphate compounds is a versatile method of producing a wide range of phosphate minerals. In addition to potential cost savings, there are a number of other potential advantages associated with this process. Biogenic hydroxyapatite has been demonstrated to have a higher uptake of contaminants, such as uranium, which is linked to the production of a poorly crystalline material with a high specific surface area and a range of different sites for the incorporation of contaminants (103,214,215). For *in situ* precipitation techniques, the slower rates of biomineralization may allow greater control over the reaction time and precipitation location compared to purely chemical methods (160,187).

Therefore, the biologically induced precipitation of phosphate minerals may be able to combine the advantages of chemical synthesis procedures (i.e. control over the production of the material) with the advantages of naturally sourced phosphate products (i.e. low costs and low energy requirements).

Despite a promising body of research that spans forty years, there has been relatively little industrial application of phosphate biomineralization procedures. One of the key limitations identified is the relatively high cost of the glycerol phosphate compounds often used in proof-of-principle studies (11,177). A range of alternatives have been proposed, but the most promising appears to be phytate (11,177), and therefore, this project focuses on the use of phytate as a phosphate donor.

1.6 Chemistry of phytate and its usage as a substrate for biomineralization

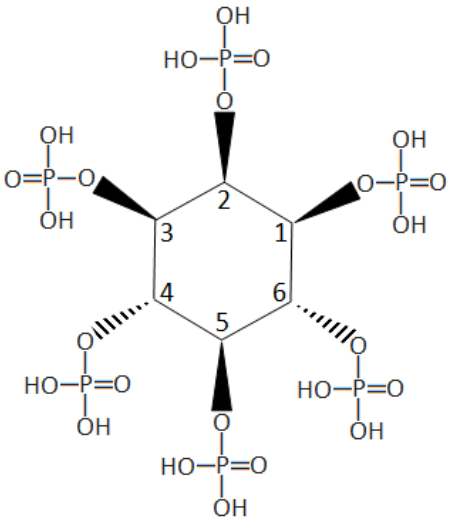

Figure 1.3 Structure of phytic acid (8,228).

Phytic acid ($C_6H_{18}O_{24}P_6$), referred to phytate in salt form, is the common name for *myo*-inositol hexakisphosphate (figure 1.3). Note that three other stereoisomers also exist in nature (*neo*-, *scyllo*-, and D-*chiro*-), but for practical purposes only the *myo*- form is important (1,8,229). Phytate is a common form of organic phosphate in soils and plant matter (1,4,6–9,230) and can be extracted from a range of plant waste products at low cost, which is an attractive property for environmental remediation purposes (11,230–237). Most research into the chemistry of phytate has occurred within agricultural sciences, where the focus is on improving the solubility (and digestibility) of phytate-phosphorus and complexed metals and/or alleviating environmental concerns such as eutrophication (1,238–243). However, there is a growing body of work investigating the application of phytate to waste management and environmental remediation problems.

There are three main ways in which phytate may be applied to environmental remediation problems. Firstly, phytate may be directly mixed with contaminated media to form insoluble phytate complexes (121,244). Secondly, phytate-containing composite materials may be used as sorbents (245–250). Thirdly, phytate may be used as a precursor for inorganic phosphate-containing materials, with the transformation induced by physicochemical (251) or enzymatic/biological methods (11).

The motivation for using phytate as a precursor for phosphate minerals over simply using phytate by itself is related to two main factors. Firstly, knowledge regarding the long-term

stability of metal phytate solids is uncertain, whereas the geological stability of uranium and other metals incorporated into phosphate minerals is well established (12–15). As *in situ* containment remediation strategies for radionuclides require contaminants to be locked up over timescales of hundreds of years (at a minimum) (91,252), it is important to use materials where their long-term stability has been established. Secondly, the performance of phytate as a contaminant host appears to be variable. Some researchers have observed calcium phytate to have a higher uptake for uranium than hydroxyapatite (253). However, in other cases, phytate amendments have been found to be ineffective or even to increase uranium mobility (121,244). Factors such as the ability of phytate to act as a soil dispersant (121) and the ability of phytate to form either insoluble or soluble complexes with metals depending on the metal:phytate ratio (188,244,253,254) may contribute towards the variable performance of phytate amendments. Therefore, taking measures to transform phytate into inorganic phosphate appears to be a more reliable method of ensuring contaminant immobilisation in both the short and long-term.

The advantage of an enzymatic process for transforming phytate over a physicochemical one is mainly because, in the absence of enzymatic hydrolysis, the chemical breakdown of phytate is extremely slow. At ambient temperatures, the chemical half-life of phytate has been calculated to be between 100 and 150 years, while at 85 °C the transformation of europium phytate to europium phosphate required around a month (251). In contrast, phytate degradation can occur at ambient temperatures over the span of hours to days in the presence of appropriate enzymes (e.g. (201,202,255)). This means the enzymatically mediated process is both less energy-intensive than a physicochemical process and is also more versatile in the sense that it could be stimulated at a contaminated site *in situ*.

Phosphatase enzymes that degrade phytate are referred to as phytate-degrading enzymes or as ‘phytases’ (229). Technically, the term ‘phytase’ should only refer to enzymes which have been demonstrated to perform phytate degradation as their *in vivo* function (229,256). In practice, however, the distinction is not usually made and the terms ‘phytase’ and ‘phytate-degrading enzyme’ can usually be considered synonymous. For brevity, the term ‘phytase’ is used throughout this thesis.

The production of phytase enzymes by plants, fungi, and bacteria is widespread in nature (257). The term phytase actually covers a broad and diverse group of enzymes which may be

categorised in various ways (258). The Enzyme Nomenclature Committee of the International Union of Biochemistry classifies phytases based upon the number of the first phosphate group (based upon the 1D-numbering convention) cleaved: these are 3-phytase (EC 3.1.3.8), 4-phytase (EC 3.1.3.26), and 5-phytase (EC 3.1.3.72) (256,259). Alternatively, phytases may be grouped according structure type, of which there are four classes: histidine acid phosphatases, β-propeller phytases, purple acid phosphatases, and cysteine phosphatases (256,258,260). Phytases may also be classified according to the gene used to express them (e.g. phyA) (258,261) or their optimum pH range (i.e. acid, neutral, or alkaline) (258). The catalytic properties and the genetic regulation of these different enzymes is complicated, and varies considerably between different types of organisms (256,258).

Table 1.1 Comparison of phytate (myo-inositol hexakisphosphate) with myo-inositol and the intermediate lower myo-inositol phosphates (8,229,262).

Name	Chemical formula	IUPAC abbreviation	Number of possible *myo*- stereoisomers
myo-Inositol	$C_6H_{12}O_6$	Ins	1
myo-Inositol monophosphate	$C_6H_{13}O_9P$	InsP_1	6
myo-Inositol bisphosphate	$C_6H_{14}O_{12}P_2$	InsP_2	15
myo-Inositol trisphosphate	$C_6H_{15}O_{15}P_3$	InsP_3	20
myo-Inositol tetrakisphosphate	$C_6H_{16}O_{18}P_4$	InsP_4	15
myo-Inositol pentakisphosphate	$C_6H_{17}O_{21}P_5$	InsP_5	6
myo-Inositol hexakisphosphate	$C_6H_{18}O_{24}P_6$	InsP_6	1

Unlike the hydrolysis of glycerol phosphates, which occurs in a single, simple step, the degradation of phytate is a complicated process involving multiple substrates (and potentially multiple enzymes). The release of phosphate groups from phytate occurs in a stepwise manner producing compounds collectively referred to as lower inositol phosphates (table 1.1) (8,256,262). Theoretically, then, the complete degradation of one mole of phytate yields six moles of inorganic phosphate plus one mole of the fully dephosphorylated *myo*-inositol. However, most phytase enzymes (in the strict sense of the term) yield either InsP_1 or InsP_3 as the final product (256) and other phosphatase enzymes are required to release all of the available phosphate.

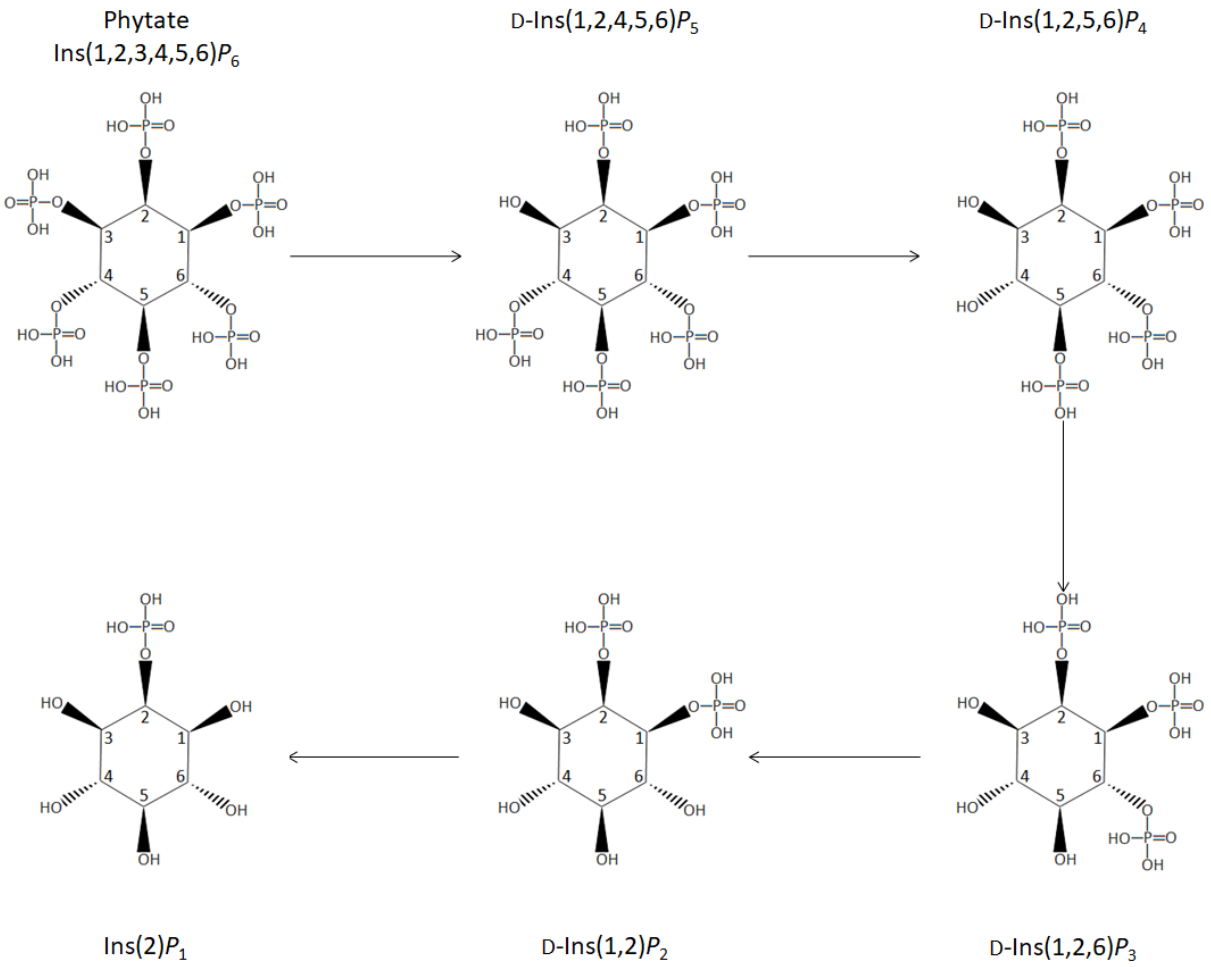

Figure 1.4 Schematic of the sequential breakdown of phytate and lower inositol phosphates, representative of the reaction pathway associated with 3-phytase (EC 3.1.3.8) enzymes. Each 'step' releases one inorganic phosphate molecule to solution.

The 'pathways' of phytate degradation are complicated and depend on the type of phytases being studied. Phytases vary in which of the phosphate groups of phytate they initiate hydrolysis at (figure 1.3), which leads to a different series of lower inositol phosphate stereoisomers produced during degradation. Figure 1.4 shows an example of one possible pathway of phytate degradation, representative of 3-phytase enzymes produced by organisms such as *Aspergillus niger*, *Aspergillus niger* var. *ficuum*, and *Saccharomyces cerevisiae* (256,263). The ability of phytase enzymes to hydrolyse these lower inositol phosphates controls the total amount of inorganic phosphate eventually made available. For example, the *A. niger* phytase follows the full pathway illustrated in figure 1.4 to produce 5 moles of phosphate from 1 mole of phytate; in contrast, the *Escherichia coli* agp phytase produces D-Ins(1,2,4,5,6)P_5 as the final product and therefore only releases 1 mole of

phosphate per mole of phytate (256). A detailed investigation of the enzymology and chemistry of the lower inositol phosphates is beyond the scope of this work. However, the fact that the complete degradation of all inositol phosphates in a system is difficult to guarantee, the ability of lower inositol phosphates to form strong soluble and insoluble complexes with metals (262,264,265), and the ability of lower inositol phosphates to inhibit mineral crystallisation/precipitation (266) means that the influence of these compounds may require further study.

Table 1.2 Example costs of some different sources of phosphate, correct as of 28/6/20. All prices were found on Alibaba.com except for Apatite II™ which was taken from the PIMS NM, Inc. website. Costs are likely to vary considerably depending on vendor, purity etc. so these prices are only to be taken as estimates of the relative costs.

Phosphate source	**Vendor (reference)**	**Cost (per kilogram)**
Sodium phytate	Qingdao Ocean Import And Export Co., Ltd. (267)	£0.8 – £81.3
Disodium glycerol phosphate	Jinan Boss Chemical Industry Co., Ltd. (268)	£16.3 – £81.3
Hydroxyapatite	Qingdao Ocean Import And Export Co., Ltd. (269)	£0.8 – £122.0
Rock phosphate fertiliser (KH_2PO_4)	Shifang Anda Chemicals Co., Ltd. (270)	£0.5 – £0.7
Apatite II™ (from fish bone)	PIMS NM, Inc. (271)	£1.0 – £17.9

Due to its abundance in plant wastes, phytate has been proposed as a low cost phosphate source for a variety of purposes (11,232). Prices at the time of writing (table 1.2) indicate that the cost of phytate is comparable to other available phosphate sources, although it is likely that sourcing phytate directly from waste producers would bring the cost down further. An aspect of future work would be to perform a more detailed cost assessment and develop an appropriate supply chain. Aside from generally being cheaper than glycerol phosphates, another advantage of phytate is the high potential yield of phosphate (1 g of phytic acid contains ~ 0.86 g of phosphate, compared to ~ 0.55 g of phosphate in 1 g of glycerol phosphate) phytate is an attractive source of phosphate (11).

Table 1.3 Results of previous work investigating the biomineralization of phosphate minerals when using phytate as a phosphate donor.

Reference	Successful?	Result
Paterson-Beedle *et al*., 2009, 2010 (182,200)	Mixed	Uranium phosphate by *E. coli* supplied with phytate. However, the *Serratia* sp. N14 bacterium – which has been well researched for its ability to precipitate phosphate minerals from glycerol phosphate – was not able to degrade phytate.
Roeselers and Van Loosdrecht, 2010 (201)	Yes	Calcium phosphate, mineralogical characterisation not performed.
Yung and Jiao, 2014 (183)	No	*Caulobacter crescentus* is able to induce uranium phosphate precipitation *via* the hydrolysis of glycerol 2-phosphate, but no phosphate release or uranium precipitation observed when using phytate as a phosphate source.
Newsome *et al*., 2015 (104)	No	Successful uranium phosphate precipitation when supplying a mixed microbial community with glycerol phosphate, but experiments with phytate were unsuccessful.
Liang *et al*., 2016 (185)	Yes	Uranium phosphate precipitated by various yeasts, but growth and phosphate release were higher when supplied with glycerol phosphate as compared to phytate.
Liang *et al.,* 2016 (202)	Yes	Lead phosphate precipitated by *Isaria javanica*, but glycerol phosphate a more efficient phosphate donor than phytate.
Salome *et al*., 2017 (188)	Mixed	Phytic acid degradation and uranium phosphate precipitation by a mixed microbial community occurred at pH 5 but not at pH 7.
Zhang *et al*., 2019 (203)	Mixed	*A. niger* used to hydrolyse phytate successfully; pyromorphite-Cl formed at pH 5.5, but anglesite ($PbSO_4$) predominated at higher or lower pH values.

Despite the attractive properties of phytate, research to date has encountered mixed success when compared to similar research using glycerol phosphates as phosphate donor molecules. To date, there have been nine published papers investigating phosphate biomineralization from a phytate precursor, with the precipitation of calcium, lead, and uranium phosphates studied (104,182,183,185,188,200–203).

Table 1.3 lists the previous research that has investigated the use of phytate as a phosphate donor and indicates whether phytate was able to be successfully used as a precursor for the formation of phosphate biominerals. The mixed results of these papers can be attributed to

several factors. Firstly, phytase enzymes appear to be less widespread than phosphatase enzymes that can hydrolyse glycerol phosphates. Secondly, even where phytase-active organisms are present, there is generally a higher yield of phosphate from glycerol phosphates than from phytate (185,202). Thirdly, most studied phytase enzymes are optimally active in the acidic pH range (~ pH 2–6) (e.g. see references in (257,272–275)), which likely contributed towards the lack of phytase activity observed by (188) at pH 7.

The pH range (~ 2–6) of most phytase enzymes may also limit the precipitation of certain phosphate minerals such as hydroxyapatite, which typically requires higher pH values to form (276–278). However, a range of other phosphate minerals (including REE, lead, and uranium phosphates) precipitate under acidic conditions (113,182,279,280) and therefore may be more suitable targets. Alternatively, although they are less well characterised, alkaline phytase enzymes do exist (256), and it may be a promising direction for a future project to focus specifically on the identification, isolation, and characterisation of alkaline phytases for biomineralization purposes.

Also of note is the fact that experiments in the presence of contaminated solids encountered mixed results, with (104) finding phytate to be an unsuitable phosphate source, and the experiments in (188) working at pH 5.5 but not pH 7.0. In addition to the previously highlighted limitations, other researchers have noted that the interactions between phytase or phytate and solid phases may limit phytate degradation (3,10,281–285). This has not been explicitly researched in relation to biomineralization but is a critical aspect to understand for *in situ* remediation studies.

1.7 Project aims and objectives

At the outset of this project there were two main directions that could have been pursued: (1) to focus attention on searching for suitable phytate-degrading organisms that produce alkaline-active phytase enzymes that may be suitable for hydroxyapatite manufacture, or (2) to focus on the better characterised acid phytase-producing organisms and study the advantages and limitations of applying these organisms/enzymes to contaminated mine sites. Because they are better characterised, and the fact that many mine tailings sites have acidic pH values, and because a number of relevant phosphate phases are insoluble under acidic conditions, it was decided to pursue the second direction of using acid phytase-producing organisms. Therefore, the main aims of this project can be described as:

- To identify suitable microorganisms that can degrade phytate under environmentally relevant conditions (with a focus on temperature).
- To investigate the precipitation of various phosphate phases (with a focus on calcium and lanthanum phosphates).
- To investigate phytate degradation and phosphate mineral precipitation in simple and complex solid matrices and to understand any factors that may limit the effectiveness of phytate degradation or phosphate mineral precipitation.
- To use purified phytase enzymes to study the precipitation of a variety of different metal phosphate phases and identify the most promising systems for further research, while also comparing metal removal by the precipitated metal phosphates to metal phytate compounds, metal phosphates precipitated directly with inorganic phosphate, and what happens in the absence of phosphate.

1.8 Thesis structure

The main work in this thesis is split into three chapters focusing on experimental results. These chapters are preceded by the introduction and literature review chapter (chapter 1) and followed by a summary/conclusions chapter at the end (chapter 5). The thesis is structured as a series of chapters in journal article format, with chapters 2–4 each representing an early paper draft. To allow a paper-like format, methodology and discussion sections are included in each of the results chapters, rather than being presented as separate chapters.

The first of the results chapters is chapter 2. This describes the identification of two promising phytate-degrading organisms (*Aspergillus niger* and *Blastobotrys adeninivorans*) and investigates the influence of environmentally relevant temperatures (4–30 °C) and carbon source on growth and phytate degradation. This is followed by studying whether either organism is a suitable candidate to produce calcium, manganese, iron, or lanthanum phosphates. The influence of pH, the presence or absence of microbial cells, and whether the metal is added before or after phytate degradation has occurred is also investigated.

Chapter 3 focuses phytate degradation and phosphate mineral precipitation by *A. niger* and *B. adeninivorans* in simple (sand) and complex (simulated mine tailings) solid matrices. Further experiments investigate the interactions between phytate or a purified phytase with

various solid phases to study how these interactions may limit phytate degradation in complex environments.

Finally, chapter 4, focuses on the use of a purified phytase enzyme rather than growing microorganisms to eliminate some of the complicating factors introduced by the presence of microorganisms (e.g. microbially induced pH decreases, production of interfering substances such as oxalic acid). The precipitation of a range of metals – aluminium, calcium, manganese, iron, cobalt, copper, barium, lanthanum, and lead – is studied, comparing the use of phytate alone or phytate followed by phytase hydrolysis. For select metals, further comparisons are made with systems where inorganic phosphate is added directly or when no source of phosphate is added.

Chapter 2
The influence of temperature and carbon source on microbial phytate degradation and the implications for phosphate biomineralization

2.0 Introduction

Phosphate biomineralization, mediated by the microbial hydrolysis of organic phosphate compounds, has been widely researched for the immobilisation of contaminants (such as lead and uranium) and the production of host/sorbent materials (such as calcium, zirconium, and lanthanum phosphates) (11,104,182,184,185,199,202). Phosphate minerals are suitable hosts for contaminants as they can incorporate a wide range of elements into their structures and natural analogues have been shown to be stable over geological timescales (12–15,110,114,116–120).

Most research to date has focused on glycerol phosphate ($C_3H_9O_6P$) compounds as phosphate donor molecules, but the cost of these substrates has been considered a limiting factor (11). As such, alternate sources of organic phosphate such as *myo*-inositol hexakisphosphate ($C_6H_{18}O_{24}P_6$) – commonly referred to as phytic acid, or phytate as a salt – have been proposed (11). Phytate is a common form of organic phosphate in soils and plant matter and can be extracted from a range of plant waste products at low cost (11,230–237).

There have only been a few studies to date using phytate as a substrate for phosphate biomineralization, and these studies have yielded mixed results (104,182,185,188,200–203). A range of bacteria and fungi have been shown to induce the formation of lead and uranium phosphates at the expense of phytate (182,185,188,200,202,203) but, where comparisons with glycerol phosphate were made, the latter compound provided a greater yield of phosphate. Newsome *et al.* (104) found that a mixed microbial community were able to hydrolyse glycerol phosphate to induce the formation of uranium phosphates, but determined that phytate was an unsuitable phosphate donor. Also, the *Serratia* sp. N14 organism widely used to biomineralize phosphates from glycerol phosphate does not hydrolyse phytate (182,200). Researchers have also shown that pH may limit phosphate precipitation; Salome *et al.* (188) found that phytate breakdown and uranium phosphate precipitation occurred at pH 5 but not at pH 7.

Most of this research has looked at immobilising contaminants through the precipitation of contaminant phosphate phases (104,182,185,188,200,202,203). However, in environments where there is a complex range of contaminants at relatively low concentrations, the direct nucleation of their phosphate phases may prove challenging (e.g. Pan *et al.* (286) only observed uranyl phosphate precipitation at uranyl concentrations above 25 µmol/L, with sorption mechanisms more important at lower concentrations). Instead, the formation of a sorption/host material with the capability to immobilise a range of contaminants may be a superior option (102). The best researched phosphate mineral in this regard is calcium hydroxyapatite, and its precipitation from a glycerol 2-phosphate precursor has been well studied (103,128,213–216). However, only one paper has investigated the precipitation of calcium phosphate from phytate, and the authors did not characterise the mineralogy of the precipitate or discuss it with regards to contaminant immobilisation (201).

Given the variability that has been encountered in previous research, the aim of this chapter was to focus attention on two organisms (the mould *Aspergillus niger* and the yeast *Blastobotrys adeninivorans*) well-researched for their production of phytate-degrading (phytase) enzymes (238,243,287,288) and establish their suitability for the production of phosphate sorbent materials that could support the remediation of contaminated uranium mine sites.

Initial experiments investigated the influence of temperature and carbon source on microbial growth and phytate breakdown, as these are important practical factors that need to be considered. Temperature is important in controlling microbial growth and phytase activity (238,287). Most research into phytase enzymes has taken place in the areas of agricultural science where the focus is on temperatures above 30 °C. For *in situ* environmental engineering applications, temperatures are usually well below this value, so it is important to establish whether the test organisms can grow, and induce phytate breakdown, at environmentally relevant temperatures.

A source of carbon is important for microbial growth, but the growth of organisms and the production of enzymes (including phytases) can vary depending on what the source of carbon is (287–290). Additionally, certain other factors need to be considered. Firstly, the type of carbon source has implications for engineering strategies: water-soluble compounds such as glucose could be injected into the subsurface, but insoluble compounds like starch could not.

Secondly, the cost needs to be considered. For example, galactose has been demonstrated to be the best source of carbon to support phytase activity by *B. adeninivorans* (288). However, galactose is more expensive than other sources of carbon, such as glucose and starch (table 2.1). Therefore, these alternatives would be preferable if they can support sufficient phytate breakdown. While there are a wide range of carbon sources that could be used for this work, attention was focused on the three listed in table 2.1. Glucose was chosen because it is the most commonly used carbon source for phytase production (291), while galactose is the best carbon source for *B. adeninivorans* (288). Starch was chosen as a complex carbohydrate representative of the type of carbon source that might be found in waste products (for example, rice bran has been researched as both a source of starch (292) and phytate (237)).

Table 2.1 Comparison of list prices for galactose, glucose, and starch, correct as of 13/4/2020. Costs can vary substantially depending on the vendor, pack size, product purity etc. so these costs are only to be taken as illustrative of the relative differences between the carbon sources. Note that product S4126 is only available in 2 kg or 5 kg pack sizes, so the cost is the price of the 2 kg pack divided by 2. All other prices indicate the cost of the 1 kg pack.

Carbon source	Vendor (product number)	Cost (per kilogram)
Galactose	Sigma-Aldrich (G0625)	£199.00
	Sigma-Aldrich (G0750)	£794.00
Glucose	Sigma-Aldrich (G7021)	£31.20
	Sigma-Aldrich (G7528)	£76.10
Starch	Sigma-Aldrich (S4126)	£20.65
	Sigma-Aldrich (S9765)	£102.00

Experiments investigating the role of temperature and carbon source were followed by precipitation tests to investigate whether calcium phosphates could be formed under the conditions tested. Further investigations also tested alternate metals (manganese, iron, or lanthanum) to see whether their formation could be a promising direction to pursue.

2.1 Experimental programme and methods

As stated above, initial experiments investigated microbial growth and phytate breakdown in a chemically defined nutrient media in which mineral precipitation was unlikely to occur.

Different temperatures (4, 12, 22, or 30 °C) with galactose as the carbon source and different carbon sources (galactose, glucose, or starch) at 22 °C were investigated to test their influence on growth, on the release of phosphate from phytate, and to understand what conditions may be favourable for mineral precipitation.

Following these experiments, investigations into phytase-mediated precipitation of metals were performed using three different experimental systems:

- Filtrate system: Microorganisms were grown in phytate-containing media; once the hydrolysis reaction was complete, the cultures were filtered, the pH of the filtrates adjusted to 2.5, 5.5, or 7.0, and calcium added.
- "Active" system: A culture media containing phytate and the metal of interest was inoculated with microorganisms to investigate how the presence of the metal influenced growth, the release of phosphate from phytate, and to test whether metal phosphate phases could be produced under these conditions.
- "Inactive" system: Microorganisms were grown in a phytate-containing media; once the hydrolysis reaction was complete, the metal of interest was added into the system to investigate precipitation in the presence of microbial cells.

The precipitation tests were all performed at room temperature (~ 22 °C).

2.1.1 Media preparation

Yeast-mold broth (YMB) was purchased from Formedium (YMBR0110). Yeast-mold agar (YMA) was prepared by supplementing YMB (at 21 g/L) with 20 g/L agar powder (either Oxoid LP0011 or Sigma A1296).

Phosphate-free Czapek-Dox agar (CD3A), based upon the media used by (202), consisted of (g/L): glucose (30), $NaNO_3$ (3), KCl (0.5), $MgSO_4.7H_2O$ (0.5), $Fe(NO_3)_3.9H_2O$ (0.01), agar (20).

Phytate minimal agar (PhyM4A), modified from the media used by (288,293), consisted of (g/L): NH_4NO_3 (5), phytic acid (3.8), KCl (0.5), $MgSO_4.7H_2O$ (0.5), $CaCl_2$ (0.1), $MnSO_4.H_2O$ (0.0079), agar (20).

Phosphate buffered saline (PBS) consisted of (g/L): NaCl (8), KCl (0.2), Na_2HPO_4 (1.44), KH_2PO_4 (0.24) (294).

Yeast nitrogen base (YN) media was prepared by supplementing yeast nitrogen base without amino acids and without phosphate powder (Formedium, CYN0801) with phytic acid (2.5 g/L) and appropriate carbon sources (galactose (YN6B), glucose (YN5B), or starch (YN9B) at 20 g/L). For the precipitation experiments, the appropriate concentration of metal being investigated was added. Yeast nitrogen base (added at a concentration of 5.9 g/L) consists of (g/L): $(NH_4)_2SO_4$ (5), $MgSO_4$ (0.5), NaCl (0.1), $CaCl_2$ (0.1), BH_3O_3 (0.0005), $CuSO_4$ (0.00004), KI (0.0001), $FeCl_3$ (0.0002), $MnSO_4$ (0.0004), Na_2MoO_4 (0.0002), $ZnSO_4$ (0.0004), Biotin (0.000002), Ca-Pantothenate (0.0004), Folic Acid (0.000002), Inositol (0.002), Nicotinic Acid (0.0004), 4-Aminobenzoic acid (0.0002), Pyridoxine HCl (0.0004), Riboflavin, (0.0002), Thiamine HCl (0.0004). Except where stated otherwise, the pH of the media was adjusted to 5.5.

All media were prepared using nanopure water (npH_2O) with a resistivity of ≥ 18.2 MΩ·cm. Media was sterilised by autoclaving at 121 °C, 15 psi for 20 minutes. Autoclave-sensitive chemicals (phytic acid, galactose, iron nitrate nonahydrate ($Fe(NO_3)_3.9H_2O$)) were sterilised by syringe filtration (0.2 µm, polyethersulfone (PES) membrane) and then mixed with autoclave-sterilised media under aseptic conditions. In all experiments, phytic acid was added at a nominal concentration of 3.8 mmol/L. Where necessary, filter sterilised 1 mol/L KOH was used to adjust the pH of media to the desired value.

2.1.2 Microorganisms

Aspergillus niger van Tieghem 1867 was supplied by the American Type Culture collection (strain number 201373). *Blastobotrys adeninivorans* (Middelhoven, Hoogk. Niet & Kreger-van Rij) Kurtzman & Robnett (2007) was supplied by CBS (strain number 8335). Long term storage of the strains involved storing spore or cell suspensions as 25% (v/v) glycerol stocks at –80 °C. Routine cultivation of the organisms involved inoculating plates of YMA with a scraping of frozen glycerol stock followed by incubating the plates at 25 °C for four to seven days.

2.1.3 Inoculum preparation

Cryopreserved organisms were revived by transferring a scraping of the frozen glycerol stock onto a YMA plate, which was then incubated at 25 °C for four to seven days. After this period, these cultures were used to inoculate an appropriate nutrient-limited agar media designed to support the induction of phytase activity. The cultures grown on the nutrient-limited agar were then used as inocula for the main experimental work. Repeated subcultures onto fresh

nutrient-limited agar were not performed due to uncertainty over the long-term survival of the cultures under these conditions.

For *A. niger*, a sterile loop was used to transfer spores from a YMA plate onto a phosphate-free CD3A plate. This culture was then incubated at 25 °C for between seven and ten days until spore formation occurred. A spore suspension was prepared by pipetting 10 mL sterile npH_2O onto the surface of the agar plate followed by very carefully 'nudging' the spores into suspension with the pipette tip. The suspension was then pipetted into a sterile 15 mL centrifuge tube. Spore suspensions prepared in this way generally had a measured optical density at 425 nm (OD_{425}) of ~ 0.1.

B. adeninivorans was grown on PhyM4A with phytate as the sole carbon source and main phosphorus source (288) (although note that an inorganic phosphate impurity did exist in the phytate stock at a concentration of about 10% of the phytate concentration). The PhyM4A plates were inoculated by using a sterile loop to transfer a single colony of *B. adeninivorans* grown on YMA followed by streaking the cells across the surface of a PhyM4A plate. The plates were incubated at 25 °C for seven days. A cell suspension was then prepared by pipetting 10 mL sterile 8.5 g/L NaCl solution onto the plate surface and using the pipette tip to gently 'nudge' the cells into suspension. This suspension was pipetted into a sterile 15 mL centrifuge tube, and an aliquot withdrawn to record the optical density at 600 nm (OD_{600}). If necessary, the OD_{600} was adjusted to achieve a value of 0.85 ± 0.05.

Both cell and spore suspensions were inoculated into sterile experimental media at a concentration of 0.5% (v/v). For both organisms, the cell or spore suspension was directly added into experimental media without multiple transfers to "equilibrate" the cultures to the new media. This was done because the transfer of multicellular *A. niger* biomass between liquid cultures is impractical, and because preliminary tests indicated that these methods were sufficient for investigating which conditions were and were not favourable towards phytate degradation.

2.1.4 Experimental setup

Experiments took place in glass Erlenmeyer flasks filled to approximately half capacity (i.e. 50 mL media in 100 mL flasks for "active" system precipitation tests, 100 mL in 250 mL flasks for all other experiments). The necks of flasks were plugged with non-absorbent cotton wool, and

for all experiments except the temperature tests, parafilm was wrapped around the opening to limit the loss of water due to evaporation while still allowing O_2 access (295). Flasks were placed inside shaking incubators set to the appropriate temperature (for 30 °C and 12 °C) or on an orbital shaker at room temperature (for 22 °C) or inside a cold room (for 4 °C). The shaking speed was set to about 130 rpm. Aseptic techniques were used for all experiments except the filtrate and "inactive" system precipitation tests which were performed under non-sterile conditions.

2.1.5 Temperature comparisons

To investigate the rate of phytate breakdown at different temperatures, organisms were inoculated into YN media with galactose as the carbon source (YN6B) and grown at four different temperatures (4 °C, 12 °C, 22 °C, and 30 °C). Triplicate cultures were grown at each temperature along with a single sterile control. Experiments at 22 °C and 30 °C lasted 45 days, while at 4 °C and 12 °C they lasted 120 days.

2.1.6 Carbon source comparisons

To investigate the influence of the carbon source on phytate breakdown, organisms were grown at 22 °C in YN media supplied with one of three carbon sources (galactose, YN6B; glucose, YN5B; or starch, YN9B) at a concentration of 20 g/L. The experiments lasted 30 days and were performed in triplicate for each organism. A single sterile control was also prepared for glucose and starch cultures, while the sterile control from the temperature experiments at 22 °C was considered to represent the galactose cultures.

2.1.7 Filtrate system precipitation tests

These tests involved taking cultures from the temperature and the carbon source tests (grown for 45 and 30 days respectively), filtering out the biomass, and adding calcium into the filtrates.

Because the final pH in the temperature and carbon source tests, of approximately 2.5, does not favour calcium phosphate precipitation, filtrates from the temperature tests were used to investigate the role of pH. Culture filtrates were either left at the final pH of ~ 2.5 or adjusted with 1 mol/L KOH to pH values of ~ 5 or ~ 7. Calcium was then added to a concentration of 10 g/L (250 mmol/L) by directly adding $CaCl_2.2H_2O$. The same amount of calcium was added to the filtrate of the sterile control (left at ~ pH 5.5).

The influence of the carbon source used during growth was investigated by taking filtrates of cultures grown with either galactose, glucose, or starch and directly adding $CaCl_2.2H_2O$ to a calcium concentration of 20 g/L (500 mmol/L). These experiments were all performed at ~ pH 2.5, so the amount of calcium was doubled compared to the pH tests, to try and test whether this could increase the likelihood of calcium phosphates forming at low pH.

After adding calcium, the flasks were gently shaken by hand and then left at room temperature (22 °C) overnight before collecting the precipitates by centrifugation. For convenience, and because microbial contamination was not likely to be significant over the short timescales used, these experiments were performed under non-sterile conditions.

2.1.8 "Active" system precipitation tests

This section investigated the precipitation of three metals (calcium, manganese, lanthanum) when microorganisms were inoculated into a media containing the metal and phytate. Calcium was added at a concentration of 50 mmol/L at pH 7.0, while for manganese and lanthanum, the metals were added at two different concentrations levels (0.5 or 50 mmol/L) at a constant pH value (5.5).

A pH of 7.0 was used for the calcium experiments to try and maximise the likelihood of calcium phosphates forming, while keeping the experiments within a pH range where it was hoped that low levels of phytase activity may still effectively break down phytate over long timescales. For pH 5.5, a value where both *A. niger* and *B. adeninivorans* show high phytase activity (238,261,288), manganese and lanthanum were investigated to test whether their precipitation was more favourable at this value than calcium. Manganese was chosen because geochemical modelling of the nutrient media used in these experiments indicated that manganese phosphates were supersaturated despite a low concentration of manganese in the media (0.15 mg/L or 2.65 µmol/L). Lanthanum was chosen because lanthanide phosphates are known to readily precipitate at acidic pH values (113,296). Additionally, while lanthanum cannot be considered a surrogate for uranium in the strict sense of the term (in solution, lanthanum exists as the trivalent La^{3+} cation, while (under oxidising conditions) uranium exists as the divalent, complex, UO_2^{2+} cation), the elements are considered to have some geochemical similarities (17). In particular both elements have a high affinity for phosphate, and natural examples of phosphate minerals such as apatite and monazite often

contain high levels of both uranium and lanthanum/lanthanides (17). Therefore, experiments with lanthanum can be used to probe conditions which will likely also be favourable towards uranium phosphate precipitation.

Experiments with lanthanum or manganese at 50 mmol/L were performed only for *B. adeninivorans*, with galactose as carbon source. The other experiments (calcium at 50 mmol/L and lanthanum or manganese at 0.5 mmol/L) were performed for both *A. niger* and *B. adeninivorans* with starch as carbon source.

Media was buffered at the appropriate pH value with either 0.2 mol/L MES (pH 5.5) or 0.2 mol/L TES (pH 7.0). Experiments were performed in triplicate at room temperature (~ 22 °C) along with single sterile controls. Cultures were grown for 20 days before collecting biomass and any precipitation that may have occurred.

2.1.9 "Inactive" system precipitation tests

As high concentrations of manganese and lanthanum were observed to inhibit growth and phytase activity of *B. adeninivorans*, experiments were performed to test whether a more viable strategy for the precipitation of these metals was to grow cultures and allow them to break down phytate in the absence of these metals, and then add the metals once inorganic phosphate had already been released to solution. In addition to manganese and lanthanum, tests were also performed with iron as, like manganese, geochemical modelling indicated supersaturation for iron phosphates despite the low concentration of iron (0.07 mg/L or 1.23 µmol/L) initially present. Due to the prevalence of oxalate/tartrate crystals forming in the presence of *A. niger* biomass, equivalent tests were not performed for *A. niger*.

To perform the "inactive" system precipitation tests, cultures of *B. adeninivorans* were grown YN media with galactose as carbon source (YN6B) until the phytate hydrolysis reaction had reached equilibrium (after four to seven days). At this point, the amount of inorganic phosphate released to solution was between 18 and 21 mmol/L which, including the initial background content, gave total inorganic phosphate concentrations of 22 and 24 mmol/L. Duplicate cultures were then spiked with individual metals to a concentration of 50 mmol/L. Lanthanum and manganese were added by pipetting in appropriate amounts of stock solutions (prepared with $LaCl_3.7H_2O$ and $MnSO_4.H_2O$ respectively), while iron was added by directly weighing in the appropriate amount of $FeSO_4.7H_2O$.

After metal addition, the flask necks were plugged with cotton wool, and the flasks shaken by hand to mix. The flasks were then left at room temperature (22 °C) overnight before collecting the biomass and any precipitates that may have formed. For convenience, and because microbial contamination was not likely to be significant over the short timescales used, these experiments were performed under non-sterile conditions.

2.1.10 Sampling

Samples were taken prior to inoculation with microorganisms (i.e. time point zero), at the final time point, and if indicated, at intermediate time points. Samples were removed in aliquots of 5 mL and treated as appropriate depending on the desired analysis:

- For growth quantification (OD_{600} and viable plate counts), cell suspensions were used directly;
- For quantification of water-soluble elements/ions and pH, samples were syringe filtered through 0.2 µm PES or hydrophilic polytetrafluoroethylene (PTFE) membranes and either measured immediately (pH) or stored at –20 °C (for the temperature and carbon tests) or acidified to 1.7 mol/L nitric acid and stored at 4 °C until analysis (for all other experiments);
- For quantification of total elements/ions, samples were acidified to a concentration of 1.7 mol/L nitric acid, filtered (0.2 µm PES or hydrophilic PTFE), and stored at 4 °C until analysis.

2.1.11 Harvesting

At the final time point, in addition to solution samples (described above), the biomass and/or precipitate was harvested for solid phase analysis. Solids were harvested either by vacuum filtration or centrifugation. Vacuum filtration was mainly used for *A. niger*-containing samples (as the *A. niger* cultures do not readily form pellets when centrifuging) and used 47 mm diameter filters (either 0.45 µm mixed cellulose ester (MCE) or, for starch containing samples, glass fibre GF/F filters). After all the liquid had passed through, an extra volume of npH_2O was passed through to wash the sample, followed by washing with isopropyl alcohol (IPA).

Centrifugation was used for *B. adeninivorans* cultures (as filtration times were extremely slow for the unicellular *B. adeninivorans*), sterile controls, and cell-free samples. Samples were

centrifuged at 10,000 rcf for 5–30 minutes as required to yield a pellet and the solids washed one to three times in npH_2O and once with IPA. Washing involved repeated cycles of centrifugation, dispensing the supernatant, mixing the solids with fresh washing solution, and centrifuging again.

Washed solids were then dried at 50 °C to a constant mass, and the dry mass of biomass/precipitates calculated by subtracting the initial mass of the filter/centrifuge tube from the final total mass. Dried samples were ground in a mortar and pestle into a fine powder and stored at room temperature until solid phase analysis was performed.

2.1.12 Analytical techniques

Microbial growth was quantified for *B. adeninivorans* by measuring the optical density at 600 nm (OD_{600}). *A. niger* spore suspensions were quantified by measuring the OD_{425}. Viable plate counts (VPCs), using either the spread plate or drop plate methods (297), were also used to quantify the number of viable cells (expressed as colony forming units per millilitre, CFU/mL) in *B. adeninivorans* cell and *A. niger* spore suspensions. Serial dilutions of cell/spore suspensions were prepared in PBS and, in general, dilution factors in the range of 10^{-4} to 10^{-7} were used. The optical density and VPC techniques are not suitable for quantifying the multicellular *A. niger* cultures, so growth was judged qualitatively based upon photographs.

Analysis of solution samples involved measurements of pH and the concentrations of phosphate and relevant metals. Solution pH was recorded using either using a Mettler-Toledo SevenMulti™ S47 pH meter and an InLab Expert Pro pH probe or a Hach HQ40d Portable Meter with a Hach PHC30101 probe. Prior to each set of measurements, the pH probe was calibrated using pH 4, pH 7, and/or pH 10 standards depending on the pH range required.

Colorimetric determination of inorganic phosphate was performed according to the Peterson method as modified by Qvirist *et al*. (298). The absorbance of the reaction mixture was read at 700 nm (A_{700}) using an Epoch Biotek multiplate reader and recorded with the Gen 5 1.11 software. Samples were compared to a standard curve of known values (0–0.32 mmol PO_4/L) measured at the same time as the samples. Standards were either prepared from KH_2PO_4 (after drying overnight at 105 °C) or by diluting commercially prepared standards (supplied by Megazyme (299) or SPEX CertiPrep).

The limit of detection (LOD) for the colorimetric phosphate procedure was defined using the equation LOD = $\bar{x} + 3\sigma$, where $\bar{x}$ and σ respectively represent the mean and standard deviation of 129 blank (npH_2O mixed with the colorimetric reagents) samples. Using this method, the limit of detection was calculated to be approximately 8 µmol/L.

The background inorganic phosphate concentration in each media tested was defined as the mean recorded value of phosphate across all samples taken prior to inoculation. The phosphate released was defined as the measured phosphate concentration recorded at each time point after the background value had been subtracted. Phosphate release is given in terms of the amount released (per millilitre of culture solution) rather than attempting to normalise to any quantitative measures of growth as it was impractical to quantify the growth of *A. niger* throughout the course of the experiments and, therefore, comparisons to the *B. adeninivorans* cultures would not have been possible.

Metal and phosphorus concentrations were measured by inductively coupled plasma optical emission spectroscopy (ICP-OES) using a Thermo Scientific iCAP 6000 Series ICP Spectrometer with the Thermo i-TEVA (version 2.4.0.81, 2010) software. Samples were compared to standards of known concentrations prepared from ICP grade commercially prepared stock solutions, supplied by BDH, Fisher Scientific, or SPEX CertiPrep. Samples and standards were diluted in 0.8 mol/L trace element grade nitric acid, which was also used as a blank. The Minimum detection limits of analytes were determined automatically by the instrument's software based upon calibration standards and blanks. Phosphorus measured by ICP-OES was expressed as phosphate (PO_4).

Phosphate concentrations were measured by the two different techniques above (colorimetry and ICP-OES) because they measure different phosphate species; that is, colorimetry is selective for inorganic phosphate, while ICP-OES measures all phosphate species (inorganic and organic). From this, inorganic phosphate concentrations were subtracted from ICP-OES measured phosphate concentrations to calculate the concentration of organic phosphate present. The calculated organic phosphate can be used as a proxy for phytate concentrations, although due to the possible presence of lower inositol phosphates and cellular phosphates, the results sections below are discussed in terms of organic phosphate.

For all analytes (inorganic phosphate, organic phosphate, and metals), two fractions are described in the results: water-soluble and total. Water-soluble concentrations are where any precipitation was filtered out of the samples prior to analysis, while total is where the precipitation was dissolved prior to filtration (as described in the sampling section above). The difference between the total and water-soluble fractions gives the concentration in the solid phase.

Solid phase analysis was performed by X-ray diffraction (XRD) using a Bruker D8 Advance X-ray diffractometer operated by the DIFFRAC Measurement Centre v6 software. Analysis used the Cu K_α radiation, a 2ϑ range of 5–80°, a 2ϑ step size of 0.02°, a step time of 1 s, a voltage of 40 kV, and a current of 40 mA. For the primary optics, either the Göbel mirror or the motorised slit was used. Phase identification was performed using the DIFFRAC EVA v4.1.1 software and the PDF-2 ICDD Release 2009 database (300). Rietveld refinements were performed using TOPAS v5, with structural models sourced from the Inorganic Crystal Structure Database (ICSD) (301) or the Crystallography Open Database (COD) (302).

Geochemical modelling was performed using PHREEQC version 3 to probe solution speciation and mineral saturation indices (303). Modelling was performed using the SIT.DAT database. As this database did not include phytate, literature values were used to construct a phytate database – the details of this are described in appendix A.

2.2 Results and discussion

2.2.1 The effect of temperature on growth and phytate degradation

The microorganisms *A. niger* and *B. adeninivorans* were grown with a source of phytic acid at four different temperatures and the concentration of inorganic phosphate in solution measured as a function of time. Negligible changes in inorganic phosphate concentration were measured in the sterile controls (Table 2.2), and phytate is known to have a chemical half-life of about 100–150 years at 25 °C and pH 5–6 in the absence of biological activity (251), so any changes in the inorganic phosphate concentration during these experiments can be attributed to phytase enzyme activity of either *A. niger* or *B. adeninivorans*.

Table 2.2 Summary of temperature experiment results (maximum phosphate release is given as a percentage of the available phosphate content of phytate). Values are given as the mean plus or minus difference between the mean and the upper or lower measured values. Experiments were performed in triplicate, except for the sterile controls which were performed as single experiments. The sterile control at 30 °C had to be discarded due to contamination. An asterisk (*) indicates that the value is the mean of two samples due to the spillage of one sample preventing dry mass measurement. The initial pH was 5.48, as determined by measuring a representative batch of media.

Organism	Temp. (°C)	Phosphate release at final time point (%)			Final pH			Dry mass (g)		
		Mean	+	-	Mean	+	-	Mean	+	-
B. adeninivorans	4 °C	**19%**	2%	2%	**2.06**	0.02	0.02	**0.30**	0.03	0.05
B. adeninivorans	12 °C	**42%**	5%	5%	**2.16**	0.03	0.11	**0.31***	0.02	0.02
B. adeninivorans	20 °C	**69%**	3%	2%	**2.31**	0.02	2.31	**0.46**	0.06	0.06
B. adeninivorans	30 °C	**50%**	15%	22%	**2.39**	0.09	0.06	**0.45***	0.01	0.01
A. niger	4 °C	**2%**	2%	2%	**5.49**	0.05	0.04	**0.00**	0.00	0.00
A. niger	12 °C	**57%**	17%	29%	**2.47**	0.50	0.36	**0.35**	0.16	0.28
A. niger	20 °C	**76%**	23%	25%	**2.52**	0.05	0.10	**0.45**	0.02	0.01
A. niger	30 °C	**122%**	30%	19%	**2.66**	0.07	0.04	**0.45**	0.01	0.02
Sterile control	4 °C	**-1%**	n/a	n/a	**5.57**	n/a	n/a	**0.00**	n/a	n/a
Sterile control	12 °C	**0%**	n/a	n/a	**5.52**	n/a	n/a	**0.00**	n/a	n/a
Sterile control	20 °C	**4%**	n/a	n/a	**5.27**	n/a	n/a	**0.01**	n/a	n/a

Table 2.2 summarises the results for the temperature experiments. *B. adeninivorans* displayed growth at every temperature investigated, along with a release of phosphate from phytate. In contrast, *A. niger* showed no signs of growth or phytase activity at 4 °C (as indicated by visual observations, the culture pH remaining at around 5.5, and measured dry mass values of 0 g), but at every other temperature grew well and released similar or greater quantities of phosphate than *B. adeninivorans*.

It is notable that, at 30 °C, *A. niger* released more than 100% of the available phosphate from phytate. This could have been due to the release of cellular phosphate, experimental or analytical error, or the evaporation of water over the course of the experiments. Water evaporation appeared to be significant at 30 °C, and to a lesser extent at 22 °C (the volumes of culture filtrates were measured at the final time point and were recorded as between 35 and 80 mL when they should have been around 95 mL – the range of values likely relates to the different shapes of conical flasks used, with some having larger openings than others).

Because corrections for evaporation could not be applied throughout the time course of the experiment the results presented in table 2.2 and figure 2.1 are presented “as-measured”.

Factors relating to analytical error or water evaporation should have been comparable between the different organisms and the controls. The slight increase in phosphate in the sterile control at 22 °C, despite no visible signs of contamination, suggests that evaporation may have been a factor in artificially increasing the measured phosphate concentrations. However, an excess (more than 100% of that theoretically available) of phosphate was only measured in the *A. niger* cultures which suggests that there was an organism-dependent difference. Further work would be required to establish this, but if the excess of phosphate was released from the *A. niger* cells then this could be an advantageous property, as it would provide more available phosphate for precipitation.

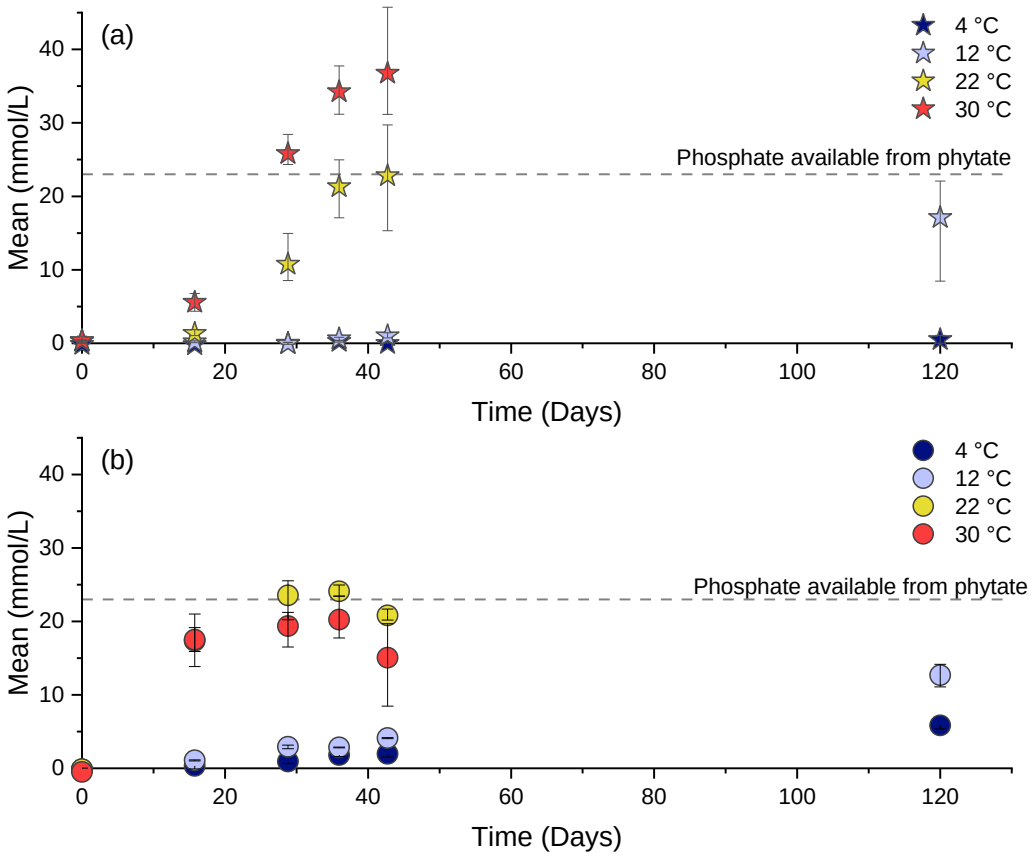

Figure 2.1 Phosphate release from phytate over time for (a) A. niger *(★), and (b)* B. adeninivorans *(●) at four different temperatures with galactose as carbon source. Data points are the mean values of triplicate samples, plus or minus the difference between the mean and the upper or lower measured values. All samples have had the background concentration of inorganic phosphate in the media (4 mmol/L) subtracted. Dashed line indicates the theoretically available phosphate in phytate.*

Plotting phosphate concentrations against time (figure 2.1) indicated a faster release of phosphate for *B. adeninivorans* compared to *A. niger*. For *B. adeninivorans,* the release of phosphate appears to reach equilibrium at 22 °C and 30 °C after between 15 and 30 days, while for *A. niger* it takes around 40 days to reach equilibrium. At the lower temperatures, *B. adeninivorans* begins to show some phytate degradation at 12 °C after about 30 days and at 4 °C after 40 days, whereas for *A. niger* the only indication of any phytate hydrolysis at lower temperatures was at 12 °C after 120 days. At 22 °C and 30 °C in the *B. adeninivorans* cultures there appeared to be a decrease in inorganic phosphate between 30 and 45 days. It is uncertain whether this is a result of analytical variability, precipitation/biosorption of phosphate, or the synthesis of organic phosphate compounds that are not detected by the colorimetric procedure for phosphate determination. Phosphate release by *B. adeninivorans* at 22 °C was also equivalent to, or better than, the phosphate release at 30 °C. While the differences may be within experimental error margins, effective phosphate release at ambient temperatures is a useful property for environmental applications.

At the final time points of the experiments, *A. niger* had released more phosphate than *B. adeninivorans* at 12 °C and 30 °C, while the reverse was true at 4 °C, and the organisms were equivalent at 22 °C. To truly compare the organisms at 30 °C, it would be necessary to understand the reasons for the greater than 100% phosphate release by *A. niger* at this temperature. However, at 12 °C and above, it appears that over long timescales, *A. niger* is more efficient at releasing phosphate to solution despite the initially faster release by *B. adeninivorans*. The minimum growth temperature for *A. niger* has been described as being in the range of 6 to 8 °C (304). Above this “cut-off” point it may be a more efficient organism for releasing phosphate from phytate, whereas at lower temperatures, *B. adeninivorans* would be more suitable.

2.2.2 Effect of carbon source on growth and phytate degradation

To investigate the role of carbon source in phytase production and activity, *A. niger* and *B. adeninivorans* were grown at 22 °C in a phytate-containing culture media with either galactose, glucose, or starch added as carbon source at 20 g/L.

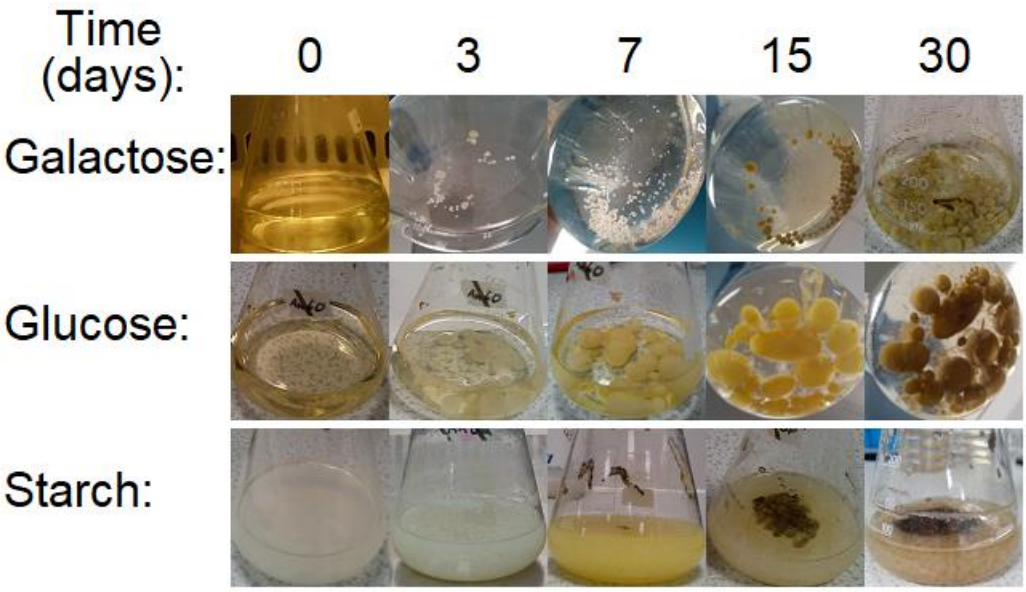

Figure 2.2 Photographs taken at each sampling time point of A. niger *cultures grown with galactose, glucose, or starch as carbon source. Turbidity in the starch culture is a result of the insoluble starch present.*

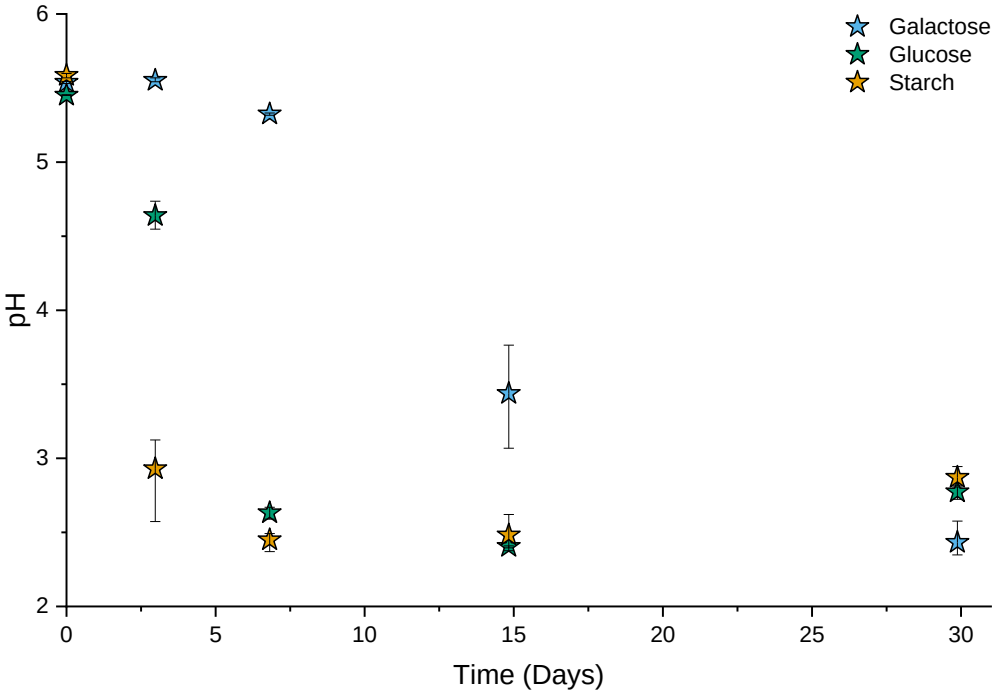

Figure 2.3 pH of media during incubation of A. niger *grown with three different carbon sources at 22 °C. Data points are the mean values of triplicate samples, plus or minus the difference between the mean and the upper or lower measured values.*

Quantitative measures of fungal growth are challenging, as multicellular organisms cannot be quantified by optical density or viable plate count methods. Instead, the growth of *A. niger*

supplied with either galactose, glucose, or starch as carbon sources was judged by a visual assessment (figure 2.2). The speed of *A. niger* growth when supplied with different carbon sources appeared to follow the order starch > glucose > galactose, and this was mirrored in the speed of the pH reduction when grown with the different carbon sources (figure 2.3).

There were also notable differences in fungal morphology between the cultures grown with the different carbon sources. The morphology of colonies with starch as a carbon source were small, filamentous, and densely packed the culture media within three days, with spore formation becoming visible at around seven days. With glucose as a carbon source, the fungal colonies formed larger, denser, "smoother" appearing pellets, with spore formation visible after thirty days. The colonies when grown with galactose appeared intermediate in size and seemed to have a similarly dense structure to the glucose cultures. A small amount of spore formation possibly occurred with galactose after thirty days. The morphology of fungal cultures (i.e. dense "pellets" in the galactose and glucose cultures, compared to more dispersed, filamentous "clumps" in the starch cultures) is an important consideration in fungal biotechnology processes and may have an influence on the production of metabolites (305–307). Previous research has indicated that smaller, filamentous morphologies favour higher phytase production than larger pellets (308) which is consistent with the fastest breakdown occurring in the starch cultures in this work (figure 2.3). A detailed examination into how this influences any subsequent biomineralization is beyond the scope of this work but may be of interest when attempting to optimise procedures.

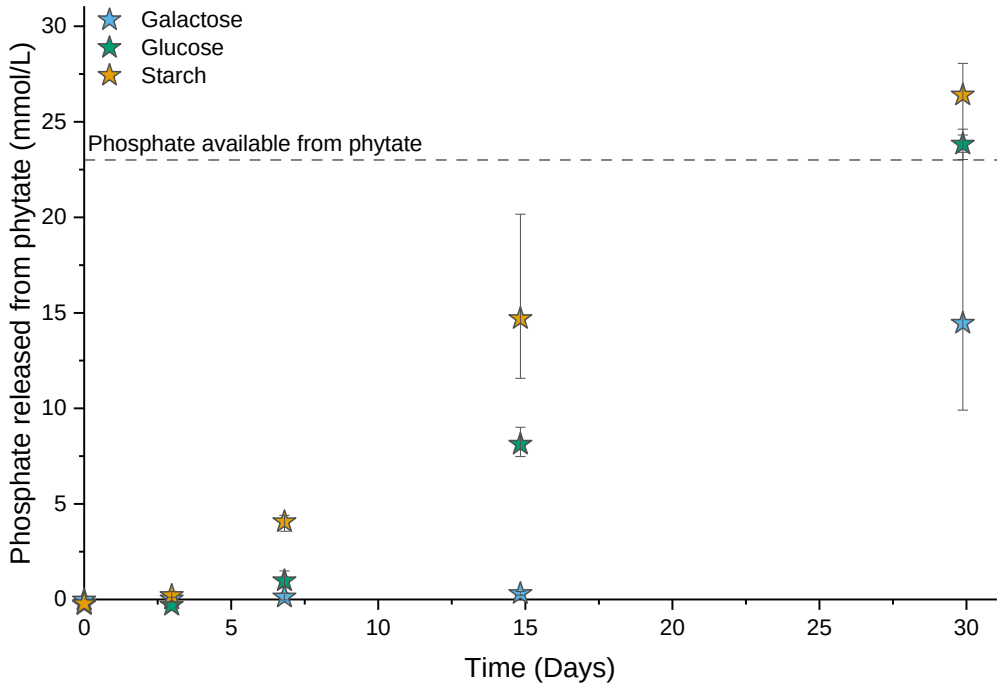

Figure 2.4 Phosphate released from phytate by A. niger *when grown with three different carbon sources at 22 °C. Data points are the mean values of triplicate samples, plus or minus the difference between the mean and the upper or lower measured values. The background concentration of phosphate in the phytate stock (5.2, 4.7, and 4.4 mmol/L for galactose, glucose, and starch cultures respectively) has been subtracted from all values. Dashed line indicates the theoretically available phosphate in phytate.*

The rates of phosphate release for *A. niger* when grown with different carbon sources follows the qualitative observations of growth and the measurements of pH, occurring in the order starch > glucose > galactose (figure 2.4). Results from the temperature experiments (figure 2.1a) indicate that the galactose cultures would require 45 days to release equivalent amounts of phosphate to the starch and glucose cultures at 30 days.

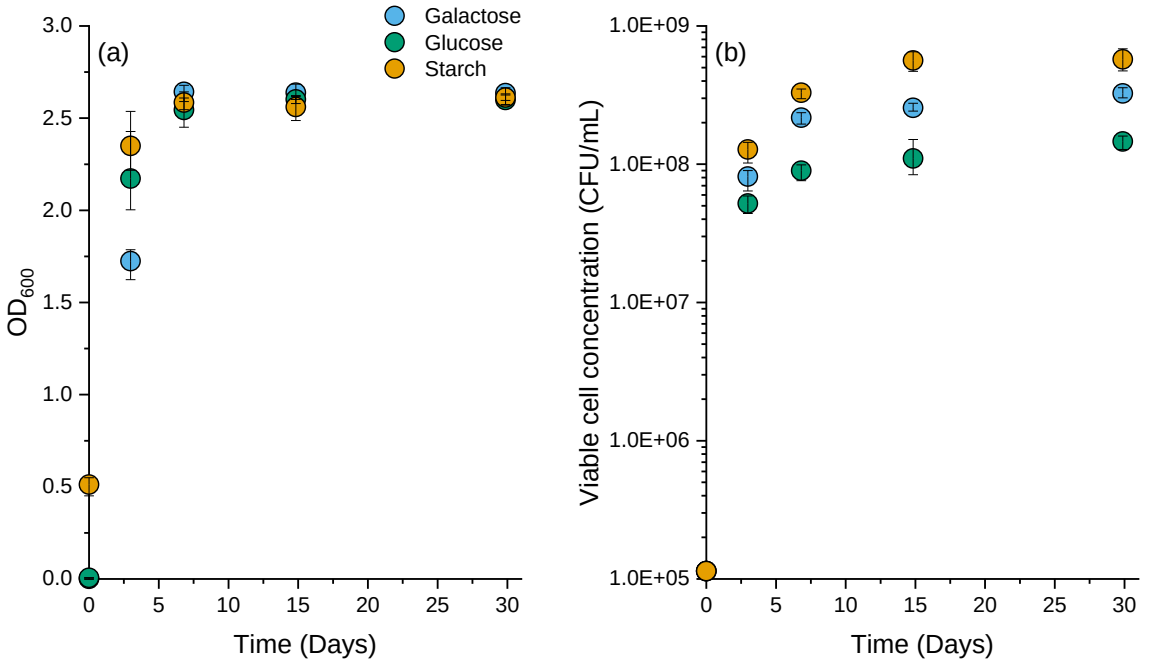

Figure 2.5 Measurements of (a) Optical density at 600 nm (OD_{600}), and (b) Viable cell concentrations (as colony forming units per millilitre) for B. adeninivorans *grown with three different carbon sources at 22 °C. Values are the mean of triplicate samples plus or minus the difference between the mean and upper or lower measured values. For OD_{600} measurements, the zero time point represents blank, sterile culture media (the non-zero reading in the starch culture is due to turbidity from starch). For viable cell concentrations, the zero time point measurement was calculated by taking the CFU/mL measured in the inoculum and multiplying it by a dilution factor (for 0.5 mL inoculum into 100 mL media).*

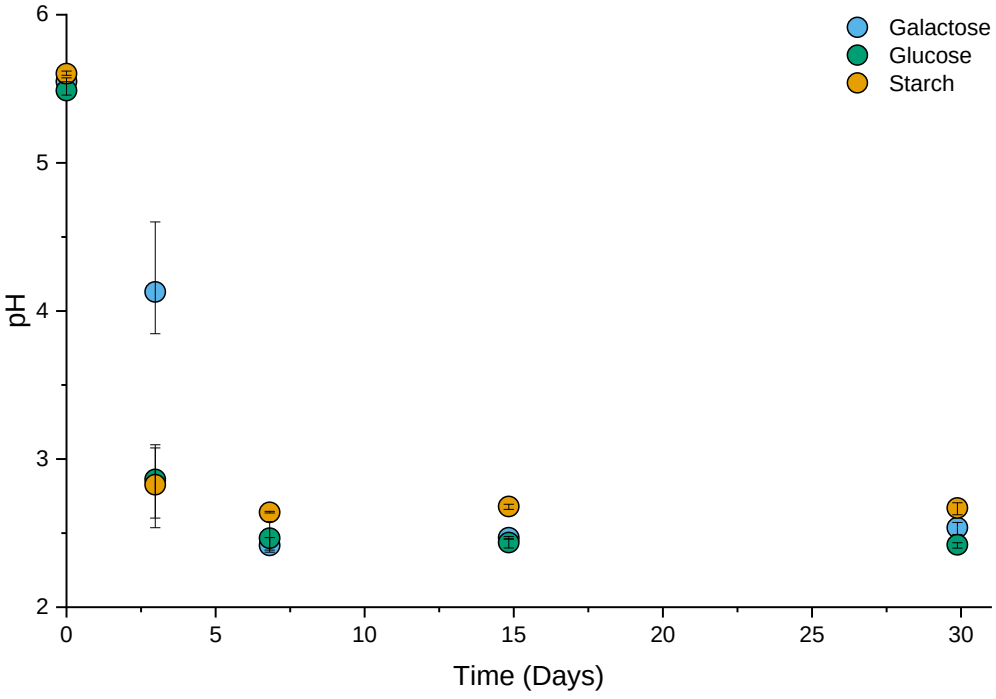

Figure 2.6 pH of media during incubation of B. adeninivorans *grown with three different carbon sources at 22 °C. Data points are the mean values of triplicate samples, plus or minus the difference between the mean and the upper or lower measured values.*

B. adeninivorans grew well with all three carbon sources (figure 2.5), with the cell density reaching a maximum after 3–7 days and remaining stable until the final time point of the experiment at 30 days. There appeared to be little difference between the carbon sources, with maximum cell density following the order starch > galactose > glucose (figure 2.5b), although OD_{600} measurements followed the order starch > glucose > galactose (figure 2.5a).

The trend of pH reduction was slightly different, with the glucose and starch grown cultures reducing the pH to around 3 after three days, while in the galactose culture, the pH after three days was slightly higher at around 4 (figure 2.6). After seven days, all cultures had reduced the pH to a similar value of around 2.5, and this remained stable for the rest of the experiment.

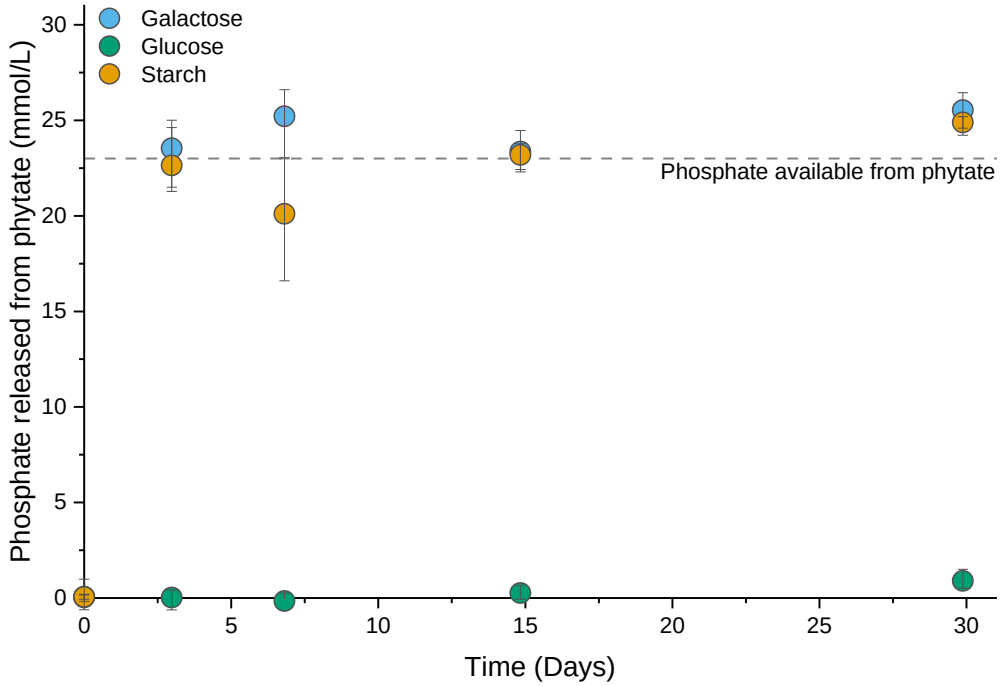

Figure 2.7 Phosphate released from phytate by B. adeninivorans *when grown with three different carbon sources at 22 °C. Data points are the mean values of triplicate samples, plus or minus the difference between the mean and the upper or lower measured values. The background concentration of phosphate in the phytate stock (5.2, 4.7, and 4.4 mmol/L for galactose, glucose, and starch cultures respectively) has been subtracted from all values. Dashed line indicates the theoretically available phosphate in phytate.*

B. adeninivorans shows a striking difference in phytate hydrolysis when supplied with different carbon sources (figure 2.7). With starch and galactose, phosphate release is rapid, reaching equilibrium after 3–7 days (the dip at seven days for the starch grown cultures is likely due to analytical variability). However, with glucose as the carbon source, no phosphate release was

observed over the thirty days of the experiment. This was despite showing equivalent growth and pH changes when compared to starch and galactose. Glucose inhibition of phytase activity by *B. adeninivorans* has previously been shown (288), but the complete lack of any phosphate release over thirty days was surprising.

The findings of the experiments comparing carbon sources indicate the importance of the nutrient requirements of microorganisms being utilised in bioremediation strategies. Starch appeared to be the best carbon source in terms of cost, supporting microbial growth, and phosphate release. However, its low solubility in water may provide either advantages or disadvantages. The low solubility may be an advantage for *in situ* soil mixing-based remediation strategies, as it will be less likely to be washed out by flowing water. However, for injection-based strategies, it is likely that starch would lead to clogging of the injection well, and a soluble carbon source such as galactose or glucose would be necessary. In that case, despite the higher cost, galactose would be a more appropriate choice for *B. adeninivorans* than glucose. In contrast, phytate breakdown by *A. niger* is faster when provided with the cheaper glucose.

2.2.3 Filtrate system precipitation tests

While the temperature and carbon tests indicate that *A. niger* and *B. adeninivorans* can effectively induce the hydrolysis of phytate across a range of conditions, the final pH of cultures in all cases being reduced to between 2 and 3 creates conditions that are unfavourable towards calcium phosphate (and particularly hydroxyapatite) precipitation (277,278,309). Therefore, culture filtrates from the temperature experiments were either left at their final growth pH value (~ 2.5) or adjusted to pH values of 5, 6, or 7 to investigate the role of pH in calcium precipitation. The role of the carbon source used during growth was also investigated at pH 2.5 only.

2.2.3.1 *Influence of pH on calcium precipitation in phytase-active culture filtrates*

Table 2.3 Summary of soluble inorganic phosphate and precipitated minerals at different pH values. N.d. indicates that the sample was not analysed by XRD.

Setup			***Results***			
Organism	**Growth temp. (°C)**	**Modified pH**	**Phosphate removed from solution (mmol/L)**	**Final pH**	**Dry mass (g/100 mL)**	**Identification by XRD**
B. adeninivorans	22	2.3	4.0	1.8	0.652	Gypsum
B. adeninivorans	30	2.5	2.1	2.0	1.050	n.d.
A. niger	30	2.5	6.2	2.0	1.497	Gypsum
A. niger	22	2.6	0.4	2.0	0.815	Gypsum
A. niger	30	5.0	9.6	4.0	0.020	n.d.
Sterile	22	5.3	3.0	3.8	0.114	n.d.
B. adeninivorans	22	5.3	8.3	4.4	0.009	n.d.
A. niger	22	5.9	8.4	3.1	0.509	Gypsum + Brushite/Ardealite
B. adeninivorans	30	6.9	19.5	4.6	0.484	Gypsum + Brushite/Ardealite
A. niger	22	7.0	12.0	4.0	0.754	Gypsum + Brushite/Ardealite
A. niger	30	7.0	30.4	4.4	0.961	Gypsum + Brushite/Ardealite
B. adeninivorans	30	7.0	13.4	5.0	0.483	Gypsum + Brushite/Ardealite
B. adeninivorans	22	7.1	18.0	4.5	0.722	Gypsum + Brushite/Ardealite

Varying solution pH appeared to influence the amount of inorganic phosphate remaining in solution, the mass of precipitates, and the mineralogy of the precipitates (table 2.3). Where, at around pH 2.5, between 1% and 17% of phosphate was removed from solution, this increased to between 26% and 57% at between pH 5 and pH 6 and increased further to between 62% and 87% at around pH 7. The original plan in this experiment was to adjust pH so that each pH value (pH 2.5, 5.5, 7.0) would be represented by two filtrates for each organism (i.e. two *A. niger* filtrates left at pH 2.5, two adjusted to pH 5.5, two adjusted to pH 7.0, and likewise for *B. adeninivorans*). However, the different filtrates had slightly different acid-base properties (for example, one *A. niger* filtrate was adjusted to pH 5.0 with 0.016 mol/L KOH while adding 0.016 mol/L KOH to another *A. niger* filtrate brought the pH to 6.0). This was likely due to varying concentrations of phosphate and phytate (and lower inositol phosphates produced during phytate hydrolysis) between different samples, as varying concentrations of the species will change the titration curves of the solutions (310,311). Therefore, one filtrate each for *A. niger* and *B. adeninivorans* ended up being adjusted to higher pH values than intended (pH 6 and 7 respectively).

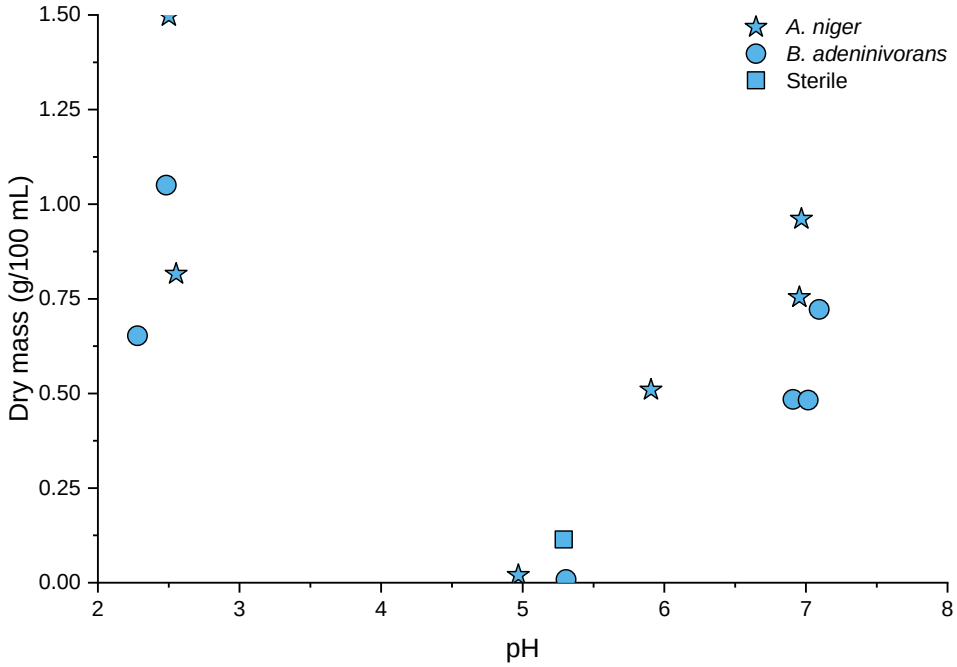

Figure 2.8 Dry mass of precipitates plotted against the initial pH of solutions prior to calcium addition. Data points represent single measurements. Symbols represent the organism that was present during growth prior to filtration of the samples (★ = A. niger, ● = B. adeninivorans, ■ = sterile control). Due to different solution volumes, the dry masses are given in terms of grams per 100 mL of solution that they were precipitated from.

The dry mass of the recovered precipitates did not follow the trend of phosphate removal. The highest masses were recorded at initial pH values of 2.5 and 7.0, with a minimum amount recorded at around pH 5.0 (figure 2.8).

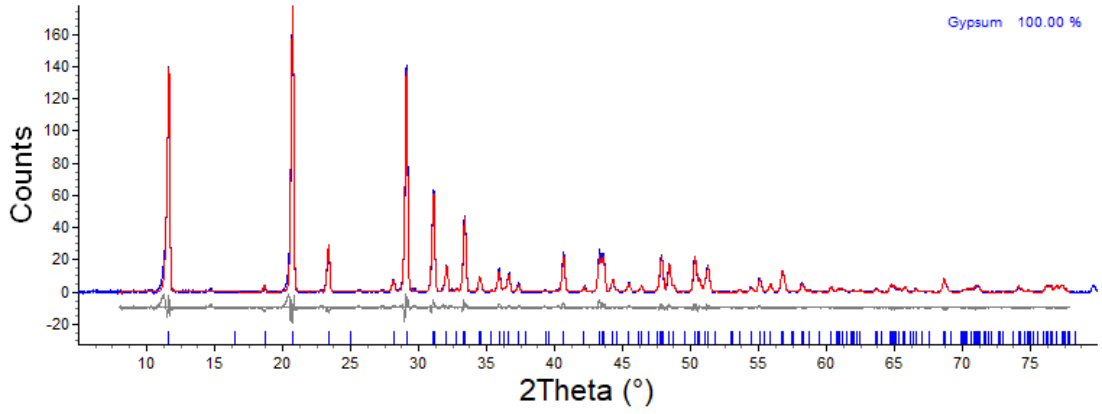

Figure 2.9 Representative XRD pattern from the filtrate system precipitation tests at an initial pH of 2.5 (blue). The fitted reference pattern (red) used the structural model for gypsum (ICSD #2058) from (312)*. The grey line shows the difference between the measured pattern and the fitted model, the blue tick marks show the positions of Bragg peaks associated with gypsum. Samples were measured using the Göbel mirror optics setup with the copper K_α radiation across a 2θ range of 5–80° with a step size of 0.02° and a step time of 1 s.*

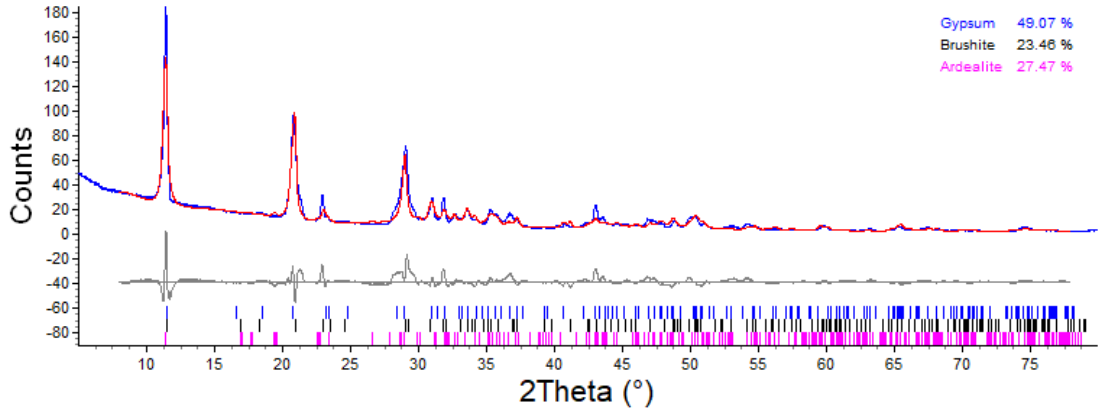

Figure 2.10 Representative XRD pattern from the filtrate system precipitation tests at an initial pH of 7.0 (blue). The fitted reference pattern (red) used the structural model for gypsum (ICSD #2058) from (312), *brushite (COD #1533075) from* (313), *and ardealite (ICSD #100626) from* (314). *The grey line shows the difference between the measured pattern and the fitted model, the blue tick marks show the positions of Bragg peaks associated with gypsum. Samples were measured using the Göbel mirror optics setup with the copper K_α radiation across a 2θ range of 5–80° with a step size of 0.02° and a step time of 1 s.*

XRD analysis of the precipitated solids (figure 2.9, figure 2.10) indicated that sulfate, present in the culture media at a concentration of 42 mmol/L, was important in all solid phases formed. At an initial pH of 2.5 the major mineral phase was gypsum ($CaSO_4.2H_2O$, figure 2.9) but at pH 7.0 peaks associated with gypsum and, potentially, brushite ($CaHPO_4.2H_2O$) and ardealite ($Ca(SO_4)(PO_3OH).4H_2O$) were present (figure 2.10). Including structural models for brushite and ardealite improved the Rietveld refinement of the pH 7.0 patterns compared to including just gypsum, but there were still substantial deviations between the fitted model and the measured pattern. The pattern shown in figure 2.10 appears visually similar to members of the $Ca(SO_4,HPO_4).2H_2O$ solid solution shown by Pinto *et al.* (315) but structural model files were not available to enable a Rietveld refinement.

This indicates an interplay between sulfate and phosphate in the speciation of calcium. At pH 2.5, calcium binds preferentially to sulfate to form gypsum, with the phosphate remaining almost entirely in solution, whereas at circumneutral pH values, the decreased solubility of calcium phosphate complexes appears to lead to the formation of mixed sulfate-phosphate coprecipitates. At around pH 5.0, however, there appears to be an antagonistic effect where competition for calcium between sulfate and phosphate inhibits the precipitation of either material. Alternatively, the strong binding of calcium by residual phytate or lower inositol phosphates produced during phytate breakdown may have had a role.

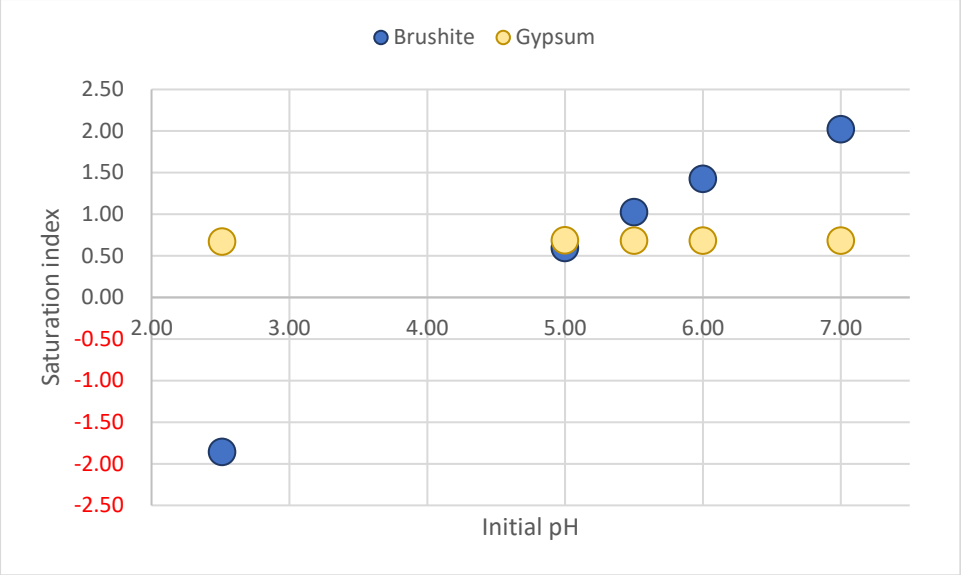

Figure 2.11 Saturation indices of brushite and gypsum versus pH in phytase-active culture filtrates calculated in PHREEQC at pH values representative of the initial pH values used in experimental work.

To examine possible antagonism between sulfate, phosphate, and phytate at ~ pH 5, geochemical modelling of the system was performed at different pH values (2.5, 5.0, 5.5, 6.0, and 7.0) based upon averaged experimental data for the pH 2.5 and pH 7.0 systems (n = 4 for pH 2.5, and n = 5 for pH 7.0) or single experiments for other pH values. Saturation indices of all possible solid phases defined in the database are shown in appendix B, table B.1. The saturation index of gypsum appears to remain constant across the range of pH values tested, while there is an increase in the saturation indices of brushite with pH, which only becomes supersaturated above pH 5.0 (figure 2.11). This explains why gypsum was the only phase observed at low pH and is consistent with a mixed calcium sulfate-phosphate forming at circumneutral pH values. Geochemical modelling was, however, unable to explain the “trough” in precipitation observed at pH 5.0–5.5.

The explanation for this U-shaped trend of precipitation in these experiments remains uncertain. Previous researchers have indicated that mixed calcium sulfate-phosphates should form in the pH 5.0–5.5 range (315,316) so something about the experimental setup differed in this work. It could be that an incomplete description of the phytate and lower inositol phosphate species in the system has introduced errors that lead to an overestimation of saturation indices in the pH 5.0–5.5 range. For example, the modelling approach used assumed that phosphorus was present either as inorganic phosphate or phytate. However,

the microbial hydrolysis of phytate produces a range of so-called lower inositol phosphates which may have an important impact on the solution speciation of calcium. Inositol trisphosphate is known to form strong complexes with calcium (317) and these complexes are more soluble than calcium complexes with phytate (264). However, without more comprehensive thermodynamic data and a quantification of which lower inositol phosphates were produced in this work it is difficult to incorporate this into any models. Additionally, no data were available for soluble mixed potassium-calcium phytate complexes. The solution speciation of phytate in the geochemical model was dominated by potassium complexes (data not shown), which indicates that potassium-calcium phytate species may have been more important than calcium phytate or calcium hydrogen phytate species. Without access to the relevant data, however, it is uncertain what influence these species would have on calcium precipitation. Alternatively, microbially secreted organic acids, such as citric acid and gluconic acid, could bind to calcium and increase its solubility at certain pH values. It may also be that the minimal precipitation at pH 5.0–5.5 was a result of experimental errors; ideally, repeat experiments would be performed to establish this – although, the fact that three independent samples in this pH range (the sterile phytate filtrate, and one filtrate each from *A. niger* and *B. adeninivorans*) produced a similar result suggests that the results are genuine.

The above results indicate that, due to their enzymes being optimally active in the acidic pH range, the direct production of hydroxyapatite by *A. niger* or *B. adeninivorans* is unlikely. However, the coprecipitation of calcium sulfate-phosphates may be more favourable. Composite calcium sulfate-phosphate materials have interesting properties and have been researched for their applications in medicine (as bone cements) (318), construction (319), and heavy metal remediation (320,321). In these materials, the sulfate component may contribute towards a higher mechanical strength (comparable to gypsum) (319) and an enhanced hydraulic performance (321) while the phosphate component may contribute towards improved water resistance (319) and contaminant immobilisation (320,321). These properties, along with a high enough porosity to allow for fluid flow (320), means calcium sulfate-phosphate composites an are interesting materials for the construction of permeable reactive barriers (321). However, if this is to be manufactured *in situ* through a phytase-mediated biomineralization strategy, further work is required to understand the lack of precipitation at pH 5.0–5.5 and how the presence of residual phytate or lower inositol phosphates influences

the precipitation of calcium sulfate-phosphates. It would also be desirable to optimise the sulfate:phosphate ratio, as these experiments were performed with an excess of sulfate, whereas it may be preferable to perform experiments with a 1:1 ratio as is found in the mineral ardealite. Furthermore, as these experiments were performed with culture filtrates, it would be necessary to study how the presence of microbial cells influences the precipitated material.

2.2.3.2 Influence of carbon source

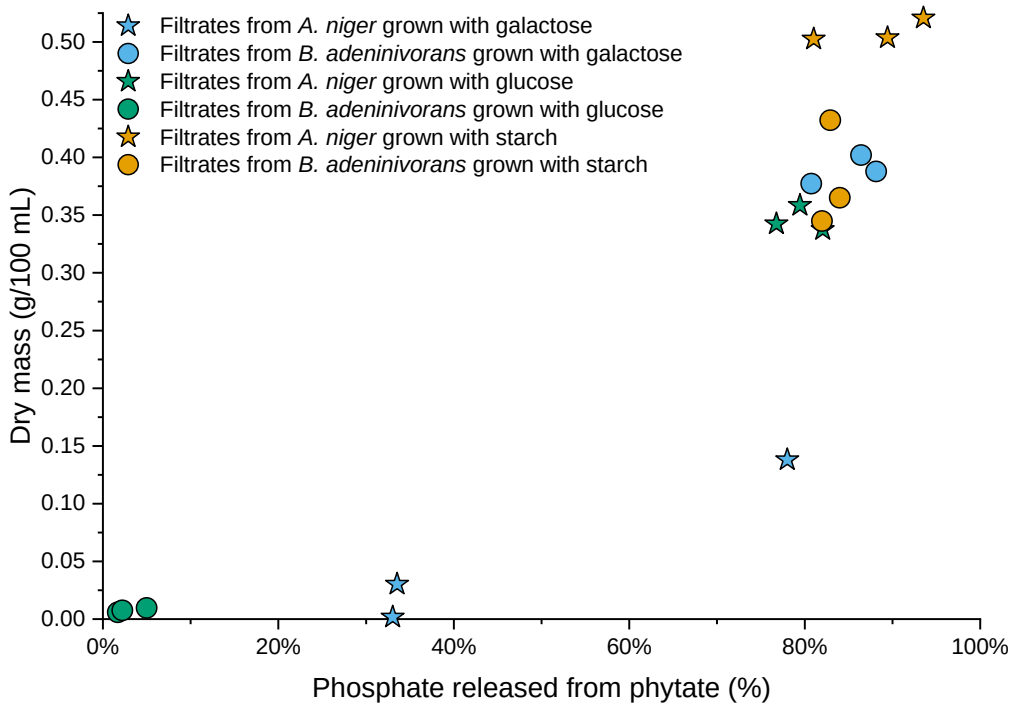

Figure 2.12 Dry mass of precipitates (given as g/100 mL of filtrate solution) plotted against the percentage of phosphate released from phytate by A. niger *(★) or* B. adeninivorans *(●) grown with galactose (blue), glucose (green), or starch (yellow) as carbon sources. Data points represent individual samples.*

Table 2.4 Summary of the results from the filtrate system precipitation tests, comparing the influence of carbon source used during microbial growth prior to filtering the cultures and adding calcium. Due to experimental errors, phosphate removal in the A. niger *galactose filtrates was not determined. The number in brackets after the mineral identification represents how many samples from that condition were analysed by XRD.*

Organism	Carbon source	Phosphate released from phytate (%)			Phosphate removed from solution (mmol/L)			Dry mass (g/100 mL)			Identification by XRD
		Mean	+	-	Mean	+	-	Mean	+	-	
A. niger	Galactose	48.2%	29.8%	15.2%	n.d.	n.d.	n.d.	0.06	0.08	0.05	n.d.
B. adeninivorans	Galactose	85.1%	3.0%	4.4%	2.38	1.15	2.26	0.39	0.01	0.01	Gypsum (1)
A. niger	Glucose	79.4%	2.6%	2.7%	0.07	3.31	2.50	0.35	0.01	0.01	Gypsum (1)
B. adeninivorans	Glucose	3.0%	2.0%	1.3%	0.41	0.58	0.46	0.01	0.00	0.00	n.d.
A. niger	Starch	88.0%	5.5%	7.0%	6.64	9.83	7.99	0.51	0.01	0.01	Gypsum (1)
B. adeninivorans	Starch	83.0%	1.0%	1.0%	2.57	6.12	3.74	0.38	0.05	0.04	Gypsum (2)

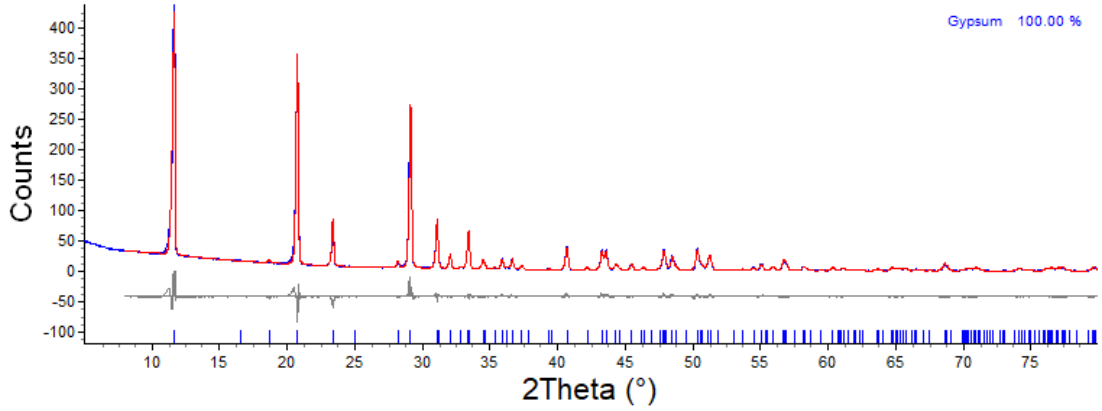

Figure 2.13 Representative XRD pattern from the filtrate system precipitation tests (blue). The fitted reference pattern (red) used the structural model for gypsum from (312) *(ICSD #2058). The grey line shows the difference between the measured pattern and the fitted model, the blue tick marks show the positions of Bragg peaks associated with gypsum. Samples were measured using the Göbel mirror optics setup with the copper K_α radiation across a 2θ range of 5–80° with a step size of 0.02° and a step time of 1 s.*

To investigate the role of the carbon source used during growth on calcium precipitation, culture filtrates (at a pH of 2.3–2.8) were supplemented with 500 mmol/L calcium. The concentration of calcium was doubled compared to the pH tests when it was noted that very little precipitation occurred in some of the samples (in particular, filtrates from *A. niger* grown with galactose and *B. adeninivorans* grown with glucose).

Results indicated that the mass of precipitates increased with increasing levels of phytate breakdown, with precipitate masses of greater than 0.1 g/100 mL only being recorded when around 80% of phosphate was released from phytate (figure 2.12). However, a negligible

amount of phosphate precipitation occurred, and XRD identified all precipitates produced as matching the database pattern for gypsum (table 2.4, figure 2.13). This suggests that phytate forms very strong soluble complexes with calcium that inhibit gypsum formation at low pH and that the microbial hydrolysis of phytate reduces this inhibitory effect.

Geochemical modelling was not able to replicate these results (appendix B, figure B.1) which may indicate that more comprehensive thermodynamic data for phytate species are required. Alternatively, kinetic factors were not accounted for in the model, and it may be that this is required to accurately model the system. Phytate (as well as the lower inositol phosphates produced during its hydrolysis) has previously been shown in inhibit the crystallisation of various minerals (266,322–327). This is likely to also be true for gypsum, and so even though gypsum remains supersaturated in the geochemical simulations performed, it may be that the presence of phytate delays the onset of precipitation. The implications this has for the addition of phytate to contaminated media should be considered, as the inhibition of mineral precipitation could conceivably lead to increased contaminant mobility under certain conditions.

2.2.4 "Active" system precipitation tests

This section investigated the precipitation of three metals (calcium, manganese, lanthanum). Calcium was added at a concentration of 50 mmol/L at pH 7.0, while manganese and lanthanum were added at two different concentrations (0.5 or 50 mmol/L) at pH 5.5.

2.2.4.1 Calcium

To address problems associated with the solubility of calcium phosphates at pH 2.5–5.5, experiments were performed with 50 mmol/L calcium at pH 7.0, where the nucleation and precipitation of calcium phosphates is more favourable (277). Given the presence of sulfate in the culture media, this may also favour the precipitation of calcium sulfate-phosphate composites, which are of interest for the formation of permeable reactive barriers (321). Starch was used as the carbon source and, to try and limit the pH reduction observed in the temperature and carbon growth tests, the culture media in these experiments was buffered with 0.2 mol/L TES. After 20 days, the pH in the sterile control and *B. adeninivorans* cultures was within 0.2 units of the starting value. However, in the *A. niger* cultures, the pH was reduced to between 2.3 and 2.9.

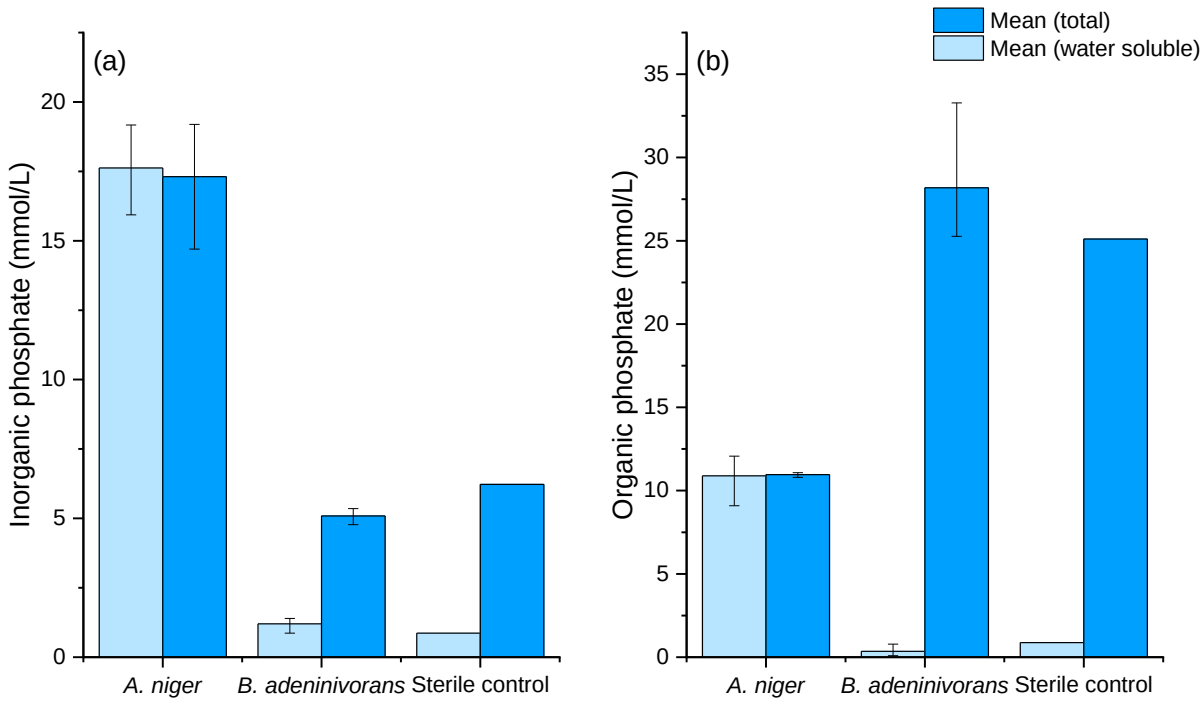

Figure 2.14 Water-soluble and total concentrations of (a) measured inorganic phosphate, and (b) calculated organic phosphate for the active system precipitation tests with 50 mmol/L calcium at pH 7.0. Values are the mean of triplicate samples plus or minus the difference between the mean and the upper or lower values (except for the sterile control, which represents a single experiment).

Figure 2.14a shows concentrations of inorganic phosphate (measured by colorimetry) in the different cultures or control experiment, while figure 2.14b shows organic phosphate concentrations (calculated by subtracting inorganic phosphate concentrations from the ICP-OES measured phosphate concentrations). Water-soluble concentrations are shown alongside total concentrations (i.e. water-soluble + insoluble concentrations) for comparative purposes.

Figure 2.14a shows an increase in inorganic phosphate for the *A. niger* cultures relative to the sterile control, with a corresponding decrease in organic phosphate concentrations displayed in figure 2.14b indicating a successful release of phosphate from phytate. In contrast, inorganic and organic phosphate concentrations for *B. adeninivorans* were effectively the same as in the sterile control (figure 2.14). This is consistent with previous reports where the *B. adeninivorans* phytase has shown a sharp decrease in activity above pH 6 (288). It had been hoped in these experiments that over long timescales, phytase activity may still occur, but after twenty days there was still no indication of phosphate release. *A. niger* has also been described as showing a low phytase activity at circumneutral pH values (261), but in this

experiment, that was counteracted by acidifying the culture media into the optimal pH range for its phytase activity.

Calculated values of organic phosphate in this work must be treated cautiously due to large variability encountered during ICP-OES measurement of phosphate concentrations. However, comparing the water-soluble and total fractions can still be used to indicate general trends. For the *A. niger* cultures at ~ pH 2.5, phosphate solubility was high, and the majority of both inorganic and organic phosphate appeared to remain in solution (figure 2.14). In contrast, both inorganic and organic phosphate solubility was low in the sterile control and *B. adeninivorans* cultures (figure 2.14).

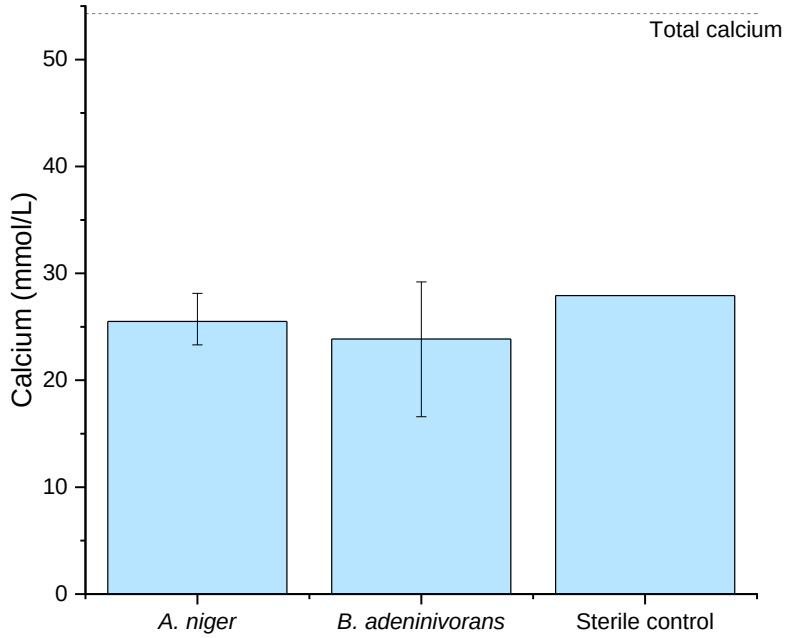

Figure 2.15 Measured water-soluble concentrations of calcium for the active system precipitation tests with 50 mmol/L calcium at pH 7.0. Values are the mean of triplicate samples plus or minus the difference between the mean and the upper or lower values (except for the sterile control, which represents a single experiment). Dashed line represents the mean total calcium in the sterile control and B. adeninivorans *cultures (values from* A. niger *samples were not included due to incomplete calcium recovery when dissolving aliquots of the solution).*

In contrast to the differences in phosphate solubility between *A. niger* and *B. adeninivorans* cultures and the sterile control, calcium solubility was effectively the same across all conditions with approximately 50% removed from solution (figure 2.15).

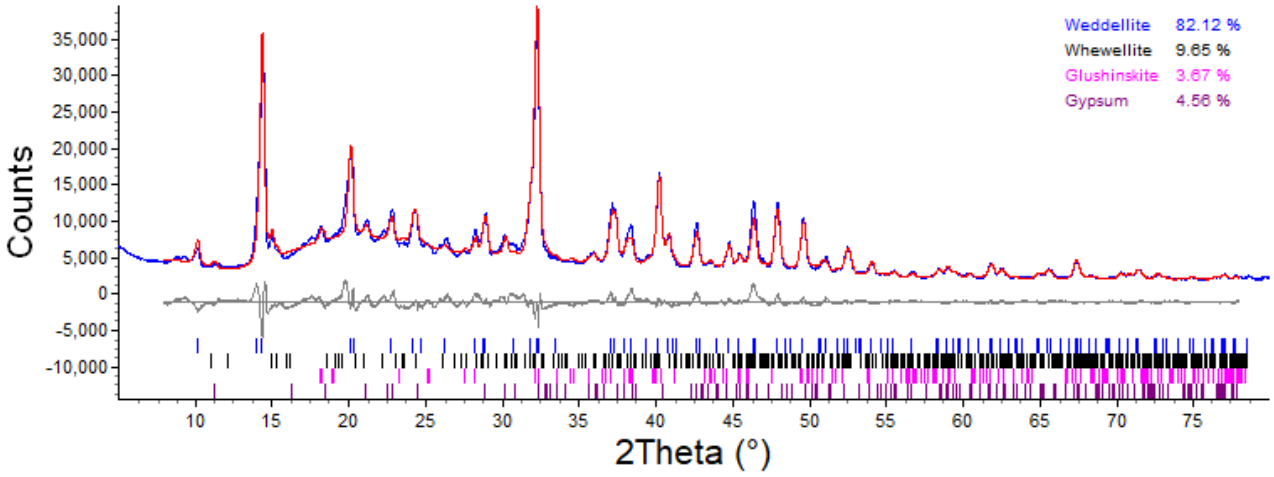

Figure 2.16 XRD pattern of a solid produced in the "active" system precipitation tests with A. niger *and 50 mmol/L calcium (blue). The fitted reference pattern (red) used the structural models for whewellite (ICSD #434201) and weddellite (ICSD #434209) from* (328)*, glushinskite (ICSD #5049) from* (329)*, and gypsum (ICSD #2058) from* (312)*. The grey line shows the difference between the measured pattern and the fitted model, the tick marks show the positions of Bragg peaks associated with each phase. Samples were measured using the Göbel mirror optics setup with the copper K_α radiation across a 2θ range of 5–80° with a step size of 0.02° and a step time of 1 s.*

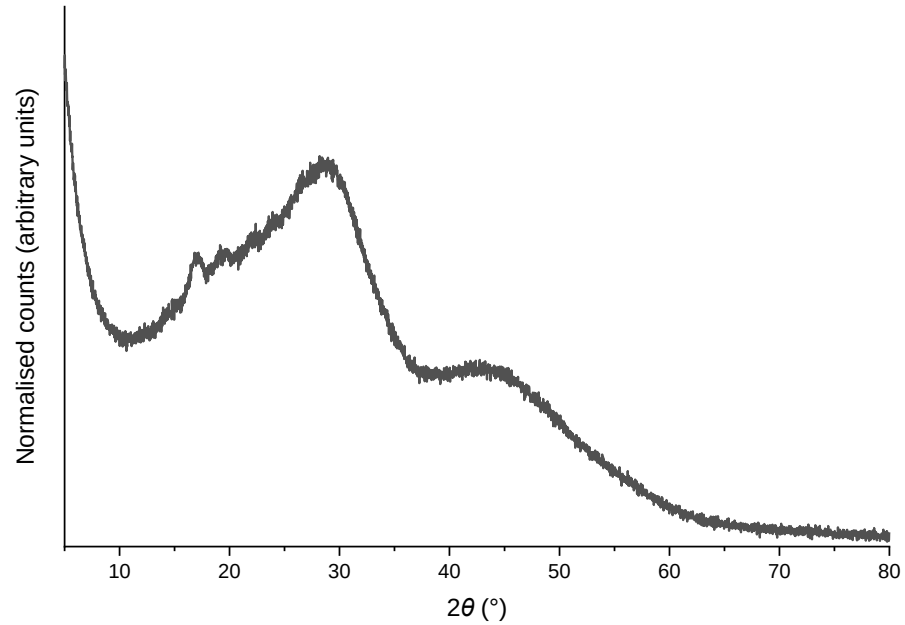

Figure 2.17 XRD pattern of a solid produced in the "active" system precipitation tests with B. adeninivorans *and 50 mmol/L calcium. Samples were measured using the Göbel mirror optics setup with the copper K_α radiation across a 2θ range of 5–80° with a step size of 0.02° and a step time of 1 s.*

Analysing solids from the *A. niger* cultures by XRD (figure 2.16) indicated the presence of weddellite, the dihydrate form of calcium oxalate ($CaC_2O_4.2H_2O$), along with minor amounts

of whewellite ($CaC_2O_4.H_2O$), glushinskite ($MgC_2O_4.2H_2O$), and gypsum ($CaSO_4.2H_2O$). The precipitation of oxalates by *A. niger* has previously been well established (330–332).

The solids recovered from *B. adeninivorans* cultures appeared to be amorphous by XRD analysis (figure 2.17), which is consistent with calcium phytate precipitation (253,333). Some small peaks could be observed in the 20–30° region, but these were hard to distinguish against the background and could not be conclusively matched to any phase. These features may have been associated with traces of inorganic calcium phosphates and/or sulfates precipitating alongside the bulk calcium phytate or unhydrolyzed starch. The precipitate from the sterile control was not analysed by XRD, as the solid was most likely an amorphous calcium phytate.

Table 2.5 Saturation indices of select phases included in the geochemical model. The different simulations are indicated as follows: (1) – sterile media at pH 7.0 media prior to the addition of phytate; (2) – sterile media at pH 7.0 after the addition of 5 mmol/L phytate, also representative of the phytase-inactive B. adeninivorans *cultures; (3) –* A. niger *cultures with 17 mmol/L phosphate, 3 mmol/L phytate, and adjusted to pH 2.5 with oxalic acid ($H_2C_2O_4$). Phytate is represented in the model by [InsP6], oxalate is represented by (Ox).*

Simulation	1	2	3
Phytates			
Ca_5K_2[InsP6].xH_2O	n/a	20.73	-0.18
Ca_5Na_2[InsP6]	n/a	17.15	-4.01
Ca_6[InsP6]	n/a	3.55	-17.66
Phosphates			
Brushite ($Ca(HPO_4).2H_2O$)	n/a	1.10	-2.32
Chloroapatite ($Ca_{10}(PO_4)_6Cl_2$)	n/a	15.40	-8.64
Hydroxyapatite ($Ca_{10}(PO_4)_6(OH)_2$)	n/a	14.29	-14.28
Oxalates			
Whewellite ($Ca(Ox).H_2O$)	n/a	n/a	3.60
Weddellite ($Ca(Ox).2H_2O$)	n/a	n/a	3.18
Caoxite ($Ca(Ox).3H_2O$)	n/a	n/a	3.08
Glushinskite ($Mg(Ox).2H_2O$)	n/a	n/a	1.59
Sulfates			
Anhydrite ($CaSO_4$)	0.18	0.14	0.05
Gypsum ($CaSO_4.2H_2O$)	0.39	0.35	0.26

Geochemical modelling (table 2.5) indicated that the calcium sulfate phases gypsum and anhydrite were supersaturated in all simulations, although in practice, no visible precipitation was observed prior to the addition of phytate (i.e. simulation 1). After the addition of 5 mmol/L phytate along with the 5 mmol/L phosphate impurity (simulation 2), calcium phytate phases become supersaturated. This is consistent with the amorphous XRD pattern as would be expected for calcium phytate (figure 2.17). Calcium phosphate and sulfates were also

supersaturated in the model. Chemical analysis did indicate that inorganic phosphate precipitated in the sterile control and the *B. adeninivorans* cultures, but as no signals for calcium phosphate could be observed in the XRD patterns, this was likely in an amorphous form. The same is true of any sulfate precipitated, although sulfate concentrations were not measured.

Simulation 3, representing the *A. niger* cultures, indicates that with the decrease in pH, all calcium phosphates and phytates become undersaturated. In the model it was assumed that the pH decrease was entirely due to oxalic acid synthesis by *A. niger*. This is an oversimplification, as *A. niger* produces other pH decreasing substances such as citric and gluconic acids, and CO_2 produced during respiration may also contribute to acidification. However, because organic acid quantification was not performed, and because the oxalic acid synthesis of *A. niger* is well studied and known to be geochemically important (331,332,334), this assumption was considered sufficient for modelling purposes. Taking this approach led to all calcium oxalate phases (the monohydrate, whewellite, the dihydrate, weddellite, and the trihydrate, caoxite) and magnesium oxalate dihydrate (glushinskite) becoming supersaturated. This is consistent with the signals for whewellite, weddellite, and glushinskite in the XRD patterns for the *A. niger* precipitates (figure 2.16), while the lack of caoxite (including caoxite in the Rietveld refinement calculated a percentage concentration of 0.00% for caoxite) is consistent with the rarity of this phase (328).

In summary, attempts to use *A. niger* and *B. adeninivorans* to mediate the formation of calcium phosphates (e.g. brushite, hydroxyapatite) or mixed calcium sulfate-phosphates (e.g. ardealite) were unsuccessful in this work. For *A. niger* a large pH decrease associated with oxalic acid production led to the formation of calcium and magnesium oxalates, while *B. adeninivorans* showed no phytase activity at pH 7 and calcium likely remained mostly associated with phytate.

While oxalates (335) and phytates (253) may still have value in the remediation of uranium and other contaminants, further work must be done if minerals such as hydroxyapatite or ardealite are to be directly produced from a phytate precursor. There are three main options that could be pursued to try and achieve this: (a) a two-stage biological process where phytate is hydrolysed under acidic conditions and the solution chemistry is then manipulated to induce the formation of desired phases, (b) focusing research on organisms that produce phytases

active in the neutral to alkaline pH range, (c) use non-biological techniques where phytate is hydrolysed into inorganic phosphate by (hydro)thermal methods.

2.2.4.2 Manganese

Experiments with manganese were performed at concentrations of 0.5 and 50 mmol/L. The first set of experiments (at 50 mmol/L) indicated that, while manganese appeared to precipitate with phytate, there were no indications of growth or phytate breakdown by *B. adeninivorans* (data not shown). Therefore, this condition was not repeated for *A. niger* and, instead, experiments were performed for both organisms at a lower manganese concentration (0.5 mmol/L). Starch was used as carbon source, and the pH was buffered at 5.5 with 0.2 mol/L MES.

The experiments lasted for 20 days. At the final time point, the pH remained at around 5.5 in the sterile control but, despite the use of a strong buffer (0.2 mol/L MES), the *B. adeninivorans* cultures reduced the pH to ~ 4.4 and the *A. niger* cultures reduced the pH to ~ 2.5.

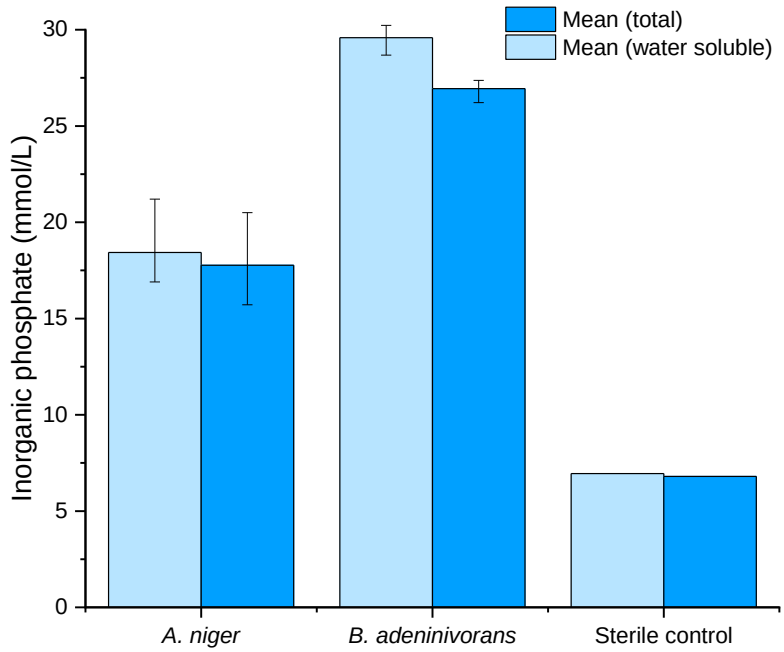

Figure 2.18 Water-soluble and total concentrations of measured inorganic phosphate for the active system precipitation tests with 0.5 mmol/L manganese at pH 5.5. Values are the mean of triplicate samples plus or minus the difference between the mean and the upper or lower values (except for the sterile control, which represents a single experiment).

Phytate degradation occurred for both *A. niger* and *B. adeninivorans* (figure 2.18), with a release of inorganic phosphate comparable to the low-manganese concentration experiments

(figure 2.4, figure 2.7). However, for all conditions, ~ 100% of inorganic phosphate remained in solution (water-soluble concentrations appearing slightly higher than total concentrations is likely a consequence of analytical error). Due to analytical errors, organic phosphate concentrations could not be calculated for this set of experiments.

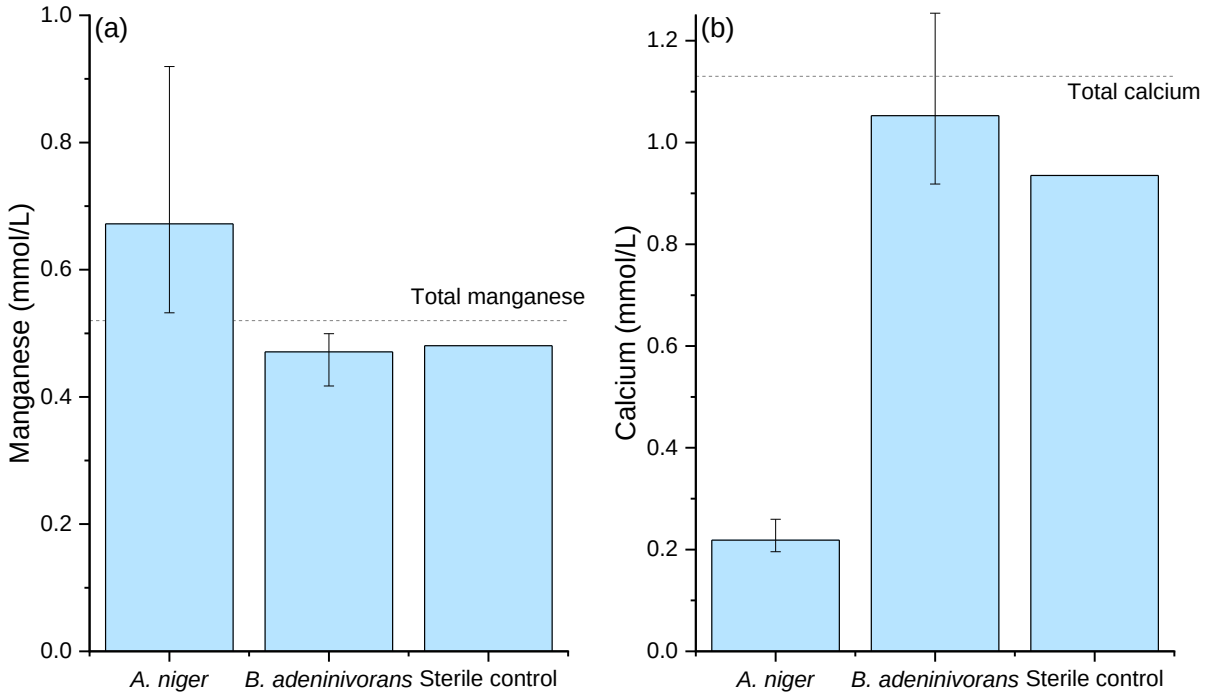

Figure 2.19 Measured water-soluble concentrations of (a) manganese, and (b) calcium for the active system precipitation tests with 0.5 mmol/L manganese at pH 5.5. Values are the mean of triplicate samples plus or minus the difference between the mean and the upper or lower values (except for the sterile control, which represents a single experiment). Dashed line represents the mean total (a) manganese in all experiments, and (b) calcium in the sterile control and B. adeninivorans *cultures (values from* A. niger *samples were not included due to incomplete calcium recovery when dissolving aliquots of the solution).*

For both organisms and the sterile control, close to 100% of the manganese appeared to remain in solution (figure 2.19a). However, calcium (which was present in the culture media at a concentration of about 1.1 mmol/L) was removed from solution in the *A. niger* cultures (figure 2.19b).

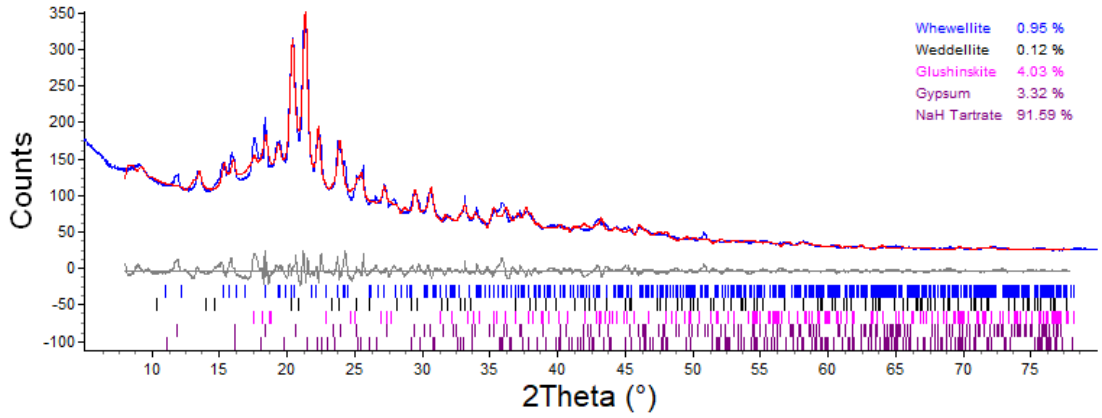

Figure 2.20 XRD pattern of a solid produced in the "active" system precipitation tests with A. niger *and 0.5 mmol/L manganese (blue). The fitted reference pattern (red) used the structural models for whewellite (ICSD #434201) and weddellite (ICSD #434209) from* (328)*, glushinskite (ICSD #5049) from* (329)*, gypsum (ICSD #2058) from* (312)*, and sodium hydrogen tartrate (COD #2005194) from* (336)*. The grey line shows the difference between the measured pattern and the fitted model, the tick marks show the positions of Bragg peaks associated with each phase. Samples were measured using the Göbel mirror optics setup with the copper K_α radiation across a 2θ range of 5–80° with a step size of 0.02° and a step time of 1 s.*

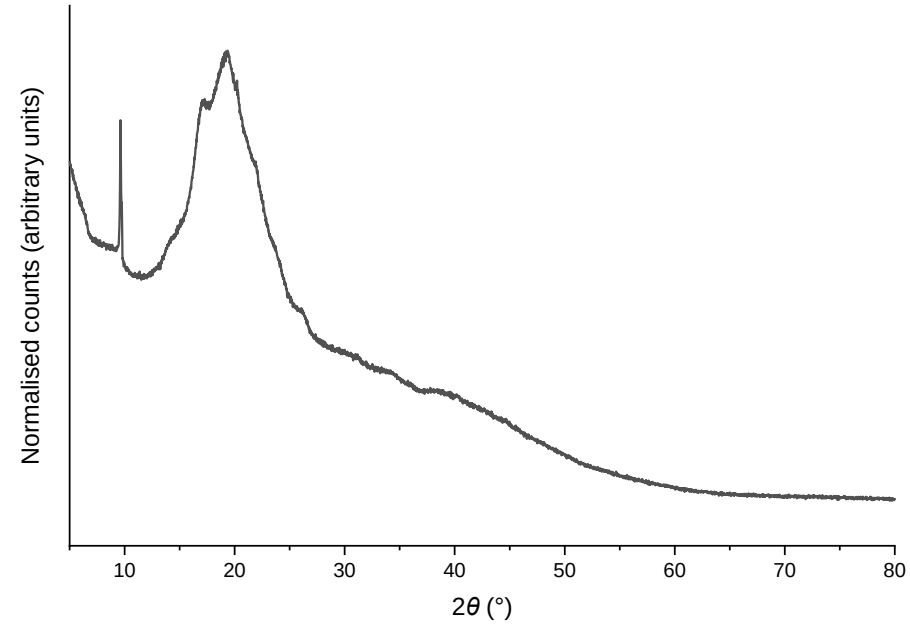

Figure 2.21 XRD pattern of a solid produced in the "active" system precipitation tests with B. adeninivorans *and 0.5 mmol/L manganese (blue). Samples were measured using the Göbel mirror optics setup with the copper K_α radiation across a 2θ range of 5–80° with a step size of 0.02° and a step time of 1 s.*

XRD analysis of the solids indicated crystalline material from the *A. niger* cultures that was challenging to identify (figure 2.20) and a mostly amorphous material from the *B. adeninivorans* cultures (figure 2.21). Applying corrections for preferred orientation during a

Rietveld refinement indicated that the majority of peaks in the *A. niger* precipitate could be assigned to NaH tartrate (note that due to the excess of potassium compared to sodium in the culture media, KH tartrate was probably more likely to form under the conditions tested, but a structural model for this phase could not be found in the ICSD or COD databases). Other peaks could be assigned to magnesium and calcium oxalates and gypsum, while the unexplained peaks are likely associated with other complexes between cations contained in the culture media (NH_4^+, Na^+, Mg^{2+}, K^+, Ca^{2+}) and organic ligands produced by *A. niger* (e.g. citrate, formate, gluconate, oxalate, tartrate). More detailed characterisation of the solution chemistry of the *A. niger* cultures would be required to establish what phases precipitated, but it appears likely that none of these phases were phosphates. Rietveld refinements were not attempted for the *B. adeninivorans* solids due to the lack of crystalline signals in the XRD pattern.

Geochemical modelling (appendix B, table B.3) indicated that the sterile control was supersaturated with respect to calcium phytate phases, $MnHPO_4$, and $Mn_3(PO_4)_2.3H_2O$. Simulations of the *B. adeninivorans* cultures indicated that only calcium phytates and $MnHPO_4$ were supersaturated. Results for the *A. niger* simulations depended on the inclusion of organic acids. In the absence of organic acids, the results were similar to *B. adeninivorans* cultures. However, with organic acids in the model (citrate, gluconate, oxalate, and tartrate, with concentrations estimated based upon literature values), magnesium and calcium oxalates became supersaturated. Manganese phytate and manganese oxalate were undersaturated in all simulations, as were all sulfate, oxide, and hydroxide phases. Other organic acid complexes were also undersaturated in the model, but the model did not account for local supersaturation that may have occurred at the *A. niger* cell surface.

These results indicate that a mixture of organic acid crystals was produced in the *A. niger* cultures, while the solid collected from the *B. adeninivorans* cultures was likely a mixture of biomass and residual starch. The explanation of a lack of manganese phosphate precipitation despite manganese phosphates being supersaturated in geochemical models (except at the higher estimated concentrations of organic acids) may be a result of low supersaturation, slow kinetics, the presence of other cations in the culture media (ammonium, sodium, magnesium, potassium, and calcium) at higher concentrations than manganese that may have competed

for sorption/precipitation sites, or production of high levels of organic acids in the microbial cultures.

Based upon the conditions tested, neither organism is a suitable candidate for the direct precipitation of manganese phosphate. Further work could focus on optimising the manganese concentrations and the solution pH (previous work has indicated that a minimum pH of ~ 5 is required for manganese phosphate precipitation (337)).

2.2.4.3 Lanthanum

The first set of experiments with lanthanum added the metal at 50 mmol/L to *B. adeninivorans* cultures. Lanthanum appeared to precipitate with phytate, but no growth or phytase activity was observed (data not shown). As such, the concentration of lanthanum was reduced to 0.5 mmol/L for the following tests with both *A. niger* and *B. adeninivorans*. Starch was used as carbon source, and the pH was buffered at 5.5 with 0.2 mol/L MES.

At 0.5 mmol/L lanthanum, growth of both *A. niger* and *B. adeninivorans* was visibly apparent. Despite the use of a relatively strong buffer (0.2 mol/L MES), both organisms decreased the pH of the media, to around 3 for *A. niger* and about 4.5 for *B. adeninivorans*. Results from the sterile control are not presented due to contamination; instead an additional batch of media that was non-sterile but kept at 4 °C during the experiment is designated an “abiotic” control. The pH remained at around 5.5 for this control, and no visible signs of obvious microbial growth were observed.

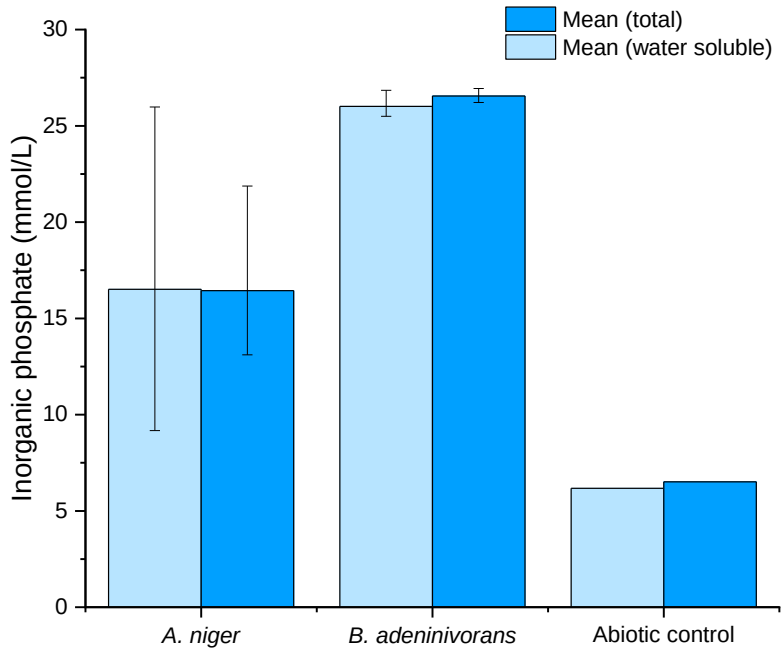

Figure 2.22 Water-soluble and total concentrations of measured inorganic phosphate for the active system precipitation tests with 0.5 mmol/L lanthanum at pH 5.5. Values are the mean of triplicate samples plus or minus the difference between the mean and the upper or lower values (except for the sterile control, which represents a single experiment).

Phytase activity occurred for both *A. niger* and *B. adeninivorans* (figure 2.22), with a release of inorganic phosphate comparable to the lanthanum-free experiments (figure 2.4, figure 2.7). Any precipitation that occurred was hard to detect, but there did appear to be a small reduction in soluble inorganic phosphate in the *B. adeninivorans* cultures and the abiotic control.

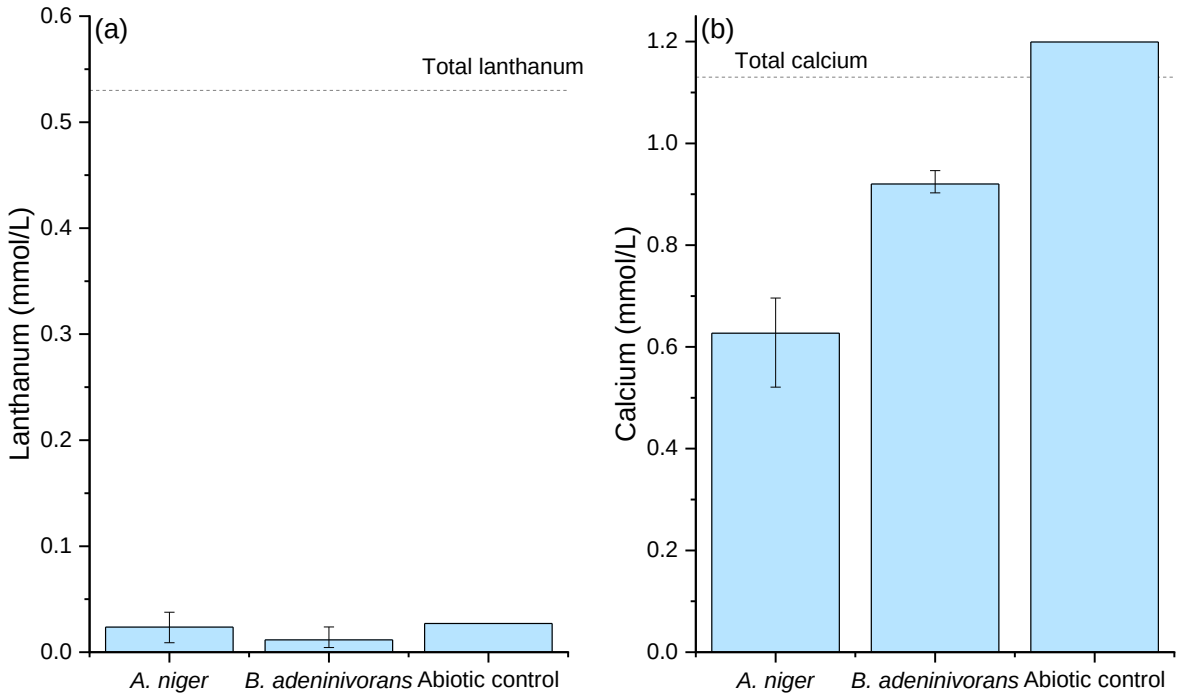

Figure 2.23 Measured water-soluble concentrations of (a) lanthanum, and (b) calcium for the active system precipitation tests with 0.5 mmol/L lanthanum at pH 5.5. Values are the mean of triplicate samples plus or minus the difference between the mean and the upper or lower values (except for the abiotic control, which represents a single experiment). Dashed line represents the mean total (a) lanthanum, and (b) calcium measured in the abiotic control and B. adeninivorans *cultures (values from* A. niger *samples were not included due to incomplete metal recovery when dissolving aliquots of the solution).*

Lanthanum had a low solubility under all tested conditions (figure 2.23a). The abiotic control removed around 95% of lanthanum from solution, while lanthanum removal ranged from 92% to 98% in the *A. niger* cultures and from 95% to 99% in the *B. adeninivorans* cultures. Additionally, a small reduction of calcium concentrations in *B. adeninovorans* cultures and a large reduction in *A. niger* cultures was measured (figure 2.23b). Soluble calcium was higher (~ 0.6 mmol/L) in the *A. niger* cultures compared to the 0.5 mmol/L manganese experiments (~ 0.2 mmol/L calcium in solution, figure 2.19b) potentially indicating some substitution of lanthanum into the precipitating phase at the expense of calcium.

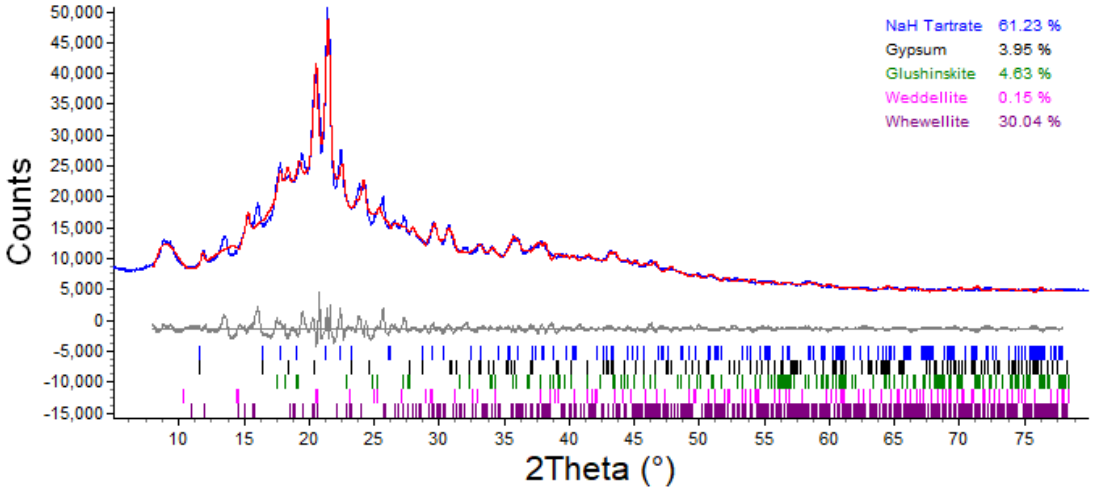

Figure 2.24 XRD pattern of a solid produced in the "active" system precipitation tests with A. niger *and 0.5 mmol/L lanthanum (blue). The fitted reference pattern (red) used the structural models for whewellite (ICSD #434201) and weddellite (ICSD #434209) from* (328)*, glushinskite (ICSD #5049) from* (329)*, gypsum (ICSD #2058) from* (312)*, and sodium hydrogen tartrate (COD #2005194) from* (336)*. The grey line shows the difference between the measured pattern and the fitted model, the tick marks show the positions of Bragg peaks associated with each phase. Samples were measured using the Göbel mirror optics setup with the copper K_α radiation across a 2θ range of 5–80° with a step size of 0.02° and a step time of 1 s.*

Solids recovered from the *A. niger* cultures (figure 2.24) had almost identical XRD patterns to the solids recovered from *A. niger* cultures in the 0.5 mmol/L manganese experiments (figure 2.20). This suggests that for both experiments the bulk material produced was some other phase rather than anything associated with manganese or lanthanum. However, these patterns both differed from the weddellite (calcium oxalate dihydrate) produced in the 50 mmol/L calcium experiments (figure 2.16) suggesting different phases predominated in the cultures with low (~ 1 mmol/L) calcium concentrations. A credible fit was achieved when including structural models for NaH tartrate, whewellite, weddellite, glushinskite, and gypsum in the Rietveld refinement (figure 2.24) but a detailed characterisation of the *A. niger* culture solution chemistry would be required to probe in more detail which phases may have precipitated. Unlike manganese, lanthanum was removed from solution in the presence of *A. niger* which may be due to incorporation into or sorption onto the organic acid phases, sorption onto biomass, or precipitation of poorly crystalline/amorphous phytate/phosphate phases.

Kang *et al.* (338) also observed the precipitation of lanthanum by *A. niger*, with precipitated minerals that matched well with the XRD database pattern for lanthanum oxalate

($La_2(C_2O_4)_3.10H_2O$), while a phosphorus containing phase (identified as $La_7P_3O_{18}$) was only observed when biomass was removed from solution prior to adding lanthanum and at a pH of > 3.5 and a lanthanum concentration > 15 mmol/L. Based upon those results, it suggests that little-to-no lanthanum phosphate precipitation occurred with *A. niger* in these experiments.

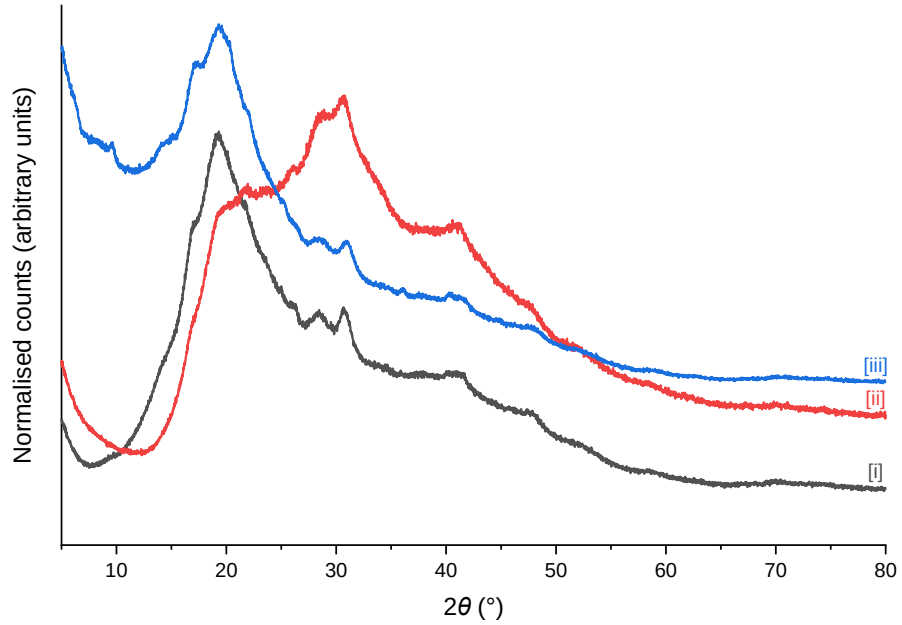

Figure 2.25 XRD pattern of solids produced in the "active" system precipitation tests with B. adeninivorans *and 0.5 mmol/L lanthanum. Samples were measured using the Göbel mirror optics setup with the copper K_α radiation across a 2θ range of 5–80° with a step size of 0.02° and a step time of 1 s. Patterns [i] and [ii] were recorded using a 'knife edge' to reduce low angle background signals but pattern [iii] was collected without the 'knife edge'. Patterns were normalised in OriginPro 2019b to a scale of 0 to 1.*

The XRD analysis of the precipitates recovered from the *B. adeninivorans* cultures indicated a very poorly crystalline or amorphous material (figure 2.25). There was also a degree of heterogeneity where patterns [i] and [iii] appeared similar but pattern [ii] differed in the lack of the broad peak around $2\vartheta \approx 20^\circ$. Features in the ~ 15–25° 2ϑ region may be associated with starch (e.g. figure 2.26 for the abiotic control) and so the lack of these signals in one pattern may indicate that that culture achieved a higher degree of starch breakdown. Other features of the patterns possibly appeared to match database patterns for rhabdophane ($LaPO_4.0.5H_2O$, PDF #00-046-1439) or $K_3La(PO_4)_2$ (ICSD #41904). However, due to the signals being small, it is difficult to identify this conclusively.

Rhabdophane is the most likely lanthanum phosphate to form under ambient conditions (113,296,339). However, if it was formed in the *B. adeninivorans* cultures, it was very poorly crystalline, and differed from previous results. For example, *Serratia* sp. N14 bacteria were able to produce a crystalline lanthanum phosphate from glycerol 2-phosphate (340,341). These experiments used similar lanthanum concentrations (0.3 mmol/L in (340), 1 mmol/L in (219,341,342)) and a slightly higher pH (6.0 for (341) or 7.0 for (340)). However, lanthanum phosphate crystallinity usually increases with decreasing pH (296) so the pH differences are unlikely to explain these results.

The main factors that may explain the differences between these results and the previously reported results for the Serratia bacterium include: the organic phosphate donor, the nutrient media used, and the lanthanum:phosphate ratio.

The organic phosphate donor may be important. Previous research indicated that the precipitation of lanthanum with glycerol 2-phosphate was negligible (219). In contrast, phytate interacts strongly with lanthanide metals (343) and is known to form insoluble lanthanide phytate precipitates (279,344). Phytate is known to inhibit mineral crystallisation, and this has been demonstrated for calcium phosphates (322,323), oxalates (325,326), fluoride (324), and carbonate (327). Other reports indicate that the lower inositol phosphates produced during phytate breakdown may also inhibit mineral crystallisation (266). Therefore, it is likely that a similar effect exists for lanthanum minerals, and that may explain the low crystallinity of phases produced in the *B. adeninivorans* cultures.

Another factor could be the much more complex media that was used for these experiments. Where the *Serratia sp.* N14 system used a very simple media consisting of phosphate source, metal, and buffer (219), this work was performed in a media containing phosphate source, metal, buffer, plus a complex carbon source (starch) and a wide range of nutrients (see methodology section for full media composition). While chemical analysis indicated minimal calcium precipitation in the *B. adeninivorans* cultures (figure 25b) other metals and ions present in the media (ammonium, sodium, magnesium, potassium, sulfate) were not quantified. Any of these coprecipitating with lanthanum and phosphate may have influenced the product's morphology and led to a more amorphous solid. Additionally, starch is known to inhibit mineral crystallisation and influence particle morphology (345,346) so this may have

been a factor, although as starch concentrations were not quantified, it is uncertain how much starch was left unutilised by *B. adeninivorans* to be available to inhibit crystallisation.

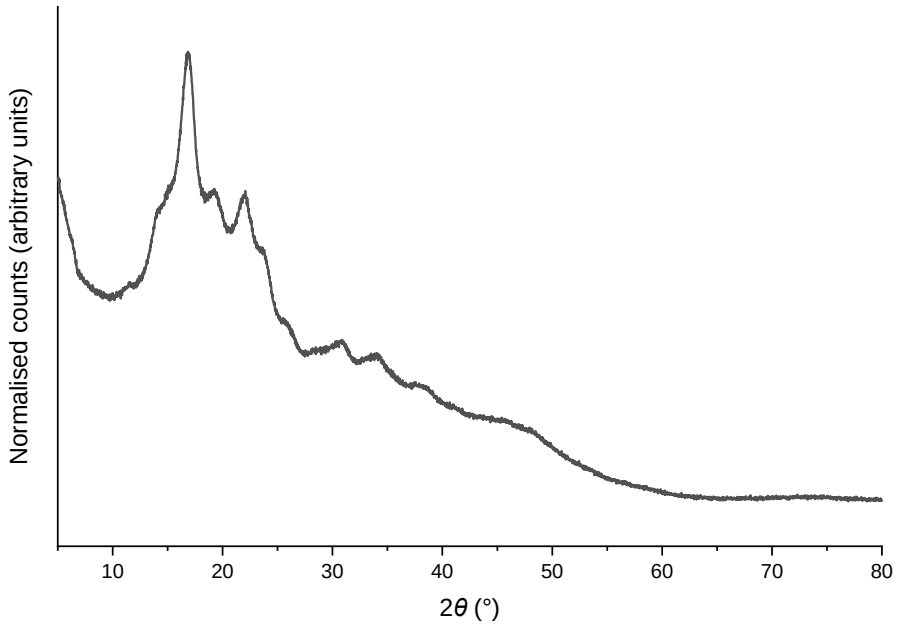

Figure 2.26 XRD pattern of solids produced in the "active" system precipitation tests for the abiotic control and 0.5 mmol/L lanthanum. Samples were measured using the Göbel mirror optics setup with the copper K_α radiation across a 2θ range of 5–80° with a step size of 0.02° and a step time of 1 s. Patterns [i] and [ii] were recorded using a 'knife edge' to reduce low angle background signals but pattern [iii] was collected without the 'knife edge'. Patterns were normalised in OriginPro 2019b to a scale of 0 to 1.

For the abiotic control, the only notable features in the XRD pattern (figure 2.26) were some broad peaks that matched database patterns for starch (PDF #00-052-2247). Lanthanum, if associated with phytate, is likely to be in an amorphous form, as has been shown for other lanthanide phytates (279,344). As starch has previously been shown to form complexes with lanthanum (347), some lanthanum removal may have been in association with the insoluble starch. However, the relative importance of phytate and starch complexes in uncertain. Starch-phytate composite materials have previously been researched as efficient ion exchangers for a range of metals, including lanthanum (348). These materials require elevated temperatures (> 100 °C) to form so it is likely that the starch and phytate remained separate in this work, but it may be of interest for further research to investigate starch-phytate composites as precursors for biogenic phosphate minerals.

Geochemical modelling (using a generic 'lanthanide' (Ln) species rather than lanthanum due to the availability of thermodynamic data) of these experiments indicated that the only supersaturated phases in the abiotic control and *B. adeninivorans* cultures were hydrated lanthanide phosphates and calcium phytates (appendix B, table B.4). Sulfates, hydroxides, oxides, and other lanthanide phases were all undersaturated. Similar results were obtained for the *A. niger* cultures, but calcium phytates became undersaturated and the saturation indices of lanthanide phosphates were reduced (although $LnPO_4.H_2O$ remained supersaturated even at the higher organic acid concentrations). Additionally, oxalates (magnesium, calcium, and mixed sodium-lanthanide oxalates) and potassium hydrogen tartrate were calculated as having positive saturation indices at potentially relevant organic acid concentrations.

In summary, lanthanum had a low solubility in these experiments, but the mechanisms of removal and speciation of precipitated lanthanum remain unclear. The most likely products were a mixture of oxalate and tartrate phases for *A. niger*, a poorly crystalline lanthanum phosphate material for *B. adeninivorans*, and a mixture of lanthanum phytate and starch for the abiotic control. While further work would be required to characterise the precipitate formed, the biologically mediated precipitation of lanthanum phosphate by *B. adeninivorans* may be a promising direction to investigate further for its application in the remediation of radionuclide-containing wastewaters. However, for *A. niger* the high production of organic acids appears to limit the options for phosphate precipitation, and so if lanthanum phosphate precipitation by *A. niger* is to be pursued in further detail, it may require the removal of biomass prior to precipitation or the use of purified *A. niger* phytase enzymes.

2.2.5 "Inactive" system precipitation tests

With high (50 mmol/L) concentrations of manganese and lanthanum appearing to inhibit growth and phytase activity of *B. adeninivorans* an alternative approach was investigated to produce phosphate minerals through a phytase-mediated strategy. Due to the prevalence of oxalate phases associated with *A. niger* biomass in the "active" system tests, these experiments were only performed with *B. adeninivorans*.

The experiments involved growing *B. adeninivorans* cultures for four to seven days until the majority of inorganic phosphate had been released from phytate. At this point, iron, manganese, or lanthanum were added to the cultures. The cells and any precipitates were

then collected for analysis. Prior to metal addition, the cultures either had a pH of ~ 2.5 or ~ 3.0. The precipitation of each metal was investigated in duplicate, with one pH 2.5 and one pH 3.0 culture used for each metal. As there appeared to be a slight pH effect for some results, results for each sample are presented individually.

Table 2.6 Summary table of the "inactive" system precipitation tests.

Metal	Initial pH	Final pH	Dry mass (g/100 mL)	Inorganic phosphate (mmol/L)		Organic phosphate (mmol/L)		Metal (mmol/L)	
				Water-soluble	Total	Water-soluble	Total	Water-soluble	Total
Manganese	2.4	2.4	0.588	23.1	27.6	12.1	3.4	53.8	51.6
Manganese	3.0	2.4	0.693	23.1	24.6	1.7	3.6	42.4	44.1
Iron (II)	2.5	2.5	0.556	26.4	27.7	-0.3	4.3	38.2	46.5
Iron (II)	3.2	2.1	0.791	25.4	26.6	-0.2	2.9	47.3	47.3
Lanthanum	2.5	1.2	0.939	6.9	22.9	1.6	13.0	17.6	44.8
Lanthanum	3.2	1.6	1.130	8.0	29.3	-1.2	-2.5	16.4	43.7

Results of the “inactive” system tests indicated that precipitation of manganese and iron was low (table 2.6). Effectively all manganese remained in solution, while there was a slight variation with pH for iron. Around 100% of iron remained in solution at an initial pH of 3.2 while around 20% precipitated at an initial pH of 2.5. Large variability encountered during ICP-OES measurements of phosphate made calculation of organic phosphate concentrations difficult (based upon the level of phytate degradation, the total organic phosphate content should have been around 4 mmol/L), but the results did appear to indicate that, where iron precipitation occurred, it was likely associated with the organic phosphate fraction rather than inorganic phosphate.

In contrast, a large amount of lanthanum was removed from solution, and this occurred alongside a large reduction in the inorganic phosphate concentrations (table 2.6). The lanthanum:inorganic phosphate ratio ranged from 1.3:1 to 1.7:1, which deviates from the expected 1:1 ratio expected for stoichiometric lanthanum phosphate ($LaPO_4$). This may indicate coprecipitation of phosphates with other anions present (e.g. residual phytate, lower inositol phosphates, sulfate), sorption of lanthanum onto the precipitated solid, or sorption onto *B. adeninivorans* biomass.

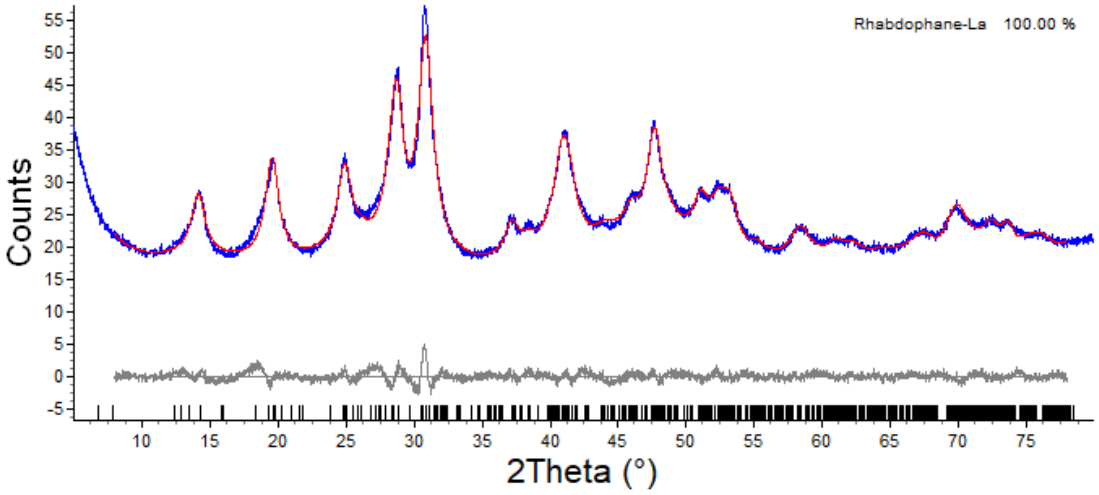

Figure 2.27 XRD pattern of a solid produced in the "inactive" system precipitation tests with B. adeninivorans *and 50 mmol/L lanthanum (blue). The fitted reference pattern (red) used the structural models for rhabdophane-Sm (ICSD #194481) from* (349) *and the lattice parameters edited in VESTA (350) to match the values for rhabdophane-La given by* (349)*. The grey line shows the difference between the measured pattern and the fitted model, the tick marks show the positions of Bragg peaks associated with each phase. Samples were measured using the Göbel mirror optics setup with the copper K_α radiation across a 2θ range of 5–80° with a step size of 0.02° and a step time of 1 s.*

XRD analysis indicated that the solid phase matched the pattern for rhabdophane ($LaPO_4.0.667H_2O$, ICSD #194481) (figure 2.27). Geochemical modelling (appendix B, table B.7) indicated that the only supersaturated lanthanum phases present were lanthanum phosphates. These results differed from the "active" system tests with lanthanum and *B. adeninivorans* cells where the XRD patterns appeared mostly amorphous (figure 2.25). These differences may be due to pH (2.5–3.2 compared to 4.5), lanthanum concentration (50 mmol/L compared to 0.5 mmol/L), carbon source present (galactose compared to starch), and timing of lanthanum addition (after phytate hydrolysis compared to before phytate hydrolysis.

These results are consistent with the known low solubility of lanthanide phosphates under acidic conditions (113,296) and indicate that the biologically mediated formation of rhabdophane may be an interesting option to research further for its applicability in contaminant remediation. Lanthanum/lanthanide phosphates have been previously researched for the immobilisation of transition and post-transition metals (351), strontium (352), thorium (340,353), uranium (354,355), and plutonium (340,356). It would be interesting to compare the performance of lanthanum phosphates produced from a phytate precursor to those produced from glycerol phosphates or by purely chemical mechanisms.

In contrast, despite geochemical modelling indicating supersaturation for manganese and iron phosphates (appendix, table B.5 and table B.6), no evidence for manganese or iron phosphate precipitation was observed in this work. If further work is to try and produce these phases, then it appears likely that a higher pH would be required for manganese (337), while it may be better to add iron as iron(III) rather than the more soluble iron(II) (357,358).

2.3 Conclusion

In this work, the low temperature degradation of phytate by *A. niger* (at 12 °C) and *B. adeninivorans* (at 4 °C and 12 °C) has been demonstrated, highlighting the possible role of both organisms in the degradation of phytic acid under environmentally relevant conditions. Alongside this, the importance of choosing appropriate sources of carbon when growing microorganisms was demonstrated as, for example, supplying *B. adeninivorans* with glucose leads to no phytase activity. In terms of cost and supporting phytase activity, starch appeared to be the most practical carbon source, but its low solubility may limit engineering options and influence the morphology of precipitated solids. Because the costs of both glucose and galactose may still be considered too expensive for bioremediation strategies, future work should investigate cheaper alternatives – ideally these would be sourced from the same waste products as phytate (e.g. ethanol by-products (233–235,359) or rice bran (237)) or from the contaminated site itself (uranium ore minerals may be associated with organic matter (360,361), and organic carbon has been found in some mine tailings (362), so it may be possible to use these materials as carbon sources). Additionally, some microorganisms, including *B. adeninivorans* have been shown to grow with phytate as the sole source of carbon (288,291), so this also merits further research

Despite both organisms being efficient at releasing phosphate from phytate, the subsequent precipitation of phosphate minerals was variable in this work. The narrow pH profile of the *B. adeninivorans* phytase enzymes and the high organic acid production by *A. niger* appear to be the main limiting factors preventing the precipitation of calcium phosphate minerals for *in situ* remediation strategies. However, these organisms may be suitable for the manufacture of a bulk material *ex situ* if they are used to hydrolyse phytate and the solution chemistry is then altered to make the formation of desired minerals (e.g. ardealite or hydroxyapatite) more favourable.

Alternatively, the formation of phosphate phases that are highly insoluble under acidic conditions (e.g. lanthanum phosphates) appears to be viable, although the different materials formed under different conditions (amorphous/poorly crystalline in the “active” system, crystalline rhabdophane in the “inactive” system for *B. adeninivorans*) may have different contaminant incorporation properties. Understanding this would be important for further work to optimise the system. Furthermore, the low solubility of lanthanum phosphate under the conditions tested indicates that uranium phosphate precipitation would likely also occur under similar conditions, although further experiments would be required to confirm this.

The usefulness of *A. niger* for producing phosphate minerals is limited by the production of organic acids, with oxalate phases observed in every condition except the filtrate tests where *A. niger* biomass was removed prior to attempting to induce precipitation. As such, removal of *A. niger* biomass after phytate hydrolysis or the use of purified phytase enzymes from *A. niger* would be the most suitable methods to research in more detail.

Chapter 3
Microbial phytate degradation and phosphate biomineralization in the presence of simple and complex solid matrices

3.0 Introduction

The release of inorganic phosphate from phytic acid ($C_6H_{18}O_{24}P_6$) by phytate-degrading enzymes (phytases) and the subsequent precipitation of phosphate minerals is a promising mechanism for the remediation of contaminated sites such as uranium mine tailings (11,182,185,188,200–203). The microorganisms *Aspergillus niger* and *Blastobotrys adeninivorans* are known for their high phytase production/activity in acidic pH ranges (238,261,287,288) and this means they may be able to support the formation of phosphate minerals that are insoluble under acidic conditions, for example lead, lanthanide, or uranium phosphates (113,184,203).

However, while the successful immobilisation of lead, lanthanum, and uranium has been achieved by the release of phosphate from phytate in relatively simple liquid systems (182,185,200,202,203) – see also chapter 2 and chapter 4 in this work – mine tailings are complex environments and the presence of mineral species, or low water content, may inhibit microbial growth and/or phytate hydrolysis and thereby limit phosphate mineral precipitation. Only two studies have investigated phytate breakdown and subsequent phosphate mineral precipitation in the presence of contaminated sediments. Salome *et al.* (188) found that natural microbial communities hydrolysed phytate and induced uranium phosphate formation in Hanford sediment slurries at pH 5.5 but not at pH 7.0. Meanwhile, studies on Sellafield sediment slurries indicated that glycerol phosphate was a suitable phosphate donor for uranium phosphate precipitation but that phytate was not (104).

Complex solid matrices may inhibit the phytase mediated precipitation of phosphate minerals in several ways. Firstly, phytate may sorb onto minerals or form insoluble metal phytate complexes, and these species may be recalcitrant towards enzymatic hydrolysis (3,10,281,284,285). Secondly, phytase enzymes may be inactivated by adsorption onto soil particles (282–285). Thirdly, the solid matrix/environment may inhibit microbial growth and/or phytase production (e.g. because of a low water content) (363–365). Low water content may also lead to the denaturing of phytase enzymes (282).

Alternatively, there may be positive consequences to the presence of complex solid matrices. For example, ternary sorption complexes between minerals (e.g. aluminium oxides, iron (oxyhydr)oxides, or clays), phosphate and metals (e.g. copper, lead, or uranium) may increase metal sorption (130,131,366–373). Furthermore, sorbed complexes on mineral surfaces may also act as precursors for the precipitation of, for example, uranium phosphate phases (371,374). Clay minerals may also stabilise proteins (including enzymes) by forming complexes that protect the proteins against degradation (283,285,375,376).

Therefore, the aim of this chapter was to determine whether the organisms *A. niger* and *B. adeninivorans* can degrade phytate, and hence induce phosphate mineral precipitation, in complex or simple solid matrices. Further attention was given to what the main limiting factors that may inhibit this process are and how those limitations may be addressed.

3.1 Experimental programme and methods

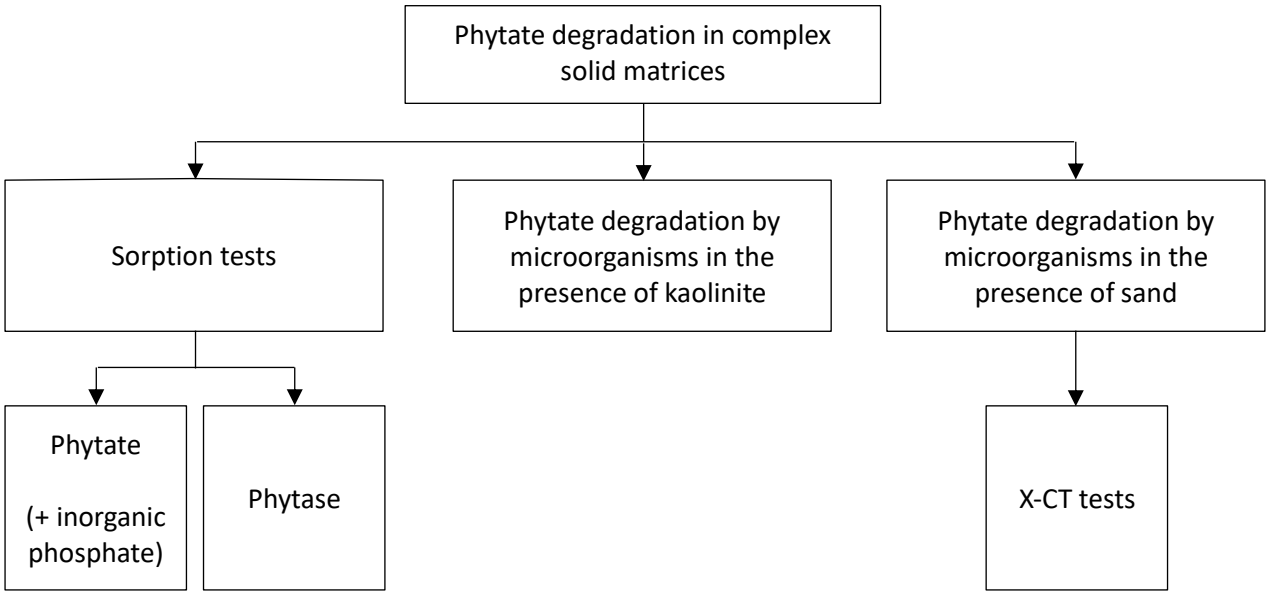

Figure 3.1 Flow chart of the experimental programme undertaken in chapter 3.

The work in this chapter (figure 3.1) began by investigating the growth of *A. niger* and *B. adeninivorans* and their ability to degrade phytate in a complex solid matrix, designed to be representative of a mine tailings material. When no phosphate release from phytate was detected in these experiments, three different directions were pursued to understand why, and what could be done to try and address this. Firstly, sorption tests were performed with the individual solids used to create the synthetic mine tailings material and either phytate or

phytase. Because the phytate stock contained an inorganic phosphate impurity, these experiments technically investigated the sorption of both phytate and inorganic phosphate.

Secondly, when the sorption tests indicated that the kaolinite fraction appeared to be the main phase interacting with both phytate and phytase, tests were performed with *A. niger* and *B. adeninivorans* growing in the presence of kaolinite to verify that it was kaolinite that inhibited phytate degradation in the presence of the microorganisms.

Thirdly, tests were performed with *A. niger* and *B. adeninivorans* growing in the presence of sand to test phytate degradation in a solid matrix with weakly interacting solids. The sand system tests were performed without any added metals, and with lanthanum added to investigate lanthanum phosphate precipitation in the solid matrix. Further tests investigated whether X-ray computed tomography (X-CT) could be used to visualise microbial growth and any lanthanum phosphate precipitation within the sand matrix.

3.1.1 Phytate degradation in a synthetic mine tailings system

Table 3.1 Composition of the synthetic mine tailings mixture. Concentrations are given on a dry mass basis.

Component	**g/100 g**	**Supplier (product number)**
K-feldspar ($KAlSi_3O_8$)	45	Mistral Industrial Chemicals (1791-o1)
Quartz (SiO_2)	35	
Coarse Leighton Buzzard sand	*28*	Departmental stock
Fine sand	*7*	Jordanhill Garden Supplies
Kaolinite ($Al_2Si_2O_5(OH)_4$)	15	Imerys Speswhite™ Quality China Clay
Marble ($CaCO_3$ + $CaMg(CO_3)_2$)	4.4	Leiths Ltd. Skye Marble
Cerium	0.5	
Cerium oxide (CeO_2)	*0.61*	Aldrich (22390)
Barium	0.1	
Barium Chloride dihydrate ($BaCl_2.2H_2O$)	*0.18*	Acros Organics (203135000)

The design of a synthetic “uranium mine” tailings material was based upon several literature reports of uranium ores (377,378), mine tailings (379–385), and sediments with naturally high uranium levels (386). Two different grades of quartz sand were chosen to represent the heterogeneity of grain sizes found in tailings, and kaolinite was chosen as a representative clay mineral. Barium and cerium were chosen as non-radioactive analogues of radium and thorium/uranium, respectively. While CeO_2 is a useful analogue for ThO_2 and UO_2 it is not a perfect analogue for uranium as cerium does not exist in a more mobile +6 oxidation state

like uranium. However, for the purposes of initial experiments, the addition of CeO_2 was considered sufficient.

X-ray diffraction (XRD) analysis of the individual solids indicated that K-feldspar was present as the microcline polymorph, while the marble consisted of a mixture of calcite and dolomite. XRD patterns of the kaolinite and fine sand indicated small peaks associated with impurity phases in addition to peaks associated with kaolinite and quartz, respectively. These impurities could not be conclusively identified but were probably other clay minerals for the kaolinite and a mixture of clays, oxides, and carbonates for the fine sand. No impurity phases could be observed in the XRD patterns of the coarse sand or CeO_2.

To prepare the synthetic tailings, the solids listed in table 3.1 were weighed out into a 250 mL Duran bottle in appropriate amounts to give a total dry mass of 50 g. The solids were then dry heat sterilised by placing the bottles in an oven set to 150 °C for 3 h. Dry heat sterilisation is the preferred method for sterilising solids as it minimises the changes in mineral composition and morphology that may occur during autoclaving (387).

After allowing to cool, the solids were mixed with approximately 100 mL of sterile nanopure water (npH_2O, resistivity ≥ 18.2 MΩ·cm) or 0.1 mol/L H_2SO_4, 0.25 mol/L H_2SO_4, or 0.5 mol/L HNO_3 to adjust the suspensions to different pH values (which ranged from ~ 2 to ~ 8). The suspensions were mixed on an overhead or orbital shaker for around 48 h. After the mixing period the suspensions were vacuum filtered (under aseptic conditions) through glass fibre (GF/D or GF/F) filters. After filtration, the amount of water retained by the solids was around 5–10 g.

The solids were then weighed out (~ 25 g, wet mass) into sterile glass beakers. To the solids, 5 mL of inoculum was added and gently mixed through with a pipette tip. The openings of beakers were either covered by sterile aluminium foil or UV-disinfected clingfilm. Experiments were conducted in the dark at room temperature (~ 22 °C) for about a month.

Inocula consisted of (1) partially homogenised *A. niger* biomass, (2) *A. niger* spores, or (3) *B. adeninivorans* cell suspensions, mixed with YN9.1B media (containing 20 g/L starch, 2.5 g/L phytate, 2.2 g/L calcium, and 5.9 g/L yeast nitrogen base (YN) – see chapter 2 for the full composition of YN) or a ~ 10 times concentrated version of YN9.1B media. Non-inoculated controls were mixed with an equivalent amount of sterile YN9.1B media.

To prepare the partially homogenised *A. niger* biomass, *A. niger* was grown in YN9B liquid media (20 g/L starch, 2.5 g/L phytate, 36 mg/L calcium, as per chapter 2) at 22 °C for 7 days. The cultures were transferred into a Stomacher bag and blended using a Seward Stomacher® Model 400 Lab Blender (388) for 15 to 30 minutes. The blending was only partially successful but did provide a cell suspension that was marginally easier to pipette than unblended *A. niger* biomass. An aliquot of the suspension was sampled, and the concentration of viable cells quantified by the viable plate count (VPC) method as per chapter 2. The *A. niger* biomass was then harvested by centrifugation (10,000 rcf, 5 minutes), washed twice in sterile 8.5 g/L NaCl by centrifuging, and resuspended in YN9.1B media. This suspension was used as the inoculum.

For *A. niger* spore suspensions, a spore suspension was prepared as described in chapter 2. This was then diluted in YN9.1B media to give an approximately equal viable cell concentration (~ 2 x 10^4 colony forming units per millilitre (CFU/mL)) to that contained in the homogenised biomass inocula. This spore suspension was then used as an inoculum.

To prepare *B. adeninivorans* cell suspensions, *B. adeninivorans* was grown in YN9B liquid media (as per chapter 2) at 22 °C for 4 days. The cell suspension was then washed and resuspended in YN9.1B media as per the blended *A. niger* biomass and subsequently used as an inoculum.

Samples were taken prior to inoculation, immediately after inoculation, and at the end of the experiment (after 30–50 days). Sampling involved weighing out 1 g (wet mass) of solids and mixing in a 1:5 ratio with either sterile npH_2O or 0.5 mol/L HNO_3 (389). After vortex mixing, an aliquot of the npH_2O samples was withdrawn and used for viable cell quantification by the VPC method. The npH_2O suspensions were then mixed on an orbital shaker for an hour before centrifuging (6,000 rcf, 5 minutes). The supernatants were then filtered and used for the determination of pH, electrical conductivity, oxidation-reduction potential, and water-soluble inorganic phosphate determination. The solids were washed twice with npH_2O and once with isopropyl alcohol (IPA) by centrifugation, dried to a constant mass at 50 °C, and used for solid phase analysis by XRD. The 0.5 mol/L HNO_3 samples were vortex mixed, then placed on an orbital shaker for 15 minutes, centrifuged (6,000 rcf, 5 minutes), filtered, and used for HNO_3 soluble inorganic phosphate determination. Water-soluble concentrations were compared to HNO_3 soluble concentrations to observe whether any inorganic phosphate precipitated.

3.1.2 Phytate sorption tests

To investigate the interactions between phytate and the solids used to create the synthetic mine tailings mixture (table 3.1) phytate was mixed with separate aqueous suspensions of each of the solids or with the full synthetic mine tailings mixture. The experiments were designed using two solid:solution ratios. One mixed the solids with water in the same ratio as was present in the synthetic mine tailings mixture and one prepared the solids with a relative excess of water. This second condition was performed for practical purposes as some solids (the kaolinite and the full synthetic tailings mixture) absorbed most of the water added and, therefore, were difficult to sample. These were designated "low water" and "high water" conditions, respectively. The low water condition was performed for kaolinite, fine sand (which was added at the same concentration as kaolinite for the low water condition), and the full synthetic tailings mixture, while the high water condition was performed for all solids. For kaolinite only, the influence of pH was tested by preparing "high water content" suspensions and adjusting the pH to 9 or 13.

Table 3.2 Solid loading used in the phytate sorption tests. N.d. indicates "low water" conditions were not performed for that solid. Note that barium chloride is water-soluble but was added in the experiments as a solid.

Component	Low water condition solids loading (g/L)	High water condition solids loading (g/L)
Synthetic mine tailings mixture	5000	1667
K-feldspar ($KAlSi_3O_8$)	n.d.	750
Coarse sand (SiO_2)	n.d.	465
Fine sand (SiO_2)	750	115
Kaolinite ($Al_2Si_2O_5(OH)_4$)	750	250
Marble ($CaCO_3$ + $CaMg(CO_3)_2$)	n.d.	75
Cerium oxide (CeO_2)	n.d.	10
Barium chloride dihydrate ($BaCl_2.2H_2O$)	n.d.	3

After weighing out the solids, they were mixed with a phytate solution (at a 2.5 g/L or 3.8 mmol/L concentration) to give the solid loadings indicated in table 3.2. Solutions of phytate without added solids were used as solid-free controls. After adding the phytate solution, the suspensions were vortex mixed and then placed on an orbital shaker (set to ~ 500 rpm) overnight. After this time, the suspensions were vortex mixed and then centrifuged (8,000 rcf, 20 min). Note that for the low water condition for the synthetic mine tailings mixture,

additional water had to be added as the solids absorbed all the water initially added. This additional water was mixed through the solids ~ 3 h before centrifugation.

After centrifuging, the supernatants were sampled, filtered, and used for pH, inorganic phosphate, and phytate measurements. Solids were washed once in npH_2O and once in IPA and then dried to a constant mass at 50 °C. Selected solids were analysed by Fourier transform infrared spectroscopy (FTIR) to investigate whether incorporation of phytate into the solid phase could be detected.

3.1.3 Phytase sorption tests

The interactions between phytase enzymes and solids used to create the synthetic mine tailings was investigated in a similar manner to the phytate sorption tests. Initial tests used the phytase enzyme provided with the Megazyme Phytic Acid assay kit (299) but, due to the limited availability of this enzyme, further tests used the wheat phytase supplied by Sigma-Aldrich (P1259-5G). Following this, additional work used an *A. niger* phytase (supplied by Hui Chem Co., Ltd.) as *A. niger* is one of the microorganisms used in this work, and different phytases may interact with solids differently (283).

Table 3.3 Conditions tested for the different phytase enzymes used in the sorption tests

Enzyme	Solids tested	Other factors investigated
A. niger	Kaolinite (1 or 250 g/L)	Time
Megazyme	K-feldspar, coarse sand, fine sand, kaolinite, marble, cerium oxide, barium chloride dihydrate (all at “high water” concentrations listed in table 2).	None
Wheat	K-feldspar, coarse sand, fine sand, kaolinite, marble, cerium oxide, barium chloride dihydrate (all at “high water” concentrations listed in table 2).	Enzyme concentration, pH, enzyme desorption, activity of sorbed enzymes.

Solutions of the phytase enzymes were prepared (at 2 mg/mL for the *A. niger* phytase, at 0.5% w/w for the Megazyme phytase, or 0.7–20 mg/mL for the wheat phytase) and mixed with solids as indicated in table 3.3. Solid-free controls involved mixing solid-free phytase solutions at room temperature for equivalent time periods; to check for the loss of activity over this time, additional solid-free controls were performed with phytase solutions freshly prepared before the enzyme assay. Suspensions were mixed on orbital shakers set to ~ 500 rpm

overnight (except where stated otherwise). After this time, suspensions were centrifuged (3,000–10,000 rcf, 5 minutes) and the supernatants withdrawn for use in enzyme assays.

Enzyme assays were performed by mixing supernatants (or suspensions) with a buffered (0.2 mol/L citrate or MES, pH 5.5) phytate (0.35 mmol/L) solution for 10 minutes at 40 °C (for Megazyme and wheat phytases) or 22 °C (for *A. niger* phytase – preliminary tests indicated a negligible difference between *A. niger* phytase activity at 22 or 40 °C). After 10 minutes, the reactions were terminated by the addition of trichloroacetic acid (TCA) to a concentration of 0.66 mol/L. The background concentration of inorganic phosphate was determined by adding TCA to the phytate solution before adding the test sample. The amount of phosphate released from phytate was calculated by subtracting the background inorganic phosphate concentration from the total inorganic phosphate concentration measured in the test sample. The amount of phosphate released from phytate was used to calculate the phytase activity in nanokatals (1 nKat = 1 nanomole of inorganic phosphate released from phytate per second of the reaction).

To investigate the desorption of enzymes or the activity of sorbed enzymes, the residual solids collected after centrifugation were resuspended in an equivalent volume of npH_2O. The suspensions were vortex mixed and placed on an orbital shaker (set to ~ 500 rpm) for 2 h. After this time, aliquots of suspension were withdrawn and used for enzyme assays as described above to test for sorbed phytase activity. Then, the suspensions were centrifuged (10,000 rcf, 1 minute), the supernatants filtered, and the filtrates assayed as described above to test for desorbed phytase activity.

Investigations of pH tested the influence of both pH and pH buffer. The kaolinite suspensions, without pH adjustment, had a pH of about 5. As a method of improving the amount of phytase remaining in solution, equivalent tests were performed by preparing the phytase solution in 0.1 mol/L citrate buffer, to test whether citrate could displace phytase from available sorption sites. Secondly, it was tested whether high pH values (~ 9) could increase the amount of phytase remaining in solution. The pH was maintained at around 9 by preparing suspensions in 0.1 mol/L TRIS buffer. The pH/buffer tests were mixed for 4 hours and assayed for phytase activity in the supernatants as described above, except that the pH 9 filtrates were re-adjusted to around pH 5 immediately before the assay.

3.1.4 Growth and phytate degradation in the presence of kaolinite

As the sorption tests indicated that kaolinite was the solid phase that interacted most strongly with both phytate and phytase, it was decided to perform growth and phytate breakdown tests with the microorganisms *A. niger* and *B. adeninivorans* to confirm the hypothesis that it was the kaolinite fraction that inhibited phytate degradation by the actively growing organisms.

These tests involved inoculating the microorganisms into YN6B liquid media (with 20 g/L galactose and 2.5 g/L phytate, prepared and sterilised as per chapter 2) with different levels of kaolinite (0, 10, or 500 g/L). The kaolinite was dry heat sterilised prior to mixing with the media (150 °C, 3 h).

Cultures were inoculated by the addition of spore or cell suspensions (prepared as described in chapter 2) at a concentration of 0.5% (v/v). The inocula were mixed through the suspension with a sterile pipette tip. Glass beakers were used as vessels and the openings covered with sterile aluminium foil, held in place with parafilm. Experiments were performed in triplicate along with single sterile controls. All experiments were performed in the dark at room temperature (22 °C) under static conditions. Samples were withdrawn at various time points using sterile pipettes and filtrates used to measure pH and inorganic phosphate concentrations. The experiments lasted for a total of 60 days.

3.1.5 Phytate degradation and lanthanum phosphate precipitation in the presence of sand

To investigate the growth of microorganisms and phytate degradation in the presence of a solid phase with a low sorption capacity towards phytate or phytase (quartz sand, Argos 365/0574), *A. niger* or *B. adeninivorans* were inoculated into a mixture of sand and YN6B nutrient media. The sand was dry heat sterilised (150 °C, 3 h), while the YN6B media was prepared and sterilised as described in chapter 2. After cooling, sand (70 g) and YN6B media (20 mL) were then mixed to give a sand concentration of 3,500 g/L. This provided a saturated solid matrix with a small amount of standing water. Spore or cell suspensions (prepared as per chapter 2) were inoculated at a concentration of 1.25% (v/v) or 0.3% (v/w). Experiments were inoculated in triplicate for each organism along with triplicate sterile controls. All experiments were performed in the dark at room temperature (22 °C) under static conditions. To test the precipitation of lanthanum, equivalent experiments were performed with 69 mg/L lanthanum added to the YN6B nutrient media.

Samples were taken after 0 (before inoculation), 7, 14, 30, and 60 days. Sampling involved using a sterile spatula to weigh out 1 g (wet mass) of sample and extracting the sample in a relevant solution which was then analysed for pH, and water-soluble and total concentrations of inorganic phosphate, ICP-OES phosphate, calcium, and lanthanum. Note that this was actually a pseudo-total concentration measurement, as quartz is insoluble in the extracting solutions used, and there was some evidence (discussed in the results) that recovery of some analytes was also low.

For pH measurements and water-soluble concentrations, solids were mixed in a 1:5 ratio with npH_2O and mixed in an overhead shaker (set to 10 rpm) for ~ 1 h. The suspensions were then centrifuged (10,000 rcf, 5 minutes) and the supernatants filtered (0.2 µm hydrophilic PTFE) and used for analysis. For total concentrations, solids were extracted in a 1:5 ratio with 1.67 mol/L HNO_3 for 15 minutes. Total concentration samples were taken at every time point for the lanthanum-containing samples or the final time point only for the lanthanum-free experiments. These extractions were either performed on separate samples (for intermediate time points) or sequentially following the npH_2O extractions (for the initial and final time points). At the final time point, samples were taken in 5 g amounts. Five samples were taken for each experiment, two samples from the upper layer, one from the middle, and two samples from the bottom. Two of the samples were only subjected to the npH_2O extraction, while the remaining three (one sample from each layer) were sequentially extracted with npH_2O and 1.67 mol/L HNO_3. In between the extractions, the solids were washed three times with npH_2O by centrifugation.

Following the extractions, the solids were washed three times in npH_2O and once in IPA by centrifugation. The solids were then dried to a constant mass at 50 °C and the dry mass of each sample measured. Solids that had only been subjected to npH_2O extractions were analysed by XRD and FTIR.

3.1.6 X-CT tests

To test whether X-CT scanning could be used to visualise microbial growth and lanthanum precipitation within a sand matrix, similar tests were performed to the sand experiments. To improve the resolution achievable, the experiments were scaled down in size (the dry mass of sand used was ~ 0.3 g rather than 70 g as in the above tests), and to improve the likelihood of observing lanthanum phases, the lanthanum concentration was increased to 695 mg/L (5

mmol/L). Experiments were performed with two organisms (*A. niger* or *B. adeninivorans*), a purified enzyme (from *A. niger*), or sterile controls (table 3.4).

Table 3.4 Conditions performed for the X-CT tests. Single experiments were performed for each condition. Lanthanum and phytate at the concentrations listed were mixed with YN6B liquid media.

Organism	Lanthanum (mmol/L)	Phytate (mmol/L)
A. niger	5	3.8
B. adeninivorans	5	3.8
Purified *A. niger* enzyme	5	3.8
Sterile control	5	3.8
Sterile control	5	0
Sterile control	0	3.8

To perform the experiments, miniature "flow through" columns were prepared by attaching 1 mL Luer-Lok™ (BD 309628) syringes to syringe filter units (0.2 µm PES, 33 mm diameter, Fisher 15206869). To stop solids falling through into the filter, an aerosol barrier (from a 200 µL Fisherbrand™ SureOne™ aerosol barrier pipette tip) and a small circle of filter paper (Green's 401) was placed at the bottom of the syringe. When not actively adding solids/liquids, the opening at the top of the syringes was plugged with sterile non-absorbent cotton wool. Dry heat sterilised sand was weighed into the syringe and was then saturated with appropriate liquid nutrient media (YN6B media with lanthanum and phytate concentrations as listed in table 4). The "columns" were then attached to a solid phase extraction (SPE) unit (Supelco Visiprep 24™ DL) and a low vacuum (~ 3–5 kPa) applied for around 30 seconds until no standing water was left. Then, a second quantity of solution was added and allowed to flow through under gravity. The liquids were collected in centrifuge tubes for zero time point analysis. The amount of liquid retained by the solids ranged from 4 to 38% (w/w). Aseptic conditions were maintained for all preparation steps.

Experiments were started by the addition of 10 µL spore or cell suspension for *A. niger* or *B. adeninivorans*, 10 µL of enzyme solution (at 1 mg/mL) for the *A. niger* phytase, or 10 µL sterile npH_2O for the controls. Experiments were left at room temperature in the dark for 40 days.

After 40 days, 1 mL of npH_2O was pipetted into each column; the columns were attached to the SPE unit and the liquid pulled through under vacuum (20 kPa). The filtrate was collected and used for measurements of water-soluble analytes. The columns were then imaged using a Nikon XT H 320 X-Ray CT scanner at the University of Strathclyde's Advanced Materials

Research Laboratory. Scan parameters included an energy of 150 kV, a current of 118 µA, recording 3,141 angular projections per scan with an angular step of 0.1146° and an exposure time of 1,000 ms. With the setup used, a voxel resolution of ~ 8 µm was achieved. 3D volumes of the scans were reconstructed using the Nikon XTekCT software. The reconstructed image stacks were then processed using the Fiji distribution (390) of ImageJ (391).

3.1.7 Analytical techniques

Microbial growth was quantified by performing VPCs using the drop plate method (297) and qualitative judgments based upon photographs. Solution samples were analysed for pH, electrical conductivity, oxidation-reduction potential (ORP), inorganic phosphate (by colorimetry), and metals and phosphorus (by ICP-OES). Methods for pH, inorganic phosphate, and ICP-OES are described in chapter 2. Organic phosphate concentrations were calculated by subtracting inorganic phosphate concentrations from ICP-OES measured phosphate concentrations.

Electrical conductivity was measured using either a Mettler Toledo InLab 731 conductivity sensor connected to either a Mettler Toledo MPC 227 pH/Conductivity Meter or a Mettler Toledo SevenMulti™ S47 - dual meter pH / conductivity, or a Hach CDC40101 Conductivity probe connected to a Hach HQ40d Multi Portable Meter. Calibrations were performed (usually two point) using standards encompassing the estimated range of values to be measured. The standards were continually mixed with a magnetic stirrer during calibration.

ORP was measured using a Mettler Toledo InLab Redox Pro probe connected to either a Mettler Toledo MPC 227 pH/Conductivity Meter or a Mettler Toledo SevenMulti™ S47 - dual meter pH / conductivity. The InLab Redox Pro probe has a platinum sensing electrode and uses the Ag/AgCl reference system with a 3 mol/L KCl electrolyte. The measured value of samples in millivolts was converted to the redox potential relative to the standard hydrogen electrode (E_h) with the equation: $E_h = E_{measured} + 207$ mV (392).

For select samples, phytate concentrations were measured using the Megazyme Phytic Acid assay kit K-PHYT (299). Phytate concentrations measured this way were similar to phytate concentrations calculated from ICP-OES measurements of phosphate after the inorganic phosphate had been subtracted.

Solid samples were analysed by X-CT (as described above), XRD (as described in chapter 2), and FTIR. FTIR analysis was carried out using an Agilent Technologies Cary 660 FTIR Spectrometer with a PIKE MIRacle™ single reflection diamond crystal Attenuated Total Reflectance (ATR) module. Each sample was scanned 32 times with a resolution of 4 cm^{-1} and a scan range of 400–4000 cm^{-1}. Spectra were acquired using the Resolutions Pro software (Agilent Technologies) and spectra were processed using OriginPro (version 2019b) (393), Spectragryph (394), and the Bio-Rad KnowItAll® Informatics System (395).

3.2 Results and discussion

3.2.1 Phytate degradation in a synthetic mine tailings system

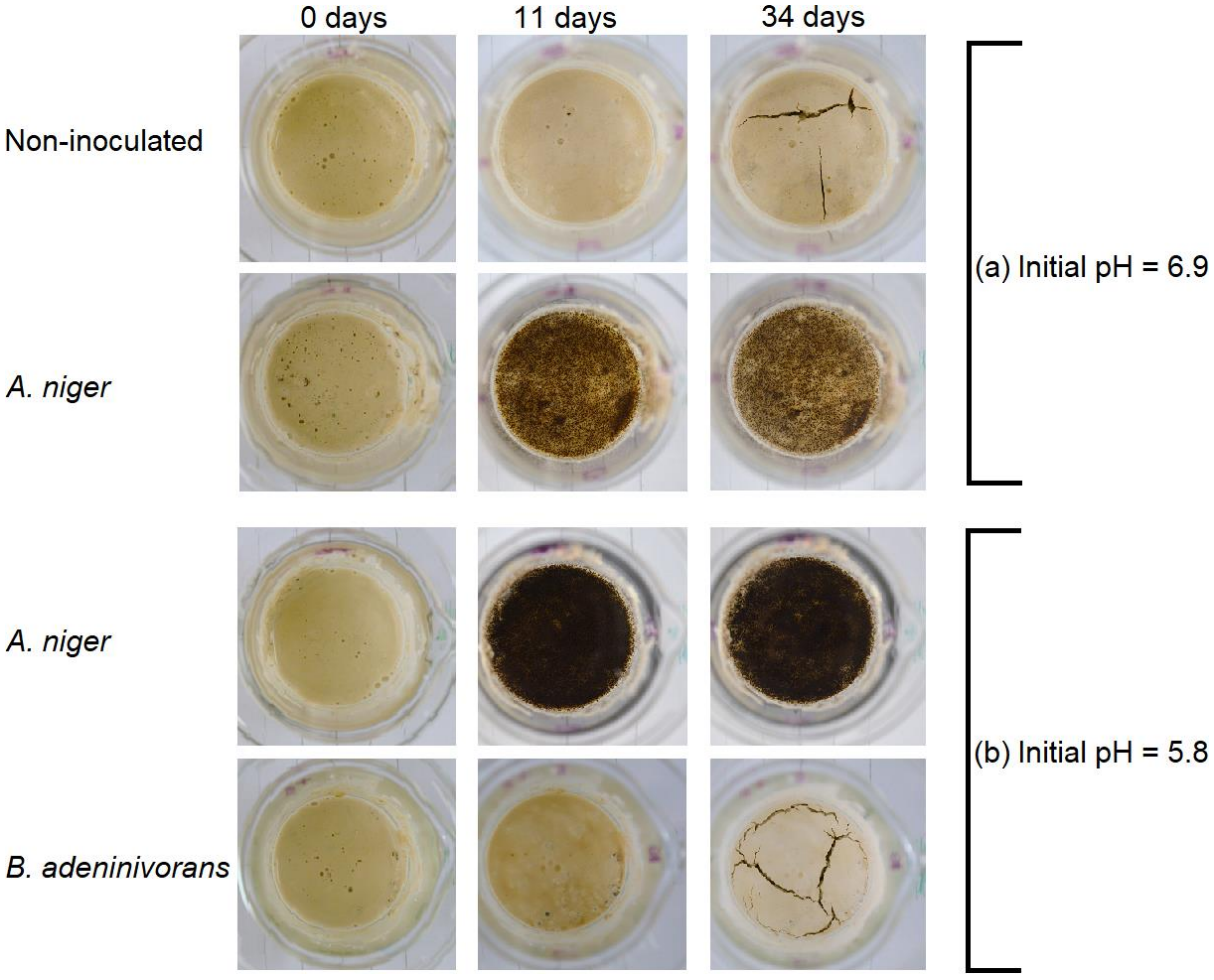

Figure 3.2 Visual comparison (top-down photographs) of select experiments from the synthetic mine tailings tests. Experiments shown are from (a) batch 3 and (b) batch 4 as indicated in table 3.5.

Visual comparisons of the synthetic mine tailings tests showed obvious signs of growth for *A. niger* with a mat of spores forming across the surface of the solids within 6–11 days (figure

3.2), although it is uncertain to what extent growth penetrated into the solid media. Visual signs of growth in the *B. adeninivorans* or non-inoculated controls were not possible to observe.

It was notable how, in the *B. adeninivorans* cultures and non-inoculated controls the solids dried out over the time of the experiment and started to crack (figure 3.2). In contrast, this effect was not observed in the *A. niger* cultures. Measurements of mass over time indicated that the *A. niger* cultures lost 9–15% of their initial mass, while other experiments lost 14–25% of their initial mass (table 3.5). This can be attributed to the evaporation of water, so it appears that the growth of *A. niger* across the surface of the solid limited water evaporation and thereby limited cracking of the solids. This effect was only observed in certain experiments, namely, batch 1, batch 3, and batch 4 as indicated in table 3.5. These experiments had the opening of the beakers covered with aluminium foil, while the other batches were covered with transparent clingfilm (to make photographing experiments easier); therefore, it appears that the clingfilm inhibited water evaporation.

Table 3.5 Summary of results from the synthetic mine tailings experiments. Concentrations are given as mmol/kg on a dry mass basis. T_0 describes samples taken immediately after mixing in the inoculum, T_1 is the final time point as indicated in the table. Data represent either single measurements or the mean of duplicate samples ± the difference between the mean and the measured values. Available phosphate in phytic acid and inorganic phosphate added were calculated from the nominal concentration of phytic acid and phosphate in the inoculum. All other values were measured directly on the relevant extracted suspensions/filtrates.

Organism	Inoculum	Available phosphate in phytic acid added (mmol/kg)	Inorganic phosphate added (mmol/kg)	Background water-soluble inorganic phosphate in solid matrix (mmol/kg)	Background nitric acid soluble inorganic phosphate in solid matrix (mmol/kg)	Water-soluble inorganic phosphate (mmol/kg)		Nitric acid soluble inorganic phosphate (mmol/kg)		$pH_{(H2O)}$		Mass loss (%)
Batch 1, initial pH 8.4, T_1 = 47 days						T_0	T_1	T_0	T_1	T_0	T_1	
A. niger	Cell suspension	29.68	4.51	< 0.06	n.d.	n.d.	0.44 *± 0.01*	n.d.	7.28 *± 0.32*	n.d.	7.4 *± 0.19*	15.21%
B. adeninivorans	Cell suspension	32.01	4.86	n.d.	n.d.	4.36	0.45 *± 0.01*	n.d.	5.23 *± 0.11*	6.0	7.3 *± 0.11*	18.85%
Unknown mould and bacteria (contamination)	None	31.33	4.76	0.11	n.d.	2.68	0.46 *± 0.26*	n.d.	6.04 *± 1.05*	6.5	7.5 *± 0.29*	16.72%
Batch 2, initial pH 7.6, T_1 = 52 days												
A. niger	Cell suspension	7.08	1.08	0.04	0.89	0.56	0.07	1.54	1.70	6.3	7.1	8.30%
A. niger	Spore suspension	9.25	1.41	< 0.04	1.16	0.25	0.15	2.37	2.83	6.6	6.5	5.87%
B. adeninivorans	Cell suspension	7.27	1.11	< 0.03	0.94	0.22	0.05	2.29	1.33	6.6	7.1	4.10%
Unknown bacteria (contamination)	None	8.58	1.30	< 0.03	0.91	0.11	0.04	2.01	2.30	6.8	7.1	5.56%

Table 3.5 (continued).

Organism	Inoculum	Available phosphate in phytic acid added (mmol/kg)	Inorganic phosphate added (mmol/kg)	Background water-soluble inorganic phosphate in solid matrix (mmol/kg)	Background nitric acid soluble inorganic phosphate in solid matrix (mmol/kg)	Water-soluble inorganic phosphate (mmol/kg)		Nitric acid soluble inorganic phosphate (mmol/kg)		$pH_{(H2O)}$		Mass loss (%)
Batch 3, initial pH 6.9, T_1 = 34 days						T_0	T_1	T_0	T_1	T_0	T_1	
A. niger	Cell suspension	7.05	1.07	< 0.05	1.26	0.94	0.16 *± 0.05*	2.37	2.27 *± 0.41*	6.5	7.4 *± 0.09*	9.00%
Unknown bacteria (contamination)	None	7.61	1.16	< 0.05	1.73	0.74	0.19 *± 0.01*	2.74	3.00 *± 0.40*	6.9	6.9 *± 0.19*	13.93%
Batch 4, initial pH 5.8, T_1 = 34 days												
A. niger	Cell suspension	5.73	0.87	< 0.06	1.52	0.53	0.12 *± 0.05*	2.54	2.13 *± 0.45*	5.2	6.4 *± 0.04*	11.58%
B. adeninivorans	Cell suspension	7.01	1.07	< 0.05	1.56	0.72	0.17 *± 0.07*	2.72	2.14 *± 0.10*	5.3	6.6 *± 0.04*	25.28%
Batch 5, initial pH 4.5, T_1 = 52 days												
A. niger	Cell suspension	7.59	1.15	0.09	0.43	0.63	0.35	3.32	1.98	4.6	6.0	4.62%
B. adeninivorans	Cell suspension	8.47	1.29	0.09	0.42	0.59	0.07	1.07	1.16	4.6	6.6	6.28%
Batch 6, initial pH 3.9, T_1 = 52 days												
A. niger	Cell suspension	7.12	1.08	< 0.03	0.07	2.04	0.39	0.61	1.34	3.9	5.9	3.84%
A. niger	Spore suspension	9.14	1.39	< 0.03	0.08	0.62	1.23	1.03	1.83	4.0	5.4	6.28%
B. adeninivorans	Cell suspension	7.26	1.10	< 0.03	0.08	0.40	0.41	0.77	1.12	3.6	5.9	5.60%
None	None	8.97	1.36	< 0.03	0.09	0.53	0.15	0.67	0.79	4.1	5.9	9.30%

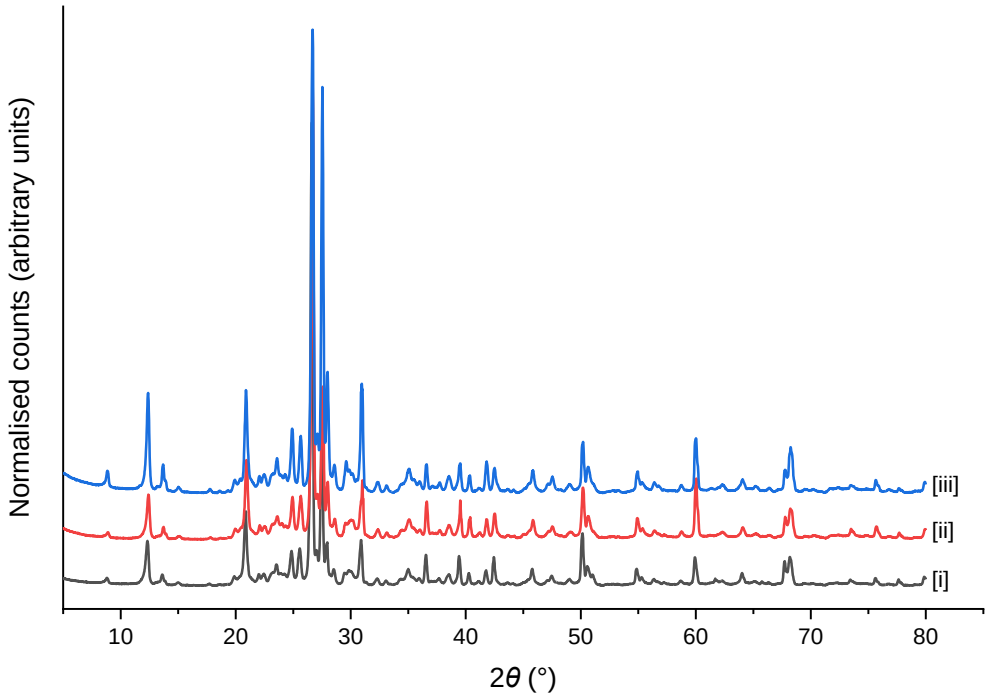

Figure 3.3 XRD patterns of [i] simulated waste tailings before addition of nutrient media, [ii] after addition of inoculum/nutrient media, and [iii] after growth of A. niger *(red). Samples were taken from experiments listed in table 5 as part of 'batch 1'. Patterns were measured using the Göbel mirror optics setups. Samples were measured using the copper K_α radiation across a 2θ range of 5–80° with a step size of 0.02° and a step time of 1 s. Patterns were normalised in OriginPro 2019b to a scale of 0 to 1.*

Despite the indications of *A. niger* growth, there was no indication of release of phosphate from phytate under any conditions, as both water-soluble and 0.5 mol/L HNO_3 soluble concentrations of inorganic phosphate were low compared to the theoretically available amount in phytate (table 3.5). Additionally, no observable changes to the bulk mineralogy occurred (figure 3.3). Measurements of pH (table 3.5) indicated that pH values generally increased over the course of the experiment but that there was little difference between different organisms. There also appeared to be no obvious trends in electrical conductivity or oxidation-reduction potential (appendix C, table C.1). Viable cell concentrations generally decreased for *B. adeninivorans* and increased for *A. niger* (appendix C, table C.1), although to what extent this was due to the abundance of spores forming on the surface of the cultures is uncertain. Additionally, all but one of the "sterile" non-inoculated controls showed contamination, indicating that refinements to the procedures to maintain sterility are required.

3.2.2 Phytate sorption tests

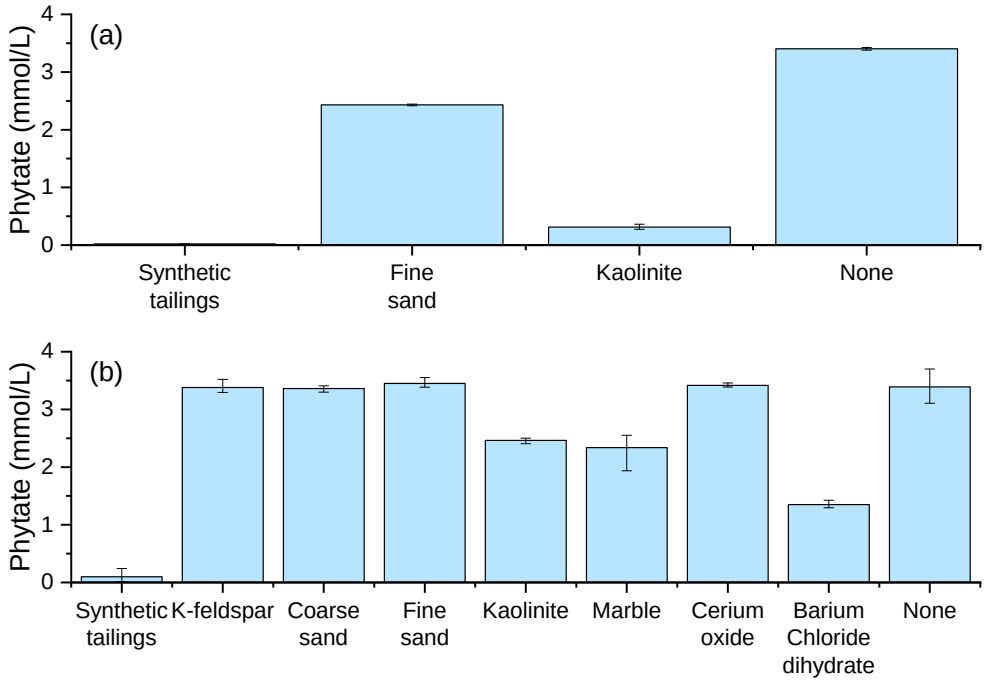

Figure 3.4 Concentration of phytate remaining in solution after mixing with various solids in (a) low water and (b) high water conditions. Columns represent the mean value of triplicate samples, error bars represent the difference between the mean and upper or lower measured values.

Mixing phytate with the synthetic mine tailings material indicated that effectively all phytate was removed from solution (figure 3.4). Tests with individual solids indicated that kaolinite, marble, and barium all removed substantial quantities of phytate from solution (figure 3.4). Summing the amount of phytate removed in each case appeared to account for the complete removal of phytate. The mechanisms of removal were likely sorption onto kaolinite, dissolution/precipitation with calcium and magnesium in the marble, and precipitation with the soluble barium. Under the low water conditions, there also appeared to be some removal of phytate by the fine sand (figure 3.4a) – this was likely associated with impurities in the sand.

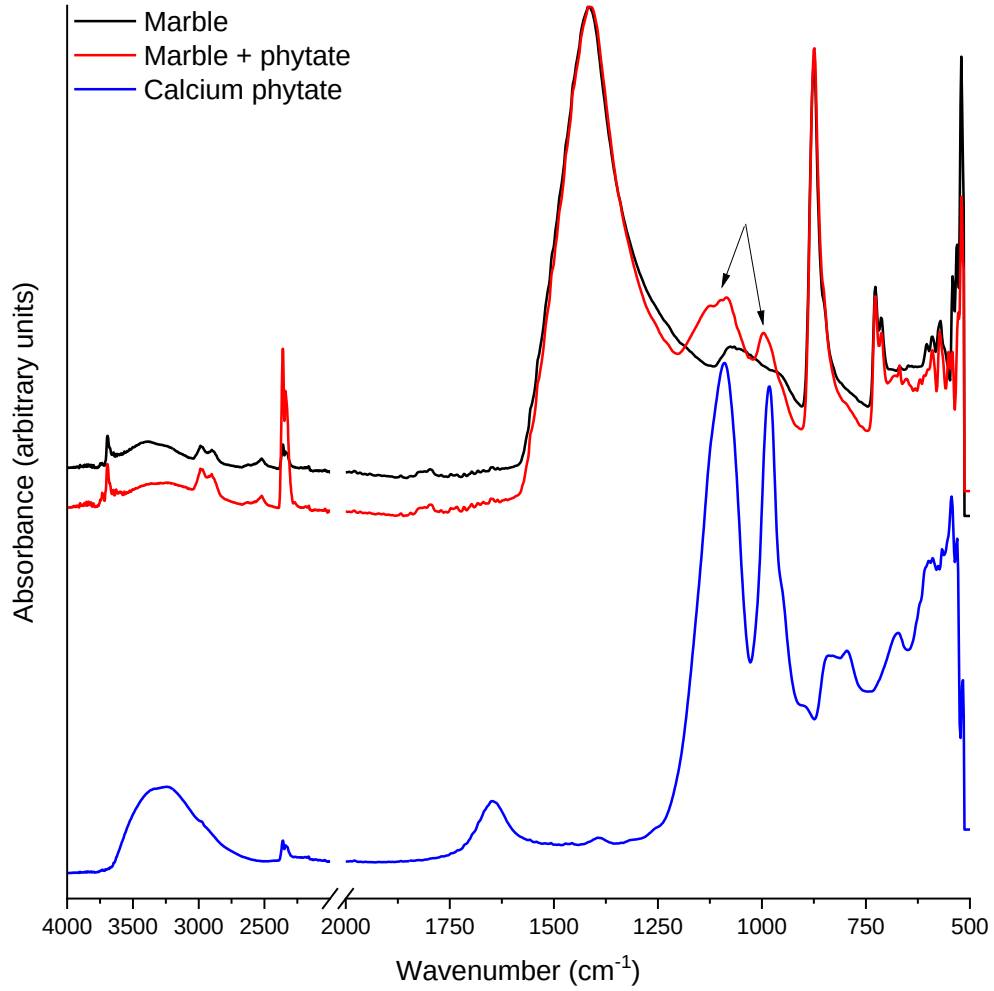

Figure 3.5 FTIR spectra of marble (black), marble reacted with phytate (red), and calcium phytate (blue). Arrows indicate the positions of peaks potentially associated with calcium phytate in the marble reacted with phytate sample. Spectra were normalised in OriginPro 2019b to a scale of 0–1.

Analysis of select solid phases (marble and kaolinite) indicated that, for marble, after mixing with phytate, two peaks emerged in the 1,200–900 cm^{-1} region (indicated by arrows) that match with the two most intense peaks in the spectrum of calcium phytate (figure 3.5). This has previously been observed by Celi *et al.* (396) who studied the interactions of phytate with calcite, and appears to be consistent with a dissolution/precipitation mechanism of phytate removal. In contrast, negligible changes to the FTIR spectrum of kaolinite could be observed after phytate sorption (data not shown). This is consistent with previous studies of phytate sorption by kaolinite and is considered to be related to the low specific surface area of kaolinite, which means that the amount of sorbed phytate will be too low compared to the amount of bulk kaolinite to be detected by FTIR (281,397).

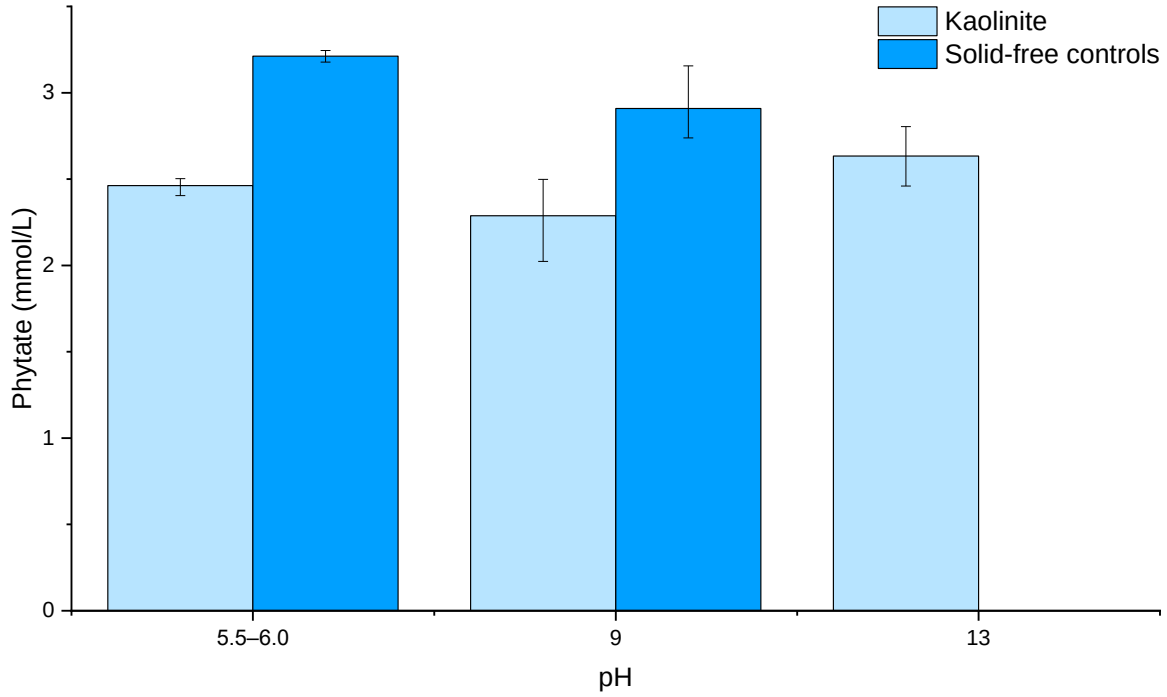

Figure 3.6 Phytate remaining in solution when mixed with kaolinite at different pH values. Columns represent the mean of triplicate samples, error bars are the difference between the mean and the upper and lower measured values. No solid-free controls were performed at pH 13.

To try and reduce the sorption of phytate onto kaolinite, tests at different pH values were performed. The kaolinite suspensions prepared without pH adjustment had a pH of 5.4–5.8. As phytate is a highly charged anion, it was decided to perform sorption tests at high pH values (9–13). These values are substantially higher than the point of zero charge (PZC) for kaolinite edges of about pH 5.5 (398). Therefore, at the high pH values used, the kaolinite edges should have been negatively charged, with the hypothesis that this would repel the phytate anion and limit sorption. However, as shown in figure 3.6, the amount of phytate removed from solution was similar regardless of pH, although there was possibly a small increase in solution phytate at pH 13.

Previous research on the sorption of phytate by kaolinite has produced contradictory results. Ruyter-Hooley *et al.* (399) found that phytate sorption increased slightly from pH 3 to pH 8 and only decreased significantly above pH 10. However, Hu *et al.* (397) found that phytate immobilisation by kaolinite reached a maximum at pH 2.5–4.0, decreased slightly at pH 5.5, and decreased substantially at pH 7.0–9.0.

Ruyter-Hooley *et al.* (399) and Hu *et al.* (397) both used the KGa-2 kaolinite sourced from the Clay Minerals Society so differences in their results may be due to sample preparation techniques.

Ruyter-Hooley *et al.* (399) used the KGa-2 kaolinite without further treatment, while Hu *et al.* (397) used hydrogen peroxide to oxidise organic matter, used wet sedimentation to separate the 2 µm size fraction, then freeze-dried the material and ground it so it would pass through a 100-mesh sieve. Therefore, it is apparent that impurities in the kaolinite influence the sorption behaviour of phytate, and that the results presented by Hu *et al.* (397) are likely a more accurate representation of the interactions between phytate and kaolinite. A different source of kaolinite was used in this work but, like Ruyter-Hooley *et al.* (399), no measures were taken to remove impurities, and this likely explains the similarities between these results and those presented by Ruyter-Hooley *et al.* (399).

Ruyter-Hooley *et al.* (399) and Hu *et al.* (397) also described different mechanisms of interaction between phytate and kaolinite. Hu *et al.* (397) observed that phytate may precipitate with aluminium dissolved from kaolinite or form inner-sphere complexes with kaolinite. The dissolution/precipitation mechanism was the predominant mode of interaction below pH 4 but may occur between pH 2.5 and 5.5; above this value, the solubility of kaolinite is too low to allow the release of sufficient quantities of aluminium (397). Instead, inner-sphere complexation was described as the main mechanism of phytate sorption at pH 5.5 and above (397). In contrast, Ruyter-Hooley *et al.* (399) claim that phytate forms an inner-sphere surface complex with kaolinite below pH 6, with outer-sphere complexes dominating at higher pH values.

Kaolinite is described as having two types of site where adsorption may occur; the face and the edge (398,399). The kaolinite faces are always negatively charged, regardless of pH (398,399), and therefore will repel anions such as phytate. The kaolinite edges, which consist of AlOH groups (399), have a pH dependent charge with a PZC (as stated above) of around 5.5 (398). It is therefore unlikely that outer-sphere complexation would occur between the negatively charged phytate anion and the negatively charged kaolinite edges above the PZC (400). Inner-sphere complexation of inorganic phosphate onto mineral phases, including kaolinite, can occur above the PZC through ligand exchange (401). A similar process may occur for phytate but, as shown by Hu *et al.* (397), the amount of inner-sphere complexation above pH 5.5 was low and does not account for phytate sorption remaining mostly constant between pH 5.5 and 13 in this work. Therefore, other mechanisms were likely important in the high pH interactions between phytate and kaolinite. These mechanisms may have included cation bridging, or interactions with organic matter or mineral impurities.

Cation bridging occurs where a cation adsorbs to a negatively charged surface, with the negatively charged adsorbate subsequently binding to the sorbed cation (402,403). Cation bridging has been described as an important mechanism for the sorption of organic phosphate compounds such as DNA and RNA onto clay minerals (402,404). Therefore, if multivalent cations (e.g. magnesium, calcium, or iron) were present as impurities it is possible that cation bridges were formed between the negatively charged kaolinite particles and phytate.

As discussed above, the differences between the reports by Ruyter-Hooley *et al.* (399) and Hu *et al.* (397) may have been due to the latter authors taking measures to destroy accompanying organic matter impurities. Phytate may interact with organic matter through direct adsorption or through cation bridging (2,3) and, as procedures to remove organic matter were not performed in this work, these interactions may have been important.

Finally, XRD analysis of the supply of kaolinite used in this work indicated that there were (unidentified) mineral impurities present. Therefore, depending on their properties, these mineral impurities may have contributed to phytate sorption across a wider range of pH values than would be expected for kaolinite alone.

The results presented here along with their comparisons to previous work (397,399) suggest that impurities co-occurring with kaolinite may have an important role in the sorption of phytate. As the solubility of phytate is an important factor determining whether it is available for enzymatic hydrolysis, it is critical that further work is performed to (a) develop an improved understanding of the interactions between phytate and kaolinite, and (b) to understand how different impurities (e.g. cations, organic matter, other minerals) influence the sorption of phytate by kaolinite.

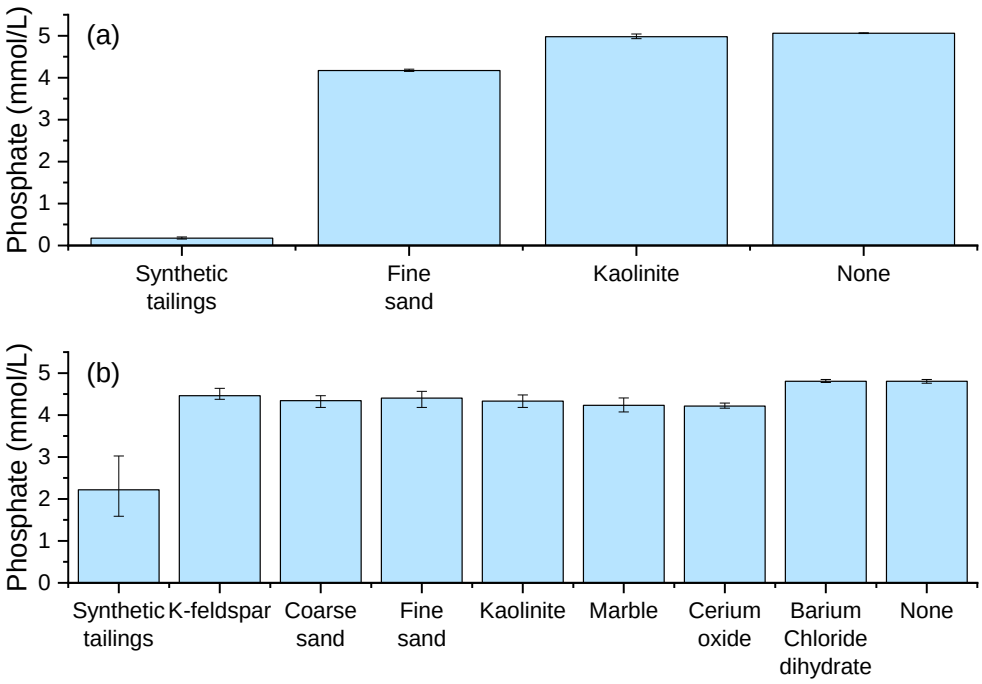

Figure 3.7 Concentration of inorganic phosphate remaining in solution after mixing with various solids in (a) low water and (b) high water conditions. Columns represent the mean value of triplicate samples, error bars represent the difference between the mean and upper or lower measured values.

As the phytate stock also contained an inorganic phosphate impurity, the interactions of inorganic phosphate with the solids used to create the synthetic mine tailings could also be investigated. Phosphate solubility was low in the synthetic mine tailings mixture but appeared to be higher than phytate (figure 3.7). When mixed with individual solids, however, the majority of inorganic phosphate remained in solution (figure 3.7). The impact of pH seemed to be similar for inorganic phosphate as for phytate, with a negligible difference between pH ~ 6 and 9 and a small increase in phosphate solubility at pH 13 (data not shown).

The low amount of phosphate sorption/precipitation when mixed with the individual solids is likely due to the strong interactions between phytate and the solids keeping phosphate in solution. However, where almost complete phytate precipitation occurred there was presumably an excess of sorption/precipitation sites compared to the phytate concentration, which therefore allowed phosphate to also sorb/precipitate. This is consistent with previous research indicating that phytate interacts more strongly with soil minerals than inorganic phosphate (10,281,405). Ideally, separate experiments would be performed with pure sources of phytate and inorganic phosphate, respectively, to understand the mechanisms of removal and the competition between the two species.

3.2.3 Phytase sorption tests

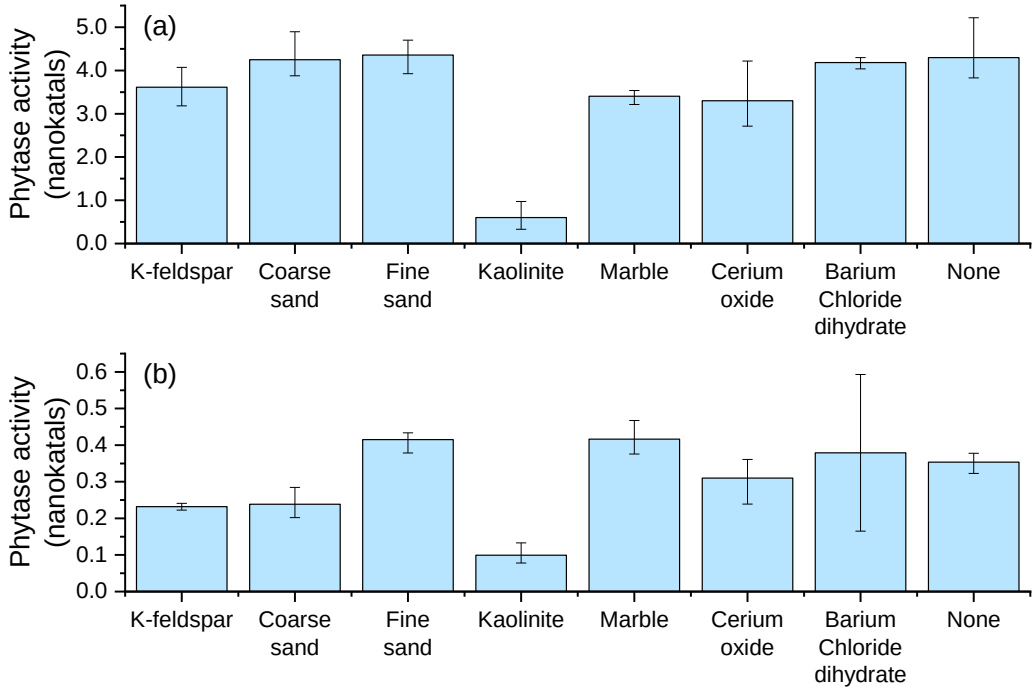

Figure 3.8 Activities of filtered supernatants after mixing (a) Megazyme (at 0.5% v/v), and (b) Wheat (at 0.7 mg/mL) phytase enzymes with solid phases (added at the concentrations listed in for the "high water" condition in table 2). Mixing took place for ~ 24 h at ~ 22 °C, enzyme assays took place for 10 minutes at 40 °C. Columns represent the mean value of triplicate samples, error bars represent the difference between the mean and the upper or lower measured values.

Mixing either Megazyme (figure 3.8a) or wheat (figure 3.8b) phytases with kaolinite showed a clear reduction of phytase activity remaining in solution. Solid-free controls showed that the phytase solutions left overnight did not lose activity compared to freshly prepared phytase solutions (data not shown). The majority of the Megazyme phytase appeared to remain in solution with the other solids (figure 3.8a), while there may have been some interaction between the wheat phytase and K-feldspar or the coarse sand (figure 3.8b). However, as the enzyme concentration was low (nominally 0.7 mg/mL, diluted to 0.4 mg/mL for the assay) and the assay time short (10 minutes) further tests would be required to verify this.

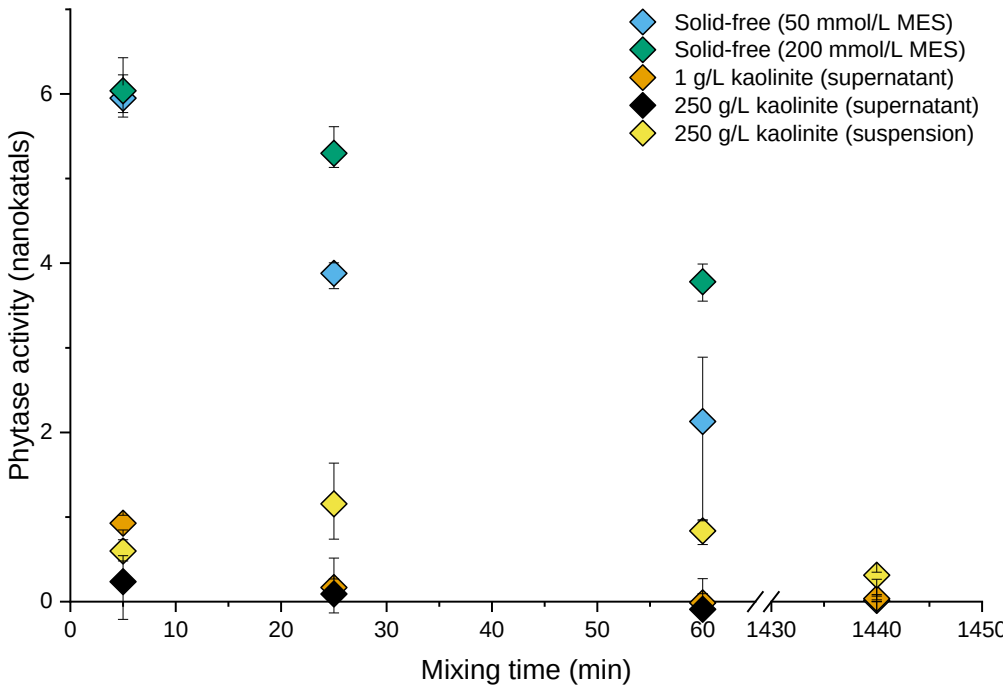

Figure 3.9 Activities of supernatants or suspensions after mixing the A. niger *phytase (nominal concentration of 2 mg/mL) with 1 g/L or 250 g/L kaolinite. Mixing took place for ~ 24 h at ~ 22 °C, enzyme assays took place for 10 minutes at ~ 22 °C. Data points represent the mean value of triplicate samples, error bars represent the difference between the mean and the upper or lower measured values. The 1 g/L kaolinite experiments used a 50 mmol/L MES buffer, the 250 g/L kaolinite experiments used a 200 mmol/L MES buffer, so solid-free controls for both buffers are presented for reference.*

Equivalent tests could not be performed with the *A. niger* phytase as, in the absence of a substrate, the phytase solutions lost activity over the span of 24 hours, even without any solids present (figure 3.9). Instead, time course experiments were performed with kaolinite only, and these indicated a rapid interaction between the *A. niger* phytase and kaolinite, with almost complete removal of the phytase from solution within 20 minutes at both solid loadings tested. This is consistent with previous research investigating the sorption of phytase by soils (283,285,406). A small amount of phytase activity possibly occurred when assaying the kaolinite suspensions but this was low.

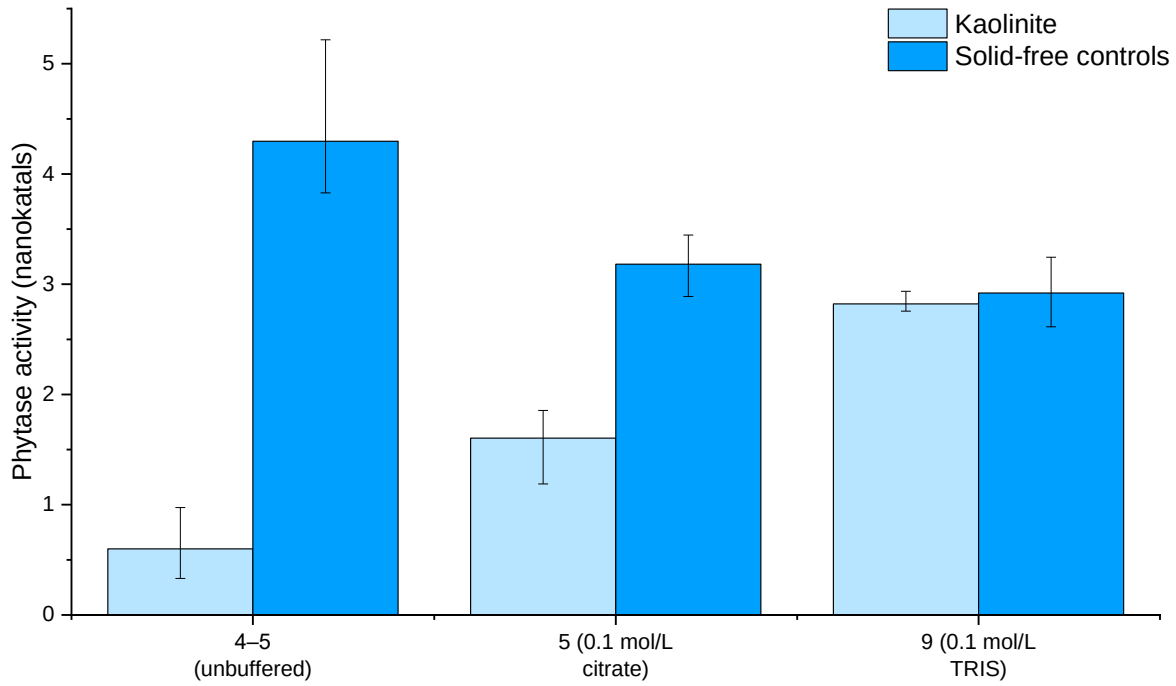

Figure 3.10 Comparison of Megazyme phytase (added at 0.5% v/v) activity remaining in solution when mixed with kaolinite or solid-free controls at pH 4–5 (unbuffered), in solutions buffered at pH 5 with 0.1 mol/L citrate, or solutions buffered at pH 9 with 0.1 mol/L TRIS. Mixing took place for ~ 24 h for unbuffered samples or 4 h for buffered samples at ~ 22 °C, enzyme assays took place for 10 minutes at ~ 22 °C. Columns represent the mean value of triplicate samples, error bars represent the difference between the mean and the upper or lower measured values.

To test whether complexing agents (citrate) or high pH could increase the amount of phytase remaining in solution, experiments were performed in buffered solutions of 0.1 mol/L citrate (pH 5, equivalent to the unbuffered kaolinite suspension, to test whether citrate could keep phytase in solution) or 0.1 mol/L TRIS (to test whether high pH values could keep the phytase in solution). These tests indicated that both citrate at pH 5 and a high pH could keep the Megazyme phytase in solution (figure 3.10). Previous research has described citrate as having a negligible effect on the sorption of *A. niger* phytase (285) so the contrasting results here underline the variable interactions of different phytase enzymes with solid phases. It is not certain to what extent the phytase remaining in solution at high pH was due to the pH or the presence of TRIS, although the solid-free control indicated that TRIS slightly inhibited phytase activity (figure 3.10). Previous research has observed that increased pH values can increase the amount of *A. niger* phytase remaining in solution (283), so it is likely that the pH is important.

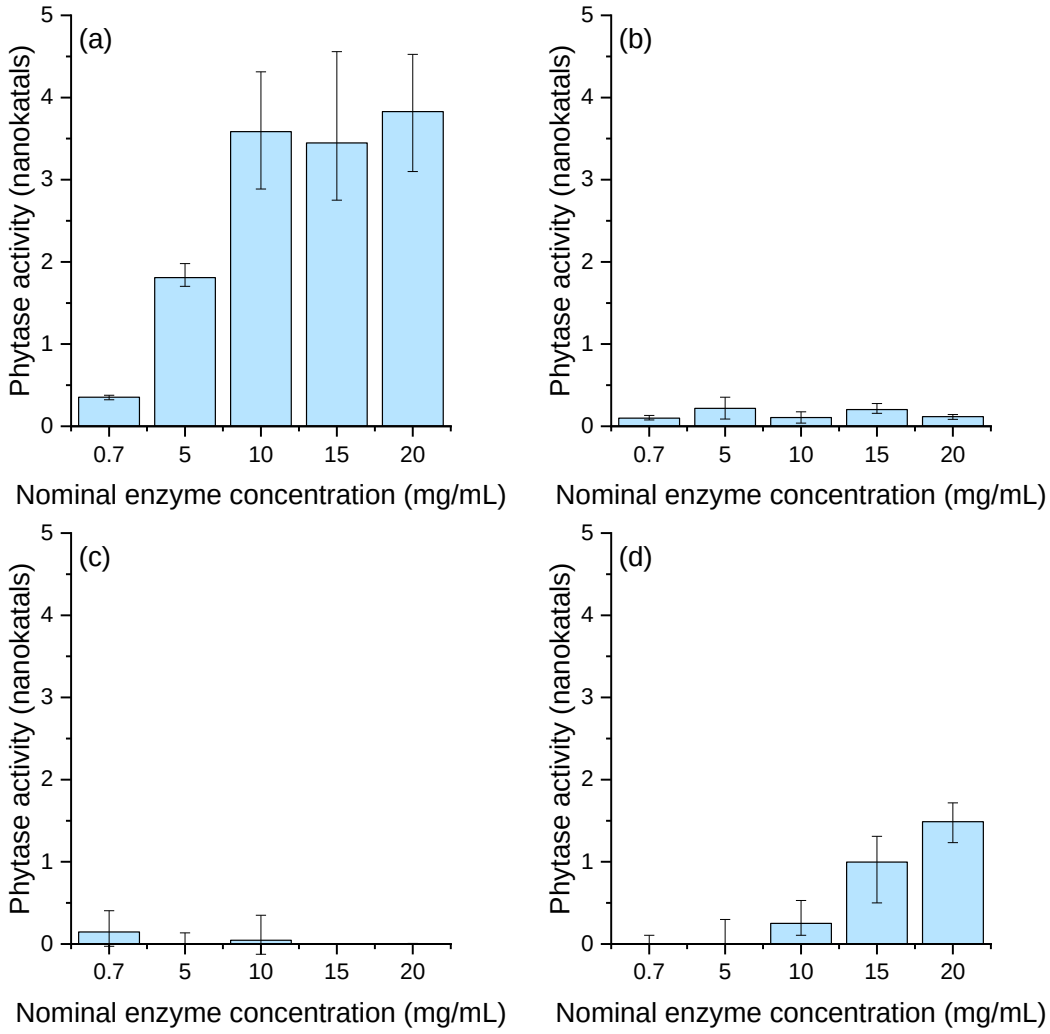

Figure 3.11 Activity of wheat phytase at different nominal initial concentrations for (a) solid-free controls, (b) supernatants taken after mixing with 250 g/L kaolinite, (c) supernatants taken after attempted desorption with npH_2O, and (d) the kaolinite resuspended in npH_2O (i.e. the sorbed phytase). The initial mixing took place for ~ 24 h (data in (a) and (b)) at 22 °C, the desorption (c) and sorbed (d) experiments were mixed for ~ 2 h before performing the assay. Assays took place at pH 5.5, 40 °C, for 10 min.

Additional tests investigated whether the Megazyme or wheat phytase could be desorbed from kaolinite or if sorbed phytase showed any activity (as has previously been indicated for *A. niger* and *Peniophora lycii* phytases (283,285)). Repeat assays of the original samples indicated that there was no loss of phytase activity in solid-free controls in the time between the original sorption tests and the desorption tests (data not shown). Negligible amounts of the Megazyme phytase could be desorbed and no activity could be detected when assaying the kaolinite suspensions (data not shown). Tests with the wheat phytase also investigated a range of wheat phytase concentrations (figure 3.11). No phytase activity could be detected in supernatants from the original mixing (figure

3.11b) or after the desorption attempts (figure 3.11c). However, at 10 mg/mL phytase and above, the sorbed phytase did show some activity (figure 3.11d). Note that, because these enzyme assays took place in a citrate buffer, it is hard to be certain to what extent the sorbed phytase activity was a function of phytase concentration, phytase desorption by citrate, or citrate inhibiting phytate sorption. However, the fact that the sorbed phytase activity increased with the initial concentration of phytase added suggests that phytase concentration has an important role. Further work would be required to fully understand the different factors influencing the activity of sorbed phytases, but the results do indicate that, if working with purified enzymes, increasing the enzyme concentration may be a simple method to exceed the sorption capacity of solid phases.

3.2.4 Growth, phytate degradation, and lanthanum precipitation in simple solid matrices

The sorption tests indicated that both phytate and phytase interacted strongly with kaolinite but weakly with quartz sand. Following this, experiments were performed to investigate growth of *A. niger* or *B. adeninivorans* and their ability to degrade phytate in simple solid matrices consisting of only kaolinite or sand.

Results indicated that at a low solids loading (10 g/L kaolinite) phytate degradation occurred at a level comparable with solid-free controls (appendix D, figure D.1). However, at 500 g/L kaolinite, no phytate degradation occurred (appendix D, figure D.1) despite evidence suggesting growth was successful (this was visually apparent for *A. niger*, while a pH decrease was recorded for both organisms, suggesting some level of metabolic activity). This verifies that the kaolinite fraction had an important role in inhibiting phytate degradation by actively growing microorganisms in the synthetic mine tailings.

In contrast, phytate degradation by both organisms was successful in the sand matrix (appendix D, figure D.3, figure D.4a) which suggested this would be a suitable solid matrix to use for biomineralization experiments. Therefore, experiments in a sand matrix spiked with lanthanum were performed.

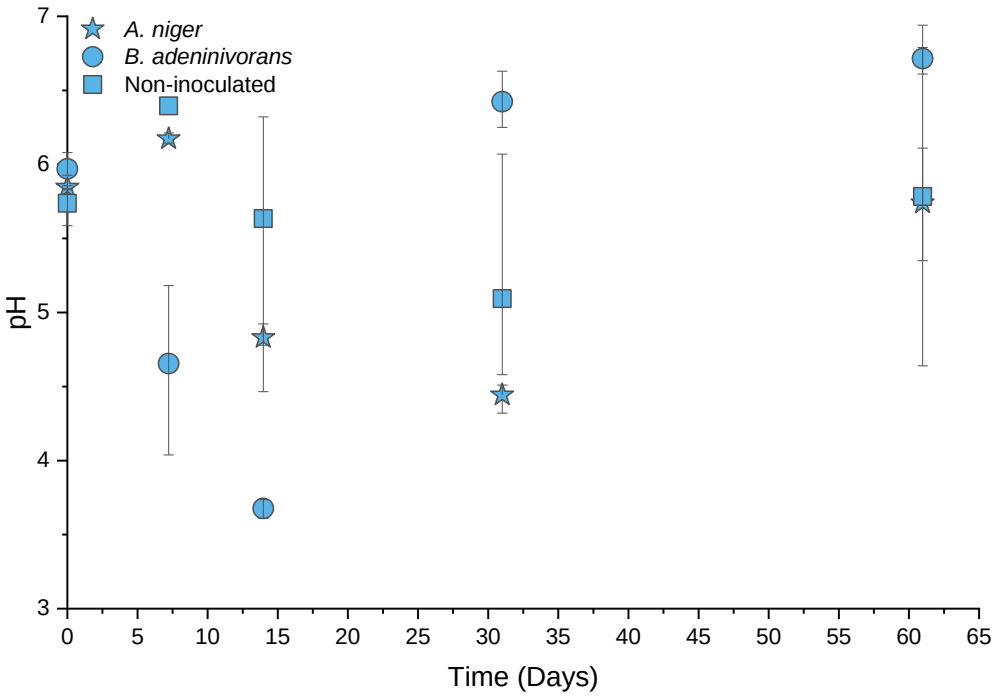

Figure 3.12 Measurements of pH over time. Experiments were performed in triplicate with single samples taken from 0–30 days and five samples from each experiment at the final time point. Data points are the mean of every measured value, error bars represent the difference between the upper and lower measured values.

The pH of aqueous extracts of the sand and nutrient media mixture was slightly higher (~ 6) than the pH of the pure nutrient media (~ 5.8). As with the lanthanum-free experiments (appendix D, figure D.2), both *A. niger* and *B. adeninivorans* cultures showed an initial decrease in pH followed by an increase between 30 and 60 days (figure 3.12). Unlike the lanthanum-free experiments, an initial pH decrease was also observed in the controls; this may be associated with microbial contamination in the system, although none was visibly apparent.

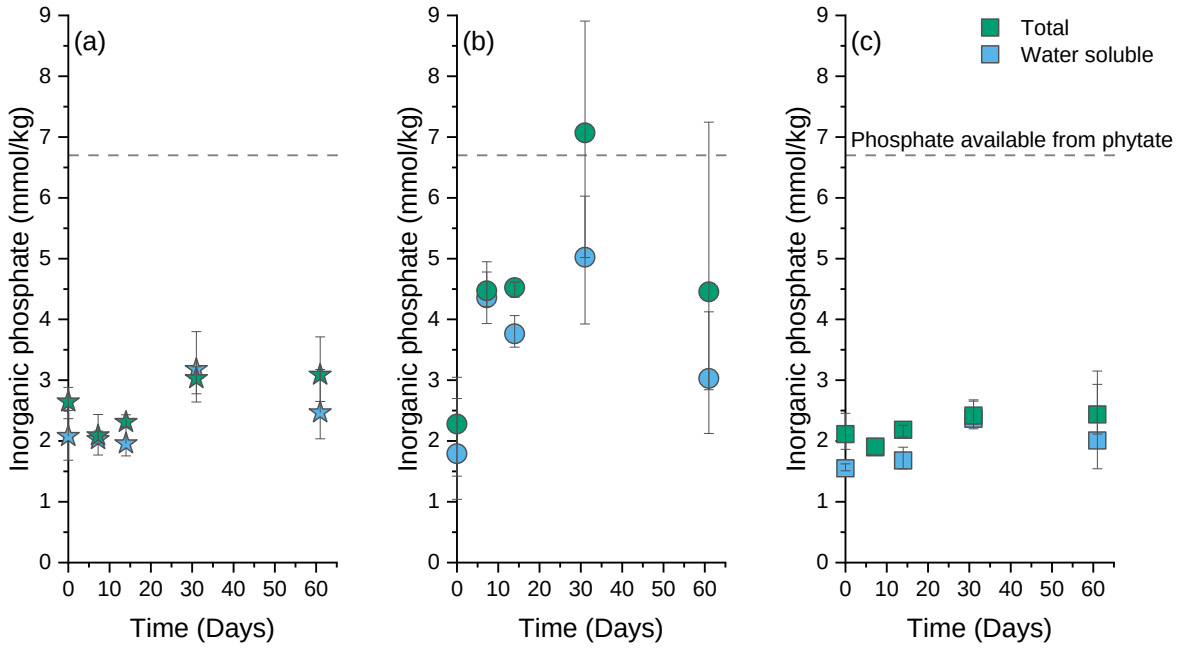

Figure 3.13 Water-soluble and total concentrations (mmol/kg dry mass) of inorganic phosphate versus time for (a) A. niger, *(b)* B. adeninivorans, *and (c) non-inoculated controls. Experiments were performed in triplicate with single samples taken from 0–30 days and five samples from each experiment at the final time point. Data points are the mean of every measured value, error bars represent the difference between the upper and lower measured values. At 0 and 60 days, sequential extractions were performed on samples with npH_2O and 1.7 mol/L nitric acid to define water-soluble and acid soluble fractions; these values were summed to calculate total concentrations. For the intermediate time point samples (7, 14, and 31 days), separate individual extractions (npH_2O or 1.7 mol/L nitric acid) were performed to determine water-soluble and total concentrations directly.*

Growth and phytate degradation tests in the presence of 0.5 mmol/L lanthanum gave similar results (figure 3.13) to the lanthanum-free experiments in terms of phosphate release (appendix D, figure D.3). The concentration of soluble inorganic phosphate did appear to decrease between 30 and 60 days for *B. adeninivorans*, but it is uncertain whether this is due to precipitation/sorption or if all these data points were within a given accuracy range (for example, a slight dip in phosphate concentrations occurred for all experiments between 7 and 15 days by a similar proportion, suggesting that this change was a legacy of the variability associated with sample handling).

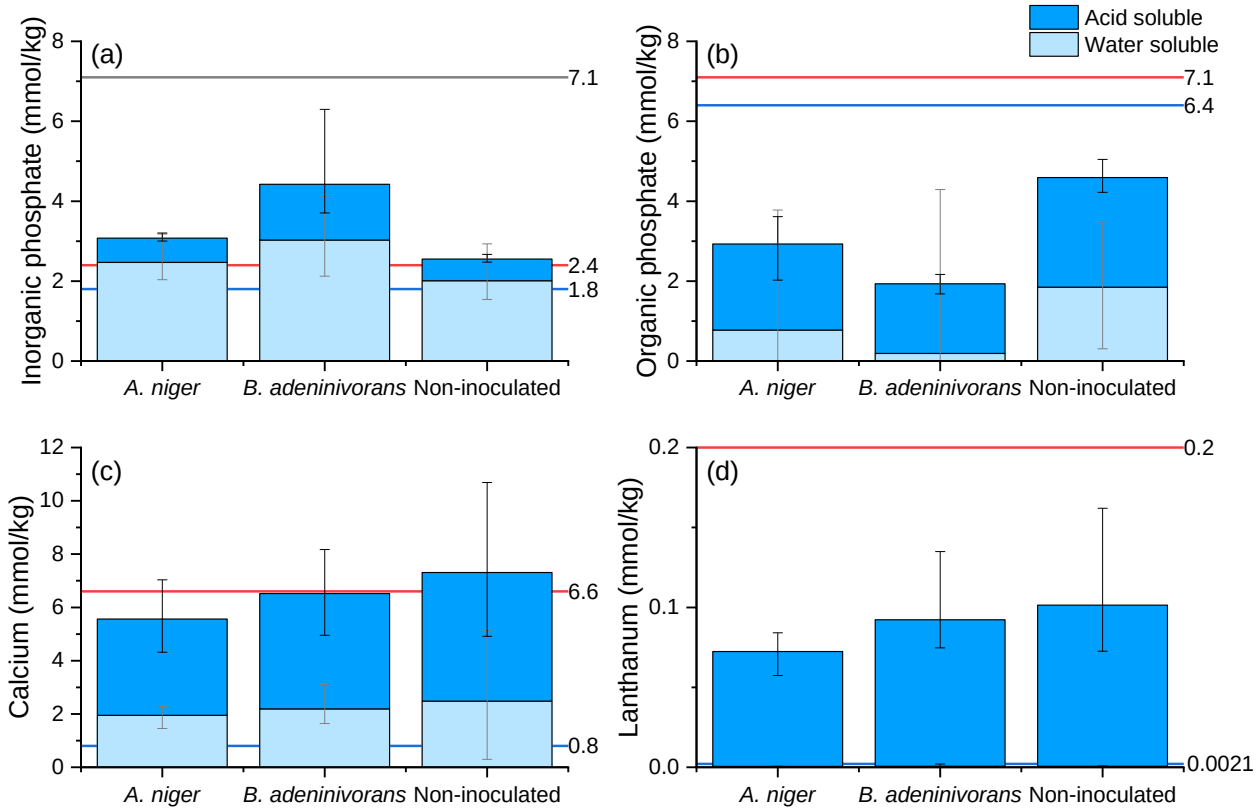

Figure 3.14 Concentrations (mmol/kg dry mass) of water-soluble and 1.7 mol/L nitric acid soluble fractions of (a) measured inorganic phosphate, (b) calculated organic phosphate, (c) measured calcium, and (d) measured lanthanum at the final time point of the sand growth and phytate degradation in the presence of lanthanum experiments. Triplicate experiments were each sampled five times, three of which were sequentially extracted with npH_2O and 1.7 mol/L nitric acid while the remaining two were only extracted with npH_2O. Columns represent the mean of all samples, error bars are the difference between the mean and the upper or lower measured value. The reference lines represent the following (in mmol/kg): blue = mean water-soluble concentrations at the zero time point; red = mean total concentrations at the zero time point; grey = phosphate available from phytate.

ICP-OES analysis (used to measure calcium and lanthanum concentrations and calculate organic phosphate concentrations) only took place for the first and final sample time points. These data indicate a decrease in soluble lanthanum and organic phosphate over time and an increase in soluble calcium in a manner that appeared to be independent of the organism present (figure 3.14). The low solubility of lanthanum at the initial time point indicates a rapid initial precipitation of lanthanum with phytate (analysis of the bulk culture media indicated that soluble lanthanum concentrations were around 3 µmol/L compared to a total concentration of 500 µmol/L). At the final time point, lanthanum concentrations were below the detection limit (which ranged from 0.7 to 2.0 µmol/kg depending on the sample dilution factor used) for *A. niger*, *B. adeninivorans*, and the non-

inoculated controls (figure 3.14d) and therefore assessing differences between the conditions is challenging. Recovery of total lanthanum at the final time point was low (~ 0.09 mmol/kg) compared to values calculated from measurements of the bulk culture media (~ 0.16 mmol/kg) or measured values at the initial time point (~ 0.20 mmol/kg) which may support the hypothesis that the decrease in inorganic phosphate observed at the final time point (figure 3.13) was a result of variability introduced during sampling. However, the fact that calcium concentrations at the final time point (figure 14c) were within reasonable margins of the theoretically known and initial time point measurements may indicate that lanthanum was precipitated with inorganic and organic phosphate phases (recovery of organic phosphate was also low compared to theoretically known values) that were recalcitrant towards complete dissolution in 1.7 mol/L nitric acid. Further experiments would be required to confirm or reject this hypothesis.

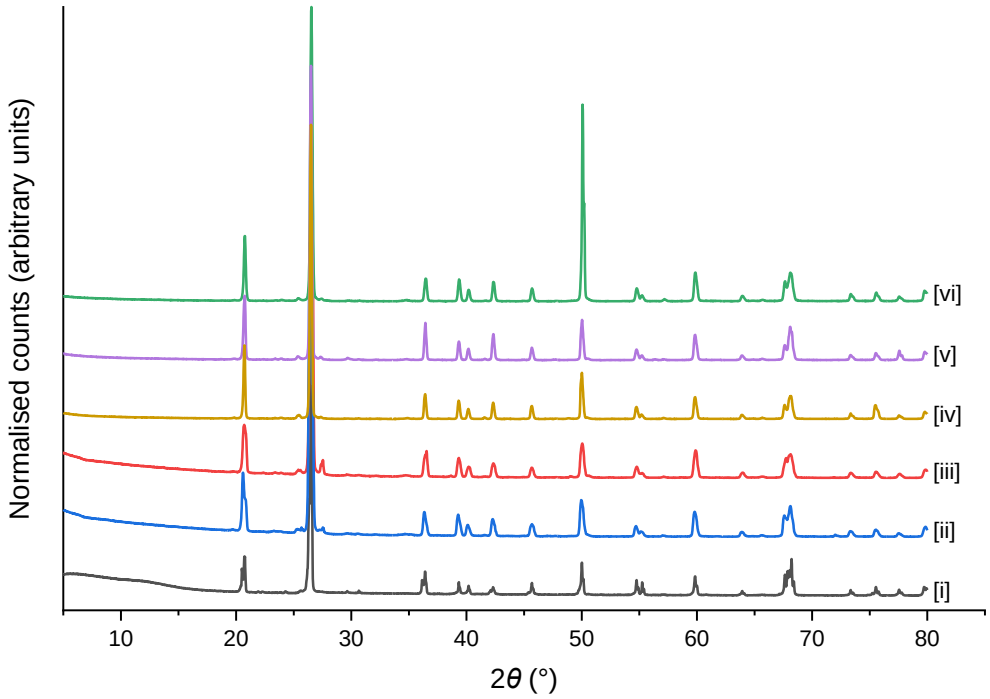

Figure 3.15 XRD patterns showing [i] the raw sand used in these experiments, [ii] sample taken from a B. adeninivorans *experiment after 30 days, [iii] sample taken from a control experiment after 30 days, [iv] sample taken from an* A. niger *experiment after 60 days, [v] sample taken from a* B. adeninivorans *experiment after 60 days, [vi] sample taken from a control experiment after 60 days. Patterns [ii]–[vi] were measured using the Göbel mirror optics setup, pattern [i] was measured using the motorised slit. Samples were measured using the copper K_α radiation across a 2θ range of 5–80° with a step size of 0.02° and a step time of 1 s. Patterns were normalised in OriginPro 2019b to a scale of 0 to 1.*

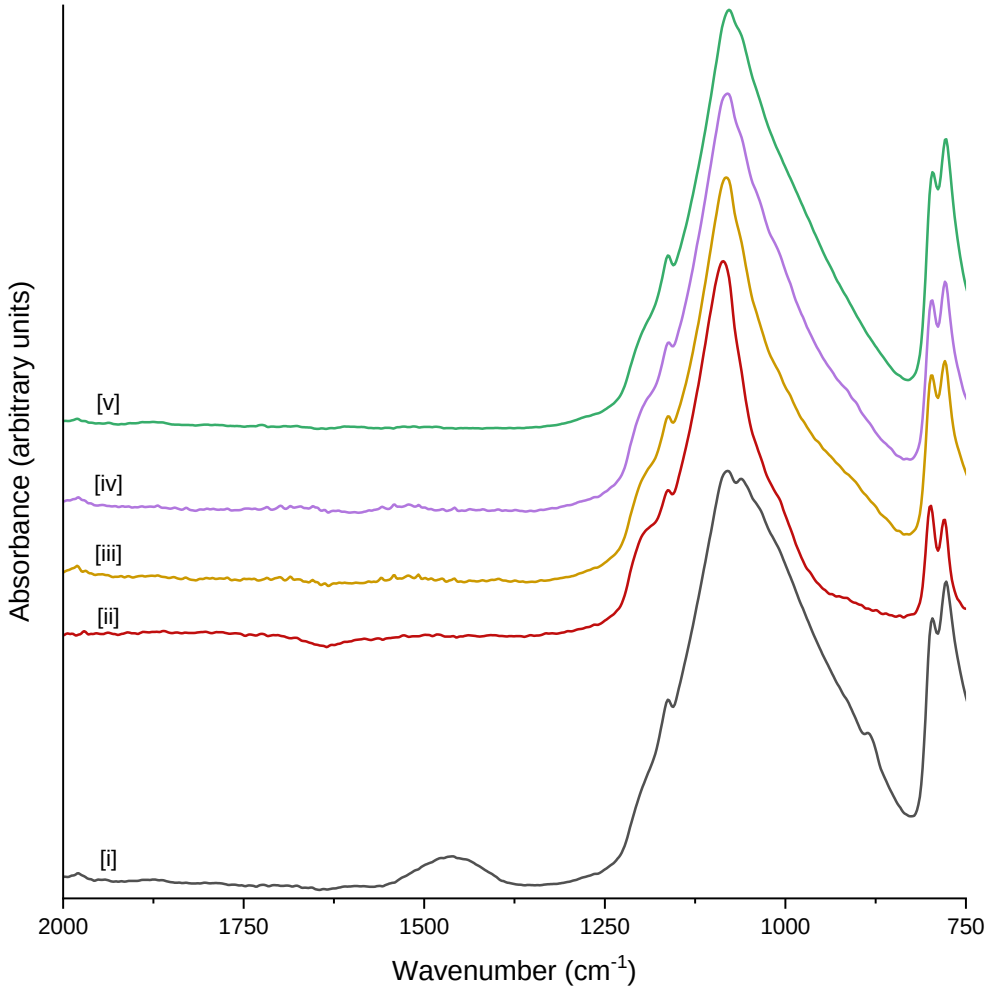

Figure 3.16 FTIR spectra showing [i] the raw sand used in these experiments, [ii] sand washed with 1.7 mol/L nitric acid, [iii] sample from an A. niger *experiment, [iv] sample from a* B. adeninivorans *experiment, [v] sample from a control experiment. Spectra were normalised in OriginPro2019b to a scale of 0–1.*

Solid phase characterisation by XRD (figure 3.15) and FTIR (figure 3.16) of samples taken at the final time point indicated that solids matched database patterns for quartz sand (PDF #01-070-7344 for XRD, WSAAX #6772 for FTIR). Few differences could be observed between the different samples. There was a broad peak at around 1,500–1,300 cm^{-1} in the FTIR spectrum of the bulk sand used in these experiments (spectrum [i], figure 3.16) that was absent in an acid washed sample of the sand (spectrum [ii]) or the experimental samples (spectra [iii]–[v]). This was likely associated with a water-soluble impurity in the supply of sand used, probably a carbonate phase based upon the position of the peak (407).

These experiments indicate that phytate is an effective sequestering agent for lanthanum. However, the speciation of lanthanum following microbial phytate hydrolysis remains elusive; further work would be required to test whether lanthanum remains bound to unhydrolyzed phytate, reprecipitates with liberated inorganic phosphate, precipitates with microbially secreted organic acids (e.g. oxalic acid), or is sorbed to biomass. Batch solution tests in chapter 2 indicated that, at 0.5 mmol/L lanthanum, discrete, crystalline lanthanum phases could not be observed by XRD. Further attempts to investigate the solids by ^{31}P or ^{139}La nuclear magnetic resonance (NMR) failed to provide usable data, although in principle NMR is a powerful tool for investigating phosphate and lanthanum speciation in solid matrices (e.g. (408)) so more work to refine the methodology used may be useful. Additionally, alternative techniques should be considered to probe in more detail the mechanisms of lanthanum removal in these experiments. Previous researchers have used density separation techniques to separate out high density materials (including zinc and lead minerals) from soils and mine wastes (186,409) so it may be useful to apply those techniques in this work.

3.2.5 X-CT tests

One technique that has been used to successfully image biomineralization (410,411) and organic matter (412,413), within solid matrices is X-CT scanning. Therefore, phytate hydrolysis and lanthanum precipitation tests were performed within small column systems and imaged by X-CT to test whether microbial growth and lanthanum precipitation could be visualised under these conditions. For these tests, the concentration of lanthanum used was increased from 0.5 mmol/L to 5 mmol/L. Additionally, one column was supplied with a purified *A. niger* phytase to compare phytase-active samples in the presence or absence of biomass. Three sterile controls were performed, consisting of lanthanum and phytate, lanthanum with no phytate, and phytate with no lanthanum.

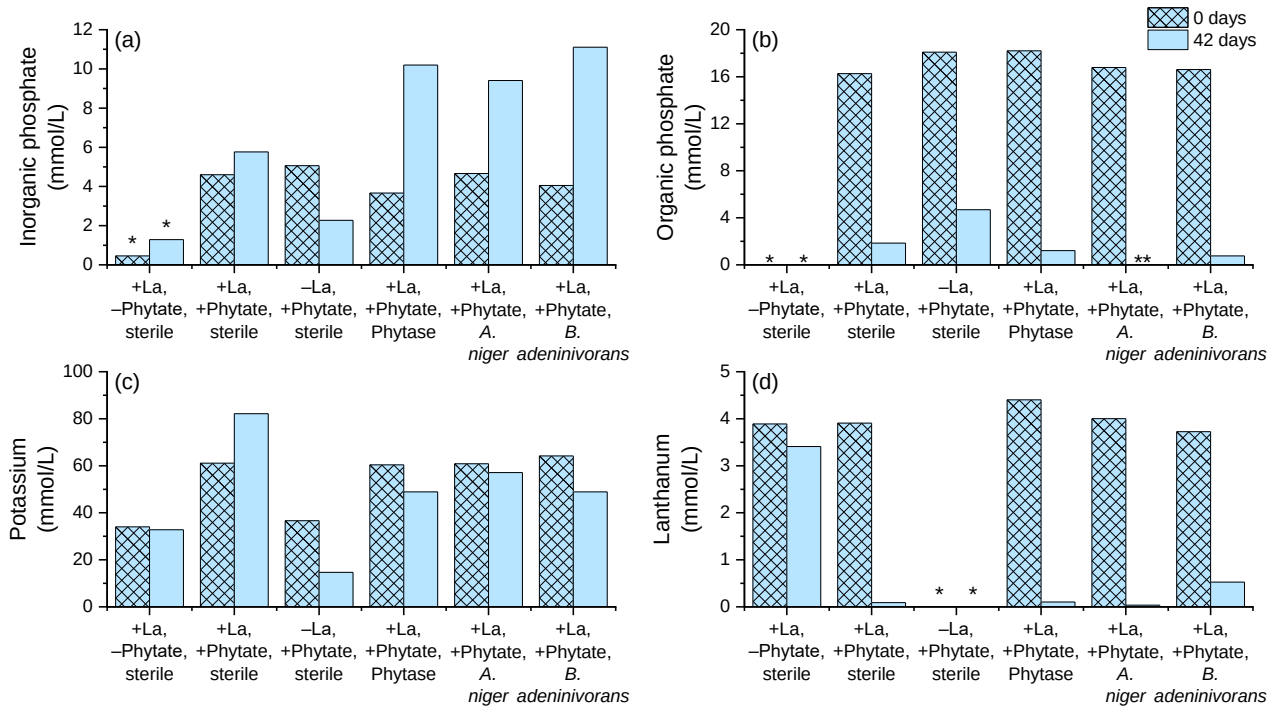

*Figure 3.17 Results of chemical analysis of filtrates from the experiments used for X-CT examinations at initial (0 days) and final (42 days) sample time points showing (a) inorganic phosphate, (b) calculated organic phosphate, (c) potassium, and (d) lanthanum concentrations. Columns labelled * are where values were below the analytical detection limit, columns labelled ** are where organic phosphate concentrations were calculated as negative due to measured inorganic phosphate concentrations being slightly higher than ICP-OES measured phosphate concentrations.*

Chemical analysis was performed on filtrates after perfusing excess culture media (at 0 days) or npH$_2$O (at 42 days) through the columns. The concentrations of analytes were calculated using dilution factors derived from measurements of filtrate masses which were compared to the known amount of solution added and used to calculate the amount of solution retained in the columns. Therefore, measurement errors could have been introduced through water being retained by the filters or inaccurate recording of filtrate masses. Replicates were not performed for these experiments, but due to possible variability in mass measurements, the data presented may have relatively large error bars. Despite this, there is convincing evidence of an increase of phosphate concentrations in the columns where *A. niger* phytase, *A. niger* spores, or *B. adeninivorans* cells were added (figure 3.17a). Similarly, the lanthanum concentrations decreased over time in the experiments where lanthanum and phytate were present, while the majority of lanthanum remained in solution for the phytate-free control (figure 3.17d). Organic phosphate concentrations decreased over time in every condition where phytate was added (figure 3.17b) but discerning between phytate lost through precipitation and phytate lost through microbial hydrolysis was

challenging. Potassium concentrations (figure 3.17c) were generally similar at both time points except in the sterile conditions where phytate was present. In the sterile condition with lanthanum and phytate, concentrations of potassium increased, while in the sterile condition with phytate but no lanthanum, potassium concentrations decreased. Further work would be required to understand these differences, but the results may indicate that, in the absence of lanthanum, phytate co-precipitated with potassium and other cations present in the culture media (e.g. calcium, magnesium). In contrast, where lanthanum was present, this bound preferentially to phytate and kept potassium in solution (and possibly induced desorption of potassium sorbed to the sand used). As with the bulk sand tests, little difference in lanthanum solubility could be observed between the phytate-only control and the experiments where phytase or phytase-producing organisms were added.

The results in figure 3.17 were broadly comparable with the results observed in the bulk sand tests (figure 3.14), and therefore indicated that these experiments were sufficient for a preliminary investigation by X-CT.

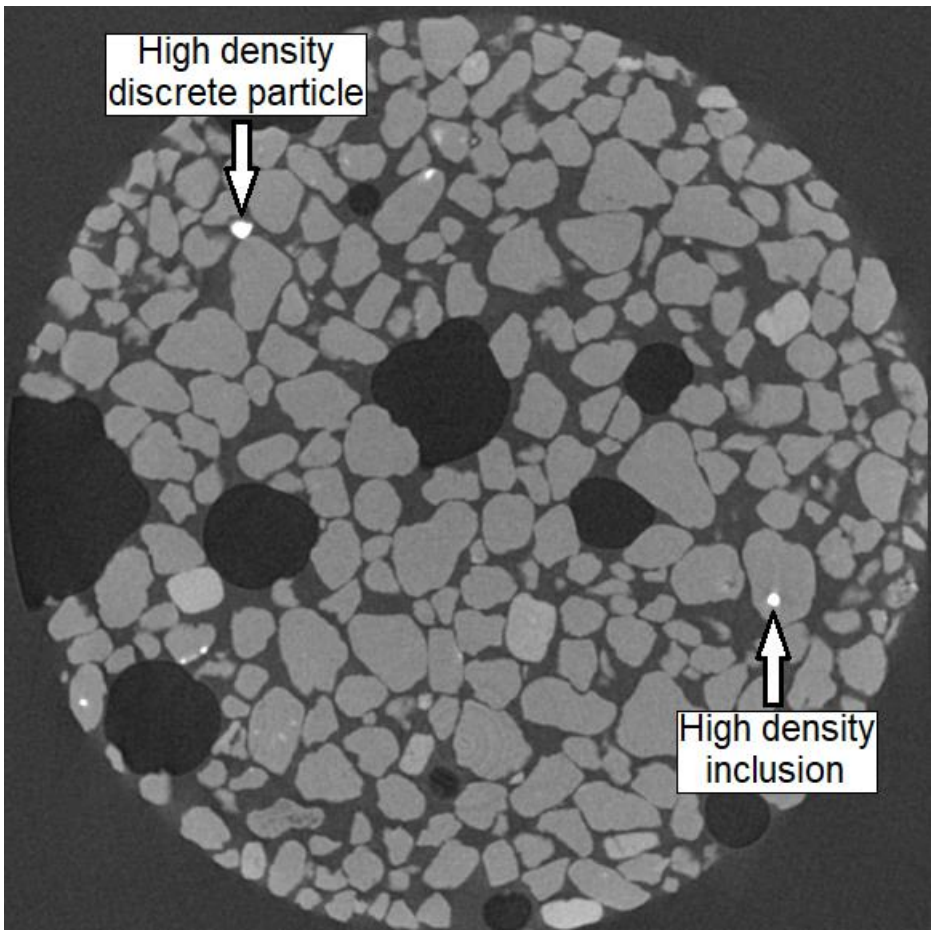

Figure 3.18 Example 'slice' from an X-CT scan of the experiment with lanthanum, phytate, and B. adeninivorans *cells. Arrows indicate bright spots associated with high density solids which exist as both discrete particles and as inclusions within the quartz sand grains.*

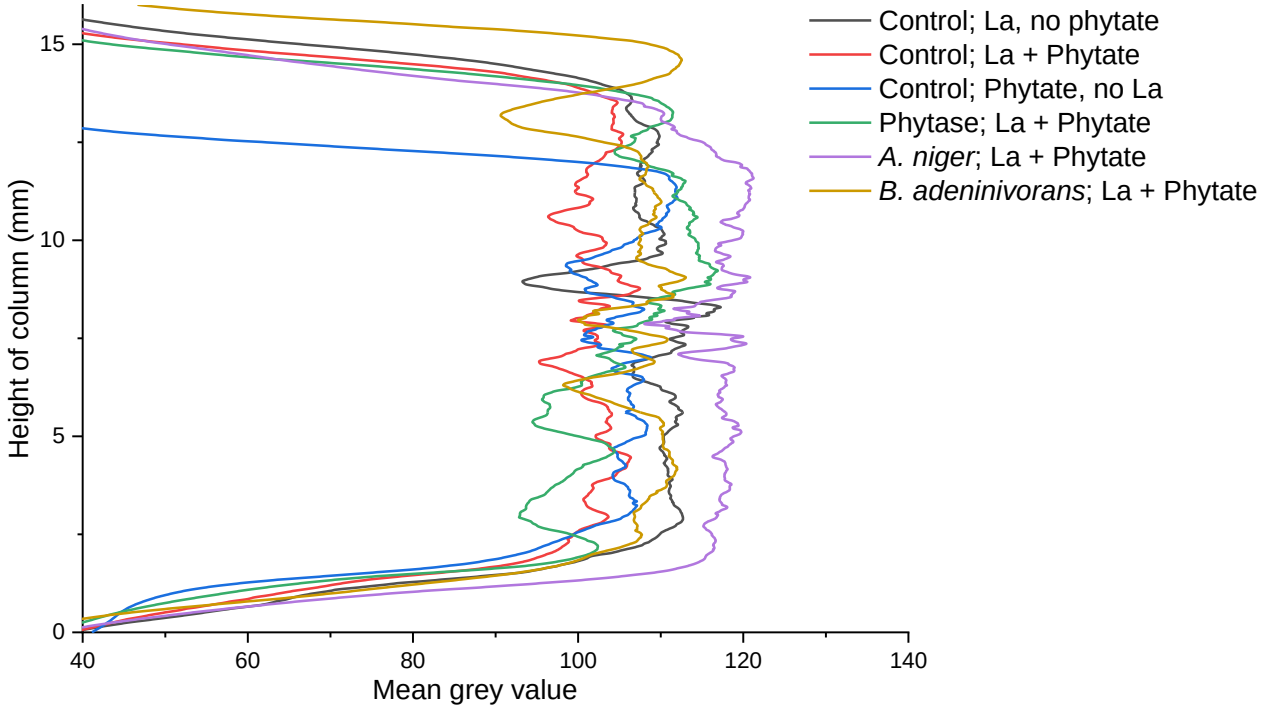

Figure 3.19 Mean grey value versus column height for the X-CT experiments.

X-CT analysis provided ambiguous results. Despite microbial growth being visible by eye (at least in the *A. niger* column) no signs of biomass could be observed in the X-CT images (e.g. figure 3.18). With the setup used, a good resolution (~ 8 µm) was achieved, but this is still larger than the size of *A. niger* or *B. adeninivorans* cells (*A. niger* hyphae have a diameter of ~ 5 µm (414), and *B. adeninivorans* cells are also on the order of ~ 5 µm in size (415,416). This, in combination with the low X-ray attenuation of biological material (which would be similar to water), meant no biomass could be visualised.

Figure 3.18 shows an example 'slice' from one of the image stacks produced as output from the X-CT scans. In this image, the black spaces represent air, dark grey areas are water, and light grey areas are quartz sand. Also, throughout the columns, patches of a high-density material (represented by the white areas) could be observed, but qualitatively, this did not appear to differ between the different conditions tested. Rather than lanthanum, these high-density areas may have been associated with impurities in the sand (e.g. iron oxides, pyrite, zircon). The different bright spots may not have all been the same material, as some appeared to exist as inclusions within the sand grains, while other bright spots appeared to exist as discrete particles. It is the latter which are more likely to be associated with lanthanum, but the conclusive identification of such bright spots is challenging, and other techniques (e.g. scanning electron microscopy, back-scattered electron imaging, and energy dispersive X-ray spectroscopy) must be used in conjunction with X-CT scanning to achieve this (417).

Previous research has used mean grey values (indicating X-ray attenuation, where low grey values indicate low X-ray attenuation and high values indicate high X-ray attenuation) versus column height as a tool for locating bulk precipitation within a solid matrix (410). However, in this work, plotting mean grey values against column height (figure 3.19) showed no obvious trends, and differences between the different samples appeared to be minimal. Variations in grey values throughout the column were most likely a result of uneven packing of sand within the column, with large decrease in mean grey values (e.g. at ~ 12 mm the *B. adeninivorans* column or at ~ 9 mm in the sterile control with lanthanum but no phytate) associated with large amounts of air filled spaces at that point in the column. This indicates that refinements to the experimental procedure would be desirable to ensure a more even packing of the solid material in the column.

X-CT has been successfully used to image bulk calcium carbonate precipitation in sandstone (411) and marble (410), while staining with lanthanum is one option that has been tested for imaging

organic matter by X-CT (413). However, for imaging low levels of metal precipitation (initial solution concentration of lanthanum in this work was 5 mmol/L compared to 400–1,000 mmol/L calcium in calcite precipitation studies (410,411)) it appears that refinements to experimental procedures are required. This may require preparing thin slices of the columns, imaging them using scanning electron microscopy (SEM), and then combining the X-CT and SEM images to create 3 dimensional chemical maps (e.g. (418)).

3.3 Conclusions

The results in this chapter indicate that phytate degradation occurs readily in the presence of solids, such as quartz sand, which do not themselves interact strongly with phytate or phytase. Depending on site specific parameters, sandy media may have a low intrinsic ability to sorb and immobilise contaminants, which means that these types of sites may be suitable targets for phosphate biomineralization strategies. In experiments with lanthanum, the low solubility of lanthanum phytate made comparisons with phytase-active experiments challenging. Further work is required to characterise the speciation of lanthanum in the presence of phytate and in systems where phytate has been degraded, and to understand the implications this has for the stability and contaminant incorporation properties of the precipitated materials. Furthermore, these experiments could act as models upon which to base similar experiments with radioactive elements such as uranium.

Experiments performed in more complex solid matrices highlighted some important challenges that need to be addressed in future work. In particular, the strong interactions between phytate or phytase with solids such as kaolinite may be significant limiting factors that constrain the environments in which phosphate biomineralization strategies are viable.

Results in this chapter indicate that phytase is sorbed onto kaolinite. However, sorption of phytase by kaolinite can be limited by the presence of complexing agents (citrate), high pH values, or increasing the concentration of phytase added. Further work would be required to understand how these options may impact biomineralization processes. For example, citrate may increase metal solubility and thereby inhibit precipitation, while the phytase enzymes studied have low activities at high pH values which would limit phytate degradation. Increasing the enzyme concentration is simple if directly adding purified enzymes, but if using actively growing organisms to produce phytase *in situ*, work is required to optimise growth conditions to increase the yield of phytase.

Attempts to increase phytate solubility were unsuccessful, and this requires further attention, as some researchers have highlighted phytate sorption/precipitation as being a main limiting factor inhibiting phytate degradation rather than phytase sorption (10). The addition of citrate (10,285) or humic acid (419) may help to achieve this, although these amendments should be added before phytate, as the desorption of phytate from minerals is challenging (419). As these amendments may also increase metal solubility, one possible strategy could involve adding citrate to temporarily increase phytate and phytase solubility for long enough to allow phytate degradation to occur followed by the addition of citrate-degrading organisms (e.g. (40,165)) which would then lead to liberated inorganic phosphate and metals dropping out of solution.

Chapter 4
Influence of different metals on the phytase-mediated precipitation of phosphate biominerals

4.0 Introduction

The mining of uranium, as well as other metals associated with naturally occurring radioactive material (NORM), produces complicated waste streams that contain a wide range of contaminants. In addition to thorium, uranium, and their decay products, these contaminants may include aluminium, sulfur (as sulfate/sulfuric acid), vanadium, chromium, manganese, iron, cobalt, nickel, copper, zinc, arsenic, selenium, molybdenum, cadmium, barium, mercury, and lead (32,37,420–427). Excesses of any of these can contribute to degrading the quality of surface and groundwaters (428).

To address the potential contamination of environments by these metals, precipitation by or sorption onto phosphate minerals has been researched as a possible remediation strategy (117). Many phosphate species are highly insoluble and non-bioavailable which makes them suitable for both *ex situ* water treatment and *in situ* stabilisation strategies where the complete removal of contaminants is unfeasible (for example, from the enormous areas covered by mine sites) (116).

Phosphate biomineralization has been researched as a method of producing phosphate minerals that alleviates supply issues and environmental concerns associated with mining rock phosphate (e.g. (116,142,143)) and produces materials that may be more efficient sorbents than synthetically prepared alternatives (103). Phosphate biomineralization is a biologically mediated process where microorganisms hydrolyse organic phosphate compounds and release inorganic phosphate to solution which can then precipitate out of solution with supplied metals (e.g. calcium) or contaminants (e.g. lead or uranium) (11).

Phytic acid ($C_6H_{18}O_{24}P_6$), or phytate as a salt, is an abundant plant waste product that has been proposed as a more cost-effective source of organic phosphate than the more commonly used glycerol 2-phosphate ($C_3H_9O_6P$) (11,230–237). Limitations with phytic acid include that it forms low solubility complexes with many metals, and that the precipitated phytates may be particularly recalcitrant to enzymatic hydrolysis (e.g. (285,429,430)). Also, most phytate-degrading (phytase) enzymes are active only within a limited pH range (typically 2–6 (257,272–275)) which is sub-optimal for the precipitation of calcium phosphate minerals such as hydroxyapatite at ambient temperatures (276–278). However, many other phosphate phases – including aluminium, iron, lead, lanthanide,

and actinide phosphates – may be readily precipitated from acidic solutions (e.g. (113,279,280,431,432)). The low solubility of many metal phytate complexes may also have benefits in terms of supporting metal removal, and phytate has itself been researched as a sequestering agent for a range of contaminants (232,244,251,253,433).

Most research into phytase-mediated phosphate mineral precipitation has involved the use of actively growing microorganisms such as *Aspergillus niger*, *Blastobotrys adeninivorans*, or *Escherichia coli* in the presence of phytic acid and the contaminant of interest (182,185,188,200–203). However, the use of actively growing microorganisms may pose several drawbacks, including variable performance, sometimes laborious and time-consuming growth requirements, the requirement for nutrient media that can introduce interfering substances (e.g. sulfate), acidification of the culture media, and the synthesis of interfering substances (e.g. citric acid, oxalic acid) ((202,330,434), also see chapter 2 in this work).

An alternative is to use a source of purified phytase enzyme; purified enzymes can be added to solution like any other laboratory chemical and begin working immediately. As purified enzymes have minimal requirements to be able to operate (although some do require the addition of cofactors such as magnesium) this enables an examination of (a) the interactions between metals and phytate, (b) the influence that this has phytate hydrolysis compared to metal-free systems, (c) and the influence this has on subsequent metal phosphate precipitation, in the absence of interfering factors. In this work, a purified form of the *A. niger* phytase was used. The *A. niger* phytase was chosen because it is one of the most widely researched organisms for the production of phytase and the *A. niger* phytase is used commercially to reduce the phytic acid content in animal feed (272,273,435). Therefore, the *A. niger* phytase is relatively easy to produce and can be purchased in bulk amounts at low costs. The pH profile of phytases produced by *A. niger* generally describe two pH optima at pH 2.5 and 5.5 with negligible activity above pH 7 (261,435,436).

The original aim of this work was to synthesise calcium hydroxyapatite from a phytic acid precursor. However, as hydroxyapatite typically only forms above pH ~ 7.5, this chapter investigated a range of metals (table 4.1) to test which metal phosphate phases are suitable targets for production by the *A. niger* phytase at pH 5.5. This pH value was chosen as it satisfies the conditions of (a) matching with one of the pH optima for the enzyme's activity, and (b) all metal phosphates investigated may achieve supersaturation at this value (hydroxyapatite doesn't form at pH 5.5 but other calcium phosphates such as brushite ($CaHPO_4.2H_2O$) may (278)). This also enabled an investigation of the

extent to which different metals may inhibit phytase activity, as this could be a limiting factor if it prevents the release of enough phosphate to support mineral precipitation.

A secondary aim was to compare the materials formed in this "phytate + phytase strategy" with the materials formed in a "phytate-only" strategy, as phytate also interacts strongly with many of the metals investigated. Previous researchers have generally either looked at phytate as a sequestering agent or phytate as a precursor for phosphate compounds and have typically not compared the advantages and disadvantages of the two approaches. For select metals (aluminium, iron, lanthanum, and lead) comparisons were also made to the direct addition of inorganic phosphate and phosphate-free conditions.

The metals listed in table 4.1 are categorised as being 'benign', 'toxic', or 'variable' and their relevance to NORM-producing mining activities is summarised. 'Benign' is defined as an element that is unlikely to be present at harmful concentrations at mining-impacted sites but may be useful as part of a remediation material (e.g. calcium). 'Toxic' refers to an element which is always harmful and where it is generally regarded that there is no lower threshold for its harmful effects (e.g. lead (437)). The elements designated 'variable' are those which may have negative, positive, or negligible impacts depending on site-specific characteristics. The metals listed in table 4.1 are not the only metals that are likely to be present at uranium mine tailings sites but have been chosen as a representative range of metals that are known to form insoluble compounds with phosphate. For iron, both common oxidation states (+2 and +3) were investigated as both may be present at mining sites, are important in redox cycles associated with acid mine drainage, and potentially form geochemically important phosphate minerals.

Table 4.1 Properties of metals investigated in chapter 4.

Element	Project category	Health impacts	Environmental toxicity	(Drinking) water limits	Relevance to NORM-producing mining industries	Importance in phosphate minerals
Aluminium	Variable	Little indication of acute toxicity; but hypotheses exist about long term exposure being a risk factor for neurotoxic effects and the onset of Alzheimer's disease (265,437).	May be toxic towards plants, fish (428), and invertebrates (438,439). May affect some species' ability to regulate ions and may inhibit respiratory functions (440). May impair the reproduction of *Daphnia Magna* (441).	No official guideline value set by World Health Organization, but recommendation that concentrations should be kept below 0.9 mg/L (33 µmol/L) (437). Recommended maximum values for acute freshwater toxicity of 1-4,800 µg/L (0.04–178 µmol/L), or 0.63-3,200 µg/L (0.02–119 µmol/L) for chronic freshwater toxicity (440).	Elevated concentrations associated with acid mine drainage (442). Sites with elevated concentrations include river sediments in the lead-zinc and uranium mining region of Sumsar-Shakaftar, Kyrgyzstan (423), the former uranium mining region of Mailuu-Suu, Kyrgyzstan (422), Antas Reservoir (a uranium mining region), Brazil (42), former uranium mine near Cunha Baixa, Portugal (421). Aluminium (as e.g. aluminium sulfate) may also be deliberately added to mine wastes to precipitate iron, uranium and other contaminants, and this may contribute to elevated aluminium levels in the local environment (426,443).	30-35% of known phosphate minerals contain "substantial" amounts of aluminium (110). Precipitates with aluminium and phosphate may also incorporate other contaminant metals (e.g. lead in plumbogummite and hinsdalite, copper in turqoise, zinc in faustite) (431). May be immobilised in contaminated media by phosphate amendment (95,444,445). As a host for other contaminants, aluminium phosphate has been investigated for the immobilisation of lead in municipal solid waste (446) and crandallite has been suggested as a suitable host for toxic and radioactive contaminants (447). Some research has found that in contaminated soils amended with apatite that aluminium phosphate phases were one of the main hosts of sequestered nickel, lead, and uranium (95,448). Aluminium hydroxyphosphates such as bolivarite, evansite, and gorceixite have been observed to accumulate uranium, in the range of 0.2 to 1.4% (449–451).
Calcium	Benign	Calcium is an essential element for life; excess concentrations can be associated with negative health impacts (452) but these are unlikely to be associated with environmental contamination.	Negligible	Maximum recommended value of 100 mg/L (2.5 mmol/L) according to Portuguese guidelines (421).	Calcium-containing materials (including oxides, hydroxides, carbonates, and phosphates) have been widely researched for the immobilisation of contaminants in mining environments (117,444,453–455).	30-35% of known phosphate minerals incorporate calcium as a major component (110), of which apatite ($Ca_{10}(PO_4)_3(F,Cl,OH)$ is the most widely researched due to its importance in medicine, geology, and environmental remediation (114,116,276,456). Apatites can incorporate a multitude of metals into their structure, including strontium, barium, lead, cadmium, magnesium, iron, manganese, cobalt, nickel, copper, zinc, thorium, uranium, and transuranics (114) and have been researched for the immobilisation of a wide range of contaminants (116,117). Apatites persist over long timescales and are stable against chemical, radiological, and geological processes (12–14,116).

Table 4.1 (continued).

Element	Project category	Health impacts	Environmental toxicity	(Drinking) water limits	Relevance to NORM-producing mining industries	Importance in phosphate minerals
Manganese	Variable	Extended exposure to high concentrations may be a risk factor for adverse neurological effects, but evidence is inconclusive (437). Excess levels cause the condition manganism (457).	Toxic to invertebrates and other animals at high concentrations (428,438,458–460). May also impair the reproduction of *Daphnia Magna* (441).	No guideline value recommended; health-based value of 0.4 mg/L (7.3 µmol/L) can be derived (437).	Sites where elevated concentrations of manganese have been measured include groundwater at a uranium mill tailings near Durango, Colorado, USA (37), river waters in the former uranium mining region of Mailuu-Suu, Kyrgyzstan (422), acid mine drainage waters of the Curilo uranium deposit, Bulgaria (425), the Antas Reservoir (in a uranium mining region), Brazil (42), groundwater at an *in situ* leaching site in Wyoming, USA (461), and effluents from the former uranium mine near Cunha Baixa, Portugal (421).	Around 25% of phosphate minerals contain manganese as a major component (110). May be immobilised in contaminated media by phosphate amendment (95,337,462).
Iron	Variable	An essential element for life, but iron overload may be associated with a range of negative health impacts, for example, symptoms linked to neurodegenerative diseases (463).	Chronic toxicity towards aquatic organisms (438,464,465). Iron(III) may impair the reproduction of *Daphnia Magna* (441).	No guideline value recommended; 2 mg/L (35.8 µmol/L) would be considered a sufficient precaution against intake and storage of excessive iron (437). Recommended maximum values to protect aquatic species range from 0.25 mg/L (4.5 µmol/L) to 1 mg/L (18 µmol/L) to protect against chronic effects on freshwater organisms (465,466).	Common pollutant associated with mining activities (465). In particular, associated with acid mine drainage where the oxidation of pyrite leads to the release of iron in addition to sulfuric acid (465). Sites where elevated levels of iron have been measured include river waters in the former uranium mining region of Mailuu-Suu, Kyrgyzstan (422), river sediments in the lead-zinc and uranium mining district of Sumsar-Shakaftar, Kyrgyzstan (423), acid mine drainage waters of the Curilo uranium deposit, Bulgaria (425), groundwater at an in situ leaching site in Wyoming, USA (461), effluents from the former uranium mine near Cunha Baixa, Portugal (421). In contrast, iron-containing materials can be important hosts of contaminants and may be used in remediation strategies (37,448).	45% of known phosphate minerals contain either iron(II) or iron(III) as major components (110). Iron and phosphate may coprecipitate with a range of other metals including lead (e.g. corkite), copper (chalcosiderite), and zinc (phosphophyllite, rockbridgeite) (431). The precipitation of iron(III) as phosphate phases may limit the ability of iron(III) to contribute towards the oxidation of sulfide phases and thereby limit acid mine drainage (467). Vivianite ($Fe_3(PO_4)_2.8H_2O$) nanoparticles have been researched for the *in situ* immobilisation of copper (468). Arey *et al.* (448) found that in contaminated soils amended with apatite that iron phosphate phases were one of the main hosts of sequestered uranium.

Table 4.1 (continued).

Element	Project category	Health impacts	Environmental toxicity	(Drinking) water limits	Relevance to NORM-producing mining industries	Importance in phosphate minerals
Cobalt	Variable	Animal and human studies indicate a range of possible health impacts at elevated levels including genotoxicity and hypoxia (469–471).	May be toxic for invertebrates, fish, and plants (438,470) and may adversely impact invertebrate reproduction (441,470).	Recommended guidance values to protect aquatic life range from 0.004 mg/L (0.07 µmol/L) to 0.11 mg/L (1.9 µmol/L) (470,472).	Sites where elevated levels of cobalt have been measured include sediments in the gold mining Wonderfonteinspurit region, South Africa (420), acid mine drainage waters of the Curilo uranium deposit, Bulgaria (425), effluents from the former uranium mine near Cunha Baixa, Portugal (421).	May be immobilised in contaminated media by phosphate amendment (95,124,165,462,473)).
Copper	Variable	Gastrointestinal effects (437,474). At very high doses, vomiting, liver damage, and other acute impacts may occur (428,474). May catalyse the generation of toxic reactive oxygen species (474). May have a role in neurodegenerative diseases but the exact role of copper is "unclear" (474).	Toxic to invertebrates, fish and aquatic life (428,439,475–478). May impair the reproduction of *Daphnia Magna* (441).	2 mg/L (31.5 µmol/L) (437).	Sites where elevated levels of copper have been measured include river sediments in the lead-zinc and uranium mining district of Sumsar-Shakaftar, Kyrgyzstan (423), and acid mine drainage waters of the Curilo uranium deposit, Bulgaria (425).	A number of copper phosphate minerals are highly insoluble (431). May also coprecipitate with uranium to give the torbernite/metatorbernite minerals (431). May be immobilised in contaminated media by phosphate amendment (115,165,462,468,479).

Table 4.1 (continued).

Element	Project category	Health impacts	Environmental toxicity	(Drinking) water limits	Relevance to NORM-producing mining industries	Importance in phosphate minerals
Barium	Variable	Insoluble barium compounds (i.e. baryte, $BaSO_4$) are non-toxic but water-soluble or stomach acid soluble compounds may cause harmful effects including hypertension and kidney damage (437,480).	Soluble barium compounds are effective insect and rat poisons (480). May harm aquatic and soil organisms (438,458–460,481,482) May impair the reproduction of Daphnia Magna (441).	0.7 mg/L (5.1 µmol/L) (437).	Sites with elevated barium concentrations include uranium mill tailings in Utah, USA (26)), effluents from the former uranium mine near Cunha Baixa, Portugal (421). Barium may also be deliberately added to waste stream to induce the coprecipitation of barium-radium sulfates (106,426,483). This may lead to increased releases of barium to the local environment (426,443,484).	May be immobilised in contaminated media by phosphate amendment (95,473,485), Suzuki et al. (1981) cited by (117)). As a host material, barium hydroxyapatite has been researched for the immobilisation of copper, lead, zinc, cadmium, and cobalt (486,487).
Lanthanum	Variable	May compete with calcium and interfere with cellular functions, may also accumulate in biological tissues (488).	More research required to establish this, but potential for bioaccumulation (particularly at base of food chain) and toxicity in high doses (489).	0.004 mg/L (0.03 µmol/L) recommended as a preliminary water quality criterion (488).	Lanthanides often co-occur with uranium and thorium, and lanthanide-containing minerals (e.g. the lanthanide phosphates monazite and xenotime) may contain elevated levels of radionuclides (490). Generally not a priority contaminant, but surface waters in Virginia Canyon, Colorado, USA (a mining region with a historical legacy of uranium mining amongst other resources) have shown levels of lanthanum (0.39 mg/L) (491) above the provisional water limit of 0.004 mg/L recommended by (488). Mining of lanthanum and other rare earth elements (REEs) is associated with contamination, including NORMs (489).	Lanthanide phosphates are one of the major "families" of phosphate mineral structure types identified by (492). Phosphate may control the mobility of lanthanum and the REEs in the environment (493). Lanthanum and lanthanide phosphates have been researched for the sorption of uranium (354,355), the coprecipitation of cadmium (494), iron, and lead (495) and as a host for thorium (353) and other actinides (163,164,356,496,497).

Table 4.1 (continued).

Element	Project category	Health impacts	Environmental toxicity	(Drinking) water limits	Relevance to NORM-producing mining industries	Importance in phosphate minerals
Lead	Toxic	Poses acute and chronic toxicity, accumulates in bodies (428). Neurodevelopmental effects, mortality, impaired renal function, hypertension, impaired fertility and adverse pregnancy outcomes (437). Radioisotopes in the uranium and thorium decay chains (most importantly Pb-210) pose an additional radiological hazard (36,437).	Poisonous towards invertebrates, fish and aquatic life (428,438,464,478). May accumulate in livestock (428). May impair the reproduction of *Daphnia Magna* (441).	0.01 mg/L (0.05 µmol/L) in drinking water (437), 0.05 mg/L (0.24 µmol/L) in groundwater (498). For radioactive lead, guidance levels of 1000 Bq/L for Pb-203 and 0.1 Bq/L for Pb-210 (437).	Sites where elevated lead concentrations have been identified include: the Sumsar Say River, associated with lead-zinc and uranium deposit mining (423); in acid mine drainage waters associated with the Curilo uranium deposit, Bulgaria (425); mine tailings at the Rabbit Lake site, Canada (32), effluents from the former uranium mine near Cunha Baixa, Portugal (421). Stable and radioactive lead (Pb-210) may pose issues in the processing of copper ores (427).	Precipitation with phosphate is widely researched and a standard method for the treatment of lead-contaminated water (13,95,115,117,186,437,462,473,499–501). Lead phosphate minerals such as pyromorphite ($Pb_{10}(PO_4)_6(Cl,OH)$ are highly stable (431) and are the least soluble lead minerals in aerobic environments (502). May coprecipitate with uranium (parsonite, dumontite, dewindtite, renardite, przhevalskite), copper (tsumebite), aluminium (plumbogummite, hinsdalite), and iron (corkite) (431).

4.1 Experimental programme and methods

To investigate the phytase-mediated precipitation of the metals listed in table 4.1, as well as the interactions between the metals and phytate, solutions of metals (at 5 mmol/L in a buffered pH 5.5 solution) were subjected to four 'treatments':

- Phytate-only (mixed with 3.8 mmol/L phytate)
- Phytate + phytase (mixed with 3.8 mmol/L phytate, 1 mg/mL *A. niger* phytase added)
- Inorganic phosphate (mixed with 35 mmol/L inorganic phosphate)
- No phosphate (no source of phosphate added to the metal solution)

The phytate-only and phytate + phytase treatments were performed for all metals, while the no phosphate and inorganic phosphate treatments were performed only for aluminium, iron (II), iron (III), lanthanum, and lead.

For calcium, two additional conditions were investigated (50 mmol/L calcium at pH 5.5 or 5 mmol/L calcium at pH 7.0) with an extra treatment (phytate + phytase + alkaline phosphatase) investigated at pH 7.0. These additional conditions were performed to try and increase the likelihood of calcium phosphates forming after it was observed that very little precipitation occurred in the 'baseline' condition (5 mmol/L calcium, pH 5.5).

After mixing the experiments for 24 hours, solution and solid samples were taken for analysis.

4.1.1 Reagent preparation

The *A. niger* phytase was purchased from Hui Chem Co. Ltd. To prepare a solution of the phytase, the powder was weighed out and mixed with nanopure water (npH_2O, resistivity ≥ 18.2 MΩ·cm) at a concentration of 100 mg/mL (285). The suspension was centrifuged at 12,500 rcf for 10 minutes and the supernatant filtered through 0.2 µm syringe filters (either using PES or hydrophilic PTFE membranes). The filtered enzyme solution was then diluted into experimental solutions to give the desired nominal enzyme concentration (1 mg/mL based upon the original amount of powder weighed out, except where stated otherwise).

Stock solutions of phytic acid (100–200 mmol/L) were prepared by diluting phytic acid (48.1% w/w, nominal concentration of 1.044 mol/L, but see methodological issues section below) in npH_2O and adjusting the pH with 10 mol/L KOH to the desired pH. Stock solutions of potassium phosphate

monobasic (KH_2PO_4) were prepared in npH_2O at a concentration of 0.74 mol/L and placed at 37 °C for 2–3 hours to fully dissolve. The K:P ratio in the potassium phosphate stocks was 1:1 compared to a ratio of about 1.14:1 in the pH 5.5 phytate stocks, thus keeping the concentration of potassium roughly consistent for the comparisons between phytate and inorganic phosphate.

Metal stock solutions were prepared from various salts at the following concentrations: $Al_2(SO_4)_3.16H_2O$ (25 mmol/L, corresponding to 50 mmol/L Al), $CaCl_2.2H_2O$ (500 mmol/L), $MnSO_4.H_2O$ (500 mmol/L), $FeSO_4.7H_2O$ (50 mmol/L), $Fe(NO_3)_3.9H_2O$ (50 mmol/L), $Co(NO_3)_2{\cdot}6H_2O$ (42 mmol/L), $CuSO_4{\cdot}5H_2O$ (39 mmol/L), $BaCl_2.2H_2O$ (500 mmol/L), $LaCl_3.7H_2O$ (500 mmol/L), $Pb(NO_3)_2$ (50 mmol/L).

Stock solutions of pH buffers (glycine–HCl for pH 2.5, citric acid–trisodium citrate or MES–KOH for pH 5.5, TES–KOH for pH 7.0, TRIS-HCl for pH 8.5) were prepared by dissolving the corresponding powders in npH_2O and adjusting to the desired pH with either 5 mol/L HCl or 10 mol/L KOH.

For terminating enzyme reactions and dissolving precipitates, stock solutions of trichloroacetic acid (TCA) were prepared at 3.06 mol/L and nitric acid (HNO_3) at 3.3 mol/L.

4.1.2 Experimental procedures

Experimental media was prepared by mixing, in the following order, npH_2O, buffer, phytate or phosphate, and metal stocks to approximately ¾ of the final desired volume. The pH was then adjusted to the desired value with 10 mol/L KOH and solutions brought to the desired completed volume with npH_2O (or npH_2O + a nominal 1 mg/mL phytase for the phytate + phytase treatment).

The buffer was added to a final concentration of 200 mmol/L, phytate at 3.8 mmol/L, and the metals at 5 mmol/L except where stated otherwise. Inorganic phosphate controls were performed by substituting phytate for 35 mmol/L inorganic phosphate (35 mmol/L, designed to correspond to the amount of phosphate in phytate, but see methodological issues section below). The no phosphate controls were performed by mixing the metal and buffer with no phosphate sources added.

The ‘baseline’ condition used for these experiments (pH 5.5, 3.8 mmol/L phytate and 5 mmol/L metal) was chosen based upon the concentrations used by other researchers in similar projects (e.g. (184)) and the pH profile of the *A. niger* phytase. Experimental work took place at room temperature (~ 22 °C).

After completing the media (for controls) or adding the phytase to start the reaction, the centrifuge tubes were shaken by hand to mix and then placed in an overhead shaker (Gerhardt Rotoshake RS12)

at 10 rpm for ~ 24 hours. After this time period, solution samples were taken and precipitated solids were harvested.

For the solution samples, two fractions were defined: water-soluble and total. The water-soluble fraction was either defined as the amount remaining in the supernatant of a sample after centrifuging (for calcium, manganese, iron(II), iron(III), and barium) or the amount passing through a filtered (0.2 or 0.45 μm) aliquot of the sample supernatant after centrifuging (for aluminium, cobalt, copper, lanthanum, and lead). Experiments performed earlier in the project sampled directly from the supernatant and acidified the sample (to 1.67 mol/L HNO_3) before filtering. After it became apparent that some solid particles remained in suspension even after centrifuging, later experiments changed to filtering the supernatants before acidification. The water-soluble samples were split into two separate volumes; one used for chemical analysis and the other (which was not acidified) for pH and electrical conductivity/total dissolved solids measurements.

For total concentrations, an aliquot of the suspension was pipetted into a centrifuge tube and acidified to a HNO_3 concentration of 1.67 mol/L. This mixture was shaken by hand, and once dissolved, filtered through 0.2 μm hydrophilic PTFE syringe filters.

A slightly different strategy was used for the lanthanum experiments, where the dried solid was dissolved in acid to determine the insoluble fraction in mmol/g of precipitate. This was converted to mmol/L of experimental solution, and the insoluble fraction added to the water-soluble fraction to calculate the total concentrations. This was done for the purpose of comparing the different sampling strategies as the lanthanum experiments were repeated several times. However, during analysis it became apparent that there were subtle differences between the batches. The repeatability of the experiments is discussed in more detail in appendix E, but for this chapter, data are reported for the batch of samples that were used for the majority of solid phase analyses.

The order of operations when sampling was: (1) take total concentration sample, (2) centrifuge suspensions (3,000–10,000 rcf for 5–20 minutes), (3) take water-soluble samples, (4) wash solid phase in npH_2O and isopropyl alcohol by repeated centrifuging/discarding supernatant/mixing with fresh solution cycles, (5) dry solid to a constant mass at 50 °C.

Washing of the solid phase used one to three cycles in npH_2O and one in isopropyl alcohol. Initial experiments involved washing precipitates in npH_2O three times, but measurements of the electrical

conductivity of the supernatants indicated one wash in npH_2O and one in isopropyl alcohol was sufficient for these experiments.

All experiments were performed in triplicate. Multiple batches of experiments (each in triplicate) were performed for aluminium (two batches), lanthanum (four batches), and lead (two batches). Slight differences in results, likely due to changing background levels of inorganic phosphate in the phytate stock, were encountered so only the results from one batch are reported. The data reported were chosen based upon which batch of samples was used in the majority of solid phase analyses. Additionally, results for the phytate + phytase treatment for manganese and the phytate + phytase + alkaline phosphatase treatment for calcium are reported in duplicate due to experimental errors in preparing one of the replicates for each of these experiments.

The performance of the *A. niger* phytase without added metals was examined by preparing buffered (0.2 mmol/L) solutions of phytate (3.8 mmol/L) as above but without metals (except potassium which was introduced through the use of KOH to adjust pH). The enzyme reaction was terminated at various time points by the addition of either TCA or HNO_3 to a concentration of ~ 11% (w/v, corresponding to 0.66 mol/L for TCA or 1.67 mol/L for HNO_3; preliminary tests (data not shown) indicated that the acid used did not influence experimental results).

4.1.3 Analytical techniques

Solution samples were analysed for the following parameters: pH, electrical conductivity, total dissolved solids (TDS), elemental composition (by ICP-OES), and inorganic phosphate content (by colorimetry). pH, ICP-OES, and inorganic phosphate concentrations were measured as per chapter 2. Electrical conductivity was measured as per chapter 3; TDS was measured equivalently but with the meter operating in TDS mode.

These measured values were used to calculate the following parameters: metal removed from solution, inorganic phosphate released from phytate, inorganic phosphate removed from solution, and water-soluble and total organic phosphate concentrations.

The percentage of metals removed from solution was calculated by comparing the measured water-soluble concentrations to the mean measured total concentrations for all samples.

Inorganic phosphate released from phytate was calculated by subtracting the mean total inorganic phosphate concentration of phytate-only samples (and inorganic phosphate content of zero time

samples where these were taken) from the measured total inorganic phosphate in each phytate + phytase sample. Inorganic phosphate removed from solution was calculated by subtracting the measured water-soluble concentrations from the measured total concentrations.

Water-soluble organic phosphate concentrations were calculated by subtracting inorganic phosphate concentrations (measured by colorimetry) from the ICP-OES measured phosphate concentrations. For total organic phosphate concentrations, the inorganic phosphate concentration of individual samples was subtracted from the mean ICP-OES measured phosphate concentration for that batch of samples (this averaging was done to try and account for the large variability in phosphate concentrations measured by ICP-OES, see methodological issues section below). Where no phytate degradation was detected, the organic phosphate concentrations were converted to phytate concentrations on the basis that 6 moles of organic phosphate = 1 mole of phytate.

Solid phases were investigated by X-ray diffraction (XRD) as per chapter 2, Fourier Transform Infrared Spectroscopy (FTIR) as per chapter 3, Scanning Electron Microscopy (SEM), Transmission Electron Microscopy (TEM), Nuclear Magnetic Resonance (NMR), and a carbon hydrogen nitrogen (CHN) analyser.

SEM analysis was performed using a JEOL JSM-IT100 InTouchScope Tungsten low-vacuum SEM, with powder samples mounted on a carbon adhesive disc attached to an aluminium stub. TEM, along with Energy Dispersive X-ray Spectroscopy (EDX), was performed using a Titan Themis 200 scanning transmission electron microscope. Fast Fourier Transform (FFT) generated diffractograms were produced using the Gatan Digital Micrograph software or the Fiji distribution (390) of ImageJ (391). The SingleCrystal® 4 software (503) was used to aid the interpretation of diffractograms and to generate simulated electron diffraction patterns. NMR analysis was performed using a 400 MHz Bruker Avance III solid-state spectrometer and the recorded spectra were processed using Bruker's TopSpin™ 3.6.2 software. Chemical shifts are reported in ppm relative to 0.1 mol/L $Al(NO_3)_3$ or 85% aqueous H_3PO_4 using aluminium acetylacetonate ($Al(acac_3)$; δ_{iso} = 0.0 ppm) and BPO_4 (δ_{iso} = -29.6 ppm) as secondary solid references. CHN analysis was performed using an Exeter Analytical Inc. CE440 Elemental analyser.

In addition to these techniques, the likely solution speciation and saturation indices of solid phases were calculated by geochemical modelling using PHREEQC version 3 (303), see appendix A for details.

4.1.4 Methodological issues

Outlined below are a number of methodological issues encountered in this work that should be considered when interpreting results – however, it should also be noted that none of these issues are severe enough to alter the main conclusions of the experimental work.

4.1.4.1 Phytate concentration

The source of phytic acid used in this project was supplied by Sigma-Aldrich (product number Sigma 593648, batch number MKBW3159V). The batch purchased was specified as having a concentration of 48.1% (w/w). When planning experimental work, it was assumed that this purity referred to the phytic acid concentration. Accounting for the solution density of 1.432 g/mL, this gave a calculated phytic acid concentration of 688.8 g/L or 1.044 mol/L. When an inorganic phosphate impurity was measured in the phytic acid solution, it was assumed that this was *in addition* to the phytic acid content.

However, the purity of the solution was determined by titration with NaOH and refers to *all phosphate* in the solution, that is, phytic acid plus lower inositol phosphate and inorganic phosphate impurities.

Based upon the erroneous assumptions above, experimental solutions were prepared with a nominal phytic acid concentration of 5 mmol/L along with an inorganic phosphate concentration of ~ 5 mmol/L; this would have corresponded to an overall phosphate concentration of 35 mmol/L. However, the actual measured overall phosphate content was around 28 mmol/L, with a concentration of phosphate in phytic acid calculated to be around 23 mmol/L. This gave an actual phytic acid concentration of ~ 3.83 mmol/L.

This also had a further consequence in introducing discrepancies between the phytic acid-containing experiments and the inorganic phosphate controls. The inorganic phosphate controls were prepared with a phosphate concentration of 35 mmol/L, based upon the nominal phytic acid content, so in practice, the inorganic phosphate treatments contained an excess of phosphate compared to the phytic acid-containing experiments.

4.1.4.2 ICP-OES measurements

ICP-OES measurements generally appeared reliable for the metals investigated in this work (as determined by comparing the measured values to the known values of quality control samples run multiple times throughout batches of analysis). However, the measurements of phosphorus concentrations by ICP-OES encountered multiple issues.

The first issue encountered in early batches of samples was that during analysis the measured concentrations of phosphorus increased over time independently of the sample phosphorus concentration. This was indicated by quality control standards being equal to their known value at the start of a run but overestimating the phosphorus concentration by 30–60% after several samples had been measured. For the phytate-only and phytate + phytase treatments of calcium (at 5 mmol/L, pH 5.5), manganese, iron(II), iron(III), and barium there was not an opportunity to re-analyse these samples, so any calculated organic phosphate measurements presented are likely overestimates.

This rising phosphorus concentration issue was accounted for by running regular additional calibrations throughout analysis. However, once this issue was solved, another potential problem became apparent. The measured values of phosphorus by colorimetry and by ICP-OES should have been the same for the inorganic phosphate treatments as no organic phosphate was present in these samples. However, for all inorganic phosphate treatments performed, the measured values by colorimetry were about 3 mmol/L higher than the ICP-OES measured values. This is despite using the same standards to calibrate both techniques. It is uncertain where this error was introduced and whether it also applies to measurements of phosphate in the phytic acid-containing samples.

Due to these issues, calculated organic phosphate concentrations presented in this work should be interpreted with caution as a semi-quantitative indication of general trends.

4.1.4.3 XRD analysis

All XRD analysis used the copper K_α radiation. This is sub-optimal for iron or cobalt containing samples due to X-ray fluorescence resulting from interactions with the copper X-rays leading to high backgrounds (504,505). However, due to time and equipment availability constraints, this configuration was deemed sufficient for an initial investigation to test whether products were amorphous or contained crystalline features.

4.1.4.4 Dry mass measurements

The dry mass of harvested precipitates was recorded for all experiments. However, the results recorded are likely not representative of the actual mass of solid formed. This is because the samples were harvested by centrifugation and therefore suspended solids may be discarded with the supernatant. This was particularly pronounced for the phytate solids as phytate may form colloidal suspensions. For example, the dry mass of lead phytate was recorded as around 1.6 grams per litre of experimental solution when a centrifugation speed of 12,500 rcf was used but only 1.2 g/L when a centrifugation

speed of 3,000 rcf was used. The different centrifugation speeds were used due to equipment availability limitations. Due to the inconsistencies, the dry mass results are not reported here, and in future, filtration would be a preferable method of dry mass determination.

Because of these issues, the amounts of analytes incorporated into precipitates are expressed in terms of mmol/L removed from solution rather than as mmol/g of precipitate. The only case where dry mass measurements have been used are for the CHN results where the results (in mmol/g) were converted to mmol/L removed from solution to be comparable with the other results – therefore it should be noted that CHN results will not account for any suspended solids that were disposed with the supernatant.

4.2 Results and discussion

4.2.1 Baseline performance of A. niger phytase

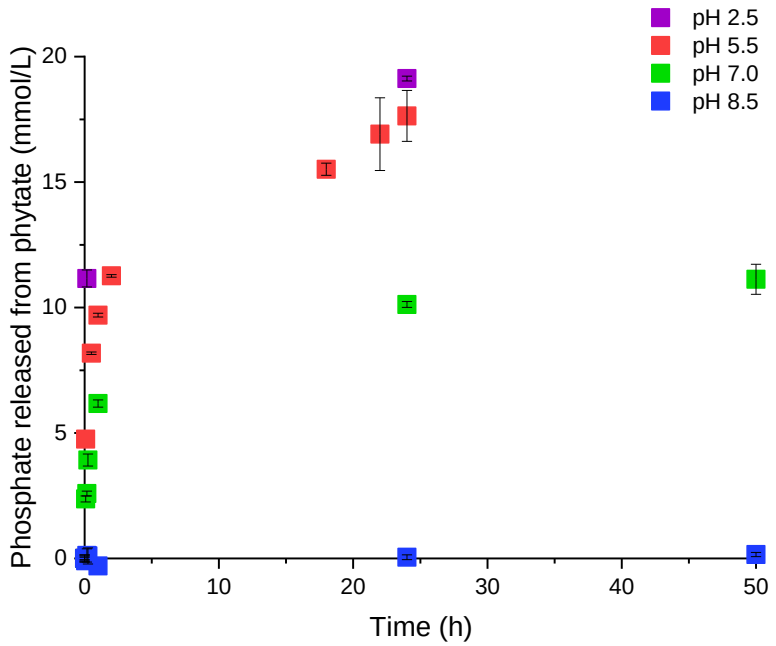

Figure 4.1 Phosphate release over time by the A. niger *phytase at room temperature at different pH values, buffered with 0.2 mol/L glycine (pH 2.5), citrate (pH 5.5), TES (pH 7.0), or TRIS (pH 8.5). Data points are the mean of duplicate samples; error bars represent the difference between the mean and the upper or lower measured values.*

To establish the baseline performance of the *A. niger* phytase, assays of the release of phosphate from phytate were performed at different pH values, temperatures, substrate concentrations, and with different buffers. The pH profile was consistent with previous reports of the *A. niger* phytase, with high levels of phytate breakdown at pH 2.5 and 5.5, moderate phosphate release at pH 7.0, and negligible

release at pH 8.5 (figure 4.1). Further tests at pH 5.5 indicated that the enzyme used was relatively insensitive to the pH buffer used (0.2 mol/L MES or citrate, data not shown), and therefore MES was used for the metal precipitation tests due to its lower ability to complex metals compared to citrate.

4.2.2 Individual metal precipitation tests

In all experiments, pH values in the experiments remained within ± 0.5 pH units of the starting value (data not shown). Where measured, there was a negligible difference in electrical conductivity or total dissolved solids values between different treatments (data not shown).

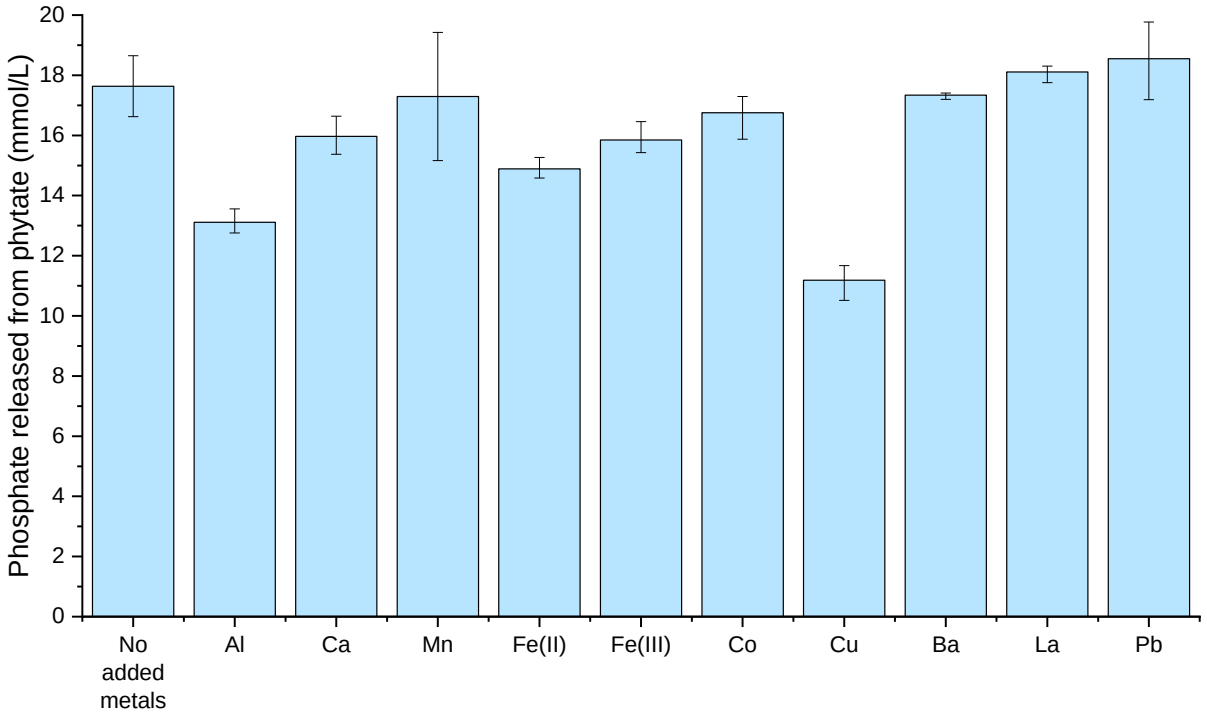

Figure 4.2 Phosphate release from 3.8 mmol/L phytate over 24 hours at pH 5.5 in the presence of different metals at 5 mmol/L (buffered with 0.2 mol/L citrate for no metals added data or 0.2 mol/L MES for all other experiments). Columns represent the mean values of experiments performed in triplicate except for no metals added (performed in duplicate) and manganese (reported in duplicate due to experimental error in the third sample). Error bars represent the difference between the mean value and the upper or lower measured values. Phosphate available from phytate was ~ 23 mmol/L. For the experiments where precipitation occurred (i.e. in all but the 'no metals added' condition), the data reported are for the 'total inorganic phosphate' concentrations after dissolving the precipitation with nitric acid.

After 24 hours, phosphate release occurred for all experiments where phytase had been added (figure 4.2). The baseline performance of the *A. niger* phytase, as indicated by the 'no added metals' condition, is to release approximately 18 mmol/L phosphate over a 24 hour experiment. In the presence of most of the metals investigated (calcium, manganese, iron(III), cobalt, barium, lanthanum, lead), a

comparable amount of phosphate (within ~ 2 mmol/L of the 'no metals added' control) was released. There was a slight indication of inhibition of phytate breakdown by iron(II) (mean phosphate release of ~ 15 mmol/L), and a much clearer indication of phytase inhibition by aluminium and copper (mean phosphate release being around 13 mmol/L and 11 mmol/L respectively). Metal inhibition of phytase and phosphatase activity has previously been described by several authors (230,285,506–508), and copper has been described as one of the more potent inhibitors of phytase activity (272).

Phosphate released was calculated by subtracting the background concentration of inorganic phosphate in the phytate-only control from the total inorganic phosphate measured in the phytate + phytase experiments. This background concentration of inorganic phosphate was determined to be around 5–6 mmol/L in all experiments except for the cobalt and copper experiments where it was measured at around 6–8 mmol/L. It is uncertain whether this discrepancy arose during preparation of the phytate stock (the cobalt and copper experiments were chronologically the last to be performed and there was evidence that the background inorganic phosphate concentration in the phytate stock increased over time) or that in the cobalt and copper experiments there was an additional level of metal catalysed phytate hydrolysis. Previous researchers have described metals having little impact on the chemical hydrolysis of phytate (references cited in (8)), although other researchers have claimed that metal catalysed phytate hydrolysis may be important (509). Metals have also been described as catalysing the hydrolysis of other organic phosphates (510,511) and so a small amount of metal catalysed hydrolysis cannot be ruled out. Regardless of explanation, this does not change the results in terms of copper being the most effective phytase inhibitor while cobalt has a low impact.

For the 'baseline' condition investigated for all metals (pH 5.5, 5 mmol/L metal) the following metal solubility trends (from least to most soluble) could be observed:

- Aluminium: No phosphate ≈ Inorganic phosphate < Phytate + Phytase < Phytate-only
- Calcium: Phytate-only < Phytate + Phytase
- Manganese: Phytate-only < Phytate + Phytase
- Iron (II): Inorganic phosphate < Phytate + Phytase < Phytate-only < No phosphate
- Iron (III): No phosphate ≈ Inorganic phosphate < Phytate + Phytase < Phytate-only
- Cobalt: Phytate-only < Phytate + Phytase

- Copper: Phytate-only + Phytase < Phytate
- Barium: Phytate-only < Phytase + Phytate
- Lanthanum: Inorganic phosphate ≈ Phytate + Phytase < Phytate-only < No phosphate
- Lead: Inorganic phosphate < Phytate + Phytase < Phytate-only < No phosphate

In summary, phytase addition improved metal removal compared to phytate alone for aluminium, iron (II), iron (III), copper, lanthanum, and lead, but increased metal solubility for calcium, manganese, cobalt, and barium. Where phytate-free inorganic phosphate controls were performed (for aluminium, iron (II), iron (III), lanthanum, and lead) metal removal was equivalent or superior to the phytate + phytase treatment. In addition, where no phosphate controls were performed, ~ 100% of the metal remained in solution for lanthanum and lead, while around 50% of iron (II) and ~ 100% of aluminium and iron (III) precipitated.

Detailed description of each of the systems investigated is given below, with the metals listed according to atomic number.

4.2.3 Aluminium

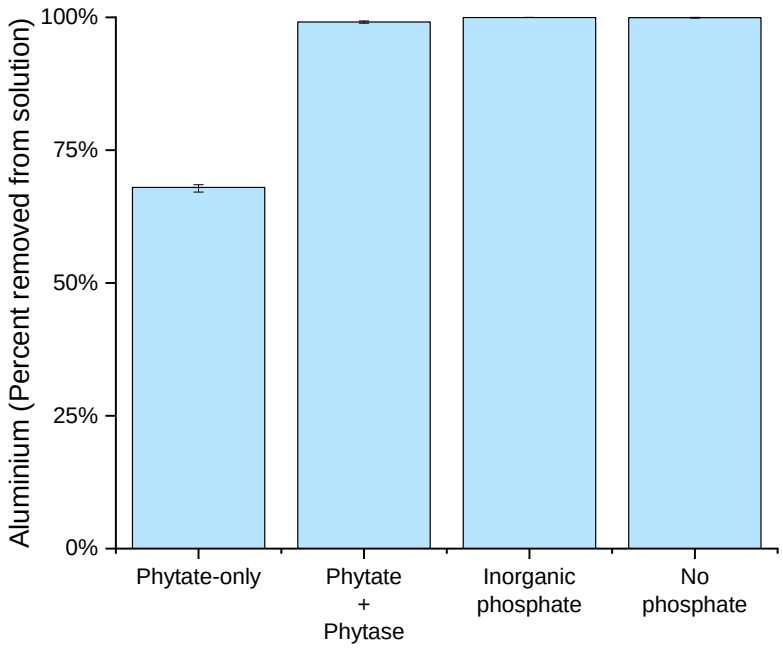

Figure 4.3 Percentage of aluminium removed from solution in the different treatments. Columns represent the mean of triplicate samples, error bars represent the difference between the mean and the upper and lower measured values.

Aluminium had a low solubility across all tested conditions, with 98–100% of aluminium removed from solution in the phytate + phytase, inorganic phosphate, and no phosphate treatments (figure 4.3). In the phytate-only treatment, however, only around 70% of aluminium was removed from solution. In comparison to suggested water limits, the inorganic phosphate and no phosphate treatments both reduced aluminium to below the limit recommended by the (437) of 33 µmol/L, while concentrations in the phytate + phytase treatment were close to the limit (between 34 and 55 µmol/L remaining in solution). In contrast, the phytate-only treatment kept aluminium in solution (~ 1.6 mmol/L) above even the upper limits for acute and chronic toxicity recommended by (440) of 178 and 119 µmol/L respectively.

For the phytate-only and phytate + phytase treatments, the data shown in figure 4.3 are for the second batch of experiments performed. It is worth noting that in the first batch only around 94% of aluminium was removed from solution for the phytate + phytase treatment. This may be because the second batch of experiments had a slightly higher background concentration of inorganic phosphate (~ 6.2 mmol/L compared to ~ 5.8 mmol/L in the first batch) which meant there was more inorganic phosphate available to precipitate with aluminium in the second batch (after phytase treatment, a total of ~ 19.5 mmol/L compared to ~ 18.8 mmol/L in the first batch). Alternatively, the first batch of samples took water-soluble samples from the supernatant while the second batch filtered the supernatant before acidifying; therefore the discrepancy may have been due to including suspended solid particles in the water-soluble fraction for the first batch of samples. In contrast, aluminium removal was similar in both batches for the phytate-only treatment.

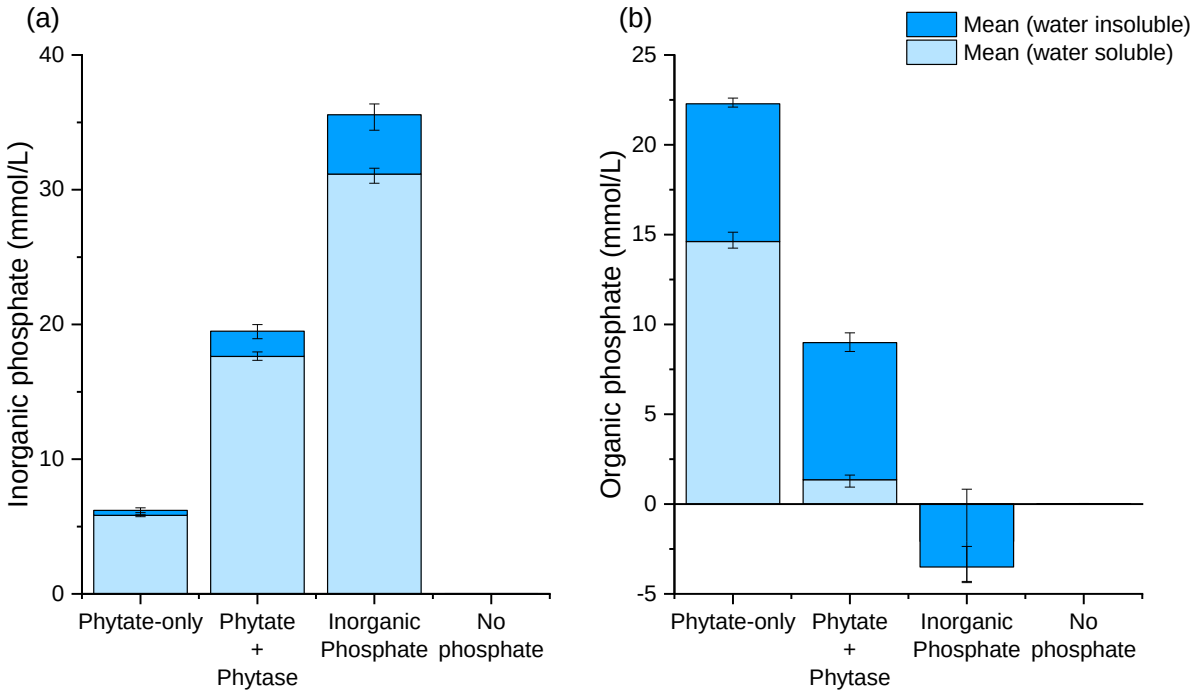

Figure 4.4 Comparison of water-soluble and total concentrations of (a) inorganic phosphate, and (b) organic phosphate across different treatments for the aluminium experiments. Columns represent the mean of value of triplicate samples, error bars represent the difference between the mean and the upper and lower measured or calculated values.

Comparisons of water-soluble to total inorganic phosphate concentrations indicated that around 1.9 mmol/L inorganic phosphate precipitated in the phytate + phytase treatment compared to around 0.4 mmol/L in the phytate-only treatment and 4.4 mmol/L in the inorganic phosphate treatment (figure 4.4a). Inorganic phosphate concentrations were close to or below the detection limit in the no phosphate treatment (< 0.02 mmol/L when accounting for dilution factors).

The calculated organic phosphate concentrations (figure 4.4b) indicated that around 7–8 mmol/L organic phosphate precipitated for both the phytate + phytase and phytate-only treatments. Inorganic + organic phosphate concentrations in the no phosphate treatment were close to or below the ICP-OES detection limit (< 0.05 mmol/L when accounting for sample dilution factor).

Table 4.2 Concentrations of analytes incorporated into precipitated solids, given in terms of mmol/L of experimental solution. Values are given as the mean of triplicate samples, columns designated as + and – represent the difference between the mean value and the upper or lower measured value respectively.

	Inorganic phosphate			Organic phosphate			Aluminium			Potassium		
Treatment	Mean	+	–	Mean	+	–	Mean	+	–	Mean	+	–
Phytate-only	**0.37**	*0.29*	*0.22*	**7.67**	*0.69*	*0.71*	**3.43**	*0.02*	*0.04*	**0.73**	*2.52*	*2.44*
Phytate + Phytase	**1.87**	*0.16*	*0.26*	**7.63**	*0.35*	*0.64*	**4.99**	*0.01*	*0.01*	**-1.62**	*2.40*	*2.32*
Inorganic Phosphate	**4.40**	*1.02*	*1.39*	**-1.44**	*1.50*	*1.75*	**5.04**	*0.00*	*0.00*	**14.76**	*23.25*	*12.38*
No phosphate	**0.00**	*0.00*	*0.00*	**0.03**	*0.02*	*0.03*	**5.04**	*0.00*	*0.00*	**2.50**	*1.80*	*1.16*

The concentrations of analytes removed from solution are shown in table 4.2. The phytate + phytase and phytate-only treatments both appeared to contain an excess of organic phosphate compared to aluminium, as would be expected for aluminium phytate precipitates (or aluminium precipitates with lower inositol phosphates). In both cases, more organic phosphate precipitated than inorganic phosphate, although there was an increase in inorganic phosphate precipitation in the phytate + phytase treatment that may be associated with the increase in aluminium precipitation.

The aluminium:phytate ratio for the phytate-only treatment was calculated to be between 2.5:1.0 and 2.9:1.0. Previous researchers have indicated that aluminium precipitates with aluminium:phyate ratios ranging from 1:1 to 4:1 (512). A 1:1 ratio, which was the approximate starting ratio in these experiments, is the most soluble, although precipitation still occurs above pH ~ 2.5 (512).

The amount of organic phosphate precipitating in the phytate + phytase treatment was similar to the phytate-only treatment at ~ 8 mmol/L (table 4.2). Assuming that the amount of aluminium associated with this fraction remained similar (~ 3.4 mmol/L), this gave an additional ~ 1.6 mmol/L aluminium removed from solution. Compared to the phytate-only treatment, an additional ~ 1.5 mmol/L inorganic phosphate precipitated in the phytate + phytase treatment. If the improvement in aluminium removal was associated with the increase in inorganic phosphate, then this means it can be calculated that the precipitation occurred in an approximate 1:1 ratio.

The inorganic phosphate treatment had an aluminium:inorganic phosphate ratio that ranged from 0.9:1 to 1.7:1. Aluminium phosphates may occur with aluminium:phosphate ratios of 1:1 (e.g. berlinite, $AlPO_4$, and variscite, $AlPO_4.2H_2O$), 1:3 (e.g. $Al(H_2PO_4)_3$), 1.3:1 (e.g. vantasselite $(Al_4(PO_4)_3(OH)_3 \cdot 9H_2O)$), 1.5:1 (e.g. wavellite, $Al_3(PO_4)_2(OH,F)_3.5H_2O$), or 3:1 (e.g. $Al_3(PO_4)(OH)_6$). This suggests that the precipitated

mineral was a non-stoichiometric aluminium hydroxyphosphate, possibly similar to vantasselite or wavellite.

Potassium concentrations were also measured for these experiments, but for the phytate + phytase, phytate-only, and inorganic phosphate treatments, the results were inconclusive with a large degree of analytical variability. In the no phosphate treatment, the potassium concentrations measured were more consistent, with 1.3 to 4.3 mmol/L potassium calculated to be removed from solution.

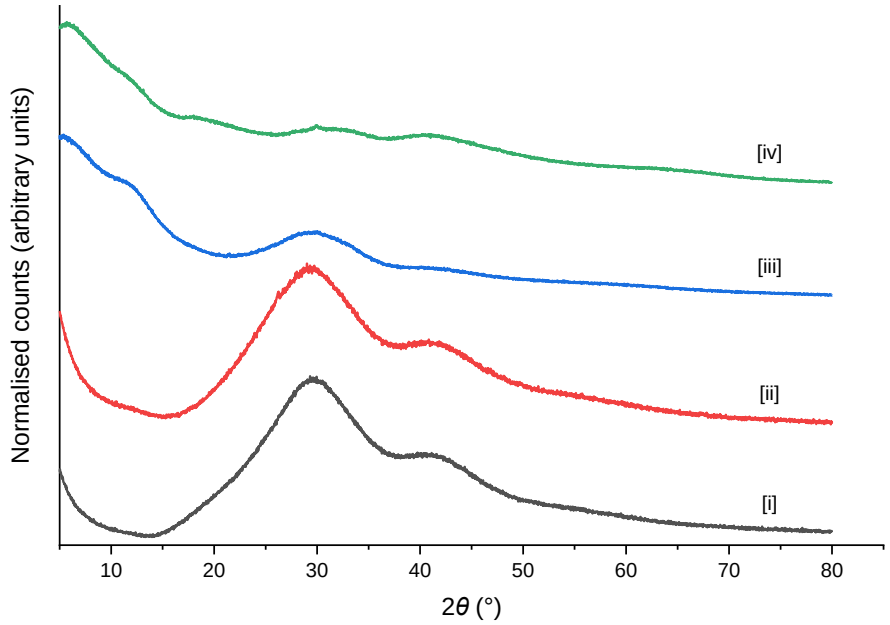

Figure 4.5 XRD patterns of solids formed in the aluminium experiments showing [i] Phytate-only; [ii] Phytate + Phytase; [iii] Inorganic phosphate; and [iv] No phosphate treatments.. Phytate-only and phytate + phytase samples were measured using the Göbel mirror optics setup, inorganic phosphate and no phosphate samples were measured using the motorised slit. Samples were measured using the copper K_α radiation across a 2θ range of 5–80° with a step size of 0.02° and a step time of 1 s. Patterns were normalised in OriginPro 2019b to a scale of 0 to 1.

XRD patterns of the precipitates all showed amorphous materials with no notable, distinctive features (figure 4.5). Phytate solids are usually known to be amorphous (8,230,513), as are aluminium hydroxyphosphates (449,451,514), and aluminium hydroxysulfates precipitated under ambient conditions (515,516).

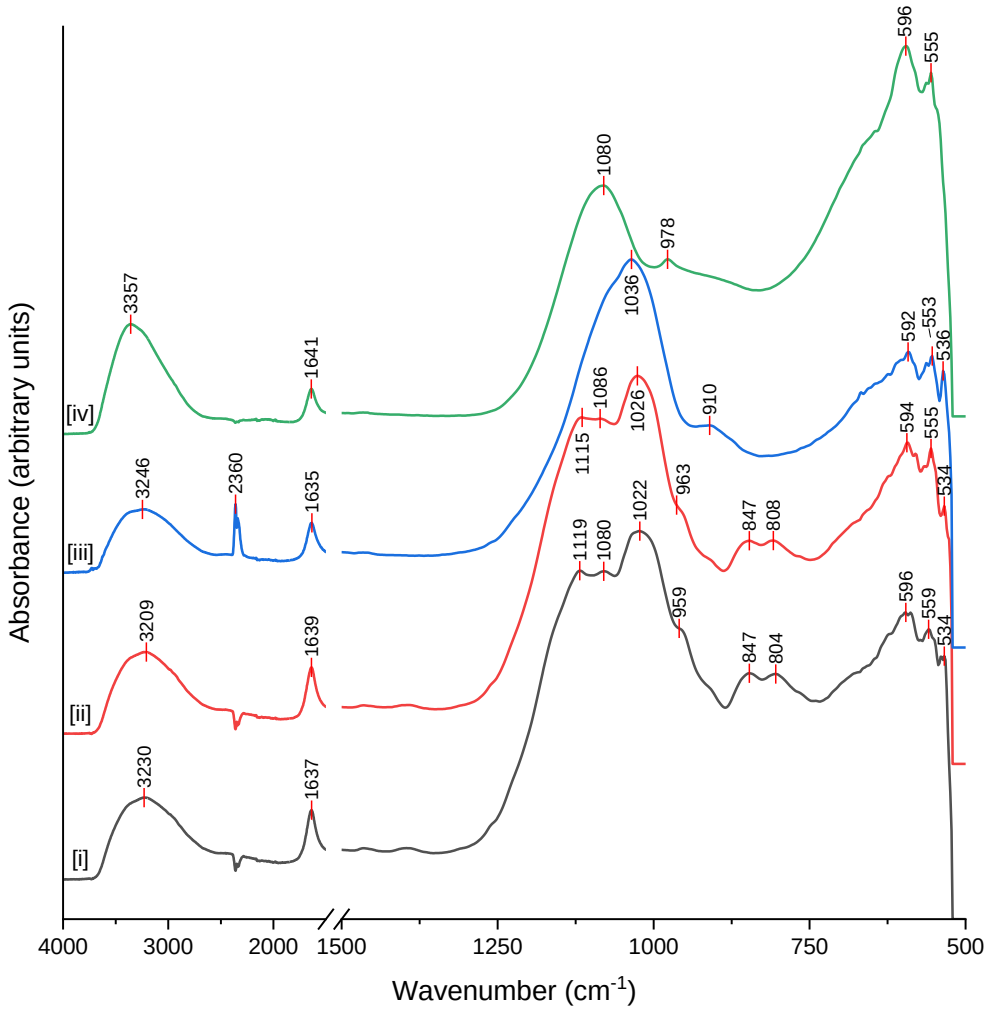

Figure 4.6 FTIR spectra of precipitates produced in the aluminium experiments showing [i] Phytate-only; [ii] Phytate + Phytase; [iii] Inorganic phosphate; and [iv] No phosphate treatments. Spectra were normalised in OriginProb2019b to a scale of 0–1.

FTIR spectra of the aluminium precipitates are shown in (figure 4.6). The spectra indicated that precipitates recovered from the phytate + phytase and phytate-only treatments were similar, while the inorganic phosphate and no phosphate treatments produced materials with their own distinct spectra.

All spectra showed a broad band between ~ 3,500 and 2,700 cm^{-1} and a narrow band at ~ 1,640 cm^{-1} associated with O–H stretching and bending modes respectively (407). These features indicate the presence of crystallised water within the solid phase (407). The peak or trough at ~ 2,360 cm^{-1} is contamination from atmospheric CO_2 (407).

The fingerprint region (~ 1,500–500 cm^{-1}) is challenging to interpret, particularly due to the possible presence of sulfate in the system, as the vibrational modes of sulfate and phosphate groups give signals

in similar regions of the infrared spectrum. The vibrational frequencies of sulfate groups generally occur at higher wavenumbers than the corresponding phosphate vibrations (407,517). A peak at 1,080 cm^{-1} in the no phosphate treatment compared to 1,036 cm^{-1} in the inorganic phosphate treatment may indicate a sulfate-containing solid for the former and a phosphate-containing solid for the latter (figure 4.6). In the same region, the phytate-only and phytate + phytase samples showed a broad band between 1,200 and 900 cm^{-1} which appeared to consist of at least four overlapping peaks (figure 4.6). Overlapping peaks in this region in phytate-containing samples have been attributed to P–O–C groups (518,519). A doublet at ~ 800 and ~ 850 cm^{-1} is another feature that may be associated with the P–O–C groups of phytate (281,407,518,520). The peaks in the 700–500 cm^{-1} are difficult to assign as signals from P–O, S–O, Al–O, and O–H may all be prominent in this region (407,521,522).

Searching spectral databases failed to provide satisfactory matches for the phytate-only and phytate + phytase samples. FTIR spectra of aluminium phytate shown in previous work differed slightly in the shape and intensities of peaks in the 1,200–900 cm^{-1} region (513,518) which may be associated with pH, aluminium source, stoichiometry of the precipitate, sample preparation, or the equipment used.

The most likely match for the inorganic phosphate treatment was wavellite ($Al_3(PO_4)_2(OH,F)_{3.5}H_2O$, database number MNX #150). The spectrum also appeared to match well (based on a visual assessment) with the spectrum of amorphous aluminium phosphate ($AlPO_4.xH_2O$) (432) or aluminium hydroxyphosphate (514) reported in the literature.

The most likely match for the no phosphate treatment sample according to database searching was chalcoalumite ($CuAl_4(SO_4)(OH)_{12}.3H_2O$; database number MNX #169). While there was no copper present in this experiment, the vibrational frequencies associated with S–O, Al–O, and O–H are likely to be similar in phases such as alunite ($KAl_3(SO_4)_2(OH)_6$) and felsobányaite ($Al_4(SO_4)(OH)_{10}·4H_2O$). The no phosphate spectrum appeared visually similar to literature descriptions of basic aluminium sulfate ($Na_{0.1}[Al_{13}O_4(OH)_{24}(H_2O)_{12}](SO_4)_{3.55}$) (523,524) and nanocrystalline basaluminite/felsobányaite ($Al_4OH_{10}(SO_4).(H_2O)_{3–5}$) (525). Alternatively, the peak at 1,080 cm^{-1} combined with the most intense peak in the spectrum appearing at around 600 cm^{-1} may be indicative of boehmite (AlO(OH)) (526).

Furthermore, ^{27}Al and ^{31}P NMR spectra for the phytate-only and phytate + phytase treatments were consistent with previous descriptions of aluminium phytate (appendix F, figures F.1–F.3) (397,513,527). The inorganic phosphate spectra matched with previous descriptions of amorphous aluminium

hydroxyphosphate (514,528,529), while the no phosphate treatment produced a ^{27}Al NMR spectrum similar to felsobányaite/basaluminite (525,530) but different from basic aluminium sulfate (523).

Despite no solubility product data being available for aluminium phytate, geochemical modelling provided some useful insights. In particular, solution modelling indicated that phytate strongly inhibited aluminium hydrolysis (appendix G, table G.2). The highest saturation index in the phytate-only, phytate + phytase and inorganic phosphate treatments was calculated for aluminium hydroxyphosphate, while in the no phosphate treatment, alunite ($KAl_3(SO_4)_2(OH)_6$) had the highest saturation index – this would be consistent with the chemical analysis indicating some potassium precipitation for the no phosphate treatment (table 4.2).

This inhibition of aluminium hydrolysis is likely the main explanation behind the increased solubility of aluminium in the phytate-only treatment, with a mixture of insoluble and soluble aluminium phytate complexes being formed. It follows that in the phytate + phytase treatment, phytase catalysed the hydrolysis of the soluble phytate while the precipitated aluminium phytate remained intact. Once the soluble phytate had been broken down, this allowed aluminium hydrolysis to occur and the subsequent precipitation of the residual soluble aluminium as (hydroxy)phosphate, (oxyhydr)oxide, and/or sulfate phases alongside the already formed aluminium phytate.

Concentrations of soluble aluminium remained higher in the phytate + phytase treatment as compared to the inorganic phosphate treatment. This may be due to a higher concentration of available inorganic phosphate in the inorganic phosphate treatment (~ 35 mmol/L compared to ~ 19 mmol/L in the phytate + phytase treatment). Alternatively, strong soluble complexes between aluminium and unhydrolyzed phytate or other organic phosphates produced during phytate breakdown (so-called lower inositol phosphates) may keep some aluminium in solution. Inositol trisphosphates ($C_6H_{15}O_{15}P_3$), for example, are known to bind aluminium strongly (265). The phytate breakdown products were not quantified in this work, but ideally this would be done in future, as the lower inositol phosphates interact strongly with metals and minerals and will likely have an impact on the speciation and mobility of contaminants.

In summary, attempts at synthesising aluminium phosphate minerals from a phytate precursor produced somewhat ambiguous results in this work. Across all conditions tested, aluminium had a low solubility at pH 5.5, but the highest concentrations of soluble aluminium were measured in the phytate-only and phytate + phytase treatments. The most likely product formed for the phytate + phytase and

phytate-only treatments was an aluminium phytate, compared to aluminium hydroxyphosphates and hydroxysulfates likely produced in the inorganic phosphate and no phosphate treatments respectively.

A multitude of different aluminium hydroxyphosphates exist, such as vantasselite ($Al_4(PO_4)_3(OH)_3 \cdot 9H_2O$), wardite ($NaAl_3(OH)_4(PO_4)_2 \cdot 2H_2O$), augelite ($Al_2(OH)_3(PO_4)$), wavellite ($Al_3(PO_4)_2(OH,F)_{3.5}H_2O$), bolivarite ($Al_2(PO_4)(OH)_3 \cdot 4\text{-}5H_2O$), and evansite ($Al_3(PO_4)(OH)_6 \cdot 6H_2O$) (449,531–534). Natural examples of these minerals have shown enriched levels of uranium (449,451) which make them of interest for the remediation of contaminated environments. However, further work would be required if these phases are to be produced from a phytate precursor.

Previous researchers have noted that, under certain circumstances, phytate amendments can increase metal solubility or mobility (121,244,535). In this case, the strength of the aluminium phytate complexes and the inhibition of aluminium hydrolysis likely had a role in keeping around 30% of the aluminium in solution. The metal:phytate ratio is known to have an important role in determining the solubility of metal phytates (244). With the 1:1 aluminium:phytate ratio used, it is likely that a mixture of insoluble and soluble aluminium phytate complexes were formed. Therefore, the phytate-only treatment could likely be improved by adjusting to the more favourable 4:1 aluminium:phytate ratio (512,536).

An additional complicating factor in these experiments was the use of aluminium sulfate as an aluminium source as, while aluminium sulfate is soluble, aluminium hydroxysulfates have a low solubility. The amount of aluminium remaining in solution in the no phosphorus treatment was equivalent to or lower than the amount of aluminium in solution in the inorganic phosphate treatment. Sulfate is likely to be present at mining-impacted sites, so this was not an unrealistic condition to investigate. Additionally, previous researchers have successfully used aluminium sulfate as a source of aluminium for the production of aluminium hydroxyphosphate vaccine adjuvants (526) and to bind and precipitate phosphate in wastes and body fluids (537–539). Experiments using other soluble sources of aluminium (e.g. chloride or nitrate salts) would be useful to probe the role of sulfate in these experiments. It should also be investigated whether the presence of phosphate and sulfate together may stabilise aluminium within solid phases or if anionic competition may increase the solubility of aluminium.

A further aspect to investigate would be the kinetics of precipitation and crystallisation. Previous researchers have described the crystallisation rates of aluminium phosphates as being extremely slow (21 days at 100 °C, which implies even slower kinetics at ambient temperatures) (432) so it would be of

interest to perform these experiments over longer timescales to investigate any transitions from amorphous products to crystalline ones.

4.2.4 Calcium

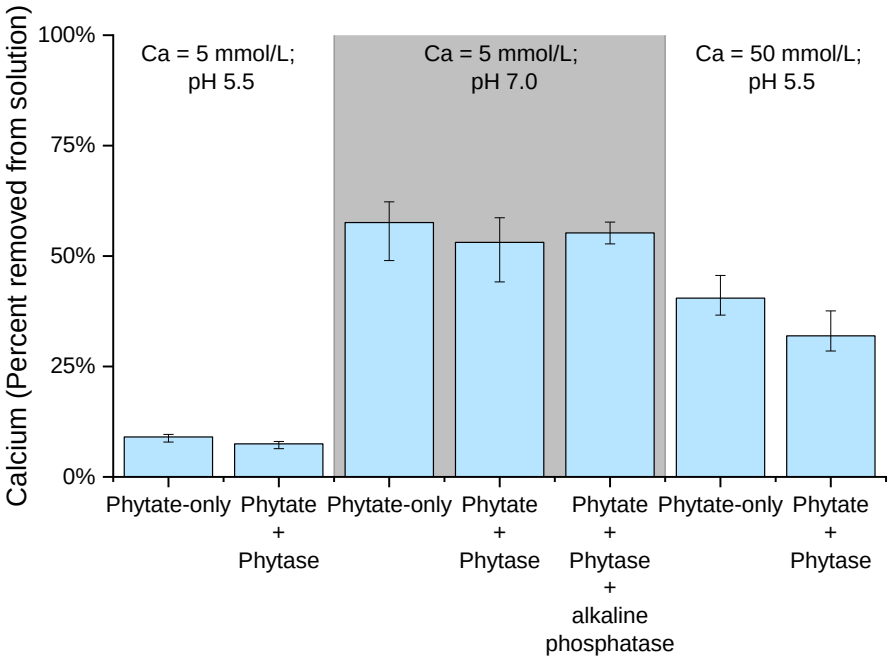

Figure 4.7 Percentage of calcium removed from solution in the different treatments. Columns represent the mean of triplicate samples (or duplicate for phytate + phytase + alkaline phosphatase treatment due to experimental errors), error bars represent the difference between the mean and the upper and lower measured values.

Calcium solubility varied between the conditions, with the lowest solubility observed at pH 7.0 and the highest solubility at pH 5.5 (figure 4.7). Increasing the calcium concentration from 5 mmol/L to 50 mmol/L reduced the solubility at pH 5.5, but calcium was still more soluble (in percentage terms) compared to 5 mmol/L at pH 7.0. The calcium concentration and pH appeared to be more important in determining calcium solubility than whether phytase was added to the system, as calcium solubility only varied by a small amount between treatments. There did appear to be a slight increase in calcium solubility in the phytate + phytase treatments, particularly at 50 mmol/L calcium, pH 5.5 but this may have been within the margins of analytical variability.

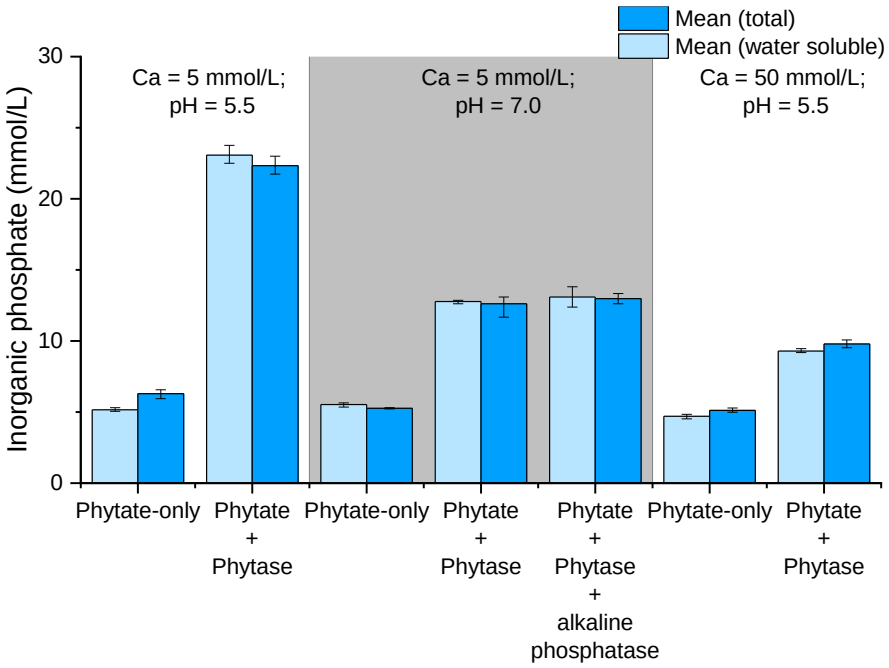

Figure 4.8 Comparison of water-soluble and total inorganic phosphate concentrations across the different conditions and treatments tested for the calcium experiments. Columns represent the mean of value of triplicate samples (or duplicate in the case of the phytate + phytase + alkaline phosphatase treatment), error bars represent the difference between the mean and the upper and lower measured values.

As indicated in figure 4.8, phosphate release from phytate was most successful at pH 5.5 with 5 mmol/L calcium (~ 16 mmol/L phosphate released from phytate). Higher pH values (pH 7.0) or higher calcium concentrations (50 mmol/L) greatly reduced the amount of phosphate being released from phytate (~ 8 mmol/L released at pH 7.0, ~ 5 mmol/L released in the presence of 50 mmol/L calcium). Inhibition at 50 mmol/L calcium, pH 5.5 was likely due to the precipitation of phytate 'protecting' it from enzymatic hydrolysis. Inhibition at pH 7.0 was likely a function of the pH profile of the *A. niger* phytase, as phosphate release was comparable to calcium-free controls (see figure 4.1 at 24 hours).

There also appeared to be a negligible difference between phosphate release in the phytate + phytase and phytate + phytase + alkaline phosphatase treatments attempted at pH 7.0. Across all conditions, it appeared that the majority of inorganic phosphate remained in solution.

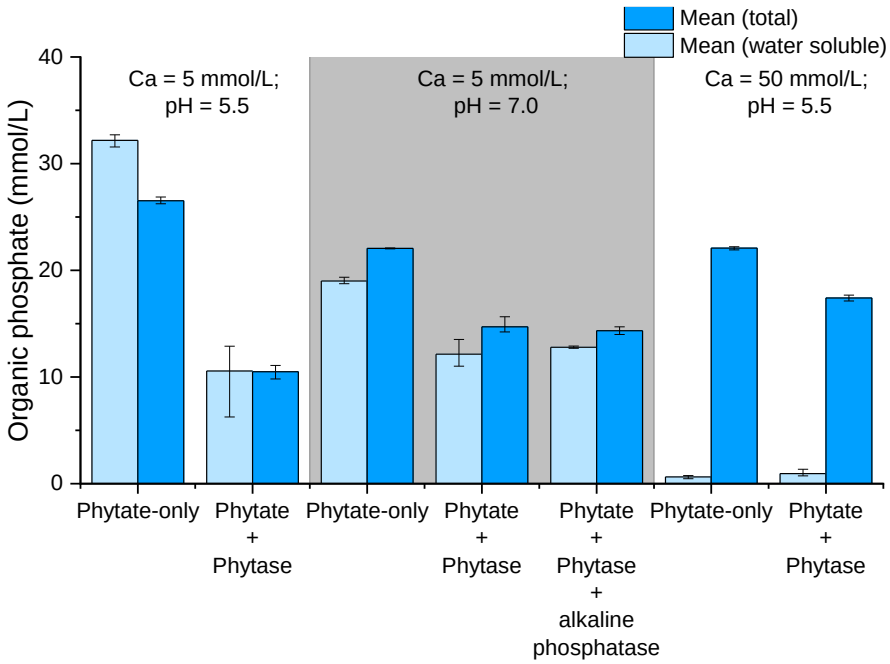

Figure 4.9 Comparison of water-soluble and total organic phosphate across different conditions and treatments tested for the calcium experiments. Organic phosphate concentrations were calculated by subtracting the inorganic phosphate concentration from the inorganic + organic phosphate concentration. Columns represent the mean of value of triplicate samples (or duplicate in the case of the phytate +phytase + alkaline phosphatase treatment), error bars represent the difference between the mean and the upper and lower measured values.

The data for calculated organic phosphate concentrations in figure 4.9 indicate that, where precipitation occurred, it was mostly with the organic phosphate fraction rather than inorganic phosphate, regardless of phytase activity. In particular, at 50 mmol/L calcium, pH 5.5, around 95% of organic phosphate was insoluble.

Table 4.3 Concentrations of analytes removed from solution into precipitated solids, given in terms of mmol per litre of experimental solution. Values are given as the mean of triplicate samples (or duplicate in the case of the phytate + phytase + alkaline phosphatase treatment), columns designated as + and – represent the difference between the mean value and the upper or lower measured value respectively. N.d. indicates not determined.

Condition	Treatment	Inorganic phosphate			Organic phosphate			Calcium			Potassium		
		Mean	+	–	Mean	+	–	Mean	+	–	Mean	+	–
5 mmol/L Ca; pH 5.5	Phytate-only	**1.13**	*0.39*	*0.50*	**-5.66**	*0.97*	*0.58*	**0.46**	*0.03*	*0.06*	**n.d.**	*n.d.*	*n.d.*
	Phytate + phytase	**-0.74**	*0.78*	*0.76*	**-0.08**	*4.39*	*2.99*	**0.38**	*0.03*	*0.05*	**n.d.**	*n.d.*	*n.d.*
5 mmol/L Ca; pH 7.0	Phytate-only	**-0.27**	*0.18*	*0.17*	**3.06**	*0.25*	*0.31*	**2.94**	*0.24*	*0.44*	**-1.46**	*1.43*	*1.06*
	Phytate + Phytase	**-0.16**	*0.64*	*1.03*	**2.55**	*0.66*	*0.43*	**2.71**	*0.29*	*0.46*	**-3.47**	*7.21*	*9.81*
	Phytate + Phytase + alkaline phosphatase	**-0.12**	*1.07*	*1.07*	**1.55**	*0.25*	*0.25*	**2.82**	*0.13*	*0.13*	**-4.14**	*5.51*	*5.51*
50 mmol/L Ca; pH 5.5	Phytate-only	**0.41**	*0.05*	*0.07*	**21.45**	*0.20*	*0.29*	**22.35**	*2.83*	*2.13*	**3.92**	*6.73*	*5.82*
	Phytate + Phytase	**0.49**	*0.11*	*0.20*	**16.47**	*0.48*	*0.68*	**17.63**	*3.12*	*1.90*	**0.58**	*3.87*	*6.53*

Due to the low amount of precipitation and large analytical variability, it was difficult to calculate stoichiometric ratios for the 5 mmol/L calcium, pH 5.5 condition (table 4.3). For the other conditions, there appeared to be an approximate 1:1 ratio between calcium and organic phosphate groups, which would correspond to a calcium:phytate ratio of around 6:1 if all the organic phosphate was present as phytate. The only exception to this was for the phytate + phytase + alkaline phosphatase treatment, where the calcium:organic phosphate ratio was closer to 1.9. It is uncertain whether this is due to analytical error, or potentially, the presence of different lower inositol phosphates when the alkaline phosphatase was introduced into the system. Potassium concentrations provided ambiguous results, with a large variability between replicate experiments (table 4.3).

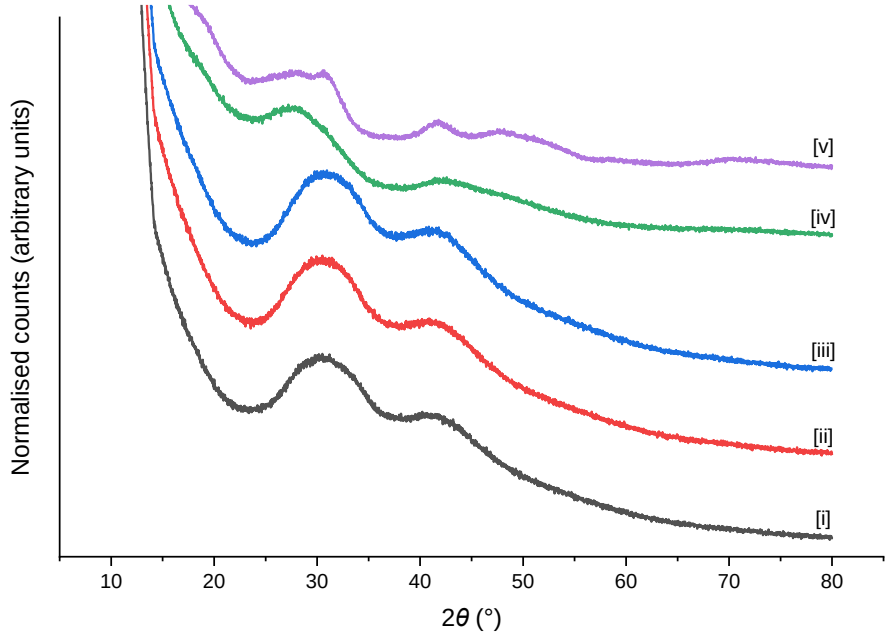

Figure 4.10 XRD patterns of precipitates produced in the calcium experiments showing [i] Phytate-only at 5 mmol/L calcium, pH 7.0; [ii] Phytate + Phytase at 5 mmol/L calcium, pH 7.0; [iii] Phytate + Phytase + Alkaline phosphatase at 5 mmol/L calcium, pH 7.0; [iv] Phytate-only at 50 mmol/L calcium, pH 5.5 treatments; and [v] Phytate + Phytase at 50 mmol/L calcium, pH 5.5. Samples were measured using the Göbel mirror optics setup, using the copper K_α radiation across a 2θ range of 5–80° with a step size of 0.02° and a step time of 1 s. Patterns were normalised in OriginPro 2019b to a scale of 0 to 1.

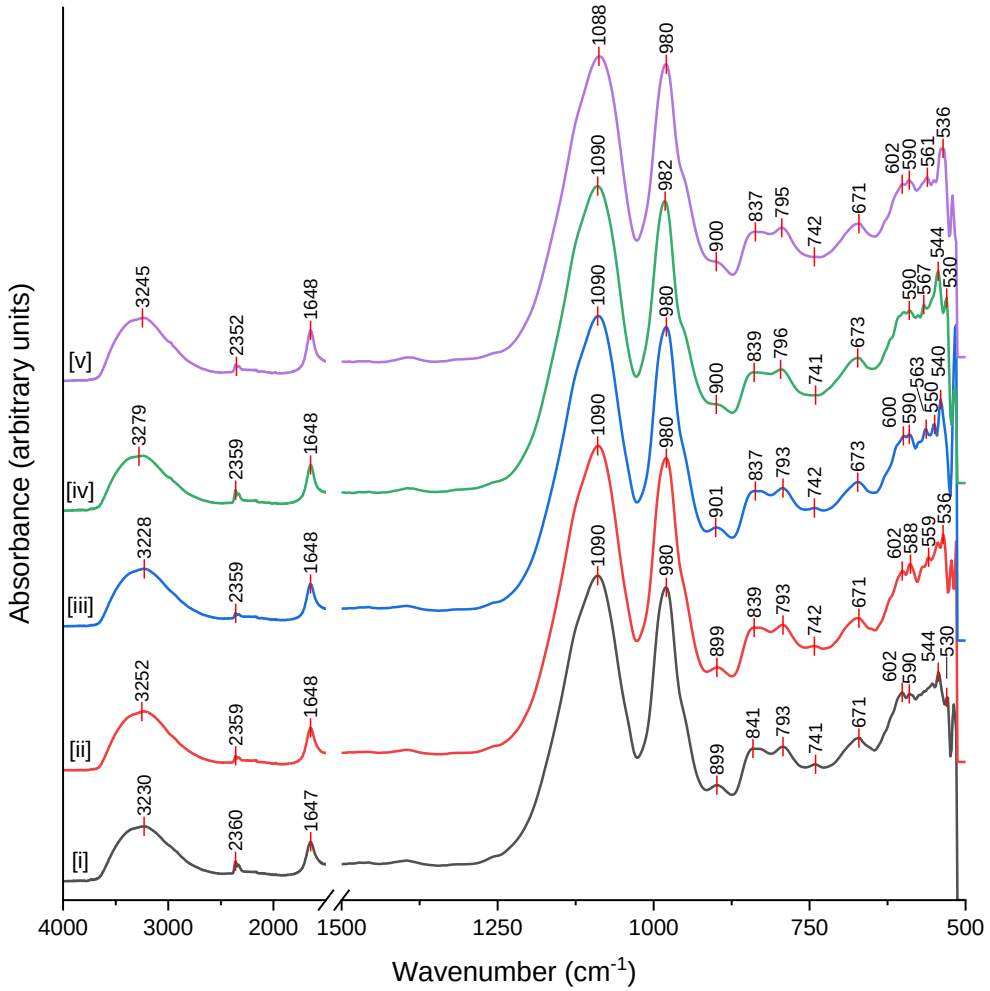

Figure 4.11 FTIR spectra of precipitates produced in the calcium experiments showing [i] Phytate-only at 5 mmol/L calcium, pH 7.0; [ii] Phytate + Phytase at 5 mmol/L calcium, pH 7.0; [iii] Phytate + Phytase + Alkaline phosphatase at 5 mmol/L calcium, pH 7.0; [iv] Phytate-only at 50 mmol/L calcium, pH 5.5 treatments; and [v] Phytate + Phytase at 50 mmol/L calcium, pH 5.5. Spectra were normalised in OriginPro 2019b to a scale of 0–1.

Solid phase analysis was only possible for the pH 7 experiments with 5 mmol/L calcium or the pH 5.5 experiments with 50 mmol/L calcium. For the experiments with 5 mmol/L calcium at pH 5.5 a negligible amount of precipitate was recovered, and therefore, solid phase analysis was not possible. The XRD patterns (figure 4.10) and the FTIR spectra (figure 4.11) were broadly similar across all samples investigated. The XRD patterns indicated that all the samples were amorphous, which is consistent with previous descriptions of calcium phytate (253,333).

The FTIR spectra (figure 4.11) showed features indicative of phytate/organic phosphate containing samples and visually matched well with previously reported spectra for Ca_6Phytate (333,518). The

double peaks at 1,090 and 980 cm^{-1} and at 840 and 800 cm^{-1} are associated with multiple P–O–C bonds in phytate, and these features have been used to distinguish between calcium phytate and calcium phosphate (518,520). However, the position of the peak at 1,090 cm^{-1} compared to ~ 1,130 cm^{-1} may indicate that the material in this work was actually a pentacalcium phytate (e.g. Ca_5H_2Phytate or Ca_5K_2Phytate) (540).

Geochemical modelling indicated that the apatite minerals hydroxyapatite ($Ca_{10}(PO_4)_6(OH)_2$) and chloroapatite ($Ca_{10}(PO_4)_6Cl_2$) were supersaturated under every condition, and brushite ($Ca(HPO_4).2H_2O$) was supersaturated at pH 7 or with 50 mmol/L calcium (appendix G, table G.3). However, the saturation indices for Ca_6Phytate and Ca_5K_2Phytate were much higher than the calculated values for any inorganic phosphate mineral across all conditions, regardless of whether phytate hydrolysis occurred. Therefore, it is likely that the strong binding of calcium by phytate inhibited inorganic phosphate precipitation, as has been previously described (266,322,323).

None of the treatments attempted in this batch of experiments were successful at manufacturing hydroxyapatite or any other inorganic calcium phosphate phase. The pH profile of the *A. niger* phytase appears to be the major limiting factor preventing the direct production of calcium hydroxyapatite. However, the use of the *A. niger* phytase may still provide an efficient mechanism of sourcing inorganic phosphate and, once phytate has been broken down, the produced inorganic phosphate could then be used to synthesise hydroxyapatite by chemical mechanisms. This method would be less suitable for an *in situ* production strategy, but may be useful in terms of the *ex situ* bulk production of hydroxyapatite. Future research into this method should also consider the potential role of residual phytate/lower inositol phosphates acting as crystallisation inhibitors, as complete phytate breakdown is generally unlikely.

Additionally, previous researchers have also considered the possibility of directly using calcium phytate as a remediation material (244,253). Using a calcium concentration of 50 mmol/L, a phytate concentration of 5 mmol/L, and a pH of 5.5 appeared to be an efficient set of conditions for precipitating the majority of phytate as calcium phytate. The bulk production of calcium phytate could then be followed up by investigating its ability to precipitate contaminants. Finally, bulk calcium phytate production could also be used as a precursor for producing calcium hydroxyapatite by other means such as (hydro)thermal methods (e.g. (251,541)).

4.2.5 Manganese

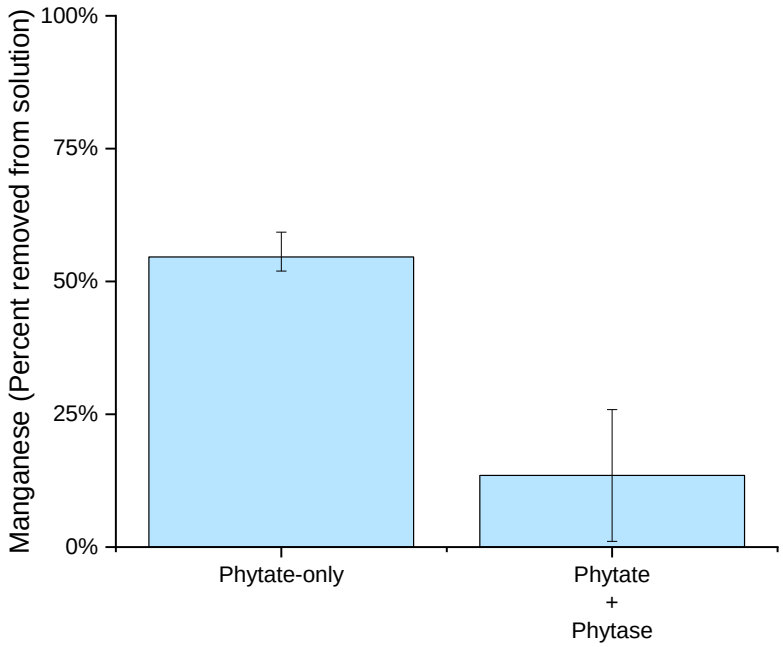

Figure 4.12 Percentage of manganese removed from solution in the different treatments. Columns represent the mean of triplicate samples for the phytate-only treatment and duplicate samples for the phytate + phytase treatment, error bars represent the difference between the mean and the upper and lower measured values.

In the phytate-only treatment, between 50 and 60% of manganese was removed from solution (figure 4.12). For the phytate + phytase treatment there was a large variation between the two data points, with either 1% or 26% of manganese removed from solution. The increase in manganese solubility coincided with the release of inorganic phosphate from phytate.

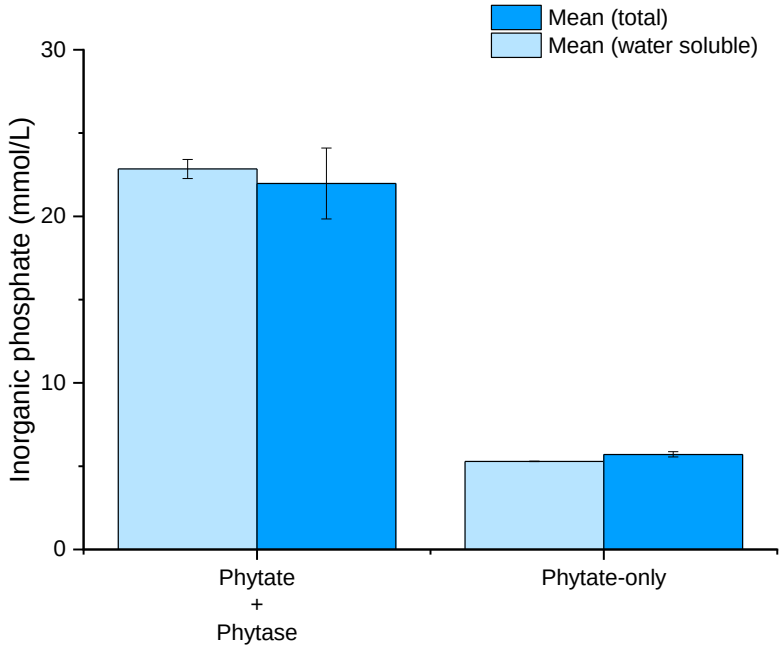

Figure 4.13 Water-soluble and total inorganic phosphate in the different treatments for the manganese experiments. Columns represent the mean of triplicate samples for the phytate-only treatment and duplicate samples for the phytate + phytase treatment, error bars represent the difference between the mean and the upper and lower measured values.

Phosphate release from phytate occurred successfully in the phytate + phytase treatment, while inorganic phosphate concentrations remained at approximate background levels in the phytate-only treatment (figure 4.13). The inorganic phosphate data (figure 4.13) indicate that, where precipitation occurred, it was most likely associated with the organic phosphate fraction. However, analytical issues encountered during ICP-OES analysis meant that organic phosphate concentrations could not be calculated for this batch of samples.

Geochemical modelling of saturation indices indicated a similar level of supersaturation for manganese phosphates ($Mn(HPO_4)$ and $Mn_3(PO_4)_2.3H_2O$) and manganese phytate ($Mn_5H_2Phytate.16H_2O$) (appendix G, table G.5). The model indicated that saturation indices increased in the phytate + phytase treatment, but this is contradicted by chemical analyses indicating higher manganese solubility in this treatment (figure 4.12). Also supersaturated were manganese dioxide (MnO_2), manganite (MnOOH), and for the phytate + phytase treatment, hausmannite (Mn_3O_4) (appendix G, table G.5). These manganese oxides/hydroxides all contain oxidised manganese in either the +3 and/or +4 state. However, solution modelling (appendix G, table G.5) indicated that manganese was mainly present in the +2 state and that negligible oxidised manganese was present. However, it would be useful to perform control experiments

without any phosphate source to test whether any of the oxides or oxyhydroxide phases are likely to precipitate under the tested conditions.

It has been previously suggested that phosphate amendments could be an effective method of reducing concentrations of bioavailable manganese in soils (117,337). However, while both treatments did remove manganese from solution, a large proportion of manganese remained soluble and was above the health-based value of 0.007 mmol/L that has been suggested (437).

These results indicate that, in some cases, phytate may be a more efficient sequestering agent than inorganic phosphate. If this direction is to be pursued, then further experiments to optimise the manganese:phytate ratio would be the first place to start, as metal:phytate ratios of 1:1 (close to that used in these experiments) typically favour a more soluble product (230,512), while the optimal ratio is more likely to be around 5:1 (542).

For the precipitation of inorganic manganese phosphates, it would be desirable to understand the apparent lack of precipitation despite manganese phosphates being supersaturated in geochemical models. Possible explanations include precipitation kinetics for these phases being relatively slow or a contribution from residual phytate/inositol phosphate molecules inhibiting precipitation. Ideally, further controls would be performed with the direct addition of inorganic phosphate to test this.

4.2.6 Iron (II)

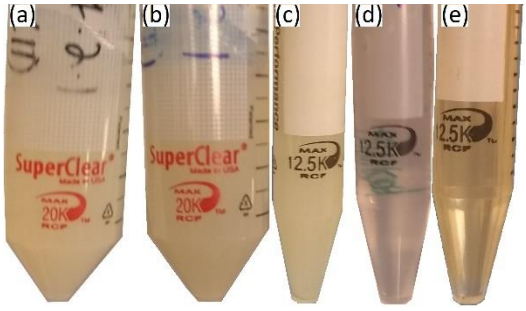

Figure 4.14 Photographs showing (a) Phytate-only, (b) Phytate + phytase, and (c) Inorganic phosphate treatments after 24 hours; (d) initial appearance of no phosphate treatment, and (e) No phosphate treatment after 24 hours.

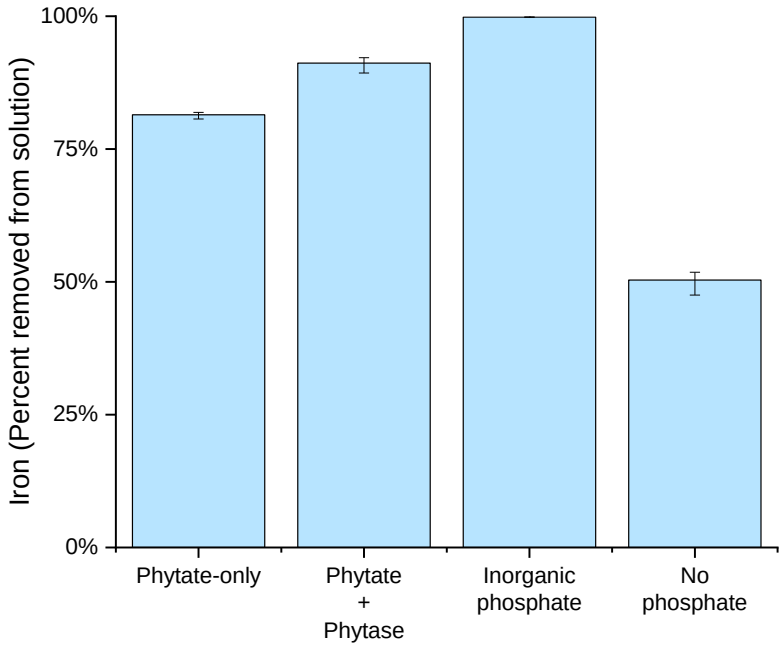

Figure 4.15 Percentage of iron (initially added as iron(II)) removed from solution. Columns represent the mean value of triplicate samples, error bars represent the difference between the mean and the upper or lower measured values.

Precipitation occurred immediately when mixing iron(II) solutions with phytate or inorganic phosphate to form a grey-white suspension (figure 4.14a, figure 4.14b). In contrast, the no phosphate treatment initially remained transparent (figure 4.14c), with an orange precipitate only forming after the overnight mixing period (figure 4.14d).

After 24 hours, around 50% of iron was removed from solution in the no phosphate treatment (figure 4.15). For the phytate + phytase and phytate-only treatments, around 90% and 80% of iron was removed,

respectively. Finally, in the inorganic phosphate treatment, around 99.8% of iron precipitated out of solution.

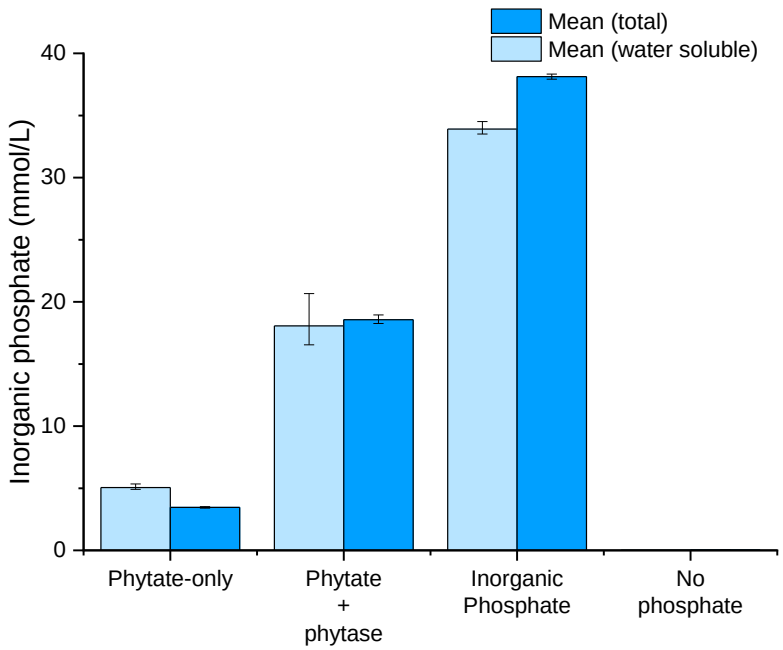

Figure 4.16 Comparison of water-soluble and total inorganic phosphate concentrations across the different conditions and treatments tested for the iron(II) experiments. Columns represent the mean of value of triplicate samples, error bars represent the difference between the mean and the upper and lower measured values.

Measurements of inorganic phosphate (figure 4.16) indicated that around 4 mmol/L inorganic phosphate precipitated for the inorganic phosphate treatment, while a low to negligible amount precipitated for the phytate + phytase and phytate-only treatments. Inorganic phosphate concentrations for the no phosphate control were close to or below the colorimetric detection limit (< 0.02 mmol/L when accounting for sample dilution factors). For the phytate-only samples, total inorganic phosphate concentrations were measured as lower than water-soluble concentrations. It is uncertain where the error here was sourced, dilution errors introduced when attempting to fully dissolve the precipitate may have been responsible.

Table 4.4 Calculated water-soluble and total organic phosphate concentrations for the iron(II) experiments. Values are given as the mean of triplicate samples, columns designated as + and – represent the difference between the mean value and the upper or lower measured value respectively.

Treatment	Water-soluble			Total		
	Mean	+	-	**Mean**	+	-
Phytate-only	**17.32**	*0.04*	*0.03*	**33.58**	*0.05*	*0.06*
Phytate + phytase	**5.73**	*0.60*	*0.43*	**18.47**	*0.31*	*0.38*
Inorganic Phosphate	**-3.98**	*1.25*	*0.88*	**-7.62**	*0.20*	*0.20*
No phosphorus	**-0.01**	*0.01*	*0.01*	**-0.02**	*0.01*	*0.01*

Quality control issues during ICP-OES analysis meant that organic phosphate concentrations were likely overestimates for the phytate + phytase and phytate-only treatments (table 4.4). However, comparing the water-soluble and total concentrations can be used to indicate that the majority of precipitation in the phytate-only and phytate + phytase treatments was associated with the organic phosphate fraction rather than inorganic phosphate.

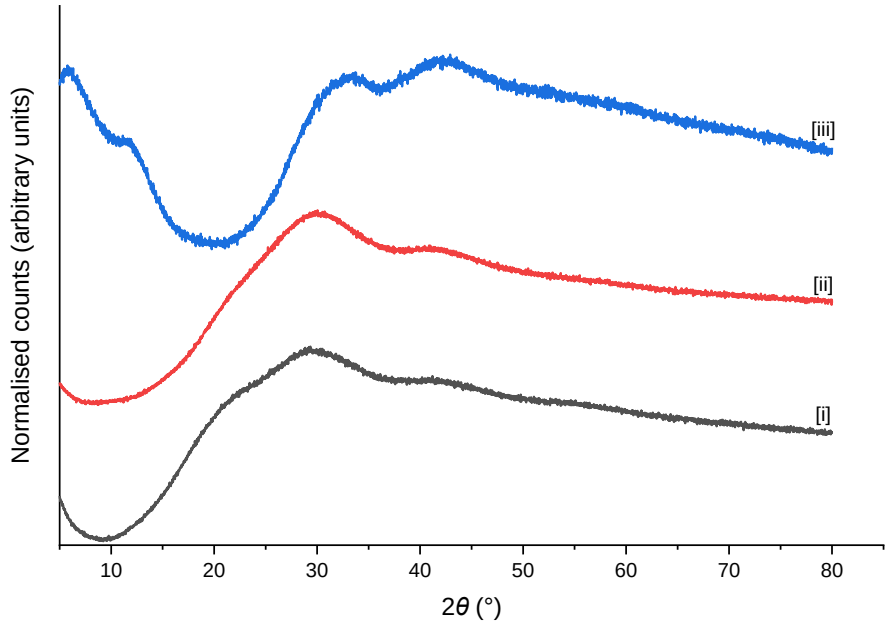

Figure 4.17 XRD patterns of precipitates produced in the iron(II) experiments showing [i] phytate-only; [ii] phytate + phytase; and [iii] inorganic phosphate treatments. Patterns [i] and [ii] were measured using the Göbel mirror optics setup, pattern [iii] was measured using the motorised slit. Samples were measured using the copper K_α radiation across a 2θ range of 5–80° with a step size of 0.02° and a step time of 1 s. Patterns were normalised in OriginPro 2019b to a scale of 0 to 1.

Solid phase analysis could not be performed on the precipitation formed in the no phosphate treatment as the physical amount of precipitate produced was small, and what precipitation did occur stuck to the

sides of the centrifuge tubes used and could not be recovered. XRD analysis of the other precipitates produced indicated that all were amorphous solids (figure 4.17).

Geochemical modelling indicated that iron(II) phosphates were supersaturated in the phytate-only, phytate + phytase, and inorganic phosphate treatments, while hematite (Fe_2O_3) was the only supersaturated phase in the no phosphate treatment (appendix G, table G.7). As discussed in the appendix, there were a number of limitations with the model – including a lack of solubility products for iron phytates, and not accurately accounting for iron(II) oxidation.

These experiments indicated that, when initially supplied as iron(II), inorganic phosphate, phytate-only, and phytate + phytase treatments can rapidly remove the majority of iron from solution. In contrast, over the same period, the precipitation of iron in the absence of any phosphate source was limited. The likely products formed were a mixed iron(II)/iron(III) phytate for the phytate + phytase and phytate-only treatments, an amorphous iron(II)/iron(III) hydroxyphosphate for the inorganic phosphate treatment, and an iron(III) oxide such as hematite for the no phosphate treatment.

The precipitation of iron was most efficient in the inorganic phosphate treatment, which was the only treatment to bring iron concentrations to below the suggested value (35.8 μmol/L) for drinking water (437). The formation of soluble complexes with phytate and/or lower inositol phosphates formed during phytate breakdown likely explains the incomplete iron precipitation in the phytate containing treatments.

Further work is required to characterise the nature of the precipitates in more detail (including a quantification of iron(II)/iron(III) ratios), investigate their long term stability against dissolution/leaching, and to test their potential contaminant-incorporation properties. Additionally, it may be desirable to optimise the iron:phytate ratio to improve iron precipitation.

4.2.7 Iron (III)

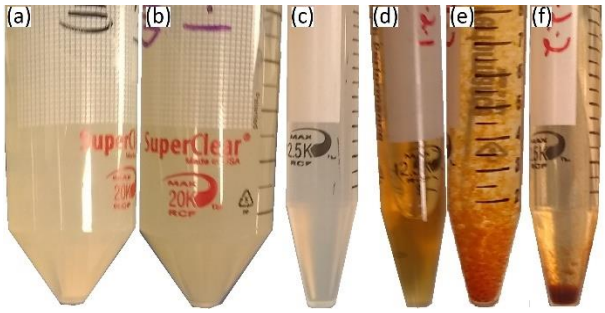

Figure 4.18 Photographs showing (a) Phytate-only, (b) Phytate + phytase, and (c) Inorganic phosphate treatments after 24 hours; (d) initial appearance of no phosphate treatment, (e) No phosphate treatment after adjusting to pH 5.5, and (f) No phosphate treatment after 24 hours.

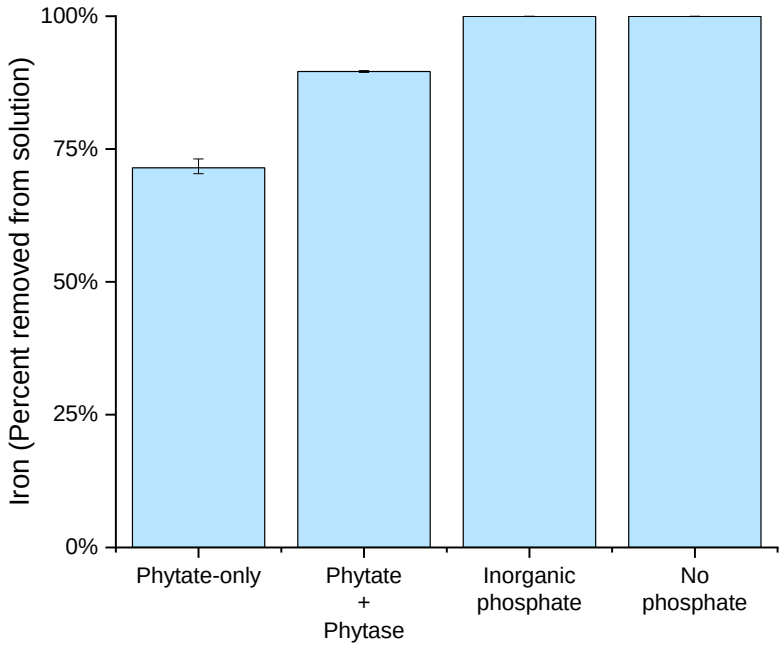

Figure 4.19 Percentage of iron (initially added as iron(III)) removed from solution in the different treatments. Columns represent the mean value of triplicate samples, error bars represent the difference between the mean and the upper or lower measured values.

Precipitation occurred immediately upon mixing iron(III) with phytate or inorganic phosphate to form a pale orange-white suspension (figure 4.18a, figure 4.18b). When preparing the no phosphate treatment, the solution (at an initial pH of 5.2) appeared clear (figure 4.18c), but when adjusting to the desired pH of ~ 5.5 precipitation occurred upon the addition of KOH (figure 4.18d).

More than 99.9% of iron was removed from solution in the no phosphate and inorganic phosphate treatments (figure 4.19). All three samples in the inorganic phosphate treatment were below the ICP-OES detection limit (< 0.26 µmol/L or < 2.9 µmol/L depending on dilution factor used). For the no

phosphate treatment two samples were below the detection limit (< 2.9 µmol/L for the dilution factor used) while the third sample was measured as containing 0.31 µmol/L iron, very close to the detection limit of 0.26 µmol/L.

The phytate + phytase and phytate-only treatments were less effective than the controls, with around 90% and 70% of iron removed from solution respectively (figure 4.19).

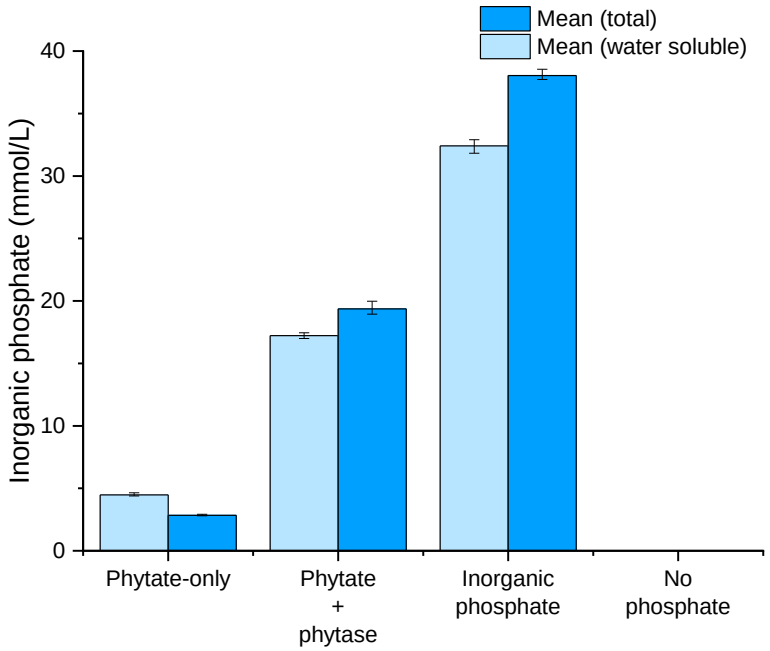

Figure 4.20 Comparison of water-soluble and total inorganic phosphate concentrations across the different conditions and treatments tested for the iron(III) experiments. Columns represent the mean of value of triplicate samples, error bars represent the difference between the mean and the upper and lower measured values.

Measurements of inorganic phosphate (figure 4.20) indicated that around 5.6 mmol/L inorganic phosphate precipitated for the inorganic phosphate treatment, compared to around 2.1 mmol/L for the phytate + phytase treatment and a low to negligible amount precipitated for the phytate-only treatment. Inorganic phosphate concentrations for the no phosphate control were close to or below the colorimetric detection limit (< 0.02 mmol/L when accounting for sample dilution factors). For the phytate-only samples, total inorganic phosphate concentrations were measured as lower than water-soluble concentrations which is likely associated with analytical error.

Table 4.5 Calculated water-soluble and total organic phosphate concentrations for the iron(III) experiments. Values are given as the mean of triplicate samples, columns designated as + and – represent the difference between the mean value and the upper or lower measured value respectively.

Treatment	Water-soluble			Total		
	Mean	*+*	-	**Mean**	*+*	-
Phytate-only	**19.95**	*0.94*	*0.98*	**30.14**	*0.04*	*0.08*
Phytate + phytase	**5.65**	*0.27*	*0.46*	**13.61**	*0.42*	*0.61*
Inorganic Phosphate	**-2.94**	*2.07*	*1.91*	**-4.47**	*0.31*	*0.51*
No phosphorus	**-0.06**	*0.06*	*0.10*	**0.03**	*0.00*	*0.00*

As discussed above, ICP-OES issues led to likely overestimates for organic phosphate concentrations for the phytate-only and phytate + phytase treatments and calculated negative concentrations for the inorganic phosphate treatment. However, comparing the water-soluble and total concentrations indicates that precipitation in the phytate-only and phytate + phytase treatments was mostly associated with the organic phosphate fraction rather than inorganic phosphate.

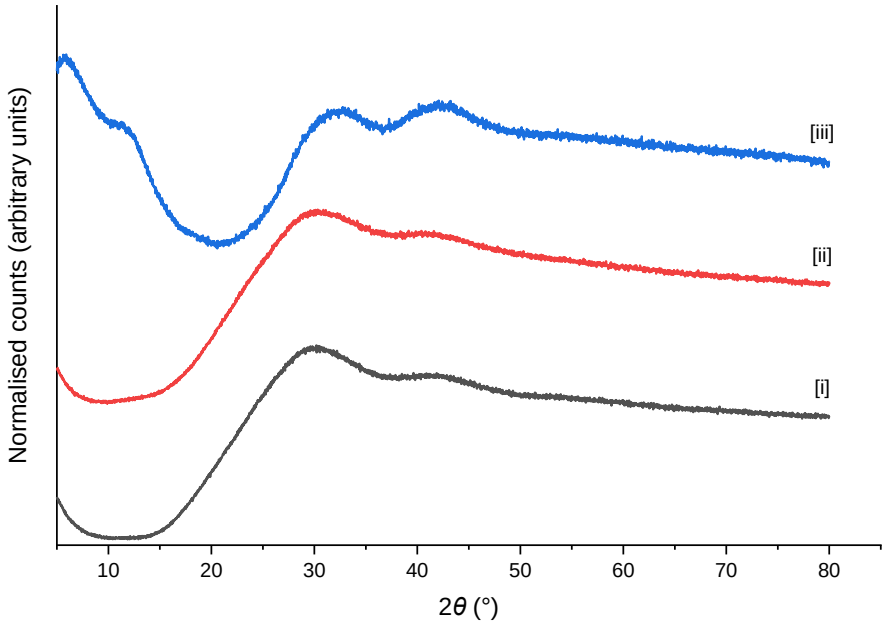

Figure 4.21 XRD patterns of precipitates produced in the iron(III) experiments showing [i] phytate-only; [ii] phytate + phytase; and [iii] inorganic phosphate treatments. Patterns [i] and [ii] were measured using the Göbel mirror optics setup, pattern [iii] was measured using the motorised slit. Samples were measured using the copper K_α radiation across a 2θ range of 5–80° with a step size of 0.02° and a step time of 1 s. Patterns were normalised in OriginPro 2019b to a scale of 0 to 1.

Solid phase analysis could not be performed on the precipitation formed in the no phosphate treatment as the physical amount of precipitate produced was small and remained stuck to the walls of the centrifuge tubes. XRD analysis of the other precipitates produced indicated that all were amorphous

solids (figure 4.21). For the phytate + phytase and phytate-only treatments, this is consistent with previous descriptions of iron(III) phytate (228,543). Previous researchers have also described the crystallisation kinetics of iron(III) phosphates as being very slow (432), so it is unsurprising that an amorphous material was produced in a 24 hour experiment at room temperature for the inorganic phosphate treatment.

As with aluminium, geochemical modelling indicated a strong inhibition of iron(III) hydrolysis in the presence of phytate (appendix G, table G.10). Saturation indices indicated that iron (hydroxy)phosphates were supersaturated in the presence of phosphate and iron (oxyhydr)oxides were supersaturated in all simulations (appendix G, table G.9).

As with iron(II), inorganic phosphate, phytate, and phytate treated with a phytase enzyme were all able to rapidly remove the majority of iron (initially supplied as iron(III)) from solution. In contrast to the iron(II) experiments, the phosphate-free control also saw the majority of iron removed from solution. As with iron(II) and aluminium, the phytate + phytase and phytate-only treatments were less efficient than the direct addition of inorganic phosphate. It appears that this is likely due to the inhibition of iron hydrolysis and formation of soluble complexes by phytate and/or lower inositol phosphates. As the no phosphate and inorganic phosphate treatments were the only ones to reduce iron concentrations to below suggested water limits (35.8 µmol/L) (437) further optimisation of phytate-based strategies would be required for the treatment of contaminated media containing high levels of iron.

Further work may also try to characterise the nature of the precipitates in more detail, investigate their long term stability against dissolution/leaching, and to test their potential contaminant-incorporation properties. Experiments at lower pH values (below pH 2) would also be interesting. Iron(III) hydroxides generally only precipitate above pH 2 where iron(III) phytates (543) and iron(III) phosphates (432) may still be insoluble below this value. Therefore, low pH studies would allow the examination of interactions between phytate, phosphate, and phosphate released from phytate in the absence of metal hydrolysis. This may then have applicability in the treatment of highly acidic iron-containing waste waters.

4.2.8 Cobalt

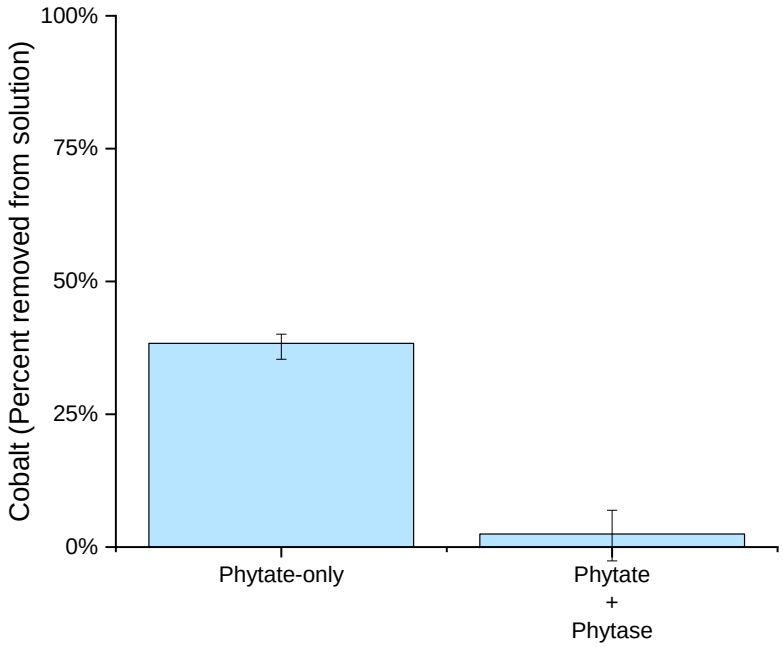

Figure 4.22 Percentage of cobalt removed from solution in the different treatments. Columns represent the mean value of triplicate samples, error bars represent the difference between the mean and the upper or lower measured values.

Precipitation occurred immediately upon mixing cobalt with phytate, but phytase treatment over the course of 24 hours appeared to return most of this to solution. Analysis indicated that around 40% of cobalt was removed from solution in the phytate-only treatment, while less than 10% was removed in the phytate + phytase treatment (figure 4.22).

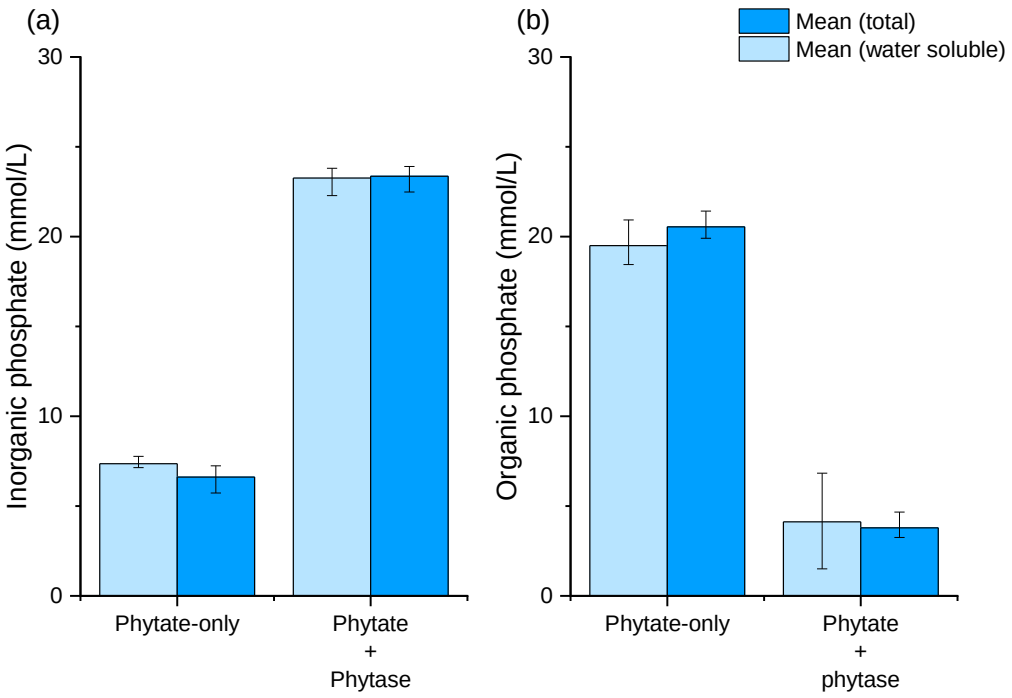

Figure 4.23 Comparison of water-soluble and total concentrations of (a) inorganic phosphate, and (b) organic phosphate across different treatments for the cobalt experiments. Columns represent the mean of value of triplicate samples, error bars represent the difference between the mean and the upper and lower measured or calculated values.

Measured values of inorganic phosphate (figure 4.23a) and calculated values of organic phosphate (figure 4.23b) gave values for water-soluble and total fractions that appeared to be the same, within the margins of analytical variability, indicating low amounts of phosphate precipitation.

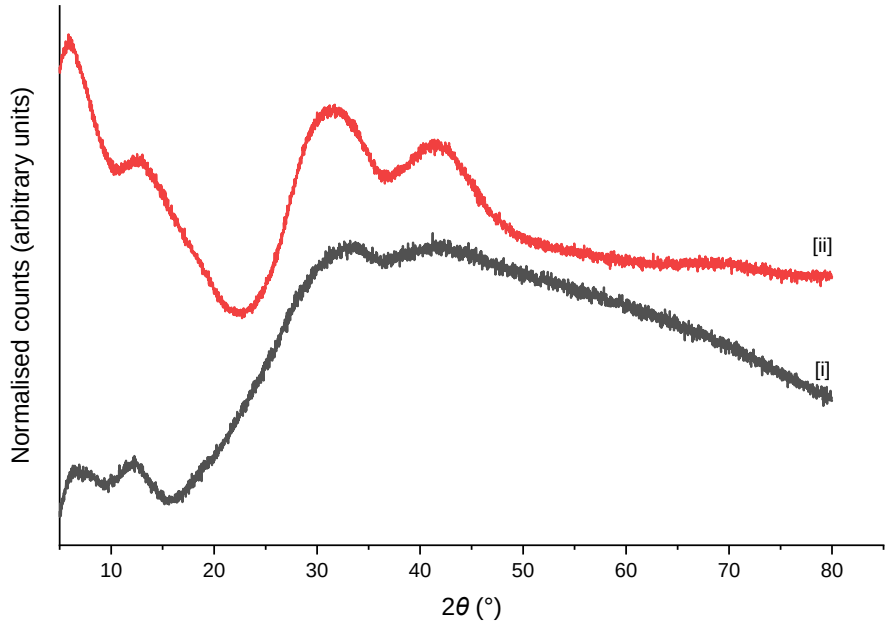

Figure 4.24 XRD patterns of precipitates produced in the cobalt experiments showing [i] phytate-only; and [ii] phytate + phytase treatments. Patterns were measured using the motorised slit optics setup. Samples were measured using the copper K_α radiation across a 2θ range of 5–80° with a step size of 0.02° and a step time of 1 s. Patterns were normalised in OriginPro 2019b to a scale of 0 to 1.

XRD analysis of the precipitates indicated amorphous materials, consistent with previous reports of cobalt phytate (543) (figure 4.24). The high background observed for the phytate-only precipitate is a result of fluorescence from the interaction of the copper X-rays with cobalt (504). The lack of such a background for the phytate + phytase treatment indicates that there was probably not enough material present to record a signal. Geochemical modelling indicated supersaturation for cobalt phosphate ($Co_3(PO_4)_2$) and Co_3O_4, with saturation indices increasing in the phytate + phytase treatment compared to the phytate-only treatment (appendix G, table G.11). This does not correspond to the experimental results, and it is likely that solubility product data for cobalt phytate would be required to model the system more accurately.

These results indicate that, under the conditions tested, neither phytate nor phytate treated with phytase are efficient mechanisms of removing cobalt from solution, with soluble cobalt remaining above suggested water limits in the range of 0.07–19 µmol/L (470,472) . The phytate-only treatment was more promising, with 40% of cobalt removed from solution, and this could potentially be improved be adjusting the cobalt:phytate ratio to 5:1 (544) compared to the 1.3:1 ratio used in this work.

Additionally, controls without added phosphate and with the direct inorganic phosphate would also be useful for comparative purposes.

4.2.9 Copper

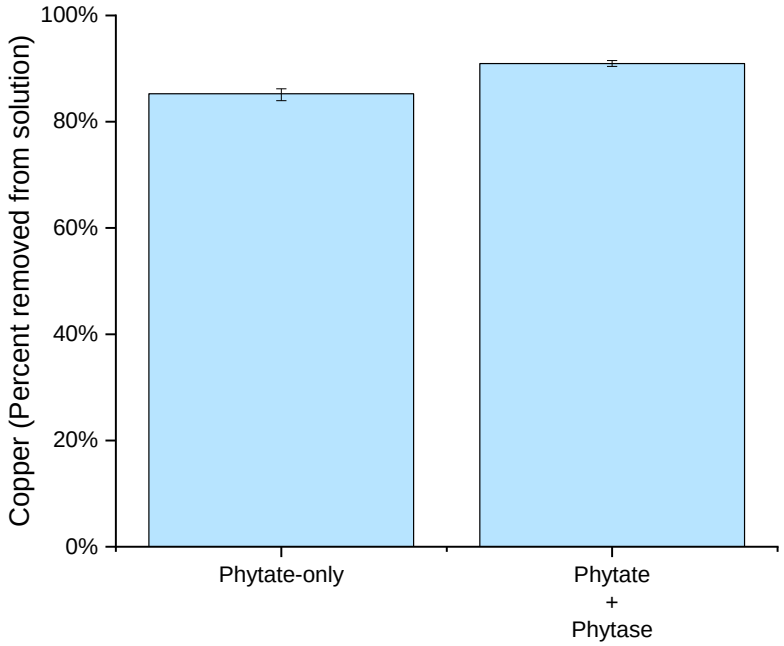

Figure 4.25 Percentage of copper removed from solution in the different treatments. Columns represent the mean value of triplicate samples, error bars represent the difference between the mean and the upper or lower measured values.

Both treatments removed similar amounts of copper from solution, with around 85% of the copper precipitating in the phytate-only treatment and around 90% precipitating in the phytate + phytase treatment (figure 4.25).

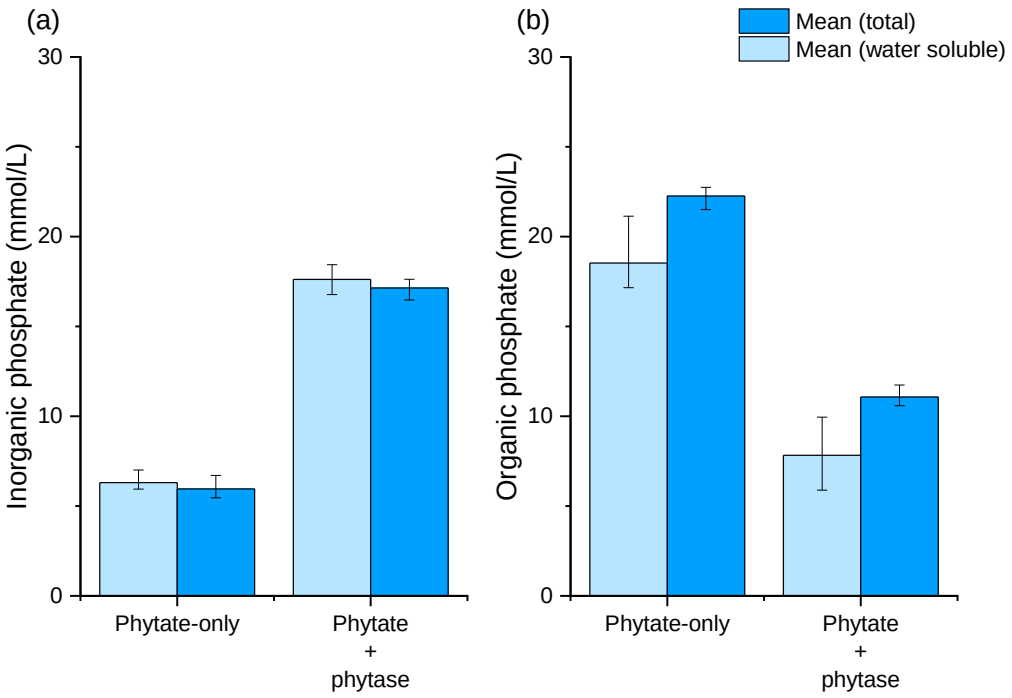

Figure 4.26 Comparison of water-soluble and total concentrations of (a) inorganic phosphate, and (b) organic phosphate across different treatments for the copper experiments. Columns represent the mean of value of triplicate samples, error bars represent the difference between the mean and the upper and lower measured or calculated values.

Measurements of inorganic phosphate indicated that water-soluble and total concentrations were effectively the same (figure 4.26a), indicating that inorganic phosphate precipitation was low. Calculated organic phosphate values (figure 4.26b) indicated that around 30% (~ 3.2 mmol/L) of organic phosphate precipitated in the phytate + phytase treatment compared to around 20% (~ 3.7 mmol/L) in the phytate-only treatment, suggesting that copper precipitation was associated with the organic phosphate fraction.

Table 4.6 Concentrations of analytes removed from solution into precipitated solids, given in terms of mmol per litre of experimental solution. Values are given as the mean of triplicate samples, columns designated as + and – represent the difference between the mean value and the upper or lower measured value respectively. The phytate concentration was calculated on the assumption that 100% of the organic phosphate in the system was present as phytate and that 1 mmol of phytate = 6 mmol of phosphate.

Treatment	Inorganic phosphate			Organic phosphate			Copper			Potassium		
	Mean	+	–	Mean	+	–	Mean	+	–	Mean	+	–
Phytate-only	**-0.35**	*0.10*	*0.15*	**3.72**	*1.72*	*2.35*	**4.29**	*0.05*	*0.07*	**1.41**	*22.56*	*32.51*
Phytate + phytase	**-0.47**	*0.17*	*0.34*	**3.24**	*1.76*	*1.46*	**4.58**	*0.03*	*0.03*	**-9.39**	*21.68*	*35.41*

Large variability in the concentrations of phosphate measured by ICP-OES made the calculations of the amount of organic phosphate precipitating challenging. Based upon the mean organic phosphate values, the precipitates from both treatments had copper:organic phosphate ratios of around 1.3:1, which corresponds to a copper:phytate ratio of about 8:1 (figure 4.6). As the maximum number of copper atoms that can be bound to a single phytate molecule is 6 this suggests either errors in the measurements of phosphate concentrations or coprecipitation of copper as hydroxide and/or sulfate phases. Large variability in potassium measurements suggested that any potassium precipitation was low.

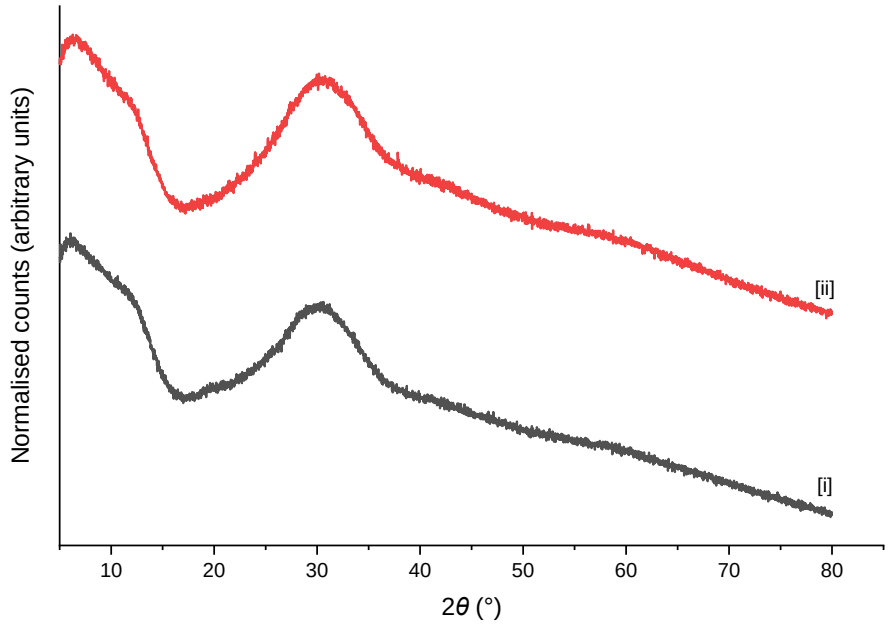

Figure 4.27 XRD patterns of precipitates produced in the copper experiments showing [i] phytate-only; and [ii] phytate + phytase treatments. Patterns were measured using the motorised slit optics setup. Samples were measured using the copper K_α radiation across a 2θ range of 5–80° with a step size of 0.02° and a step time of 1 s. Patterns were normalised in OriginPro 2019b to a scale of 0 to 1.

The XRD patterns indicated that the materials were amorphous (figure 4.27), as has previously been described for copper phytate (543). Geochemical modelling calculated that multiple copper (hydroxy)phosphates were supersaturated for both treatments, along with a copper hydroxysulfate (appendix G, table G.13). Copper oxides and hydroxides were all undersaturated. The model was limited by the lack of solubility product data for copper phytate, but it is likely that copper phytate was supersaturated under the conditions tested (545). Furthermore, solution modelling indicated that

around 50% of copper was bound to phytate (with the remaining 50% as free Cu^{2+}), even after phytate hydrolysis had been simulated (appendix G, table G.14).

The lack of copper phosphate precipitation was likely a result of the strength of copper binding by phytate. Previous research has indicated that the crystallisation rate of copper phosphates is extremely slow (2 months at 37 °C in the absence of crystallisation inhibitors (115). As phytate is a well-known crystallisation inhibitor (266,322,323,327), the crystallisation rates for copper phosphates may be even slower in the presence of phytate or lower inositol phosphates. The very slight improvement in copper removal in the phytate + phytase treatment may be related to the reduced amount of phytate allowing small amounts of precipitation of amorphous copper hydroxyphosphate or copper hydroxysulfate species.

In these experiments, phytate or phytate treated with phytase was able to remove the majority of copper from solution, although values were still around an order of magnitude higher than the recommended drinking water limit of 31.5 µmol/L (437). In both cases, copper appeared to be mostly associated with the organic phosphate fraction. This indicates that phytate could be an effective sequestering agent for the removal of copper from wastewaters, although further work is required if the transformation of copper phytates into copper phosphates is to be achieved.

Copper was the most effective inhibitor of phytase activity out of all the metals investigated in this project (figure 4.1) which limits the transformation of phytate into inorganic phosphate. Further work should look at whether increasing the amount of enzyme could overcome this limitation or if alternative sources of phytase would need to be looked at. Additionally, controls comparing these treatments to a phosphate-free system and a system where phosphate is directly added in an inorganic form would be useful. The stability of the precipitates against leaching and any contaminant incorporation properties should also be investigated.

The potential indication of copper-catalysed phytate hydrolysis is also interesting, although further tests would be required to test that the increase background level of inorganic phosphate was not due to hydrolysis in the phytic acid stock. If copper does catalyse phytate hydrolysis, then it may be interesting to investigate the use of copper phytate as a precursor for the formation of the highly insoluble torbernite mineral ($Cu(UO_2)_2(PO_4)_2.8–12H_2O$).

4.2.10 Barium

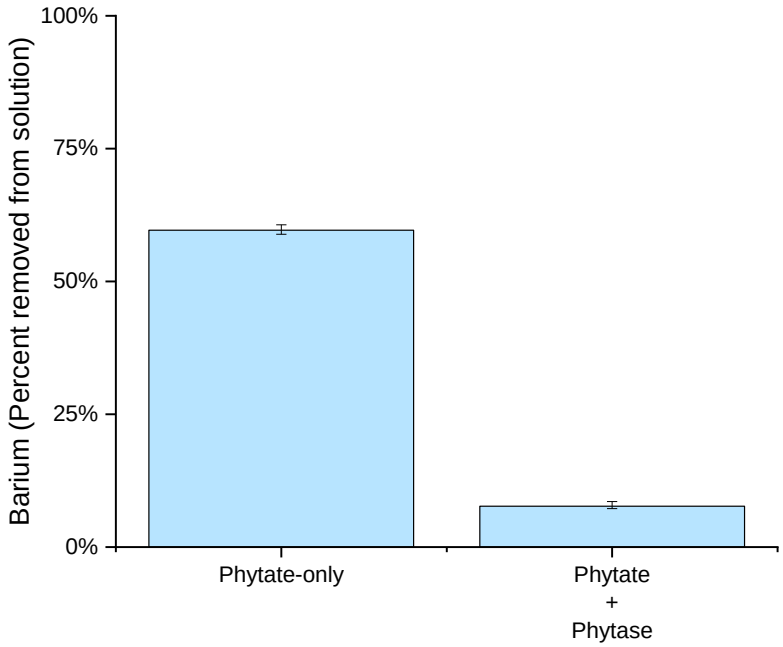

Figure 4.28 Percentage of barium removed from solution in the different treatments. Columns represent the mean value of triplicate samples, error bars represent the difference between the mean and the upper or lower measured values.

In the phytate-only treatment, around 60% of barium was removed from solution, while less than 10% precipitated in the phytate + phytase treatment (figure 4.28).

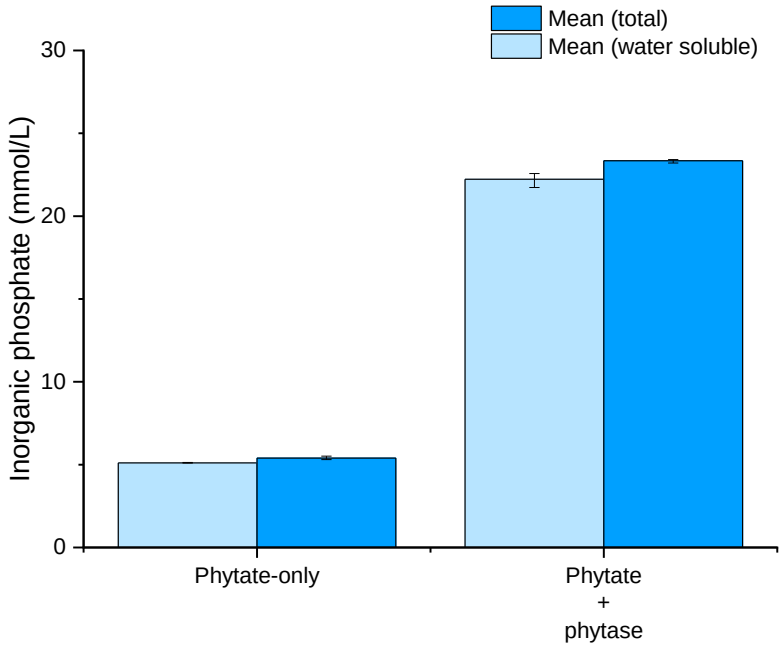

Figure 4.29 Comparison of water-soluble and total inorganic phosphate concentrations across the different conditions and treatments tested for the barium experiments. Columns represent the mean of value of triplicate samples, error bars represent the difference between the mean and the upper and lower measured values.

Table 4.7 Water-soluble and total organic phosphate concentrations from the barium experiments. Values are given as the mean of triplicate samples, columns designated as + and – represent the difference between the mean value and the upper or lower measured value respectively.

Treatment	Water-soluble			Total		
	Mean	*+*	-	**Mean**	*+*	-
Phytate-only	**18.41**	*0.94*	*1.09*	**28.11**	*0.09*	*0.12*
Phytate + phytase	**4.13**	*0.29*	*0.54*	**10.16**	*0.14*	*0.07*

Measurements of inorganic phosphate indicated that phosphate release from phytate occurred successfully in the presence of barium (figure 4.29). Analytical variability influenced the organic phosphate calculations, but, comparing the water-soluble and total fractions indicated that, where precipitation occurred, it was likely associated with organic phosphate (table 4.7).

Due to the low amount of precipitation, solid phase characterisation was not performed for the barium experiments. Geochemical modelling indicated that the only supersaturated phases were barium phytate and barium hydrogen phosphate (appendix G, table G.15). Saturation indices increased following simulated phytase treatment, which is contradicted by the experimental results, indicating that more comprehensive thermodynamic data are required.

These results indicate that, at mildly acidic pH values, phytate may be a more effective sequestering agent for barium than inorganic phosphate. However, in both cases, barium concentrations remained above the recommended value of 5.1 µmol/L (437). As these experiments were not designed with using phytate as a precipitating agent being the primary aim, it may be interesting to pursue this angle in more detail. In particular, the metal:phytate ratio is known to be important in determining the solubility of metal phytate complexes. These experiments were setup with a metal:phytate ratio of 1.3:1, and 1:1 complexes are known to usually be relatively soluble (540). Reducing the phytate concentration to give, for example, a ratio between 2:1 and 6:1 may improve metal removal further.

4.2.11 Lanthanum

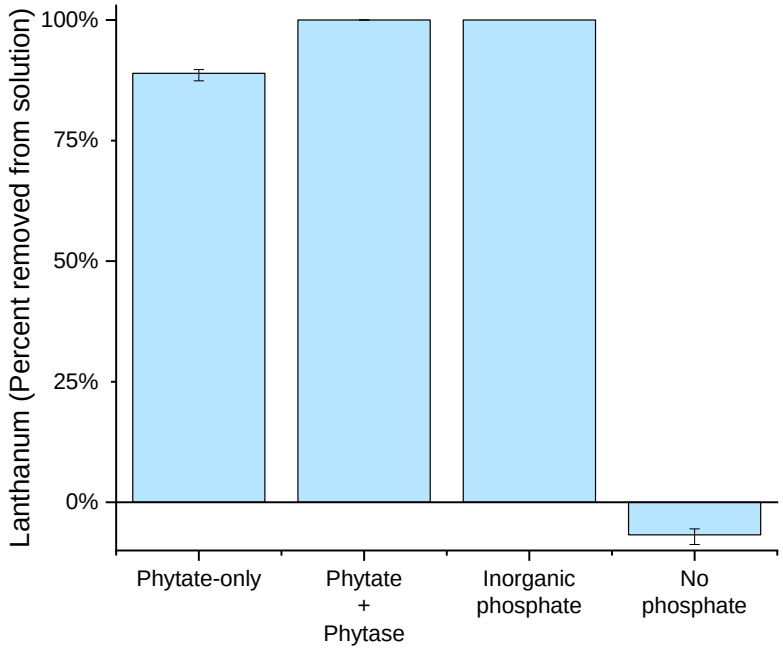

Figure 4.30 Percentage of lanthanum removed from solution in the different treatments. Columns represent the mean value of triplicate samples, error bars represent the difference between the mean and the upper or lower measured values.

The majority of lanthanum was removed from solution in the phytate-only, phytate + phytase, and inorganic phosphate treatments, while effectively all of the lanthanum remained soluble in the no phosphate treatment (figure 4.30). For the inorganic phosphate treatment, all samples gave lanthanum concentrations below the ICP-OES detection limit (< 0.029 µmol/L when accounting for dilution factors), while for the phytate + phytase treatment, measured lanthanum values (between 0.04 and 0.30 µmol/L) were very slightly higher than the detection limit. Lanthanum removal was less efficient for the phytate-

only treatment, with around 89% of lanthanum removed from solution, leaving around 0.56 mmol/L lanthanum in solution.

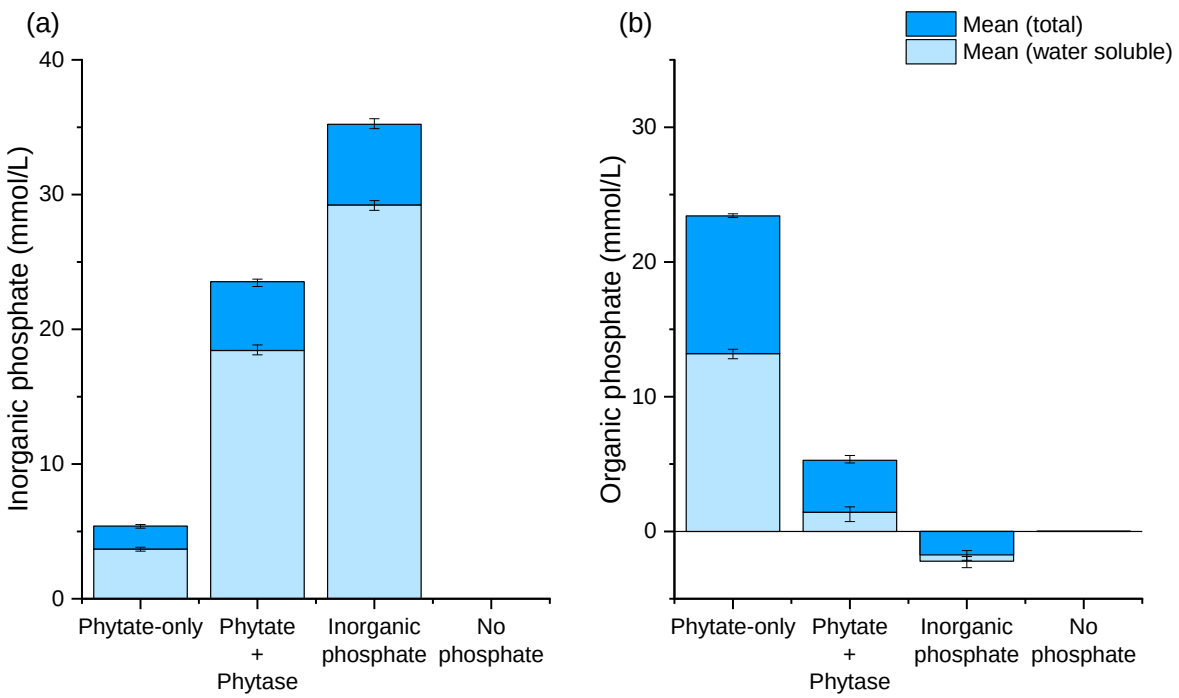

Figure 4.31 Comparison of water-soluble and total concentrations of (a) inorganic phosphate, and (b) organic phosphate across different treatments for the lanthanum experiments. Columns represent the mean of value of triplicate samples, error bars represent the difference between the mean and the upper and lower measured or calculated values.

Measurements of inorganic phosphate (figure 4.31a) and calculated values for organic phosphate (figure 4.31b) indicated that phosphate release from phytate occurred successfully in the phytate + phytase treatment. Around 5.1 mmol/L inorganic phosphate and around 3.9 mmol/L organic phosphate precipitated for the phytate + phytase treatment. In the phytate-only treatment, around 1.7 mmol/L inorganic phosphate and around 10.2 mmol/L organic phosphate (equivalent to 1.7 mmol/L phytate) precipitated. For the inorganic phosphate treatment, around 6.0 mmol/L inorganic phosphate precipitated out of solution.

Table 4.8 Concentrations of analytes incorporated into precipitated solids, given in terms of mmol/L of experimental solution. Values are given as the mean of triplicate samples, columns designated as + and – represent the difference between the mean value and the upper or lower measured value respectively. N.d. indicates not determined, n.c. indicates not calculated.

Treatment	Inorganic phosphate			Organic phosphate			Lanthanum			Potassium			Hydrogen	Carbon	Nitrogen
	Mean	*+*	*-*	**Mean**	*+*	*-*	**Mean**	*+*	*-*	**Mean**	*+*	*-*	**Mean**	**Mean**	**Mean**
Phytate-only	**1.70**	*0.09*	*0.09*	**10.18**	*0.27*	*0.36*	**4.53**	*0.04*	*0.08*	**1.77**	*0.26*	*0.33*	**38.75**	**12.09**	**0.81**
Phytate + Phytase	**5.10**	*0.24*	*0.21*	**3.82**	*0.54*	*0.60*	**5.10**	*0.00*	*0.00*	**0.23**	*0.07*	*0.12*	**26.60**	**6.67**	**0.42**
Inorganic phosphate	**5.99**	*0.81*	*0.40*	**n.c.**	*n.c.*	*n.c.*	**5.10**	*0.00*	*0.00*	**2.76**	*1.26*	*1.10*	**n.d.**	**n.d.**	**n.d.**

Chemical analyses indicated that, at most, around 0.2 mmol/L potassium precipitated in the phytate + phytase treatment, compared to around 1.8 mmol/L in the phytate-only treatment and around 2.8 mmol/L in the inorganic phosphate treatment (table 4.8). Of the other analytes measured, there was no evidence of sodium or sulfur precipitation (data not shown). Traces of magnesium, which may have been present as an impurity in the phytate stock, appeared to precipitate for the phytate-only (~ 0.08 mmol/L) and phytate + phytase (~ 0.03 mmol/L) treatments, while no magnesium was detected in the inorganic phosphate treatment (data not shown).

CHN analysis was also performed for the phytate + phytase and phytate-only treatments (table 4.8). Hydrogen and carbon concentrations were higher for the phytate-only treatment than the phytate + phytase treatment, likely associated with the higher proportion of organic phosphate precipitating in the former. Nitrogen also appeared to be present in the solids, but it is not certain where this came from – nitrogen was present in the MES ($C_6H_{13}NO_4S$) buffer used, but if the buffer had been incorporated into the solid phase, then sulfur should have also been detectable.

The phytate + phytase treatment had an inorganic phosphate:lanthanum ratio of 1.0:1.0 (table 4.8). However, as evidence suggested that organic phosphate, potassium, and magnesium also precipitated in this system, it is likely that the product was not a stoichiometric lanthanum phosphate (i.e. $LaPO_4.xH_2O$) but a complex mixture of inorganic and organic phosphate precipitated with lanthanum and the other metals in the system. The carbon:organic phosphate ratio of 1.7:1.0 (table 4.8) indicated that some of the organic phosphate in the precipitate was not present as phytate, but rather, as lower inositol phosphates. Phytate has a carbon:phosphate ratio of 1.0:1.0; in comparison, inositol tetrakisphosphates ($C_6H_{16}O_{18}P_4$) have a ratio of 1.5:1.0 and inositol trisphosphates ($C_6H_{15}O_{15}P_3$) have a

ratio of 2.0:1.0. Fully deprotonated inositol phosphates have a carbon:hydrogen ratio of 1.0:1.0. The excess of hydrogen to carbon indicates the presence of hydrogen phosphate groups and water molecules in the solid structure. The distribution between these forms of hydrogen is uncertain.

The phytate-only treatment had a carbon:organic phosphate ratio of 1.4:1.0 (table 4.8), which deviates from the expected ratio of 1.0:1.0 for pure phytate. This may be a result of analytical variability encountered in the ICP-OES measurement of phosphate content, errors associated with collecting the solid used for CHN analysis (see section 4.1.4.4), or be indicative of lower inositol phosphate impurities contained in the phytate stock used.

The inorganic phosphate treatment had an inorganic phosphate:lanthanum ratio of about 1.1:1.0 (table 25). The slight excess of phosphate to lanthanum may be a result of a mixed lanthanum-potassium phosphate phase being formed and/or due to sorbed phosphate (296).

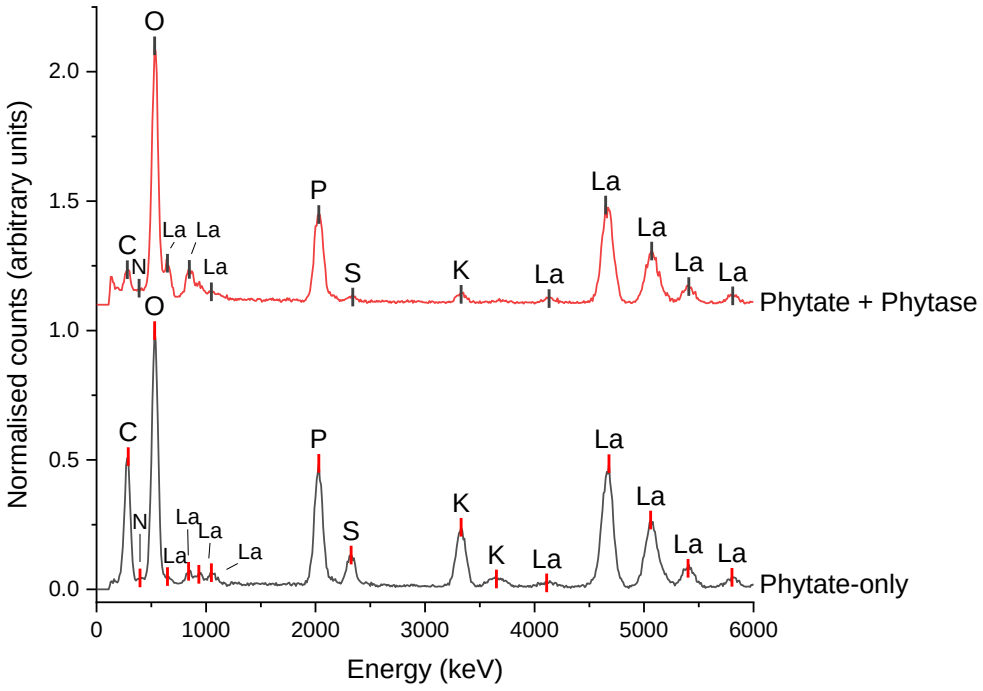

Figure 4.32 EDX spectra recorded during TEM analysis of precipitates produced in phytate-only and phytate + phytase treatments.

EDX spectra recorded during TEM analysis of samples produced in the phytate + phytase treatments confirmed the presence of oxygen, phosphorus, and lanthanum in the samples (figure 4.32). Both samples also showed signals for carbon, sulfur, and potassium but the peaks were notably higher for

the phytate-only treatment. A peak for nitrogen has also been labelled based upon CHN analysis indicating the presence of nitrogen, although it is difficult to observe this peak against the much larger signals for carbon and oxygen. In contrast to the chemical analyses (table 4.8), the EDX analysis appeared to confirm the presence of sulfur in the precipitate but showed no signs of detectable magnesium (figure 4.32). The only source of sulfur (and nitrogen) deliberately added to the experiments was in the form of the MES buffer so it appears likely that the buffer either sorbed onto or coprecipitated with the solid phases, and was preferentially incorporated into phytate rather than an inorganic phosphate precipitate. The alternate explanation could be the presence of nitrogen and sulfur impurities in the stock of phytate used.

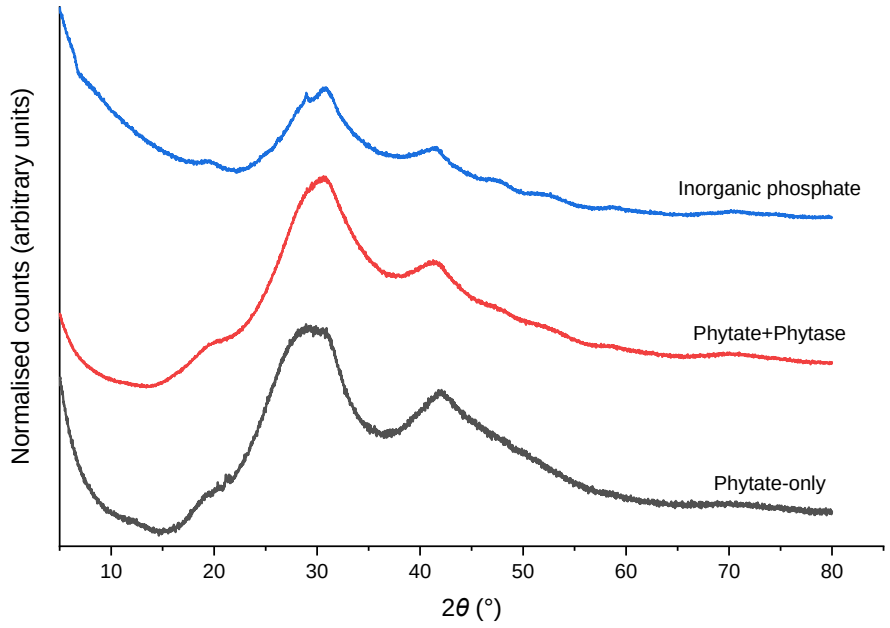

Figure 4.33 XRD patterns of precipitates produced in the lanthanum experiments showing [i] phytate-only; [ii] phytate + phytase; and [iii] inorganic phosphate treatments. Patterns were measured using the Göbel mirror optics setup. Samples were measured using the copper K_α radiation across a 2θ range of 5–80° with a step size of 0.02° and a step time of 1 s. Patterns were normalised in OriginPro 2019b to a scale of 0 to 1.

XRD patterns indicated amorphous or very poorly crystalline materials for all treatments (figure 4.33), except for the no phosphate treatment where no precipitate was recovered. This matches with previous XRD investigations of lanthanide phytates (279,344) but differs from previous investigations of lanthanum phosphates, where phases such as rhabdophane ($LaPO_4.0.667H_2O$) would be expected to form (113,296,339).

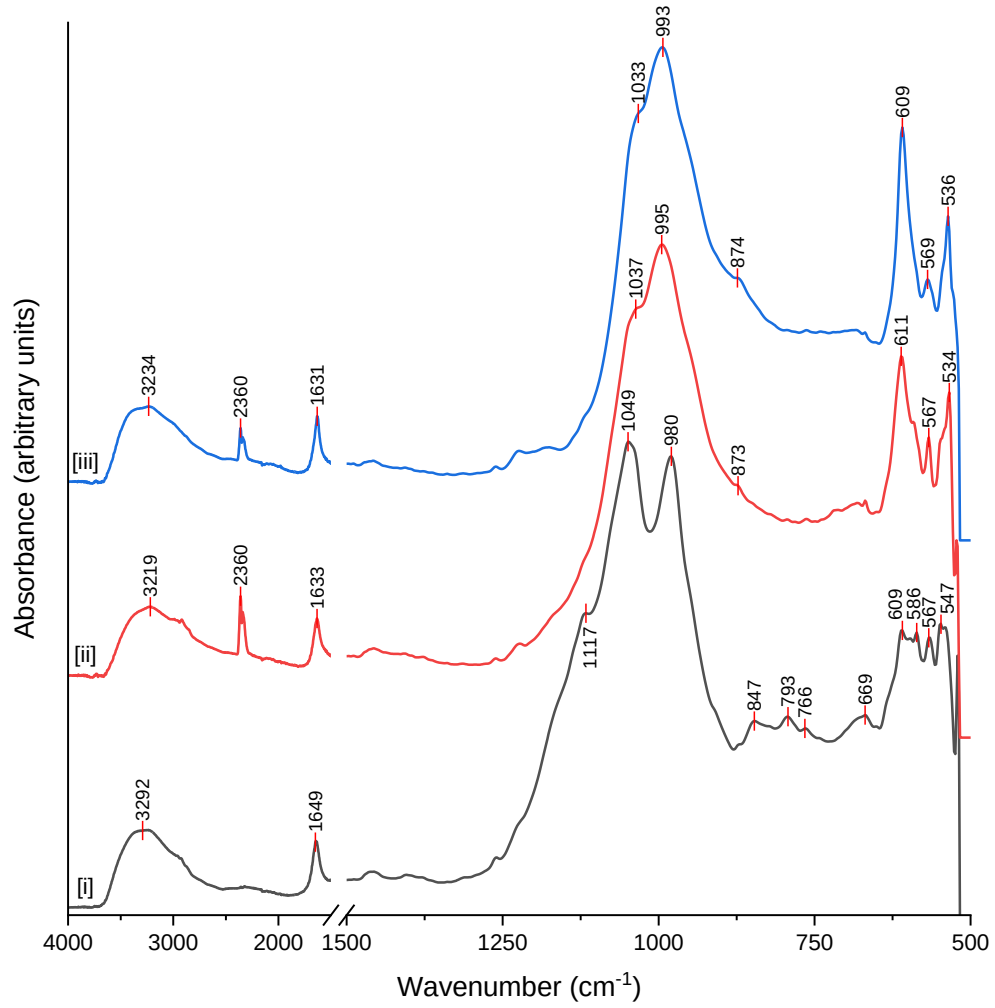

Figure 4.34 FTIR spectra of precipitates produced in [i] Phytate-only; [ii] Phytate + Phytase; [iii] and inorganic phosphate treatments for the lanthanum experiments. Spectra were normalised in OriginPro 2019b to a scale of 0–1.

FTIR spectra of samples produced in the lanthanum experiments are shown in figure 4.34. The functional group region (4,000–1,500 cm^{-1}) was broadly similar for all samples and was dominated by the signals for O–H stretching (the broad band around 3,200 cm^{-1}) and O–H bending (at ~ 1,640 cm^{-1}) associated with water molecules in the solid structure (407). Contamination from atmospheric CO_2 can be observed at around 2,360 cm^{-1} (407).

The fingerprint region (1,500–500 cm^{-1}) shows signals associated with the stretching and bending modes of phosphate are observed in the 1,200–900 cm^{-1} and 650–500 cm^{-1} regions, respectively. The split double peak at 1,049 and 980 cm^{-1} and the triplet at 847, 793, and 766 cm^{-1} in the phytate-only

spectrum are features that arise from the multiple P–O–C groups in phytate and can be used to distinguish between metal phytates and metal phosphates (518,520).

The phytate + phytase treatment showed a spectrum more closely resembling that of the inorganic phosphate treatment, with a single peak with shoulders at ~ 995 cm^{-1} and two sharp peaks emerging at ~ 610 and ~ 535 cm^{-1}. A similar change in the FTIR spectra has been previously observed in the hydrothermal transformation of europium phytate into europium phosphate (251).

Finding database patterns for lanthanum phosphates proved challenging, but a number of researchers have published infrared investigations of rare earth (REE) phosphate minerals. Making qualitative comparisons, the products from the phytate + phytase and inorganic phosphate treatments appeared similar to examples of rhabdophane ($REEPO_4.0.667H_2O$) (113,119,296,339,546,547) or europium phosphate monohydrate ($EuPO_4.H_2O$) (251). In particular, a single peak for the water O–H bending at 1,630 cm^{-1} contrasts with a doublet observed for churchite ($REEPO_4.2H_2O$) or no signal for the anhydrous REE phosphates (547). In addition, the triplet of peaks observed at around 609, 569, and 536 cm^{-1} matched well with the triplet observed in this region for rhabdophane where other REE phosphate polymorphs were either more (the anhydrous $REEPO_4$ phases monazite and xenotime) or less (churchite) complex (547).

However, some differences from previously published FTIR do exist, notably that the most intense peak at around 1,000 cm^{-1} for rhabdophane showed more prominent signs of peak splitting in the work by (547). This may be due to different spectral resolutions used ((547) used a resolution of 2 cm^{-1} compared to 4 cm^{-1}) or the fact that the product investigated by (547) was more crystalline than the X-ray amorphous product investigated in this work. The FTIR spectra in this work also matched well with the FTIR spectrum for an amorphous lanthanum phosphate shown by (548). This amorphous product was transformed to rhabdophane with a hydrothermal treatment at 100 °C (548) which may indicate that the initially precipitated solid is an amorphous rhabdophane precursor.

Previous researchers have described trivalent metal phytates (aluminium and iron phytate in (518,549), neodymium phytate in (279), europium phytate in (251)) as having a broad band with shoulders in the 1,200–900 cm^{-1}. In contrast, the well-defined double peak feature in this work for the phytate-only treatment (figure 4.34) showed more in common with divalent metal phytates (518,520,549). The differences may be a result of different pH values used in experimental work. The solution pH will

influence the degree of protonation on the phosphate groups of phytate, with $H_8Phytate^{4-}$ and $H_7Phytate^{5-}$ expected to be the predominant species at pH 2–3 compared to $H_6Phytate^{6-}$ at pH 5–6 (550). The degree of protonation of phosphate groups is known to influence the position and number of peaks in the FTIR spectra of phosphate compounds (551). The previous investigations of aluminium, iron, and neodymium phytates took place at pH values of around 2–3 (279,518,549) compared to the pH in this work (5.5). However, the europium phytate was precipitated at pH 5 (251). The differences, then, may be related to equipment setup (e.g. measuring samples in transmittance or attenuated total reflectance mode or using different spectral resolutions).

Techniques such as FTIR have value in the characterisation of amorphous and poorly crystalline materials, but the variability between the results reported here and elsewhere need to be understood before the technique could be used to examine the behaviour of lanthanum phytate – and its transformation into lanthanum phosphate – in more complex samples.

As with the FTIR results, ^{31}P NMR analysis (appendix F, figures F.4 and F.5) showed that the spectrum for the inorganic phosphate treatment was similar to literature reports of rhabdophane (408) but with slight differences that, again, may indicate the presence of a rhabdophane precursor material. The phytate-only treatment appeared similar to a previous report of lanthanum phytate (552), while the phytate + phytase treatment showed features of both inorganic phosphate and phytate-only treatments.

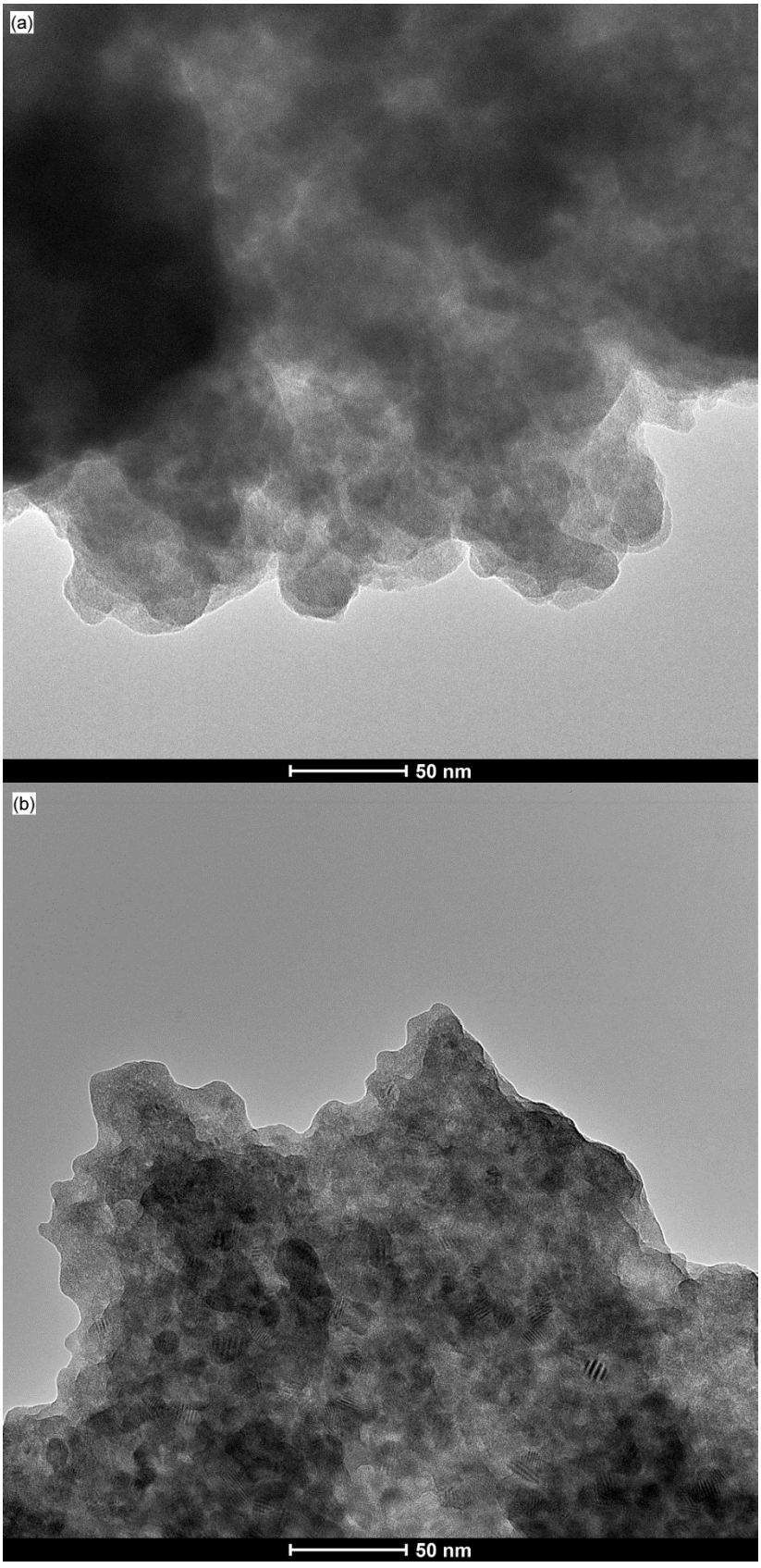

Figure 4.35 (continued).

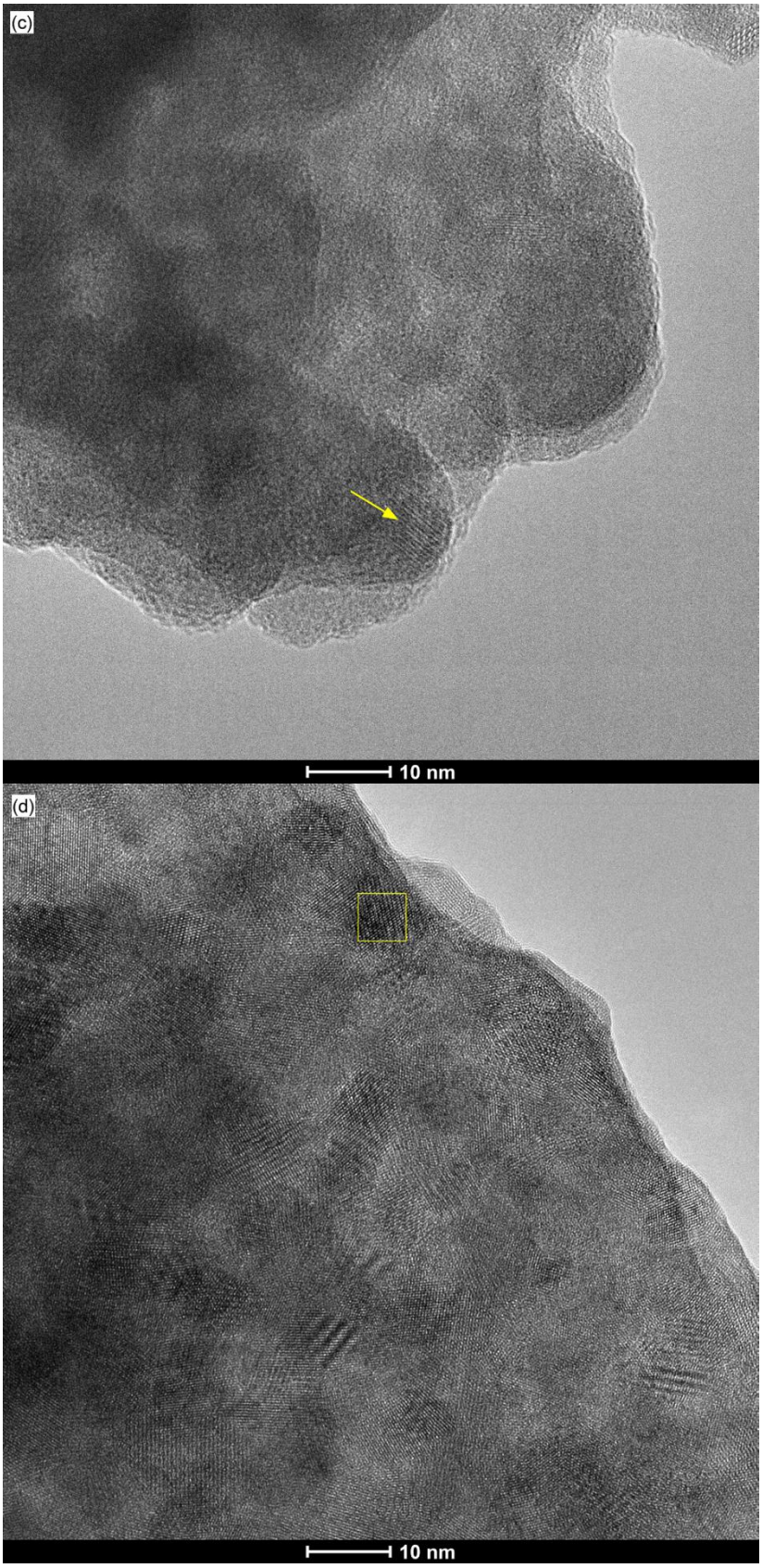

Figure 4.35 TEM images of precipitates produced in (a, c) phytate-only, and (b, d) phytate + phytase treatments. Arrow points to crystalline material, square shows area used for the generation of the diffractogram shown in figure 4.36c.

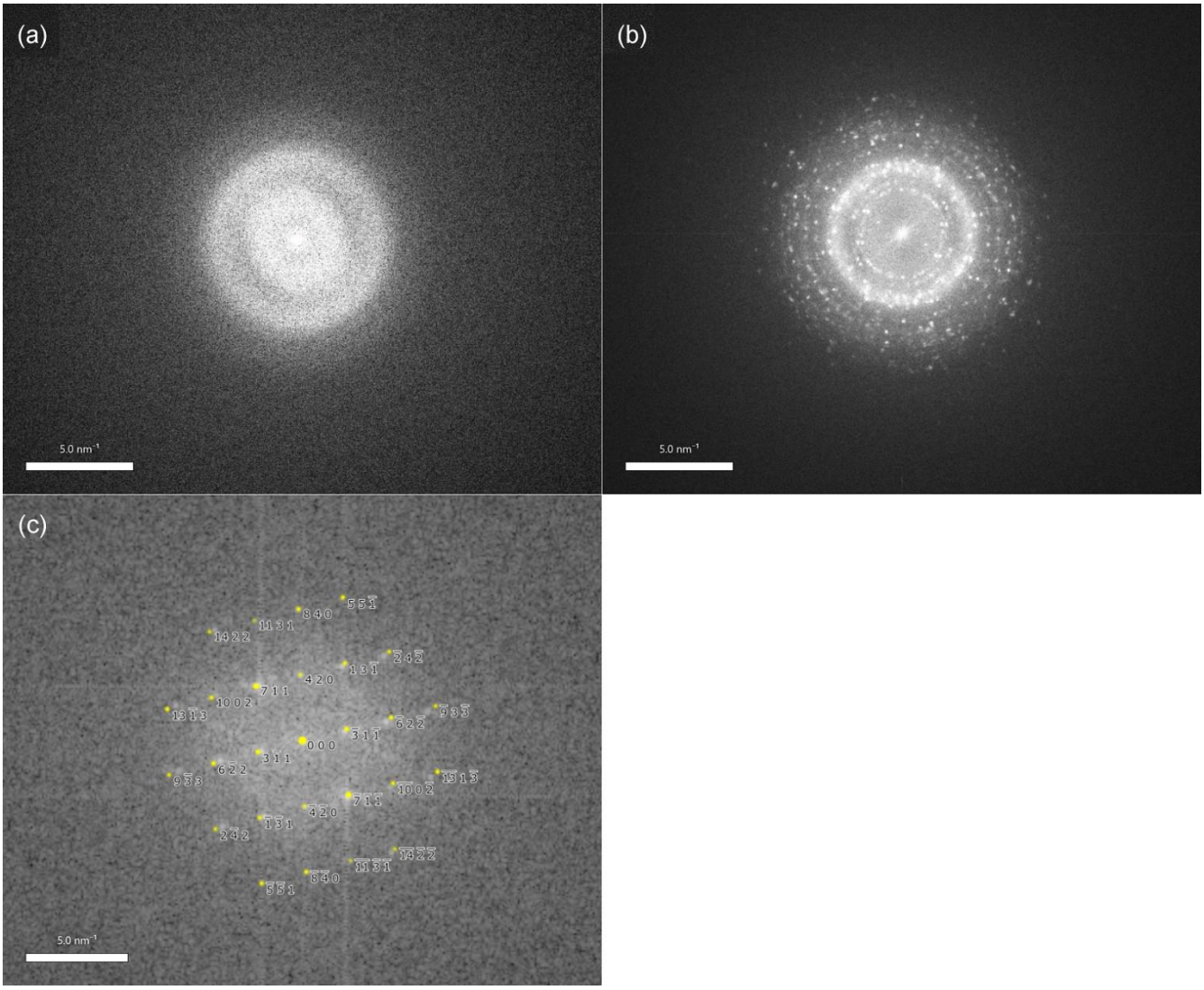

Figure 4.36 FFT-generated diffractograms of TEM images of samples produced by (a) phytate-only, and (b, c) phytate + phytase treatments. Diffractograms (a) and (b) were produced in Gatan's DigitalMicrograph software from whole images, while (c) was produced using ImageJ from the selected area shown by the yellow square in figure 4.35d. The yellow spots in (c) represent the simulated electron diffraction pattern for rhabdophane viewed along the [$\bar{1}$25] direction, produced using the SingleCrystal® 4 software (503).

Analysis by SEM (at the micrometre scale) indicated little in the way of distinctive features when comparing samples produced in phytate + phytase and phytate-only treatments (appendix H). However, TEM analysis (at the nanometre scale) potentially provided some insight. While XRD analysis appeared to show that all materials were amorphous, TEM showed that the material produced in the phytate + phytase treatment (figure 4.35b, figure 4.35d) was polynanocrystalline as indicated by the diffuse rings containing intermittently spaced Bragg reflections shown in the diffractogram (figure 4.36b). The

phytate-only sample appeared to be mostly amorphous (figure 4.35a, figure 4.35c) as indicated by diffuse rings in the diffractogram (figure 4.36a), although patches of a nanocrystalline material could be observed in some images (shown by the arrow in figure 4.35c).

To try and identify the crystalline material, FFT-generated diffractograms were produced using small areas in the TEM images corresponding to zone-axis patterns (see appendix I for details). The generated diffractograms matched reasonably well with simulated electron diffraction patterns for rhabdophane, as shown by figure 4.36c. However, the identification could not be confirmed unambiguously and further analysis with well-defined reference materials would be required to confirm the identity of the crystalline phase present and understand the influence of potential impurities (e.g. carbonates) and electron beam damage. Comparisons to the material produced in the inorganic phosphate treatment (which was not analysed by TEM due to time constraints) would also be useful to understand the influence of phytate on the precipitated crystal's morphology.

As the phytate stock contained an inorganic phosphate impurity and analysis indicated a fraction of this impurity was insoluble (figure 4.31a, table 4.8) it is likely that the crystalline material observed in the phytate-only treatment was a result of lanthanum precipitating with inorganic phosphate alongside the bulk amorphous lanthanum phytate (although this crystalline material may also have been formed as a result of electron beam damage, e.g. figure I.3). Following phytase treatment, the proportion of crystalline material appeared to increase, consistent with an increased precipitation of inorganic phosphate at the expense of phytate.

Previous TEM investigations of lanthanum phosphates formed at ambient temperatures have observed the formation of rod-shaped nanocrystals (113,339) in contrast to the aggregated spherical nanocrystals formed in this work. The differences are likely related to pH (the previous work took place at pH 2–3) and the presence of organic phosphate in this work. The comparatively slow release of phosphate from phytate (compared to just mixing solutions of lanthanum and inorganic phosphate together) may have also influenced the rates of precipitation and crystallisation.

Geochemical modelling indicated that the only supersaturated phases in the presence of phosphate were hydrated lanthanum phosphates, while all phases were undersaturated in the no phosphate treatment (appendix G, table G.17). It is likely that lanthanum phytate would also be supersaturated under the conditions tested, but solubility product data for this phase are not available.

In summary, the addition of phytate, inorganic phosphate, or inorganic phosphate sourced from phytate are all efficient methods of precipitating lanthanum out of solution. Therefore, the use of phytase enzymes to hydrolyse phytate may prove to be a simple and cost-effective method of producing lanthanum phosphates for environmental remediation applications.

Questions around the morphology and identity of the lanthanum phosphate precipitated remain unanswered. The structure of the material may have important implications for contaminant incorporation properties and long-term stability, so this should be a key aspect of future research.

Rhabdophane is the most likely lanthanum phosphate to form under ambient conditions (113,296,339) but the lanthanum phosphate phase produced in this work could not be conclusively identified. Factors influencing the crystal structure and morphology of lanthanum phosphate include pH, temperature, time, and the La:P ratio (113,296,339,553). Furthermore, phytate and the lower inositol phosphates formed in its breakdown are known to inhibit mineral crystallisation (266,322,323) and to stabilise amorphous mineral precursors (327). This has not been directly investigated for lanthanum phosphates but may be important. Together, the FTIR, ^{31}P NMR, and TEM results suggest that the product formed in the phytate + phytase and inorganic phosphate treatments was a poorly crystalline rhabdophane but further work would be required to verify this.

A preliminary attempt to investigate the controls on lanthanum phosphate morphology in the phytate + phytase system (described in appendix E) indicated that lower pH values, longer experiment times, or adding lanthanum after phytate had been hydrolysed all produced slightly more crystalline materials, with broad peaks in the XRD patterns matching the positions of the main peaks in the XRD pattern of well crystallised rhabdophane (appendix E, figure E.6). However, in all cases, the product remained very poorly crystalline.

Further experiments should also be performed to investigate the influence of solution chemistry on the structure of the materials, the stability of the materials across different solution conditions, and their ability to sorb contaminants such as uranium. An initial test to investigate the leachability of the phytate-only and phytate + phytase materials in a pH 5.5 artificial groundwater indicated that less than 0.05% of lanthanum was leached from either material over multiple cycles (appendix E, figure E.3) which is a highly promising basis for further research to build on.

4.2.12 Lead

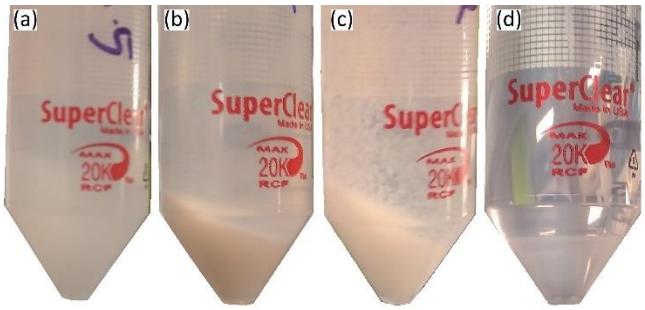

Figure 4.37 Appearances of the lead experiments after 24 hours of mixing. Photographs were taken around 5 minutes after removing the experiments from the overhead shaker. (a) Phytate-only; (b) Phytate + Phytase; (c) Inorganic phosphate; (d) No phosphate.

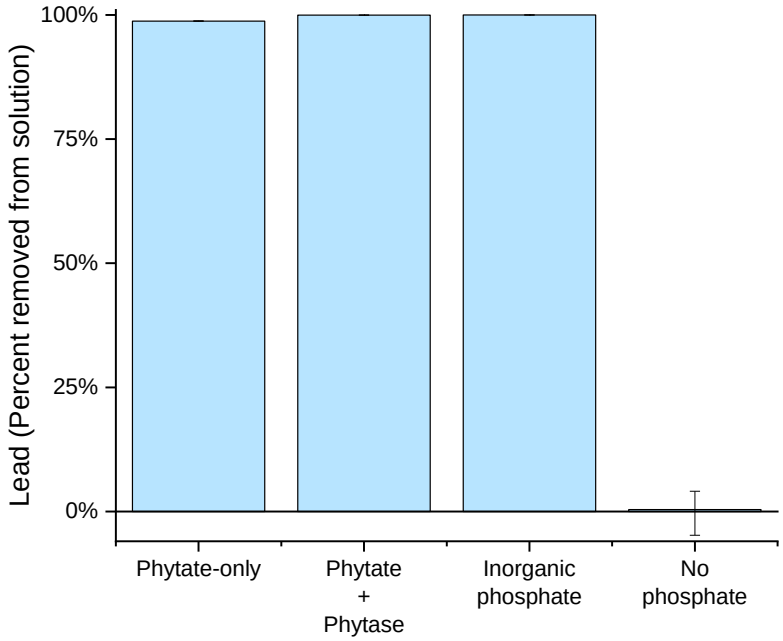

Figure 4.38 Percentage of lead removed from solution in the different treatments. Columns represent the mean value of triplicate samples, error bars represent the difference between the mean and the upper or lower measured values.

Precipitation occurred immediately upon mixing lead with either phytate or inorganic phosphate, while the solution remained clear in the no phosphate treatment (figure 4.37). After 24 hours, the phytate + phytase and inorganic phosphate treatments had produced a material that settled under gravity (figure 4.37b, figure 4.37c), while solids in the phytate-only treatment remained suspended, potentially indicating the formation of lead phytate colloids (figure 4.37a). Upwards of 98% of lead was removed in the phytate + phytase, phytate-only, and inorganic phosphate treatments, while effectively all the lead

remained soluble in the no phosphate treatment (figure 4.38). In terms of absolute concentrations, the amount of lead remaining solution was ~ 0.2 µmol/L for the inorganic phosphate treatment, ~ 0.8 µmol/L for the phytate + phytase treatment, 55 µmol/L for the phytate-only treatment, and 4.45 mmol/L for the no-phosphate treatment.

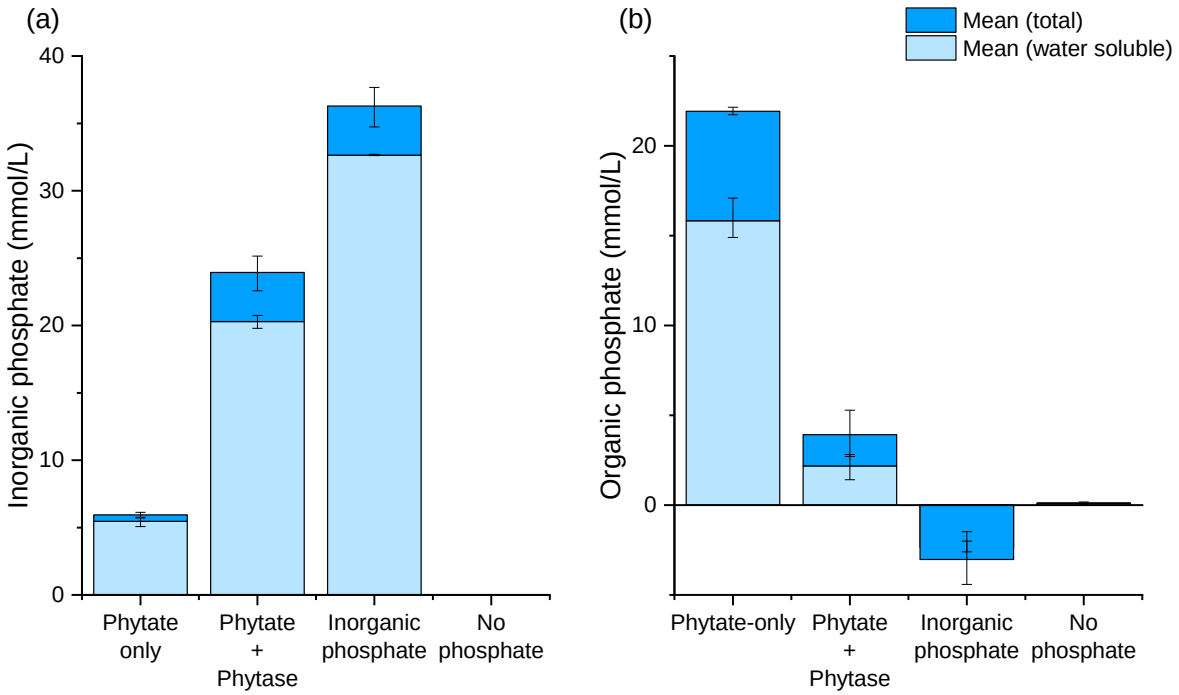

Figure 4.39 Comparison of water-soluble and total concentrations of (a) inorganic phosphate, and (b) organic phosphate across different treatments for the lead experiments. Columns represent the mean of value of triplicate samples, error bars represent the difference between the mean and the upper and lower measured or calculated values.

Compared to the inorganic phosphate control, the total concentration of inorganic phosphate in the phytate + phytase condition was about 10 mmol/L lower, but the insoluble fraction was similar for both conditions (~ 3.5 mmol/L) (figure 4.39a). In contrast, for the phytate-only control, only around 0.5 mmol/L inorganic phosphate precipitated (figure 4.39a). For the no phosphate control, inorganic phosphate concentrations were below the detection limit (< 0.02 mmol/L) for both water-soluble and total concentration samples. Calculated organic phosphate values indicated that around 1.7 mmol/L organic phosphate precipitated in the phytate + phytase treatment compared to around 6 mmol/L in the phytate-only treatment (figure 4.39b).

Table 4.9 Concentrations of analytes removed from solution (mmol/L) into precipitated solids for different treatments for the lead experiments. Values are given as the mean of triplicate samples, columns designated as + and – represent the difference between the mean value and the upper or lower measured value respectively.

Treatment	Inorganic phosphate			Organic phosphate			Lead			Potassium		
	Mean	+	–	Mean	+	–	Mean	+	–	Mean	+	–
Phytate-only	**0.47**	*0.17*	*0.11*	**6.09**	*0.73*	*1.03*	**4.42**	*0.002*	*0.001*	**-0.07**	*1.08*	*1.84*
Phytate + Phytase	**3.65**	*1.72*	*1.41*	**1.74**	*2.14*	*1.36*	**4.47**	*0.000*	*0.000*	**-1.18**	*1.97*	*1.70*
Inorganic phosphate	**3.64**	*1.32*	*1.52*	**-0.67**	*1.80*	*1.27*	**4.47**	*0.000*	*0.000*	**0.17**	*1.81*	*3.04*
No phosphate	**0.00**	*0.00*	*0.00*	**0.00**	*0.05*	*0.07*	**0.02**	*0.16*	*0.23*	**-0.80**	*2.39*	*4.26*

Comparing the amounts of lead and phosphate removed from solution indicated that lead precipitated in a 1.5:1.0 ratio with inorganic phosphate for both phytate + phytase and inorganic phosphate treatments (table 4.9). However, the materials appeared to differ with the incorporation of some organic phosphate into the phytate + phytase treatment precipitate. The phytate-only precipitate contained a lead:organic phosphate ratio of about 0.8:1.0, which corresponds to a lead:phytate ratio of about 4.6:1.0. Analysis indicated that the majority (between 97% and 113%) of potassium remained in solution for all treatments (table 4.9).

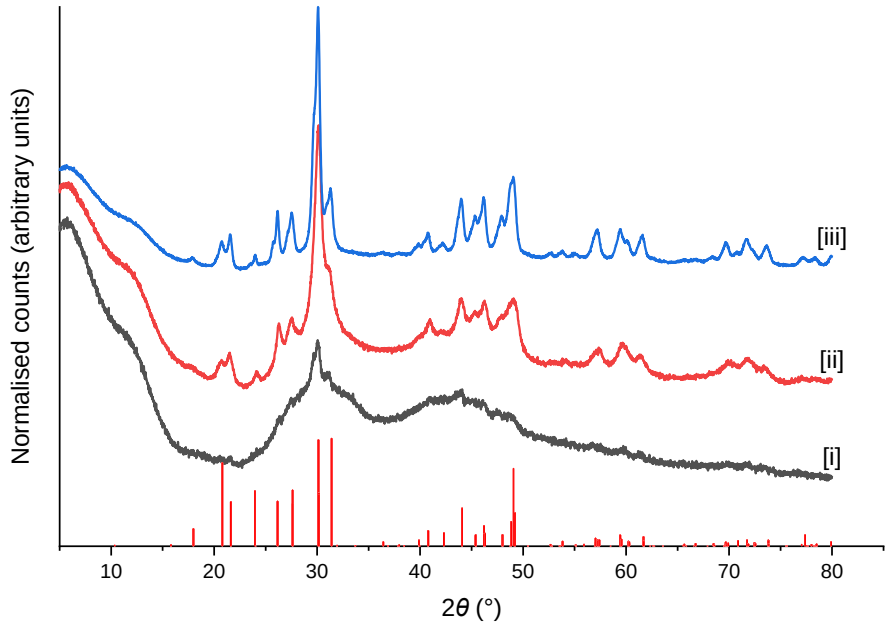

Figure 4.40 XRD patterns of precipitates produced in the lead experiments showing [i] phytate-only; [ii] phytate + phytase; and [iii] inorganic phosphate treatments. Patterns were measured using the Göbel mirror optics setup. Samples were measured using the copper K_α radiation across a 2θ range of 5–80° with a step size of 0.02° and a step time of 1 s. Patterns were normalised in OriginPro 2019b to a scale of 0 to 1. Reference pattern is pyromorphite-OH, $Pb_{10}(PO_4)_6(OH)_2$ (PDF 01-086-0236).

XRD indicated that the precipitates recovered from the phytate + phytase and inorganic phosphate treatments matched the database pattern for pyromorphite-OH ($Pb_{10}(PO_4)_6(OH)_2$), PDF number 01-086-0236 (figure 4.40). The pattern for the phytate-only precipitate appeared to be mostly amorphous but did show some features possibly also matching the database pattern for pyromorphite-OH (figure 4.40). As the phytate stock was known to contain an inorganic phosphate impurity, and a fraction of this was insoluble (figure 4.39, table 4.9), it is likely that small traces of pyromorphite-OH were formed in this experiment alongside the bulk lead phytate.

The broader peaks in the phytate + phytase pattern as compared to the inorganic phosphate treatment indicate a less crystalline material. Phytate has previously been shown to inhibit the crystallisation rate of calcium hydroxyapatite (554) and it is likely that this is also true for the lead analogue pyromorphite-OH.

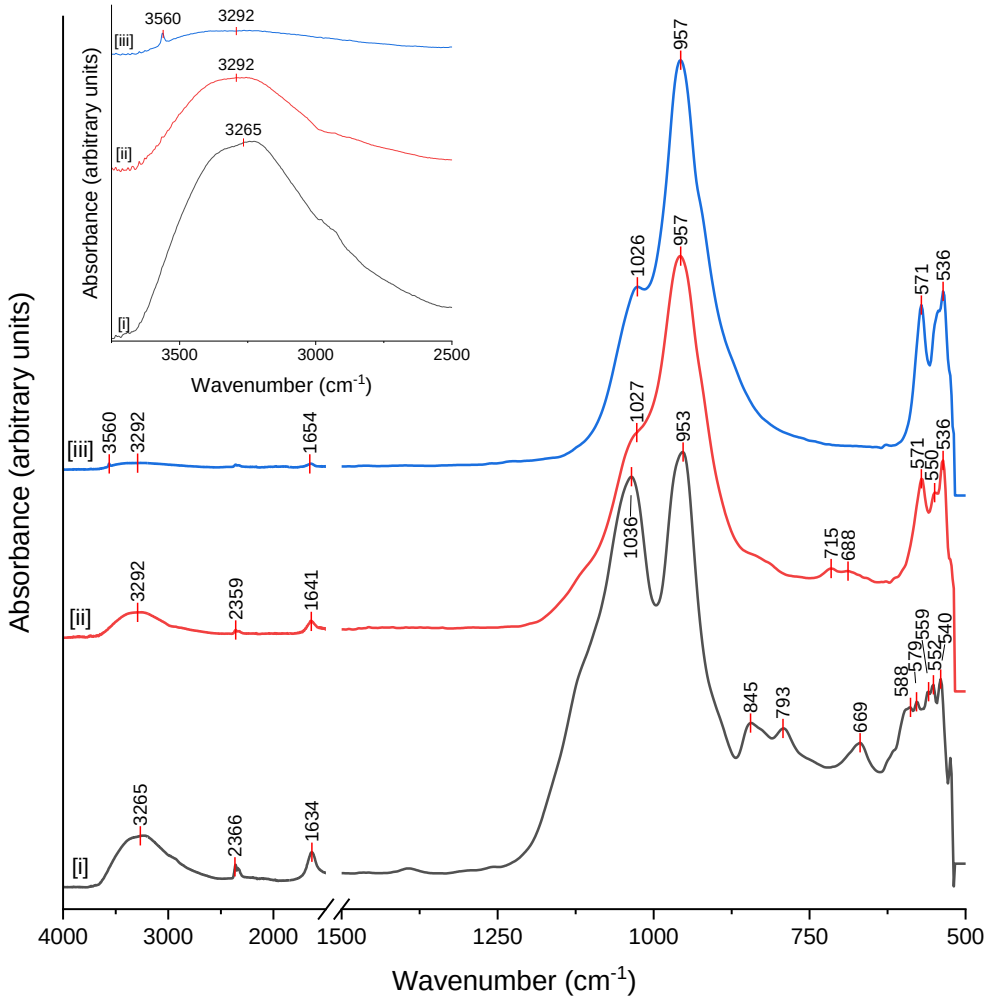

Figure 4.41 FTIR spectra of precipitates produced in [i] Phytate-only; [ii] Phytate + Phytase; [iii] and inorganic phosphate treatments for the lead experiments. Inset focuses on the O–H stretching region of the spectrum. Spectra were normalised in OriginPro 2019b to a scale of 0–1.

FTIR spectra of precipitates produced in the lead experiments are shown in figure 4.41 and show a similar trend to the lanthanum experiments. The lead phytate spectrum showed prominent bands associated with crystallised water (at ~ 3,600–2,700 cm^{-1} and ~ 1640 cm^{-1}) and the P–O–C groups of phytate (1036, 953, 845, and 793 cm^{-1}) (518,520). Following phytase treatment, a single peak with a shoulder replaced the double peak in the 1,200–900 cm^{-1} range (associated with P–O stretching (555)), two narrow peaks became apparent at 571 and 536 cm^{-1} (associated with P–O bending (555,556)), and the signals associated with crystallised water became less intense (figure 41).

The phytate + phytase sample's spectrum also closely resembled the spectrum for the inorganic phosphate treatment (figure 4.41). Both spectra resembled previously reported FTIR spectra for

pyromorphite-OH (115,500,501). Differences between the phytate + phytase and inorganic phosphate spectra were that the inorganic phosphate sample showed much weaker signals for crystallised water as well as a small, sharp peak at 3560 cm^{-1} (figure 4.41 inset). Additionally, the shoulder peak at ~ 1,026 cm^{-1} appeared to be more separated from the main peak at 957 cm^{-1} in the inorganic phosphate sample as compared to the phytate + phytase sample.

^{31}P NMR analysis (appendix F, figures F.6 and F.7) indicated similarities between the phytate-only treatment and previous reports of metal phytates (520,527), while the inorganic phosphate treatment was similar to reported spectra of pyromorphite (557–560). The phytate + phytase treatment resembled the inorganic phosphate treatment but with some features (i.e. more prominent spinning side bands) associated with the residual phytate/organic phosphate incorporated into the precipitate.

Despite the lack of any solubility data for lead phytate, geochemical modelling results were consistent with the experimental data (appendix G, table G.19). All phases were undersaturated in the no phosphate treatment while, in the presence of phosphate, pyromorphite-OH was calculated to have the highest saturation index. The saturation index of pyromorphite-OH increased for the different treatments in the order phytate-only < phytate + phytase < inorganic phosphate, consistent with lead solubility trends in the experiments.

In these experiments, phytate has been shown to be a highly efficient sequestering agent for lead, with phytase treatment improving lead removal to a level comparable with the direct addition of inorganic phosphate. Phytase treatment also mediated the transformation of lead phytate into pyromorphite-OH, one of the most stable and insoluble known lead minerals (502). This indicates that either the direct addition of phytate to contaminated soils/waters or the addition of phytate in combination with phytase enzymes/phytase producing organisms could be promising remediation mechanisms.

The concentrations of soluble lead were still slightly higher than the recommended drinking water limit of 0.05 µmol/L (437). However, concentrations in the inorganic phosphate (0.22 µmol/L) and phytate + phytase (0.84 µmol/L) treatments were below or close to the limit (0.24 µmol/L) recommended for groundwater in the vicinity of uranium and thorium mill tailings (498) which may be a more relevant standard to work towards.

Further work should investigate similar experiments across different pH values and concentrations of lead/phytate/phosphate and how the treatments perform in more complex, environmental matrices.

Additionally, for *in situ* remediation strategies it is important to investigate the long-term stability and leachability of both lead phytate and the phytase-mediated pyromorphite-OH in comparison to pyromorphite-OH precipitated from the direct addition of inorganic phosphate. The potential formation of lead phytate colloids (figure 4.37a) may also have important implications for lead mobility.

4.3 Conclusions

In this chapter the immobilisation of nine different metals (ten different species when discussing iron(II) and iron(III) separately) by phytic acid and the subsequent transformation by a phytase enzyme has been investigated. The metals investigated can be grouped according to whether the phytate + phytase strategy was effective (lanthanum and lead), yielded mixed results (aluminium, iron(II), iron(III), and copper), or was ineffective (calcium, manganese, cobalt, barium).

These results suggest that a combined phytate + phytase strategy is an efficient mechanism of precipitating lanthanum and lead phosphates which may have applications in the production of a bulk material for use as a sorbent or waste form (lanthanum phosphate) or the clean-up of lead contaminated environments. Based upon the similar solubilities of lanthanum, lead, and uranium phosphates under acidic conditions, these experiments could also be used as models upon which to build similar tests investigating uranium precipitation.

The experiments with mixed results were able to remove the majority of metals from solution by precipitation with phytate and were able to improve this by the addition of phytase. However, the metals (aluminium, iron(II), iron(III), and copper) appeared to remain mostly associated with phytate even after phytase treatment and further work would be required to produce the corresponding phosphate minerals through this method. Because metal precipitation under phosphate-free conditions for aluminium and iron(III) was equivalent to precipitation in the presence of phosphate, tests of leachability and contaminant incorporation properties would need to be performed to compare the advantages and disadvantages of corresponding phytate, phosphate, and (oxyhydr)oxide species. Furthermore, the ability of phytate to increase the solubility of aluminium and iron(III) through the inhibition of metal hydrolysis may have important implications for contaminant mobility and requires further attention if phytate is to be added to contaminated systems with high concentrations of these metals. Hypothetically, this property could be advantageous if aluminium and iron are not priority contaminants, as phytate/lower inositol phosphates could keep these elements in solution while allowing the targeted precipitation of certain other metals (e.g. lanthanum or lead).

The experiments where the phytate + phytase strategy was ineffective were notable because phytase treatment increased the concentration of metal in solution. This was particularly important for manganese, cobalt, and barium where phytate precipitated 40–60% of the metal while phytase treatment almost completely solubilised the precipitate. This suggests that for certain metals phytate may be a more efficient sequestering agent than phosphate, particularly with refinements to the experimental procedure to optimise the metal:phytate ratio. For the precipitation of these metals as metal phosphates, particularly calcium as hydroxyapatite, the procedures used in this experimental work were ineffective. To improve the procedures, several different options could be pursued: (a) by using an enzyme with a different pH profile allowing reactions to take place under alkaline conditions, (b) by using a two-stage process where the experiments in this work are followed by pH adjustments to make mineral precipitation more favourable, or (c) by using non-biologically based methods, e.g. (hydro)thermal treatments to decompose phytate into inorganic phosphate.

The work in this chapter has used very simple single metal systems as a precursor to more complex waste streams. Mining wastes typically contain a wide range of contaminants together. Therefore for future work, experiments in more complex, realistic systems would be required.

Chapter 5
Conclusions and Future Directions

5.0 Introduction

This project has studied the use of phytic acid as a precursor to various phosphate minerals with a view to using these phases to support the chemical stabilisation of NORM-containing mine wastes. This has been studied through, firstly, investigating the ability of microorganisms (*Aspergillus niger* and *Blastobotrys adeninivorans*) to hydrolyse phytate at environmentally relevant temperatures and testing whether the organisms were suitable for precipitating calcium, manganese, iron, or lanthanum phosphates. Secondly, the same organisms were investigated for their ability to degrade phytate and induce phosphate mineral precipitation in simple and complex solid matrices. Thirdly, experiments were performed using a purified phytase enzyme to hydrolyse phytate in the presence of various potentially relevant metals to identify the most promising metal phosphates to precipitate under the optimum conditions of the enzyme (i.e. in the mildly acidic pH range).

Phytic acid is an attractive source of phosphate due to its availability as a low-cost waste product. However, the complexity of its chemistry and its recalcitrance towards enzymatic or chemical hydrolysis (relative to other organic phosphates) may be a factor that has contributed towards its limited practical application in environmental remediation technologies to date. The results presented in this thesis will aid an improved understanding of the use of phytate as a phosphate mineral precursor and have implications for phosphate biomineralization as a remediation strategy for radiologically contaminated sites – both in the mining industry and other sectors.

5.1 The influence of temperature and carbon source on microbial phytate degradation and the implications for phosphate biomineralization

Most previous research has only investigated phytate degradation at temperatures above room temperature. This work revealed that the yeast *B. adeninivorans* can grow and hydrolyse phytate across a range of temperatures from 4 °C to 30 °C, while the mould *A. niger* can only grow and degrade phytate at 12 °C and above. Furthermore, the importance of different carbon sources was highlighted: with starch, both organisms were efficient at degrading phytate, while for *A. niger*, galactose as a carbon source led to a slower release of phosphate, and for *B. adeninivorans*, no phosphate release at all was observed when grown with glucose.

This shows the importance of matching the organism(s) used in a bioremediation strategy to the site characteristics (i.e. average temperature) and the importance of a careful choice of nutrients, balancing efficacy, practicality, and cost.

Subsequent precipitation tests, using three different experimental systems, provided mixed results with important implications. In the "filtrate" system (i.e. where microorganisms were used to hydrolyse phytate, the biomass filtered out of the cultures, and calcium added to the filtrates) it was found that at the low pH (~ 2.5) representative of the final pH in the microbial cultures, the predominant mineral phase was the calcium sulfate gypsum – except where phytate degradation did not occur, in which case, no precipitation was formed, likely due to the formation of strong soluble calcium phytate complexes. Experiments where the pH was adjusted prior to precipitation did highlight that, at pH 6–7, mixed calcium phosphate-sulfate composites may form; these materials have a range of interesting physicochemical properties and are a highly promising direction for future research.

In the "active" system (where the metal of interest was added to a phytate-containing nutrient media prior to inoculation with microorganisms) promising results included phytate removing the majority of lanthanum from solution, and the transformation of lanthanum phytate into a poorly crystalline lanthanum phosphate by *B. adeninivorans*. Less successful was the lack of calcium phosphate by *B. adeninivorans* at pH 7 (as no phosphate release occurred at this pH value), the lack of manganese precipitation under any conditions, and the ubiquitous formation of organic crystals (particularly oxalates) by *A. niger* under every condition tested.

In the "inactive" system (where metals were added to *B. adeninivorans* cell suspensions after phytate hydrolysis had occurred) lanthanum phosphate precipitation occurred readily to produce rhabdophane, while a low amount of iron and no manganese precipitation occurred.

Together, these results indicate that *B. adeninivorans* is a good candidate organism to produce phosphate phases that are insoluble under acidic conditions, particularly lanthanum phosphates. However, neither organism tested is suitable for the direct formation of phases that require pH values of 7 and above to form (e.g. hydroxyapatite). Additionally, the high levels of organic acid production by *A. niger* means that, to successfully produce phosphate minerals using this organism, it may be necessary to either first remove the biomass prior to metal addition or work with purified *A. niger* phytase enzymes.

5.2 Microbial phytate degradation and phosphate biomineralization in the presence of simple and complex solid matrices

Building upon the results obtained in batch solution cultures, experiments were undertaken to investigate phytate degradation and phosphate mineral precipitation in the presence of simple (sand) or complex (simulated mine tailings) solid matrices.

In the simple sand systems, the low solubility of lanthanum phytate was again demonstrated. Both microorganisms (*A. niger* and *B. adeninivorans*) were able to grow and induce phytate degradation with a probable transformation of lanthanum phytate to lanthanum phosphate, although conclusive identification of the lanthanum phases formed could not be performed. Techniques such as X-CT and solid-state NMR may be valuable in answering questions around the localisation and identity of the precipitation but further work is required to optimise the procedures. In contrast, the utility of XRD and FTIR were limited by the strong signals of quartz in XRD patterns and Si–O groups in FTIR spectra (although, for solid media where, for example, carbonates are predominant rather than silicates, FTIR may prove useful).

Also of note was the fact that the sand (or, more likely, impurities in the supply of sand used) buffered the pH of the cultures – where batch solution experiments reduced pH values from 5.5 to 2.5–4.5, in the presence of sand, pH values initially decreased over the first 17–30 days of the experiment before increasing to around pH 6 after 2 months. This means that, while a microbial pH decrease in batch solution experiments may be a considerable limitation for the production of some phosphate phases, this limitation may not be so important in solid matrices.

Furthermore, experiments in complex solid matrices representative of mine tailings found no evidence of phytate hydrolysis. It was demonstrated that phytate interacted strongly with kaolinite, marble, and barium while phytase enzymes were sorbed onto kaolinite. Both of these factors may have contributed towards the lack of phytate hydrolysis observed in the simulated mine tailings and highlights the need for further research into methods that can both increase the solubility of phytate/phytase to allow phytate hydrolysis to occur while also still allowing inorganic phosphate phases to precipitate out of solution.

5.3 Influence of different metals on the phytase-mediated precipitation of phosphate biominerals

While the phytase enzyme of *A. niger* is one of the best studied phytase enzymes and was a logical place to start with this project, there are a number of potential limitations. Firstly, *A. niger* is well known for its ability to secrete huge quantities of organic acids, which decrease solution pH and may preferentially precipitate over phosphate phases. Secondly, the *A. niger* phytase only degrades phytate within the pH range of 2–7 which limits the range of phosphate minerals that may be successfully precipitated.

To address the problems associated with organic acid synthesis, work was performed with a purified form of the *A. niger* phytase. Experiments with this purified enzyme were then performed to investigate which metal phosphate phases were appropriate targets to try and produce in the mildly acidic pH range (pH 5.5) at which the *A. niger* phytase displays its optimum activity. The metals investigated were: aluminium, calcium, manganese, iron(II), iron(III), cobalt, copper, barium, lanthanum, and lead.

Results indicated that the phytase-mediated precipitation of lanthanum or lead was a highly promising system to work with, with metal removal comparable to systems where inorganic phosphate was added directly, and where close to 100% of the metal remained in solution in the absence of any phosphate source. These results could be applied directly to the production of lanthanum phosphate waste hosts, the treatment of lead contaminated wastes, or as model systems used as the basis for experiments with uranium.

For aluminium, iron(II), iron(III), and copper results were ambiguous. The use of phytase to hydrolyse phytate improved metal removal compared to phytate-only experiments, but regardless, the metal appeared to remain mostly associated with phytate, with only a small amount of metal phosphate coprecipitating. Additionally, in the presence of phytate or hydrolysed phytate, metal removal from aluminium, iron(II), and iron(III) was lower than when directly mixing the metal with inorganic phosphate. For aluminium and iron(III), metal removal was also lower than in a phosphate-free system. The phytase-mediated materials produced may still have value in environmental remediation, but more work is required to effectively characterise the materials and to understand what the implications of phytate inhibiting aluminium and iron hydrolysis means for metal mobility at contaminated sites.

For calcium, manganese, cobalt, and barium the results indicated that the metal phytate complexes were less soluble than the corresponding metal phosphates under the conditions tested, indicating that

the pH profile of the *A. niger* phytase means that this enzyme is not suitable for the direct production of any of these metal phosphates.

5.4 Outlook

This project has demonstrated the precipitation of a range of metal phosphate phases under a range of conditions using either purified enzymes or actively growing organisms, in batch solution experiments or in the presence of solid phases. This highlights the utility of phytase-mediated phosphate mineral precipitation as a process that may be applicable to range of *ex situ* and *in situ* processes to aid the remediation of NORM-contaminated sites. Further work remains before any of these processes can be applied on an industrial scale, with some of the most promising future directions highlighted below.

A study of uranium phosphate precipitation and a comparison of properties to materials produced through alternate mechanisms

As stated earlier in the thesis, lanthanum, lead, and uranium phosphates have some similar properties in terms of being very insoluble under acidic conditions. This fact, along with previous research into uranium phosphate precipitation from organic phosphate precursors (e.g. (104,182,184,188)) indicates that conditions used for lanthanum and lead phosphate precipitation in this work would also be favourable towards uranium phosphate precipitation.

Therefore, the question is not whether or not uranium phosphate precipitation is favourable, but what form of uranium phosphate is formed and how does this compare to uranium phosphate prepared from alternative sources of phosphate? For example, the enzymatically-mediated pyromorphite was less crystalline that pyromorphite precipitated directly with inorganic phosphate. The picture was slightly less clear for lanthanum phosphate, which was mostly amorphous, but there were indications that the precipitate produced from the direct addition of inorganic phosphate was slightly more crystalline than the phytase-mediated version. If a similar picture emerges for the uranium phosphate system, then what does this mean for the solubility and long-term stability of the precipitated mineral?

Experiments should be performed to precipitate uranium phosphate from a phytate precursor and comparisons made to uranium phosphate precipitated with inorganic phosphate (as well as uranium phytate and, potentially, any uranium minerals precipitated in the absence of phosphate) to understand any differences, including possible benefits of the phytase-mediated process or any limitations that need to be addressed.

Further experiments – either with uranium or lanthanum/lead as stable "analogue" systems – could be performed to investigate the influence of solution chemistry parameters and any residual phytate hydrolysis products in the system on the morphology of the precipitated solid. Understanding these factors could be used to optimise processes to produce a mineral phase with the desired properties.

Biogenic ardealite/calcium sulfate-phosphates as a permeable reactive barrier material

While the *A. niger* phytase appears to be unsuitable for the direct precipitation of hydroxyapatite, results in this project suggest that calcium sulfate-phosphate phases such as ardealite may be more suitable targets, as they form within the pH range that encompasses the optimum activity of the *A. niger* phytase. Calcium sulfate-phosphate composites have previously been researched as possible materials for use in permeable reactive barriers (PRB) (321). PRBs have been widely researched in the mining industry for the remediation of groundwater contamination, and the biogenic formation of calcium sulfate-phosphate may be a highly promising direction for future work – particularly if the sulfate component can be "scavenged" from the environment, as sulfate concentrations are typically high in mining wastewaters.

Calcium phytate as an ex situ wastewater treatment material

Calcium phytate has previously been described as a more efficient sorbent for uranium than hydroxyapatite (253). While certain properties of phytate may limit its applicability for use *in situ* (e.g. acting as a soil dispersant (121), uncertainty over long-term stability), these concerns would not be relevant for an *ex situ* wastewater treatment system. One option would be to produce bulk amounts of calcium phytate, providing a low-cost sorbent that could be used to rapidly remove metals from a wastewater. Following this, (hydro)thermal (or potentially enzymatic) treatments could be used to convert the phytate and sorbed contaminants into a stable crystalline phosphate phase, suitable as a host material for disposal.

Colloidal calcium phytate to support alternate engineering strategies

The low solubility of phytate is considered to be a limiting factor for the remediation of groundwater at depth, as the rapid precipitation of phytate may lead to an undesired loss in permeability, a lack of control over the localisation of precipitation, and the clogging of injection wells (104,561). However, in this project, qualitative evidence of the formation of phytate colloids was observed. Furthermore, phytate colloids have been well researched for their medical applications (232,333,562). This raises the

possibility injecting a colloidal phytate suspension into a contaminated aquifer and then, once the phytate is in place, using phytase to induce the formation of phosphate minerals.

It should be noted that what makes a colloidal suspension appropriate in a medical context won't necessarily be appropriate for groundwater remediation, so initial experiments would need to characterise phytate colloidal suspensions and understand how to produce a suspension with the right properties (for example, particle sizes may range from 5 to 1000 nm and the suspensions may remain stable for between six hours and two weeks depending on preparation techniques (333,562)). However, once these factors have been understood, the injection of phytate colloidal suspensions into the subsurface may be an interesting engineering mechanism.

Further work could also investigate including phytate within a colloidal silica grout (e.g. (563)) as an alternative engineering strategy. In that case, the influence of phytate on the colloidal silica gelling time would need to be studied, as would what phytate being embedded within a colloidal silica matrix would mean for phytate hydrolysis by phytase.

Options to pursue to manufacture hydroxyapatite from a phytate precursor

All attempts at producing hydroxyapatite, the most widely researched phosphate mineral for environmental remediation purposes, in this work were unsuccessful. The principle reason for this was the narrow pH profile of the phytase enzymes produced by *A. niger* and *B. adeninivorans* which show a negligible ability to hydrolyse phytate above pH 7 – at ambient temperatures, hydroxyapatite typically requires the pH to be above ~ 7.5 before nucleation will occur (276–278).

There are three main options that could be pursued to successfully manufacture hydroxyapatite from a phytate precursor: (a) by focusing attention on microorganisms that produce alkaline-active phytase enzymes, (b) by using *A. niger* or *B. adeninivorans* to hydrolyse phytate, followed by adjusting the pH to ~ 9, or (c) prepare calcium phytate and use a (hydro)thermal treatment to decompose phytate into inorganic phosphate.

Option (b) would be the easiest to achieve; an experimental setup similar to the "filtrate" system tests used in chapter 2 could be used, simply increasing the pH until hydroxyapatite precipitation becomes favourable. Option (c) would be the most energy intensive due to the stability of the phytate molecule – previous research found that 2 weeks at 85 °C was required to transform europium phytate into europium phosphate (251), while 24 hours at 180 °C was required to convert lead phytate into lead

hydrogen phosphate (541). However, these procedures do allow microorganisms to be eliminated from the process, which may enable a more easily repeatable procedure that is not subject to the variability sometimes encountered in microbial processes.

Option (a) would potentially be the most challenging to achieve, but also the most interesting, as it would allow hydroxyapatite formation to take place *in situ*. While less well-researched than their acidic counterparts, alkaline phytases do exist. Sources of alkaline phytases (pH optimum determined to be ≥ 7) include members of the *Bacillus* spp. genus, lily pollen, and mung beans (256,257,564) and so these would appear to be the logical places to start a search for a suitable organism/enzyme to produce hydroxyapatite from phytate.

Preliminary work in this project (data not shown) indicated no phytate degradation by the bacterium *Bacillus subtilis* subsp. *spizizenii* NCTC 10400 – however, only one set of conditions (i.e. pH, nutrient media, carbon source) was tested and, as shown with the results for *B. adeninivorans* grown with glucose as carbon source, if one of these parameters is "wrong" it can lead to the phytase activity of an organism being missed. Future work should probe a range of organisms that are likely to be capable of producing alkaline phytase enzymes. Once a suitable organism has been identified, it should be a relatively simple matter to optimise the system to enable hydroxyapatite formation.

References

1. Turner BL. Inositol phosphates in soil: amounts, forms and significance of the phosphorylated inositol stereoisomers. In: Turner BL, Richardson AE, Mullaney EJ, editors. Inositol phosphates: linking agriculture and the environment [Internet]. Wallingford: CABI; 2007 [cited 2016 Jan 15]. p. 186–206. Available from: http://www.cabi.org/cabebooks/ebook/20073069294

2. Turner BL, Papházy MJ, Haygarth PM, Mckelvie ID. Inositol phosphates in the environment. Philosophical Transactions of the Royal Society of London B: Biological Sciences. 2002 Apr 29;357(1420):449–69.

3. Celi L, Barberis E. Abiotic reactions of inositol phosphates in soil. In: Turner BL, Richardson AE, Mullaney EJ, editors. Inositol phosphates: linking agriculture and the environment [Internet]. Wallingford: CABI; 2007 [cited 2016 Jan 15]. p. 207–20. Available from: http://www.cabi.org/cabebooks/ebook/20073069295

4. El-Batal AI, Abdel Karem H. Phytase production and phytic acid reduction in rapeseed meal by Aspergillus niger during solid state fermentation. Food Research International. 2001;34(8):715–20.

5. Duffin PA. The Effect of Phytate on Mineral Bioavailability and Heavy Metal Contaminants [Doctor of Philosophy]. [Guildford, Surrey, United Kingdom]: University of Surrey; 1989.

6. Ebune A, Al-Asheh S, Duvnjak Z. Effects of phosphate, surfactants and glucose on phytase production and hydrolysis of phytic acid in canola meal by Aspergillus ficuum during solid-state fermentation. Bioresource Technology. 1995;54(3):241–7.

7. Erdman JW. Oilseed phytates: Nutritional implications. Journal of the American Oil Chemists' Society. 1979 Aug;56(8):736–41.

8. Frank AW. 2 - Phytic Acid. In: Frank AW, editor. Chemistry of Plant Phosphorus Compounds [Internet]. Oxford: Elsevier; 2013. p. 75–134. Available from: http://www.sciencedirect.com/science/article/pii/B9780124071940000020

9. Frank AW. 8 - Distribution of Phosphorus Compounds in Plants. In: Frank AW, editor. Chemistry of Plant Phosphorus Compounds [Internet]. Oxford: Elsevier; 2013. p. 457–74. Available from: http://www.sciencedirect.com/science/article/pii/B9780124071940000081

10. Gerke J. Phytate (Inositol Hexakisphosphate) in Soil and Phosphate Acquisition from Inositol Phosphates by Higher Plants. A Review. Plants (Basel). 2015 May 22;4(2):253–66.

11. Macaskie LE, Yong P, Paterson-Beedle M. Bacterial precipitation of metal phosphates. In: Valsami-Jones E, editor. Phosphorus in Environmental Technologies: Principles and Applications. IWA Publishing; 2004. p. 549–81.

12. Murray FH, Brown JR, Fyfe WS, Kronberg BI. Immobilization of U-Th-Ra in mine wastes by phosphate mineralization. The Canadian Mineralogist. 1983 Nov 1;21(4):607–10.

13. Conca JL, Wright J. An Apatite II permeable reactive barrier to remediate groundwater containing Zn, Pb and Cd. Applied Geochemistry. 2006 Dec;21(12):2188–200.

14. Oelkers EH, Montel J-M. Phosphates and Nuclear Waste Storage. Elements. 2008 Apr 1;4(2):113–6.

15. Jerden JL, Sinha AK. Phosphate based immobilization of uranium in an oxidizing bedrock aquifer. Applied Geochemistry. 2003 Jun 1;18(6):823–43.

16. Egidi P. Introduction to naturally occurring radioactive material. In: Health Physics Society annual meeting, San Antonio [Internet]. San Antonio, TX (United States): Oak Ridge National Lab; 1997. Available from: http://www.osti.gov/scitech/servlets/purl/560732

17. International Atomic Energy Agency. Extent of Environmental Contamination by Naturally Occurring Radioactive Material (NORM) and Technological Options for Mitigation [Internet]. Vienna: International Atomic Energy Agency; 2003 [cited 2016 Jul 29]. (Technical Reports Series). Report No.: 419. Available from: http://www-pub.iaea.org/books/IAEABooks/6789/Extent-of-Environmental-Contamination-by-Naturally-Occurring-Radioactive-Material-NORM-and-Technological-Options-for-Mitigation

18. World Nuclear Association. Naturally Occurring Radioactive Materials (NORM) [Internet]. World Nuclear Association. 2016 [cited 2016 Sep 12]. Available from: http://www.world-nuclear.org/information-library/safety-and-security/radiation-and-health/naturally-occurring-radioactive-materials-norm.aspx

19. International Atomic Energy Agency. Management of NORM residues. Vienna: International Atomic Energy Agency; 2013. 66 p. (TECDOC).

20. Hore-Lacy I. 6 - Mining and milling of uranium. In: Crossland I, editor. Nuclear Fuel Cycle Science and Engineering [Internet]. Woodhead Publishing; 2012. p. 129–50. Available from: http://www.sciencedirect.com/science/article/pii/B9780857090737500064

21. Merkel BJ, Hoyer M. 16 - Remediation of sites contaminated by radionuclides. In: Poinssot C, Geckeis H, editors. Radionuclide Behaviour in the Natural Environment [Internet]. Woodhead Publishing; 2012. p. 601–45. Available from: http://www.sciencedirect.com/science/article/pii/B978085709132150016X

22. Falck WE. 1 - Radioactive and other environmental contamination from uranium mining and milling. In: van Velzen L, editor. Environmental Remediation and Restoration of Contaminated Nuclear and Norm Sites [Internet]. Woodhead Publishing; 2015. p. 3–34. Available from: http://www.sciencedirect.com/science/article/pii/B9781782422310000016

23. Abundance in Earth's crust: periodicity [Internet]. WebElements. [cited 2016 Nov 9]. Available from: https://www.webelements.com/periodicity/abundance_crust/

24. Wendel G. Radioactivity in mines and mine water—sources and mechanisms. J South Afr Inst Min Metall. 1998;(2).

25. Hashim MA, Mukhopadhyay S, Sahu JN, Sengupta B. Remediation technologies for heavy metal contaminated groundwater. Journal of Environmental Management. 2011 Oct;92(10):2355–88.

26. Abdelouas A. Uranium Mill Tailings: Geochemistry, Mineralogy, and Environmental Impact. Elements. 2006 Dec 1;2(6):335–41.

27. Winde F, Brugge D, Nidecker A, Ruegg U. Uranium from Africa – An overview on past and current mining activities: Re-appraising associated risks and chances in a global context. Journal of African Earth Sciences. 2017 May;129:759–78.

28. WISE Uranium Project. Uranium Maps and Statistics [Internet]. [cited 2020 May 22]. Available from: http://www.wise-uranium.org/umaps.html

29. Biele H, Hurst S. Long-term Aspects of Uranium Mining Remediation. In: Merkel BroderJ, Hasche-Berger A, editors. Uranium in the Environment [Internet]. Springer Berlin Heidelberg; 2006. p. 1–9. Available from: http://dx.doi.org/10.1007/3-540-28367-6_1

30. Mudd GM. The future of Yellowcake: A global assessment of uranium resources and mining. Science of The Total Environment. 2014 Feb 15;472:590–607.

31. Wiles DR. The radiochemistry of radium and thorium in uranium mine tailings. Water Air Soil Pollut. 1983 Jul 1;20(1):99–108.

32. Donahue R, Hendry MJ, Landine P. Distribution of arsenic and nickel in uranium mill tailings, Rabbit Lake, Saskatchewan, Canada. Applied Geochemistry. 2000 Sep;15(8):1097–119.

33. Bondici VF, Lawrence JR, Khan NH, Hill JE, Yergeau E, Wolfaardt GM, et al. Microbial communities in low permeability, high pH uranium mine tailings: characterization and potential effects. Journal of Applied Microbiology. 2013 Jun;114(6):1671–86.

34. Lottermoser BG, Ashley PM. Tailings dam seepage at the rehabilitated Mary Kathleen uranium mine, Australia. Journal of Geochemical Exploration. 2005 Apr;85(3):119–37.

35. Lottermoser BG. Colonisation of the rehabilitated Mary Kathleen uranium mine site (Australia) by Calotropis procera: Toxicity risk to grazing animals. Journal of Geochemical Exploration. 2011 Oct;111(1–2):39–46.

36. U.S. Environmental Protection Agency. Radium-226, Uranium and Other Radiological Data from Water Quality Surveillance Stations Located in the Colorado River Basin of Colorado, Utah, New Mexico, and Arizona, January 1961 Through June 1972 [Internet]. U.S. Environmental Protection Agency; 1973 [cited 2020 Feb 7]. Report No.: 8SA/TIB-24. Available from: https://nepis.epa.gov/Exe/ZyNET.exe/91023CNY.TXT?ZyActionD=ZyDocument&Client=EPA&Index=Prior+to+1976&Docs=&Query=&Time=&EndTime=&SearchMethod=1&TocRestrict=n&Toc=&TocEntry=&QField=&QFieldYear=&QFieldMonth=&QFieldDay=&IntQFieldOp=0&ExtQFieldOp=0&XmlQuery=&File=D%3A%5Czyfiles%5CIndex%20Data%5C70thru75%5CTxt%5C00000029%5C91023CNY.txt&User=ANONYMOUS&Password=anonymous&SortMethod=h%7C-&MaximumDocuments=1&FuzzyDegree=0&ImageQuality=r75g8/r75g8/x150y150g16/i425&Display=hpfr&DefSeekPage=x&SearchBack=ZyActionL&Back=ZyActionS&BackDesc=Results%20page&MaximumPages=1&ZyEntry=1&SeekPage=x&ZyPURL

37. Morrison SJ, Metzler DR, Dwyer BP. Removal of As, Mn, Mo, Se, U, V and Zn from groundwater by zero-valent iron in a passive treatment cell: reaction progress modeling. Journal of Contaminant Hydrology. 2002 May;56(1–2):99–116.

38. Landa ER. Uranium mill tailings: nuclear waste and natural laboratory for geochemical and radioecological investigations. Journal of Environmental Radioactivity. 2004;77(1):1–27.

39. U.S. Department of Energy. Summary: Final Uranium Leasing Program Programmatic Environmental Impact Statement [Internet]. U.S. Department of Energy; 2014 Mar p. 102. Report No.: DOE/EIS-0472. Available from: https://www.energy.gov/sites/prod/files/2019/10/f67/Final_ULP_PEIS_Summary.pdf

40. Moore R, Szecsody J, Rigali M, Vermuel V, Luellen J. Assessment of a Hydroxyapatite Permeable Reactive Barrier to Remediate Uranium at the Old Rifle Site, Colorado – 16193. In Phoeniz, Arizona, USA; 2016.

41. Rodgher S, de Azevedo H, Ferrari CR, Roque CV, Ronqui LB, de Campos MB, et al. Evaluation of surface water quality in aquatic bodies under the influence of uranium mining (MG, Brazil). Environ Monit Assess. 2013 Mar 1;185(3):2395–406.

42. Ferrari CR, Nascimento H de AF do, Rodgher S, Almeida T, Bruschi AL, Nascimento MRL do, et al. Effects of the discharge of uranium mining effluents on the water quality of the reservoir: an integrative chemical and ecotoxicological assessment. Sci Rep. 2017 Oct 24;7(1):1–10.

43. Green A. Cleaning up a toxic legacy: environmental remediation of former uranium production sites in Central Asia. IAEA Bulletin. 2016 Apr;57(1):10–1.

44. Scheele F, Wilde-Ramsing J. Uranium from Africa mitigation of uranium mining impacts on society and environment by industry and governments. Amsterdam; Amsterdam: WISE ; SOMO; 2011.

45. Chareyon B. Impact of the Kayelekera uranium mine [Internet]. Environmental Justice Organisations, Liabilities and Trade; 2015 p. 77. Report No.: EJOLT Report No. 21. Available from: https://mininginmalawi.files.wordpress.com/2013/05/chareyron-2015-impact-of-kum-malawi.pdf

46. WISE Uranium Project. Issues at Operating Uranium Mines and Mills - Africa [Internet]. [cited 2020 May 15]. Available from: https://www.wise-uranium.org/umopafr.html

47. EURSSEM. Table A2 Candidate Radiological contaminants - 103 [Internet]. 2011 [cited 2017 Oct 28]. Available from: http://eurssem.eu/assets/103

48. Marcinowski F. Potential for Radiation Contamination Associated With Mineral and Resource Extraction Industries [Internet]. US Environmental Protection Agency; 2003 [cited 2016 Sep 7]. Available from: https://www.epa.gov/sites/production/files/2015-04/documents/mineguide.pdf

49. Sweeck L, Kanyár B, Krajewski P, Kryshev A, Lietava P, Nenyei A, et al. Model testing for the remediation assessment of a radium contaminated site in Olen, Belgium. Journal of Environmental Radioactivity. 2005;84(2):245–58.

50. Carvalho FP, Madruga MJ, Reis MC, Alves JG, Oliveira JM, Gouveia J, et al. Radioactivity in the environment around past radium and uranium mining sites of Portugal. Journal of Environmental Radioactivity. 2007 Jul 1;96(1):39–46.

51. Tyler AN, Dale P, Copplestone D, Bradley S, Ewen H, McGuire C, et al. The radium legacy: Contaminated land and the committed effective dose from the ingestion of radium contaminated materials. Environment International. 2013 Sep 1;59:449–55.

52. International Atomic Energy Agency. The environmental behaviour of radium. Vienna; 2014. (Technical Reports).

53. EURSSEM. Table A3 Hazardous contaminants - 104 [Internet]. 2011 [cited 2017 Oct 28]. Available from: http://eurssem.eu/assets/104

54. Winde F. Uranium pollution of the Wonderfonteinspruit, 1997-2008 Part 1: uranium toxicity, regional background and mining-related sources of uranium pollution. Water SA. 2010 Apr;36(3):239–56.

55. Winde F. Uranium pollution of the Wonderfonteinspruit, 1997-2008 Part 2: Uranium in water - concentrations, loads and associated risks. Water SA. 2010 Apr;36(3):257–78.

56. U.S. Environmental Protection Agency. TENORM: Gold, Silver, Zircon and Titanium Mining Wastes [Internet]. [cited 2016 Sep 12]. Available from: https://www.epa.gov/radiation/tenorm-gold-silver-zircon-and-titanium-mining-wastes

57. Winde F, Wade P, Van der Walt IJ. Gold tailings as a source of waterborne uranium contamination of streams - the Koekemoerspruit (Klerksdorp goldfield, South Africa) as a case study - part I of III: uranium migration along the aqueous pathway. Water SA [Internet]. 2004 Aug 3 [cited 2016 Oct 4];30(2). Available from: http://www.ajol.info/index.php/wsa/article/view/5067

58. Winde F, Sandham LA. Uranium pollution of South African streams – An overview of the situation in gold mining areas of the Witwatersrand. GeoJournal. 2004;61(2):131–49.

59. The Expert Team of the Inter-Ministerial Committee under the Coordination of the Council for Geoscience. Mine water management in the Witwatersrand gold fields with special emphasis on acid mine drainage. 2010 Dec.

60. Balch O. Radioactive city: how Johannesburg's townships are paying for its mining past. The Guardian [Internet]. 2015 Jul 6 [cited 2016 Oct 4]; Available from: https://www.theguardian.com/cities/2015/jul/06/radioactive-city-how-johannesburgs-townships-are-paying-for-its-mining-past

61. British Geological Survey. Rare Earth Elements [Internet]. Nottingham, United Kingdom: British Geological Survey, Natural Environment Research Council; 2011 p. 54. Available from: www.mineralsuk.com

62. International Atomic Energy Agency. Radiation Protection and NORM Residue Management in the Production of Rare Earths from Thorium containing Minerals. [Internet]. Vienna: International Atomic Energy Agency; 2011 [cited 2019 Feb 11] p. 259. (Safety Reports Series). Report No.: 68. Available from: http://public.ebookcentral.proquest.com/choice/publicfullrecord.aspx?p=5267085

63. National Nuclear Laboratory. Thorium and uranium fuel cycles: comparison by the National Nuclear Laboratory [Internet]. Department of Energy & Climate Change; 2012 Sep [cited 2016 Oct 4]. Report No.: NNL (11) 11593 Issue 5. Available from: https://www.gov.uk/government/publications/thorium-and-uranium-fuel-cycles-comparison-by-the-national-nuclear-laboratory

64. World Nuclear Association. Uranium from Rare Earths deposits [Internet]. World Nuclear Association. 2016 [cited 2016 Oct 1]. Available from: http://world-nuclear.org/information-library/nuclear-fuel-cycle/uranium-resources/uranium-from-rare-earths-deposits.aspx

65. Yusoff M, Latifah A. Rare earth processing in Malaysia: case study of ARE and MAREC. In: Omar R, Ali Rahman Z, Latif MT, Lihan T, Adam JH, editors. Proceedings of the Regional Symposium on Environment and Natural Resources [Internet]. Kuala Lumpur, Malaysia; 2002 [cited 2016 Oct 4]. p. 287–295. Available from: https://www.scribd.com/document/47811051/Malaysia-RE

66. Castor SB, Hedrick JB. Rare Earth Elements. In: Industrial Minerals and Rocks: Commodities, Markets, and Uses. 7th ed. Society for Mining, Metallurgy, and Exploration; 2006. p. 767–92.

67. Bradsher K. Mitsubishi Is Quietly Cleaning Up a Former Rare Earth Refinery - The New York Times [Internet]. 2011 [cited 2019 Feb 11]. Available from: https://www.nytimes.com/2011/03/09/business/energy-environment/09rareside.html?ref=energy-environment

68. Schmidt G. Description and critical environmental evaluation of the REE refining plant LAMP near Kuantan/Malaysia [Internet]. Darmstadt, Germany: Öko-Institut e.V.; 2013 Jan p. 114. Available from: https://waste-management-world.com/l.php?u=http%3A%2F%2Fwww.oeko.de%2Foekodoc%2F1628%2F2013-001-en.pdf

69. AL-Areqi WM, Majid AAb, Sarmani S, Bahri CNACZ. Thorium: Issues and prospects in Malaysia. In Skudai, Johor, Malaysia; 2015 [cited 2019 Feb 11]. p. 040005. Available from: http://aip.scitation.org/doi/abs/10.1063/1.4916865

70. Jegathesan M. Toxic legacy in Malaysia rare-earths village [Internet]. phys.org. [cited 2016 Oct 4]. Available from: http://phys.org/news/2012-06-toxic-legacy-malaysia-rare-earths-village.html

71. Gilmore JC, Jackson RG. Radiological Hazards from Deposits of Tin-Smelting Slag and the Problems of Site Clearance and Disposal. In: IRPA 8 [Internet]. Montreal, Canada; 1992. Available from: http://www.irpa.net/irpa8/cdrom/VOL.2/M2_97.PDF

72. National Research Council. Major Sources of Technologically Enhanced Naturally-Occurring Radioactive Materials. In: Evaluation of Guidelines for Exposures to Technologically Enhanced Naturally Occurring Radioactive Materials [Internet]. Washington, D.C.: National Academies Press (US); 1999 [cited 2016 Sep 12]. Available from: http://www.ncbi.nlm.nih.gov/books/NBK230641/

73. Ismail B, Teng IL, Muhammad Samudi Y. Relative radiological risks derived from different TENORM wastes in Malaysia. Radiation Protection Dosimetry. 2011 Nov 1;147(4):600–7.

74. WISE Uranium Project. Issues at Operating Uranium Mines and Mills - Olympic Dam, Australia [Internet]. WISE Uranium Project. 2016 [cited 2016 Oct 4]. Available from: http://www.wise-uranium.org/umopauod.html

75. U.S. Environmental Protection Agency. TENORM: Oil and Gas Production Wastes [Internet]. [cited 2016 Sep 12]. Available from: https://www.epa.gov/radiation/tenorm-oil-and-gas-production-wastes#tab-1

76. U.S. Environmental Protection Agency. TENORM: Aluminum Production Wastes [Internet]. [cited 2016 Sep 12]. Available from: https://www.epa.gov/radiation/tenorm-aluminum-production-wastes

77. U.S. Environmental Protection Agency. TENORM: Fertilizer and Fertilizer Production Wastes [Internet]. [cited 2016 Sep 12]. Available from: https://www.epa.gov/radiation/tenorm-fertilizer-and-fertilizer-production-wastes

78. U.S. Environmental Protection Agency. TENORM: Copper Mining and Production Wastes [Internet]. [cited 2016 Sep 12]. Available from: https://www.epa.gov/radiation/tenorm-copper-mining-and-production-wastes#tab-1

79. International Atomic Energy Agency. Advancing Implementation of Decommissioning and Environmental Remediation Programmes [Internet]. Vienna: International Atomic Energy Agency; 2016 [cited 2016 Jul 29]. (IAEA Nuclear Energy Series). Report No.: NW-T-1.10. Available from: http://www-pub.iaea.org/books/IAEABooks/10993/CIDER

80. International Atomic Energy Agency. Estimation of global inventories of radioactive waste and other radioactive materials. Vienna: International Atomic Energy Agency; 2008. (Tecdoc).

81. Hartman HL, Mutmansky JM. Introductory Mining Engineering. 2nd ed. John Wiley & Sons; 2002. 586 p.

82. Thiel R, Smith ME. State of the practice review of heap leach pad design issues. Geotextiles and Geomembranes. 2004 Dec;22(6):555–68.

83. Groundwater Engineering. Mine Dewatering [Internet]. Groundwater Engineering; 2013 [cited 2016 Sep 30]. Available from: http://www.groundwatereng.com/uploads/groundwater_engineering/files/TDS_-_Mine_Dewatering1.pdf

84. Wills BA, Finch JA. Chapter 1 - Introduction. In: Wills' Mineral Processing Technology (Eighth Edition) [Internet]. Boston: Butterworth-Heinemann; 2016. p. 1–27. Available from: http://www.sciencedirect.com/science/article/pii/B9780080970530000017

85. Wills BA, Finch JA. Chapter 16 - Tailings Disposal. In: Wills' Mineral Processing Technology (Eighth Edition) [Internet]. Boston: Butterworth-Heinemann; 2016. p. 439–48. Available from: http://www.sciencedirect.com/science/article/pii/B9780080970530000169

86. Klohn ES. Seepage Control for Tailings Dams. In: Argall GO, Brawner CO, editors. Mine Drainage – Proceedings of the First International Mine Drainage Symposium [Internet]. San Francisco: Freeman; 1979 [cited 2016 Sep 30]. p. 671–725. Available from: https://www.imwa.info/imwaconferencesandcongresses/proceedings/193-proceedings-1979.html

87. Smith ES, Connell DH. The Role of Water in the Failure of Tailings Dams. In: Argall GO, Brawner CO, editors. Mine Drainage – Proceedings of the First International Mine Drainage Symposium [Internet]. San Francisco: Freeman; 1979 [cited 2016 Sep 30]. p. 627–650. Available from: https://www.imwa.info/imwaconferencesandcongresses/proceedings/193-proceedings-1979.html

88. Villavicencio G, Espinace R, Palma J, Fourie A, Valenzuela P. Failures of sand tailings dams in a highly seismic country. Can Geotech J. 2013 Dec 21;51(4):449–64.

89. International Atomic Energy Agency, editor. Monitoring and surveillance of residues from the mining and milling of Uranium and Thorium. Vienna: International Atomic Energy Agency; 2002. 65 p. (Safety reports series).

90. Potocki M, Mayewski PA, Kurbatov AV, Simões JC, Dixon DA, Goodwin I, et al. Recent increase in Antarctic Peninsula ice core uranium concentrations. Atmospheric Environment. 2016 Sep;140:381–5.

91. Morrison SJ, Spangler RR. Extraction of uranium and molybdenum from aqueous solutions: a survey of industrial materials for use in chemical barriers for uranium mill tailings remediation. Environ Sci Technol. 1992 Oct 1;26(10):1922–31.

92. Winde F, Erasmus E. Assessing risks associated with the flooding of mine voids on underground infrastructure and water resources in and around Johannesburg (South Africa). In: Merkel BJ, Arab A, editors. Uranium - Past and Future Challenges. Cham: Springer International Publishing; 2015. p. 201–10.

93. EURSSEM. 4.5.6 Pump and treat for surface and groundwater (SRT) [Internet]. EURSSEM. [cited 2016 Oct 3]. Available from: http://eurssem.eu/pages/4-5-6-pump-and-treat-for-surface-and-groundwater-srt

94. EURSSEM. 4.3.1 Planning approach: monitored non-intervention [Internet]. [cited 2016 Oct 5]. Available from: http://eurssem.eu/pages/4-3-1-planning-approach-monitored-non-intervention

95. Seaman JC, Arey JS, Bertsch PM. Immobilization of Nickel and Other Metals in Contaminated Sediments by Hydroxyapatite Addition. Journal of Environmental Quality. 2001;30(2):460–9.

96. Scullion J. Remediating polluted soils. Naturwissenschaften. 2006 Feb;93(2):51–65.

97. International Atomic Energy Agency. Policy and Strategies for Environmental Remediation [Internet]. Vienna: International Atomic Energy Agency; 2015 [cited 2016 Jul 29]. (IAEA Nuclear Energy Series). Report No.: NW-G-3.1. Available from: http://www-pub.iaea.org/books/IAEABooks/10622/Policy

98. Wismut GmbH. Tailings Pond Remediation, tailings management areas [Internet]. [cited 2020 May 23]. Available from: https://www.wismut.de/www/webroot/en/tailings_pond_remediation.php

99. WISE Uranium Project. Chronology of major tailings dam failures [Internet]. WISE Uranium Project. 2016 [cited 2016 Aug 3]. Available from: http://wise-uranium.org/mdaf.html

100. Waggitt P. Sustainability: the Balanced Approach to Modern Uranium Mining. In: Merkel B, Schipek M, editors. The New Uranium Mining Boom: Challenge and Lessons learned [Internet]. Berlin, Heidelberg: Springer; 2012 [cited 2020 May 22]. p. 193–9. (Springer Geology). Available from: https://doi.org/10.1007/978-3-642-22122-4_23

101. Gadd GM. Bioremedial potential of microbial mechanisms of metal mobilization and immobilization. Current Opinion in Biotechnology. 2000 Jun 1;11(3):271–9.

102. Newsome L, Morris K, Lloyd JR. The biogeochemistry and bioremediation of uranium and other priority radionuclides. Chemical Geology. 2014 Jan 10;363:164–84.

103. Handley-Sidhu S, Hriljac JA, Cuthbert MO, Renshaw JC, Pattrick RAD, Charnock JM, et al. Bacterially Produced Calcium Phosphate Nanobiominerals: Sorption Capacity, Site Preferences, and Stability of Captured Radionuclides. Environ Sci Technol. 2014 Jun 17;48(12):6891–8.

104. Newsome L, Morris K, Trivedi D, Bewsher A, Lloyd JR. Biostimulation by Glycerol Phosphate to Precipitate Recalcitrant Uranium(IV) Phosphate. Environ Sci Technol. 2015 Sep 15;49(18):11070–8.

105. Koch-Steindl H, Pröhl G. Considerations on the behaviour of long-lived radionuclides in the soil. Radiat Environ Biophys. 2001 Jun 1;40(2):93–104.

106. Fedorak PM, Westlake DW, Anders C, Kratochvil B, Motkosky N, Anderson WB, et al. Microbial release of 226Ra2+ from (Ba,Ra)SO4 sludges from uranium mine wastes. Appl Environ Microbiol. 1986 Aug;52(2):262–8.

107. Ekström SM, Regnell O, Reader HE, Nilsson PA, Löfgren S, Kritzberg ES. Increasing concentrations of iron in surface waters as a consequence of reducing conditions in the catchment area. Journal of Geophysical Research: Biogeosciences. 2016;121(2):479–93.

108. Hemmings RT, Cornelies BJ. Process for enhanced remediation of contaminated wastewaters, soils and wasteforms [Internet]. WO2010144149A1, 2010 [cited 2020 Feb 28]. Available from: https://patents.google.com/patent/WO2010144149A1/en

109. Fuller CC, Bargar JR, Davis JA. Molecular-Scale Characterization of Uranium Sorption by Bone Apatite Materials for a Permeable Reactive Barrier Demonstration. Environmental Science & Technology. 2003 Oct;37(20):4642–9.

110. Nriagu JO. Phosphate Minerals: Their Properties and General Modes of Occurrence. In: Nriagu JO, Moore PB, editors. Photosphate Minerals [Internet]. Berlin, Heidelberg: Springer Berlin Heidelberg; 1984 [cited 2019 Dec 2]. p. 1–136. Available from: http://link.springer.com/10.1007/978-3-642-61736-2_1

111. Rard JA, Wolery TJ. The Standard Chemical-Thermodynamic Properties of Phosphorus and Some of its Key Compounds and Aqueous Species: An Evaluation of Differences between the Previous Recommendations of NBS/NIST and CODATA. Journal of Solution Chemistry. 2007 Nov 27;36(11–12):1585–99.

112. Eighmy TT, Crannell BS, Butler LG, Cartledge FK, Emery EF, Oblas D, et al. Heavy Metal Stabilization in Municipal Solid Waste Combustion Dry Scrubber Residue Using Soluble Phosphate. Environmental Science & Technology. 1997 Nov;31(11):3330–8.

113. Roncal-Herrero T, Rodríguez-Blanco JD, Oelkers EH, Benning LG. The direct precipitation of rhabdophane (REEPO4·nH2O) nano-rods from acidic aqueous solutions at 5–100 °C. Journal of Nanoparticle Research. 2011 Sep;13(9):4049–62.

114. Hughes JM, Rakovan JF. Structurally Robust, Chemically Diverse: Apatite and Apatite Supergroup Minerals. Elements. 2015 Jun 1;11(3):165–70.

115. Ayati M, Lundager Madsen HE. Crystallization of some heavy-metal phosphates alone and in the presence of calcium ion. Journal of Crystal Growth. 2000 Jan;208(1–4):579–91.

116. Rakovan JF, Pasteris JD. A Technological Gem: Materials, Medical, and Environmental Mineralogy of Apatite. Elements. 2015 Jun 1;11(3):195–200.

117. Hafsteinsdóttir EG, Camenzuli D, Rocavert AL, Walworth J, Gore DB. Chemical immobilization of metals and metalloids by phosphates. Applied Geochemistry. 2015 Aug;59:47–62.

118. Cetiner ZS, Wood SA, Gammons CH. The aqueous geochemistry of the rare earth elements. Part XIV. The solubility of rare earth element phosphates from 23 to 150 °C. Chemical Geology. 2005 Apr 15;217(1):147–69.

119. Heuser J, Bukaemskiy AA, Neumeier S, Neumann A, Bosbach D. Raman and infrared spectroscopy of monazite-type ceramics used for nuclear waste conditioning. Progress in Nuclear Energy. 2014 Apr 1;72:149–55.

120. Mesbah A, Clavier N, Elkaim E, Szenknect S, Dacheux N. In pursuit of the rhabdophane crystal structure: from the hydrated monoclinic LnPO 4 .0.667H 2 O to the hexagonal LnPO 4 (Ln = Nd, Sm, Gd, Eu and Dy). Journal of Solid State Chemistry. 2017 May;249:221–7.

121. Baker MR, Coutelot FM, Seaman JC. Phosphate amendments for chemical immobilization of uranium in contaminated soil. Environment International. 2019 Aug;129:565–72.

122. Rieuwerts JS, Austin S, Harris EA. Contamination from historic metal mines and the need for non-invasive remediation techniques: a case study from Southwest England. Environmental Monitoring and Assessment. 2009 Jan;148(1–4):149–58.

123. Boisson J, Ruttens A, Mench M, Vangronsveld J. Evaluation of hydroxyapatite as a metal immobilizing soil additive for the remediation of polluted soils. Part 1. Influence of hydroxyapatite on metal

exchangeability in soil, plant growth and plant metal accumulation. Environmental Pollution. 1999 Feb;104(2):225–33.

124. Kaplan DI, Knox AS. Enhanced Contaminant Desorption Induced by Phosphate Mineral Additions to Sediment. Environmental Science & Technology. 2004 Jun;38(11):3153–60.

125. Szrek D, Bajda T, Manecki M. A comparative study of the most effective amendment for Pb, Zn and Cd immobilization in contaminated soils. Journal of Environmental Science and Health, Part A. 2011 Nov;46(13):1491–502.

126. Saxena S, Prasad M, D'Souza SF. Radionuclide Sorption onto Low-Cost Mineral Adsorbent. Industrial & Engineering Chemistry Research. 2006 Dec;45(26):9122–8.

127. da Silva EAB, Costa CAE, Vilar VJP, Botelho CMS, Larosi MB, Saracho JMP, et al. Water Remediation Using Calcium Phosphate Derived From Marine Residues. Water, Air, & Soil Pollution. 2012 Mar;223(3):989–1003.

128. Handley-Sidhu S, Mullan TK, Grail Q, Albadarneh M, Ohnuki T, Macaskie LE. Influence of pH, competing ions, and salinity on the sorption of strontium and cobalt onto biogenic hydroxyapatite. Sci Rep. 2016 Mar 18;6:23361.

129. Lammers LN, Rasmussen H, Adilman D, deLemos JL, Zeeb P, Larson DG, et al. Groundwater uranium stabilization by a metastable hydroxyapatite. Applied Geochemistry. 2017 Sep 1;84(Supplement C):105–13.

130. Cheng T, Barnett MO, Roden EE, Zhuang J. Effects of Phosphate on Uranium(VI) Adsorption to Goethite-Coated Sand. Environmental Science & Technology. 2004 Nov;38(22):6059–65.

131. Payne TE, Davis JA, Waite TD. Uranium Adsorption on Ferrihydrite - Effects of Phosphate and Humic Acid. Radiochimica Acta [Internet]. 1996 Jan 1 [cited 2019 Jan 24];74(s1). Available from: http://www.degruyter.com/view/j/ract.1996.74.issue-s1/ract.1996.74.special-issue.239/ract.1996.74.special-issue.239.xml

132. Duc M, Lefevre G, Fedoroff M, Jeanjean J, Rouchaud JC, Monteil-Rivera F, et al. Sorption of selenium anionic species on apatites and iron oxides from aqueous solutions. Journal of Environmental Radioactivity. 2003;70(1–2):61–72.

133. Thomson B, Smith C, Busch R, Siegel M, Baldwin C. Removal of Metals and Radionuclides Using Apatite and Other Natural Sorbents. J Environ Eng. 2003 May 15;129(6):492–9.

134. Czerniczyniec M, Farías S, Magallanes J, Cicerone D. Arsenic(V) Adsorption onto Biogenic Hydroxyapatite: Solution Composition Effects. Water, Air, and Soil Pollution. 2007 Mar 1;180(1):75–82.

135. Zhai H, Wang L, Qin L, Zhang W, Putnis CV, Putnis A. Direct Observation of Simultaneous Immobilization of Cadmium and Arsenate at the Brushite–Fluid Interface. Environ Sci Technol. 2018 Mar 20;52(6):3493–502.

136. Impellitteri CA. Effects of pH and phosphate on metal distribution with emphasis on As speciation and mobilization in soils from a lead smelting site. Science of The Total Environment. 2005 Jun 1;345(1):175–90.

137. Hodson ME, Valsami-Jones E, Cotter-Howells JD, Dubbin WE, Kemp AJ, Thornton I, et al. Effect of bone meal (calcium phosphate) amendments on metal release from contaminated soils — a leaching column study. Environmental Pollution. 2001 Apr;112(2):233–43.

138. Ma QYing, Logan TJ, Traina SJ. Lead Immobilization from Aqueous Solutions and Contaminated Soils Using Phosphate Rocks. Environ Sci Technol. 1995 Apr 1;29(4):1118–26.

139. Chen, Wright JV, Conca JL, Peurrung LM. Effects of pH on Heavy Metal Sorption on Mineral Apatite. Environmental Science & Technology. 1997 Mar;31(3):624–31.

140. Hong CO, Chung DY, Lee DK, Kim PJ. Comparison of phosphate materials for immobilizing cadmium in soil. Arch Environ Contam Toxicol. 2010 Feb;58(2):268–74.

141. Park JH, Bolan N. Lead immobilization and bioavailability in microbial and root interface. Journal of Hazardous Materials. 2013 Oct;261:777–83.

142. Butusov M, Jernelöv A. Fertilizers: 100 Years of Supremacy. In: Phosphorus [Internet]. New York, NY: Springer New York; 2013 [cited 2019 Feb 18]. p. 37–52. Available from: http://link.springer.com/10.1007/978-1-4614-6803-5_5

143. Butusov M, Jernelöv A. Silent Underground Life. In: Phosphorus [Internet]. New York, NY: Springer New York; 2013 [cited 2019 Feb 18]. p. 23–35. Available from: http://link.springer.com/10.1007/978-1-4614-6803-5_4

144. Frankel RB, Bazylinski DA. Biologically Induced Mineralization by Bacteria. Reviews in Mineralogy and Geochemistry. 2003 Jan 3;54(1):95–114.

145. Weiner S, Dove PM. An Overview of Biomineralization Processes and the Problem of the Vital Effect. Reviews in Mineralogy and Geochemistry. 2003 Jan 3;54(1):1–29.

146. Admassu W, Breese T. Feasibility of using natural fishbone apatite as a substitute for hydroxyapatite in remediating aqueous heavy metals. Journal of Hazardous Materials. 1999 Oct;69(2):187–96.

147. Conca JL, Lu N, Parker G, Moore B, Adams A, Wright J, et al. PIMS - REMEDIATION OF METAL CONTAMINATED WATERS AND SOILS. In: Proceedings of the Second International Conference on Remediation of Chlorinated and Recalcitrant Compounds [Internet]. 2000 [cited 2016 Aug 1]. Available from: http://www.pimsnw.com/papers/apatite2/

148. Chattanathan SA, Clement TP, Kanel SR, Barnett MO, Chatakondi N. Remediation of Uranium-contaminated Groundwater by Sorption onto Hydroxyapatite Derived from Catfish Bones. Water, Air, & Soil Pollution [Internet]. 2013 Feb [cited 2019 Feb 21];224(2). Available from: http://link.springer.com/10.1007/s11270-012-1429-5

149. Hwang A, Ji W, Khim J. Characteristics of phosphorus containing waste-bones. Materials Letters. 2007 Feb;61(3):677–9.

150. Goto T, Sasaki K. Effects of trace elements in fish bones on crystal characteristics of hydroxyapatite obtained by calcination. Ceramics International. 2014 Aug;40(7):10777–85.

151. Dybowska A, Manning DAC, Collins MJ, Wess T, Woodgate S, Valsami-Jones E. An evaluation of the reactivity of synthetic and natural apatites in the presence of aqueous metals. Science of The Total Environment. 2009 Apr 1;407(8):2953–65.

152. Hodson ME, Valsami-Jones É, Cotter-Howells JD. Bonemeal Additions as a Remediation Treatment for Metal Contaminated Soil. Environmental Science & Technology. 2000 Aug;34(16):3501–7.

153. Ashry A, Bailey EH, Chenery SRN, Young SD. Kinetic study of time-dependent fixation of U VI on biochar. Journal of Hazardous Materials. 2016 Dec;320:55–66.

154. Yong P, Macaskie LE, Sammons R l., Marquis PM. Synthesis of nanophase hydroxyapatite by a Serratia sp. from waste-water containing inorganic phosphate. Biotechnology Letters. 2004 Nov 1;26(22):1723–30.

155. Hupfer M, Gloess S, Grossart H. Polyphosphate-accumulating microorganisms in aquatic sediments. Aquatic Microbial Ecology. 2007 May 30;47:299–311.

156. Mañas A, Pocquet M, Biscans B, Sperandio M. Parameters influencing calcium phosphate precipitation in granular sludge sequencing batch reactor. Chemical Engineering Science. 2012 Jul 30;77:165–75.

157. Isanta E, Suárez-Ojeda ME, Val del Río Á, Morales N, Pérez J, Carrera J. Long term operation of a granular sequencing batch reactor at pilot scale treating a low-strength wastewater. Chemical Engineering Journal. 2012 Aug 1;198–199:163–70.

158. Akiyama M, Kawasaki S. Improvement in the unconfined compressive strength of sand test pieces cemented with calcium phosphate compound by addition of calcium carbonate. Ecological Engineering. 2012 Oct;47:264–7.

159. Akiyama M, Kawasaki S. Microbially mediated sand solidification using calcium phosphate compounds. Engineering Geology. 2012 Jun;137–138:29–39.

160. Akiyama M, Kawasaki S. Novel grout material comprised of calcium phosphate compounds: In vitro evaluation of crystal precipitation and strength reinforcement. Engineering Geology. 2012 Jan;125:119–28.

161. Turner RJ, Renshaw JC, Hamilton A. Biogenic Hydroxyapatite: A New Material for the Preservation and Restoration of the Built Environment. ACS Appl Mater Interfaces. 2017 Sep 20;9(37):31401–10.

162. Volkland H-P, Harms H, Muller B, Repphun G, Wanner O, Zehnder AJB. Bacterial Phosphating of Mild (Unalloyed) Steel. Applied and Environmental Microbiology. 2000 Oct 1;66(10):4389–95.

163. Jiang M, Ohnuki T, Kozai N, Tanaka K, Suzuki Y, Sakamoto F, et al. Biological nano-mineralization of Ce phosphate by Saccharomyces cerevisiae. Chemical Geology. 2010 Oct 1;277(1):61–9.

164. Jiang M, Ohnuki T, Tanaka K, Kozai N, Kamiishi E, Utsunomiya S. Post-adsorption process of Yb phosphate nano-particle formation by Saccharomyces cerevisiae. Geochimica et Cosmochimica Acta. 2012 Sep 15;93(Supplement C):30–46.

165. Thomas RA, Beswick AJ, Basnakova G, Moller R, Macaskie LE. Growth of naturally occurring microbial isolates in metal-citrate medium and bioremediation of metal-citrate wastes. Journal of Chemical Technology & Biotechnology. 2000 Mar;75(3):187–95.

166. Li Z, Wang F, Bai T, Tao J, Guo J, Yang M, et al. Lead immobilization by geological fluorapatite and fungus Aspergillus niger. Journal of Hazardous Materials. 2016 Dec;320:386–92.

167. Hu N, Li K, Sui Y, Ding D, Dai Z, Li D, et al. Utilization of phosphate rock as a sole source of phosphorus for uranium biomineralization mediated by *Penicillium funiculosum*. RSC Advances. 2018;8(24):13459–65.

168. Andrès Y, MacCordick HJ, Hubert JC. Selective biosorption of thorium ions by an immobilized mycobacterial biomass. Applied Microbiology and Biotechnology. 1995 Dec;44(1–2):271–6.

169. Templeton AS, Trainor TP, Spormann AM, Newville M, Sutton SR, Dohnalkova A, et al. Sorption versus Biomineralization of Pb(II) within *Burkholderia cepacia* Biofilms. Environmental Science & Technology. 2003 Jan;37(2):300–7.

170. Mire CE, Tourjee JA, O'Brien WF, Ramanujachary KV, Hecht GB. Lead Precipitation by Vibrio harveyi: Evidence for Novel Quorum-Sensing Interactions. Applied and Environmental Microbiology. 2004 Feb 1;70(2):855–64.

171. Nie X, Dong F, Bian L, Liu M, Ding C, He H, et al. Uranium Binding on *Landoltia punctata* as a Result of Formation of Insoluble Nano-U (VI) and U (IV) Phosphate Minerals. ACS Sustainable Chemistry & Engineering. 2017 Feb 6;5(2):1494–502.

172. Huang W, Cheng W, Nie X, Dong F, Ding C, Liu M, et al. Microscopic and Spectroscopic Insights into Uranium Phosphate Mineral Precipitated by Bacillus Mucilaginosus. ACS Earth Space Chem [Internet]. 2017 Aug 11; Available from: http://dx.doi.org/10.1021/acsearthspacechem.7b00060

173. Sharma J, Shamim K, Dubey SK. Phosphatase mediated bioprecipitation of lead as pyromorphite by Achromobacter xylosoxidans. Journal of Environmental Management. 2018 Jul 1;217:754–61.

174. Aickin RM, Dean ACR. Lead Accumulation by Pseudomonas-Fluorescens and by a Citrobacter Sp. Microbios Letters. 1979;9(34):55–66.

175. Macaskie LE, Dean ACR. Cadmium accumulation by micro-organisms. Environmental Technology Letters. 1982 Jan 1;3(1–11):49–56.

176. Macaskie LE, Dean ACR. Cadmium Accumulation by a Citrobacter sp. Microbiology. 1984 Jan 1;130(1):53–62.

177. Michel LJ, Macaskie LE, Dean ACR. Cadmium accumulation by immobilized cells of aCitrobacter sp. using various phosphate donors. Biotechnology and Bioengineering. 1986 Sep;28(9):1358–65.

178. Hambling SG, Macaskie LE, Dean ACR. Phosphatase Synthesis in a Citvobacter sp. Growing in Continuous Culture. Microbiology. 1987;133(10):2743–9.

179. Macaskie LE, Dean ACR, Cheetham AK, Jakeman RJB, Skarnulis AJ. Cadmium Accumulation by a Citrobacter sp.: the Chemical Nature of the Accumulated Metal Precipitate and its Location on the Bacterial Cells. Microbiology. 1987 Mar 1;133(3):539–44.

180. Macaskie LE. An immobilized cell bioprocess for the removal of heavy metals from aqueous flows. J Chem Technol Biotechnol. 1990 Jan 1;49(4):357–79.

181. Watson JHP, Ellwood DC. Biomagnetic separation and extraction process for heavy metals from solution. Minerals Engineering. 1994 Aug;7(8):1017–28.

182. Paterson-Beedle M, Readman JE, Hriljac JA, Macaskie LE. Biorecovery of uranium from aqueous solutions at the expense of phytic acid. Hydrometallurgy. 2010 Oct;104(3–4):524–8.

183. Yung MC, Jiao Y. Biomineralization of Uranium by PhoY Phosphatase Activity Aids Cell Survival in Caulobacter crescentus. Appl Environ Microbiol. 2014 Aug 15;80(16):4795–804.

184. Liang X, Hillier S, Pendlowski H, Gray N, Ceci A, Gadd GM. Uranium phosphate biomineralization by fungi. Environmental Microbiology. 2015;17(6):2064–75.

185. Liang X, Csetenyi L, Gadd GM. Uranium bioprecipitation mediated by yeasts utilizing organic phosphorus substrates. Appl Microbiol Biotechnol. 2016;100(11):5141–51.

186. Cotter-Howells J, Caporn S. Remediation of contaminated land by formation of heavy metal phosphates. Applied Geochemistry. 1996 Jan;11(1–2):335–42.

187. Martinez RJ, Wu CH, Beazley MJ, Andersen GL, Conrad ME, Hazen TC, et al. Microbial Community Responses to Organophosphate Substrate Additions in Contaminated Subsurface Sediments. PLoS ONE. 2014 Jun 20;9(6):e100383.

188. Salome KR, Beazley MJ, Webb SM, Sobecky PA, Taillefert M. Biomineralization of U(VI) phosphate promoted by microbially-mediated phytate hydrolysis in contaminated soils. Geochimica et Cosmochimica Acta. 2017 Jan 15;197:27–42.

189. Selvaraj U, Venu-Babu P, Thilagaraj WR. Application of H412R mutant alkaline phosphatase for removal of heavy metals from single-ion solutions and effluents. International Journal of Environmental Science and Technology [Internet]. 2018 May 31 [cited 2019 Feb 25]; Available from: http://link.springer.com/10.1007/s13762-018-1730-y

190. Basnakova G, Macaskie LE. Microbially enhanced chemisorption of nickel into biologically synthesized hydrogen uranyl phosphate: A novel system for the removal and recovery of metals from aqueous solutions. Biotechnol Bioeng. 1997 May 20;54(4):319–28.

191. Basnakova G, Spencer AJ, Palsgard E, Grime GW, Macaskie LE. Identification of the Nickel Uranyl Phosphate Deposits on *Citrobacter* sp. Cells by Electron Microscopy with Electron Probe X-ray Microanalysis and by Proton-Induced X-ray Emission Analysis. Environmental Science & Technology. 1998 Mar;32(6):760–5.

192. Basnakova G, Macaskie LE. Microbially-enhanced chemisorption of Ni2+ ions into biologically-synthesised hydrogen uranyl phosphate (HUP) and selective recovery of concentrated Ni2+ using citrate or chloride ion. Biotechnology Letters. 2001 Jan 1;23(1):67–70.

193. Paterson-Beedle M, Macaskie LE, Lee CH, Hriljac JA, Jee KY, Kim WH. Utilisation of a hydrogen uranyl phosphate-based ion exchanger supported on a biofilm for the removal of cobalt, strontium and caesium from aqueous solutions. Hydrometallurgy. 2006 Sep;83(1–4):141–5.

194. Beazley MJ, Martinez RJ, Sobecky PA, Webb SM, Taillefert M. Uranium Biomineralization as a Result of Bacterial Phosphatase Activity: Insights from Bacterial Isolates from a Contaminated Subsurface. Environ Sci Technol. 2007 Aug 1;41(16):5701–7.

195. Nilgiriwala KS, Alahari A, Rao AS, Apte SK. Cloning and Overexpression of Alkaline Phosphatase PhoK from Sphingomonas sp. Strain BSAR-1 for Bioprecipitation of Uranium from Alkaline Solutions. Applied and Environmental Microbiology. 2008 Sep 1;74(17):5516–23.

196. Shelobolina ES, Konishi H, Xu H, Roden EE. U(VI) Sequestration in Hydroxyapatite Produced by Microbial Glycerol 3-Phosphate Metabolism. Applied and Environmental Microbiology. 2009 Sep;75(18):5773–8.

197. Mennan C, Paterson-Beedle M, Macaskie L. Accumulation of zirconium phosphate by a Serratia sp.: a benign system for the removal of radionuclides from aqueous flows. Biotechnol Lett. 2010 Oct 1;32(10):1419–27.

198. Beazley MJ, Martinez RJ, Webb SM, Sobecky PA, Taillefert M. The effect of pH and natural microbial phosphatase activity on the speciation of uranium in subsurface soils. Geochimica et Cosmochimica Acta. 2011 Oct;75(19):5648–63.

199. Newsome L, Morris K, Lloyd JonathanR. Uranium Biominerals Precipitated by an Environmental Isolate of Serratia under Anaerobic Conditions. Janssen PJ, editor. PLOS ONE. 2015 Jul 1;10(7):e0132392.

200. Paterson-Beedle M, Macaskie LE, Readman JE, Hriljac JA. Biorecovery of Uranium from Minewaters into Pure Mineral Product at the Expense of Plant Wastes. Advanced Materials Research. 2009 May;71–73:621–4.

201. Roeselers G, Van Loosdrecht MCM. Microbial phytase-induced calcium-phosphate precipitation — a potential soil stabilization method. Folia Microbiol. 2010 Nov 1;55(6):621–4.

202. Liang X, Kierans M, Ceci A, Hillier S, Gadd GM. Phosphatase-mediated bioprecipitation of lead by soil fungi. Environ Microbiol. 2016 Jan 1;18(1):219–31.

203. Zhang L, Song X, Shao X, Wu Y, Zhang X, Wang S, et al. Lead immobilization assisted by fungal decomposition of organophosphate under various pH values. Sci Rep. 2019 Sep 16;9(1):1–9.

204. Chaudhuri G, Venu-Babu P, Dalal D, Thilagaraj WR. Application of alkaline phosphatase for heavy metals precipitation using ascorbic acid 2-phosphate as an effective natural substrate. International Journal of Environmental Science and Technology. 2015 Dec;12(12):3877–86.

205. Chaudhuri G, Chatterjee S, Venu-Babu P, Ramasamy K, Thilagaraj WR. Kinetic behaviour of calf intestinal alkaline phosphatase with pNPP. Indian J Biochem Biophys. 2013 Feb;50(1):64–71.

206. Chaudhuri G, Shah GA, Dey P, S. G, Venu-Babu P, Thilagaraj WR. Enzymatically mediated bioprecipitation of heavy metals from industrial wastes and single ion solutions by mammalian alkaline phosphatase. Journal of Environmental Science and Health, Part A. 2013 Jan;48(1):79–85.

207. Lucas J, Prévôt L. Synthèse d'apatite a partir de matière organique phosphorée (ARN) et de calcite par voie bacterienne. CR Acad Sci (Paris) Ser II. 1981;(292):1203–8.

208. Lucas J, Prévôt L. Synthèse de l'apatite par voie bactérienne à partir de matière organique phosphatée et de divers carbonates de calcium dans des eaux douce et marine naturelles. Chemical Geology. 1984 Jan 1;42(1):101–18.

209. Lucas J, Prévôt L. The synthesis of apatite by bacterial activity : mechanism. Sciences Géologiques, bulletins et mémoires. 1985;77(1):83–92.

210. Hirschler A, Lucas J, Hubert J-C. Bacterial involvement in apatite genesis. FEMS Microbiology Letters. 1990 Apr 1;73(3):211–20.

211. Macaskie LE, Yong P, Paterson-Beedle M, Thackray AC, Marquis PM, Sammons RL, et al. A novel non line-of-sight method for coating hydroxyapatite onto the surfaces of support materials by biomineralization. Journal of Biotechnology. 2005 Aug 4;118(2):187–200.

212. Macaskie L, Yong P, Handley-Sidhu S, Moriyama S, Sasaki K, Renshaw J. Biogenic Hydroxyapatite: New Nanophase Material for Radionuclide Removal. Geochimica et Cosmochimica Acta. 2010;74(12, Supplement):651.

213. Holliday K, Handley-Sidhu S, Renshaw J, Macaskie L, Stumpf T. Using TRLFS to Explain Increased Uptake of Eu(III) and Cm(III) into Biologically Produced Apatite. Mineralogical Magazine. 2011;75(3):1039.

214. Handley-Sidhu S, Renshaw JoannaC, Yong P, Kerley R, Macaskie LynneE. Nano-crystalline hydroxyapatite bio-mineral for the treatment of strontium from aqueous solutions. Biotechnol Lett. 2011 Jan 1;33(1):79–87.

215. Handley-Sidhu S, Renshaw JC, Moriyama S, Stolpe B, Mennan C, Bagheriasl S, et al. Uptake of Sr2+ and Co2+ into Biogenic Hydroxyapatite: Implications for Biomineral Ion Exchange Synthesis. Environ Sci Technol. 2011 Aug 15;45(16):6985–90.

216. Holliday K, Handley-Sidhu S, Dardenne K, Renshaw J, Macaskie L, Walther C, et al. A New Incorporation Mechanism for Trivalent Actinides into Bioapatite: A TRLFS and EXAFS Study. Langmuir. 2012 Feb 28;28(8):3845–51.

217. Ballester A, Castro L, Costa MC, Carlier J, García-Roig M, Pérez-Galende P, et al. Design of remediation pilot plants for the treatment of industrial metal-bearing effluents (BIOMETAL DEMO project): Lab tests. Hydrometallurgy. 2017 Mar;168:103–15.

218. Macaskie LE, Hewitt CJ, Shearer JA, Kent CA. Biomass production for the removal of heavy metals from aqueous solutions at low pH using growth-decoupled cells of a Citrobacter sp. International Biodeterioration & Biodegradation. 1995;35(1–3):73–92.

219. Tolley MR, Strachan LF, Macaskie LE. Lanthanum accumalation from acidic solutions using aCitrobacter sp. immobilized in a flow-through bioreactor. Journal of Industrial Microbiology. 1995 Mar;14(3–4):271–80.

220. Yong P, Macaskie LE. The role of sulfate as a competitive inhibitor of enzymatically-mediated heavy metal uptake by Citrobacter sp: implications in the bioremediation of acid mine drainage water using biogenic phosphate precipitant. Journal of Chemical Technology & Biotechnology. 1999;74(12):1149–56.

221. Macaskie LE, Empson RM, Cheetham AK, Grey CP, Skarnulis AJ. Uranium bioaccumulation by a Citrobacter sp. as a result of enzymically mediated growth of polycrystalline HUO2PO4. Science. 1992 Aug 7;257(5071):782–4.

222. Macaskie LE, Empson RM, Lin F, Tolley MR. Enzymatically-mediated uranium accumulation and uranium recovery using a Citrobacter sp. Immobilised as a biofilm within a plug-flow reactor. J Chem Technol Biotechnol. 1995 May 1;63(1):1–16.

223. Yong P, Macaskie LE. Enhancement of uranium bioaccumulation by aCitrobacter sp. via enzymically-mediated growth of polycrystalline NH4UO2PO4. Journal of Chemical Technology AND Biotechnology. 1995 Jun;63(2):101–8.

224. Yong P, Macaskie LE. Role of citrate as a complexing ligand which permits enzymically-mediated uranyl ion bioaccumulation. Bull Environ Contam Toxicol. 1995 Jun 1;54(6):892–9.

225. Finlay JA, Allan VJM, Conner A, Callow ME, Basnakova G, Macaskie LE. Phosphate release and heavy metal accumulation by biofilm-immobilized and chemically-coupled cells of a citrobacter sp. pre-grown in continuous culture. Biotechnol Bioeng. 1999 Apr 5;63(1):87–97.

226. Basnakova G, Macaskie LE. Accumulation of zirconium and nickel by Citrobacter sp. J Chem Technol Biotechnol. 1999 Jun 1;74(6):509–14.

227. Macaskie LE, Paterson-Beedle M, Mennan C, Readman JE, Hriljac JA, Graf von der Schulenburg DA, et al. Uptake of cobalt, strontium and caesium by zirconium bioaccumulation. Journal of Biotechnology. 2008 Oct;136:S681.

228. Mali G, Šala M, Arčon I, Kaučič V, Kolar J. Insight into the Short-Range Structure of Amorphous Iron Inositol Hexaphosphate as Provided by ^{31} P NMR and Fe X-ray Absorption Spectroscopy. J Phys Chem B. 2006 Nov;110(46):23060–7.

229. Shears SB, Turner BL. Nomenclature and terminology of inositol phosphates: clarification and a glossary of terms. In: Turner BL, Richardson AE, Mullaney EJ, editors. Inositol phosphates: linking agriculture and the environment [Internet]. Wallingford: CABI; 2007 [cited 2016 Jan 15]. p. 1–6. Available from: http://www.cabi.org/cabebooks/ebook/20073069289

230. Duffin PA. The effect of phytate on mineral bioavailability and heavy metal contaminants. [Internet] [Doctor of Philosophy]. [Guildford, Surrey, United Kingdom]: University of Surrey; 1989 [cited 2020 Mar 2]. Available from: http://epubs.surrey.ac.uk/595/

231. Brown EC, Heit ML, Ryan DE. PHYTIC ACID: AN ANALYTICAL INVESTIGATION. Canadian Journal of Chemistry. 1961 Jun 1;39(6):1290–7.

232. Graf E. Applications of phytic acid. Journal of the American Oil Chemists' Society. 1983 Nov;60(11):1861–7.

233. Shetty JK, Paulson B, Pepsin M, Chotani G, Dean B, Hruby M. Phytase in fuel ethanol production offers economical and environmental benefits. International Sugar Journal. 2008;110(1311):160–74.

234. Noureddini H, Malik M, Byun J, Ankeny AJ. Distribution of phosphorus compounds in corn processing. Bioresour Technol. 2009 Jan;100(2):731–6.

235. Khullar E, Shetty JK, Rausch KD, Tumbleson ME, Singh V. Use of Phytases in Ethanol Production from E-Mill Corn Processing. Cereal Chemistry Journal. 2011 May;88(3):223–7.

236. He Q, Rodrigues Reis CE, Wang F, Hu B. Phytate extraction from coproducts of the dry-grind corn ethanol process. RSC Advances. 2017;7(9):5466–72.

237. Madsen CK, Brearley CA, Brinch-Pedersen H. Lab-scale preparation and QC of phytase assay substrate from rice bran. Analytical Biochemistry. 2019 Aug;578:7–12.

238. Dvořáková J. Phytase: Sources, preparation and exploitation. Folia Microbiol. 1998 Aug 1;43(4):323–38.

239. Boyce A, Casey A, Walsh G. A phytase enzyme-based biochemistry practical particularly suited to students undertaking courses in biotechnology and environmental science. Biochemistry and Molecular Biology Education. 2004 Sep;32(5):336–40.

240. Lei XG, Porres JM. Phytase and inositol phosphates in animal nutrition: dietary manipulation and phosphorus excretion by animals. In: Turner BL, Richardson AE, Mullaney EJ, editors. Inositol phosphates: linking agriculture and the environment [Internet]. Wallingford: CABI; 2007 [cited 2016 Jan 15]. p. 133–49. Available from: http://www.cabi.org/cabebooks/ebook/20073069291

241. Leytem AB, Maguire RO. Environmental implications of inositol phosphates in animal manures. In: Turner BL, Richardson AE, Mullaney EJ, editors. Inositol phosphates: linking agriculture and the environment [Internet]. Wallingford: CABI; 2007 [cited 2016 Jan 15]. p. 150–68. Available from: http://www.cabi.org/cabebooks/ebook/20073069292

242. Gulati HK, Chadha BS, Saini HS. Production and characterization of thermostable alkaline phytase from Bacillus laevolacticus isolated from rhizosphere soil. J Ind Microbiol Biotechnol. 2007 Jan 1;34(1):91–8.

243. Olstorpe M, Schnürer J, Passoth V. Screening of yeast strains for phytase activity. FEMS Yeast Research. 2009 May 1;9(3):478–88.

244. Seaman JC, Hutchison JM, Jackson BP, Vulava VM. In Situ Treatment of Metals in Contaminated Soils with Phytate. Journal of Environment Quality. 2003;32(1):153.

245. Şimşek S, Ulusoy U, Ceyhan Ö. Adsorption of UO22+, Tl+, Pb2+, Ra2+ and Ac3+ onto polyacrylamide-bentonite composite. Journal of Radioanalytical and Nuclear Chemistry. 2003 May 1;256(2):315–21.

246. Ulusoy U, Şimşek S, Ceyhan Ö. Investigations for Modification of Polyacrylamide-Bentonite by Phytic Acid and its Usability in Fe3+, Zn2+ and UO22+ Adsorption. Adsorption. 2003 Jun 1;9(2):165–75.

247. Şimşek S, Ulusoy U. UO22+, Tl+, Pb2+, Ra2+, Bi3+ and Ac3+ adsorption onto polyacrylamide-zeolite composite and its modified composition by phytic acid. Journal of Radioanalytical and Nuclear Chemistry. 2004 Jul 1;261(1):79–86.

248. Ulusoy U, Simsek S. Lead removal by polyacrylamide-bentonite and zeolite composites: Effect of phytic acid immobilization. Journal of Hazardous Materials. 2005 Dec 9;127(1–3):163–71.

249. Baybaş D, Ulusoy U. The use of polyacrylamide-aluminosilicate composites for thorium adsorption. Applied Clay Science. 2011 Jan;51(1–2):138–46.

250. Faghihian H, Farsani SN. Modification of Polyacrylamide–β–Zeolite Composite by Phytic Acid for the Removal of Lead from Aqueous Solutions. Polish Journal of Chemical Technology. 2013 Mar 1;15(1):1–6.

251. Jensen MP, Nash KL, Morss LR, Appelman EH, Schmidt MA. Immobilization of Actinides in Geomedia by Phosphate Precipitation. In: Gaffney JS, Marley NA, Clark SB, editors. Humic and Fulvic Acids [Internet]. Washington, DC: American Chemical Society; 1996 [cited 2019 Jan 24]. p. 272–85. Available from: http://pubs.acs.org/doi/abs/10.1021/bk-1996-0651.ch017

252. Falck WE. The long-term safety of uranium mine and mill tailing legacies in an enlarged EU. Luxembourg: Publications Office; 2008.

253. Nash KL, Jensen MP, Schmidt MA. In-Situ Mineralization of Actinides for Groundwater Cleanup: Laboratory Demonstration with Soil from the Fernald Environmental Management Project [Internet]. Argonne National Lab., IL (United States); 1997 Nov [cited 2015 Dec 18]. Report No.: ANL/CHM/CP--93218; CONF-970962--. Available from: http://www.osti.gov/scitech/biblio/554810-SGLlj1/webviewable/

254. Tovar-Valdín G, Ordóñez-Regil E, Almazán-Torres M-G, Martínez-Gallegos S. Synthesis and characterization of phytate–uranium (VI) complexes. Journal of Radioanalytical and Nuclear Chemistry. 2018 Dec;318(3):2129–37.

255. Greenwood AJ, Lewis DH. Phosphatases and the utilisation of inositol hexaphosphate by soil yeasts of the genus Cryptococcus. Soil Biology and Biochemistry. 1977;9(3):161–6.

256. Greiner R. Phytate-degrading enzymes: regulation of synthesis in microorganisms and plants. In: Turner BL, Richardson AE, Mullaney EJ, editors. Inositol phosphates: linking agriculture and the environment [Internet]. Wallingford: CABI; 2007 [cited 2016 Jan 15]. p. 78–96. Available from: http://www.cabi.org/cabebooks/ebook/20073069303

257. Hill JE, Richardson AE. Isolation and assessment of microorganisms that utilize phytate. In: Turner BL, Richardson AE, Mullaney EJ, editors. Inositol phosphates: linking agriculture and the environment [Internet]. Wallingford: CABI; 2007 [cited 2016 Jan 15]. p. 61–77. Available from: http://www.cabi.org/cabebooks/ebook/20073069301

258. Mullaney EJ, Ullah AHJ. The term phytase comprises several different classes of enzymes. Biochemical and Biophysical Research Communications. 2003 Dec 5;312(1):179–84.

259. ExplorEnz: Search Results for ‘phytase’ [Internet]. [cited 2017 Sep 18]. Available from: http://www.enzyme-database.org/query.php?name=phytase&search=search_all&display=show_all&order=ec_num&nr=50

260. Mullaney EJ, Ullah AHJ. Phytases: attributes, catalytic mechanisms and applications. In: Turner BL, Richardson AE, Mullaney EJ, editors. Inositol phosphates: linking agriculture and the environment [Internet]. Wallingford: CABI; 2007 [cited 2016 Jan 15]. p. 97–110. Available from: http://www.cabi.org/cabebooks/ebook/20073069304

261. Han Y, Wilson DB, Lei X gen. Expression of an Aspergillus niger Phytase Gene (phyA) in Saccharomyces cerevisiae. Applied and Environmental Microbiology. 1999 May;65(5):1915–8.

262. Frank AW. 3 - Lower myo-Inositol Phosphates. In: Frank AW, editor. Chemistry of Plant Phosphorus Compounds [Internet]. Oxford: Elsevier; 2013. p. 135–58. Available from: http://www.sciencedirect.com/science/article/pii/B9780124071940000032

263. Greiner R, Silva LG da, Couri S. Purification and characterisation of an extracellular phytase from Aspergillus niger 11T53A9. Brazilian Journal of Microbiology. 2009 Dec;40(4):795–807.

264. Xu P, Price J, Wise A, Aggett PJ. Interaction of inositol phosphates with calcium, zinc, and histidine. Journal of Inorganic Biochemistry. 1992 Aug 1;47(2):119–30.

265. Kiss T, Zatta P, Corain B. Interaction of aluminium (III) with phosphate-binding sites: biological aspects and implications. Coordination Chemistry Reviews. 1996 May 1;149:329–46.

266. Van Den Berg CJ, Hill LF, Stanbury SW. Inositol Phosphates and Phytic Acid as Inhibitors of Biological Calcification in the Rat. Clinical Science. 1972 Sep 1;43(3):377–83.

267. High Purity And Top Cas 14306-25-3 Sodium Phytate With Reasonable Price On Hot Selling!! - Buy Sodium Phytate,14306-25-3,Sodium Phytate Food Grade Product on Alibaba.com [Internet]. www.alibaba.com. [cited 2020 Jun 28]. Available from: //www.alibaba.com/product-detail/High-Purity-and-Top-CAS-14306_62368970639.html

268. Cas:1334-74-3 Sodium Glycerol Phosphate - Buy Sodium Glycerol Phosphate,Sodium Glycerol Phosphate 1334-74-3,Disodium Glycerophosphate Cas 1334-74-3 Product on Alibaba.com [Internet]. [cited 2020 Jun 28]. Available from: https://www.alibaba.com/product-detail/CAS-1334-74-3-Sodium-glycerol_817540172.html?spm=a2700.galleryofferlist.0.0.13b41008EjoTdU

269. Hot Selling High Quality Cas 1306-06-5 Hydroxyapatite With Reasonable Price And Fast Delivery !! - Buy Hydroxyapatite,Hydroxyapatite Powder,1306-06-5 Product on Alibaba.com [Internet]. www.alibaba.com. [cited 2020 Jun 28]. Available from: //www.alibaba.com/product-detail/Hot-selling-high-quality-CAS-1306_62337813766.html

270. Higher Crop Productivity Up Fertilizer Rock Phosphate Fertilizer Phosphate Fertilizer - Buy Up Fertilizer,Rock Phosphate Fertilizer,Phosphate Fertilizer Product on Alibaba.com [Internet]. [cited 2020 Jun 28]. Available from: https://www.alibaba.com/product-detail/higher-crop-productivity-up-fertilizer-rock_1600059293109.html?spm=a2700.galleryofferlist.0.0.479372f1IC8uJJ

271. PIMS NW Inc. - Pricing [Internet]. [cited 2020 Jun 28]. Available from: http://www.pimsnw.com/pricing.php

272. Konietzny U, Greiner R. Molecular and catalytic properties of phytate-degrading enzymes (phytases). International Journal of Food Science & Technology. 2002;37(7):791–812.

273. Mittal A, Gupta V, Singh G, Yadav A, Aggarwal NK. Phytase: A Boom in Food Industry. Octa Journal of Biosciences. 2013;1(2):158–69.

274. Azeem M, Riaz A, Chaudhary AN, Hayat R, Hussain Q, Tahir MI, et al. Microbial phytase activity and their role in organic P mineralization. Archives of Agronomy and Soil Science. 2015 Jun 3;61(6):751–66.

275. Balwani I, Chakravarty K, Gaur S. Role of phytase producing microorganisms towards agricultural sustainability. Biocatalysis and Agricultural Biotechnology. 2017 Oct;12:23–9.

276. LeGeros RZ, Legeros JP. Phosphate Minerals in Human Tissues. In: Nriagu JO, Moore PB, editors. Phosphate Minerals [Internet]. Berlin, Heidelberg: Springer; 1984 [cited 2020 Feb 26]. p. 351–85. Available from: https://doi.org/10.1007/978-3-642-61736-2_12

277. Mekmene O, Quillard S, Rouillon T, Bouler J-M, Piot M, Gaucheron F. Effects of pH and Ca/P molar ratio on the quantity and crystalline structure of calcium phosphates obtained from aqueous solutions. Dairy Science and Technology. 2009 May;89(3–4):301–16.

278. Dorozhkin SV. Calcium orthophosphates: Occurrence, properties, biomineralization, pathological calcification and biomimetic applications. Biomatter. 2011 Oct;1(2):121–64.

279. Morss LR, Schmidt MAJ, Nash KL, Allen PG, Bucher JJ, Edelstein N, et al. EXAFS studies of lanthanide coordination in crystalline phosphates and amorphous phytates. In Illinois: Argonne National

Laboratory; 1995 [cited 2019 Nov 9]. p. 1–8. Available from: https://digital.library.unt.edu/ark:/67531/metadc665455/

280. Cao X, Ma LQ, Singh SP, Zhou Q. Phosphate-induced lead immobilization from different lead minerals in soils under varying pH conditions. Environmental Pollution. 2008 Mar 1;152(1):184–92.

281. Celi L, Lamacchia S, Marsan FA, Barberis E. INTERACTION OF INOSITOL HEXAPHOSPHATE ON CLAYS: ADSORPTION AND CHARGING PHENOMENA. Soil Science. 1999;164(8):574–85.

282. George TS, Quiquampoix H, Simpson RJ, Richardson AE. Interactions between phytases and soil constituents: implications for the hydrolysis of inositol phosphates. In: Turner BL, Richardson AE, Mullaney EJ, editors. Inositol phosphates: linking agriculture and the environment [Internet]. Wallingford: CABI; 2007 [cited 2016 Jan 15]. p. 221–41. Available from: http://www.cabi.org/cabebooks/ebook/20073069296

283. George TS, Simpson RJ, Gregory PJ, Richardson AE. Differential interaction of Aspergillus niger and Peniophora lycii phytases with soil particles affects the hydrolysis of inositol phosphates. Soil Biology and Biochemistry. 2007 Mar 1;39(3):793–803.

284. Giaveno C, Celi L, Richardson AE, Simpson RJ, Barberis E. Interaction of phytases with minerals and availability of substrate affect the hydrolysis of inositol phosphates. Soil Biology and Biochemistry. 2010 Mar 1;42(3):491–8.

285. Mezeli MM, Menezes-Blackburn D, George TS, Giles CD, Neilson R, Haygarth PM. Effect of citrate on Aspergillus niger phytase adsorption and catalytic activity in soil. Geoderma. 2017 Nov;305:346–53.

286. Pan Z, Giammar DE, Mehta V, Troyer LD, Catalano JG, Wang Z. Phosphate-Induced Immobilization of Uranium in Hanford Sediments. Environmental Science & Technology. 2016 Dec 20;50(24):13486–94.

287. Vats P, Banerjee UC. Studies on the production of phytase by a newly isolated strain of Aspergillus niger var teigham obtained from rotten wood-logs. Process Biochemistry. 2002 Oct;38(2):211–7.

288. Sano K, Fukuhara H, Nakamura Y. Phytase of the yeast Arxula adeninivorans. Biotechnology Letters. 1999 Jan 1;21(1):33–8.

289. Margaris NS, Mitrakos K, Markou S. Carbon sources forAspergillus niger growth under different shaking programmes. Folia Microbiol. 1974 Sep 1;19(5):394–6.

290. Meier AK, Worch S, Böer E, Hartmann A, Mascher M, Marzec M, et al. Agdc1p – a Gallic Acid Decarboxylase Involved in the Degradation of Tannic Acid in the Yeast Blastobotrys (Arxula) adeninivorans. Frontiers in Microbiology [Internet]. 2017 Sep 15 [cited 2020 Apr 13];8. Available from: http://journal.frontiersin.org/article/10.3389/fmicb.2017.01777/full

291. Vohra A, Satyanarayana T. Phytases: Microbial Sources, Production, Purification, and Potential Biotechnological Applications. Critical Reviews in Biotechnology. 2003 Jan 1;23(1):29–60.

292. Fabian C, Ayucitra A, Ismadji S, Ju Y-H. Isolation and characterization of starch from defatted rice bran. Journal of the Taiwan Institute of Chemical Engineers. 2011 Jan;42(1):86–91.

293. Lambrechts C, Boze H, Moulin G, Galzy P. Utilization of phytate by some yeasts. Biotechnol Lett. 1992 Jan 1;14(1):61–6.

294. Cold Spring Harbor Protocols. Phosphate-buffered saline (PBS). Cold Spring Harbor Protocols. 2006 Jun 1;2006(1):pdb.rec8247.

295. Bemis. Parafilm® M All-Purpose Laboratory Film [Internet]. Available from: http://www.bemis.com/na/products/parafilm-floratape/parafilm-lab

296. Lucas S, Champion E, Bregiroux D, Bernache-Assollant D, Audubert F. Rare earth phosphate powders RePO4·nH2O (Re=La, Ce or Y)—Part I. Synthesis and characterization. Journal of Solid State Chemistry. 2004 Apr;177(4–5):1302–11.

297. Herigstad B, Hamilton M, Heersink J. How to optimize the drop plate method for enumerating bacteria. J Microbiol Methods. 2001 Mar 1;44(2):121–9.

298. Qvirist L, Carlsson N-G, Andlid T. Assessing phytase activity–methods, definitions and pitfalls. J Biol Methods. 2015 Jun 4;2(1):e16.

299. Megazyme. Phytic Acid (Phytate)/Total Phosphorus [Internet]. Megazyme International Ireland; 2014. Available from: https://secure.megazyme.com/files/Booklet/K-PHYT_DATA.pdf

300. PDF-2 [Internet]. ICDD. [cited 2019 Jun 9]. Available from: http://www.icdd.com/index.php/pdf-2/

301. Inorganic Crystal Structure Database (ICSD) | Physical Sciences Data science Service [Internet]. [cited 2019 Nov 22]. Available from: https://www.psds.ac.uk/icsd

302. Crystallography Open Database [Internet]. [cited 2020 May 26]. Available from: http://crystallography.net/cod/

303. Parkhurst DL, Appelo CAJ. Description of input and examples for PHREEQC version 3—A computer program for speciation, batch-reaction, one-dimensional transport, and inverse geochemical calculations. In: US Geological Survey Techniques and Methods, book 6, chap A43 [Internet]. 2013. p. 497. Available from: https://pubs.usgs.gov/tm/06/a43/

304. Pitt JI, Hocking AD. Aspergillus and Related Teleomorphs. In: Pitt JI, Hocking AD, editors. Fungi and Food Spoilage [Internet]. Boston, MA: Springer US; 2009 [cited 2020 Apr 6]. p. 275–337. Available from: https://doi.org/10.1007/978-0-387-92207-2_8

305. Pera LM, Callieri DA. Influence of calcium on fungal growth, hyphal morphology and citric acid production inaspergillus niger. Folia Microbiol. 1997 Dec 1;42(6):551–6.

306. Papagianni M, Mattey M, Kristiansen B. The influence of glucose concentration on citric acid production and morphology of Aspergillus niger in batch and culture. Enzyme and Microbial Technology. 1999 Nov 1;25(8):710–7.

307. Wucherpfennig T, Hestler T, Krull R. Morphology engineering - Osmolality and its effect on Aspergillus niger morphology and productivity. Microbial Cell Factories. 2011 Jul 29;10(1):58.

308. Papagianni M, Nokes SE, Filer K. Production of phytase by Aspergillus niger in submerged and solid-state fermentation. Process Biochemistry. 1999 Nov;35(3–4):397–402.

309. Recillas S, Rodríguez-Lugoc V, Monterod ML, Viquez-Canoc S, Hernandeze L, Castaño VM. Studies on the precipitation behavior of calcium phosphate solutions. JCPR. 2012 Feb;013(01):5–10.

310. Persson H, Türk M, Nyman M, Sandberg A-S. Binding of Cu2+, Zn2+, and Cd2+ to Inositol Tri-, Tetra-, Penta-, and Hexaphosphates. J Agric Food Chem. 1998 Aug 17;46(8):3194–200.

311. Marolt G, Pihlar B. Potentiometric Determination of Phytic Acid and Investigations of Phytate Interactions with Some Metal Ions. Acta Chimica Slovenica. 2015 Jun 15;62(2):319–27.

312. Cole WF, Lancucki CJ. A refinement of the crystal structure of gypsum $CaSO_4.2H_2O$. Acta Crystallographica Section B Structural Crystallography and Crystal Chemistry. 1974 Apr 1;30(4):921–9.

313. Sainz-Díaz CI, Villacampa A, Otálora F. Crystallographic properties of the calcium phosphate mineral, brushite, by means of First Principles calculations. American Mineralogist. 2004 Feb 1;89(2–3):307–13.

314. Sakae T, Nagata H, Sudo T. The crystal structure of synthetic calcium phosphate-sulfate hydrate, Ca<2) HPO<4) SO<4) .4H<2) O, and its relation to brushite and gypsum. American Mineralogist. 1978 Jun 1;63(5–6):520–7.

315. Pinto AJ, Carneiro J, Katsikopoulos D, Jiménez A, Prieto M. The Link between Brushite and Gypsum: Miscibility, Dehydration, and Crystallochemical Behavior in the $CaHPO_4 \cdot 2H_2O$–$CaSO_4 \cdot 2H_2O$ System. Crystal Growth & Design. 2012 Jan 4;12(1):445–55.

316. Rinaudo C, Lanfranco AM, Boistelle R. The gypsum-brushite system: crystallization from solutions poisoned by phosphate ions. Journal of Crystal Growth. 1996 Jan;158(3):316–21.

317. Bieth H, Spiess B, Jost P. Complexation studies on inositol-phosphates. I. Ca(II) and Mg(II) complexes of D-myo-inositol 1,2,6-trisphosphate. Journal of Inorganic Biochemistry. 1990 May 1;39(1):59–73.

318. Greish YE. Phase evolution during the low temperature formation of calcium-deficient hydroxyapatite–gypsum composites. Ceramics International. 2011 Jul;37(5):1493–500.

319. Fisher RD, Hanna JV, Rees GJ, Walton RI. Calcium sulfate-phosphate composites with enhanced water resistance. Journal of Materials Chemistry. 2012;22(11):4837.

320. Belaicha N, Lemlikchi W, Mecherri MO, Sharrock P, Nzihou A. Composite Material with Calcium Sulfate and Calcium Phosphate for Heavy Metals Retention. Procedia Engineering. 2014;83:403–6.

321. Raii M. Formulation, caracterization and implementation of Permeable Reactive Barrier (PRB) made of calcium phosphate. [Internet]. Institut National Polytechnique de Toulouse; 2012 [cited 2019 Nov 24]. Available from: https://tel.archives-ouvertes.fr/tel-00842771

322. Koutsoukos PG, Amjad Z, Nancollas GH. The influence of phytate and phosphonate on the crystal growth of fluorapatite and hydroxyapatite. Journal of Colloid and Interface Science. 1981 Oct;83(2):599–605.

323. Amjad Z. Constant composition study of crystal growth of dicalcium phosphate dihydrate. The influence of polyphosphates, phosphonates, and phytate. Canadian Journal of Chemistry. 1988 Sep;66(9):2181–7.

324. Amjad Zahid. Constant composition study of crystal growth of calcium fluoride. Influence of poly(carboxylic acids), polyphosphates, phosphonates, and phytate. Langmuir. 1991 Mar;7(3):600–3.

325. Conte A, Pizá P, García-Raja A. Urinary lithogen risk test: usefulness in the evaluation of renal lithiasis treatment using crystallization inhibitors (citrate and phytate). Arch Esp Urol. 1999 Feb;52(1):94–9.

326. Grases F, March JG, Prieto RM, Simonet BM, Costa-Bauzá A, García-Raja A, et al. Urinary Phytate in Calcium Oxalate Stone Formers and Healthy People: Dietary Effects on Phytate Excretion. Scandinavian Journal of Urology and Nephrology. 2000 Jan;34(3):162–4.

327. Xu A-W, Yu Q, Dong W-F, Antonietti M, Cölfen H. Stable Amorphous CaCO3 Microparticles with Hollow Spherical Superstructures Stabilized by Phytic Acid. Advanced Materials. 2005 Sep 16;17(18):2217–21.

328. Izatulina AR, Gurzhiy VV, Krzhizhanovskaya MG, Kuz'mina MA, Leoni M, Frank-Kamenetskaya OV. Hydrated Calcium Oxalates: Crystal Structures, Thermal Stability, and Phase Evolution. Crystal Growth & Design. 2018 Sep 5;18(9):5465–78.

329. Wilson MJ, Jones D, Russell JD. Glushinskite, a naturally occurring magnesium oxalate. Mineralogical Magazine. 1980 Sep;43(331):837–40.

330. Gharieb MM, Gadd GM. Influence of nitrogen source on the solubilization of natural gypsum (CaSO4.2H2O) and the formation of calcium oxalate by different oxalic and citric acid-producing fungi. Mycological Research. 1999 Apr;103(04):473–481.

331. Gadd GM. Fungal Production of Citric and Oxalic Acid: Importance in Metal Speciation, Physiology and Biogeochemical Processes. In: R.K. Poole, editor. Advances in Microbial Physiology [Internet]. Academic Press; 1999. p. 47–92. Available from: http://www.sciencedirect.com/science/article/pii/S0065291108601654

332. Gadd GM. Geomycology: biogeochemical transformations of rocks, minerals, metals and radionuclides by fungi, bioweathering and bioremediation. Mycological Research. 2007 Jan;111(1):3–49.

333. Ganesan K, Epple M. Calcium phosphate nanoparticles as nuclei for the preparation of colloidal calcium phytate. New J Chem. 2008;32(8):1326–30.

334. Strasser H, Burgstaller W, Schinner F. High-yield production of oxalic acid for metal leaching processes by Aspergillus niger. FEMS Microbiol Lett. 1994 Jun 1;119(3):365–70.

335. Sharma S, Singh B, Thulasidas SK, Kulkarni MJ, Natarajan V, Manchanda VK. Evaluation of terrestrial plants extracts for uranium sorption and characterization of potent phytoconstituents. International Journal of Phytoremediation. 2016 Jan 2;18(1):10–5.

336. Matsumoto S, Kashino S. Sodium Hydrogen l-Tartrate. Acta Cryst C. 1996 Aug 15;52(8):1948–50.

337. HEINTZE SG. MANGANESE-PHOSPHATE REACTIONS IN AQUEOUS SYSTEMS AND THE EFFECTS OF APPLICATIONS OF MONOCALCIUM PHOSPHATE, ON THE AVAILABILITY OF MANGANESE TO OATS IN AN ALKALINE FEN SOIL. Plant and Soil. 1968;29(3):407–23.

338. Kang X, Csetenyi L, Gadd GM. Biotransformation of lanthanum by Aspergillus niger. Applied Microbiology and Biotechnology. 2019 Jan 1;103(2):981–93.

339. Ochiai A, Utsunomiya S. Crystal Chemistry and Stability of Hydrated Rare-Earth Phosphates Formed at Room Temperature. Minerals. 2017 May;7(5):84.

340. Yong P, Macaskie LE. Bioaccumulation of lanthanum, uranium and thorium, and use of a model system to develop a method for the biologically-mediated removal of plutonium from solution. Journal of Chemical Technology & Biotechnology. 1998 Jan;71(1):15–26.

341. Nott KP, Paterson-Beedle M, Macaskie LE, Hall LD. Visualisation of metal deposition in biofilm reactors by three-dimensional magnetic resonance imaging (MRI). Biotechnology Letters. 2001 Nov 1;23(21):1749–57.

342. Nott KP, Heese FP, Paterson-Beedle M, Macaskie LE, Hall LD. Visualization of the Function of a Biofilm Reactor by Magnetic Resonance Imaging. The Canadian Journal of Chemical Engineering. 2005 May 19;83(1):68–72.

343. Crea F, De Stefano C, Milea D, Sammartano S. Thermodynamic data for lanthanoid(III) sequestration by phytate at different temperatures. Monatshefte für Chemie - Chemical Monthly. 2010;141(5):511–20.

344. Leadbetter J. Rare Earth Separation Using Monazite and Xenotime [Internet]. UC Irvine; 2016 [cited 2019 Apr 23]. Available from: https://escholarship.org/uc/item/6sd0p2tg

345. Sadjadi MS, Meskinfam M, Sadeghi B, Jazdarreh H, Zare K. In situ biomimetic synthesis, characterization and in vitro investigation of bone-like nanohydroxyapatite in starch matrix. Materials Chemistry and Physics. 2010 Nov;124(1):217–22.

346. Kuusisto JE, Maloney TC. The Effect of Carbonation Conditions on the Properties of Carbohydrate-Calcium Carbonate Hybrid Pigments. BioResources [Internet]. 2015 Apr 16 [cited 2019 Nov 27];10(2). Available from: http://ojs.cnr.ncsu.edu/index.php/BioRes/article/view/6792

347. Tomasik P, Schilling C, Anderegg J, Refvik M. Starch–lanthanum complexes. Carbohydrate Polymers. 2000 Jan;41(1):61–8.

348. Lehrfeld J. Cation exchange resins prepared from phytic acid. Journal of Applied Polymer Science. 1997 Oct 17;66(3):491–7.

349. Mesbah A, Clavier N, Elkaim E, Gausse C, Kacem IB, Szenknect S, et al. Monoclinic Form of the Rhabdophane Compounds: $REEPO_4 \cdot 0.667H_2O$. Crystal Growth & Design. 2014 Oct;14(10):5090–8.

350. Momma K, Izumi F. *VESTA 3* for three-dimensional visualization of crystal, volumetric and morphology data. J Appl Crystallogr. 2011 Dec 1;44(6):1272–6.

351. Anbia M, Rofouei MK, Husain SW. Synthesis of Mesoporous Lanthanum Phosphate and Its Use as a Novel Sorbent. Chinese Journal of Chemistry. 2006 Aug;24(8):1026–30.

352. Vats BG, Rawat D, Shafeeq M, Shelke GP, Keskar M, Krishnan K. Ternary U (IV) containing phosphates: Synthesis, structure and thermodynamic studies. Journal of Alloys and Compounds. 2019 Aug;798:174–86.

353. Qin D, Mesbah A, Gausse C, Szenknect S, Dacheux N, Clavier N. Incorporation of thorium in the rhabdophane structure: Synthesis and characterization of Pr 1-2x Ca x Th x PO 4 ·nH 2 O solid solutions. Journal of Nuclear Materials. 2017 Aug;492:88–96.

354. Ordoñez-Regil E, Drot R, Simoni E, Ehrhardt JJ. Sorption of Uranium(VI) onto Lanthanum Phosphate Surfaces. Langmuir. 2002 Oct;18(21):7977–84.

355. Ordoñez-Regil E, Drot R, Simoni E. Surface complexation modeling of uranium(VI) sorbed onto lanthanum monophosphate. Journal of Colloid and Interface Science. 2003 Jul;263(2):391–9.

356. Arinicheva Y, Popa K, Scheinost AC, Rossberg A, Dieste-Blanco O, Raison P, et al. Structural investigations of (La,Pu)PO 4 monazite solid solutions: XRD and XAFS study. Journal of Nuclear Materials. 2017 Sep;493:404–11.

357. Nriagu JO, Dell CI. Diagenetic formation of iron phosphates in recent lake sediments. American Mineralogist. 1974 Oct 1;59(9–10):934–46.

358. Li R, Cui J, Li X, Li X. Phosphorus Removal and Recovery from Wastewater using Fe-Dosing Bioreactor and Cofermentation: Investigation by X-ray Absorption Near-Edge Structure Spectroscopy. Environ Sci Technol. 2018 Dec 18;52(24):14119–28.

359. He Q, Rodrigues Reis CE, Wang F, Hu B. Phytate extraction from coproducts of the dry-grind corn ethanol process. RSC Adv. 2017;7(9):5466–72.

360. Meunier J-D, Landais P, Monthioux M, Pagel M. Oxidation-reduction processes in the genesis of the uranium-vanadium tabular deposits of the Cottonwood Wash mining area (Utah, U.S.A.) : evidence from petrological study and organic matter analysis. Bulletin de Minéralogie. 1987;110(2):145–56.

361. Deditius AP, Utsunomiya S, Ewing RC. The chemical stability of coffinite, USiO4·nH2O; 0. Chemical Geology. 2008 Jun 1;251(1):33–49.

362. Dhal PK, Sar P. Microbial communities in uranium mine tailings and mine water sediment from Jaduguda U mine, India: A culture independent analysis. Journal of Environmental Science and Health, Part A. 2014 May 12;49(6):694–709.

363. Awad G, Elnashar M, Danial E. Optimization of phytase production by Penicillium funiculosum NRC467 under solid state fermentation by using full factorial design. World Applied Sciences Journal. 2011;15(11):1635–44.

364. Jafari-Tapeh H, Hamidi-Esfahani Z, Azizi MH. Culture Condition Improvement for Phytase Production in Solid State Fermentation by Aspergillus ficuum Using Statistical Method [Internet]. Vol. 2012, ISRN Chemical Engineering. Hindawi; 2012 [cited 2020 Apr 28]. p. e479167. Available from: https://www.hindawi.com/journals/isrn/2012/479167/

365. McKinney K, Combs J, Becker P, Humphries A, Filer K, Vriesekoop F. Optimization of Phytase Production from Escherichia coli by Altering Solid-State Fermentation Conditions. Fermentation. 2015 Jul 30;1(1):13–23.

366. Bostick BC, Fendorf S, Barnett MO, Jardine PM, Brooks SC. Uranyl Surface Complexes Formed on Subsurface Media from DOE Facilities. Soil Science Society of America Journal. 2002;66(1):99–108.

367. Bachmaf S, Planer-Friedrich B, Merkel BJ. Uranium sorption and desorption behavior on bentonite. In: Merkel BJ, Hasche-Berger A, editors. Uranium, Mining and Hydrogeology [Internet]. Berlin, Heidelberg: Springer Berlin Heidelberg; 2008 [cited 2019 Jan 24]. p. 515–24. Available from: http://link.springer.com/10.1007/978-3-540-87746-2_63

368. Bachmaf S, Planer-Friedrich B, Merkel BJ. Effect of sulfate, carbonate, and phosphate on the uranium(VI) sorption behavior onto bentonite. Radiochimica Acta [Internet]. 2008 Jan 1 [cited 2020 Apr 27];96(6). Available from: http://www.degruyter.com/view/j/ract.2008.96.issue-6/ract.2008.1496/ract.2008.1496.xml

369. Guo Z, Yan C, Xu J, Wu W. Sorption of U(VI) and phosphate on γ-alumina: Binary and ternary sorption systems. Colloids and Surfaces A: Physicochemical and Engineering Aspects. 2009 Mar 20;336(1):123–9.

370. Bachmaf S. Uranium Sorption on Clay Minerals: Laboratory Experiments and Surface Complexation Modeling. Universität Bergakademie Freiberg; 2010.

371. Singh A, Ulrich K-U, Giammar DE. Impact of phosphate on U(VI) immobilization in the presence of goethite. Geochimica et Cosmochimica Acta. 2010 Nov 15;74(22):6324–43.

372. Singh A, Catalano JG, Ulrich K-U, Giammar DE. Molecular-Scale Structure of Uranium(VI) Immobilized with Goethite and Phosphate. Environ Sci Technol. 2012 Jun 19;46(12):6594–603.

373. Tiberg C, Sjöstedt C, Persson I, Gustafsson JP. Phosphate effects on copper(II) and lead(II) sorption to ferrihydrite. Geochimica et Cosmochimica Acta. 2013 Nov 1;120:140–57.

374. Sato T, Murakami T, Yanase N, Isobe H, Payne TE, Airey PL. Iron Nodules Scavenging Uranium from Groundwater. Environ Sci Technol. 1997 Oct 1;31(10):2854–8.

375. Menezes-Blackburn D, Jorquera M, Gianfreda L, Rao M, Greiner R, Garrido E, et al. Activity stabilization of Aspergillus niger and Escherichia coli phytases immobilized on allophanic synthetic compounds and montmorillonite nanoclays. Bioresource Technology. 2011 Oct 1;102(20):9360–7.

376. Yu WH, Li N, Tong DS, Zhou CH, Lin CX (Cynthia), Xu CY. Adsorption of proteins and nucleic acids on clay minerals and their interactions: A review. Applied Clay Science. 2013 Aug 1;80–81:443–52.

377. Wang J, Liu J, Li H, Chen Y, Xiao T, Song G, et al. Uranium and thorium leachability in contaminated stream sediments from a uranium minesite. Journal of Geochemical Exploration. 2017 May;176:85–90.

378. Ito M, Azam S. Dewatering Behaviour of a Uranium Ore Slurry Containing Clays. Geotechnical and Geological Engineering. 2017 Dec;35(6):2549–69.

379. Abdelouas A. Uranium Mill Tailings: Geochemistry, Mineralogy, and Environmental Impact. Elements. 2006 Dec 1;2(6):335–41.

380. Shaw SA, Hendry MJ, Essilfie-Dughan J, Kotzer T, Wallschläger D. Distribution, characterization, and geochemical controls of elements of concern in uranium mine tailings, Key Lake, Saskatchewan, Canada. Applied Geochemistry. 2011 Dec;26(12):2044–56.

381. Schindler M, Legrand CA, Hochella MF. Alteration, adsorption and nucleation processes on clay–water interfaces: Mechanisms for the retention of uranium by altered clay surfaces on the nanometer scale. Geochimica et Cosmochimica Acta. 2015 Mar;153:15–36.

382. Déjeant A, Galoisy L, Roy R, Calas G, Boekhout F, Phrommavanh V, et al. Evolution of uranium distribution and speciation in mill tailings, COMINAK Mine, Niger. Science of The Total Environment. 2016 Mar;545–546:340–52.

383. Chautard C, Beaucaire C, Gérard M, Phrommavanh V, Nos J, Galoisy L, et al. Geochemical Characterization of U Tailings (Bois Noirs Limouzat, France). Procedia Earth and Planetary Science. 2017 Jan 1;17:308–11.

384. Liu B, Peng T, Sun H, Yue H. Release behavior of uranium in uranium mill tailings under environmental conditions. Journal of Environmental Radioactivity. 2017 May;171:160–8.

385. Liu B, Peng T, Sun H. Leaching behavior of U, Mn, Sr, and Pb from different particle-size fractions of uranium mill tailings. Environmental Science and Pollution Research. 2017 Jun;24(18):15804–15.

386. Alam MdS, Cheng T. Uranium release from sediment to groundwater: Influence of water chemistry and insights into release mechanisms. Journal of Contaminant Hydrology. 2014 Aug;164:72–87.

387. Jenneman GE, McInerney MJ, Crocker ME, Knapp RM. Effect of Sterilization by Dry Heat or Autoclaving on Bacterial Penetration through Berea Sandstone. Appl Environ Microbiol. 1986 Jan;51(1):39–43.

388. van Wollingen P, Seviour RJ. Using the Stomacher for preparing standard inocula from non-spore-forming fungi. Transactions of the British Mycological Society. 1986 Jan 1;86(3):487–90.

389. Mehta S. Geochemical evaluation of uranium sequestration from field-scale infiltration and injection of polyphosphate solutions in contaminated Hanford sediments. Applied Geochemistry. 2017 Sep 1;84(Supplement C):133–53.

390. Schindelin J, Arganda-Carreras I, Frise E, Kaynig V, Longair M, Pietzsch T, et al. Fiji: an open-source platform for biological-image analysis. Nature Methods. 2012 Jul;9(7):676–82.

391. Rueden CT, Schindelin J, Hiner MC, DeZonia BE, Walter AE, Arena ET, et al. ImageJ2: ImageJ for the next generation of scientific image data. BMC Bioinformatics [Internet]. 2017 Dec [cited 2019 May 27];18(1). Available from: https://bmcbioinformatics.biomedcentral.com/articles/10.1186/s12859-017-1934-z

392. Mettler-Toledo AG. InLab® Redox combination electrodes (ORP). 2007.

393. OriginPro. Northampton, MA, USA: OriginLab Corporation;

394. Menges F. Spectragryph - optical spectroscopy software [Internet]. 2019. Available from: http://www.effemm2.de/spectragryph/

395. Bio-Rad KnowItAll® Informatics System Vibrational Spectroscopy Edition. Bio-Rad Laboratories, Inc.;

396. Celi L, Lamacchia S, Barberis E. Interaction of inositol phosphate with calcite. Nutrient Cycling in Agroecosystems. 2000 Jul 1;57(3):271–7.

397. Hu Z, Jaisi DP, Yan Y, Chen H, Wang X, Wan B, et al. Adsorption and precipitation of myo-inositol hexakisphosphate onto kaolinite. European Journal of Soil Science. 2020;71(2):226–35.

398. Pedrotti M, Tarantino A. An experimental investigation into the micromechanics of non-active clays. Géotechnique. 2017 Nov 8;68(8):666–83.

399. Ruyter-Hooley M, Johnson BB, Morton DW, Angove MJ. The adsorption of myo-inositol hexaphosphate onto kaolinite and its effect on cadmium retention. Applied Clay Science. 2017 Jan 1;135:405–13.

400. Sposito G. The Chemistry of Soils. Oxford University Press, USA; 2008. 342 p.

401. He LM, Zelazny LW, Martens DC, Baligar VC, Ritchey KD. Ionic Strength Effects on Sulfate and Phosphate Adsorption on γ-Alumina and Kaolinite: Triple-Layer Model. Soil Science Society of America Journal. 1997;61(3):784–93.

402. Franchi M, Ferris JP, Gallori E. Cations as Mediators of the Adsorption of Nucleic Acids on Clay Surfaces in Prebiotic Environments. Orig Life Evol Biosph. 2003 Feb 1;33(1):1–16.

403. Wang X, Lee SY, Miller K, Welbourn R, Stocker I, Clarke S, et al. Cation Bridging Studied by Specular Neutron Reflection. Langmuir. 2013 May 7;29(18):5520–7.

404. Sheng X, Qin C, Yang B, Hu X, Liu C, Waigi MG, et al. Metal cation saturation on montmorillonites facilitates the adsorption of DNA via cation bridging. Chemosphere. 2019 Nov 1;235:670–8.

405. Giaveno C, Celi L, Cessa RMA, Prati M, Bonifacio E, Barberis E. INTERACTION OF ORGANIC PHOSPHORUS WITH CLAYS EXTRACTED FROM OXISOLS. Soil Science. 2008 Oct;173(10):694–706.

406. George TS, Richardson AE, Simpson RJ. Behaviour of plant-derived extracellular phytase upon addition to soil. Soil Biology and Biochemistry. 2005 May 1;37(5):977–88.

407. Socrates G. Infrared and Raman characteristic group frequencies: tables and charts. 3. ed., repr. as paperback. Chichester: Wiley; 2001. 347 p.

408. Dithmer L, Lipton AS, Reitzel K, Warner TE, Lundberg D, Nielsen UG. Characterization of Phosphate Sequestration by a Lanthanum Modified Bentonite Clay: A Solid-State NMR, EXAFS, and PXRD Study. Environ Sci Technol. 2015 Apr 7;49(7):4559–66.

409. Cotter-Howells J. Separation of high density minerals from soil. Science of The Total Environment. 1993 Apr 15;132(1):93–8.

410. Minto JM, Tan Q, Lunn RJ, El Mountassir G, Guo H, Cheng X. 'Microbial mortar'-restoration of degraded marble structures with microbially induced carbonate precipitation. Construction and Building Materials. 2018 Aug;180:44–54.

411. Tobler DJ, Minto JM, El Mountassir G, Lunn RJ, Phoenix VR. Microscale Analysis of Fractured Rock Sealed With Microbially Induced $CaCO_3$ Precipitation: Influence on Hydraulic and Mechanical Performance. Water Resour Res. 2018 Oct;54(10):8295–308.

412. Sleutel S, Cnudde V, Masschaele B, Vlassenbroek J, Dierick M, Van Hoorebeke L, et al. Comparison of different nano- and micro-focus X-ray computed tomography set-ups for the visualization of the soil microstructure and soil organic matter. Computers & Geosciences. 2008 Aug;34(8):931–8.

413. Van Loo D, Bouckaert L, Leroux O, Pauwels E, Dierick M, Van Hoorebeke L, et al. Contrast agents for soil investigation with X-ray computed tomography. Geoderma. 2014 Jan;213:485–91.

414. Bowen AD, Davidson FA, Keatch R, Gadd GM. Induction of contour sensing in Aspergillus niger by stress and its relevance to fungal growth mechanics and hyphal tip structure. Fungal Genetics and Biology. 2007 Jun;44(6):484–91.

415. Wartmann T, Erdmann J, Kunze I, Kunze G. Morphology-related effects on gene expression and protein accumulation of the yeast Arxula adeninivorans LS3. Arch Microbiol. 2000 Apr 1;173(4):253–61.

416. Malak A, Baronian K, Kunze G. Blastobotrys (Arxula) adeninivorans: a promising alternative yeast for biotechnology and basic research. Yeast. 2016;33(10):535–47.

417. Cnudde V, Masschaele B, Dierick M, Vlassenbroeck J, Hoorebeke LV, Jacobs P. Recent progress in X-ray CT as a geosciences tool. Applied Geochemistry. 2006 May;21(5):826–32.

418. Hapca SM, Wang ZX, Otten W, Wilson C, Baveye PC. Automated statistical method to align 2D chemical maps with 3D X-ray computed micro-tomographic images of soils. Geoderma. 2011 Sep;164(3–4):146–54.

419. Ruyter-Hooley M, Morton DW, Johnson BB, Angove MJ. The effect of humic acid on the sorption and desorption of myo-inositol hexaphosphate to gibbsite and kaolinite. European Journal of Soil Science. 2016;67(3):285–93.

420. Coetzee H, South Africa, Water Research Commission. An assessment of sources, pathways, mechanisms and risks of current and potential future pollution of water and sediments in gold-mining areas of the Wonderfonteinspruit Catchment: report to the Water Research Commission. Gezina: Water Research Comission; 2006.

421. Marques SM, Chaves S, Gonçalves F, Pereira R. Evaluation of growth, biochemical and bioaccumulation parameters in Pelophylax perezi tadpoles, following an in-situ acute exposure to three different effluent ponds from a uranium mine. Science of The Total Environment. 2013 Feb 15;445–446:321–8.

422. Djenbaev B, Karmisheva U, Tilenbaev A, Egemberdieva A. The modern hydrochemical state of the Mailuu-Suu river and radioecological problem of the Fergana Valley. In: Merkel BJ, Arab A, editors. Uranium - Past and Future Challenges. Cham: Springer International Publishing; 2015. p. 73–8.

423. Torgoev I, Jakubick A. Environmental Issues and Proposed Assessment of Feasibility of Remediation of the Legacy Sites of Mining and Milling in the Area of Sumsar-Shekaftar in Kyrgyzstan. In: Merkel BJ, Arab A, editors. Uranium - Past and Future Challenges. Cham: Springer International Publishing; 2015. p. 147–54.

424. Gagnaire B, Bado-Nilles A, Betoulle S, Amara R, Camilleri V, Cavalié I, et al. Former uranium mine-induced effects in caged roach: a multiparametric approach for the evaluation of in situ metal toxicity. Ecotoxicology. 2015 Jan 1;24(1):215–31.

425. Groudev S, Spasova I, Georgiev P, Nicolova M. Passive treatment of heavily polluted drainage waters in a uranium deposit. In: Merkel BJ, Arab A, editors. Uranium - Past and Future Challenges. Cham: Springer International Publishing; 2015. p. 355–62.

426. Le Guernic A, Sanchez W, Bado-Nilles A, Palluel O, Turies C, Chadili E, et al. In situ effects of metal contamination from former uranium mining sites on the health of the three-spined stickleback (Gasterosteus aculeatus, L.). Ecotoxicology. 2016 Aug 1;25(6):1234–59.

427. Rollog M, Cook NJ, Guagliardo P, Ehrig K, Ciobanu CL, Kilburn M. Detection of Trace Elements/Isotopes in Olympic Dam Copper Concentrates by nanoSIMS. Minerals. 2019 May 30;9(6):336.

428. Schlager P. Requirements for an Adequate Site Characterisation of Tailings Facilities [Internet]. Karlsruhe, Germany: Karlsruhe University; 2004 May p. 39. (Sustainable Improvement in Safety of Tailings Facilities TAILSAFE). Available from: http://www.tailsafe.com/pdf-documents/TAILSAFE_Site_Characterisation_Concept_Paper.pdf

429. Dao TH. Polyvalent Cation Effects on myo-Inositol Hexakis Dihydrogenphosphate Enzymatic Dephosphorylation in Dairy Wastewater. Journal of Environmental Quality. 2003;32(2):694–701.

430. Tang J, Leung A, Leung C, Lim BL. Hydrolysis of precipitated phytate by three distinct families of phytases. Soil Biology and Biochemistry. 2006 Jun;38(6):1316–24.

431. Nriagu JO. Formation and Stability of Base Metal Phosphates in Soils and Sediments. In: Nriagu JO, Moore PB, editors. Phosphate Minerals [Internet]. Berlin, Heidelberg: Springer; 1984 [cited 2020 Feb 26]. p. 318–29. Available from: https://doi.org/10.1007/978-3-642-61736-2_10

432. Roncal-Herrero T, Rodríguez-Blanco JD, Benning LG, Oelkers EH. Precipitation of Iron and Aluminum Phosphates Directly from Aqueous Solution as a Function of Temperature from 50 to 200 °C. Crystal Growth & Design. 2009 Dec 2;9(12):5197–205.

433. Evans WJ, Martin CJ. Interactions of inositol hexaphosphate with Pb(II) and Be(II). A calorimetric study. XVIII. Journal of Inorganic Biochemistry. 1992 Feb 1;45(2):105–13.

434. Ceci A, Rhee YJ, Kierans M, Hillier S, Pendlowski H, Gray N, et al. Transformation of vanadinite [Pb5(VO4)3Cl] by fungi. Environmental Microbiology. 2015;17(6):2018–34.

435. Mullaney EJ, Daly CB, Kim T, Porres JM, Lei XG, Sethumadhavan K, et al. Site-directed mutagenesis of Aspergillus niger NRRL 3135 phytase at residue 300 to enhance catalysis at pH 4.0. Biochemical and Biophysical Research Communications. 2002 Oct 4;297(4):1016–20.

436. Kim T, Mullaney EJ, Porres JM, Roneker KR, Crowe S, Rice S, et al. Shifting the pH Profile of Aspergillus niger PhyA Phytase To Match the Stomach pH Enhances Its Effectiveness as an Animal Feed Additive. Appl Environ Microbiol. 2006 Jun 1;72(6):4397–403.

437. World Health Organization, editor. Guidelines for drinking-water quality. 4th ed. Geneva: World Health Organization; 2011. 541 p.

438. Khangarot BS, Ray PK. Investigation of correlation between physicochemical properties of metals and their toxicity to the water flea Daphnia magna Straus. Ecotoxicology and Environmental Safety. 1989 Oct 1;18(2):109–20.

439. Bass J, Great Britain, Environment Agency. Using science to create a better place. Bristol: Environment Agency; 2008.

440. U.S. Environmental Protection Agency. Aquatic Life Ambient Water Quality Criteria for Aluminum in Freshwater [Internet]. Federal Register. 2018 [cited 2020 Feb 24]. Available from: https://www.federalregister.gov/documents/2018/12/21/2018-27745/aquatic-life-ambient-water-quality-criteria-for-aluminum-in-freshwater

441. Biesinger KE, Christensen GM. Effects of Various Metals on Survival, Growth, Reproduction, and Metabolism of Daphnia magna. J Fish Res Bd Can. 1972 Dec 1;29(12):1691–700.

442. World Health Organization. Aluminium in drinking-water: background document for development of WHO Guidelines for drinking-water quality [Internet]. Geneva: World Health Organization; 2003. Available from: https://apps.who.int/iris/handle/10665/75362

443. Herlory O, Bonzom J-M, Gilbin R, Frelon S, Fayolle S, Delmas F, et al. Use of diatom assemblages as biomonitor of the impact of treated uranium mining effluent discharge on a stream: case study of the Ritord watershed (Center-West France). Ecotoxicology. 2013 Oct 1;22(8):1186–99.

444. U.S. Environmental Protection Agency. The Use of Soil Amendments for Remediation, Revitalization, and Reuse [Internet]. U.S. Environmental Protection Agency; 2007 Dec. Report No.: EPA 542-R-07-013. Available from: https://semspub.epa.gov/work/11/176023.pdf

445. Wang W, Yang H, Wang X, Jiang J, Zhu W. Factors effecting aluminum speciation in drinking water by laboratory research. Journal of Environmental Sciences. 2010 Jan;22(1):47–55.

446. Kaikake K, Sekito T, Tsunomori M, Dote Y. Lead Stabilization Mechanisms of AlPO4 Prepared from Waste Acid Etchant in Municipal Solid Waste Incineration Fly Ash. 廃棄物資源循環学会論文誌. 2013;24(3):53–62.

447. Kolitsch U, Pring A. Crystal chemistry of the crandallite, beudantite and alunite groups: a review and evaluation of the suitability as storage materials for toxic metals. Journal of Mineralogical and Petrological Sciences. 2001;96(2):67–78.

448. Arey JS, Seaman JC, Bertsch PM. Immobilization of Uranium in Contaminated Sediments by Hydroxyapatite Addition. Environ Sci Technol. 1999 Jan 1;33(2):337–42.

449. Garcia-Guinea J, Chagoyen AM, Nickel EH. A re-investigation of bolivarite and evansite. The Canadian Mineralogist. 1995 Feb 1;33(1):59–65.

450. Jerden JL. Uranium Sequestration by Aluminum Phosphate Minerals in Unsaturated Soils. MRS Proceedings [Internet]. 2006 Jan [cited 2019 Jan 24];985. Available from: http://journals.cambridge.org/abstract_S1946427400060450

451. Sanchez-Moral S, Fernandez-Cortes A, Cuezva S, Cañaveras JC, Correcher V, Miller AZ, et al. Uranyl-Evansites from Porto (Northwest Portugal) and Galicia (Northwest Spain): Structure and Assignment of Spectra Catholuminescence and Raman Bands. Spectroscopy Letters. 2011 Oct 1;44(7–8):511–5.

452. Brini M, Ottolini D, Calì T, Carafoli E. Calcium in Health and Disease. In: Sigel A, Sigel H, Sigel RKO, editors. Interrelations between Essential Metal Ions and Human Diseases [Internet]. Dordrecht: Springer Netherlands; 2013 [cited 2020 Feb 25]. p. 81–137. (Metal Ions in Life Sciences). Available from: https://doi.org/10.1007/978-94-007-7500-8_4

453. O'Day PA, Vlassopoulos D. Mineral-Based Amendments for Remediation. Elements (Que). 2010 Dec;6(6):375–81.

454. Wuana RA, Okieimen FE. Heavy Metals in Contaminated Soils: A Review of Sources, Chemistry, Risks and Best Available Strategies for Remediation. ISRN Ecology. 2011;2011:1–20.

455. Dowling A, O'Dwyer J, Adley CC. Lime in the limelight. Journal of Cleaner Production. 2015 Apr 1;92:13–22.

456. Posner AS, Blumenthal NC, Betts F. Chemistry and Structure of Precipitated Hydroxyapatites. In: Nriagu JO, Moore PB, editors. Phosphate Minerals [Internet]. Berlin, Heidelberg: Springer; 1984 [cited 2020 Feb 26]. p. 330–50. Available from: https://doi.org/10.1007/978-3-642-61736-2_11

457. Avila DS, Puntel RL, Aschner M. Manganese in Health and Disease. In: Sigel A, Sigel H, Sigel RKO, editors. Interrelations between Essential Metal Ions and Human Diseases [Internet]. Dordrecht: Springer Netherlands; 2013 [cited 2020 Feb 25]. p. 199–227. (Metal Ions in Life Sciences). Available from: https://doi.org/10.1007/978-94-007-7500-8_7

458. Kuperman RG, Checkai RT, Phillips CT, Simini M, Speicher JA, Barclift DJ. Toxicity Assessments of Antimony, Barium, Beryllium, and Manganese for Development of Ecological Soil Screening Levels (ECO-

SSL) Using Enchytraeid Reproduction Benchmark Levels. Aberdeen Proving Ground, MD: U. S. Army Edgewood Chemical Biological Center; 2002. Report No.: ECBC-TR-324.

459. Phillips CT, Checkai RT, Kuperman RG, Simini M, Speicher JA, Barclift DJ. Toxicity Assessments of Antimony, Barium, Beryllium, and Manganese for Development of Ecological Soil Screening Levels (ECO-SSL) Using Folsomia Reproduction Benchmark Levels. Aberdeen Proving Ground, MD: U. S. Army Edgewood Chemical Biological Center; 2002. Report No.: ECBC-TR-326.

460. Simini M, Checkai RT, Kuperman RG, Phillips CT, Speicher JA, Barclift DJ. Toxicity Assessments of Antimony, Barium, Beryllium, and Manganese for Development of Ecological Soil Screening Levels (ECO-SSL) Using Earthworm (Eisenia Fetida) Benchmark Levels. Aberdeen Proving Ground, MD: U. S. Army Edgewood Chemical Biological Center; 2002. Report No.: ECBC-TR-325.

461. Borch T, Roche N, Johnson TE. Determination of contaminant levels and remediation efficacy in groundwater at a former in situ recovery uranium mine. J Environ Monit. 2012 Jun 27;14(7):1814–23.

462. Suzuki T, Hatsushika T, Miyake M. Synthetic hydroxyapatites as inorganic cation exchangers. Part 2. J Chem Soc, Faraday Trans 1. 1982 Jan 1;78(12):3605–11.

463. Hider RC, Kong X. Iron: Effect of Overload and Deficiency. In: Sigel A, Sigel H, Sigel RKO, editors. Interrelations between Essential Metal Ions and Human Diseases [Internet]. Dordrecht: Springer Netherlands; 2013 [cited 2020 Feb 25]. p. 229–94. (Metal Ions in Life Sciences). Available from: https://doi.org/10.1007/978-94-007-7500-8_8

464. Shuhaimi-Othman M, Nadzifah Y, Nur-Amalina R, Umirah NS. Deriving Freshwater Quality Criteria for Iron, Lead, Nickel, and Zinc for Protection of Aquatic Life in Malaysia. The Scientific World Journal. 2012;2012:1–7.

465. Cadmus P, Brinkman SF, May MK. Chronic Toxicity of Ferric Iron for North American Aquatic Organisms: Derivation of a Chronic Water Quality Criterion Using Single Species and Mesocosm Data. Arch Environ Contam Toxicol. 2018;74(4):605–15.

466. U.S. Environmental Protection Agency. Quality Criteria for Water. U.S. Environmental Protection Agency; 1986. Report No.: EPA 440/5-86-001.

467. Vigneault B. Geochemical changes in sulfidic mine tailings stored under a shallow water cover. Water Research. 2001 Mar;35(4):1066–76.

468. Liu R, Zhao D. In situ immobilization of Cu(II) in soils using a new class of iron phosphate nanoparticles. Chemosphere. 2007 Aug 1;68(10):1867–76.

469. De Boeck M, Kirsch-Volders M, Lison D. Cobalt and antimony: genotoxicity and carcinogenicity. Mutat Res. 2003 Dec 10;533(1–2):135–52.

470. Kim JH, Gibb HJ, Howe P, Sheffer M. Cobalt and inorganic cobalt compounds. Geneva: World Health Organization; 2006. 88 p. (Concise international chemical assessment document).

471. Yamada K. Cobalt: Its Role in Health and Disease. In: Sigel A, Sigel H, Sigel RKO, editors. Interrelations between Essential Metal Ions and Human Diseases [Internet]. Dordrecht: Springer Netherlands; 2013 [cited 2020 Feb 25]. p. 295–320. (Metal Ions in Life Sciences). Available from: https://doi.org/10.1007/978-94-007-7500-8_9

472. Nagpal NK, British Columbia, Water Protection Section, Golder Associates, British Columbia, Ministry of Water L and AP. Ambient water quality guidelines for cobalt: overview report. Victoria, B.C.: Water Protection Section, Water, Air and Climate Change Branch, Ministry of Water, Land and Air Protection; 2004.

473. Knox AS, Kaplan DI, Adriano DC, Hinton TG, Wilson MD. Apatite and Phillipsite as Sequestering Agents for Metals and Radionuclides. Journal of Environmental Quality. 2003;32(2):515–25.

474. Scheiber I, Dringen R, Mercer JFB. Copper: Effects of Deficiency and Overload. In: Sigel A, Sigel H, Sigel RKO, editors. Interrelations between Essential Metal Ions and Human Diseases [Internet]. Dordrecht: Springer Netherlands; 2013 [cited 2020 Feb 25]. p. 359–87. (Metal Ions in Life Sciences). Available from: https://doi.org/10.1007/978-94-007-7500-8_11

475. Flemming CA, Trevors JT. Copper toxicity and chemistry in the environment: a review. Water Air Soil Pollut. 1989 Mar 1;44(1):143–58.

476. Genderen EJV, Ryan AC, Tomasso JR, Klaine SJ. Evaluation of acute copper toxicity to larval fathead minnows (Pimephales promelas) in soft surface waters. Environmental Toxicology and Chemistry. 2005;24(2):408–14.

477. Ezeonyejiaku CD, Obiakor MO, Ezenwelu CO. TOXICITY OF COPPER SULPHATE AND BEHAVIORAL LOCOMOTOR RESPONSE OF TILAPIA (Oreochromis Niloticus) AND CATFISH (Clarias Gariepinus) SPECIES. Online Journal of Animal and Feed Research. 2011;1(4):130–4.

478. Ubani-Rex OA, Saliu JK, Bello TH. Biochemical Effects of the Toxic Interaction of Copper, Lead and Cadmium on Clarias gariepinus. J Health Pollut. 2017 Dec 18;7(16):38–48.

479. Cao X, Wahbi A, Ma L, Li B, Yang Y. Immobilization of Zn, Cu, and Pb in contaminated soils using phosphate rock and phosphoric acid. Journal of Hazardous Materials. 2009 May 30;164(2–3):555–64.

480. Agency for Toxic Substances and Disease Registry (ATSDR). Toxicological Profile for Barium [Internet]. Atlanta, GA: U.S. Department of Health and Human Services, Public Health Service; 2007 Aug [cited 2020 Feb 25]. Available from: https://www.atsdr.cdc.gov/ToxProfiles/tp.asp?id=327&tid=57

481. Spangenberg JV, Cherr GN. Developmental effects of barium exposure in a marine bivalve (Mytilus californianus). Environmental Toxicology and Chemistry. 1996;15(10):1769–74.

482. Lira VF, Santos GAP, Derycke S, Larrazabal MEL, Fonsêca-Genevois VG, Moens T. Effects of barium and cadmium on the population development of the marine nematode Rhabditis (Pellioditis) marina. Marine Environmental Research. 2011 Oct;72(4):151–9.

483. Beneš P, Šebesta F, Sedláček J, Obdržálek M, Šandrik R. Particulate forms of radium and barium in uranium mine waste waters and receiving river waters. Water Research. 1983 Jan 1;17(6):619–24.

484. Cazala C, Andrès C, Decossas J-L, Cathelineau M, Peiffert C. Impact of uranium mines water treatment on uranium and radium behaviour. In: Merkel BJ, Hasche-Berger A, editors. Uranium, Mining and Hydrogeology [Internet]. Berlin, Heidelberg: Springer; 2008 [cited 2020 Feb 27]. p. 829–38. Available from: https://doi.org/10.1007/978-3-540-87746-2_109

485. Suzuki T, Hatsushika T, Hayakawa Y. Synthetic hydroxyapatites employed as inorganic cation-exchangers. J Chem Soc, Faraday Trans 1. 1981 Jan 1;77(5):1059–62.

486. Sugiyama S, Matsumoto H, Hayashi H, Moffat JB. Sorption and ion-exchange properties of barium hydroxyapatite with divalent cations. Colloids and Surfaces A: Physicochemical and Engineering Aspects. 2000 Sep 1;169(1):17–26.

487. Sugiyama S, Matsumoto H, Ichii T, Hayashi H, Hiraga Y, Shigemoto N. Enhancement of Lead–Barium Exchangeability of Barium Hydroxyapatite. Journal of Colloid and Interface Science. 2001 Jun 1;238(1):183–7.

488. Herrmann H, Nolde J, Berger S, Heise S. Aquatic ecotoxicity of lanthanum – A review and an attempt to derive water and sediment quality criteria. Ecotoxicology and Environmental Safety. 2016 Feb;124:213–38.

489. MacMillan GA, Chételat J, Heath JP, Mickpegak R, Amyot M. Rare earth elements in freshwater, marine, and terrestrial ecosystems in the eastern Canadian Arctic. Environ Sci: Processes Impacts. 2017 Oct 18;19(10):1336–45.

490. Peelman S, Sun ZHI, Sietsma J, Yang Y. Leaching of Rare Earth Elements. In: Rare Earths Industry [Internet]. Elsevier; 2016 [cited 2019 Nov 9]. p. 319–34. Available from: https://linkinghub.elsevier.com/retrieve/pii/B9780128023280000218

491. Zielinski RA, Otton JK, Schumann RR, Wirt L. Uranium in Surface Waters and Sediments Affected by Historical Mining in the Denver West 1:100,000 Quadrangle, Colorado [Internet]. U.S. Geological Survey; 2008 p. 54. Report No.: 2007–5246. Available from: http://pubs.usgs.gov/sir/2007/5246

492. Moore PB. Crystallochemical Aspects of the Phosphate Minerals. In: Nriagu JO, Moore PB, editors. Phosphate Minerals [Internet]. Berlin, Heidelberg: Springer; 1984 [cited 2020 Feb 26]. p. 155–70. Available from: https://doi.org/10.1007/978-3-642-61736-2_3

493. Byrne RH, Kim K-H. Rare earth precipitation and coprecipitation behavior: The limiting role of PO43− on dissolved rare earth concentrations in seawater. Geochimica et Cosmochimica Acta. 1993 Feb 1;57(3):519–26.

494. Kagaya S, Hosomori Y, Arai H, Hasegawa K. Determination of cadmium in river water by electrothermal atomic absorption spectrometry after internal standardization-assisted rapid coprecipitation with lanthanum phosphate. Anal Sci. 2003 Jul;19(7):1061–4.

495. Kagaya S, Malek ZA, Araki Y, Hasegawa K. Application of internal standardization to rapid coprecipitation technique using lanthanum phosphate for flame atomic absorption spectrometric determination of iron and lead. Anal Sci. 2002 Aug;18(8):923–6.

496. Brandt F, Neumeier S, Schuppik T, Arinicheva Y, Bukaemskiy A, Modolo G, et al. Conditioning of minor actinides in lanthanum monazite ceramics: A surrogate study with Europium. Progress in Nuclear Energy. 2014 Apr;72:140–3.

497. Arinicheva Y, Gausse C, Neumeier S, Brandt F, Rozov K, Szenknect S, et al. Influence of temperature on the dissolution kinetics of synthetic LaPO4-monazite in acidic media between 50 and 130 °C. Journal of Nuclear Materials. 2018 Oct;509:488–95.

498. 40 CFR Part 192 - Health and Environmental Protection Standards for Uranium and Thorium Mill Tailings [Internet]. 1995. Available from: https://www.govinfo.gov/content/pkg/CFR-2018-title40-vol27/pdf/CFR-2018-title40-vol27-part192.pdf

499. Cao X, Ma LQ, Rhue DR, Appel CS. Mechanisms of lead, copper, and zinc retention by phosphate rock. Environmental Pollution. 2004 Oct 1;131(3):435–44.

500. Sternlieb MP, Pasteris JD, Williams BR, Krol KA, Yoder CH. The structure and solubility of carbonated hydroxyl and chloro lead apatites. Polyhedron. 2010 Jul 28;29(11):2364–72.

501. Hopwood JD, Derrick GR, Brown DR, Newman CD, Haley J, Kershaw R, et al. The Identification and Synthesis of Lead Apatite Minerals Formed in Lead Water Pipes. Journal of Chemistry. 2016;2016:1–11.

502. Powell KJ, Brown PL, Byrne RH, Gajda T, Hefter G, Leuz A-K, et al. Chemical speciation of environmentally significant metals with inorganic ligands. Part 3: The Pb2+ + OH–, Cl–, CO32–, SO42–, and PO43– systems (IUPAC Technical Report). Pure and Applied Chemistry. 2009 Oct 31;81(12):2425–76.

503. Palmer DC. SingleCrystal 4: real-time multi-phase diffraction simulation. J Appl Cryst. 2020 Jun 1;53(3):860–860.

504. He BB. X-Ray Source and Optics. In: Two-Dimensional X-Ray Diffraction [Internet]. John Wiley & Sons, Ltd; 2009 [cited 2020 Mar 15]. p. 51–84. Available from: https://onlinelibrary.wiley.com/doi/abs/10.1002/9780470502648.ch3

505. Mos YM, Vermeulen AC, Buisman CJN, Weijma J. X-Ray Diffraction of Iron Containing Samples: The Importance of a Suitable Configuration. Geomicrobiology Journal. 2018 Jul 3;35(6):511–7.

506. Svenson A. Effects of copper, zinc, and cadmium ions on the production of phosphate from phytic acid by the phytase system in spruce forest soil. Plant Soil. 1986 Jun 1;94(2):227–34.

507. Maenz DD, Engele-Schaan CM, Newkirk RW, Classen HL. The effect of minerals and mineral chelators on the formation of phytase-resistant and phytase-susceptible forms of phytic acid in solution and in a slurry of canola meal. Animal Feed Science and Technology. 1999 Oct;81(3–4):177–92.

508. Heighton L, Schmidt WF, Siefert RL. Kinetic and Equilibrium Constants of Phytic Acid and Ferric and Ferrous Phytate Derived from Nuclear Magnetic Resonance Spectroscopy. Journal of Agricultural and Food Chemistry. 2008 Oct 22;56(20):9543–7.

509. Nash KL. Thermally unstable complexants/phosphate mineralization of actinides [Internet]. Richland, WA (United States): Pacific Northwest Lab.; 1996. Available from: https://inis.iaea.org/collection/NCLCollectionStore/_Public/28/002/28002198.pdf?r=1&r=1

510. Butcher WW, Westheimer FH. The Lanthanum Hydroxide Gel Promoted Hydrolysis of Phosphate Esters. J Am Chem Soc. 1955 May 1;77(9):2420–4.

511. Frank AW. 1 - Sugar Phosphates. In: Frank AW, editor. Chemistry of Plant Phosphorus Compounds [Internet]. Oxford: Elsevier; 2013. p. 1–74. Available from: http://www.sciencedirect.com/science/article/pii/B9780124071940000019

512. Evans WJ, Martin CJ. Heat of complex formation of Al(III) and Cd(II) with phytic acid. IX. Journal of Inorganic Biochemistry. 1988 Sep 1;34(1):11–8.

513. Yan Y, Li W, Yang J, Zheng A, Liu F, Feng X, et al. Mechanism of Myo-inositol Hexakisphosphate Sorption on Amorphous Aluminum Hydroxide: Spectroscopic Evidence for Rapid Surface Precipitation. Environ Sci Technol. 2014 Jun 17;48(12):6735–42.

514. Burrell LS, Johnston CT, Schulze D, Klein J, White JL, Hem SL. Aluminium phosphate adjuvants prepared by precipitation at constant pH. Part I: composition and structure. Vaccine. 2000 Sep;19(2–3):275–81.

515. Singh SS. Neutralization of dilute aqueous aluminium sulfate solutions with a base. Canadian Journal of Chemistry. 1969 Feb 15;47(4):663–7.

516. Adams F, Rawajfih Z. Basaluminite and Alunite: A Possible Cause of Sulfate Retention by Acid Soils. Soil Science Society of America Journal. 1977;41(4):686.

517. Lutz HD, Haeuseler H. Infrared and Raman spectroscopy in inorganic solids research. Journal of Molecular Structure. 1999 Nov;511–512:69–75.

518. He Z, Honeycutt CW, Zhang T, Bertsch PM. Preparation and FT–IR Characterization of Metal Phytate Compounds. Journal of Environment Quality. 2006;35(4):1319–28.

519. Carli LD, Schnitzler E, Ionashiro M, Szpoganicz B, Rosso ND. Equilibrium, thermoanalytical and spectroscopic studies to characterize phytic acid complexes with Mn(II) and Co(II). Journal of the Brazilian Chemical Society. 2009;20(8):1515–22.

520. He Z, Honeycutt CW, Xing B, McDowell RW, Pellechia PJ, Zhang T. SOLID-STATE FOURIER TRANSFORM INFRARED AND 31P NUCLEAR MAGNETIC RESONANCE SPECTRAL FEATURES OF PHOSPHATE COMPOUNDS: Soil Science. 2007 Jul;172(7):501–15.

521. Miller FA, Mayo DW, Hannah RW. Course notes on the interpretation of infrared and Raman spectra. Hoboken, N.J: Wiley-Interscience; 2004. 567 p.

522. Capitelli F, Della Ventura G, Bellatreccia F, Sodo A, Saviano M, Ghiara MR, et al. Crystal-chemical study of wavellite from Zbirov, Czech Republic. Mineralogical Magazine. 2014 Aug;78(4):1057–70.

523. Kloprogge JT, Geus JW, Jansen JBH, Seykens D. Thermal stability of basic aluminum sulfate. Thermochimica Acta. 1992 Nov 1;209:265–76.

524. Contreras CA, Sugita S, Ramos E. Preparation of Sodium Aluminate From Basic Aluminium Sulfate. The AZo Journal of Materials Online [Internet]. 2006 Aug 1 [cited 2020 Jun 6];2. Available from: https://www.azom.com/article.aspx?ArticleID=3517

525. Wanner C, Pöthig R, Carrero S, Fernandez-Martinez A, Jäger C, Furrer G. Natural occurrence of nanocrystalline Al-hydroxysulfates: Insights on formation, Al solubility control and As retention. Geochimica et Cosmochimica Acta. 2018 Oct 1;238:252–69.

526. Shirodkar S, Hutchinson RL, Perry DL, White JL, Hem SL. Aluminum Compounds Used as Adjuvants in Vaccines. Pharm Res. 1990 Dec 1;7(12):1282–8.

527. He Z, Honeycutt CW, Zhang T, Pellechia PJ, Caliebe WA. Distinction of Metal Species of Phytate by Solid-State Spectroscopic Techniques. Soil Science Society of America Journal. 2007 May;71(3):940–3.

528. Lookman R, Grobet P, Merckx R, Van Riemsdijk WH. Application of 31P and 27Al MAS NMR for phosphate speciation studies in soil and aluminium hydroxides: promises and constraints. Geoderma. 1997 Nov 1;80(3):369–88.

529. Klein J, Ushio M, Burrell LS, Wenslow B, Hem SL. Analysis of Aluminum Hydroxyphosphate Vaccine Adjuvants by 27Al MAS NMR. JPharmSci. 2000 Mar 1;89(3):311–21.

530. Carrero S, Fernandez-Martinez A, Pérez-López R, Lee D, Aquilanti G, Poulain A, et al. The nanocrystalline structure of basaluminite, an aluminum hydroxide sulfate from acid mine drainage. American Mineralogist. 2017 Dec 20;102(12):2381–9.

531. Breitinger DK, Mohr J, Colognesi D, Parker SF, Schukow H, Schwab RG. Vibrational spectra of augelites Al2(OH)3(XO4) (X=P, As, V). Journal of Molecular Structure. 2001 May 28;563–564:377–82.

532. Breitinger DK, Belz H-H, Hajba L, Komlósi V, Mink J, Brehm G, et al. Combined vibrational spectra of natural wardite. Journal of Molecular Structure. 2004 Nov 12;706(1):95–9.

533. Frost RL, Weier ML. Vibrational spectroscopy of natural augelite. Journal of Molecular Structure. 2004 Jul 16;697(1):207–11.

534. Frost RL, Scholz R, Belotti FM, López A, Theiss FL. A vibrational spectroscopic study of the phosphate mineral vantasselite Al4(PO4)3(OH)3·9H2O. Spectrochimica Acta Part A: Molecular and Biomolecular Spectroscopy. 2015 Aug 5;147:185–92.

535. Majs F. Potential Adverse Effects of Applying Phosphate Amendments to Immobilize Soil Contaminants. Journal of Environment Quality. 2011;40(4):1135.

536. Bullock JI, Duffin PA, Nolan KB, Smith TK. Effect of phytate on the in-vitro solubility of Al+, Ca2+, Hg2+ and Pb2+ as a function of pH at 37°C. Journal of the Science of Food and Agriculture. 1995 Apr;67(4):507–9.

537. Peak D, Sims JT, Sparks DL. Solid-State Speciation of Natural and Alum-Amended Poultry Litter Using XANES Spectroscopy. Environ Sci Technol. 2002 Oct 1;36(20):4253–61.

538. Hunger S, Cho H, Sims JT, Sparks DL. Direct Speciation of Phosphorus in Alum-Amended Poultry Litter: Solid-State 31P NMR Investigation. Environ Sci Technol. 2004 Feb 1;38(3):674–81.

539. Peitsch T, Matthes M, Brandenburg V, Epple M. An in vitro crystallization setup to assess the efficiency of different phosphate binders in nephrology: quantitative analytical considerations. Anal Methods. 2010 Jul 1;2(7):901–11.

540. Torres J, Veiga N, Gancheff JS, Domínguez S, Mederos A, Sundberg M, et al. Interaction of myo-inositol hexakisphosphate with alkali and alkaline earth metal ions: Spectroscopic, potentiometric and theoretical studies. Journal of Molecular Structure. 2008 Feb 28;874(1–3):77–88.

541. Chen G-Y, Qu W-G, Ye F, Zhang W-X, Xu A-W. Hydrothermal Synthesis of Ferroelectric PbHPO4 Nanowires from a Single-Source Precursor. J Phys Chem C. 2008 Oct 30;112(43):16818–23.

542. Evans WJ, Hinojosa O, Martin CJ, Marshall WE. Phytic acid-manganese(II) ion interactions: A calorimetric and EPR study. Journal of Inorganic Biochemistry. 1988 Jan 1;32(1):67–75.

543. Evans WJ, Pierce AG. Interaction of Phytic Acid with the Metal Ions, Copper (II), Cobalt (II), Iron (III), Magnesium (II), and Manganese (II). Journal of Food Science. 1982 May;47(3):1014–5.

544. Bebot-Brigaud A, Dange C, Fauconnier N, Gérard C. 31P NMR, potentiometric and spectrophotometric studies of phytic acid ionization and complexation properties toward Co2+, Ni2+, Cu2+, Zn2+ and Cd2+. Journal of Inorganic Biochemistry. 1999 May 30;75(1):71–8.

545. Evans WJ, Martin CJ. The heat of complex formation of copper(II) with phytic acid. Journal of Inorganic Biochemistry. 1987 Nov 1;31(3):155–60.

546. Assaaoudi H, Ennaciri A, Rulmont A. Vibrational spectra of hydrated rare earth orthophosphates. Vibrational Spectroscopy. 2001 Feb 18;25(1):81–90.

547. Clavier N, Mesbah A, Szenknect S, Dacheux N. Monazite, rhabdophane, xenotime & churchite: Vibrational spectroscopy of gadolinium phosphate polymorphs. Spectrochimica Acta Part A: Molecular and Biomolecular Spectroscopy. 2018 Dec;205:85–94.

548. Zhang Y, Guan H. The growth of lanthanum phosphate (rhabdophane) nanofibers via the hydrothermal method. Materials Research Bulletin. 2005 Sep;40(9):1536–43.

549. Sakai H, Ikemoto Y, Kinoshita T, Moriwaki T, Yoshida KT. Fourier-transform spectra of metal salts of phytic acid in the mid- to far-infrared spectral range. Vibrational Spectroscopy. 2017 Sep 1;92:215–9.

550. Bieth H, Spiess B. A comparative study of the protonation of myo-inositol hexakis(phosphate). Journal of the Chemical Society, Faraday Transactions 1: Physical Chemistry in Condensed Phases. 1986;82(6):1935.

551. Arai Y, Sparks DL. ATR–FTIR Spectroscopic Investigation on Phosphate Adsorption Mechanisms at the Ferrihydrite–Water Interface. Journal of Colloid and Interface Science. 2001 Sep 15;241(2):317–26.

552. Fair GE, Hay RS, Boakye EE, Morgan PED, Marzke RF, Sharma R. Precipitation Coating of Monazite on Woven Ceramic Fibers: III—Coating without Strength Degradation Using a Phytic Acid Precursor. Journal of the American Ceramic Society. 2010;93(2):420–8.

553. Chen P, Mah T-I. Synthesis and characterization of lanthanum phosphate sol for fibre coating. Journal of Materials Science. 1997 Jul 1;32(14):3863–7.

554. Koutsoukos PG, Amjad Z, Nancollas GH. The Influence of Phytate and Phosphonate on the Crystal Growth of Fluorapatite and Hydroxyapatite. J Colloid Interface Sci. 1981;83(2):599–605.

555. Assaaoudi H, Ennaciri A, Rulmont A, Harcharras M. Gadolinium orthophosphate weinschenkite type and phase change in rare earth orthophosphates. Phase Transitions. 2000 Aug 1;72(1):1–13.

556. Persson P, Nilsson N, Sjöberg S. Structure and Bonding of Orthophosphate Ions at the Iron Oxide–Aqueous Interface. Journal of Colloid and Interface Science. 1996 Jan 15;177(1):263–75.

557. Burchill P, Howarth OW, Richards DG, Sword BJ. Solid-state nuclear magnetic resonance studies of phosphorus and boron in coals and combustion residues. Fuel. 1990 Apr 1;69(4):421–8.

558. Pizzala H, Caldarelli S, Eon J-G, Rossi AM, Laurencin D, Smith ME. A Solid-State NMR Study of Lead and Vanadium Substitution into Hydroxyapatite. J Am Chem Soc. 2009 Apr 15;131(14):5145–52.

559. Mason HE, Hirner JJ, Xu W, Parise JB, Phillips BL. Solid-state NMR spectroscopy of Pb-rich apatite. Magnetic Resonance in Chemistry. 2009;47(12):1062–70.

560. Zeman OEO, Moudrakovski IL, Hoch C, Hochleitner R, Schmahl WW, Karaghiosoff K, et al. Determination of the 31P and 207Pb Chemical Shift Tensors in Pyromorphite, Pb5(PO4)3Cl, by Single-Crystal NMR Measurements and DFT Calculations. Zeitschrift für anorganische und allgemeine Chemie. 2017;643(21):1635–41.

561. Wellman DM, Icenhower JP, Owen AT. Comparative Analysis of Soluble Phosphate Amendments for the Remediation of Heavy Metal Contaminants: Effect on Sediment Hydraulic Conductivity. Environ Chem. 2006 Jul 28;3(3):219–24.

562. Tsopelas C, Hsieh W. Preparation of ^{68} Ga-Mg-Ca-phytate colloid and its evaluation as a liver imaging agent. Journal of Labelled Compounds and Radiopharmaceuticals. 2017 Sep;60(11):528–41.

563. Bots P, Renshaw JC, Payne TE, Comarmond MJ, Schellenger AEP, Pedrotti M, et al. Geochemical evidence for the application of nanoparticulate colloidal silica gel for in situ containment of legacy nuclear wastes. Environ Sci: Nano. 2020 May 22;7(5):1481–95.

564. Greiner R, Konietzny U. Phytase for Food Application. Food Technol Biotechnol. 2006;44(2):125–140.

Appendix A
Geochemical modelling methods

Geochemical modelling in this project was performed using PHREEQC version 3 (1). The SIT.DAT database was used. This database is based upon the ThermoChimie database developed by Andra (the French radioactive waste management agency) (2–4) and was chosen because it includes many of the elements and chemical species relevant to this project.

However, a number of important species – in particular phytate, but also various phosphate, sulfate, and organic acid complexes – were not present in the SIT.DAT database. Therefore, a literature search was performed for relevant species. In general, preference was given to any data available in the NIST46 database (5) before searching peer reviewed journal articles and text books. In some cases, equations were taken from other databases included with the PHREEQC download – these were the LLNL.DAT and MINTEQ.DAT databases.

Where possible, data that had been extrapolated to zero ionic strength was used. If data were provided for multiple temperatures, the data recorded at 20–25 °C were given preference. No data outside the temperature range of 20–40 °C were used.

For rare earth/lanthanide elements a major simplification was made due to the variability in the literature regarding which of the lanthanides there is data available for. Instead of specifying any single lanthanide, data from different lanthanide elements were grouped together in a generic lanthanide species in the model. Some researchers do provide thermodynamic data in the form of an averaged value for the lanthanides (e.g. (6)) so, if available, this was used. Otherwise, preference was given to data specified for lanthanum, due to that being the main lanthanide used in the experimental work of this thesis. However, the species specified in the SIT.DAT database describe europium – for the current work, europium in the database was redefined as the generic lanthanide species. This simplification was considered sufficient for the current work due to the time constraints associated with compiling thermodynamic data and because the thermodynamic data for different lanthanides are usually similar (no reducing conditions were encountered in this work, so the differences in redox chemistry between europium and other lanthanides were not considered relevant).

Note that this database is far from comprehensive and, as described above, has some considerable limitations. However, it was deemed sufficient as a 'starting point' for performing geochemical modelling in the presence of phytate and, with future work, refinements to the database (including providing definitions for different lanthanides) can be made.

The relevant species added to the database used in geochemical modelling are listed below in the PHREEQC input format. Annotations (lines preceded by a #) describe the source of the data, experimental conditions used to derive the data, and any adjustments that were made to the data (e.g. re-arranging an equation that describes a precipitation reaction so that it describes the reverse dissolution reaction).

The following abbreviations are used:

[InsP6]	Phytate
Mes	2-(*N*-morpholino)ethanesulfonic acid (MES buffer)
Tes	N-tris(hydroxymethyl)methyl-2-aminoethanesulfonic acid (TES buffer)
Tris	tris(hydroxymethyl)aminomethane (TRIS buffer)
Tar	Tartrate
Cit	Citrate
Glu	Gluconate
Ox	Oxalate
Ln	Lanthanide

The species as added to the PHREEQC input file are as follows:

SOLUTION_MASTER_SPECIES

#element	species	alk	gfw_formula	element_gfw
Mes	Mes-	0	Mes	194.2
Tes	Tes-	0	Tes	229.25
Tris	Tris-	0	C4H10NO3	120.136

[InsP6] [InsP6]-12 0 C6H6O24P6 647.944

Tar Tar-2 0 C4H4O6 148.09

SOLUTION_SPECIES

#Protonation constants for MES, TES, and TRIS from (7)

Mes- = Mes-

log_k 0

H+ + Mes- = HMes

log_k 6.15

Tes- = Tes-

log_k 0

H+ + Tes- = HTes

log_k 7.5

Tris- = Tris-

log_k 0

H+ + Tris- = HTris

log_k 8.3

#For defining phytate acid-base chemistry: using protonation constants from (8) as reported by (9), in KCl, ionic strength = 0.2 mol/L, at 25 C.

[InsP6]-12 = [InsP6]-12 #primary master species definition

log_k 0.000

delta_h 0.000 #kJ/mol

[InsP6]-12 + H+ = H[InsP6]-11 #definition of H[InsP6]-11 related to the primary master species

log_k 9.530

H[InsP6]-11 + H+ = H2[InsP6]-10

log_k 9.530

H2[InsP6]-10 + H+ = H3[InsP6]-9

log_k 9.190

H3[InsP6]-9 + H+ = H4[InsP6]-8

log_k 7.980

H4[InsP6]-8 + H+ = H5[InsP6]-7

log_k 6.250

H5[InsP6]-7 + H+ = H6[InsP6]-6

log_k 5.200

H6[InsP6]-6 + H+ = H7[InsP6]-5

log_k 3.160

H7[InsP6]-5 + H+ = H8[InsP6]-4

log_k 2.380

H8[InsP6]-4 + H+ = H9[InsP6]-3

log_k 2.380

H9[InsP6]-3 + H+ = H10[InsP6]-2

log_k 1.920

H10[InsP6]-2 + H+ = H11[InsP6]-

log_k 1.920

H11[InsP6]- + H+ = H12[InsP6]

log_k 1.920

#Log stability constants for the Na[InsP6] system taken from (10), calculated for zero ionic strength at 25 C.

[InsP6]-12 + 6Na+ = Na6[InsP6]-6

log_k 35.1

[InsP6]-12 + 5Na+ + H+ = Na5H[InsP6]-6

log_k 43.3

[InsP6]-12 + 4Na+ + 2H+ = Na4H2[InsP6]-6

log_k 52.6

[InsP6]-12 + 3Na+ + 3H+ = Na3H3[InsP6]-6

log_k 59.0

[InsP6]-12 + 2Na+ + 4H+ = Na2H4[InsP6]-6

log_k 63.9

[InsP6]-12 + Na+ + 5H+ = NaH5[InsP6]-6

log_k 67.4

[InsP6]-12 + Na+ + 6H+ = NaH6[InsP6]-5

log_k 72.4

[InsP6]-12 + 2Na+ + 5H+ = Na2H5[InsP6]-5

log_k 69.4

[InsP6]-12 + 3Na+ + 4H+ = Na3H4[InsP6]-5

log_k 65.6

[InsP6]-12 + 4Na+ + 3H+ = Na4H3[InsP6]-5

log_k 60.7

[InsP6]-12 + 5Na+ + 2H+ = Na5H2[InsP6]-5

log_k 53.8

[InsP6]-12 + 6Na+ + H+ = Na6H[InsP6]-5

log_k 45.1

[InsP6]-12 + 7Na+ = Na7[InsP6]-5

log_k 36.2

#Log stability constants for the K[InsP6] system taken from (10), calculated for zero ionic strength at 25 C.

[InsP6]-12 + 6K+ = K6[InsP6]-6

log_k 33.8

[InsP6]-12 + 5K+ + H+ = K5H[InsP6]-6

log_k 43.0

[InsP6]-12 + 4K+ + 2H+ = K4H2[InsP6]-6

log_k 51.5

[InsP6]-12 + 3K+ + 3H+ = K3H3[InsP6]-6

log_k 58.5

[InsP6]-12 + 2K+ + 4H+ = K2H4[InsP6]-6

log_k 63.6

[InsP6]-12 + K+ + 5H+ = KH5[InsP6]-6

log_k 67.3

[InsP6]-12 + K+ + 6H+ = KH6[InsP6]-5

log_k 72.4

[InsP6]-12 + 2K+ + 5H+ = K2H5[InsP6]-5

log_k 69.3

[InsP6]-12 + 3K+ + 4H+ = K3H4[InsP6]-5

log_k 65.3

[InsP6]-12 + 4K+ + 3H+ = K4H3[InsP6]-5

log_k 60.1

[InsP6]-12 + 5K+ + 2H+ = K5H2[InsP6]-5

log_k 53.0

[InsP6]-12 + 6K+ + H+ = K6H[InsP6]-5

log_k 44.4

[InsP6]-12 + 7K+ = K7[InsP6]-5

log_k 35.0

#Log stability constants for the Al[InsP6] system taken from (11) in 0.15 mol/L NaClO4 at 37 C.

H2[InsP6]-10 + Al+3 = AlH2[InsP6]-7

log_k 23.7

H3[InsP6]-9 + Al+3 = AlH3[InsP6]-6

log_k 20.1

H4[InsP6]-8 + Al+3 = AlH4[InsP6]-5

log_k 16.4

H5[InsP6]-7 + Al+3 = AlH5[InsP6]-4

log_k 12.2

H6[InsP6]-6 + Al+3 = AlH6[InsP6]-3

log_k 8.48

#Log Stability constants for the Ca[InsP6] system from (12), calculated for infinite dilution at 25 C.

H3[InsP6]-9 + Ca+2 = CaH3[InsP6]-7

log_k 7.64

H4[InsP6]-8 + Ca+2 = CaH4[InsP6]-6

log_k 5.82

H5[InsP6]-7 + Ca+2 = CaH5[InsP6]-5

log_k 5.41

H3[InsP6]-9 + 2Ca+2 = Ca2H3[InsP6]-5

log_k 13.99

H4[InsP6]-8 + 2Ca+2 = Ca2H4[InsP6]-4

log_k 11.87

H5[InsP6]-7 + 2Ca+2 = Ca2H5[InsP6]-3

log_k 9.81

H2[InsP6]-10 + 3Ca+2 = Ca3H2[InsP6]-4

log_k 22.52

H3[InsP6]-9 + 3Ca+2 = Ca3H3[InsP6]-3

log_k 19.34

H4[InsP6]-8 + 3Ca+2 = Ca3H4[InsP6]-2

log_k 15.93

H5[InsP6]-7 + 3Ca+2 = Ca3H5[InsP6]-

log_k 13.54

#Log stability constants for manganese-[InsP6] system from (13), calculated for zero ionic strength at 25 C.

[InsP6]-12 + Mn+2 = Mn[InsP6]-10

log_k 3.9

H[InsP6]-11 + Mn+2 = MnH[InsP6]-9

log_k 10.2

H2[InsP6]-10 + Mn+2 = MnH2[InsP6]-8

log_k 9.3

H3[InsP6]-9 + Mn+2 = MnH3[InsP6]-7

log_k 8.3

H4[InsP6]-8 + Mn+2 = MnH4[InsP6]-6

log_k 7.2

H5[InsP6]-7 + Mn+2 = MnH5[InsP6]-5

log_k 5.8

#Log stability constants for iron(II)-[InsP6] system from (13), calculated for zero ionic strength at 25 C.

[InsP6]-12 + Fe+2 = Fe[InsP6]-10

log_k 5.1

H[InsP6]-11 + Fe+2 = FeH[InsP6]-9

log_k 9.8

H2[InsP6]-10 + Fe+2 = FeH2[InsP6]-8

log_k 9

H3[InsP6]-9 + Fe+2 = FeH3[InsP6]-7

log_k 8.1

H4[InsP6]-8 + Fe+2 = FeH4[InsP6]-6

log_k 7

H5[InsP6]-7 + Fe+2 = FeH5[InsP6]-5

log_k 5.5

#Log stability constants for iron(III)-[InsP6] system from (14), measured in NaNO3 background, with 0.1 mol/L ionic strength, at 25 C.

[InsP6]-12 + Fe+3 = Fe[InsP6]-9

log_k 28.5

H[InsP6]-11 + Fe+3 = FeH[InsP6]-8

log_k 24.78

H2[InsP6]-10 + Fe+3 = FeH2[InsP6]-7

log_k 20.61

H3[InsP6]-9 + Fe+3 = FeH3[InsP6]-6

log_k 15.42

H4[InsP6]-8 + Fe+3 = FeH4[InsP6]-5

log_k 10.23

#Log stability constants for cobalt-[InsP6] system from (13), calculated for zero ionic strength at 25 C.

[InsP6]-12 + Co+2 = Co[InsP6]-10

log_k 11.4

H[InsP6]-11 + Co+2 = CoH[InsP6]-9

log_k 11.2

H2[InsP6]-10 + Co+2 = CoH2[InsP6]-8

log_k 10.7

H3[InsP6]-9 + Co+2 = CoH3[InsP6]-7

log_k 9.6

H4[InsP6]-8 + Co+2 = CoH4[InsP6]-6

log_k 8.1

H5[InsP6]-7 + Co+2 = CoH5[InsP6]-5

log_k 6.2

#Log stability constants for copper-[InsP6] system from (15), with NaNO3 as background electrolyte and ionic strength = 0.15 at 25 C.

H[InsP6]-11 + Cu+2 = CuH[InsP6]-9

log_k 10.74

H2[InsP6]-10 + Cu+2 = CuH2[InsP6]-8

log_k 9.30

H3[InsP6]-9 + Cu+2 = CuH3[InsP6]-7

log_k 7.51

H4[InsP6]-8 + Cu+2 = CuH4[InsP6]-6

log_k 5.98

H5[InsP6]-7 + Cu+2 = CuH5[InsP6]-5

log_k 4.35

H6[InsP6]-6 + Cu+2 = CuH6[InsP6]-4

log_k 3.04

#Log stability constants for barium-[InsP6] system from (16)], with tetramethylammonium hydroxide as background electrolyte and ionic strength = 0.15 at 37 C.

H2[InsP6]-10 + Ba+2 = BaH2[InsP6]-8

log_k 6.18

H3[InsP6]-9 + Ba+2 = BaH3[InsP6]-7

log_k 5

H2[InsP6]-10 + 5Ba+2 = Ba5H2[InsP6]

log_k 23.22

#Average log stability constants for the lanthanide-[InsP6] system from (6), measured at 25 C and I = 0.15 mol/L in aqueous NaCl. Represented as Ln for a generic lanthanide

[InsP6]-12 + Ln+3 = Ln[InsP6]-9

log_k 15.4

H[InsP6]-11 + Ln+3 = LnH[InsP6]-8

log_k 14.6

H2[InsP6]-10 + Ln+3 = LnH2[InsP6]-7

log_k 13.7

H3[InsP6]-9 + Ln+3 = LnH3[InsP6]-6

log_k 10.6

H4[InsP6]-8 + Ln+3 = LnH4[InsP6]-5

log_k 7.8

H5[InsP6]-7 + Ln+3 = LnH5[InsP6]-4

log_k 4.9

H6[InsP6]-6 + Ln+3 = LnH6[InsP6]-3

log_k 3.2

#Log stability constants for lead-[InsP6] system from (15), with NaNO3 as background electrolyte and ionic strength = 0.15 at 25 C.

H[InsP6]-11 + Pb+2 = PbH[InsP6]-9

log_k 10.29

H2[InsP6]-10 + Pb+2 = PbH2[InsP6]-8

log_k 8.62

H3[InsP6]-9 + Pb+2 = PbH3[InsP6]-7

log_k 7.10

H4[InsP6]-8 + Pb+2 = PbH4[InsP6]-6

log_k 5.68

H5[InsP6]-7 + Pb+2 = PbH5[InsP6]-5

log_k 4.39

H6[InsP6]-6 + Pb+2 = PbH6[InsP6]-4

log_k 3.23

#Aqueous AlPO4 stability constant taken from (17)

Al+3 + PO4-3 = AlPO4

log_k 14.1

#Aqueous Al(OH)PO4- stability constant taken from (17)

Al+3 + PO4-3 + H2O = Al(OH)PO4- + H+

log_k 8.37

#Data from NIST46 (5)

2Al+3 + PO4-3 = Al2PO4+3

log_k 16.7

#Data from NIST46 (5)

Al+3 + HPO4-2 = AlHPO4+

log_k 6.12

#Data from NIST46 (5)

Al+3 + H2(PO4)- = AlH2PO4+2

log_k 2.02

#Data from NIST46 (5)

Al+3 + 2H2(PO4)- = Al(H2PO4)2+

log_k 4.82

#Data from NIST46 (5), equation in database specified as dissociation reaction, so rearranged to define the association of the Al2(OH)PO4+2 species

Al2PO4+3 + H2O = Al2(OH)PO4+2 + H+

log_k -2.44

#Data from NIST46 (5), equation in database specified as dissociation reaction, so rearranged to define the association of the Al2(OH)2PO4+ species

Al2PO4+3 + 2H2O = Al2(OH)2PO4+ + 2H+

log_k -6.79

#Data from NIST46 (5), for ionic strengh = 0.1, temperature = 25 C

Cu+2 + HPO4-2 = Cu(HPO4)

log_k 3.27

#Data from NIST46 (5), for ionic strengh = 0.15, temperature = 37 C

Cu+2 + H2(PO4)- = Cu(H2PO4)+

log_k 1.3

#Data from NIST46 (5), for ionic strengh = 3, temperature = 25 C

Cu+2 + 2H2(PO4)- = Cu(H2PO4)2

log_k 1.03

#Data from NIST46 (5), for ionic strengh = 0.1, temperature = 25 C

Ba+2 + HPO4-2 = Ba(HPO4)

log_k 1.36

#Data from NIST46 (5), for ionic strengh = 3, temperature = 25 C

Ba+2 + H2(PO4)- = Ba(H2PO4)+

log_k 0.00

#Data from NIST46 (5), for ionic strengh = 3, temperature = 25 C

Ba+2 + 2H2(PO4)- = Ba(H2PO4)2

log_k -0.01

#Data from NIST46 (5), calculated for zero ionic strength at 25 C

Cu+2 + SO4-2 = Cu(SO4)

log_k 2.36

#Data from NIST46 (5), calculated for zero ionic strength at 25 C

Cu+2 + OH- = Cu(OH)+

log_k 6.5

#Data from NIST46 (5), for ionic strength = 3, temperature = 25 C

2Cu+2 + OH- = Cu2(OH)+3

log_k 8.4

#Data from NIST46 (5), calculated for zero ionic strength at 25 C

2Cu+2 + 2OH- = Cu2(OH)2+2

log_k 17.5

#Data from NIST46 (5), calculated for zero ionic strength at 25 C

3Cu+2 + 4OH- = Cu3(OH)4+2

log_k 35.2

#Citrate species from the NIST46 database and references therein (5)

NH4+ + Cit-3 = NH4(Cit)-2

log_k 0.95

Na+ + Cit-3 = Na(Cit)-2

log_k 0.75

K+ + Cit-3 = K(Cit)-2

log_k 1.17

Mn+2 + Cit-3 = Mn(Cit)-

log_k 4.15

Mn+2 + H(Cit)-2 = MnH(Cit)

log_k 2.3

Mn+2 + H2(Cit)- = MnH2(Cit)+

log_k 1.5

Cu+2 + H(Cit)-2 = CuH(Cit)

log_k 3.9

2Cu+2 + 2Cit-3 = Cu2(Cit)2-2

log_k 14.8

Zn+2 + Cit-3 = Zn(Cit)-

log_k 4.93

Zn+2 + 2Cit-3 = Zn(Cit)2-4

log_k 6.8

Zn+2 + H(Cit)-2 = ZnH(Cit)

log_k 3

Zn+2 + H2(Cit)- = ZnH2(Cit)+

log_k 1.2

#using data for Lanthanum citrate from NIST46

Ln+3 + Cit-3 = Ln(Cit)

log_k 9.18

#Gluconate species from NIST46 database and references therein (5), except for manganese gluconate

#B(OH)4- + HGlu- = B(OH)2H(Glu)

log_k 2.83

Mg+2 + HGlu- = Mg(HGlu)+

log_k 0.7

#Manganese gluconate data from (18)

Mn+2 + 2HGlu- = Mn(HGlu)2

log_k 14.7

Fe+3 + HGlu- = Fe(HGlu)+2

log_k 3.1

Cu+2 + HGlu- = Cu(HGlu)+

log_k 2.51

Cu+2 + 2HGlu- = Cu(HGlu)2

log_k 4.59

Zn+2 + HGlu- = Zn(HGlu)+

log_k 1.7

#using data for Lanthanum gluconate from NIST46 (5)

Ln+3 + HGlu- = Ln(HGlu)+2

log_k 2.32

Ln+3 + 2HGlu- = Ln(HGlu)2+

log_k 4.25

#Oxalate species from NIST46 database and references therein (5)

NH4+ + Ox-2 = (NH4)(Ox)-

log_k 0.9

Na+ + Ox-2 = Na(Ox)-

log_k 0.9

K+ + Ox-2 = K(Ox)-

```
        log_k   0.8

B(OH)3 + H(Ox)- = B(OH)2(Ox)- + H2O

        log_k   0.35

Mn+2 + Ox-2 = Mn(Ox)

        log_k   3.95

Mn+2 + 2Ox-2 = Mn(Ox)2-2

        log_k   5.25

Cu+2 + Ox-2 = CuOx

        log_k   4.85

Cu+2 + 2Ox-2 = CuOx2-2

        log_k   10.23

Zn+2 + Ox-2 = Zn(Ox)

        log_k   4.87

Zn+2 + 2Ox-2 = Zn(Ox)2-2

        log_k   7.69

MoO4-2 + Ox-2 + 2H+ = MoO3(Ox)-2 + H2O

        log_k   13.82

#Tartrate data taken from MINTEQ.DAT file

Tar-2 = Tar-2

      log_k   0

      delta_h 0       kcal

Tar-2 + H+ = H(Tar)-

      log_k   4.16
```

```
        delta_h 0       kcal
        #-gamma  0      0.01
Tar-2 + 2H+ = H2(Tar)
        log_k   6.67
        delta_h 0       kcal
        #-gamma  0      0.01
#Tartrate species from NIST46 database and references therein      (5)
K+ + Tar-2 = K(Tar)-
            log_k   0.4
Na+ + Tar-2 = Na(Tar)-
            log_k   0.9
Na+ + H(Tar)- = NaH(Tar)
            log_k   0.2
NH4+ + Tar-2 = NH4(Tar)-
            log_k   0.3
Ca+2 + Tar-2 = Ca(Tar)
            log_k   2.64
Ca+2 + H(Tar)- = CaH(Tar)+
            log_k   1.41
Mg+2 + Tar-2 = Mg(Tar)
            log_k   1.44
Mg+2 + H(Tar)- = MgH(Tar)+
            log_k   0.95
```

Mn+2 + Tar-2 = Mn(Tar)

log_k 3.38

Mn+2 + H(Tar)- = MnH(Tar)+

log_k 1.17

Fe+2 + Tar-2 = Fe(Tar)

log_k 2.24

Fe+3 + Tar-2 = Fe(Tar)+

log_k 6.49

Cu+2 + Tar-2 = Cu(Tar)

log_k 3.97

Cu+2 + 2Tar-2 = Cu(Tar)2-2

log_k 4.5

2Cu+2 + 2Tar-2 = Cu2(Tar)2

log_k 8.77

Cu+2 + H(Tar)- = CuH(Tar)+

log_k 1.88

#using data for Lanthanum tartrate from NIST46 (5)

Ln+3 + Tar-2 = Ln(Tar)+

log_k 4.6

Ln+3 + 2Tar-2 = Ln(Tar)2-

log_k 7.59

Ln+3 + H(Tar)- = LnH(Tar)+2

log_k 2.48

```
PHASES
#Data for pentamagnesium dihydrogen phytate from (19) measured at 37 C in 0.15 mol/L NaClO4
Mg5H2[InsP6]:22H2O(s)
        Mg5H2[InsP6]:22H2O = 5Mg+2 + H2[InsP6]-10 + 22H2O
        log_k -32.93
#Data for hexacalcium phytate from (20)
Ca6[InsP6](s)
        Ca6[InsP6] = 6Ca+2 + [InsP6]-12
        log_k = -58.3
        #delta_h 7.6    #kj/mol Enthalpy of formation
#Data for pentacalcium dihydrogen phytate from (19) measured at 37 C in 0.15 mol/L NaClO4
Ca5H2[InsP6]:16H2O(s)
        Ca5H2[InsP6]:16H2O = 5Ca+2 + H2[InsP6]-10 + 16H2O
        log_k -39.3
#Data for pentacalcium disodium phytate from (20)
Ca5Na2[InsP6](s)
        Ca5Na2[InsP6] = 5Ca+2 + 2Na+ + [InsP6]-12
        log_k -75.7
        #delta_h 3.7    #kj/mol Enthalpy of formation
#Data for pentacalcium dipotassium phytate from (21)
Ca5K2[InsP6]:xH2O(s)
        Ca5K2[InsP6] = 5Ca+2 + 2K+ + [InsP6]-12
```

log_k -75.7

#delta_h 19.9 kcal/mol Enthalpy of formation

#Data for pentabarium dihydrogen phytate from (16) measured at 37 C in 0.15 mol/L NaClO4

Ba5H2[InsP6]:16H2O(s)

Ba5H2[InsP6]:16H2O = 5Ba+2 + H2[InsP6]-10 + 16H2O

log_k -38.3

#Data for manganese phytate from (22), background media = NaClO4; ionic strength = 0.1 mol/L; temperature = 37 C.

Mn5H2[InsP6]:16H2O(s)

Mn5H2[InsP6]:16H2O = 5Mn+2 + H2[InsP6]-10 + 16H2O

log_k -39.9

#Anhydrous calcium citrate from NIST46 (5)

Ca3(Cit)2(s)

Ca3(Cit)2 = 3Ca+2 + 2Cit-3

log_k -17.0

#Calcium hydrogen citrate from NIST46 (5)

CaH(Cit)(s)

CaH(Cit) = Ca+2 + H+ + Cit-3

log_k -11.4

#Magnesium oxalate from NIST46 (5)

Mg(Ox)(s)

Mg(Ox) = Mg+2 + Ox-2

log_k -5.7

#Magnesium oxalate dihydrate from (23)

Mg(Ox):2H2O(s)

Mg(Ox):2H2O = Mg+2 + Ox-2 + 2H2O

log_k -8.0

#Iron(II) oxalate from (23)

FeOx:2H2O(s)

Fe(Ox):2H2O = Fe+2 + Ox-2 + 2H2O

log_k -6.5

#Manganese oxalate dihydrate from (23)

MnOx:2H2O(s)

Mn(Ox):2H2O = Mn+2 + Ox-2 + 2H2O

log_k -5.3

#Data a generic lanthanide oxalate taken from the NIST46 data for lanthanum oxalate (5)

Ln2(Ox)3(s)

Ln2(Ox)3 = 2Ln+3 + 3Ox-2

log_k -25.0

#Data for a mixed sodium-lanthanide salt taken from (24) for sodium ytterbium oxalate hydrate

LnNa(Ox)2(s)

LnNa(Ox)2 = Ln+3 + Na+ + 2Ox-2

log_k -19.0

#Potassium hydrogen tartrate data from (25)

KH(Tar)(s)

KH(Tar) = K+ + H(Tar)-

log_k -2.9

#Anhydrous calcium tartrate from (26)

Ca(Tar)(s)

Ca(Tar) = Ca+2 + Tar-2

log_k -4.0

#Calcium tartrate dihydrate from (23)

Ca(Tar):2H2O(s)

Ca(Tar):2H2O = Ca+2 + Tar-2 + 2H2O

log_k -6.1

#Copper tartrate from Dean (1985) cited by (27)

Cu(Tar)(s)

Cu(Tar) = Cu+2 + Tar-2

log_k -3.4

#Lanthanide tartrate defined based upon data in (23) for cerium tartrate nonahydrate

Ln2(Tar)3:9H2O(s)

Ln2(Tar)3:9H2O = 2Ln+3 + 3Tar-2 + 9H2O

log_k -19.0

#Struvite data taken from (28) using data from tap water at 20 C.

Struvite

NH4MgPO4:6H2O = NH4+ + Mg+2 + PO4-3 + 6H2O

log_k -13.73

#Aluminium sulfate phase data taken from llnl.dat database

Al2(SO4)3

Al2(SO4)3 = + 2.0000 Al+++ + 3.0000 SO4--

log_k 19.0535

-delta_H -364.566 kJ/mol # Calculated enthalpy of reaction Al2(SO4)3

#Aluminium sulfate hexahydrate phase data taken from llnl.dat database

Al2(SO4)3:6H2O

Al2(SO4)3:6H2O = + 2.0000 Al+++ + 3.0000 SO4-- + 6.0000 H2O

log_k 1.6849

-delta_H -208.575 kJ/mol # Calculated enthalpy of reaction Al2(SO4)3:6H2O

#Aluminium hydroxysulfate data taken from (29)

Al(OH)2.5(SO4)0.25(s)

Al(OH)2.5(SO4)0.25 = Al+3 + 2.5OH- + 0.25SO4-2

log_k -28.6

#Alunite data taken from (30)

Alunite

KAl3(SO4)2(OH)6 = K+ + 3Al+3 + 2SO4-2 + 6OH-

log_k -85.4

#Natroalunite data taken from (30)

Natroalunite

NaAl3(SO4)2(OH)6 = Na+ + 3Al+3 + 2SO4-2 + 6OH-

log_k -79.7

#Crystaline felsobányaite (aka basaluminite) taken from (30)

Felsobányaite(cr)

Al4(SO4)(OH)10:4H2O = 4Al+3 + SO4-2 + 10OH- + 4H2O

log_k -117.7

#Amorphous felsobányaite (aka basaluminite) taken from (30)

Felsobányaite(am)

Al4(SO4)(OH)10:4H2O = 4Al+3 + SO4-2 + 10OH- + 4H2O

log_k -116.0

#Copper sulfate data taken from (31) for 1.5 mol/kg ionic strength

CuSO4:5H2O(s)

CuSO4:5H2O = Cu+2 + SO4-2 + 5H2O

log_k -2.61

#Copper hydroxysulfate data taken from NIST46 (5)

Cu(OH)1.5(SO4)0.25 (s)

Cu(OH)1.5(SO4)0.25 = Cu+2 + 1.5OH- + 0.25SO4-2

log_k -17.19

#Copper hydroxide data taken from NIST46 (5)

Cu(OH)2(s)

Cu(OH)2 = Cu+2 + 2OH-

log_k -18.7

#Copper oxide data taken from NIST46 (5)

CuO(s)

CuO + H2O = Cu+2 + 2OH-

log_k -19.5

#Copper(II) phosphate data taken from (32)

Cu3(PO4)2(s)

Cu3(PO4)2 = 3Cu+2 + 2PO4-3

log_k -36.85

#Copper hydroxyphosphate data taken from (33)

Cornetite

Cu3(PO4)(OH)3 = 3Cu+2 + PO4-3 + 3OH-

log_k -48.0

#Copper hydroxyphosphate data taken from (33)

Libenthenite

Cu2(PO4)OH = 2Cu+2 + PO4-3 + OH-

log_k -28.0

#Copper hydroxyphosphate data taken from (33)

Pseudomalachite

Cu5(PO4)2(OH)4 = 5Cu+2 + 2PO4-3 + 4OH-

log_k -75.8

#Copper hydroxyphosphate data taken from (33)

Tagilite

Cu2(PO4)OH:H2O = 2Cu+2 + PO4-3 + OH- + H2O

log_k -27.9

#Copper hydroxyphosphate data taken from (33)

Cu-hydroxypyromorphite

Cu5(PO4)3OH = 5Cu+2 + 3PO4-3 + OH-

log_k -65.6

#Lanthanide sodium sulfate data based upon lanthanum data taken from (34)

LnNa(SO4)2.H2O(s)

LnNa(SO4)2:H2O = Ln+3 + Na+ + 2SO4-2 + H2O

log_k -6.83

#Lanthanide potassium sulfate data based upon lanthanum data taken from (34)

LnK(SO4)2.H2O(s)

LnK(SO4)2:H2O = Ln+3 + K+ + 2SO4-2 + H2O

log_k -5.79

Appendix A References

1. Parkhurst DL, Appelo CAJ. Description of input and examples for PHREEQC version 3—A computer program for speciation, batch-reaction, one-dimensional transport, and inverse geochemical calculations. In: US Geological Survey Techniques and Methods, book 6, chap A43 [Internet]. 2013. p. 497. Available from: https://pubs.usgs.gov/tm/06/a43/

2. Thermo-Chimie (version applicative 4.4.0) [Internet]. [cited 2020 May 29]. Available from: https://www.thermochimie-tdb.com/

3. Giffaut E, Grivé M, Blanc Ph, Vieillard Ph, Colàs E, Gailhanou H, et al. Andra thermodynamic database for performance assessment: ThermoChimie. Applied Geochemistry. 2014 Oct 1;49:225–36.

4. Grivé M, Duro L, Colàs E, Giffaut E. Thermodynamic data selection applied to radionuclides and chemotoxic elements: An overview of the ThermoChimie-TDB. Applied Geochemistry. 2015 Apr 1;55:85–94.

5. Martell AE, Smith RM, Motekaitis RJ. NIST standard reference database 46 version 8.0: NIST critically selected stability constants of metal complexes. In 2004.

6. Crea F, De Stefano C, Milea D, Sammartano S. Thermodynamic data for lanthanoid(III) sequestration by phytate at different temperatures. Monatshefte für Chemie - Chemical Monthly. 2010;141(5):511–20.

7. Good NE, Winget GD, Winter W, Connolly TN, Izawa S, Singh RMM. Hydrogen Ion Buffers for Biological Research *. Biochemistry. 1966 Feb;5(2):467–77.

8. Evans WJ, McCourtney EJ, Shrager RI. Titration studies of phytic acid. Journal of the American Oil Chemists' Society. 1982 Apr;59(4):189–91.

9. Crea F, De Stefano C, Milea D, Sammartano S. Formation and stability of phytate complexes in solution. Coordination Chemistry Reviews. 2008 May;252(10–11):1108–20.

10. De Stefano C, Milea D, Pettignano A, Sammartano S. Speciation of phytate ion in aqueous solution. Alkali metal complex formation in different ionic media. Analytical and Bioanalytical Chemistry. 2003 Aug;376(7):1030–40.

11. Torres J, Domínguez S, Cerdá MF, Obal G, Mederos A, Irvine RF, et al. Solution behaviour of myo-inositol hexakisphosphate in the presence of multivalent cations. Prediction of a neutral pentamagnesium species under cytosolic/nuclear conditions. Journal of Inorganic Biochemistry. 2005 Mar;99(3):828–40.

12. Crea P, de Robertis A, de Stefano C, Sammartano S. Speciation of phytate ion in aqueous solution. Sequestration of magnesium and calcium by phytate at different temperatures and ionic strengths, in NaClaq. Biophysical Chemistry. 2006 Oct 20;124(1):18–26.

13. Bretti C, Cigala RM, De Stefano C, Lando G, Sammartano S. Interaction of Phytate with Ag+, CH3Hg+, Mn2+, Fe2+, Co2+, and VO2+: Stability Constants and Sequestering Ability. J Chem Eng Data. 2012 Oct 11;57(10):2838–47.

14. Bretti C, Cigala RM, Lando G, Milea D, Sammartano S. Sequestering Ability of Phytate toward Biologically and Environmentally Relevant Trivalent Metal Cations. J Agric Food Chem. 2012 Aug 22;60(33):8075–82.

15. Cigala RM, Crea F, Stefano CD, Lando G, Milea D, Sammartano S. Electrochemical Study on the Stability of Phytate Complexes with Cu2+, Pb2+, Zn2+, and Ni2+: A Comparison of Different Techniques. J Chem Eng Data. 2010 Nov 11;55(11):4757–67.

16. Torres J, Veiga N, Gancheff JS, Domínguez S, Mederos A, Sundberg M, et al. Interaction of myo-inositol hexakisphosphate with alkali and alkaline earth metal ions: Spectroscopic, potentiometric and theoretical studies. Journal of Molecular Structure. 2008 Feb 28;874(1–3):77–88.

17. Harris WR. Equilibrium model for speciation of aluminum in serum. Clin Chem. 1992 Sep;38(9):1809–18.

18. Nagy L, Horváth I, Burger K. The electrochemical investigation of the manganese complexes of lactobionic acid. Inorganica Chimica Acta. 1985 Jul;107(3):179–85.

19. Veiga N, Torres J, Domínguez S, Mederos A, Irvine RF, Díaz A, et al. The behaviour of myo-inositol hexakisphosphate in the presence of magnesium(II) and calcium(II): Protein-free soluble InsP6 is limited to 49 µM under cytosolic/nuclear conditions. Journal of Inorganic Biochemistry. 2006 Nov;100(11):1800–10.

20. Crea F, Crea P, De Robertis A, Sammartano S. Speciation of phytate ion in aqueous solution. Characterisation of Ca-phytate sparingly soluble species. Chemical Speciation & Bioavailability. 2004 Jan 1;16(1–2):53–9.

21. Evans WJ, Marini MA, Martin CJ. Heats of precipitation of calcium phytate. Journal of Inorganic Biochemistry. 1983 Oct 1;19(2):129–32.

22. Quiñone D, Veiga N, Torres J, Bazzicalupi C, Bianchi A, Kremer C. Self-Assembly of Manganese(II)-Phytate Coordination Polymers: Synthesis, Crystal Structure, and Physicochemical Properties. ChemPlusChem. 2017 May;82(5):721–31.

23. Meites L. Handbook of analytical chemistry. New York: McGraw-Hill; 1963. (McGraw-Hill handbooks.).

24. Gammons CH, Wood SA. The aqueous geochemistry of REE.: Part 8: Solubility of ytterbium oxalate and the stability of Yb(III)–oxalate complexes in water at 25°C to 80°C. Chemical Geology. 2000 May;166(1–2):103–24.

25. Marzzacco CJ. The Effects of Salts and Nonelectrolytes on the Solubility of Potassium Bitartrate: An Introductory Chemistry Discovery Experiment. Journal of Chemical Education. 1998 Dec;75(12):1628.

26. Gácsi A, Kutus B, Csendes Z, Faragó T, Peintler G, Pálinkó I, et al. Calcium L -tartrate complex formation in neutral and in hyperalkaline aqueous solutions. Dalton Transactions. 2016;45(43):17296–303.

27. Thomsen MW. Determination of the solubility product of copper(II) tartrate. Journal of Chemical Education. 1992 Apr;69(4):328.

28. Rahaman MS, Mavinic DS, Bhuiyan MIH, Koch FA. Exploring the determination of struvite solubility product from analytical results. Environ Technol. 2006 Sep;27(9):951–61.

29. Singh SS. Neutralization of dilute aqueous aluminium sulfate solutions with a base. Canadian Journal of Chemistry. 1969 Feb 15;47(4):663–7.

30. Adams F, Rawajfih Z. Basaluminite and Alunite: A Possible Cause of Sulfate Retention by Acid Soils. Soil Science Society of America Journal. 1977;41(4):686.

31. Christov C. Thermodynamic study of the Na-Cu-Cl-SO4- H2O system at the temperature 298.15 K. The Journal of Chemical Thermodynamics. 2000 Mar 1;32(3):285–95.

32. Lide DR, editor. CRC handbook of chemistry and physics: a ready-reference book of chemical and physical data. 84th ed. Boca Raton: CRC Press; 2003. 2500 p.

33. Nriagu JO. Formation and Stability of Base Metal Phosphates in Soils and Sediments. In: Nriagu JO, Moore PB, editors. Phosphate Minerals [Internet]. Berlin, Heidelberg: Springer; 1984 [cited 2020 Feb 26]. p. 318–29. Available from: https://doi.org/10.1007/978-3-642-61736-2_10

34. Lokshin EP, Tareeva OA, Ivlev KG, Kashulina TG. Solubility of Double Alkali Metal (Na, K) Rare-Earth (La, Ce) Sulfates in Sulfuric-Phosphoric Acid Solutions at 20°C. Russ J Appl Chem. 2005 Jul 1;78(7):1058–63.

Appendix B
Geochemical modelling results for chapter 2

B.1 "Filtrate" system tests – pH comparisons

Table B.1 Saturation indices of different solid phases at different pH values. The phases in the model deemed most likely to be present (brushite, pentacalcium dipotassium phytate, and gypsum) are highlighted. Phytate is represented in the model by [InsP6].

Simulation	1	2	3	4	5	6
Description	Ca added to pH 5.5 control	Ca added to pH 2.5 phytase-active culture filtrate	Ca added to pH 5 phytase-active culture filtrate	Ca added to pH 5.5 phytase-active culture filtrate	Ca added to pH 6.0 phytase-active culture filtrate	Ca added to pH 7.0 phytase-active culture filtrate
Alabandite	-80.26	-85.30	-81.77	-80.90	-80.05	-78.20
Anapaite	1.33	-11.25	-0.37	1.41	3.11	6.21
Anhydrite	0.47	0.46	0.47	0.47	0.47	0.47
Antarcticite	-6.23	-6.23	-6.24	-6.24	-6.24	-6.25
Arcanite	-3.92	-4.42	-3.90	-3.87	-3.81	-3.54
B(cr)	-90.20	-92.10	-90.78	-90.44	-90.11	-89.34
B(OH)3(cr)	-4.96	-4.96	-4.96	-4.96	-4.96	-4.96
B2O3(am)	-18.12	-18.12	-18.12	-18.12	-18.12	-18.13
B2O3(cr)	-15.95	-15.95	-15.95	-15.95	-15.95	-15.96
Bassanite	-0.05	-0.06	-0.05	-0.05	-0.05	-0.05
Bischofite	-8.66	-8.65	-8.65	-8.66	-8.66	-8.68
Bloedite	-11.95	-11.95	-11.89	-11.88	-11.88	-11.87
Brucite	-9.79	-16.09	-11.33	-10.43	-9.53	-7.59
Brushite	0.57	-1.86	0.59	1.02	1.42	2.02
C3FH6	-37.58	-70.70	-45.34	-41.04	-36.76	-27.61
C4FH13	-51.07	-90.51	-60.38	-55.18	-50.01	-38.91
Ca(HPO4)(s)	0.83	-1.60	0.85	1.29	1.69	2.28
Ca(NO3)2(s)	-21.34	-23.84	-21.37	-21.35	-21.36	-21.55
Ca(s)	-115.18	-122.75	-117.11	-115.99	-114.86	-112.40
Ca(SO3)(s)	-27.22	-28.49	-27.60	-27.37	-27.15	-26.64
Ca2Cl2(OH)2:H2O(s)	-19.34	-25.64	-20.89	-19.99	-19.10	-17.16
Ca2Fe2O5(s)	-31.30	-58.12	-37.52	-34.12	-30.74	-23.54
Ca3(PO4)2(alfa)	1.31	-9.85	-0.19	1.58	3.27	6.42
Ca3B2O6(s)	-41.76	-60.69	-46.40	-43.71	-41.01	-35.17
Ca4Cl2(OH)6:13H2O(s)	-43.44	-62.37	-48.09	-45.39	-42.70	-36.86
Ca4H(PO4)3:2.5H2O(s)	1.28	-12.31	-0.19	2.00	4.10	7.84
Ca5H2[InsP6]:16H2O(s)	-7.72	-17.82	-10.28	-9.06	-8.00	-6.43
Ca5K2[InsP6]:xH2O(s)	17.30	0.40	13.21	15.36	17.37	21.17
Ca5Na2[InsP6](s)	14.62	-1.77	10.56	12.68	14.65	18.19
Ca6[InsP6](s)	1.83	-14.58	-2.28	-0.16	1.79	5.31
CaB2O4(s)	-17.23	-23.53	-18.77	-17.87	-16.98	-15.03
CaB4O7(s)	-24.49	-30.80	-26.04	-25.14	-24.24	-22.31
CaCl2:2H2O(cr)	-10.40	-10.39	-10.40	-10.40	-10.40	-10.41
CaCl2:4H2O(cr)	-7.71	-7.70	-7.71	-7.71	-7.71	-7.72
CaCl2:H2O(s)	-10.31	-10.30	-10.31	-10.31	-10.32	-10.32
CaFe2O4(s)	-4.66	-25.16	-9.32	-6.82	-4.34	0.91
CaI2(s)	-36.76	-36.75	-36.75	-36.75	-36.76	-36.76
CaMoO4(s)	-0.27	-3.07	-0.28	-0.27	-0.26	-0.27
CaO(cr)	-23.78	-30.09	-25.33	-24.43	-23.53	-21.58
Carnallite	-10.59	-10.82	-10.58	-10.56	-10.54	-10.43
Chloroapatite	11.10	-5.63	8.86	11.50	14.05	18.75
Cornetite	-11.98	-27.00	-15.03	-12.82	-10.66	-6.35
Cu(cr)	-11.16	-18.73	-13.08	-11.97	-10.85	-8.45

Table B.1 (continued).

Simulation	1	2	3	4	5	6
Description	Ca added to pH 5.5 control	Ca added to pH 2.5 phytase-active culture filtrate	Ca added to pH 5 phytase-active culture filtrate	Ca added to pH 5.5 phytase-active culture filtrate	Ca added to pH 6.0 phytase-active culture filtrate	Ca added to pH 7.0 phytase-active culture filtrate
Cu(OH)1.5(SO4)0.25	-3.96	-8.68	-5.11	-4.44	-3.78	-2.38
Cu(OH)2(s)	-6.18	-12.48	-7.72	-6.83	-5.94	-4.05
Cu-hydroxypyromorphite	-14.83	-34.69	-17.82	-14.75	-11.81	-6.44
Cu3(PO4)2(s)	-8.48	-19.61	-9.96	-8.21	-6.54	-3.59
CuO(s)	-5.37	-11.67	-6.91	-6.02	-5.13	-3.25
CuSO4:5H2O(s)	-7.37	-7.38	-7.36	-7.37	-7.38	-7.45
Epsonite	-3.88	-3.89	-3.87	-3.87	-3.88	-3.89
Ettringite-Fe	-31.14	-64.31	-38.90	-34.60	-30.33	-21.19
Fe(OH)2(cr)	-9.09	-16.83	-10.85	-9.93	-9.03	-7.12
Fe(PO4)(cr)	1.83	-1.39	1.84	2.17	2.47	2.76
Fe(s)	-38.37	-47.36	-40.50	-39.36	-38.23	-35.81
Fe5(OH)(PO4)3(s)	397.27	370.27	393.23	396.39	399.42	404.89
FeMoO4(s)	-5.39	-9.61	-5.61	-5.58	-5.57	-5.62
FeO(s)	-9.71	-17.44	-11.46	-10.55	-9.65	-7.74
Ferrihydrite(am)	1.39	-5.71	-0.17	0.63	1.42	3.07
Ferryhydrite	2.74	-4.36	1.18	1.98	2.77	4.42
FeS(am)	-76.88	-83.37	-78.61	-77.70	-76.79	-74.79
Glaserite	-18.19	-19.70	-18.10	-18.00	-17.80	-16.98
Glauberite	-14.45	-14.45	-14.40	-14.39	-14.38	-14.36
Goethite	3.36	-3.74	1.80	2.60	3.39	5.04
Gypsum	0.68	0.67	0.68	0.68	0.68	0.68
H2MoO4(s)	-4.36	-0.86	-2.83	-3.71	-4.61	-6.56
Halite	-5.03	-5.02	-5.01	-5.01	-5.00	-5.00
Hausmannite	-22.64	-40.23	-26.85	-24.44	-22.13	-17.38
Hematite	8.53	-5.67	5.40	7.01	8.59	11.89
Hexahydrite	-4.16	-4.17	-4.15	-4.15	-4.16	-4.17
Hydrophilite	-14.31	-14.30	-14.32	-14.32	-14.32	-14.33
Hydroxyapatite	7.72	-12.17	4.70	7.80	10.79	16.48
K(cr)	-59.56	-63.59	-60.52	-59.94	-59.35	-57.98
K(NO3)(s)	-8.59	-10.09	-8.59	-8.57	-8.54	-8.50
K(OH)(s)	-20.81	-24.22	-21.58	-21.12	-20.64	-19.53
K2O(s)	-77.81	-84.61	-79.34	-78.42	-77.46	-75.24
Kainite	-7.73	-7.98	-7.71	-7.70	-7.67	-7.56
KH2PO4(cr)	-4.08	-3.60	-3.28	-3.28	-3.30	-3.54
KI(s)	-9.83	-10.07	-9.82	-9.81	-9.78	-9.65
Lawrencite	-16.97	-18.38	-17.17	-17.16	-17.16	-17.21
Leonhardtite	-4.96	-4.97	-4.95	-4.95	-4.95	-4.97
Leonite	-7.59	-8.10	-7.56	-7.53	-7.47	-7.22
Lepidocrocite	2.99	-4.11	1.43	2.23	3.02	4.68
Libenthenite	-7.10	-15.82	-8.61	-7.29	-6.02	-3.60
Mackinawite	-76.23	-82.72	-77.96	-77.05	-76.14	-74.14
Maghemite(disord)	4.12	-10.08	1.00	2.60	4.18	7.49
Maghemite(ord)	3.91	-10.29	0.79	2.39	3.97	7.28
Magnetite	0.79	-21.14	-4.09	-1.57	0.92	6.13
Manganite	-8.15	-13.81	-9.49	-8.73	-7.99	-6.50
Melanterite	-7.22	-8.65	-7.42	-7.41	-7.40	-7.45
Mercallite	-8.23	-5.33	-7.45	-7.88	-8.30	-9.14
Mg(cr)	-99.72	-107.29	-101.64	-100.52	-99.40	-96.95
Mg(HPO4):3H2O(s)	-2.07	-4.49	-2.03	-1.60	-1.20	-0.62
Mg(NO3)2(s)	-32.79	-35.29	-32.81	-32.79	-32.80	-33.00
Mg(NO3)2:6H2O(s)	-19.91	-22.40	-19.92	-19.91	-19.92	-20.12
Mg(SO4)(s)	-15.19	-15.20	-15.18	-15.18	-15.19	-15.20
Mg(SO4):H2O(s)	-5.79	-5.80	-5.78	-5.78	-5.79	-5.80
Mg-oxychlorur	-17.10	-26.55	-19.41	-18.06	-16.72	-13.82
Mg3(PO4)2(cr)	-10.07	-21.21	-11.54	-9.78	-8.09	-4.98
Mg3(PO4)2:22H2O(s)	-9.74	-20.89	-11.22	-9.46	-7.77	-4.66
Mg3(PO4)2:8H2O(s)	-7.56	-18.70	-9.03	-7.27	-5.58	-2.47

Table B.1 (continued).

Simulation	1	2	3	4	5	6
Description	Ca added to pH 5.5 control	Ca added to pH 2.5 phytase-active culture filtrate	Ca added to pH 5 phytase-active culture filtrate	Ca added to pH 5.5 phytase-active culture filtrate	Ca added to pH 6.0 phytase-active culture filtrate	Ca added to pH 7.0 phytase-active culture filtrate
Mg5H2[InsP6]:22H2O(s)	-23.31	-33.39	-25.83	-24.62	-23.58	-22.05
MgCl2(s)	-26.64	-26.63	-26.64	-26.64	-26.64	-26.66
MgCl2:2H2O(s)	-17.05	-17.04	-17.04	-17.05	-17.05	-17.07
MgCl2:4H2O(s)	-11.60	-11.59	-11.60	-11.60	-11.60	-11.62
MgCl2:H2O(s)	-20.36	-20.35	-20.36	-20.36	-20.36	-20.38
MgI2(s)	-51.09	-51.08	-51.08	-51.09	-51.09	-51.11
MgMoO4(s)	-9.56	-12.36	-9.57	-9.55	-9.55	-9.56
Mirabilite	-7.12	-7.11	-7.07	-7.06	-7.05	-7.03
Mn(HPO4)(s)	1.88	-0.52	1.92	2.33	2.68	3.08
Mn(SO4)(s)	-6.30	-6.28	-6.28	-6.30	-6.35	-6.55
Mn3(PO4)2(s)	-18.60	-29.69	-20.05	-18.35	-16.81	-14.26
Mn3(PO4)2:3H2O(s)	-5.62	-16.71	-7.07	-5.37	-3.83	-1.28
Mn5H2[InsP6]:16H2O(s)	-32.43	-42.41	-34.90	-33.80	-33.00	-32.41
MnCl2:2H2O(s)	-11.35	-11.32	-11.34	-11.36	-11.42	-11.62
MnCl2:4H2O(s)	-10.10	-10.06	-10.08	-10.11	-10.16	-10.36
MnCl2:H2O(s)	-12.90	-12.86	-12.88	-12.91	-12.96	-13.17
MnO(s)	-13.46	-19.75	-14.99	-14.12	-13.27	-11.52
MnO2(s)	-12.20	-17.22	-13.34	-12.69	-12.07	-10.83
Mo(s)	-76.27	-76.55	-75.88	-76.10	-76.32	-76.73
Mo3O8(s)	-14.83	-5.57	-10.61	-13.04	-15.49	-20.85
Monosulfate-Fe	-35.09	-68.23	-42.86	-38.55	-34.28	-25.13
MoO2(s)	-13.51	-11.27	-12.36	-13.02	-13.69	-15.13
MoO3(s)	-5.59	-2.08	-4.06	-4.94	-5.84	-7.79
MoS2(s)	-140.40	-135.68	-139.21	-139.89	-140.55	-141.80
MoS3(s)	-199.93	-192.69	-198.32	-199.24	-200.12	-201.79
Na(cr)	-57.27	-61.04	-58.21	-57.64	-57.08	-55.83
Na(NO3)(s)	-11.12	-12.36	-11.11	-11.10	-11.09	-11.18
Na2B4O7(cr)	-36.50	-42.78	-38.00	-37.09	-36.18	-34.23
Na2B4O7:10H2O(s)	-27.62	-33.91	-29.12	-28.22	-27.31	-25.36
Na2HPO4(cr)	-12.76	-15.16	-12.68	-12.24	-11.83	-11.21
Na2O(cr)	-63.62	-69.91	-65.12	-64.22	-63.31	-61.33
Na3PO4(cr)	-24.80	-30.35	-25.48	-24.58	-23.72	-22.11
NaBO2(s)	-15.65	-18.79	-16.40	-15.95	-15.49	-14.51
NaH2PO4(cr)	-8.18	-7.44	-7.35	-7.37	-7.41	-7.78
P(cr)	-107.32	-106.60	-106.70	-106.62	-106.55	-106.62
Pentahydrite	-4.54	-4.55	-4.53	-4.54	-4.54	-4.55
Periclase	-14.37	-20.67	-15.91	-15.01	-14.12	-12.18
Picromerite	-7.19	-7.71	-7.17	-7.14	-7.08	-6.83
Polyhalite	-5.69	-6.23	-5.66	-5.63	-5.57	-5.32
Portlandite	-13.71	-20.02	-15.25	-14.35	-13.46	-11.51
Pseudomalachite	-19.28	-43.03	-23.85	-20.31	-16.87	-10.14
Pyrite	-121.49	-125.47	-122.82	-122.14	-121.46	-119.87
Pyrochroite	-10.87	-17.15	-12.40	-11.52	-10.68	-8.92
Pyrrhotite	-71.34	-76.66	-72.79	-72.03	-71.27	-69.58
S(cr)	-55.50	-52.99	-55.09	-55.33	-55.55	-55.96
Sacchite	-16.13	-16.10	-16.12	-16.14	-16.19	-16.40
Struvite	-2.39	-7.96	-3.12	-2.24	-1.40	0.17
Sylvite	-2.93	-3.17	-2.92	-2.91	-2.88	-2.75
Syngenite	-2.34	-2.86	-2.32	-2.29	-2.23	-1.97
Tachyhydrite	-28.02	-27.99	-28.02	-28.02	-28.03	-28.08
Tagilite	-7.21	-15.93	-8.72	-7.40	-6.12	-3.70
Thernardite	-8.17	-8.16	-8.12	-8.11	-8.10	-8.08
Troilite	-74.51	-81.00	-76.24	-75.34	-74.43	-72.43
Vivianite	-7.89	-23.31	-10.00	-8.19	-6.47	-3.46
ZnB2O4(s)	-13.98	-20.28	-15.51	-14.61	-13.71	-11.76

B.2 "Filtrate" system tests – carbon source during growth comparisons

Table B.2 Parameters used as the basis for geochemical modelling of the filtrate precipitation tests following carbon source experiments

Summary for geochemical modelling	Experimental conditions represented	Inorganic phosphate released from phytate rounded to the nearest 10 (%)	Inorganic phosphate concentration to use for geochemical modelling (mmol/L)	Remaining organic phosphate (mg/L)	Calculated remaining phytate (mg/L)
No phytase activity	*B. adeninivorans* grown with glucose	0%	5	30	5
Low phytase activity	*A. niger* grown with galactose (average of two lowest cultures)	30%	14	21	3.5
Medium phytase activity	*A. niger* grown with galactose (average of three cultures)	50%	20	15	2.5
High phytase activity	*A. niger* grown with glucose or starch; *B. adeninivorans* grown with starch or galactose	80%	29	6	1
All phytate degraded	Hypothetical	100%	35	0	0

As there did not appear to be a substantial difference between *A. niger* and *B. adeninivorans* in these experiments, the system was simplified to five generic conditions to describe different levels of phosphate release from phytate (table B.2).

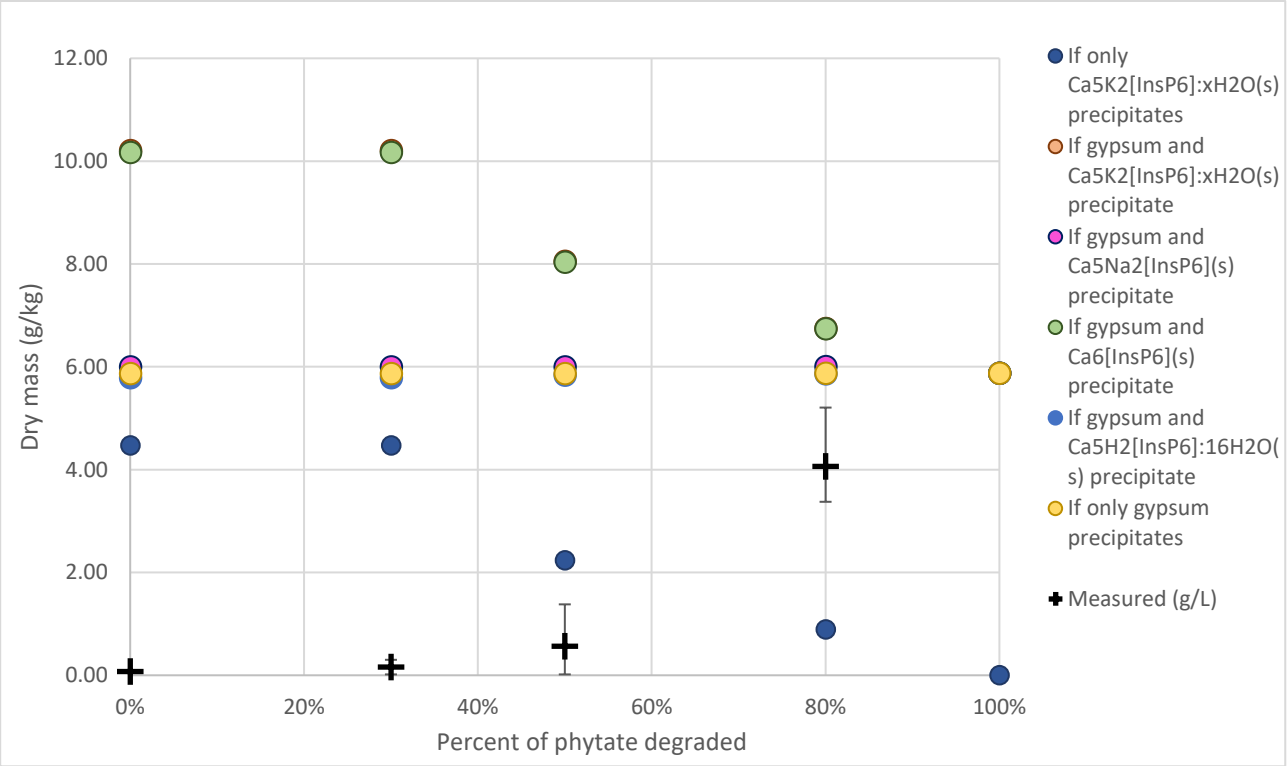

*Figure B.1 Calculated mass of precipitate from geochemical simulations where different phases are allowed to precipitate, compared to experimentally measured values. Error bars for the experimentally measured values represent the upper and lower measured values, while the data point is the average value (*n = *3, 2, 3, and 12 for 0%, 30%, 50%, and 80% phytate degraded respectively)*

Comparing the calculated total mass of precipitate (that is, gypsum and/or calcium phytate) shows a substantial deviation from the observed experimental results (figure B.1). Where the experimental results indicated an increase in precipitate mass with phytate breakdown, the modelling either suggests a decrease (where calcium phytates are precipitating) or practically no impact (where only gypsum precipitates).

The modelling approach taken does indicate some degree of competition between phytate, phosphate, and sulfate for calcium complexation (data not shown). However, it does not help to validate any ideas about phytate inhibiting gypsum precipitation. There could be a number of reasons for this:

- An incomplete range of data for soluble calcium phytate complexes has been included in the model, thereby underestimating the strength of calcium complexation by phytate
- The model has not taken account for kinetic factors; in the experiments performed where no precipitation was observed, gypsum and/or calcium phytate may indeed still have been supersaturated, and the influence of phytate could be in slowing down the nucleation of gypsum, rather than stopping it altogether
- The microorganisms used in these experiments secreted organic acids such as citric acid and gluconic acid that added further complexation for calcium speciation

B.3 "Active" system tests with 0.5 mmol/L manganese

To try and explain these results, geochemical modelling was performed using six simulations:

1. Preparation of the media prior to phytate addition
2. Sterile media at pH 5.5 after phytate addition (0.005 mol/L phosphate and 0.005 mol/L phytate)
3. *B. adeninivorans* cultures after 20 days (with 0.027 mol/L phosphate and 0.001 mol/L phytate, pH adjusted to 4.5 with HCl)
4. *A. niger* cultures after 20 days (0.016 mol/L phosphate and 0.003 mol/L phytate, pH adjusted to 3.0 with HCl)

5. *A. niger* cultures after 20 days with low concentrations of organic acids (0.016 mol/L phosphate and 0.003 mol/L phytate; 46 mmol/L oxalate, 22.6 µmol/L citrate, 1.47 µmol/L gluconate (1), and 0.666 mmol/L tartrate (2), pH adjusted to 3.0 with HCl)

6. *A. niger* cultures after 20 days with high concentrations of organic acids (0.016 mol/L phosphate and 0.003 mol/L phytate; 88 mmol/L oxalate (3), 11 mmol/L citrate (4), 18.86 mmol/L gluconate (4), 26.65 mmol/L tartrate (2); pH adjusted to 3.0 with KOH)

The different *A. niger* simulations were used as it was suspected that organic acids would have an important influence on manganese speciation. However, as organic acids were not quantified, simulations with no organic acids present or with low or high estimates of organic acids based upon literature results were performed. The acids chosen (citric, gluconic, oxalic, and tartaric) were those known to be produced by *A. niger* in high quantities.

Table B.3 Saturation indices in simulations representing the "active" system tests with manganese. Phytate is represented in the model by [InsP6].

Simulation	1	2	3	4	5	6
Anapaite	n/a	-2.61	-5.49	-14.82	-24.92	-27.77
Anhydrite	-1.33	-1.56	-1.43	-1.44	-1.45	-1.61
Bassanite	-1.85	-2.08	-1.95	-1.96	-1.97	-2.13
Brushite	n/a	-1.54	-1.75	-4.04	-4.05	-4.22
Ca(HPO4)(s)	n/a	-1.28	-1.50	-3.79	-3.79	-3.96
Ca3(PO4)2(alfa)	n/a	-5.21	-7.71	-16.25	-16.27	-16.73
Ca4H(PO4)3:2.5H2O(s)	n/a	-7.34	-10.06	-20.89	-20.91	-21.55
Ca5Na2[InsP6](s)	n/a	22.65	20.22	10.21	10.17	9.13
Ca6[InsP6](s)	n/a	7.24	4.81	-5.17	-5.21	-6.35
Chloroapatite	n/a	-2.10	-5.03	-17.35	-17.43	-19.41
Gypsum	-1.12	-1.34	-1.22	-1.23	-1.24	-1.40
Hydroxyapatite	n/a	-3.21	-8.00	-22.77	-22.81	-23.58
Mg(Ox):2H2O(s)	n/a	n/a	n/a	n/a	0.57	1.60
Mg(Ox)(s)	n/a	n/a	n/a	n/a	-1.72	-0.69
Ca(Ox):H2O(s)	n/a	n/a	n/a	n/a	0.68	1.82
Ca(Ox):2H2O(s)	n/a	n/a	n/a	n/a	0.26	1.40
Ca(Ox):3H2O(s)	n/a	n/a	n/a	n/a	0.16	1.30
FeOx:2H2O(s)	n/a	n/a	n/a	n/a	-15.83	-17.07
MnOx:2H2O(s)	n/a	n/a	n/a	n/a	-3.06	-9.36
Alabandite	-76.98	-77.46	-79.25	-82.21	-79.40	-86.97
Hausmannite	-14.83	-15.85	-21.07	-31.86	-32.69	-55.43
Manganite	-5.56	-5.90	-7.55	-11.02	-11.41	-19.00
Mn(HPO4)(s)	n/a	4.36	4.30	2.11	2.07	-5.53
Mn(SO4)(s)	-3.26	-3.74	-3.46	-3.37	-3.41	-11.01
Mn3(PO4)2(s)	n/a	-11.37	-13.40	-21.63	-21.74	-44.52
Mn3(PO4)2:3H2O(s)	n/a	1.63	-0.41	-8.64	-8.75	-31.54
Mn5H2[InsP6]:16H2O(s)	n/a	-1.73	-1.32	-6.84	-7.03	-45.23
MnCl2:2H2O(s)	-13.18	-13.60	-11.80	-10.75	-10.86	-20.86
MnCl2:4H2O(s)	-11.91	-12.34	-10.53	-9.48	-9.60	-19.60
MnCl2:H2O(s)	-14.73	-15.15	-13.35	-12.29	-12.41	-22.41
MnO(s)	-10.84	-11.18	-13.09	-16.94	-16.98	-24.56
MnO2(s)	-9.63	-9.97	-11.37	-14.46	-15.20	-22.79
Pyrochroite	-8.24	-8.58	-10.50	-14.35	-14.38	-21.96
Sacchite	-17.96	-18.38	-16.58	-15.53	-15.64	-25.64

Table B.3 (continued).

Simulation	1	2	3	4	5	6
H3Cit:H2O(cr)	n/a	n/a	n/a	n/a	-6.04	-3.55
Ca3(Cit)2:4H2O(s)	n/a	n/a	n/a	n/a	-16.75	-12.18
CaH(Cit)(s)	n/a	n/a	n/a	n/a	-6.50	-4.15
Ca3(Cit)2(s)	n/a	n/a	n/a	n/a	-17.63	-13.06
Ca(HGlu)2(s)	n/a	n/a	n/a	n/a	-16.43	-6.12
KH(Tar)(s)	n/a	n/a	n/a	n/a	-1.93	-0.11
Ca(Tar)(s)	n/a	n/a	n/a	n/a	-5.07	-3.61
Ca(Tar):2H2O(s)	n/a	n/a	n/a	n/a	-2.98	-1.52
Cu(Tar)(s)	n/a	n/a	n/a	n/a	-10.71	-11.69

Table B.3 indicates the saturation indices across the six simulations representing the manganese experiments. The addition of phytate leads to supersaturation for calcium phytates and manganese phosphates ($MnHPO_4$ and $Mn_3(PO_4)_2.3H_2O$), but not manganese phytate or any other manganese phase (simulation 2). For simulation 3, representing the *B. adeninivorans* cultures, the $Mn_3(PO_4)_2.3H_2O$ phase became undersaturated and there was a slight reduction in supersaturation for $MnHPO_4$ and the calcium phytate phases.

For the *A. niger* simulations (simulations 4–6), one of the calcium phytate phases became undersaturated, while the mixed calcium-sodium phytate and $MnHPO_4$ remained supersaturated in simulations 4 (no organic acids) and 5 (low organic acids). However, at the high organic acid condition (simulation 6), $MnHPO_4$ became undersaturated. With the addition of organic acids the three calcium oxalate species and magnesium oxalate dihydrate became supersaturated. However, manganese oxalate and solid phases of the other likely organic acids (citrate, gluconate, tartrate) remained undersaturated.

B.4 "Active" system tests with 0.5 mmol/L lanthanum

Geochemical modelling of this system involved performing six simulations, as described for the "active" system tests with manganese above. As with manganese, an approach was used where estimates of low and high levels of likely organic acids were used in the construction of the models.

Table B.4 Saturation indices in simulations representing the "active" system tests with manganese. Phases most likely to be present are highlighted. Phytate is represented in the model by [InsP6].

Simulation	1	2	3	4	5	6
Alabandite	-79.27	-79.45	-81.38	-83.89	-81.33	-89.74
Anapaite	n/a	-2.56	-5.42	-12.28	-22.53	-25.75
Anhydrite	-1.34	-1.44	-1.40	-1.42	-1.43	-1.76
Antarcticite	-12.58	-12.65	-11.73	-10.71	-10.87	-12.96
Arcanite	-2.87	-2.52	-2.91	-2.67	-2.66	-1.98
B(cr)	-90.12	-90.14	-90.90	-91.83	-90.81	-90.85
B(OH)3(cr)	-4.96	-4.96	-4.96	-4.96	-4.96	-5.02
B2O3(am)	-18.13	-18.13	-18.13	-18.13	-18.13	-18.24

Table B.4 (continued).

Simulation	1	2	3	4	5	6
B2O3(cr)	-15.96	-15.96	-15.96	-15.96	-15.96	-16.08
Bassanite	-1.86	-1.96	-1.92	-1.94	-1.95	-2.28
Bischofite	-12.47	-12.54	-11.61	-10.60	-10.78	-13.13
Bloedite	-10.42	-10.65	-10.54	-10.62	-10.65	-11.34
Brucite	-9.47	-9.55	-11.58	-14.58	-14.61	-15.15
Brushite	n/a	-1.50	-1.72	-3.47	-3.49	-3.83
C3FH6	-43.35	-44.00	-54.50	-69.51	-90.69	-96.65
C4FH13	-59.04	-59.76	-72.32	-90.31	-111.51	-117.75
Ca(HGlu)2(s)	n/a	n/a	n/a	n/a	-14.19	-5.32
Ca(HPO4)(s)	n/a	-1.24	-1.46	-3.22	-3.23	-3.57
Ca(NO3)2(s)	-23.69	-23.75	-23.77	-24.80	-30.25	-30.67
Ca(Ox):2H2O(s)	n/a	n/a	n/a	n/a	0.60	1.68
Ca(Ox):3H2O(s)	n/a	n/a	n/a	n/a	0.50	1.58
Ca(Ox):H2O(s)	n/a	n/a	n/a	n/a	1.03	2.10
Ca(s)	-117.34	-117.42	-119.98	-123.58	-122.92	-123.19
Ca(SO3)(s)	-28.97	-29.08	-29.54	-30.18	-29.51	-29.83
Ca(Tar)(s)	n/a	n/a	n/a	n/a	-4.48	-3.18
Ca(Tar):2H2O(s)	n/a	n/a	n/a	n/a	-2.39	-1.09
Ca2Cl2(OH)2:H2O(s)	-27.91	-28.06	-29.20	-31.15	-31.33	-33.70
Ca2Fe2O5(s)	-34.88	-35.45	-43.89	-55.93	-77.09	-82.76
Ca3(Cit)2(s)	n/a	n/a	n/a	n/a	-15.06	-10.92
Ca3(Cit)2:4H2O(s)	n/a	n/a	n/a	n/a	-14.17	-10.04
Ca3(PO4)2(alfa)	n/a	-5.12	-7.63	-14.11	-14.16	-15.10
Ca3B2O6(s)	-48.42	-48.65	-54.81	-63.75	-63.81	-64.76
Ca4Cl2(OH)6:13H2O(s)	-56.40	-56.70	-61.96	-69.87	-70.08	-73.03
Ca4H(PO4)3:2.5H2O(s)	n/a	-7.21	-9.94	-18.18	-18.24	-19.52
Ca5H2[InsP6]:16H2O(s)	n/a	-18.85	-21.15	-26.08	-26.16	-28.40
Ca5K2[InsP6]:xH2O(s)	n/a	7.14	2.35	-5.30	-5.38	-6.86
Ca5Na2[InsP6](s)	n/a	3.72	-0.62	-8.56	-8.64	-10.92
Ca6[InsP6](s)	n/a	-11.65	-16.00	-23.91	-24.01	-26.50
CaB2O4(s)	-19.45	-19.53	-21.58	-24.56	-24.58	-24.97
CaB4O7(s)	-26.72	-26.80	-28.85	-31.83	-31.86	-32.36
CaCl2:2H2O(cr)	-16.75	-16.82	-15.91	-14.88	-15.04	-17.13
CaCl2:4H2O(cr)	-14.06	-14.13	-13.21	-12.19	-12.35	-14.44
CaCl2:H2O(s)	-16.67	-16.74	-15.83	-14.80	-14.96	-17.05
CaFe2O4(s)	-6.02	-6.51	-12.90	-21.95	-43.10	-48.49
CaH(Cit)(s)	n/a	n/a	n/a	n/a	-5.71	-3.50
CaI2(s)	-39.00	-39.07	-39.06	-39.05	-39.07	-39.38
CaMoO4(s)	-2.43	-2.54	-2.55	-4.13	-6.42	-8.11
CaO(cr)	-26.00	-26.07	-28.13	-31.11	-31.12	-31.40
Carnallite	-16.15	-16.03	-14.86	-13.21	-13.46	-16.34
Chloroapatite	n/a	-1.76	-5.06	-14.27	-14.42	-16.89
Cornetite	n/a	-11.27	-15.59	-23.30	-29.76	-38.11
Cu(cr)	-10.87	-10.95	-13.51	-17.11	-18.58	-21.34
Cu(OH)1.5(SO4)0.25	-3.62	-3.70	-5.22	-7.46	-9.61	-12.39
Cu(OH)2(s)	-5.94	-6.01	-8.06	-11.04	-13.20	-15.96
Cu(Tar)(s)	n/a	n/a	n/a	n/a	-10.79	-11.98
Cu-hydroxypyromorphite	n/a	-13.36	-18.11	-29.32	-40.08	-54.08
Cu3(PO4)2(s)	n/a	-7.55	-10.04	-16.52	-22.97	-31.38
CuO(s)	-5.14	-5.21	-7.26	-10.24	-12.39	-15.16
CuSO4:5H2O(s)	-6.71	-6.82	-6.77	-6.79	-8.93	-11.76
Epsonite	-3.13	-3.24	-3.18	-3.22	-3.25	-3.84
Ettringite-Fe	-42.26	-43.22	-53.59	-68.67	-89.88	-96.86
Fe(OH)2(cr)	-8.63	-8.85	-11.27	-14.62	-24.84	-27.39
Fe(PO4)(cr)	n/a	2.27	1.93	0.12	-10.44	-13.05
Fe(s)	-37.85	-38.08	-41.00	-44.97	-54.52	-57.05
Fe5(OH)(PO4)3(s)	n/a	399.14	392.54	379.48	328.36	315.46
FeMoO4(s)	-4.88	-5.13	-5.50	-7.45	-19.94	-23.91
FeO(s)	-9.26	-9.47	-11.89	-15.24	-25.46	-28.01
FeOx:2H2O(s)	n/a	n/a	n/a	n/a	-15.21	-16.41

Table B.4 (continued).

Simulation	1	2	3	4	5	6
Ferrihydrite(am)	1.82	1.61	-0.56	-3.59	-14.16	-16.71
Ferryhydrite	3.17	2.96	0.79	-2.24	-12.81	-15.36
FeS(am)	-75.78	-76.07	-78.41	-81.28	-88.78	-91.33
Glaserite	-14.25	-13.34	-14.45	-13.79	-13.76	-11.82
Glauberite	-15.46	-15.69	-15.60	-15.67	-15.67	-16.11
Goethite	3.79	3.58	1.41	-1.62	-12.19	-14.74
Gypsum	-1.12	-1.23	-1.18	-1.20	-1.21	-1.55
H2MoO4(s)	-4.31	-4.34	-2.30	-0.89	-3.16	-4.58
H3Cit:H2O(cr)	n/a	n/a	n/a	n/a	-6.23	-3.75
Halite	-6.91	-6.96	-6.50	-6.00	-6.07	-7.00
Hausmannite	-21.66	-21.98	-27.49	-35.81	-37.01	-62.23
Hematite	9.38	8.96	4.63	-1.45	-22.58	-27.68
Hexahydrite	-3.42	-3.53	-3.47	-3.50	-3.53	-4.12
Hydrophilite	-20.67	-20.74	-19.83	-18.80	-18.96	-21.05
Hydroxyapatite	n/a	-3.07	-7.86	-19.07	-19.15	-20.71
K(cr)	-59.21	-59.03	-60.52	-62.19	-61.85	-61.48
K(NO3)(s)	-8.33	-8.14	-8.36	-8.75	-11.47	-11.17
K(OH)(s)	-20.49	-20.31	-21.55	-22.91	-22.91	-22.54
K2O(s)	-77.17	-76.79	-79.28	-82.00	-82.00	-81.27
Kainite	-8.75	-8.67	-8.37	-7.76	-7.86	-8.98
KH(Tar)(s)	n/a	n/a	n/a	n/a	-1.89	0.06
KH2PO4(cr)	n/a	-3.35	-2.76	-2.90	-2.90	-2.59
KI(s)	-9.52	-9.33	-9.54	-9.41	-9.41	-9.06
Lawrencite	-20.66	-20.87	-20.32	-19.66	-30.02	-34.38
Leonhardtite	-4.22	-4.33	-4.27	-4.30	-4.33	-4.92
Leonite	-5.80	-5.56	-5.89	-5.69	-5.71	-5.62
Lepidocrocite	3.42	3.21	1.05	-1.99	-12.56	-15.11
Libenthenite	n/a	-6.56	-8.82	-13.56	-17.86	-23.45
Ln(cr)	-130.28	-130.62	-134.37	-139.63	-140.05	-143.03
Ln(NO3)3:6H2O(s)	-28.03	-28.35	-28.28	-29.68	-39.28	-42.50
Ln(OH)3(am)	-6.21	-6.54	-9.53	-13.86	-15.30	-18.30
Ln(OH)3(cr)	-4.46	-4.78	-7.77	-12.10	-13.54	-16.54
Ln(PO4):xH2O(s)	n/a	7.83	6.67	3.57	2.13	-0.92
Ln2(Ox)3(s)	n/a	n/a	n/a	n/a	-0.15	-2.09
Ln2(SO4)3:8H2O(s)	-6.33	-7.07	-6.75	-6.53	-9.39	-15.55
Ln2(Tar)3:9H2O(s)	n/a	n/a	n/a	n/a	-8.33	-9.59
Ln2O3(cubic)	-30.83	-31.49	-37.46	-46.12	-49.00	-55.00
Ln2O3(monoclinic)	-31.94	-32.60	-38.57	-47.23	-50.11	-56.11
Ln3O4(s)	-73.98	-74.97	-84.18	-97.48	-101.46	-110.46
LnCl(OH)2(s)	-5.71	-6.04	-7.54	-9.87	-11.38	-15.29
LnCl2(s)	-29.19	-29.52	-29.79	-30.42	-31.67	-36.47
LnCl3(s)	-32.76	-33.08	-31.61	-29.93	-31.58	-37.29
LnCl3:6H2O(s)	-17.87	-18.19	-16.72	-15.04	-16.69	-22.41
LnK(SO4)2.H2O(s)	-4.73	-4.92	-4.95	-4.72	-6.15	-8.89
LnNa(Ox)2(s)	n/a	n/a	n/a	n/a	1.52	1.21
LnNa(SO4)2.H2O(s)	-5.16	-5.59	-5.40	-5.32	-6.74	-9.88
LnO(s)	-47.35	-47.68	-50.92	-55.56	-56.66	-59.66
LnOCl(s)	-12.85	-13.18	-14.68	-17.01	-18.52	-22.42
LnPO4:H2O(cr)	n/a	9.42	8.27	5.17	3.73	0.67
LnSO4(s)	-12.45	-12.81	-13.95	-15.63	-16.72	-19.77
Mackinawite	-75.13	-75.42	-77.76	-80.63	-88.13	-90.68
Maghemite(disord)	4.97	4.55	0.22	-5.85	-26.98	-32.09
Maghemite(ord)	4.76	4.34	0.01	-6.06	-27.19	-32.30
Magnetite	2.10	1.46	-5.29	-14.71	-46.06	-53.72
Manganite	-7.83	-7.94	-9.69	-12.36	-12.87	-21.28
Melanterite	-6.33	-6.57	-6.89	-7.28	-17.50	-20.11
Mercallite	-7.50	-7.34	-6.49	-4.89	-4.88	-4.56
Mg(cr)	-99.34	-99.43	-101.98	-105.59	-104.95	-105.47
Mg(HPO4):3H2O(s)	n/a	-1.60	-1.80	-3.57	-3.60	-4.19
Mg(NO3)2(s)	-32.60	-32.67	-32.67	-33.71	-39.18	-39.86

Table B.4 (continued).

Simulation	1	2	3	4	5	6
Mg(NO3)2:6H2O(s)	-19.70	-19.77	-19.77	-20.81	-26.28	-26.96
Mg(Ox)(s)	n/a	n/a	n/a	n/a	-1.39	-0.57
Mg(Ox):2H2O(s)	n/a	n/a	n/a	n/a	0.91	1.73
Mg(SO4)(s)	-14.47	-14.58	-14.52	-14.55	-14.58	-15.16
Mg(SO4):H2O(s)	-5.06	-5.17	-5.11	-5.14	-5.17	-5.76
Mg-oxychlorur	-18.52	-18.68	-21.28	-25.26	-25.40	-27.38
Mg3(PO4)2(cr)	n/a	-8.91	-11.37	-17.89	-17.99	-19.70
Mg3(PO4)2:22H2O(s)	n/a	-8.52	-10.97	-17.50	-17.60	-19.34
Mg3(PO4)2:8H2O(s)	n/a	-6.38	-8.83	-15.36	-15.46	-17.17
Mg5H2[InsP6]:22H2O(s)	n/a	-21.78	-23.99	-28.99	-29.16	-32.67
MgCl2(s)	-30.47	-30.55	-29.62	-28.60	-28.78	-31.12
MgCl2:2H2O(s)	-20.87	-20.95	-20.02	-19.00	-19.18	-21.52
MgCl2:4H2O(s)	-15.42	-15.49	-14.56	-13.55	-13.73	-16.07
MgCl2:H2O(s)	-24.19	-24.26	-23.33	-22.32	-22.50	-24.84
MgI2(s)	-50.81	-50.88	-50.85	-50.85	-50.89	-51.45
MgMoO4(s)	-9.19	-9.31	-9.30	-10.89	-13.19	-15.14
Mirabilite	-6.29	-6.42	-6.37	-6.42	-6.42	-6.54
Mn(HPO4)(s)	n/a	2.34	2.16	0.41	0.24	-8.22
Mn(SO4)(s)	-5.54	-5.68	-5.59	-5.61	-5.77	-14.23
Mn3(PO4)2(s)	n/a	-17.45	-19.80	-26.29	-26.80	-52.12
Mn3(PO4)2:3H2O(s)	n/a	-4.46	-6.81	-13.30	-13.81	-39.13
Mn5H2[InsP6]:16H2O(s)	n/a	-30.91	-32.96	-37.91	-38.76	-81.61
MnCl2:2H2O(s)	-15.14	-15.25	-14.29	-13.26	-13.58	-23.79
MnCl2:4H2O(s)	-13.88	-13.99	-13.02	-12.00	-12.31	-22.53
MnCl2:H2O(s)	-16.69	-16.80	-15.83	-14.81	-15.12	-25.33
MnO(s)	-13.12	-13.23	-15.23	-18.21	-18.38	-26.79
MnO2(s)	-11.91	-12.00	-13.50	-15.87	-16.72	-25.13
MnOx:2H2O(s)	n/a	n/a	n/a	n/a	-5.11	-12.16
Mo(s)	-76.04	-76.11	-75.58	-76.04	-76.27	-77.65
Mo3O8(s)	-14.61	-14.73	-9.09	-5.50	-11.64	-15.87
Monosulfate-Fe	-42.66	-43.41	-53.86	-68.90	-90.09	-96.38
MoO2(s)	-13.40	-13.45	-11.91	-11.12	-12.71	-14.12
MoO3(s)	-5.54	-5.57	-3.53	-2.12	-4.39	-5.81
MoS2(s)	-139.01	-139.20	-137.51	-135.77	-131.91	-133.33
MoS3(s)	-197.95	-198.20	-195.93	-193.09	-187.19	-188.62
Na(cr)	-57.04	-57.10	-58.37	-60.19	-59.85	-59.87
Na(NO3)(s)	-10.99	-11.04	-11.04	-11.57	-14.29	-14.39
Na2B4O7(cr)	-36.13	-36.23	-38.27	-41.28	-41.30	-41.58
Na2B4O7:10H2O(s)	-27.22	-27.32	-29.37	-32.38	-32.39	-32.69
Na2HPO4(cr)	n/a	-12.24	-12.46	-14.24	-14.24	-14.35
Na2O(cr)	-63.23	-63.33	-65.38	-68.39	-68.39	-68.45
Na3PO4(cr)	n/a	-24.15	-25.38	-28.67	-28.68	-28.81
NaBO2(s)	-15.46	-15.51	-16.53	-18.04	-18.04	-18.13
NaH2PO4(cr)	n/a	-7.81	-7.00	-7.28	-7.28	-7.36
P(cr)	n/a	-106.98	-106.42	-106.74	-105.04	-105.06
Pentahydrite	-3.80	-3.91	-3.85	-3.89	-3.91	-4.50
Periclase	-14.05	-14.13	-16.17	-19.17	-19.20	-19.73
Picromerite	-5.40	-5.17	-5.49	-5.29	-5.31	-5.22
Polyhalite	-7.53	-7.50	-7.74	-7.57	-7.61	-8.18
Portlandite	-15.92	-15.99	-18.05	-21.03	-21.05	-21.33
Pseudomalachite	n/a	-18.03	-24.61	-37.05	-47.81	-61.76
Pyrite	-119.81	-120.16	-121.92	-123.69	-129.15	-131.72
Pyrochroite	-10.52	-10.63	-12.63	-15.62	-15.79	-24.19
Pyrrhotite	-70.31	-70.57	-72.53	-74.88	-81.14	-83.37
S(cr)	-54.92	-54.98	-54.40	-53.30	-51.25	-51.27
Sacchite	-19.93	-20.04	-19.07	-18.04	-18.36	-28.57
Struvite	n/a	-1.78	-2.99	-6.26	-6.30	-6.92
Sylvite	-4.68	-4.49	-4.25	-3.61	-3.68	-4.22
Syngenite	-3.08	-2.84	-3.18	-2.96	-2.97	-2.62
Tachyhydrite	-42.00	-42.23	-39.46	-36.40	-36.91	-43.70

Table B.4 (continued).

Simulation	1	2	3	4	5	6
Tagilite	n/a	-6.66	-8.93	-13.66	-17.96	-23.55
Thernardite	-7.37	-7.50	-7.45	-7.50	-7.50	-7.60
Troilite	-73.41	-73.70	-76.04	-78.91	-86.41	-88.97
Vivianite	n/a	-6.69	-10.29	-17.88	-48.55	-56.31
ZnB2O4(s)	-13.59	-13.71	-15.69	-18.71	-19.34	-21.51

The saturation indices of a range of possible solid phases are shown in table B.4 for the six simulations. Prior to the addition of phytate, the only supersaturated phases present were iron (oxyhydr)oxides (simulation 1) which, due to the low concentration of iron present, were not likely to be relevant. After the addition of phytate (simulation 2), calcium phytate and lanthanum phosphate phases showed positive saturation indices. Note that, while no literature data could be found for the solubility product of lanthanum phytate, where calcium phytate is insoluble, it can be assumed that lanthanum phytate is also insoluble. The same trend was apparent in simulation 3, representing the *B. adeninivorans* cultures where phytase activity had occurred, although there was a slight decrease in saturation indices likely associated with the decrease in pH from 5.5 to 4.5.

For *A. niger*, assuming that the pH reduction came from HCl, left the lanthanum phosphate solids supersaturated along with one of the calcium phytate phases (simulation 4). Upon incorporating organic acids into the model (simulations 5 and 6), the saturation indices of the lanthanum phosphates and calcium phytates were reduced, while a number of oxalates became supersaturated (magnesium, calcium, and lanthanum sodium oxalates). Using the higher concentrations of organic acids, one of the lanthanum phosphate phases becomes undersaturated, and one of the tartrate phases (potassium hydrogen tartrate) becomes very slightly supersaturated.

B.5 "Inactive" system tests with 50 mmol/L manganese

Table B.5 Saturation indices for geochemical models of systems adding manganese to pH 2.5 and pH 3.0 cultures of B. adeninivorans *with hydrolysed phytate. Phytate is represented in the model by [InsP6].*

Simulation	1	2
Description	Add Mn to pH 2.5 solution	An Mn to pH 3 solution
Anapaite	-14.46	-12.34
Anhydrite	-1.38	-1.38
Bassanite	-1.90	-1.90
Brushite	-3.87	-3.41
Ca(HPO4)(s)	-3.62	-3.16
Ca3(PO4)2(alfa)	-15.86	-14.10
Ca4H(PO4)3:2.5H2O(s)	-20.33	-18.11
Ca5Na2[InsP6](s)	9.66	11.88
Ca6[InsP6](s)	-5.75	-3.53
Chloroapatite	-18.12	-15.48
Gypsum	-1.16	-1.16

Table B.5 (continued).

Simulation	1	2
Description	Add Mn to pH 2.5 solution	An Mn to pH 3 solution
Hydroxyapatite	-22.17	-19.12
Alabandite	-80.04	-79.57
Hausmannite	-25.85	-23.46
Manganite	-9.02	-8.25
Mn(HPO4)(s)	4.24	4.70
Mn(SO4)(s)	-1.34	-1.34
Mn3(PO4)2(s)	-15.36	-13.60
Mn3(PO4)2:3H2O(s)	-2.36	-0.60
Mn5H2[InsP6]:16H2O(s)	2.37	3.75
MnCl2:2H2O(s)	-11.45	-11.47
MnCl2:4H2O(s)	-10.19	-10.20
MnCl2:H2O(s)	-13.00	-13.02
MnO(s)	-14.93	-14.09
MnO2(s)	-12.48	-11.76
Pyrochroite	-12.33	-11.49
Sacchite	-16.24	-16.26

Geochemical modelling of the manganese-spiked cultures (table B.5) indicated that calcium and manganese phytates and manganese hydrogen phosphate ($Mn(HPO_4)$) were supersaturated. Chemical analysis of the initial pH 3 solution indicated a potential decrease in soluble phytate, but effectively all the manganese and inorganic phosphate appeared to remain soluble. As such, if any precipitation occurred, it was more likely to be some complex of phytate with calcium, magnesium, sodium, potassium, and other metals present.

The lack of manganese phosphate precipitation observed experimentally suggests that some critical component (e.g. complexing agents produced by *B. adeninivorans* keeping manganese in solution, the kinetics of these phases precipitating at the pH values tested being very slow) was not accounted for in the modelling approach used.

B.6 "Inactive" system tests with 50 mmol/L iron

Table B.6 Saturation indices for geochemical models of systems adding iron(II) to pH 2.5 and pH 3.0 cultures of B. adeninivorans *with hydrolysed phytate*

Simulation	1	2
Description	Add FeSO4 to pH 2.5 sample	Add FeSO4 to pH 3.0 sample
Ca5Na2[InsP6](s)	9.37	11.80
Ca6[InsP6](s)	-6.09	-3.67
Ettringite-Fe	-73.86	-68.73
Fe(OH)2(cr)	-10.45	-9.57
Fe(PO4)(cr)	-0.78	0.04
Fe(s)	-30.18	-30.01
Fe5(OH)(PO4)3(s)	401.05	404.19
FeMoO4(s)	-3.25	-2.40
FeO(s)	-11.07	-10.19
Ferrihydrite(am)	-4.74	-3.50
Ferrihydrite	-3.39	-2.15

Table B.6 (continued).

Simulation	1	2
Description	Add FeSO4 to pH 2.5 sample	Add FeSO4 to pH 3.0 sample
FeS(am)	-33.40	-36.24
Goethite	-2.77	-1.54
Gypsum	-1.09	-1.08
H2MoO4(s)	-0.86	-0.89
Hausmannite	-49.73	-46.37
Hematite	-3.74	-1.27
Lawrencite	-16.73	-16.75
Lepidocrocite	-3.14	-1.91
Mackinawite	-32.75	-35.59
Maghemite(disord)	-8.15	-5.68
Maghemite(ord)	-8.36	-5.89
Magnetite	-12.84	-9.49
Melanterite	-1.90	-1.90
Mn(HPO4)(s)	-0.44	0.03
Mo3O8(s)	5.22	4.42
Monosulfate-Fe	-74.35	-69.23
Pyrite	-42.73	-48.57
Pyrrhotite	-28.93	-31.79
Troilite	-31.04	-33.87
Vivianite	-4.88	-3.07

Geochemical modelling indicated supersaturation for the iron phase $Fe_5(OH)(PO_4)_3$ at both pH values as well as $FePO_4$ at pH 3.2 (table B.6). Melanterite ($FeSO_4.7H_2O$) was undersaturated in the model, verifying that this salt would be soluble under the conditions it was added to the media. Solubility product data for iron phytate phases could not be found, but supersaturation for calcium phytate phases indicates that iron phytates would probably also be supersaturated under these conditions. However, it appears that more comprehensive thermodynamic data would be required to model these experiments accurately.

The other questionable aspect of this model is the extremely high saturation indices (~ 400) for the iron phosphate phase ($Fe_5(OH)(PO_4)_3$) seems at odds with the lack of any detectable inorganic phosphate precipitation. Examining the sit.dat database used indicates that the solubility product for this phase is log K_{sp} = -402.320 for the dissolution reaction, with Falck *et al.* (5) cited as the source. Note, however, that Falck *et al.* (5) is a compilation of data; the original source appears to be Nriagu and Dell (6) but they only describe the free energy of formation (ΔG^o_f) which is given as -1510.2 kcal/mol. It is uncertain how the log K_{sp} has subsequently been derived from this value, and the data relating to this phase should be treated cautiously.

B.7 “Inactive” system tests with 50 mmol/L lanthanum

Table B.7 Saturation indices in the geochemical modelling of adding lanthanum to B. adeninivorans *cultures with hydrolysed phytate*

Simulation	1	2
Description	Add La to pH 2.5 sample	Add La to pH 3.0 sample
Alabandite	-84.96	-84.35
Anapaite	-15.65	-12.86
Anhydrite	-1.75	-1.73
Antarcticite	-9.79	-9.80
Arcanite	-4.28	-3.85
B(cr)	-92.13	-91.91
B(OH)3(cr)	-4.99	-4.99
B2O3(am)	-18.20	-18.20
B2O3(cr)	-16.03	-16.03
Bassanite	-2.27	-2.25
Bischofite	-9.71	-9.72
Bloedite	-11.48	-11.41
Brucite	-15.91	-14.82
Brushite	-4.17	-3.55
C3FH6	-77.20	-70.96
C4FH13	-99.30	-91.96
Ca(HPO4)(s)	-3.91	-3.30
Ca(NO3)2(s)	-26.14	-25.13
Ca(s)	-125.06	-123.83
Ca(SO3)(s)	-30.70	-30.53
Ca2Cl2(OH)2:H2O(s)	-31.55	-30.47
Ca2Fe2O5(s)	-62.33	-57.17
Ca3(PO4)2(alfa)	-16.81	-14.49
Ca3B2O6(s)	-67.74	-64.47
Ca4Cl2(OH)6:13H2O(s)	-72.85	-69.60
Ca4H(PO4)3:2.5H2O(s)	-21.57	-18.64
Ca5H2[InsP6]:16H2O(s)	-28.29	-26.42
Ca5K2[InsP6]:xH2O(s)	-10.11	-6.74
Ca5Na2[InsP6](s)	-12.26	-9.27
Ca6[InsP6](s)	-27.45	-24.49
CaB2O4(s)	-25.94	-24.85
CaB4O7(s)	-33.29	-32.20
CaCl2:2H2O(cr)	-13.97	-13.98
CaCl2:4H2O(cr)	-11.27	-11.28
CaCl2:H2O(s)	-13.89	-13.90
CaFe2O4(s)	-27.05	-22.98
CaI2(s)	-39.08	-39.09
CaMoO4(s)	-5.43	-4.37
CaO(cr)	-32.41	-31.32
Carnallite	-12.50	-12.31
Chloroapatite	-17.87	-14.40
Cornetite	-26.58	-23.79
Cu(cr)	-18.58	-17.34
Cu(OH)1.5(SO4)0.25	-8.51	-7.69
Cu(OH)2(s)	-12.34	-11.25
Cu-hydroxypyromorphite	-33.98	-29.96
Cu3(PO4)2(s)	-19.19	-16.88
CuO(s)	-11.53	-10.45
CuSO4:5H2O(s)	-7.11	-7.09
Epsonite	-3.57	-3.55
Ettringite-Fe	-77.34	-71.04
Fe(OH)2(cr)	-16.60	-15.03
Fe(PO4)(cr)	-1.17	-0.15
Fe(s)	-47.13	-45.42
Fe5(OH)(PO4)3(s)	371.38	377.78

Table B.7 (continued).

Simulation	1	2
Description	Add La to pH 2.5 sample	Add La to pH 3.0 sample
FeMoO4(s)	-9.43	-7.89
FeO(s)	-17.22	-15.66
Ferrihydrite(am)	-5.49	-4.00
Ferryhydrite	-4.14	-2.65
FeS(am)	-83.00	-81.92
Glaserite	-19.11	-17.79
Glauberite	-16.50	-16.43
Goethite	-3.52	-2.03
Gypsum	-1.54	-1.52
H2MoO4(s)	-0.89	-0.92
Halite	-5.63	-5.62
Hausmannite	-39.63	-36.50
Hematite	-5.24	-2.25
Hexahydrite	-3.86	-3.84
Hydrophilite	-17.89	-17.91
Hydroxyapatite	-23.77	-19.75
K(cr)	-63.57	-62.75
K(NO3)(s)	-10.05	-9.35
K(OH)(s)	-24.20	-23.45
K2O(s)	-84.58	-83.08
Kainite	-8.30	-8.08
KH2PO4(cr)	-3.58	-3.31
KI(s)	-10.06	-9.86
Lawrencite	-19.43	-18.96
Leonhardtite	-4.66	-4.64
Leonite	-7.65	-7.21
Lepidocrocite	-3.89	-2.40
Libenthenite	-15.54	-13.84
Ln(cr)	-139.77	-137.93
Ln(NO3)3:6H2O(s)	-29.61	-28.11
Ln(OH)3(am)	-13.73	-12.12
Ln(OH)3(cr)	-11.98	-10.36
Ln(PO4):xH2O(s)	4.30	5.44
Ln2(SO4)3:8H2O(s)	-3.37	-3.35
Ln2O3(cubic)	-45.87	-42.64
Ln2O3(monoclinic)	-46.98	-43.75
Ln3O4(s)	-97.20	-92.28
LnCl(OH)2(s)	-8.64	-7.57
LnCl2(s)	-28.18	-27.59
LnCl3(s)	-26.49	-26.52
LnCl3:6H2O(s)	-11.59	-11.62
LnK(SO4)2.H2O(s)	-3.95	-3.73
LnNa(SO4)2.H2O(s)	-3.99	-3.95
LnO(s)	-55.53	-53.84
LnOCl(s)	-15.78	-14.71
LnPO4:H2O(cr)	5.90	7.04
LnSO4(s)	-14.63	-14.00
Mackinawite	-82.35	-81.27
Maghemite(disord)	-9.65	-6.66
Maghemite(ord)	-9.86	-6.87
Magnetite	-20.49	-15.94
Manganite	-13.61	-12.59
Melanterite	-8.29	-7.80
Mercallite	-5.21	-5.53
Mg(cr)	-107.10	-105.86
Mg(HPO4):3H2O(s)	-4.29	-3.68
Mg(NO3)2(s)	-35.08	-34.07
Mg(NO3)2:6H2O(s)	-22.17	-21.16
Mg(SO4)(s)	-14.91	-14.89

Table B.7 (continued).

Simulation	1	2
Description	Add La to pH 2.5 sample	Add La to pH 3.0 sample
Mg(SO4):H2O(s)	-5.51	-5.49
Mg-oxychlorur	-26.81	-25.18
Mg3(PO4)2(cr)	-20.67	-18.35
Mg3(PO4)2:22H2O(s)	-20.26	-17.93
Mg3(PO4)2:8H2O(s)	-18.13	-15.81
Mg5H2[InsP6]:22H2O(s)	-31.34	-29.45
MgCl2(s)	-27.72	-27.73
MgCl2:2H2O(s)	-18.12	-18.13
MgCl2:4H2O(s)	-12.66	-12.67
MgCl2:H2O(s)	-21.44	-21.45
MgI2(s)	-50.91	-50.92
MgMoO4(s)	-12.22	-11.15
Mirabilite	-6.91	-6.86
Mn(HPO4)(s)	-0.32	0.30
Mn(SO4)(s)	-5.97	-5.95
Mn3(PO4)2(s)	-29.08	-26.75
Mn3(PO4)2:3H2O(s)	-16.09	-13.76
Mn5H2[InsP6]:16H2O(s)	-40.27	-38.37
MnCl2:2H2O(s)	-12.38	-12.39
MnCl2:4H2O(s)	-11.11	-11.12
MnCl2:H2O(s)	-13.93	-13.94
MnO(s)	-19.55	-18.45
MnO2(s)	-17.02	-16.08
Mo(s)	-76.57	-76.15
Mo3O8(s)	-5.68	-5.61
Monosulfate-Fe	-76.92	-70.65
MoO2(s)	-11.30	-11.18
MoO3(s)	-2.12	-2.15
MoS2(s)	-135.43	-136.26
MoS3(s)	-192.31	-193.77
Na(cr)	-61.01	-60.38
Na(NO3)(s)	-12.32	-11.80
Na2B4O7(cr)	-42.90	-41.78
Na2B4O7:10H2O(s)	-33.99	-32.87
Na2HPO4(cr)	-15.10	-14.46
Na2O(cr)	-69.86	-68.74
Na3PO4(cr)	-30.27	-29.06
NaBO2(s)	-18.81	-18.25
NaH2PO4(cr)	-7.40	-7.32
P(cr)	-106.58	-106.68
Pentahydrite	-4.24	-4.22
Periclase	-20.50	-19.41
Picromerite	-7.25	-6.81
Polyhalite	-10.21	-9.73
Portlandite	-22.33	-21.24
Pseudomalachite	-42.32	-37.82
Pyrite	-124.98	-124.52
Pyrochroite	-16.95	-15.86
Pyrrhotite	-76.33	-75.46
S(cr)	-52.86	-53.49
Sacchite	-17.17	-17.17
Struvite	-7.70	-6.54
Sylvite	-3.79	-3.59
Syngenite	-4.90	-4.46
Tachyhydrite	-33.71	-33.74
Tagilite	-15.64	-13.94
Thernardite	-8.00	-7.95
Troilite	-80.64	-79.55
Vivianite	-22.61	-18.86

Table B.7 (continued).

Simulation	1	2
Description	Add La to pH 2.5 sample	Add La to pH 3.0 sample
ZnB2O4(s)	-20.20	-19.10

Appendix B references

1. Gharieb MM, Gadd GM. Influence of nitrogen source on the solubilization of natural gypsum (CaSO4.2H2O) and the formation of calcium oxalate by different oxalic and citric acid-producing fungi. Mycological Research. 1999 Apr;103(04):473–481.

2. Mulligan C, Kamali M, Gibbs BF. Bioleaching of heavy metals from a low-grade mining ore using Aspergillus niger. Journal of Hazardous Materials. 2004 Jul;110(1–3):77–84.

3. Jang JY, Choi YH, Shin TS, Kim TH, Shin K-S, Park HW, et al. Biological Control of Meloidogyne incognita by Aspergillus niger F22 Producing Oxalic Acid. Han K-H, editor. PLOS ONE. 2016 Jun 3;11(6):e0156230.

4. Liaud N, Giniés C, Navarro D, Fabre N, Crapart S, Gimbert IH-, et al. Exploring fungal biodiversity: organic acid production by 66 strains of filamentous fungi. Fungal Biology and Biotechnology [Internet]. 2014 Dec [cited 2019 Nov 7];1(1). Available from: http://fungalbiolbiotech.biomedcentral.com/articles/10.1186/s40694-014-0001-z

5. Falck WE, Read D, Thomas JB. Chemval 2: thermodynamic database: final report. Luxembourg: Office for Official Publ. of the European Communities; 1996. 164 p. (EUR).

6. Nriagu JO, Dell CI. Diagenetic formation of iron phosphates in recent lake sediments. American Mineralogist. 1974 Oct 1;59(9–10):934–46.

Appendix C
Additional results from the synthetic mine tailings experiments

Table C.1 Summary of additional results from the synthetic mine tailings experiments. Concentrations are given as CFU/g on a dry mass basis. T_0 describes samples taken immediately after mixing in the inoculum, T_1 is the final time point as indicated in the table. Data represent either single measurements or the mean of duplicate samples ± the difference between the mean and the measured values. Calculated T_0 concentrations for viable cells were calculated from the measured viable cell concentration in the inoculum.

Organism	Inoculum	Electrical Conductivity $_{(H2O)}$ (µS/cm)			$E_{h\,(H2O)}$ (mV)			Viable cell concentration (CFU/g)			
Batch 1, initial pH 8.4, T_1 = 47 days		T_0	T_1		T_0	T_1		Calculated T_0	Measured T_0	Measured T_1	
A. niger	Cell suspension	n.d.	2,880	*± 20*	n.d.	390	*± 3*	2.40E+04	n.d.	1.31E+07	*± 3.66E+06*
B. adeninivorans	Cell suspension	2,690	2,885	*± 305*	489	366	*± 5*	5.51E+07	1.05E+09	2.02E+07	*± 8.71E+06*
Unknown mould and bacteria (contamination)	None	3,000	3,105	*± 945*	460	369	*± 11*	0.00E+00	n.d.	5.41E+07	*± 4.39E+07*
Batch 2, initial pH 7.6, T_1 = 52 days											
A. niger	Cell suspension	8,390	7,180	n.d.	471	454	n.d.	3.20E+04	1.67E+05	4.13E+04	n.d.
A. niger	Spore suspension	6,020	7,620	n.d.	482	432	n.d.	4.22E+03	< 5.42E+02	1.06E+05	n.d.
B. adeninivorans	Cell suspension	5,730	3,920	n.d.	480	445	n.d.	5.80E+07	5.07E+07	3.81E+07	n.d.
Unknown bacteria (contamination)	None	4,660	4,180	n.d.	481	449	n.d.	0.00E+00	9.40E+04	3.42E+07	n.d.
Batch 3, initial pH 6.9, T_1 = 34 days											
A. niger	Cell suspension	1,485	1,113	*± 81*	421	484	*± 3*	3.11E+04	n.d.	3.98E+07	*± 3.77E+07*
Unknown bacteria (contamination)	None	1,209	252	*± 100*	412	542	*± 15*	0.00E+00	n.d.	> 1.00E+05	*± 0.00E+00*
Batch 4, initial pH 5.8, T_1 = 34 days											
A. niger	Cell suspension	2,090	2715	*± 345*	442	442	*± 6*	3.02E+04	1.38E+05	7.68E+06	*± 7.06E+06*
B. adeninivorans	Cell suspension	2,300	2760	*± 20*	434	414	*± 15*	5.23E+07	9.08E+07	4.03E+06	*± 8.86E+05*
Batch 5, initial pH 4.5, T_1 = 52 days											
A. niger	Cell suspension	5,880	5,680	n.d.	610	398	n.d.	3.64E+04	5.86E+04	1.33E+05	n.d.
B. adeninivorans	Cell suspension	6,050	7,390	n.d.	537	392	n.d.	7.16E+07	5.85E+07	2.17E+05	n.d.
Batch 6, initial pH 3.9, T_1 = 52 days											
A. niger	Cell suspension	8,920	4,030	n.d.	477	458	n.d.	3.24E+04	1.56E+05	3.64E+06	n.d.
A. niger	Spore suspension	6,450	6,900	n.d.	512	386	n.d.	4.20E+03	< 4.75E+03	6.60E+04	n.d.
B. adeninivorans	Cell suspension	5,080	5,450	n.d.	545	443	n.d.	5.83E+07	3.25E+07	1.17E+08	n.d.
None	None	5,430	5,120	n.d.	549	445	n.d.	0.00E+00	< 4.94E+02	< 6.50E+03	n.d.

Appendix D
Phytate degradation in simple solid matrices

D.1 Phytate degradation in the presence of kaolinite

As the sorption tests indicated both phytate and phytase interact strongly with kaolinite it was decided to perform growth and phytate degradation tests with *A. niger* and *B. adeninivorans* to confirm that sorption by kaolinite was the likely explanation for no observable phytate breakdown in the synthetic mine tailings tests.

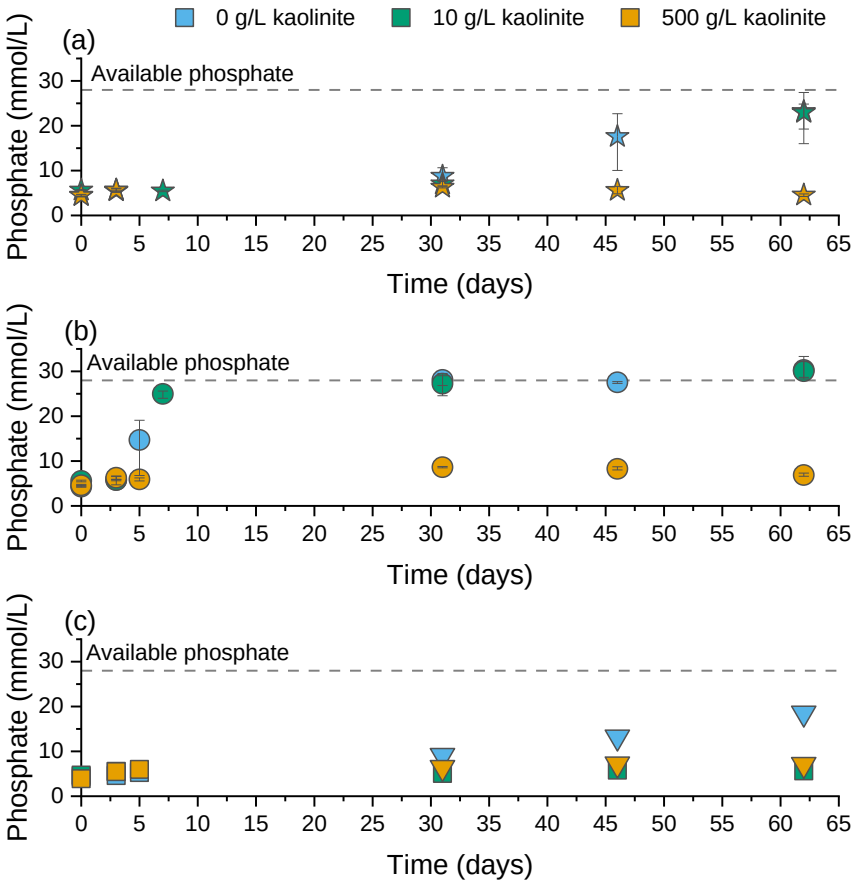

Figure D.1 Phosphate concentrations over time for (a) A. niger (★), *(b)* B. adeninivorans (●), *and (c) non-inoculated controls (■ or ▼ for experiments where contamination was visibly apparent) with different levels of kaolinite. Data points in (a) and (b) are the mean of triplicate samples, error bars are the difference between the mean and the upper or lower measured values. Data points in (c) represent single measurements.*

Experiments were performed at kaolinite concentrations of 0, 10, and 500 g/L in YN6B nutrient media under static conditions, in the dark, at ~ 22 °C at an initial pH of ~ 5.5. The final

pH of the experiments was between 2.0 and 2.5 for *A. niger* and between 2.9 and 3.5 for *B. adeninivorans* regardless of the amount of solid present. The controls at 0 g/L and 10 g/L kaolinite ended at a pH of ~ 5.3, while the control at 500 g/L kaolinite ended at a pH of ~ 4.6. These experiments indicated that, at the lower kaolinite concentration, phytate degradation was equivalent to solid-free controls (figure D.1). However, at the higher kaolinite concentration, negligible amounts of phosphate release could be detected. While it cannot be ruled out that liberated phosphate may have sorbed onto the kaolinite and gone undetected, the fact that the background level of inorganic phosphate remained constant throughout the experiment and was similar to the initial value in the solid-free experiments indicates that this was likely not the case.

Further work with this system could either use kaolinite-only systems or kaolinite mixed with an inert solid (e.g. quartz sand) to determine what level of kaolinite is required to start inhibiting the phytate degradation process. This system could then be used for further experiments to optimise experimental procedures to mitigate this limitation.

D.2 Phytate degradation in the presence of sand

A. niger or *B. adeninivorans* were inoculated into a nutrient media (YN6B, 20 g/L galactose as carbon source) mixed with sand to investigate phytate degradation and phosphate mineral precipitation in a simple solid system. Experiments were performed without and with 0.5 mmol/L lanthanum.

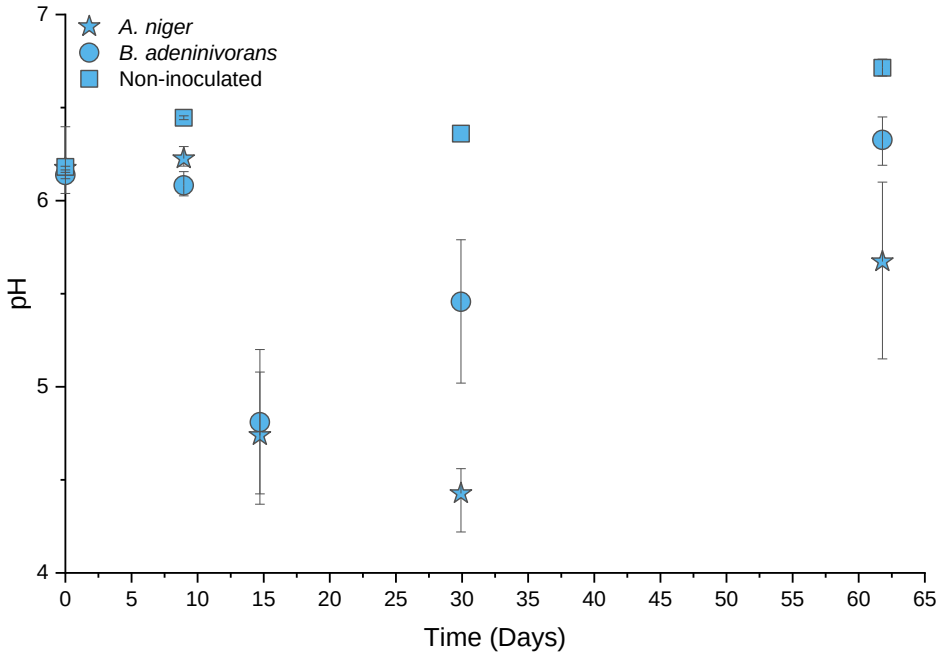

Figure D.2 Measured pH of aqueous extracts of solid samples taken over the duration of the experiment. Experiments were performed in triplicate with single samples taken from 0–30 days and five samples from each experiment at the final time point. Data points are the mean of every measured value, error bars represent the difference between the upper and lower measured values. Due to visible contamination in one of the sterile/non-inoculated controls, the data from this experiment are not presented.

The pH of aqueous extracts of the sand and nutrient media mixture was slightly higher (~ 6) than the pH of the pure nutrient media (~ 5.5). As with batch solution experiments (see chapter 2), there was a decrease in pH over the first two weeks of the experiments in the *A. niger* and *B. adeninivorans* cultures (figure D.2). However, unlike in the solid-free systems, the pH then began to increase again after 30 days. As a microbially induced pH decrease was one of the main factors identified in chapter 2 limiting the options for calcium phosphate precipitation, the apparent pH buffering of the solid phases present may be an advantage.

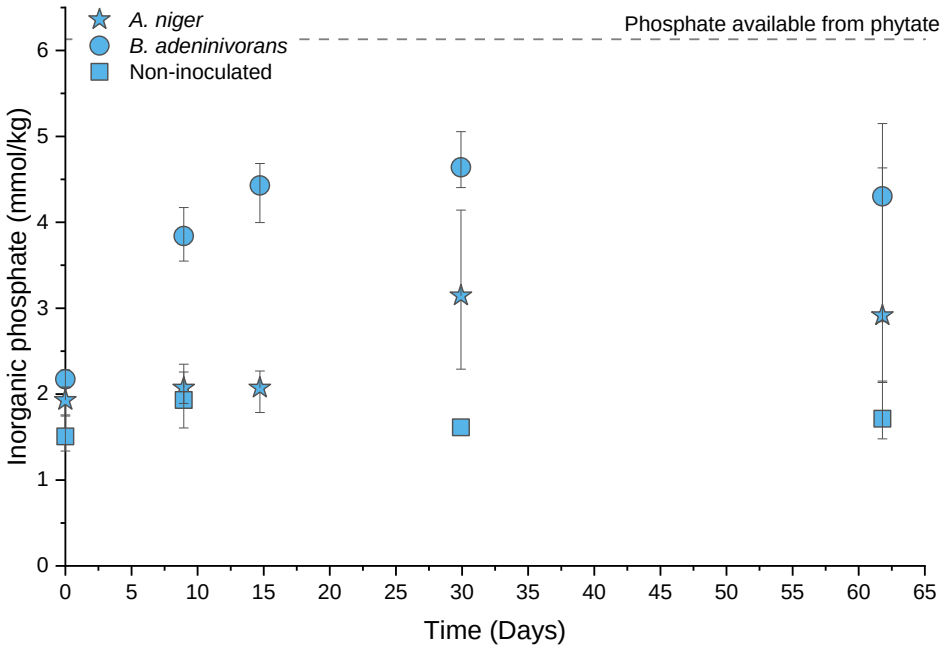

Figure D.3 Water soluble concentrations (mmol/kg dry mass) of inorganic phosphate over time. Experiments were performed in triplicate with single samples taken from 0–30 days and five samples from each experiment at the final time point. Data points are the mean of every measured value, error bars represent the difference between the upper and lower measured values. Due to visible contamination in one of the sterile/non-inoculated controls, the data from this experiment are not presented.

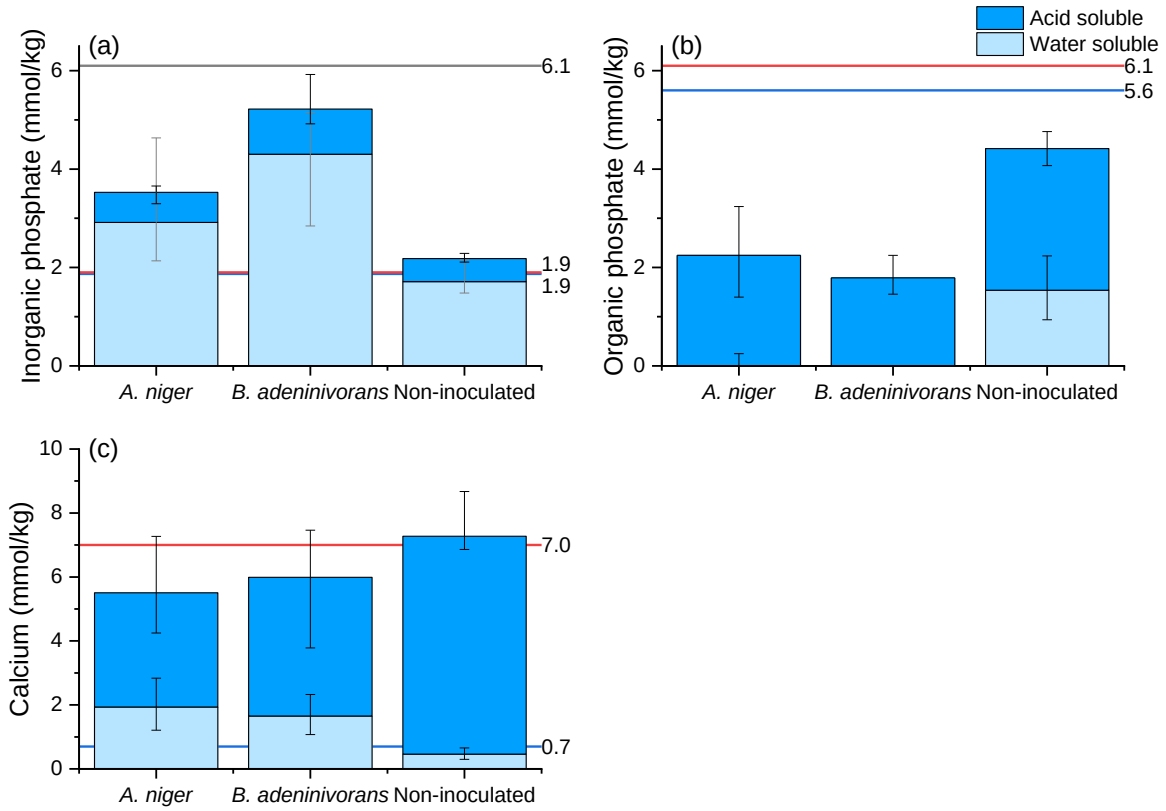

Figure D.4 Concentrations (mmol/kg dry mass) of water soluble and 1.7 mol/L nitric acid soluble fractions of (a) measured inorganic phosphate, (b) calculated organic phosphate, (c) measured calcium at the final time point of the sand growth and phytate degradation experiments. Triplicate experiments (or duplicate for the non-inoculated controls) were each sampled five times, three of which were sequentially extracted with npH_2O and 1.7 mol/L nitric acid while the remaining two were only extracted with npH_2O. Columns represent the mean of all samples, error bars are the difference between the mean and the upper or lower measured value. The reference lines represent the following: blue = mean measured water soluble values at zero time point; red = calculated total concentrations (from background measurements of culture media and sand); grey = total phosphate available from phytate.

Growth and phytate degradation tests in the sand system indicated successful phytate degradation by both *A. niger* and *B. adeninivorans* (figure D.3, figure D.4a). *B. adeninivorans* produced more phosphate than *A. niger*, which is likely a consequence of the carbon source used (galactose, see chapter 2 for details). Phytate degradation in the controls appeared negligible. A fraction of the inorganic phosphate appeared to be insoluble in each condition but due to overlapping error bars it is hard to be conclusive about how much inorganic phosphate precipitated. Calculated organic phosphate concentrations showed a corresponding decrease in organic phosphate content in the *A. niger* and *B. adeninivorans*

cultures (figure D.4b). Water soluble organic phosphate concentrations in the *A. niger* and *B. adeninivorans* cultures were calculated to be zero or negative numbers suggesting that any residual organic phosphate was not water soluble. Measurements of calcium indicated that the amount of soluble calcium increased in both *A. niger* and *B. adeninivorans* cultures compared to the zero time point measurements but remained unchanged in the non-inoculated control (figure D.4c).

Appendix E
Factors influencing the phytase-mediated precipitation of lanthanum phosphate

The results in chapter 4 of this thesis indicate that using phytase enzymes to hydrolyse phytic acid and release inorganic phosphate to solution is a promising method of producing lanthanum phosphates. However, the morphology of the precipitate remained uncertain, and this may have implications for contaminant uptake and long-term stability.

Work in this section investigated repeatability of the experiments, leachability of the precipitated materials, and the influence of solution chemistry on phytate hydrolysis and lanthanum precipitation.

E.1 Experimental programme and methods

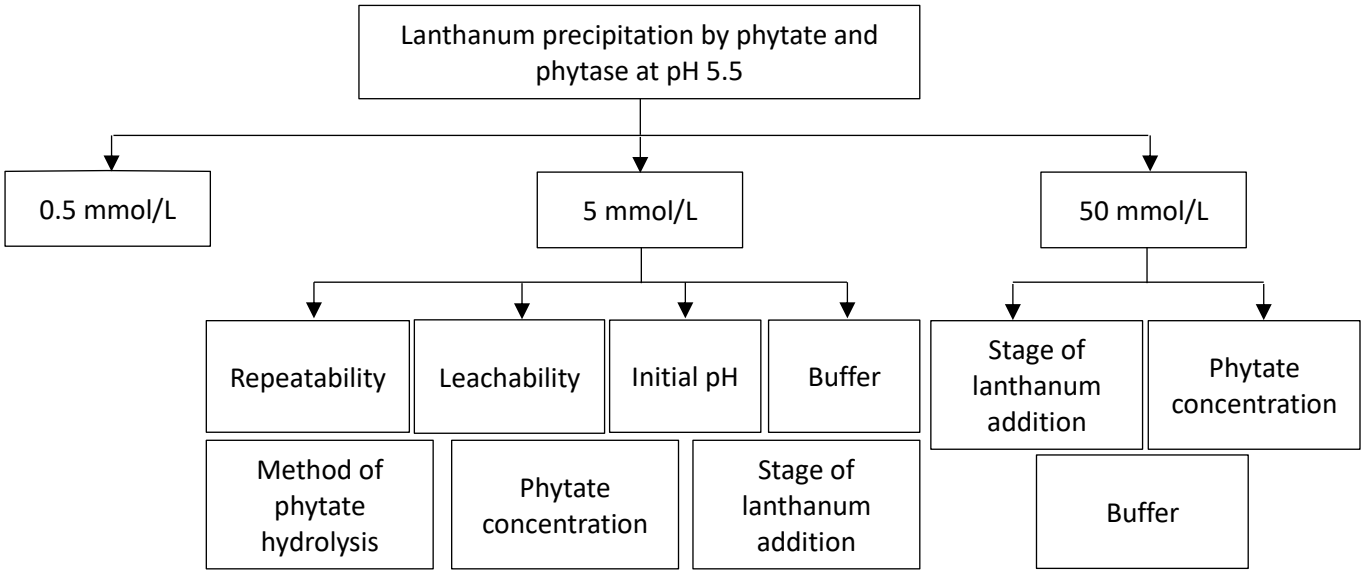

Figure E.1 Flow chart of experiments undertaken in appendix E.

Figure E.1 summarises the experiments undertaken in this appendix. Methods were as described in chapter 4, with variations to the procedure as appropriate to attain the desired conditions.

In this section, the term "condition" describes the combination of lanthanum concentration, initial pH, and pH buffer used while "treatment" describes the combination of phytate concentration, method of phytate hydrolysis used, time, and stage of lanthanum addition.

Conditions are described by numbers as listed in table E.1, while treatments are described by letters listed in table E.2.

Table E.1 List of conditions investigated in appendix E (refer to table E.2 for explanation of the treatments investigated)

Condition Code	Lanthanum concentration (mmol/L)	Initial pH	Buffer (mol/L)	Treatments investigated
1	0.5	5.5	MES (0.2 mol/L)	B, F
2	5	2.5	Glycine (0.2 mol/L)	B, F
3	5	5.5	None	B, F
4	5	5.5	MES (0.2 mol/L)	A, B, C, E, F, G, H, J, K, L, M
5	5	7.0	TES (0.2 mol/L)	B, F
6	50	5.5	MES (0.2 mol/L)	B, D, F, G, I
7	50	5.5	Citrate (0.2 mol/L)	B, F

Table E.2 List of treatments investigated in this appendix E.

Treatment Code	Phytate concentration (mmol/L)	Method of phytate hydrolysis	Experiment time	Stage of lanthanum addition
A	0.63	None	24 hours	Start
B	3.8	None	24 hours	Start
C	3.8	None	7 days	Start
D	38	None	24 hours	Start
E	0.63	*A. niger* phytase	24 hours	Start
F	3.8	*A. niger* phytase	24 hours	Start
G	3.8	*A. niger* phytase	24 hours	After phytase reaction
H	3.8	*A. niger* phytase	7 days	Start
I	38	*A. niger* phytase	24 hours	Start
J	3.8	*A. niger* cells	7 days	Start
K	3.8	*B. adeninivorans* cells (OD_{600} = 0.2)	7 days	Start
L	3.8	*B. adeninivorans* cells (OD_{600} = 1.5)	30 days	Start
M	3.8	Autoclave	3 cycles	Start

Phytate-only and phytate + phytase treatments were performed as described in chapter 4 under non-sterile conditions. For the treatment with *A. niger* cells, cultures of *A. niger* were grown in YN9B media as per chapter 2. After 7 days (based upon the time course shown in figure 2.4, phytase production should have been high at this point in time) 0.5 g of *A. niger*

biomass was weighed out, washed twice (by centrifugation at 10,000 rcf) in sterile 8.5 g NaCl, and the biomass then aseptically transferred into sterile experimental media.

For *B. adeninivorans*, cultures were grown in YN6B media as per chapter 2 and cells harvested after 2 days (with an OD_{600} of ~ 0.2) or 3 days (with an OD_{600} of ~ 1.5). The cells were centrifuged (6,000 rcf), washed twice (by centrifugation at 10,000 rcf) in sterile 8.5 g NaCl, resuspended in sterile npH_2O, and 0.5 mL of this suspension pipetted into sterile experimental media.

For the autoclave treatment, experimental media was prepared as per the phytate-only treatments in chapter 4 and then autoclaved (121 °C, 15 psi, 20 minutes) three times.

E.2 Repeatability

When repeating the experiments performed with 5 mmol/L lanthanum, 3.8 mmol/L phytate, at pH 5.5 (0.2 mol/L MES) to produce more solid material for analysis, it was noticed that results varied slightly across different batches. Therefore, comparisons were made across the four batches of experiments performed to try and understand the cause of the variability.

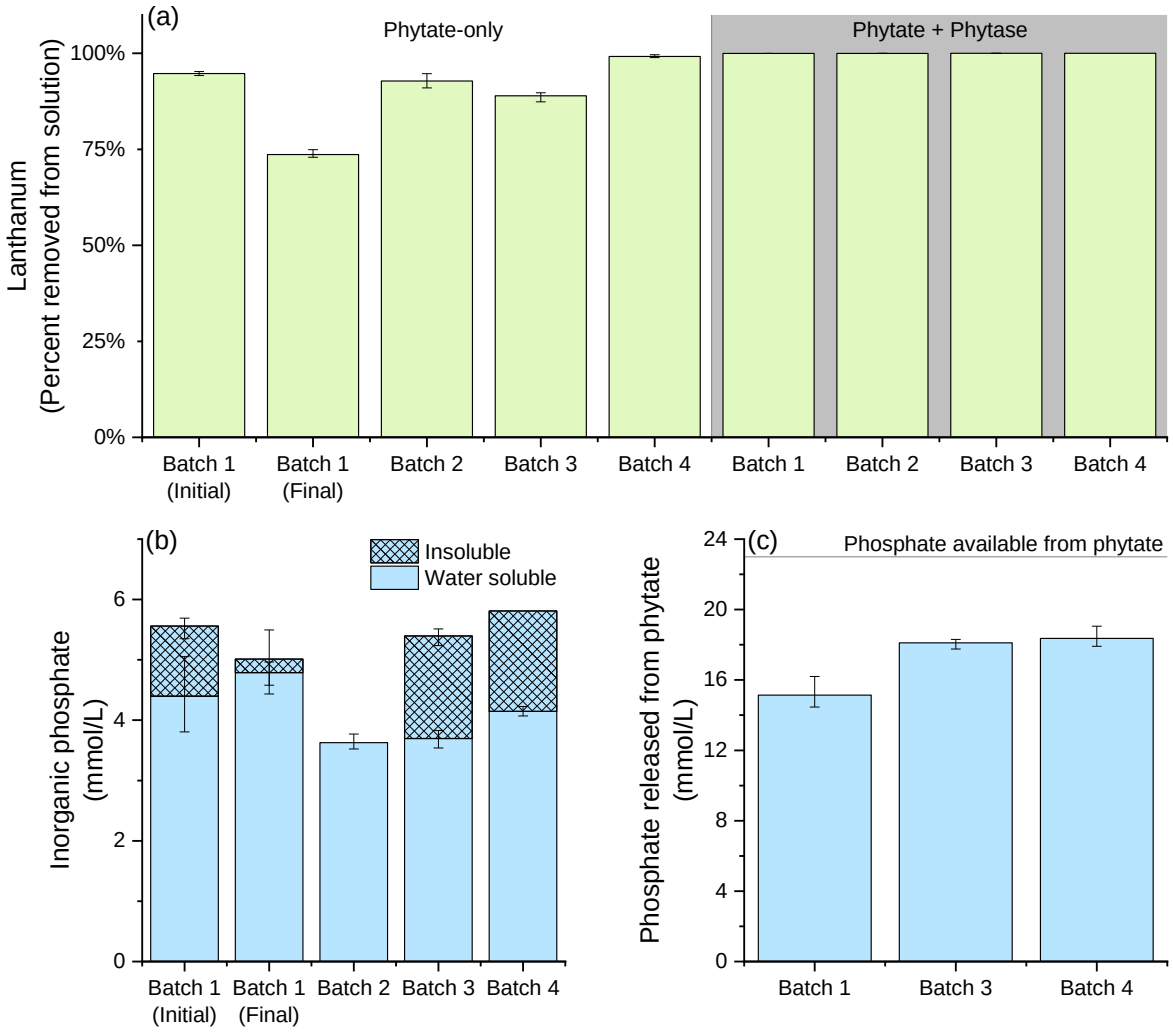

Figure E.2 Comparisons of repeat experiments at 5 mmol/L lanthanum, 3.8 mmol/L phytate, at pH 5.5 (0.2 mol/L MES) for one day, showing (a) lanthanum removal, (b) background inorganic phosphate concentrations associated with phytate, and (c) phosphate released from phytate in the experiments where the A. niger *phytase was added. Columns represent the mean value of triplicate samples, error bars are the difference between the upper and lower measured values. 'Total' concentrations were not measured for the batch 2 experiments, so insoluble background inorganic phosphate and total release of phosphate from phytate could not be calculated for this batch.*

Repeatability was investigated from experiments 4B (phytate-only) and 4F (phytate + phytase). The variability in experimental results were most notable for the phytate-only treatment (figure E.2a, figure E.2b). Lanthanum removal ranged from 73% to 99% depending on the batch of experiments (figure E.2a). It should be noted that the 73% removal figure is likely a legacy of the sampling technique used. For batch 1 experiments, water soluble concentrations were measured at the final time point by centrifuging samples (12,500 rcf), pipetting out an aliquot of the supernatant and acidifying this aliquot – therefore, any solids

remaining in suspension would have been dissolved. In contrast, batches 2 to 4 involved centrifuging samples followed by filtering the supernatant before acidifying it – therefore, any suspended solids would have been filtered out before acidification. Also shown are initial, zero time point samples for the phytate-only treatment in batch 1. This shows a much higher lanthanum removal percentage (~ 95%) for batch 1, more consistent with the other batches. Although the initial time point sample used the same strategy as the final time point sample for batch 1, a smaller sample (1 mL compared to the whole ~ 25 mL experiment) was used, which likely led to a higher proportion of the solid becoming 'pelleted' due to the different shapes of the centrifuge tubes used.

Even accounting for the sampling issues, lanthanum removal in the phytate-only treatment still varied from 88% to 99% depending on the batch. If the initial time point is taken as representative of the batch 1 samples, then lanthanum removal efficiency decreased in the order batch 4 > batch 1 > batch 2 > batch 3. Two possible explanations for this variation are subtle variations in pH or background inorganic phosphate in the phytate stock. Initial pH values ranged from ~ 5.46 (batch 4) to ~ 5.58 (batch 2) and final pH values ranged from 5.44 (batch 4) to ~ 5.57 (batch 2). Lanthanum phytate solubility has been shown to increase with increasing pH (figure E.4) but an almost 10% difference in solubility based upon a pH shift of less than 0.15 units seems extreme. Background inorganic phosphate concentrations may be a more plausible explanation. The batch 4 samples had a background inorganic phosphate content of about 5.8 mmol/L, compared to 5.6 mmol/L in batch 1, and 5.4 mmol/L in batch 3 (total inorganic phosphate was not measured for batch 2, but as the water soluble concentrations were the same as batch 3, it can be assumed that the total concentrations were similar). Therefore, the trend of inorganic phosphate concentrations decreasing in the order batch 4 > batch 1 > batch 3 does match with the lanthanum solubility trends. As one of the key advantages of using phytate as a phosphate source is its low cost as a waste product, natural sources of phytate are likely to contain variable levels of inorganic phosphate. If these varying levels of impurities can be responsible for variations in metal solubility on the order of 10% then this subject requires further study to understand its implications for phytate-based remediation strategies.

Variations between batches of the phytate + phytase treatment were much less pronounced than the phytate-only treatment but did still exist. Most notably, the release of inorganic

phosphate was inhibited in batch 1 (~ 15 mmol/L) compared to batches 3 and 4 (~ 18 mmol/L) (figure E.2c). The only difference between the preparation of phytase between batch 1 and batches 2, 3, and 4 (total concentrations in batch 2 were not measured, so total phosphate release cannot be calculated, but as water soluble inorganic phosphate concentrations were similar between the batches, batch 2 and 3 are considered equivalent) is that insoluble matter in the batch 1 preparation was removed by centrifugation, while in batches 2, 3, and 4, insoluble matter was removed by centrifugation and filtration. Therefore, some insoluble matter was carried over into the experimental media in batch 1, and if this insoluble matter carried inhibitory substances, that may explain inhibited phytase activity.

In percentage terms, lanthanum removal in all phytate + phytase treatment batches was greater than 99.98% (figure E.2a). However, in absolute terms, there were still differences in water soluble lanthanum concentrations between the different batches. Batch 1 had the highest soluble lanthanum concentrations at around 0.9 µmol/L, which is likely due to a combination of the sampling strategy (see discussion of the phytate-only experiments above) and lower inorganic phosphate concentrations. For the remaining three batches, all samples gave values very close to the ICP-OES detection limit so it is hard to be certain to what extent the differences are significant. In batch 2, two replicates were below the detection limit (< 0.11 µmol/L for the dilution factors used) while the third was measured at around 0.8 µmol/L. In batch 3, all replicates were above the detection limit, and ranged from 0.04 to 0.3 µmol/L. In batch 4, all replicates were below the detection limit (< 0.02 µmol/L for the dilution factor used). While these differences are low and potentially subject to analytical variability due to being close to the equipment's detection limit, variation by almost two orders of magnitude could be significant when considering trace metal immobilisation.

Despite the small differences in solution chemistry, solid phase analysis by FTIR and XRD indicated negligible differences between precipitates produced in different batches (data not shown).

E.3 Material leachability

To investigate leachability, materials produced with 5 mmol/L lanthanum, 3.8 mmol/L phytate, at pH 5.5 (0.2 mol/L MES) were subjected to eight cycles (each cycle = 24 hours) of leaching in an artificial groundwater, prepared as per (1). Both lanthanum phytate and the

phytase-mediated lanthanum phosphate were used and the release of lanthanum, inorganic phosphate, and organic phosphate measured.

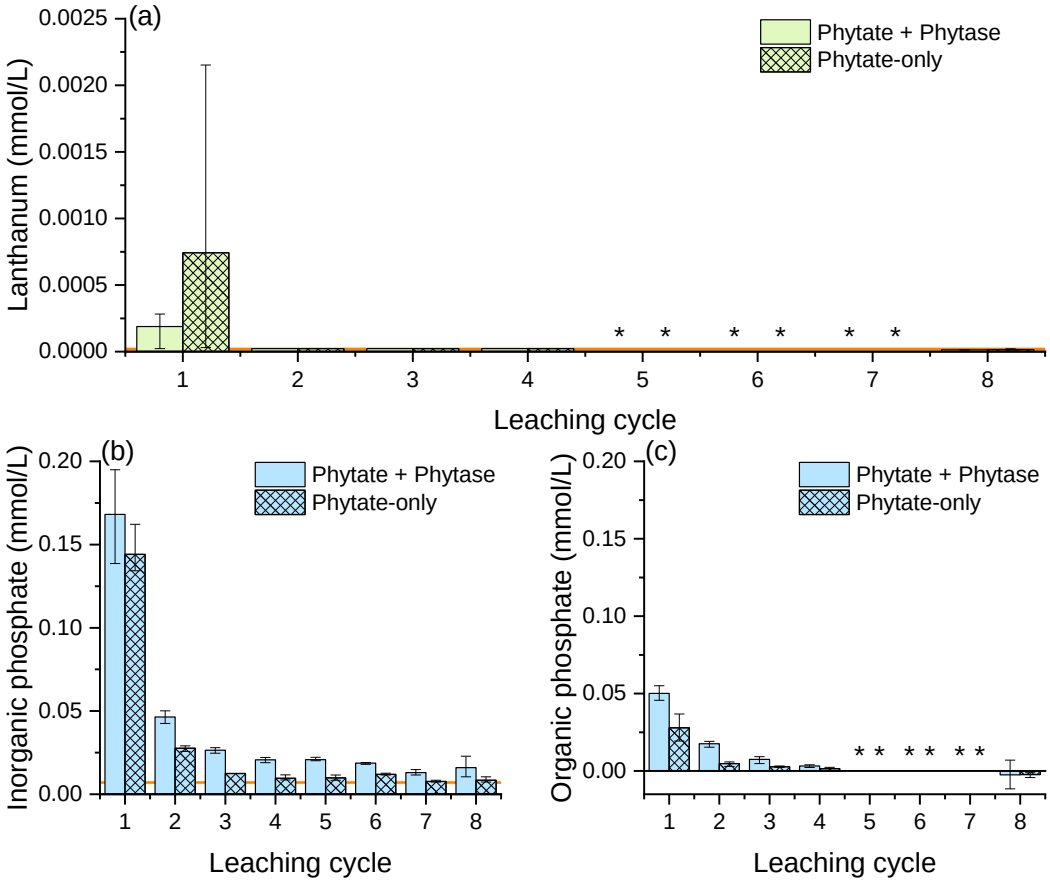

*Figure E.3 Results from the leaching experiments, showing (a) lanthanum, (b) inorganic phosphate, and (c) calculated organic phosphate released to solution after each leaching cycle. Samples from leaching cycle 5–7 were not analysed by ICP-OES (indicated by *) and so lanthanum and organic phosphate concentrations are not available for these cycles. Columns represent the mean value of triplicate samples, error bars are the difference between the upper and lower measured values. Orange reference lines represent detection limits.*

Results of the leaching experiments indicate that dissolution of lanthanum and phosphate was low and incongruent (figure E.3). Detectable lanthanum was only present in filtrates from the first leaching cycle (figure E.3a). For the phytase-mediated lanthanum phosphate, two replicates leached around 0.27 µmol/L lanthanum while the third replicate was below the ICP-OES detection limit (< 0.02 µmol/L). For the lanthanum phytate, the amount of lanthanum detected in solution was measured as 0.03, 0.05, and 2.15 µmol/L. For the second, third, fourth, and eighth leaching cycles, soluble lanthanum was ≤ 0.02 µmol/L, and it can be assumed that this would hold true for the fifth, sixth, and seventh leaching cycles. In percentage terms, the amount of lanthanum leached from the solids was at most 0.05%. As

all of these values were close to the ICP-OES detection limit, they may be subject to high degrees of analytical uncertainty, so a more sensitive technique (e.g. ICP-MS) may be required to more robustly establish the actual amount of lanthanum being leached.

The leaching of phosphate was one to three orders of magnitude higher than lanthanum, although in percentage terms was still low (at most 10% for inorganic phosphate or 1% for organic phosphate). Inorganic phosphate (figure E.3b) leaching was higher than organic phosphate (figure E.3c) and the phytase-mediated lanthanum phosphate leached more inorganic and organic phosphate than lanthanum phytate. For lanthanum phytate, inorganic phosphate leaching was negligible after the third cycle while organic phosphate leaching was negligible after the second cycle. For the phytase-mediated lanthanum phosphate, organic phosphate leaching was negligible after the fourth cycle, while inorganic phosphate concentrations were above the colorimetric detection limit after every cycle.

Non-stoichiometric dissolution of lanthanide phosphates has previously been described, with an excess of phosphate leaching from the solid compared to the lanthanide (2). This may be due to the presence of more soluble phosphate impurities or the presence of non-phosphate secondary phases (e.g. oxides, hydroxides, carbonates) (2) or the presence of excess sorbed phosphate species (3).

E.4 Influence of solution chemistry on phytate hydrolysis, lanthanum precipitation, and solid phase morphology

In this appendix, various parameters have been investigated to study their role in the interactions between lanthanum, phytate, and phytase and how these factors influence lanthanum precipitation, the release of phosphate from phytate, and the morphology of the precipitates. Previous research has established that pH, time, and lanthanum:phosphate ratios are all important. In an enzymatically/biologically mediated system, further important factors are the lanthanum:phytate ratio, the amount of phosphate released from phytate, and whether lanthanum is added before or after the release of phosphate from phytate.

E.4.1 Comparison of lanthanum removal

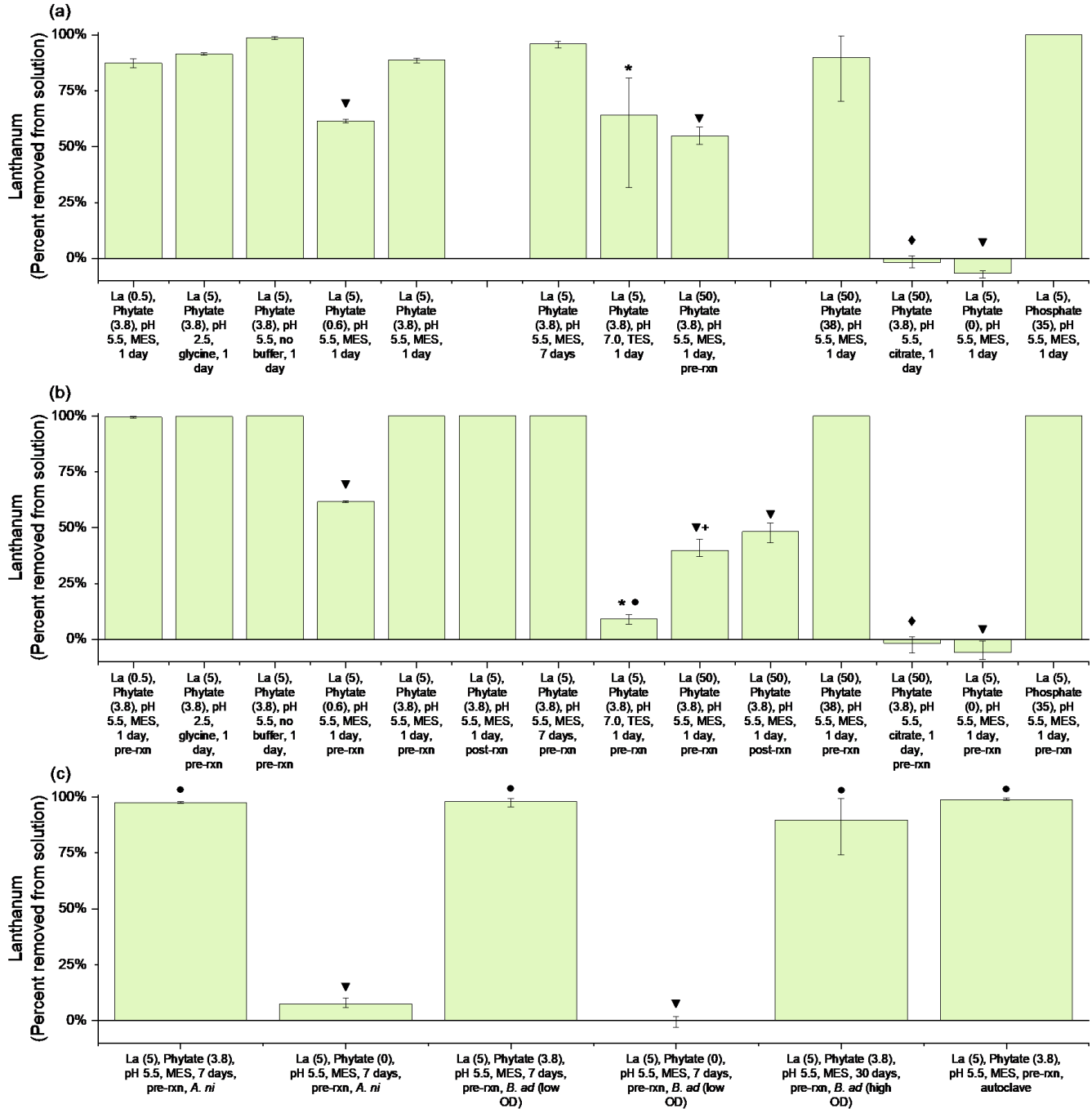

Figure E.4 Percent of lanthanum removed from solution showing (a) phytate-only experiments and inorganic phosphate or no phosphate controls, (b) phytate + A. niger *phytase experiments, plus no phosphate and inorganic phosphate controls mixed with phytase, and (c) experiments where alternative methods of phytate hydrolysis were attempted, plus no phosphate controls. Columns are the mean value of triplicate samples, error bars are the difference between the upper and lower measured values. Symbols above the columns indicate the main factor inhibiting lanthanum precipitation: ● = method of phytate hydrolysis used, * = pH, ▼ = phytate or phosphate concentration, ♦ = citrate, + = methodological issues. 'Pre-rxn' refers to experiments where lanthanum was mixed with phytate before attempting phytate hydrolysis, 'post-rxn' is where lanthanum was added after phytate hydrolysis had been performed.*

Under the 'baseline' conditions investigated (5 mmol/L lanthanum, pH 5.5, 0.2 mol/L MES buffer), the general trend was for phytate to remove 90–99% of lanthanum from solution (figure E.4a), while in the experiments where phytase hydrolysed phytate, upwards of 99.9% of lanthanum precipitated (figure E.4b). Where lower levels of lanthanum precipitation were achieved, this could be attributed to inefficient phytate hydrolysis (●), pH (*), limited phytate or phosphate available (▼), presence of citrate (♦), or methodological issues (+).

Inefficient phytate hydrolysis can be used to explain why the alternate phytate hydrolysis methods (figure E.4c) achieved lanthanum removal percentages that were closer to the phytate-only experiments than the phytate + phytase experiments. Inefficient phytate hydrolysis may also have contributed to the low percentage of lanthanum removal in the phytate + phytase treatment at pH 7 (figure E.4b) but the relative importance of this compared to an increased solubility of lanthanum phosphate at higher pH values is uncertain.

The concentration of phytate or phosphate was important. In the absence of any phytate or phosphate, effectively 100% of lanthanum remained in solution (figure E.4). Experiments with different lanthanum:phytate ratios indicated that at 5 mmol/L lanthanum, 0.6 mmol/L phytate (lanthanum:phytate ratio of 8:1, lanthanum:phosphate ratio of 1.7:1) lanthanum removal was reduced to ~ 60% and at 50 mmol/L lanthanum, 3.8 mmol/L phytate (lanthanum:phytate ratio of 13:1, lanthanum:phosphate ratio of 2.2:1) lanthanum removal was reduced to ~ 50%. This appeared to be true regardless of whether phytate was intact or had been hydrolysed (figure E.4a, figure E.4b). In contrast, the higher levels of lanthanum removal were achieved at a lanthanum:phytate ratio of 1.3:1 (corresponding to a lanthanum:phosphate ratio of 0.2:1). Therefore, the excess of phosphate ligands compared to lanthanum appeared to be required for efficient lanthanum removal.

Citrate led to the complete solubilisation of lanthanum in the phytate-only (figure E.4a) and phytate + phytase treatments (figure E.4b), likely due to the strong complexation of lanthanum by citrate.

The methodological issues have been discussed in more detail in the repeatability section but relate to sampling of the supernatant and therefore including suspended particles in the water-soluble fraction. This is apparent in the data for the phytate + phytase treatment at 50 mmol/L lanthanum, 3.8 mmol/L phytate (figure E.4b), while for phytate-only treatments

(figure E.4a) zero timepoint measurements for the 0.5 mmol/L lanthanum, 3.8 mmol/L phytate and 50 mmol/L lanthanum, 3.8 mmol/L conditions have been used on the assumption they provided better estimates of water soluble lanthanum in the presence of phytate.

E.4.2 Comparison of phosphate release

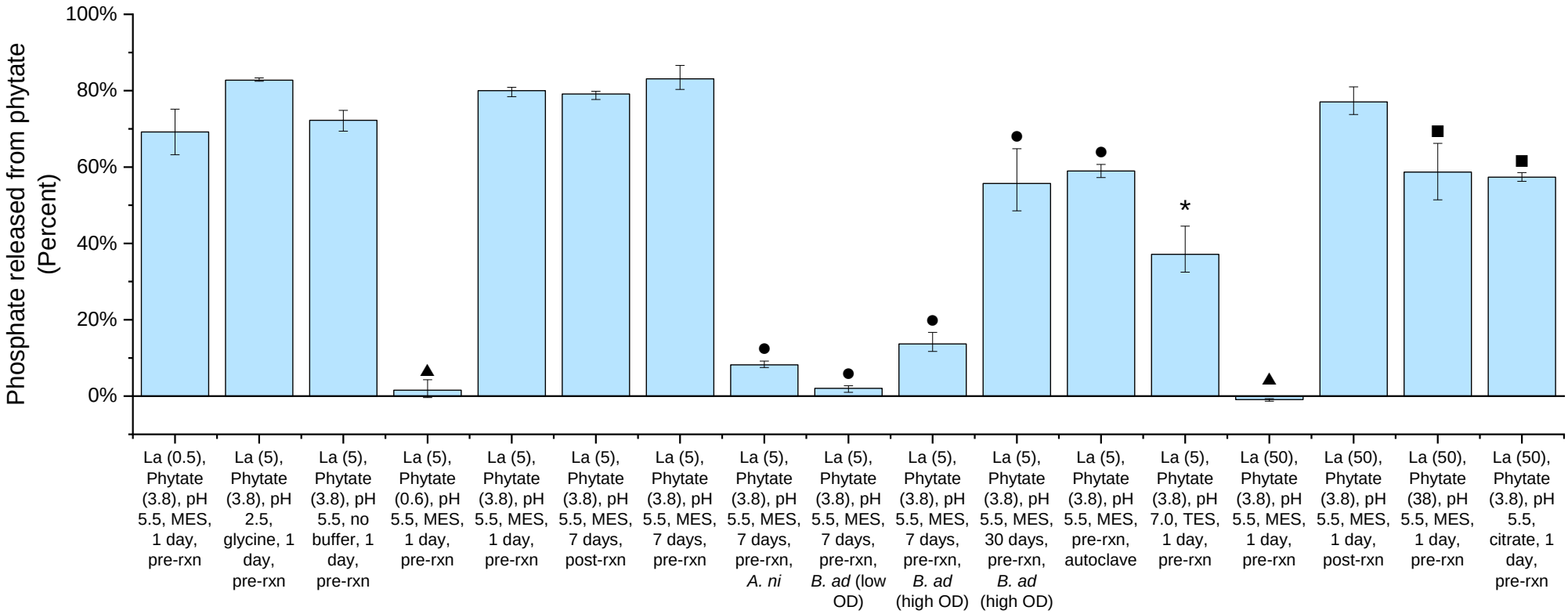

Figure E.5 Percent of phosphate released from phytate under the different conditions and treatments investigated in this work. The purified A. niger *phytase was the method of phytate hydrolysis used except where indicated otherwise (*A. ni = A. niger *cells,* B. ad = B. adeninivorans *cells). Columns represent the mean value of triplicate samples, error bars are the difference between the upper and lower measured values. Symbols above the columns indicate the main factor inhibiting phosphate release: ▲ = La:Phytate ratio, ● = inefficient method of phytate breakdown (either low phytase production by the microorganism tested or inefficient chemical breakdown in the autoclave), * = pH profile of the phytase enzyme, ■ = lanthanum concentration. 'Pre-rxn' refers to experiments where lanthanum was mixed with phytate before attempting phytate hydrolysis, 'post-rxn' is where lanthanum was added after phytate hydrolysis had been performed.*

Figure E.4 compares the amount of phosphate released from phytate under different conditions and treatments tested in this work. Due to varying phytate concentrations used, phosphate release is expressed in percentage terms. The baseline performance of the purified *A. niger* phytase enzyme used was to release 70–80% of available phosphate at pH 2.5 and 5.5. Factors responsible for lower amounts of phosphate release included the lanthanum:phytate ratio, lanthanum concentration, the method of phytate hydrolysis used, pH profile of the enzyme.

The lanthanum:phytate ratio was found to be inhibitory at 5 mmol/L lanthanum, 0.6 mmol/L phytate and 50 mmol/L lanthanum, 3.8 mmol/L phytate with lanthanum:phytate ratios of 8:1 and 13:1 respectively (columns marked ▲). Strictly speaking, the ratio was not the inhibitory factor, but rather, the complete precipitation of phytate that made it unavailable for enzymatic hydrolysis.

This leads to the second inhibitory factor: lanthanum concentration (columns marked ■). At 50 mmol/L lanthanum, even when phytate was available for enzymatic hydrolysis (either through the use of citrate buffer or increasing the phytate concentration to 38 mmol/L and a lanthanum:phytate ratio of 1.3:1), only around 60% of phosphate was released, compared to 70–80% at lower lanthanum concentrations or in the absence of lanthanum.

The third factor is related to the pH profile of the *A. niger* phytase, which is known to be less effective at pH 7 (column marked *). Finally, the alternate methods of phytate hydrolysis attempted (columns marked ●) – that is *A. niger* cells, *B. adeninivorans* cells, and the autoclave – were inefficient at releasing phosphate compared to the purified *A. niger* phytase. It is likely that further work could optimise the point at which the microorganisms are transferred from their growth media to the nutrient-limited experimental media used in this work. The autoclave treatment could be improved by performing the treatment over longer timescales or at higher temperatures.

E.4.3 XRD comparisons

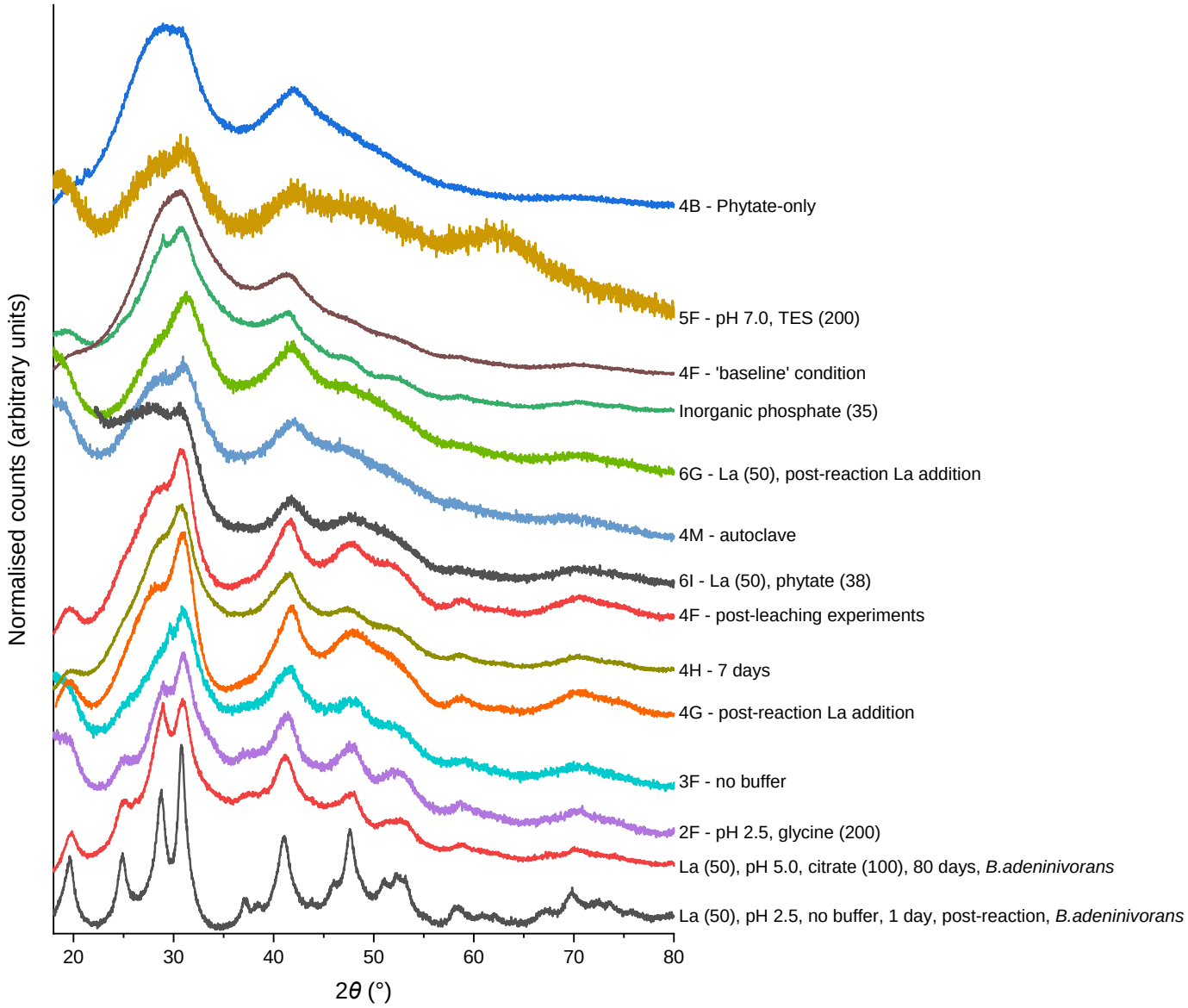

Figure E.6 XRD patterns of lanthanum phosphate precipitates produced from a lanthanum phytate precursor under different conditions. Patterns are labelled with the codes as indicated in tables E.1 and E.2 (where appropriate) and the key parameters that varied compared to the 'baseline' condition of 5 mmol/L lanthanum, 3.8 mmol/L phytate, pH 5.5, 0.2 mol/L MES buffer, lanthanum added before phytase (pre-reaction), 1 day experiment time. Numbers in brackets are concentrations in mmol/L. Also shown for reference are patterns for lanthanum phytate, lanthanum phosphate precipitated from the direct addition of inorganic phosphate, and two examples of rhabdophane (bottom two patterns) produced in other experiments (see main text for details). Patterns were measured using the Göbel mirror optics setup except for patterns labelled 2F, 3F, 6I, 4M, 6G, 5F which were measured using the motorised slit. Samples were measured using the copper K_α radiation across a 2θ range of 5–80° with a step size of 0.02° and a step time of 1 s. Patterns were normalised in OriginPro 2019b to a scale of 0 to 1.

Figure E.6 shows XRD patterns for lanthanum precipitates produced under different conditions. Patterns are arranged from the most crystalline at the bottom (all peaks matched the database pattern for rhabdophane, PDF #00-046-1439) to the most amorphous at the top (lanthanum phytate). The most crystalline patterns are 'references' that were produced using different methodologies than those described in this appendix. The bottom pattern has been described in more detail in chapter 2; briefly, *B. adeninivorans* cells were grown in a complex nutrient media until the majority of phytate had been degraded, followed by the addition of lanthanum. The second from bottom pattern was part of a batch of experiments that was not pursued in more detail due to methodological issues but used a similar strategy to that outlined in this appendix. Briefly, *B. adeninivorans* cells were grown under conditions known to induce phytase activity (i.e. grown in YN6B media as per chapter 2 for four days with an OD_{600} of ~ 2.7). A 5 mL cell suspension was then sampled from these cultures, separated from the culture media, washed, and resuspended in a solution of lanthanum and phytate, buffered at pH 5 with 0.1 mol/L citrate, without any added nutrients. The experiment then lasted for 80 days before collecting the solid phase. Also shown for reference is a lanthanum phosphate precipitated at pH 5.5 in 0.2 mol/L MES buffer using inorganic phosphate, as described in chapter 4.

In comparison to the two 'reference' patterns that show clear matches to rhabdophane, all the precipitates produced according to tables E.1 and E.2 were very poorly crystalline or amorphous. Some general trends can be observed, however. A number of patterns (2F, 3F, 4G, 4H, 4F) shown in figure E.6 showed the emergence of broad peaks that matched with the positions of peaks in the rhabdophane pattern. The increased crystallinity of these patterns compared to the 'baseline' condition (5 mmol/L lanthanum, 3.8 mmol/L phytate, pH 5.5, 0.2 mol/L MES buffer, lanthanum added before phytase (pre-reaction), 1 day experiment time) can be attributed to a lower pH (2F), no MES buffer (3F), adding lanthanum after phytate degradation has occurred (4G), increased time of experiment (4H), and performing leaching tests on the solid (which is likely a function of increased time in contact with water).

While there are multiple differences between the precipitates produced in this section and the reference patterns, it appears likely that all the factors have some level of influence on lanthanum phosphate morphology. Therefore, the bottom pattern was formed under a combination of favourable conditions – low pH, no buffer, lanthanum added after phytate

degradation had occurred – while the second from bottom pattern was formed over much longer timescales (80 days) than the other precipitates.

It is curious that rhabdophane precipitation occurred in the second from bottom pattern, in the presence of 0.1 mol/L citrate buffer, while no precipitation occurred in the presence of 0.2 mol/L citrate buffer. Further work would be required to establish whether this was purely a function of the buffer concentration or if the presence of *B. adeninivorans* cells had a role (either by providing nucleation sites or by degrading citrate as a source of carbon for growth).

E.4.4 FTIR comparisons

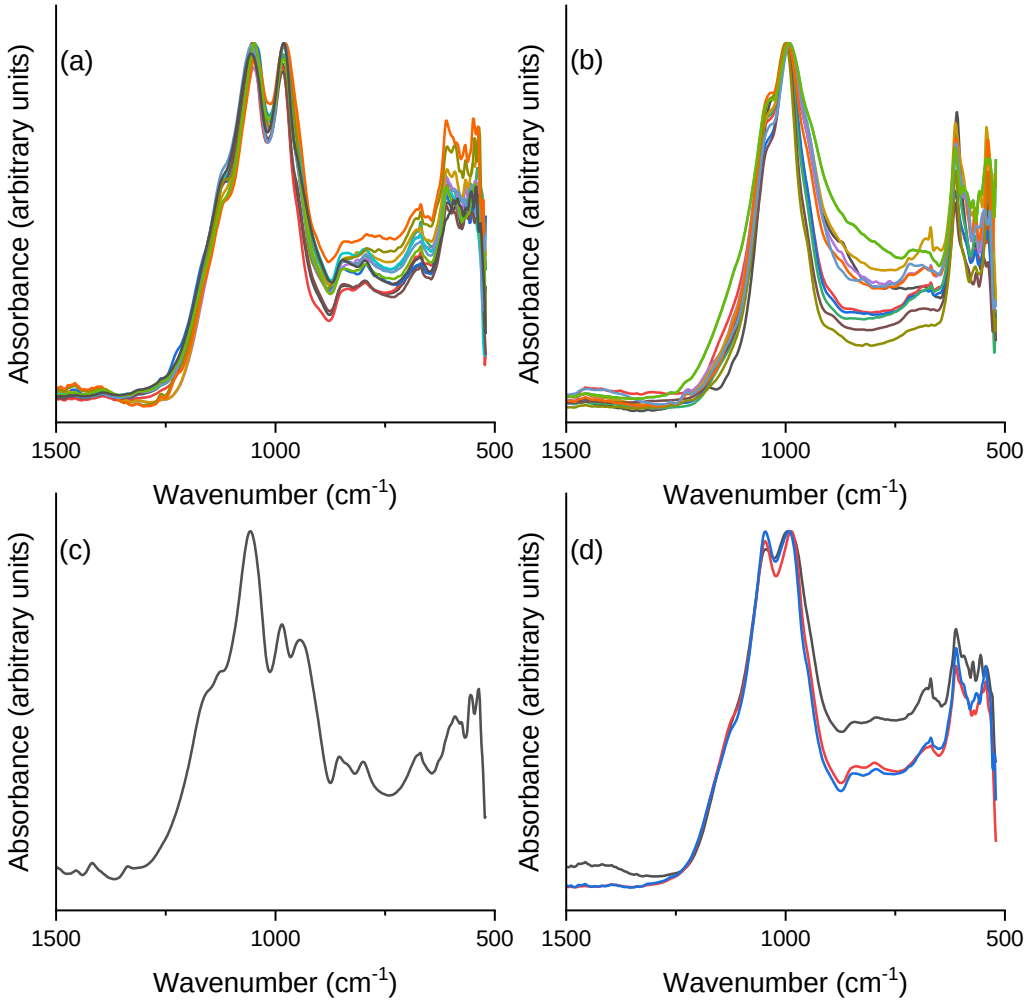

Figure E.7 Examples of the different types of FTIR spectra recorded on precipitates produced during experimental work, showing samples with spectra characteristics of (a) lanthanum phytate produced at pH 5.5, (b) a rhabdophane-like lanthanum phosphate, (c) lanthanum phytate produced at pH 2.5, (d) materials which appear to be intermediate between pH 5.5 lanthanum phytate and lanthanum phosphate. Spectra were normalised in OriginPro 2019b to a scale of 0–1.

There were essentially four types of FTIR spectrum encountered in this work – lanthanum phytate precipitated at pH 5.5 (figure E.7a), characterised by a double peak at 1,050 and 980 cm^{-1}; a rhabdophane-like lanthanum phosphate (figure E.7b), characterised by a single peak at 995 cm^{-1} with a shoulder at 1,050 cm^{-1}; lanthanum phytate precipitated at pH 2.5 (figure E.7c), characterised by a triplet at 1,050, 980, and 940 cm^{-1}; and spectra with intermediate properties between the pH 5.5 lanthanum phytate and lanthanum phosphate (figure E.7d), characterised by double peaks at 1,050 cm^{-1} and 980 cm^{-1} that were less well separated than in the lanthanum phytate spectrum.

The pH 5.5 lanthanum phytate spectra were observed for phytate-only treatments where the initial pH was set at 5.5, as well as in the treatments where the methods of phytate hydrolysis attempted released less than 10% of the available phosphate (figure E.7a). The pH 2.5 lanthanum phytate sample was only observed for the phytate-only treatment at an initial pH of 2.5 (figure E.7c); the differences between the pH 2.5 and 5.5 samples are likely related to differing levels of protonation on the phosphate groups of phytate, a parameter which is dependent on pH and is known to influence the FTIR spectra of phosphate-containing compounds (4).

The rhabdophane-like lanthanum phosphate spectra (figure E.7b) were characteristic of experiments where at least 60% of the available phosphate was released from phytate, as well as controls where lanthanum was precipitated directly with inorganic phosphate. Unlike lanthanum phytate, there did not appear to a pH dependence on the shape of the FTIR spectra of the precipitated lanthanum phosphates.

The 'intermediate' spectra (figure E.7d) were formed where between 40 and 60% of available phosphate from phytate was released, likely leading to a mixture of both lanthanum phytate and lanthanum phosphate in the final precipitate.

Appendix E References

1. Salome KR, Beazley MJ, Webb SM, Sobecky PA, Taillefert M. Biomineralization of U(VI) phosphate promoted by microbially-mediated phytate hydrolysis in contaminated soils. Geochimica et Cosmochimica Acta. 2017 Jan 15;197:27–42.

2. Cetiner ZS, Wood SA, Gammons CH. The aqueous geochemistry of the rare earth elements. Part XIV. The solubility of rare earth element phosphates from 23 to 150 °C. Chemical Geology. 2005 Apr 15;217(1):147–69.

3. Lucas S, Champion E, Bregiroux D, Bernache-Assollant D, Audubert F. Rare earth phosphate powders RePO4·nH2O (Re=La, Ce or Y)—Part I. Synthesis and characterization. Journal of Solid State Chemistry. 2004 Apr;177(4–5):1302–11.

4. Arai Y, Sparks DL. ATR–FTIR Spectroscopic Investigation on Phosphate Adsorption Mechanisms at the Ferrihydrite–Water Interface. Journal of Colloid and Interface Science. 2001 Sep 15;241(2):317–26.

Appendix F
Nuclear Magnetic Resonance results

F.1 Aluminium

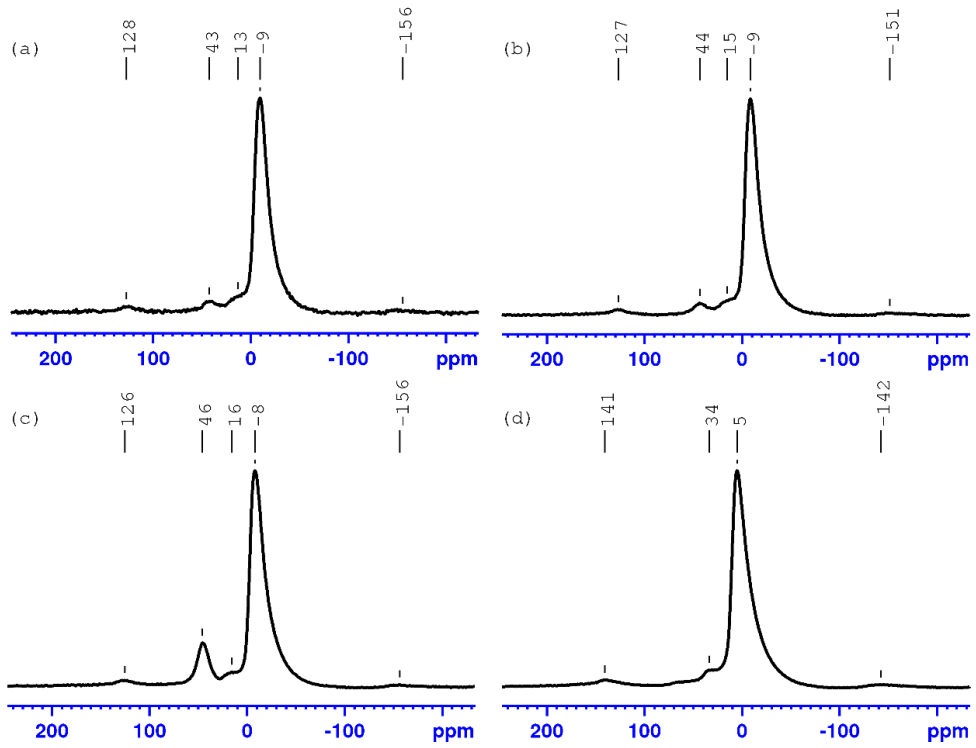

Figure F.1 ^{27}Al NMR spectra of samples produced in the aluminium experiments, showing (a) phytate-only, (b) phytate + phytase, (c) inorganic phosphate, and (d) no phosphate treatments.

The results of ^{27}Al NMR analysis of precipitates from the aluminium experiments are shown in figure F.1. Both the phytate-only and phytate + phytase treatments produced a material with a spectrum consistent with previous descriptions of aluminium phytate, including the peak at -9 ppm (1)

The spectrum of the inorganic phosphate treatment appeared similar to previously reported spectra of amorphous aluminium hydroxyphosphates (2–4). Lookman *et al.* (2) described the material they produced as consisting of a mixture of octahedral aluminium phosphate ($Al(OH)_2H_2PO_4$, peak at ~ -8 ppm) and tetrahedral aluminium phosphate ($AlPO_4$, peak at ~ 46 ppm). Lookman *et al.* (2) showed samples dried at 20, 75, and 180 °C which demonstrated that intensity of the tetrahedral aluminium peak increased with temperature while the

intensity of the octahedral aluminium peak decreased. This samples in this work were dried at 50 °C, which is consistent with the spectrum in figure F.1 having intermediate properties between the samples dried at 20 and 75 °C shown by Lookman *et al.* (2).

The spectrum for the no phosphate treatment appeared similar to previously reported spectra for basaluminite or felsöbányaite ($Al_4OH_{10}(SO_4).(H_2O)_{3–5}$; note that there is some debate in the literature as to whether basaluminite and felsöbányaite are distinct phases) (5,6) or amorphous aluminium hydroxide (1). However, the spectrum differed from alunite ($KAl_3(SO_4)_2(OH)_6$) in the lack of a broad resonance between -10 and -95 ppm (7) and differed from basic aluminium sulfate ($Na_{0.1}[Al_{13}O_4(OH)_{24}(H_2O)_{12}](SO_4)_{3.55}$) in the lack of any signals for tetrahedral aluminium (8).

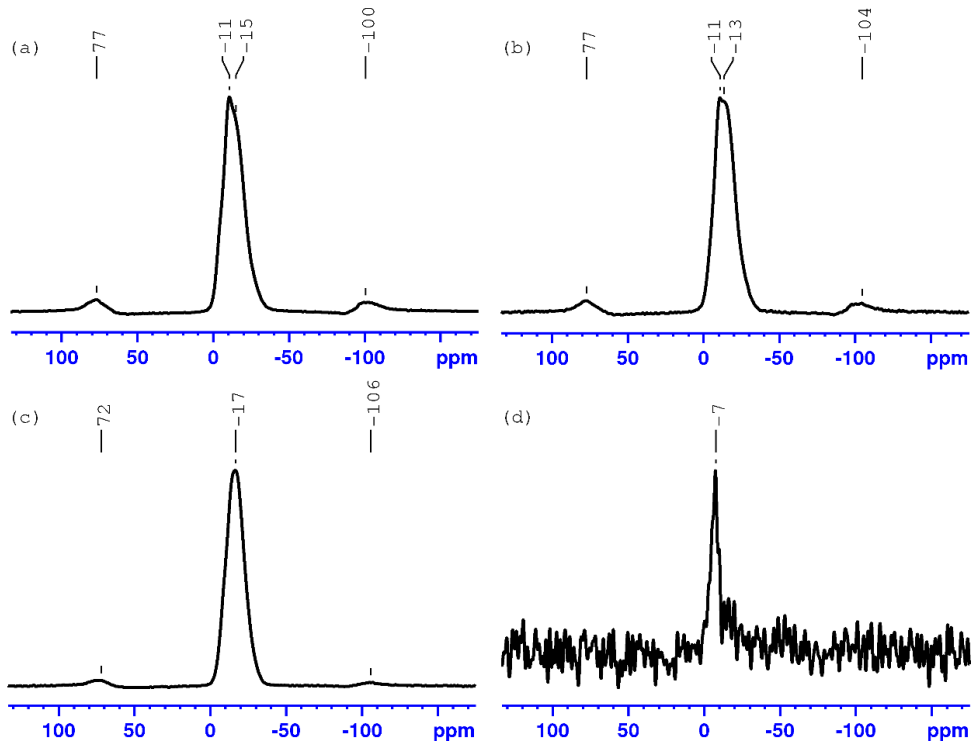

Figure F.2 ^{31}P NMR spectra of samples produced in the aluminium experiments, showing (a) phytate-only, (b) phytate + phytase, (c) inorganic phosphate, and (d) no phosphate treatments.

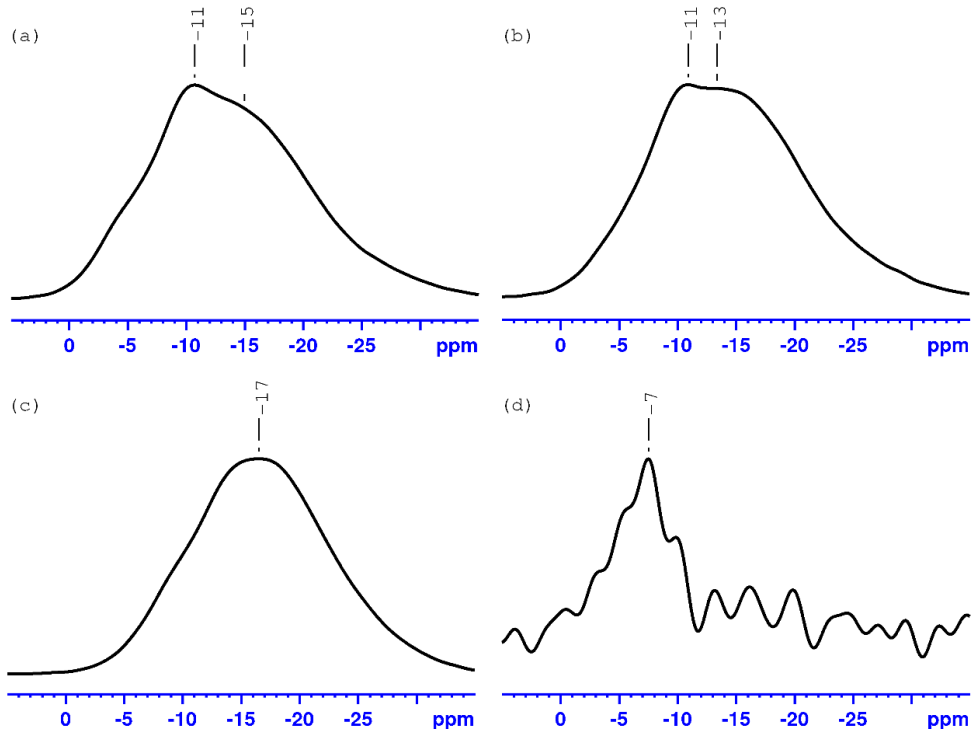

Figure F.3 ^{31}P NMR spectra of samples produced in the aluminium experiments, focused on the 5 to -35 ppm region, showing (a) phytate-only, (b) phytate + phytase, (c) inorganic phosphate, and (d) no phosphate treatments.

For ^{31}P NMR spectra, the peak at around -11 ppm for the phytate-only and phytate + phytase treatments (figure F.2) was consistent with previous descriptions of aluminium phytate *(1,9)*, although other researchers have observed the peak at around -15 ppm *(10)*. The spectra in this work appeared to consist of two peaks, centred at around -11 and -15 ppm (figure F.3), which may indicate the presence of two different types of aluminium phytate. The more prominent spinning side bands at around 80 and -100 ppm in the phytate-containing spectra compared to the inorganic phosphate spectrum is also consistent with previous comparisons of aluminium phosphate and aluminium phytate *(10)*.

The material produced in the inorganic phosphate treatment had a peak at -16.5 ppm (figure F.2c). In Lookman *et al.* (2) the amorphous aluminium hydroxyphosphate they produced had a peak at -13 ppm when dried at 20 °C and a peak at -17.5 ppm when dried at 75 °C. Therefore, as with the ^{27}Al NMR data, this suggests that an aluminium hydroxyphosphate, similar to the one produced by Lookman *et al.* (2), was produced in this work, with the difference in chemical shift a function of drying temperature.

For the phytate or inorganic phosphate containing precipitates, chemical shifts in the -10 to -20 range are indicative of aluminium phosphate or aluminium phytate precipitates (see Yan *et al.* (11) and references therein), whereas peaks for phosphate adsorbed onto aluminium (oxyhydr)oxide surfaces usually occur in the 0 to -6 ppm range (2,11).

A small peak was apparent in the ^{31}P NMR spectrum of the no phosphate treatment, but this was barely distinguishable against the background (figure F.2d). This peak may have been associated with a phosphate impurity in the stock of aluminium used (which was only of technical grade).

F.2 Lanthanum

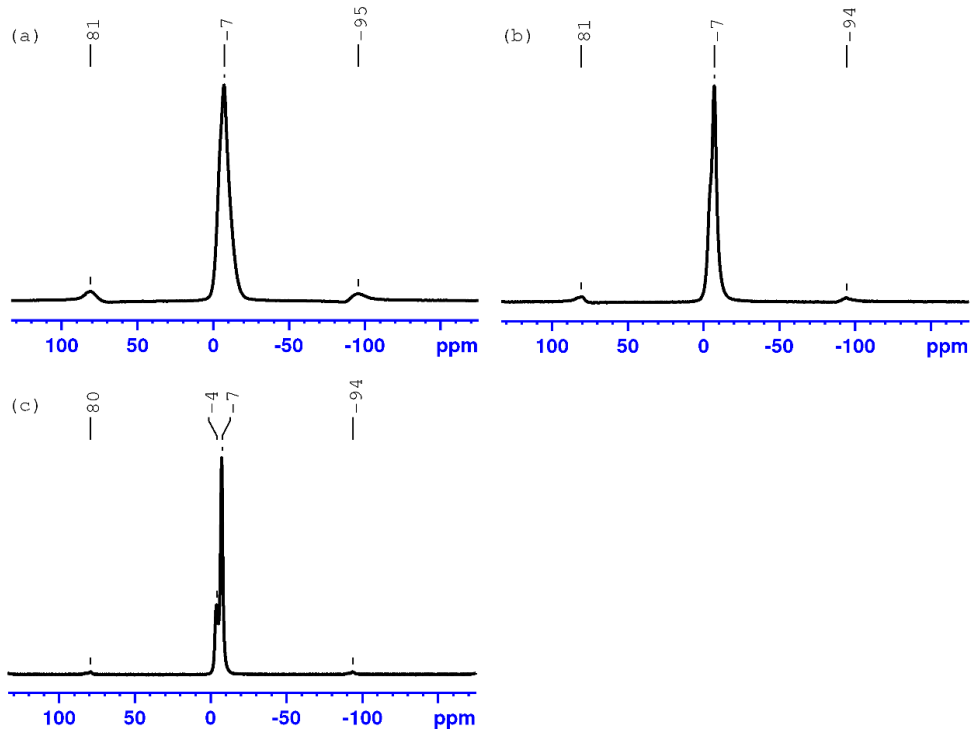

Figure F.4 ^{31}P NMR spectra of samples produced in the lanthanum experiments, showing (a) phytate-only, (b) phytate + phytase, and (c) inorganic phosphate treatments.

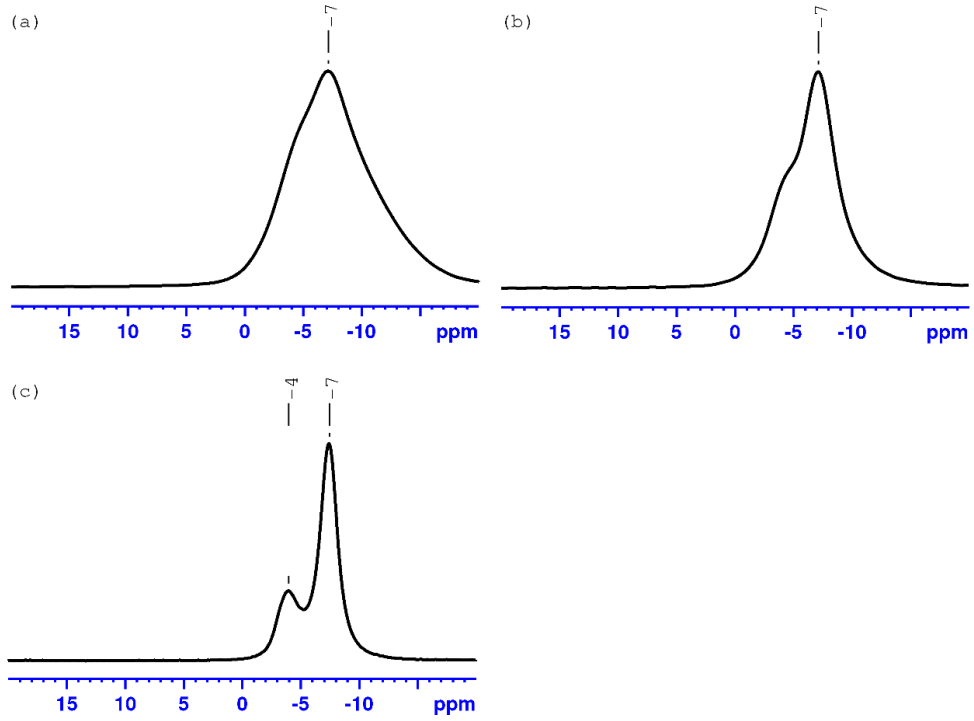

Figure F.5 ^{31}P NMR spectra of samples produced in the lanthanum experiments, focused on the 20 to -20 ppm region, showing (a) phytate-only, (b) phytate + phytase, and (c) inorganic phosphate treatments.

For the lanthanum experiments, the main ^{31}P NMR peak in all samples was observed at around -7 ppm (figure F.4), however there were notable differences in the peak shapes (figure F.5). The inorganic phosphate treatment showed a main peak at -7 ppm and a small peak at -4 ppm, while the phytate + phytase treatment showed a prominent shoulder at around -4 ppm. The phytate-only treatment only had a broad peak at -7 ppm. This appears similar to a previous comparison of lanthanum phytate and rhabdophane (12). The double peak feature in the inorganic phosphate treatment has previously been described for rhabdophane, with the smaller peak being attributed to the presence of adsorbed phosphate onto the bulk lanthanum phosphate (13). However, in Dithmer *et al.* (13) the peaks were described as being at -0.5 and -3.5 ppm compared to -4.0 and -7.4 ppm in this work. As with the FTIR results that showed spectra similar to but slightly different from literature descriptions of rhabdophane, this could be indicative of a rhabdophane precursor material being formed in these experiments.

Also notable was that the spinning side bands (at 80 and -95 ppm) were largest for the phytate-only treatment, followed by the phytate + phytase, and then the inorganic phosphate treatment (figure F.4). Larger spinning side bands for metal phytates compared to corresponding metal phosphates has previously been described for other metals (10,14) and the phytate + phytase spectrum showing intermediate properties illustrates the transition from lanthanum phytate to lanthanum phosphate.

F.3 Lead

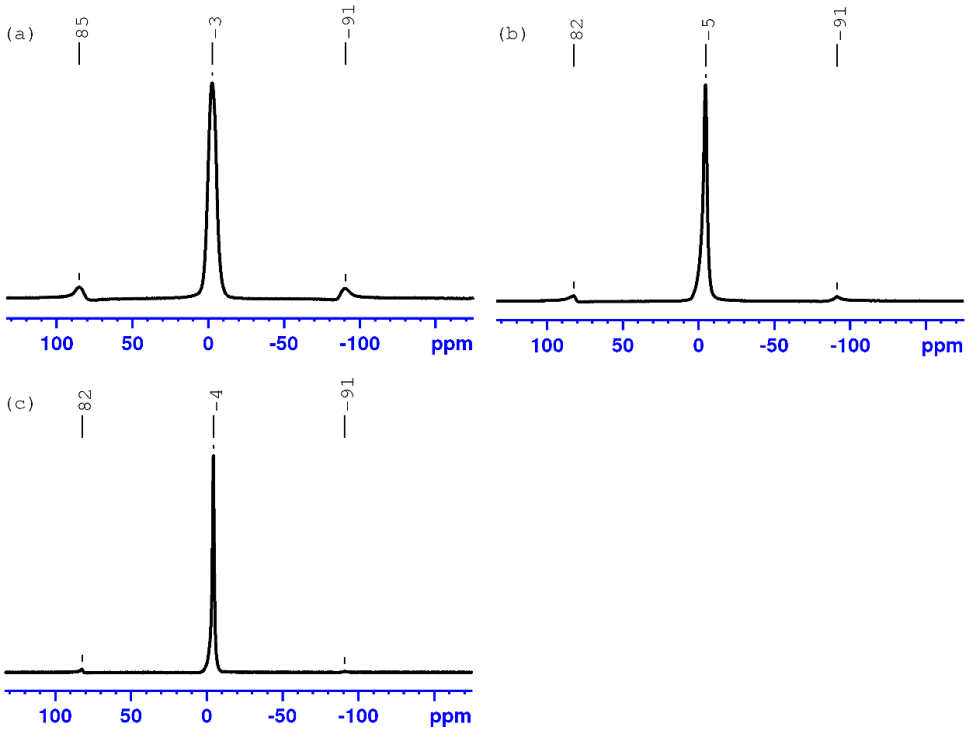

Figure F.6 ^{31}P NMR spectra of samples produced in the lead experiments, showing (a) phytate-only, (b) phytate + phytase, and (c) inorganic phosphate treatments.

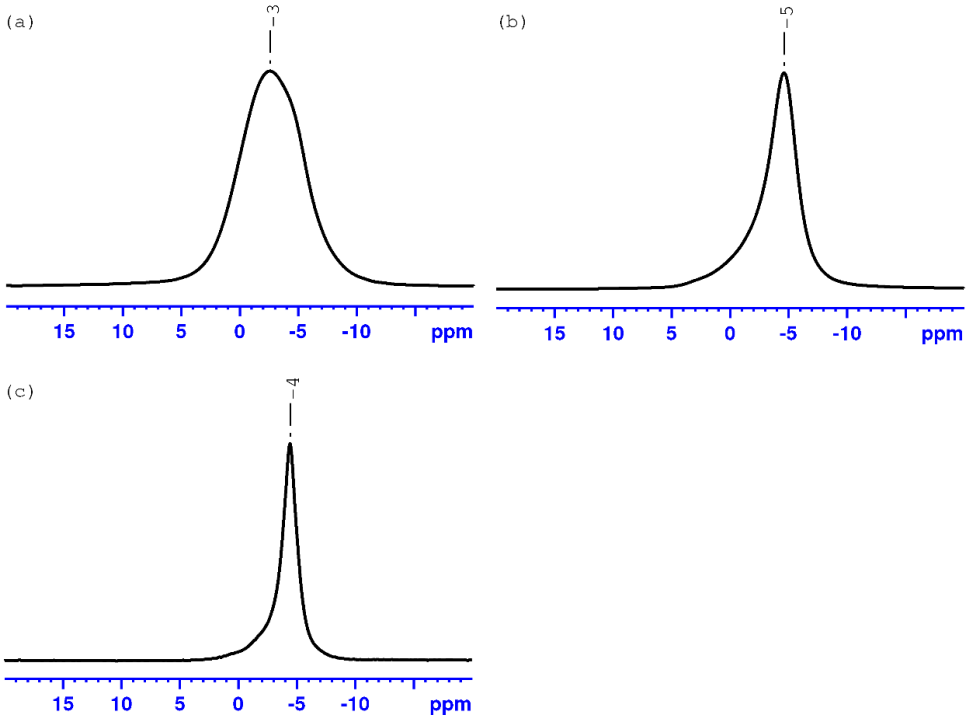

Figure F.7 ^{31}P NMR spectra of samples produced in the lead experiments, focused on the 20 to -20 ppm region, showing (a) phytate-only, (b) phytate + phytase, and (c) inorganic phosphate treatments.

As with the lanthanum experiments, the main peak in the ^{31}P NMR spectra of the lead experiments became broader when progressing from the inorganic phosphate to the phytate + phytase and then phytate-only treatments (figure F.6). Also, as observed for aluminium, lanthanum, and other previously studied metals (10,14), the spinning side bands (at around 85 and -90 ppm) were the most intense for the phytate-only treatment, decreased for the phytate + phytase treatment, and were small in the inorganic phosphate treatment.

XRD analysis indicated that the inorganic phosphate and phytate + phytase produced precipitates were pyromorphite-OH ($Pb_{10}(PO_4)_6(OH)_2$). Pyromorphite does not appear to have been well-studied by ^{31}P NMR, although a few studies have been conducted and report the ^{31}P chemical shift as being between -0.5 and -2 ppm (15–18). This is a at a slightly higher frequency than the material produced in the inorganic phosphate treatment in this work (-4 ppm). However, as XRD appeared conclusive and FTIR analysis also matched with previous descriptions of pyromorphite-OH, it can be assumed that a chemical shift of -4 ppm is representative of pyromorphite-OH under the experimental conditions used, with differences attributed to experimental or analytical variability.

Appendix F references

1. Yan Y, Li W, Yang J, Zheng A, Liu F, Feng X, et al. Mechanism of Myo-inositol Hexakisphosphate Sorption on Amorphous Aluminum Hydroxide: Spectroscopic Evidence for Rapid Surface Precipitation. Environ Sci Technol. 2014 Jun 17;48(12):6735–42.

2. Lookman R, Grobet P, Merckx R, Van Riemsdijk WH. Application of 31P and 27Al MAS NMR for phosphate speciation studies in soil and aluminium hydroxides: promises and constraints. Geoderma. 1997 Nov 1;80(3):369–88.

3. Klein J, Ushio M, Burrell LS, Wenslow B, Hem SL. Analysis of Aluminum Hydroxyphosphate Vaccine Adjuvants by 27Al MAS NMR. JPharmSci. 2000 Mar 1;89(3):311–21.

4. Burrell LS, Johnston CT, Schulze D, Klein J, White JL, Hem SL. Aluminium phosphate adjuvants prepared by precipitation at constant pH. Part I: composition and structure. Vaccine. 2000 Sep;19(2–3):275–81.

5. Carrero S, Fernandez-Martinez A, Pérez-López R, Lee D, Aquilanti G, Poulain A, et al. The nanocrystalline structure of basaluminite, an aluminum hydroxide sulfate from acid mine drainage. American Mineralogist. 2017 Dec 20;102(12):2381–9.

6. Wanner C, Pöthig R, Carrero S, Fernandez-Martinez A, Jäger C, Furrer G. Natural occurrence of nanocrystalline Al-hydroxysulfates: Insights on formation, Al solubility control and As retention. Geochimica et Cosmochimica Acta. 2018 Oct 1;238:252–69.

7. Grube E, Nielsen UG. The stoichiometry of synthetic alunite as a function of hydrothermal aging investigated by solid-state NMR spectroscopy, powder X-ray diffraction and infrared spectroscopy. Phys Chem Minerals. 2015 May 1;42(5):337–45.

8. Kloprogge JT, Geus JW, Jansen JBH, Seykens D. Thermal stability of basic aluminum sulfate. Thermochimica Acta. 1992 Nov 1;209:265–76.

9. Hu Z, Jaisi DP, Yan Y, Chen H, Wang X, Wan B, et al. Adsorption and precipitation of myo-inositol hexakisphosphate onto kaolinite. European Journal of Soil Science. 2020;71(2):226–35.

10. He Z, Honeycutt CW, Zhang T, Pellechia PJ, Caliebe WA. Distinction of Metal Species of Phytate by Solid-State Spectroscopic Techniques. Soil Science Society of America Journal. 2007 May;71(3):940–3.

11. Yan Y, Koopal LK, Li W, Zheng A, Yang J, Liu F, et al. Size-dependent sorption of myo-inositol hexakisphosphate and orthophosphate on nano-γ-Al2O3. Journal of Colloid and Interface Science. 2015 Aug 1;451:85–92.

12. Fair GE, Hay RS, Boakye EE, Morgan PED, Marzke RF, Sharma R. Precipitation Coating of Monazite on Woven Ceramic Fibers: III—Coating without Strength Degradation Using a Phytic Acid Precursor. Journal of the American Ceramic Society. 2010;93(2):420–8.

13. Dithmer L, Lipton AS, Reitzel K, Warner TE, Lundberg D, Nielsen UG. Characterization of Phosphate Sequestration by a Lanthanum Modified Bentonite Clay: A Solid-State NMR, EXAFS, and PXRD Study. Environ Sci Technol. 2015 Apr 7;49(7):4559–66.

14. He Z, Honeycutt CW, Xing B, McDowell RW, Pellechia PJ, Zhang T. SOLID-STATE FOURIER TRANSFORM INFRARED AND 31P NUCLEAR MAGNETIC RESONANCE SPECTRAL FEATURES OF PHOSPHATE COMPOUNDS: Soil Science. 2007 Jul;172(7):501–15.

15. Burchill P, Howarth OW, Richards DG, Sword BJ. Solid-state nuclear magnetic resonance studies of phosphorus and boron in coals and combustion residues. Fuel. 1990 Apr 1;69(4):421–8.

16. Pizzala H, Caldarelli S, Eon J-G, Rossi AM, Laurencin D, Smith ME. A Solid-State NMR Study of Lead and Vanadium Substitution into Hydroxyapatite. J Am Chem Soc. 2009 Apr 15;131(14):5145–52.

17. Mason HE, Hirner JJ, Xu W, Parise JB, Phillips BL. Solid-state NMR spectroscopy of Pb-rich apatite. Magnetic Resonance in Chemistry. 2009;47(12):1062–70.

18. Zeman OEO, Moudrakovski IL, Hoch C, Hochleitner R, Schmahl WW, Karaghiosoff K, et al. Determination of the 31P and 207Pb Chemical Shift Tensors in Pyromorphite, Pb5(PO4)3Cl, by Single-Crystal NMR Measurements and DFT Calculations. Zeitschrift für anorganische und allgemeine Chemie. 2017;643(21):1635–41.

Appendix G
Geochemical modelling results for chapter 4

G.1 Aluminium

Table G.1 Saturation indices for geochemical simulations of the different treatments tested for the aluminium experiments. Black numbers indicate supersaturated phases, red numbers indicate undersaturated phases. N/a indicates that one or more of the elements in a particular phase was not present in a particular model.

Phase \ Treatment	Phytate-only	Phytate + Phytase	Inorganic phosphate	No Phosphate
$Al(OH)_{2.5}(SO4)_{0.25}(s)$	-5.62	-0.12	-0.19	2.95
$Al(PO_4)(cr)$	-0.91	5.09	5.44	n/a
$Al(PO_4)\cdot 2H_2O(s)$	-1.34	4.66	5.00	n/a
Al(s)	-137.15	-131.64	-131.88	-128.67
$Al_2(OH)(PO_4)_2(s)$	26.84	38.84	39.53	n/a
$Al_2(SO_4)_3$	-52.14	-41.28	-39.77	-34.13
$Al_2(SO_4)_3\cdot 6H_2O$	-34.78	-23.93	-22.41	-16.77
Alunite ($KAl_3(SO_4)_2(OH)_6$)	-9.09	7.38	7.60	16.59
Arcanite (K_2SO_4)	-3.04	-2.99	-3.14	-3.60
Berlinite ($AlPO_4$)	-3.28	2.72	3.07	n/a
Boehmite (AlO(OH))	-3.37	2.14	1.91	5.11
Corundum (Al_2O_3)	-9.80	1.22	0.75	7.17
Diaspore (AlO(OH))	-2.61	2.90	2.67	5.87
Felsobányaite(am) ($Al_4(SO_4)(OH)_{10}\cdot 4H_2O$)	-20.87	1.11	0.83	13.40
Felsobányaite(cr) ($Al_4(SO_4)(OH)_{10}\cdot 4H_2O$)	-19.17	2.81	2.53	15.10
Gibbsite ($Al(OH)_3$)	-3.49	2.02	1.78	4.99
K(OH)(s)	-20.12	-20.07	-20.47	-20.57
$KAl(SO_4)_2(s)$	-22.73	-17.28	-16.59	-14.01
$KAl(SO_4)_2\cdot 12H_2O(s)$	-12.33	-6.88	-6.20	-3.61
$KH_2PO_4(cr)$	-3.25	-2.71	-2.53	n/a
Mercallite ($KHSO_4$)	-7.98	-7.98	-7.72	-8.09
P(cr)	-134.42	-133.93	-133.37	n/a
S(cr)	-89.97	-90.03	-89.38	-89.63

Table G.2 Concentrations (mol/kg) of different groups of aluminium species across the simulations of different experiments. Species are grouped according to type of ligand, i.e., free aluminium (Al^{3+}), hydroxyl complexes, sulfate complexes, (hydroxy)phosphate complexes, and phytate ([InsP6]) complexes.

Species \ Treatment	Phytate-only	Phytate + Phytase	Inorganic phosphate	No phosphate
Total Aluminium	**4.99E-03**	**4.99E-03**	**4.99E-03**	**4.99E-03**
Al^{3+}	5.75E-12	1.08E-06	2.48E-06	1.49E-03
$Al(OH)_x^{3-x}$	7.39E-12	1.89E-06	2.53E-06	2.48E-03
$Al(SO_4)^+$	1.30E-12	3.25E-07	1.55E-06	1.03E-03
$Al_i(OH)_j(H_kPO_4)_l^{3i-j+l(k-3)}$	1.02E-09	1.71E-03	3.41E-03	0.00E+00
$AlH_q[InsP6]^{-12+3+q}$	4.99E-03	2.63E-03	0.00E+00	0.00E+00

Geochemical modelling of the aluminium experiments was performed to probe the likely identity of precipitates formed in each treatment, as well as to try and understand why the solubility of aluminium was much higher in the phytate-only treatment.

Based upon calculated saturation indices (table G.1) it appears likely that in the no phosphate condition, the precipitate was a mixture of aluminium hydroxysulfates (e.g. (1–4)) and (oxyhydr)oxides. For the inorganic phosphate treatment, it appears likely that an aluminium hydroxyphosphate was formed, potentially along with sulfate and (oxyhydr)oxide species. However, the presence of phytate appears to inhibit aluminium hydrolysis (table G.2) which, therefore, would inhibit the formation of hydroxide-containing solids. In the phytate-only model, the concentration of free aluminium, aluminium hydroxyl, and aluminium sulfate species were all in the order of 10^{-12} mol/kg, while in the models where phytate had been degraded or was not present, the concentrations of these species were between five and nine orders of magnitude higher (~ 10^{-6} mol/kg in the presence of phosphate, ~ 10^{-3} mol/kg in the absence of phosphate).

G.2 Calcium

Table G.3 Saturation indices for geochemical simulations of the different conditions and treatments tested for the calcium experiments. As the experimental results for the phytate + phytase and phytate + phytase + alkaline phosphatase treatments were similar for the 5 mmol/L calcium, pH 7.0 condition both treatments were represented by a single simulation. Black numbers indicate supersaturated phases, red numbers indicate undersaturated phases. Phytate is represented in the model by [InsP6].

Condition:	5 mmol/L Ca, pH 5.5		5 mmol/L Ca, pH 7.0		50 mmol/L Ca, pH 5.5	
Phase \ Treatment	Phytate-only	Phytate + Phytase	Phytate-only	Phytate + Phytase	Phytate-only	Phytate + Phytase
Antarcticite ($CaCl_2.6H_2O$)	-11.58	-11.70	-11.32	-11.32	-8.28	-8.26
Brushite ($Ca(HPO_4).2H_2O$)	-0.83	-0.26	0.32	0.72	0.38	0.68
$Ca(HPO_4)(s)$	-0.53	0.05	0.62	1.02	0.68	0.99
Ca(s)	-126.23	-126.21	-121.66	-122.70	-124.93	-124.87
$Ca_2Cl_2(OH)_2.H_2O(s)$	-26.23	-26.33	-23.07	-23.03	-21.61	-21.53
A-$Ca_3(PO_4)_2$	-2.74	-1.58	2.45	3.31	1.00	1.66
$Ca_4Cl_2(OH)_6.13H_2O(s)$	-52.59	-52.67	-43.66	-43.51	-45.36	-45.16
$Ca_4H(PO_4)_3:2.5H_2O(s)$	-4.56	-2.83	1.78	3.03	0.38	1.35
Ca_5H_2[InsP6]:$16H_2O(s)$	4.44	4.64	2.32	3.20	7.95	7.91
Ca_5K_2[InsP6]:$xH_2O(s)$	30.88	31.29	31.37	32.34	34.43	34.44
Ca_6[InsP6](s)	12.36	12.57	13.11	14.05	17.19	17.22
$CaCl_2.2H_2O(cr)$	-15.59	-15.70	-15.32	-15.32	-12.27	-12.26
$CaCl_2.4H_2O(cr)$	-12.99	-13.11	-12.72	-12.73	-9.68	-9.67
$CaCl_2.H_2O(s)$	-15.48	-15.60	-15.22	-15.22	-12.17	-12.16
CaO(cr)	-24.76	-24.75	-21.88	-21.83	-23.45	-23.39
Chloroapatite ($Ca_{10}(PO_4)_6Cl_2$)	2.20	3.88	10.11	11.40	9.45	10.46

Table G.3 (continued).

Condition:	5 mmol/L Ca, pH 5.5		5 mmol/L Ca, pH 7.0		50 mmol/L Ca, pH 5.5	
Phase \ Treatment	Phytate-only	Phytate + Phytase	Phytate-only	Phytate + Phytase	Phytate-only	Phytate + Phytase
Hydrophilite ($CaCl_2$)	-19.40	-19.52	-19.13	-19.14	-16.09	-16.07
Hydroxyapatite ($Ca_{10}(PO_4)_6(OH)_2$)	0.84	2.59	10.06	11.37	7.10	8.13
K(cr)	-63.62	-63.52	-61.47	-61.97	-63.61	-63.59
K(OH)(s)	-20.07	-19.97	-18.76	-18.72	-20.06	-20.04
K_2O(s)	-75.05	-74.85	-72.43	-72.35	-75.02	-74.98
KH_2PO_4(cr)	-3.26	-2.60	-3.69	-3.30	-3.35	-3.09
P(cr)	-134.49	-133.93	-132.03	-134.39	-134.61	-134.37
Portlandite ($Ca(OH)_2$)	-14.88	-14.86	-11.99	-11.94	-13.57	-13.50
Sylvite (KCl)	-4.12	-4.09	-4.12	-4.11	-3.11	-3.11

Table G.4 Concentrations (mol/kg) of different groups of calcium species across the simulations of different experiments. Species are grouped according to type of ligand, i.e., free calcium (Ca^{2+}), hydroxyl complexes, phosphate complexes, and phytate ([InsP6]) complexes

Condition:	5 mmol/L Ca, pH 5.5		5 mmol/L Ca, pH 7.0		50 mmol/L Ca, pH 5.5	
Species \ Treatment	Phytate-only	Phytate + Phytase	Phytate-only	Phytate + Phytase	Phytate-only	Phytate + Phytase
Total Calcium	**4.99E-03**	**4.99E-03**	**4.99E-03**	**4.99E-03**	**4.98E-02**	**4.98E-02**
Ca^{2+}	1.75E-03	9.89E-04	4.65E-03	4.12E-03	3.38E-02	3.49E-02
$Ca(OH)^{+}$	4.61E-11	3.70E-11	1.96E-09	2.00E-09	9.31E-10	1.02E-09
$Ca(H_xPO4)^{-1+x}$	6.89E-05	2.18E-04	3.30E-04	8.25E-04	1.11E-03	2.14E-03
$Ca_pH_q[InsP6]^{-12+(2p)+q}$	1.66E-03	1.60E-03	2.62E-06	1.54E-05	5.02E-03	4.27E-03

Geochemical modelling indicated that, for every condition and treatment tested, hydroxyapatite ($Ca_{10}(PO_4)_6(OH)_2$), chloroapatite ($Ca_{10}(PO_4)_6Cl_2$), and three calcium phytate species were supersaturated (table G.3). Previous researchers have indicated that a saturation index of at least 10–11 is required before apatites will form (5). This explains the lack of apatite formation at pH 5.5 with 5 mmol/L calcium, but apatite precipitation should at least have been possible in the pH 7.0 with 5 mmol/L calcium experiment. The formation of apatite is known to occur *via* precursor phases such as amorphous calcium phosphate and brushite ($CaHPO_4.2H_2O$) (6–9) and so low saturation indices for these precursor phases may be a factor, although Pinto *et al.* (10) claimed that spontaneous precipitation of brushite occurred above a saturation index of 0.27. The treatments performed at pH 7 with 5 mmol/L calcium and at pH 5.5 with 50 mmol/L calcium both achieved supersaturation values for brushite above this value, so this was likely not the limiting factor by itself.

Aside from the fact that the pH in these experiments was sub-optimal for apatite precipitation at ambient temperatures (11,12), the presence of phytate and/or lower inositol phosphates likely contributed to inhibiting the formation of inorganic calcium phosphates (9,13,14).

G.3 Manganese

Table G.5 Saturation indices for geochemical simulations of the different conditions and treatments tested for the manganese experiments. Black numbers indicate supersaturated phases, red numbers indicate undersaturated phases. Phytate is represented in the model by [InsP6].

Phase \ Treatment	Phytate-only	Phytate + Phytase
Alabandite (MnS)	-122.75	-122.65
Arcanite (K_2SO_4)	-3.26	-3.18
Hausmannite (Mn_3O_4)	-0.42	0.16
K(cr)	-63.63	-63.54
K(OH)(s)	-20.08	-19.99
K_2O(s)	-75.07	-74.89
KH_2PO_4(cr)	-3.27	-2.65
Manganite (MnOOH)	1.25	1.44
Mercallite ($KHSO_4$)	-8.23	-8.24
$Mn(HPO_4)$(s)	5.44	6.17
$Mn(SO_4)$(s)	-3.61	-3.51
$Mn_3(PO_4)_2$(s)	-8.06	-6.40
$Mn_3(PO_4)_2$:$3H_2O$(s)	4.94	6.59
Mn_5H_2[InsP6]:$16H_2O$(s)	4.45	5.30
MnO(s)	-10.04	-9.84
MnO_2(s)	3.17	3.37
P(cr)	-134.48	-133.94
Pyrochroite	-7.44	-7.25
S(cr)	-90.26	-90.35

Table G.6 Concentrations (mol/kg) of different groups of calcium species across the simulations of different experiments. Species are grouped according to type of ligand, i.e., free manganese (Mn^{2+}), sulfate complexes, phosphate complexes, phytate ([InsP6]) complexes, and all others

Species \ Treatment	Phytate-only	Phytate + Phytase
Total manganese	**4.99E-03**	**4.99E-03**
Mn^{2+}	1.60E-03	1.48E-03
Mn(SO4)	9.19E-05	1.15E-04
$Mn(HPO4)_x^{2-(2x)}$	2.77E-04	1.53E-03
$MnH_q[InsP6]^{-12+2+q}$	3.02E-03	1.87E-03
Others	6.34E-09	7.89E-09

G.4 Iron(II)

Table G.7 Saturation indices for geochemical simulations of the different conditions and treatments tested for the iron(II) experiments. Black numbers indicate supersaturated phases, red numbers indicate undersaturated phases.

Phase \ Treatment	Phytate	Phytate + Phytase	Inorganic phosphate	No phosphate
Arcanite (K_2SO_4)	-3.27	-3.20	-3.32	-3.75
$Fe(OH)_2$(cr)	-4.87	-4.88	-5.32	-4.45
$Fe(PO_4)$(cr)	-3.18	-2.65	-1.01	n/a
Fe(s)	-15.82	-15.90	-19.41	-17.63
$Fe_5(OH)(PO_4)_3$(s)	417.10	418.58	417.98	n/a
FeO(s)	-5.48	-5.48	-5.93	-5.06
Ferrihydrite(am) ($Fe(OH)_3$)	-3.73	-3.71	-2.62	-2.19
Ferrihydrite ($Fe(OH)_3$)	-2.38	-2.36	-1.27	-0.84
FeS(am)	-1.06	-1.41	-13.57	-9.17
Goethite (FeOOH)	-1.58	-1.55	-0.47	-0.04
Hematite (Fe_2O_3)	-1.35	-1.30	0.86	1.72
K(cr)	-48.90	-48.85	-50.72	-50.45
K(OH)(s)	-20.08	-20.00	-20.34	-20.52
K_2O(s)	-75.07	-74.91	-75.58	-75.95
KH_2PO_4(cr)	-3.34	-2.76	-2.54	n/a
Lepidocrocite (FeOOH)	-1.94	-1.91	-0.83	-0.40
Mackinawite (FeS)	-0.41	-0.76	-12.92	-8.52
Maghemite(disord) (Fe_2O_3)	-5.68	-5.63	-3.47	-2.61
Maghemite(ord) (Fe_2O_3)	-5.89	-5.84	-3.68	-2.82
Magnetite (Fe_3O_4)	-4.89	-4.85	-3.13	-1.40
Melanterite ($FeSO_4.7H_2O$)	-4.07	-4.17	-4.07	-3.25
Mercallite ($KHSO_4$)	-8.24	-8.25	-8.04	-8.29
P(cr)	-60.92	-60.57	-67.68	n/a
Pyrite (FeS_2)	7.74	7.10	-13.70	-6.67
Pyrrhotite ($Fe_{0.87}S$)	1.58	1.23	-10.47	-6.30
S(cr)	-1.90	-2.19	-10.83	-8.20
Troilite (FeS)	1.30	0.95	-11.21	-6.81
Vivianite ($Fe_3(PO_4)_2.8H_2O$)	4.09	5.07	4.82	n/a

Table G.8 Concentrations (mol/kg) of different groups of iron(II) and iron(III) species across the simulations of different experiments. Species are grouped according to type of ligand, i.e., free iron (Fe^{2+} or Fe^{3+}), sulfate complexes, phosphate complexes, phytate ([InsP6]) complexes, and all others

Species \ Treatment	Phytate-only	Phytate + Phytase	Inorganic phosphate	No phosphate
Total iron(II)	**4.88E-03**	**4.97E-03**	**4.99E-03**	**4.99E-03**
Fe^{2+}	1.70E-03	1.06E-03	7.62E-04	4.43E-03
$Fe(H_xPO4)^{-1+x}$	8.59E-04	2.28E-03	4.14E-03	0.00E+00
$FeH_q[InsP6]^{-12+2+q}$	2.23E-03	1.57E-03	0.00E+00	0.00E+00
$Fe(H_xSO4)^{+x}$	8.64E-05	6.89E-05	8.61E-05	5.62E-04
Other Fe(II) species	7.18E-06	2.63E-06	3.58E-08	2.44E-07
Total iron(III)	**1.60E-04**	**6.73E-05**	**1.79E-11**	**1.87E-11**
Fe^{3+}	1.84E-17	8.90E-18	2.52E-16	4.22E-16
$Fe(H_xPO4)^{+x}$	5.63E-14	1.55E-13	1.02E-11	0.00E+00
$FeH_q[InsP6]^{-12+3+q}$	1.60E-04	6.73E-05	0.00E+00	0.00E+00

Table G.8 (continued).

Species \ Treatment	Phytate-only	Phytate + Phytase	Inorganic phosphate	No phosphate
$Fe(H_xSO4)_y^{+3+y(x-2)}$	1.94E-17	1.37E-17	8.94E-16	1.88E-15
Other Fe(III) species	4.85E-13	4.22E-13	7.71E-12	1.87E-11

Geochemical modelling indicated that in the phytate-only and phytate + phytase treatments, the solution speciation of iron consisted of similar concentrations of free iron(II) and as either phosphate or phytate complexes (table G.8). The model also calculated that concentrations of iron(III) would be higher in the presence of phytate compared to the simulations where phytate was not present. Effectively all of this iron(III) was calculated to be associated with phytate. This is consistent with previous descriptions of phytate accelerating the oxidation of iron(II) (15). For the no phosphate treatment, almost all of the iron was present as free iron(II), with about 10% present as complexes with sulfate (table G.8). In the inorganic phosphate treatment, iron was mostly present as iron(II) phosphate complexes, with around 10% present as free iron(II).

Solubility product data for iron phytate species could not be found, but it is likely that iron phytates would be insoluble under the conditions tested. The models also indicated, in the presence of phosphate, that vivianite ($Fe_3(PO_4)_2.8H_2O$) was supersaturated (table G.7). An extremely high saturation index (> 400) was also calculated for the phase $Fe_5(OH)(PO_4)_3$ which may indicate that phosphate phases precipitating under the conditions tested are likely to be iron hydroxyphosphates. For the no phosphate treatment, the only supersaturated phase was hematite (Fe_2O_3).

The model likely requires some refinement. Firstly, precipitation in the no phosphate treatment was most likely due to the oxidation of iron(II) to iron(III) and the subsequent precipitation of iron(III) oxides, but the model does not reflect this. Secondly, despite the indication of iron oxidation, the phytate-only and phytate + phytase simulations were the only ones where iron(II) sulfide phases (pyrite, pyrrhotite, and troilite) – phases that form under reducing conditions – were indicated as being supersaturated. Therefore, adjustments of the model to reflect the aerobic atmosphere in which the experiments took place would be desirable.

G.5 Iron(III)

Table G.9 Saturation indices for geochemical simulations of the different conditions and treatments tested for the iron(III) experiments. Black numbers indicate supersaturated phases, red numbers indicate undersaturated phases.

Phase \ Treatment	Phytate	Phytate + Phytase	Inorganic phosphate	No phosphate
$Fe(OH)_2(cr)$	-12.22	-10.79	-10.64	-10.27
$Fe(PO_4)(cr)$	4.75	6.97	7.38	n/a
Fe(s)	-53.24	-52.52	-52.51	-51.97
$Fe_5(OH)(PO4)_3(s)$	381.09	389.54	390.86	n/a
FeO(s)	-12.83	-11.40	-11.25	-10.88
Ferrihydrite(am) ($Fe(OH)_3$)	3.94	5.73	5.96	6.23
Ferrihydrite ($Fe(OH)_3$)	5.29	7.08	7.31	7.58
Goethite (FeOOH)	6.09	7.88	8.11	8.39
Hematite (Fe_2O_3)	13.99	17.57	18.03	18.57
K(cr)	-64.10	-64.33	-64.57	-64.62
$K(NO_3)(s)$	-3.00	-2.98	-3.05	-3.17
K(OH)(s)	-20.26	-20.13	-20.29	-20.43
$K_2O(s)$	-75.42	-75.16	-75.49	-75.77
$KH_2PO_4(cr)$	-3.26	-2.70	-2.68	n/a
Lepidocrocite (FeOOH)	5.73	7.52	7.75	8.03
Maghemite(disord) (Fe_2O_3)	9.66	13.24	13.70	14.24
Maghemite(ord) (Fe_2O_3)	9.45	13.03	13.49	14.03
Magnetite (Fe_3O_4)	3.10	8.11	8.72	9.63
P(cr)	-135.80	-137.16	-137.35	n/a
Vivianite ($Fe_3(PO_4)_2.8H_2O$)	-17.47	-12.31	-11.48	n/a

Table G.10 Concentrations (mol/kg) of different groups of iron(II) and iron(III) species across the simulations of different experiments. Species are grouped according to type of ligand, i.e., free iron (Fe^{2+} or Fe^{3+}), phosphate complexes, phytate ([InsP6]) complexes, hydroxyl complexes, and all others.

Species \ Treatment	Phytate-only	Phytate + Phytase	Inorganic phosphate	No phosphate
Total iron(II)	**2.67E-10**	**7.63E-09**	**1.51E-08**	**6.50E-09**
Total iron(III)	**5.05E-03**	**5.05E-03**	**5.00E-03**	**5.00E-03**
Fe^{3+}	2.96E-09	5.80E-08	6.85E-08	1.07E-07
$Fe(H_xPO4)^{+x}$	7.25E-06	8.63E-04	2.31E-03	0.00E+00
$FeH_q[InsP6]^{-12+3+q}$	5.00E-03	2.66E-03	0.00E+00	0.00E+00
$Fe_j(OH)_k^{+3j-k}$	3.40E-05	1.52E-03	2.68E-03	4.98E-03
Other Fe(III) species	4.84E-11	1.15E-09	2.21E-09	4.06E-09

Geochemical modelling indicated that iron(II) and free iron(III) (as Fe^{3+}) were present at negligible concentrations in these experiments (table G.10). Almost all the iron in the phytate-only treatment was calculated to be associated with phytate. Following phytase treatment, iron phytate complexes were still the most abundant iron species, but there was now an approximately equal level of iron hydroxyl species and a slightly lower but similar level of iron phosphate complexes. In the no phosphorus treatment, effectively all of the iron was present

as hydroxyl complexes, while in the inorganic phosphate treatment there was an approximate 50/50 split between iron hydroxyl and iron phosphate complexes.

As with aluminium, the geochemical model indicated a strong inhibition of iron(III) hydrolysis by phytate. A number of iron (oxyhydr)oxides were supersaturated in all simulations, but the lowest saturation indices were calculated for the phytate-only treatment, followed by the phytate + phytase treatment (table G.9). It appears that the inhibition of iron(III) hydrolysis by phytate and/or lower inositol phosphates was the main limiting factor for iron precipitation. In the absence of phytate, the uninhibited hydrolysis of iron(III) allowed the near complete precipitation of iron as iron (oxyhydr)oxides or iron hydroxyphosphates for the no phosphate and inorganic phosphate treatments respectively.

G.6 Cobalt

Table G.11 Saturation indices for geochemical simulations of the different conditions and treatments tested for the cobalt experiments. Black numbers indicate supersaturated phases, red numbers indicate undersaturated phases.

Phase \ Treatment	Phytate	Phytate + Phytase
Co(cr)	-39.76	-38.71
$Co(OH)_2$(s,blue)	-6.51	-5.46
$Co(OH)_2$(s,rose1)	-4.91	-3.86
$Co(OH)_2$(s,rose2)	-5.91	-4.86
$Co_3(PO_4)_2$(s)	1.23	5.49
Co_3O_4(s)	4.33	7.48
$CoHPO_4$(s)	-1.34	0.26
CoO(s)	-6.48	-5.43
K(cr)	-63.63	-63.52
$K(NO_3)$(s)	-3.16	-3.14
K(OH)(s)	-20.08	-19.98
K_2O(s)	-75.07	-74.87
KH_2PO_4(cr)	-3.25	-2.60
P(cr)	-134.46	-133.91

Table G.12 Concentrations (mol/kg) of different groups of cobalt species across the simulations of different experiments. Species are grouped according to type of ligand, i.e., free cobalt (Co^{2+}), phosphate complexes, phytate ([InsP6]) complexes, hydroxyl complexes.

Species \ Treatment	Phytate-only	Phytate + Phytase
Total cobalt	**4.95E-03**	**4.95E-03**
Co^{2+}	4.09E-04	2.57E-03
$CoHPO_4$	9.96E-06	4.02E-04
$CoH_q[InsP6]^{-12+2+q}$	4.53E-03	1.97E-03
$Co_j(OH)_k^{2j-k}$	3.79E-08	3.30E-07

Geochemical modelling indicated that in the phytate-only treatment the majority of cobalt was associated with phytate (table G.12). In the phytate + phytase treatment, free cobalt (Co^{2+}) was the most abundant species, while the concentration of cobalt phytate complexes was slightly lower (table G.12). The proportion of cobalt phosphate species increased in the phytate + phytase treatment compared to the phytate-only treatment but was almost an order of magnitude lower than free cobalt and cobalt phytate complexes.

Two solids phases ($Co_3(PO_4)_2$ and Co_3O_4) were supersaturated in both simulations (table G.11). Following phytase treatment, the saturation indices of both phases increased and a third phase ($CoHPO_4$) became supersaturated. This is counterintuitive when considering that, in reality, phytase activity was followed by increased cobalt solubility. It may be that residual phytate or lower inositol phosphates formed soluble complexes with cobalt that inhibited the formation of inorganic cobalt phosphates.

It cannot be ruled out that the phase formed in both treatments was actually Co_3O_4. However, Co_3O_4 requires the partial oxidation of cobalt(II) to cobalt(III). Also, geochemical modelling indicated that the stock solution of cobalt nitrate was supersaturated with respect to Co_3O_4 (saturation index = 2.78) but no precipitation was observed in the stock.

G.7 Copper

Table G.13 Saturation indices for geochemical simulations of the different conditions and treatments tested for the copper experiments. Black numbers indicate supersaturated phases, red numbers indicate undersaturated phases.

Phase \ Treatment	Phytate	Phytate + Phytase
Arcanite (K_2SO_4)	-3.30	-3.24
Cornetite ($Cu_3(PO_4)(OH)_3$)	2.08	3.15
Cu(cr)	-18.00	-17.79
$Cu(OH)_{1.5}(SO_4)_{0.25}$	0.58	0.77
$Cu(OH)_2$(s)	-1.38	-1.17
Cu-hydroxypyromorphite ($Cu_{10}(PO_4)_6(OH)_2$)	8.15	10.54
$Cu_3(PO_4)_2$(s)	5.24	6.77
CuO(s)	-0.58	-0.37
$CuSO_4$:$5H_2O$(s)	-3.60	-3.49
K(cr)	-63.66	-63.58
K(OH)(s)	-20.11	-20.04
K_2O(s)	-75.14	-74.98
KH_2PO_4(cr)	-3.28	-2.75
Libenthenite ($Cu_2(PO_4)OH$)	2.16	3.02
Mercallite ($KHSO_4$)	-8.23	-8.26
P(cr)	-134.46	-134.01
Pseudomalachite ($Cu_5(PO_4)_2(OH)_4$)	4.04	5.98

Table G.13 (continued).

Phase \ Treatment	Phytate	Phytate + Phytase
S(cr)	-90.23	-90.33
Tagilite ($Cu_2(PO_4)OH.H_2O$)	2.06	2.92

Table G.14 Concentrations (mol/kg) of different groups of copper species across the simulations of different experiments. Species are grouped according to type of ligand, i.e., free copper (Cu^{2+}), phosphate complexes, phytate complexes, sulfate complexes, hydroxyl complexes.

Species \ Treatment	Phytate-only	Phytate + Phytase
Total copper	**4.94E-03**	**4.94E-03**
Cu^{2+}	2.15E-03	2.25E-03
$Cu(H_xPO4)_y^{(-3+x)y+2}$	1.15E-04	4.90E-04
$CuH_q[InsP6]^{-12+2+q}$	2.50E-03	1.97E-03
Cu(SO4)	1.46E-04	1.89E-04
$Cu_j(OH)_k^{2j-k}$	2.17E-05	3.05E-05

Geochemical modelling indicated that copper speciation was dominated by free copper (Cu^{2+}) and copper phytate complexes (table G.14). There was a slightly higher concentration of copper phytate complexes in the phytate-only treatment, while in the phytate + phytase treatment, concentrations of free copper were slightly higher than copper phytate. For both treatments, copper phosphate and copper sulfate complexes were around an order of magnitude lower in concentration.

The modelling of saturation indices (table G.13) was limited by the fact that solubility product data for copper phytate solids could not be found, but it is likely that copper phytate solids would be supersaturated under the conditions studied (16). The geochemical model calculated that copper phosphate ($Cu_3(PO_4)_2$) and a number of copper hydroxyphosphates were supersaturated, with the saturation indices increasing slightly for the phytate + phytase treatment. In addition, a copper hydroxysulfate was also calculated to be supersaturated in both simulations.

G.8 Barium

Table G.15 Saturation indices for geochemical simulations of the different conditions and treatments tested for the barium experiments. Black numbers indicate supersaturated phases, red numbers indicate undersaturated phases. Phytate is represented in the model by [InsP6].

Phase \ Treatment	Phytate	Phytate + Phytase
Ba(cr)	-126.67	-126.40
$Ba(OH)_2:8H_2O(cr)$	-15.55	-15.28
$Ba_5H_2[InsP6]:16H_2O(s)$	5.10	6.69
$BaCl_2(cr)$	-9.52	-9.41
$BaCl_2:2H_2O(s)$	-6.89	-6.78
$BaCl_2:H_2O(s)$	-7.51	-7.39
$BaHPO_4(s)$	0.37	1.21
BaO(cr)	-39.73	-39.46
K(cr)	-63.63	-63.52
K(OH)(s)	-20.08	-19.98
$K_2O(s)$	-75.08	-74.86
$KH_2PO_4(cr)$	-3.27	-2.60
P(cr)	-134.48	-133.92
Sylvite (KCl)	-4.14	-4.11

Table G.16 Concentrations (mol/kg) of different groups of barium species across the simulations of different experiments. Species are grouped according to type of ligand, i.e., free barium (Ba^{2+}), phosphate complexes, phytate ([InsP6]) complexes, sulfate complexes, hydroxyl complexes.

Species \ Treatment	Phytate-only	Phytate + Phytase
Total barium	**4.99E-03**	**4.99E-03**
Ba^{2+}	4.98E-03	4.94E-03
$Ba(H_xPO4)_y^{(-3+x)y+2}$	7.26E-06	4.15E-05
$Ba_pH_q[InsP6]^{-12+2p+q}$	7.25E-06	1.06E-05
$Ba(OH)^+$	2.49E-11	3.53E-11

Geochemical modelling indicated that solution speciation for barium was dominated by the Ba^{2+} ion (table G.16). The calculated concentration of barium phosphate and barium phytate species increased by an order of magnitude following phytase treatment but was still two orders of magnitude lower than the concentration of Ba^{2+}.

Both simulations indicated supersaturation for barium phytate and barium hydrogen phosphate (table G.15). The saturation index of both phases increased following phytase treatment, which appears to be contradicted by the increase in soluble barium measured experimentally (figure 4.28).

The enhanced solubility of barium following phytase treatment may be due to the formation of soluble complexes between barium and the lower inositol phosphates produced during

phytate breakdown. Due to the lack of available thermodynamic data, this was not something that could be incorporated into the geochemical modelling. Alternatively, it may simply be an issue of barium phosphate being more soluble than barium phytate under the conditions tested or slow kinetics of barium phosphate precipitation. Ideally, additional controls with the direct addition of inorganic phosphate and with varying levels of phytate breakdown would be performed to investigate this further.

G.9 Lanthanum

Table G.17 Saturation indices for geochemical simulations of the different conditions and treatments tested for the lanthanum (represented in the model by a generic lanthanide (Ln)) experiments. Black numbers indicate supersaturated phases, red numbers indicate undersaturated phases.

Phase \ Treatment	Phytate-only	Phytate + Phytase	Inorganic phosphate	No phosphate
K(cr)	-63.67	-63.58	-63.98	-64.08
K(OH)(s)	-20.12	-20.03	-20.43	-20.53
K_2O(s)	-75.14	-74.97	-75.77	-75.97
KH_2PO_4(cr)	-3.38	-2.70	-2.59	n/a
Ln(cr)	-144.70	-145.00	-145.55	-143.27
$Ln(OH)_3$(am)	-5.68	-5.98	-6.53	-4.26
$Ln(OH)_3$(cr)	-3.54	-3.84	-4.39	-2.12
$Ln(PO_4).xH_2O$(s)	8.54	8.83	8.78	n/a
Ln_2O_3(cubic)	-28.55	-29.15	-30.25	-25.71
Ln_2O_3(monoclinic)	-29.62	-30.22	-31.32	-26.78
Ln_3O_4(s)	-75.90	-76.80	-78.46	-71.65
$LnCl(OH)_2$(s)	-4.76	-5.12	-5.37	-3.23
$LnCl_2$(s)	-33.06	-33.49	-33.43	-31.41
$LnCl_3$(s)	-30.46	-30.94	-30.59	-28.69
$LnCl_3:6H_2O$(s)	-15.95	-16.44	-16.08	-14.19
LnO(s)	-51.50	-51.81	-52.36	-50.08
LnOCl(s)	-11.44	-11.80	-12.05	-9.91
$LnPO_4.H_2O$(cr)	10.14	10.43	10.38	n/a
P(cr)	-134.57	-133.98	-133.47	n/a
Sylvite (KCl)	-3.94	-3.92	-4.01	-4.24

Table G.18 Concentrations (mol/kg) of different groups of lanthanum (represented in the model by a generic lanthanide (Ln)) species across the simulations of different experiments. Species are grouped according to type of ligand, i.e., free lanthanide (Ln^{3+}), phosphate complexes, phytate ([InsP6]) complexes, chloride complexes, hydroxyl complexes.

Species \ Treatment	Phytate-only	Phytate + Phytase	Inorganic phosphate	No phosphate
Total lanthanide (lanthanum)	**4.99E-03**	**4.99E-03**	**5.00E-03**	**5.00E-03**
Ln^{3+}	2.85E-04	5.95E-05	6.52E-05	4.88E-03
$Ln(H_xPO4)_y^{3+(x-3)y}$	1.05E-03	3.53E-03	4.93E-03	0.00E+00
$LnH_q[InsP6]^{-12+3+q}$	3.65E-03	1.40E-03	0.00E+00	0.00E+00
$LnCl_j^{3-j}$	3.38E-06	8.89E-07	1.40E-06	1.07E-04
$Ln(OH)_k^{3-k}$	3.36E-07	1.02E-07	7.96E-08	8.17E-06

Geochemical modelling showed that for the phytate-only and phytate + phytase treatments, lanthanum speciation was dominated by phytate and phosphate complexes (table G.18). The model calculated that in the phytate-only treatment, around 70% of lanthanum was associated with phytate and around 20% associated with inorganic phosphate. Following phytase treatment, the reverse trend was apparent, with around 70% of lanthanum associated with inorganic phosphate and around 30% associated with phytate. In the no phosphate treatment close to 100% of lanthanum was present as free La^{3+} while in the inorganic phosphate treatment around 100% of lanthanum was present as lanthanum phosphate complexes.

The geochemical model also indicated that all phases were undersaturated in the no phosphate treatment, while for the other three treatments, the only supersaturated phases were hydrated lanthanum phosphates (table G.17). The saturation indices for the lanthanum phosphate phases were similar for the phytate-only, phytate + phytase, and inorganic phosphate treatments. Solubility data for lanthanum phytate could not be found, so the model used is incomplete, but it can be assumed that lanthanum phytate solids would be supersaturated under the conditions tested.

G.10 Lead

Table G.19 Saturation indices for geochemical simulations of the different treatments tested for the lead experiments. Black numbers indicate supersaturated phases, red numbers indicate undersaturated phases.

Phase \ Treatment	Phytate-only	Phytate + Phytase	Inorganic phosphate	No phosphate
K(cr)	-63.78	-63.66	-63.79	-64.06
$K(NO_3)(s)$	-3.22	-3.19	-3.22	-3.45
K(OH)(s)	-20.24	-20.12	-20.25	-20.52
$K_2O(s)$	-75.38	-75.14	-75.40	-75.94
$KH_2PO_4(cr)$	-3.31	-2.63	-2.49	n/a
Litharge (PbO)	-4.67	-4.41	-4.46	-4.28
Massicot (PbO)	-4.78	-4.52	-4.57	-4.39
Minimum (Pb_3O_4)	-12.33	-11.56	-11.70	-11.16
P(cr)	-134.37	-133.81	-133.55	n/a
Pb(cr)	-33.60	-33.35	-33.40	-33.21
$Pb(H_2PO_4)_2(cr)$	1.71	3.09	3.57	n/a
$Pb(HPO_4)(s)$	4.17	4.99	5.20	n/a
$Pb(OH)_2(s)$	-5.55	-5.29	-5.34	-5.16
$Pb_3(PO_4)_2(s)$	13.05	14.95	15.34	n/a
$Pb_4O(PO_4)_2(cr)$	13.51	15.67	16.01	n/a
Plattnerite (PbO_2)	-4.32	-4.07	-4.11	-3.93
Pyromorphite-OH ($Pb_{10}(PO_4)_6(OH)_2$)	19.82	22.80	23.35	n/a

Table G.20 Concentrations (mol/kg) of different groups of lead species across the simulations of different experiments. Species are grouped according to type of ligand, i.e., free lead (Pb^{2+}), phosphate complexes, phytate ([InsP6]) complexes, nitrate complexes, hydroxyl complexes.

Species \ Treatment	Phytate-only	Phytate + Phytase	Inorganic phosphate	No phosphate
Total lead	**5.00E-03**	**5.00E-03**	**5.00E-03**	**5.00E-03**
Pb^{2+}	3.36E-03	3.02E-03	3.14E-03	4.74E-03
$Pb(H_xPO_4)^{2+(x-3)}$	1.75E-04	9.69E-04	1.71E-03	0.00E+00
$PbH_q[InsP6]^{-12+2+q}$	1.35E-03	8.88E-04	0.00E+00	0.00E+00
$Pb(NO_3)_j^{2-j}$	9.49E-05	1.04E-04	1.31E-04	2.29E-04
$Pb_m(OH)_n^{2m-n}$	1.24E-05	1.65E-05	1.67E-05	2.64E-05

Geochemical modelling indicated that the most abundant lead species in solution across all simulations was free Pb^{2+}, which was calculate to comprise around 60–70% of lead in the presence of phosphate/phytate and around 95% in the no phosphate treatment (table G.20). In the phytate-only treatment, lead phytate complexes accounted for around 25% of lead, with around 5% of lead associated with inorganic phosphate. Following phytase treatment, lead phytate and lead phosphate complexes each accounted for around 20% of lead. For the inorganic phosphate treatment, lead phosphate complexes were calculated to comprise around 35% of lead in solution.

The geochemical model also indicated that all solid phases were undersaturated in the no phosphate treatment (table G.19). In the treatments where phosphate was present, multiple lead phosphates were supersaturated, with pyromorphite-OH calculated to have the highest saturation index across all simulations. The phytate-only treatment was calculated to have slightly lower saturation indices for the lead phosphate phases than the phytate + phytase and inorganic phosphate treatments which is consistent with the lower lead removal achieved in this treatment (figure 4.38). A lack of solubility product data meant that saturation indices for lead phytate solids could not be calculated but it is likely that lead phytate is supersaturated under the conditions tested.

Appendix G References

1. Singh SS. Neutralization of dilute aqueous aluminium sulfate solutions with a base. Canadian Journal of Chemistry. 1969 Feb 15;47(4):663–7.

2. Adams F, Rawajfih Z. Basaluminite and Alunite: A Possible Cause of Sulfate Retention by Acid Soils. Soil Science Society of America Journal. 1977;41(4):686.

3. Bigham JM, Nordstrom DK. Iron and Aluminum Hydroxysulfates from Acid Sulfate Waters. Reviews in Mineralogy and Geochemistry. 2000 Jan 1;40(1):351–403.

4. Hammarstrom JM, Seal RR, Meier AL, Kornfeld JM. Secondary sulfate minerals associated with acid drainage in the eastern US: recycling of metals and acidity in surficial environments. Chemical Geology. 2005 Feb;215(1–4):407–31.

5. Van Der Houwen JAM, Valsami-Jones E. The Application of Calcium Phosphate Precipitation Chemistry to Phosphorus Recovery: The Influence of Organic Ligands. Environmental Technology. 2001 Nov;22(11):1325–35.

6. Amjad Z, Koutsoukos PG, Nancollas GH. The crystallization of fluoroapatite. A constant composition study. Journal of Colloid and Interface Science. 1981 Aug 1;82(2):394–400.

7. Nancollas GH. The Nucleation and Growth of Phosphate Minerals. In: Nriagu JO, Moore PB, editors. Phosphate Minerals [Internet]. Berlin, Heidelberg: Springer; 1984 [cited 2020 Mar 18]. p. 137–54. Available from: https://doi.org/10.1007/978-3-642-61736-2_2

8. Posner AS, Blumenthal NC, Betts F. Chemistry and Structure of Precipitated Hydroxyapatites. In: Nriagu JO, Moore PB, editors. Phosphate Minerals [Internet]. Berlin, Heidelberg: Springer; 1984 [cited 2020 Feb 26]. p. 330–50. Available from: https://doi.org/10.1007/978-3-642-61736-2_11

9. Amjad Z. Constant composition study of crystal growth of dicalcium phosphate dihydrate. The influence of polyphosphates, phosphonates, and phytate. Canadian Journal of Chemistry. 1988 Sep;66(9):2181–7.

10. Pinto AJ, Ruiz-Agudo E, Putnis CV, Putnis A, Jimenez A, Prieto M. AFM study of the epitaxial growth of brushite (CaHPO4{middle dot}2H2O) on gypsum cleavage surfaces. American Mineralogist. 2010 Nov 1;95(11–12):1747–57.

11. Mekmene O, Quillard S, Rouillon T, Bouler J-M, Piot M, Gaucheron F. Effects of pH and Ca/P molar ratio on the quantity and crystalline structure of calcium phosphates obtained from aqueous solutions. Dairy Science and Technology. 2009 May;89(3–4):301–16.

12. Dorozhkin SV. Calcium orthophosphates: Occurrence, properties, biomineralization, pathological calcification and biomimetic applications. Biomatter. 2011 Oct;1(2):121–64.

13. Van Den Berg CJ, Hill LF, Stanbury SW. Inositol Phosphates and Phytic Acid as Inhibitors of Biological Calcification in the Rat. Clinical Science. 1972 Sep 1;43(3):377–83.

14. Koutsoukos PG, Amjad Z, Nancollas GH. The influence of phytate and phosphonate on the crystal growth of fluorapatite and hydroxyapatite. Journal of Colloid and Interface Science. 1981 Oct;83(2):599–605.

15. Graf E, Empson KL, Eaton JW. Phytic acid. A natural antioxidant. J Biol Chem. 1987 Aug 25;262(24):11647–50.

16. Evans WJ, Martin CJ. The heat of complex formation of copper(II) with phytic acid. Journal of Inorganic Biochemistry. 1987 Nov 1;31(3):155–60.

Appendix H
Scanning Electron Microscope images

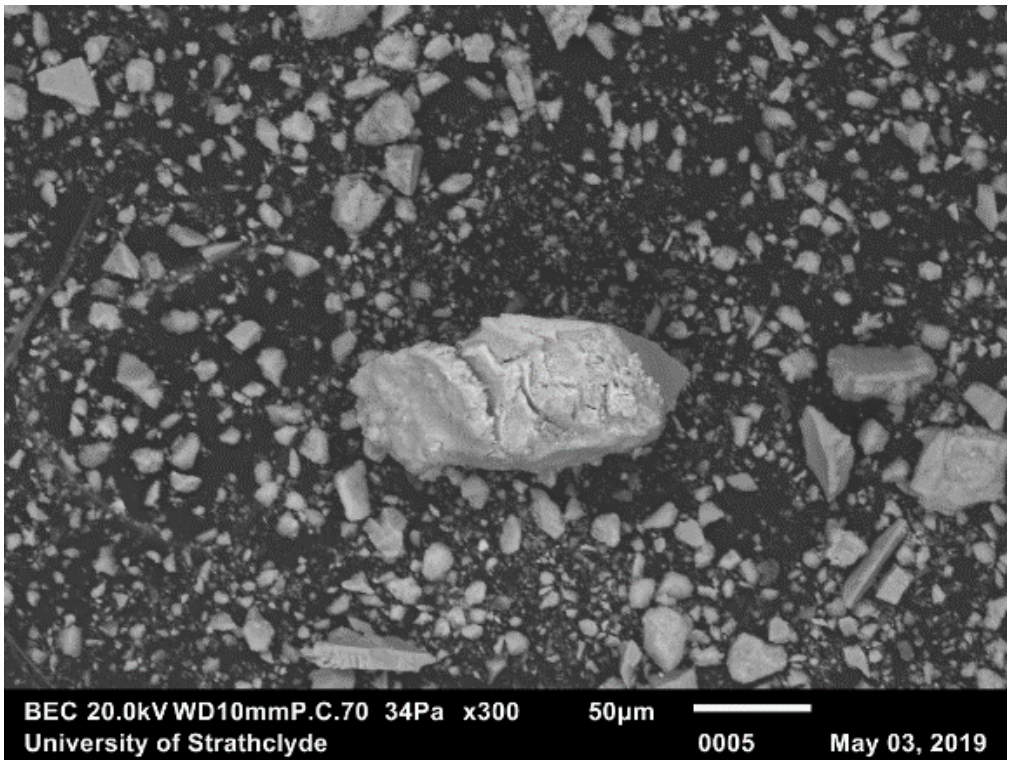

Figure H.1 Image of a phytate-only sample (non-carbon coated sample).

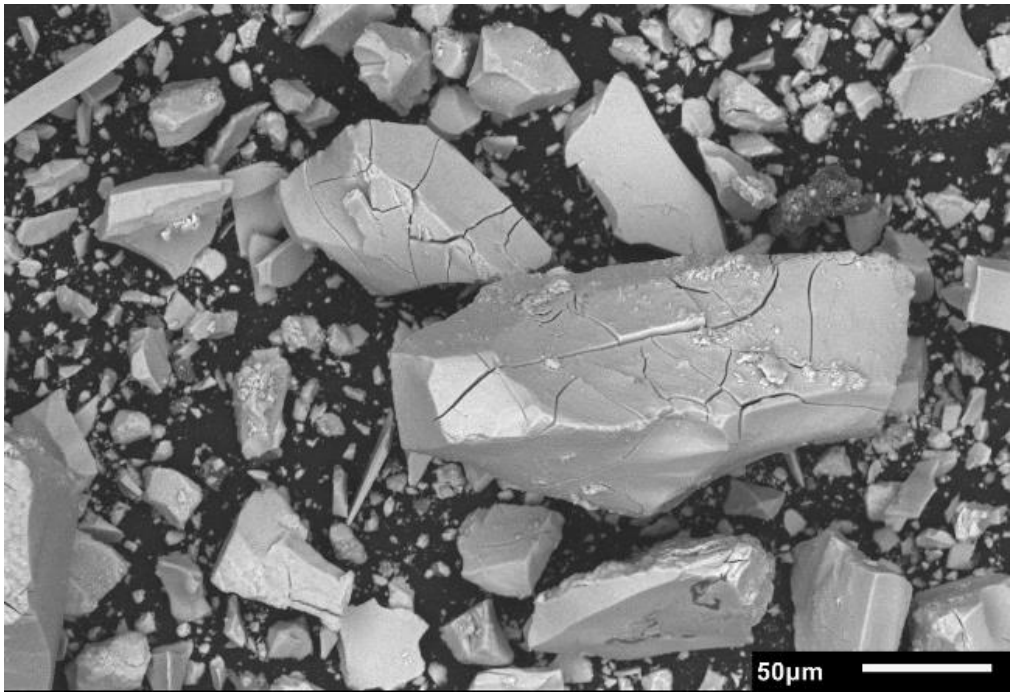

Figure H.2 Image of a sample from the phytate + phytase treatment (non-carbon coated sample).

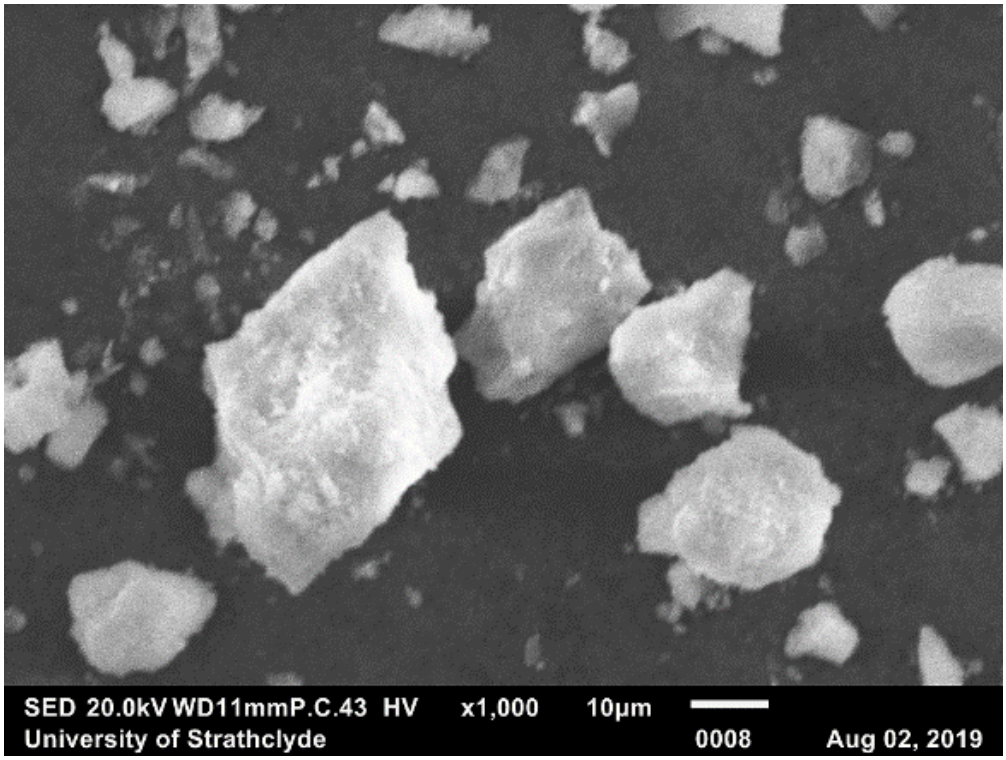

Figure H.3 Image of a phytate-only sample (carbon coated sample).

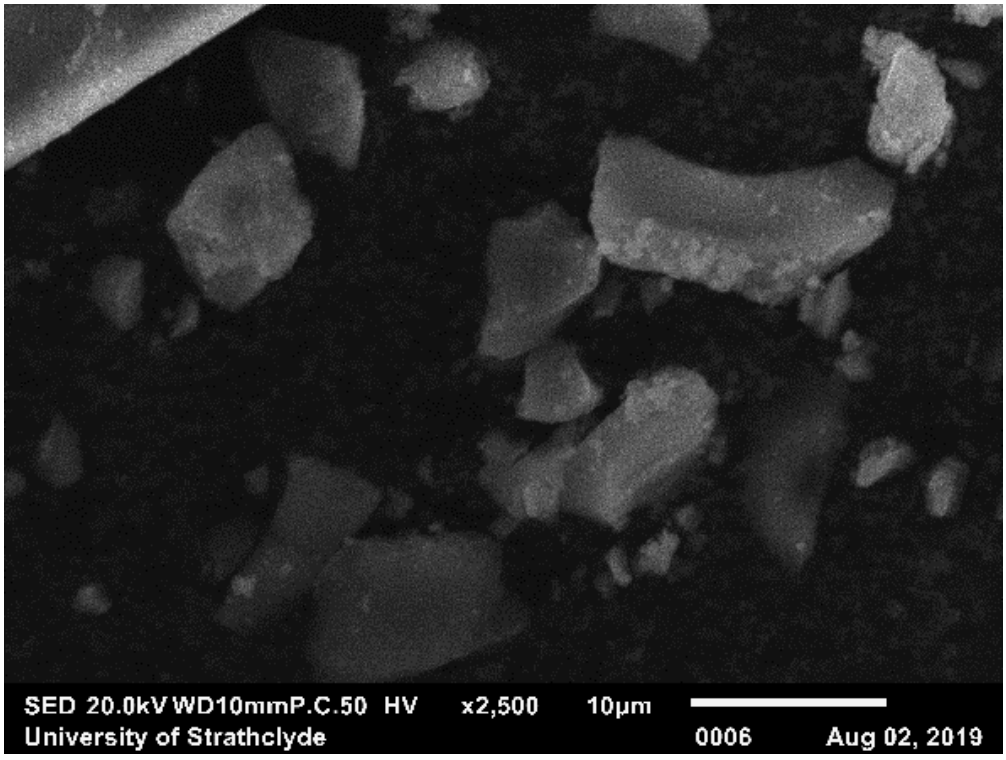

Figure H.4 Image of a sample from the phytate + phytase treatment (carbon coated sample).

Appendix I
Transmission Electron Microscope diffractograms

In chapter 4, lanthanum-containing materials produced by the precipitation of lanthanum with phytate (the phytate-only treatment) or phytate hydrolysed by phytase (the phytate + phytase treatment) were investigated by transmission electron microscopy (TEM). Where X-ray diffraction (XRD) had indicated that both materials were amorphous, TEM was informative as it indicated that the material produced in the phytate + phytase treatment was polynanocrystalline, while the material produced in the phytate-only treatment was mostly amorphous interspersed with small regions of crystalline material. To investigate the identity of the crystalline material(s) present Fast Fourier Transform (FFT) generated diffractograms were produced from selected areas in the TEM images. These diffractograms were used to calculate d-spacings for the precipitated material which could be compared to the d-spacings of possible phases, while the diffractograms were compared to simulated electron diffraction patterns for possible phases.

I.1 Methodology

TEM images were examined for regions that appeared to correspond to individual nanocrystals, and these areas used to generate diffractograms using the FFT function of the Fiji distribution (1) of ImageJ (2). In total, 15 areas from the phytate + phytase treatment and 6 areas from the phytate-only treatment samples were investigated.

The SingleCrystal® 4 software (3) was used to aid the interpretation of diffractograms and to generate simulated electron diffraction patterns. Electron diffraction patterns were generated using .cif files downloaded from the Inorganic Crystal Structure Database (ICSD) (4). For rhabdophane ($LaPO_4.0.667H_2O$), the ICSD record represents the data for rhabdophane-Sm (ICSD #194481) reported by Mesbah *et al.* (5). Therefore, the lattice parameters were edited using the VESTA software (6) to match the values for rhabdophane-La provided in the publication by Mesbah *et al.* (5). For some other phases investigated, data for lanthanum-containing forms could not be found, so phases containing other REEs were used as analogues in these cases.

I.2 Possible phases

Previous research into rare earth (REE) phosphates precipitated at ambient temperatures has indicated that rhabdophane is the most likely crystalline phase to form for the light REEs such as lanthanum (7–9), and the FTIR (figure 4.34) and ^{31}P NMR (figure F.4, figure F.5) analysis in this work showed similarities to previously reported spectra for rhabdophane. However, these analyses were not conclusive, and it could not be discounted that a different phosphate phase or a non-phosphate phase was present instead of or alongside rhabdophane. Therefore, the ICSD was examined for possible alternate phases.

Phases requiring reducing conditions to form (e.g. phosphites, phosphides, hydrides) were not considered as this work was conducted under aerobic conditions without any strong reducing agents present.

There are four main crystalline forms described for the 1:1 REE orthophosphate ($REEPO_4.xH_2O$) minerals: rhabdophane, monazite, churchite/weinschenkite, and xenotime. Monazite ($LaPO_4$), as well as dehydrated forms of rhabdophane, were considered unlikely as they require elevated temperatures (≥ 100 °C) to form (5,8,10–14). Additionally, unlike the material produced in this work (table I.2), monazite has no d-spacings larger than 0.6 nm. Churchite and xenotime preferentially incorporate heavy REEs (yttrium and terbium–lutetium) so lanthanum forms of these minerals are unlikely (10,12,15); their d-spacings also do not match up with those reported here.

ICP-OES (table 4.8) and EDX (figure 4.32) analysis indicated the presence of potassium in the precipitate, while ICP-OES (but not EDX) indicated the possible presence of magnesium. Therefore, the ICSD was also searched for phases containing alkali and alkaline earth metals. The phases found ($K_3La(PO_4)_2$, $Na_7Mg_{13}Eu(PO_4)_{12}$, $Sr_3La(PO_4)_3$, and $Ca_9La(PO_4)_7$) all contain an excess of the alkali or alkaline earth metal to the REE which makes them (or the potassium, magnesium, and lanthanum-containing analogues) unlikely. These phases were also all formed at high (> 1,000 °C) temperatures (16–20), and FTIR spectra of $Rb_3La(PO_4)_2$ (21) and $K_3Nd(PO_4)_2$ (22) (both structurally similar to $K_3La(PO_4)_2$) and $Ca_9La(PO_4)_7$ (20) were different to the FTIR spectra reported in this work. It is possible that similar phases formed as impurities alongside the bulk precipitates, but considering that the amounts of precipitated potassium and magnesium appeared to decrease in the phytate + phytase treatment compared to the

phytate-only treatment, it is more likely that these elements were mostly associated with the organic phosphate in the system.

Condensed phosphates, including $NaLaP_2O_7$, $La(HP_2O_7).3H_2O$, $KLa(P_4O_{12})$, $KLa(PO_3)_4$, were also considered but could be ruled by comparing published FTIR and/or ^{31}P NMR spectra to the spectra reported in this work (23–26). These materials are also typically prepared at high temperatures (> 300 °C) (23,25,26) or from appropriate condensed phosphate precursors (24). Note that there is a report of the phase $La_7P_3O_{18}$ forming under ambient conditions from an orthophosphate (PO_4) precursor (27), but detailed research into this phase has indicated that it only forms at temperatures above 1,200 °C (28,29), so this was likely a misidentification. $La_7P_3O_{18}$ does, in fact, have similar d-spacings to rhabdophane (29), which is the more likely phase to form under ambient conditions.

Due to the lack of any precipitation in the no phosphate treatment (figure 4.30, figure 4.31), non-phosphate containing solids were unlikely to form under the conditions tested, but it was considered that their formation might be possible if the bulk phytate/phosphate solids acted as nucleation points. The d-spacings of lanthana (La_2O_3), lanthanum hydroxide ($La(OH)_3$), and lanthanum oxyhydroxide (LaOOH) could be used to rule these materials out. The picture for carbonate phases was less clear-cut, however. No carbonate was deliberately added to the experimental solutions, but as the experiments were conducted under atmospheric conditions with no attempt made to purge the system of CO_2 it is possible that this led to the formation of carbonate-containing impurities.

Table I.1 Saturation indices for selected phases when including atmospheric CO_2 in geochemical modelling. Black numbers indicate supersaturated phases, red numbers indicate undersaturated phases. N/a indicates that one or more of the elements in a particular phase was not present in a particular model. Ln is a generic representation of lanthanum/REEs.

Phase \ Treatment	Phytate-only	Phytate + Phytase	Inorganic phosphate	No Phosphate
$Ln(OH)_3$(am)	-5.68	-5.98	-6.53	-4.26
$Ln(OH)_3$(cr)	-3.54	-3.84	-4.39	-2.12
$Ln(PO_4).xH_2O$(s)	8.54	8.83	8.78	n/a
Ln_2O_3(cubic)	-28.55	-29.15	-30.25	-25.71
Ln_2O_3(monoclinic)	-29.62	-30.22	-31.32	-26.78
$LnPO_4.H_2O$(cr)	10.14	10.43	10.38	n/a
K_2CO_3(cr)	-17.99	-17.82	-18.62	-18.82
Kalicinite ($KHCO_3$)	-7.01	-6.92	-7.32	-7.42
$Ln(CO_3)(OH)$(cr)	0.0044	-0.30	-0.85	1.42
$Ln(CO_3)(OH)$:0.5H2O(s)	-1.83	-2.13	-2.68	-0.41
$Ln_2(CO_3)_3.3H_2O$(s)	-5.81	-6.41	-7.51	-2.97

To test the likelihood of carbonate phases forming, geochemical modelling with PHREEQC was performed as per chapter 4 and appendix G but with atmospheric CO_2 included in the model (using the equilibrium phases keyword data block and a log partial pressure value for CO_2 of -3.4, based upon an atmospheric CO_2 concentration of ~ 410 ppm (30,31)). Results indicated that the phase $Ln(CO_3)(OH)$ (equivalent to the mineral hydroxylbastnäsite) was supersaturated in the no phosphate and phytate-only treatments (table I.1). Although these saturation indices were low, and the phase became undersaturated in the phytate + phytase treatment, and no precipitation was observed in the no phosphate treatment, the results do confirm that the most likely impurity phases to occur would be (hydroxy)carbonates.

The ICSD contains four REE carbonate phases: hydroxylbastnäsite ($Ce(CO_3)(OH)$), kozoite ($Nd(CO_3)(OH)$), lanthanite ($La_2(CO_3)_3.8H_2O$), and tengerite ($Y_2(CO_3)_3.2–3H_2O$). Kozoite could be ruled out as it has no d-spacings larger than 0.55 nm. However, the other three phases were plausible matches for the observed d-spacings (table I.2). The excess of phosphorus to carbon in the precipitate as shown by chemical (table 4.8) and EDX (figure 4.32) analyses shows that the bulk material was not a carbonate phase, but carbonates may have been present as impurities. However, while CHN and EDX data confirm that carbon was present in the precipitates, a large proportion of this would be assumed to be associated with the phytate molecule or lower inositol phosphates that precipitated. Therefore, further work to quantify the distribution of carbon between organic and inorganic forms would be required to demonstrate whether any carbonate actually precipitated alongside the bulk lanthanum phosphate/phytate.

I.3 Results

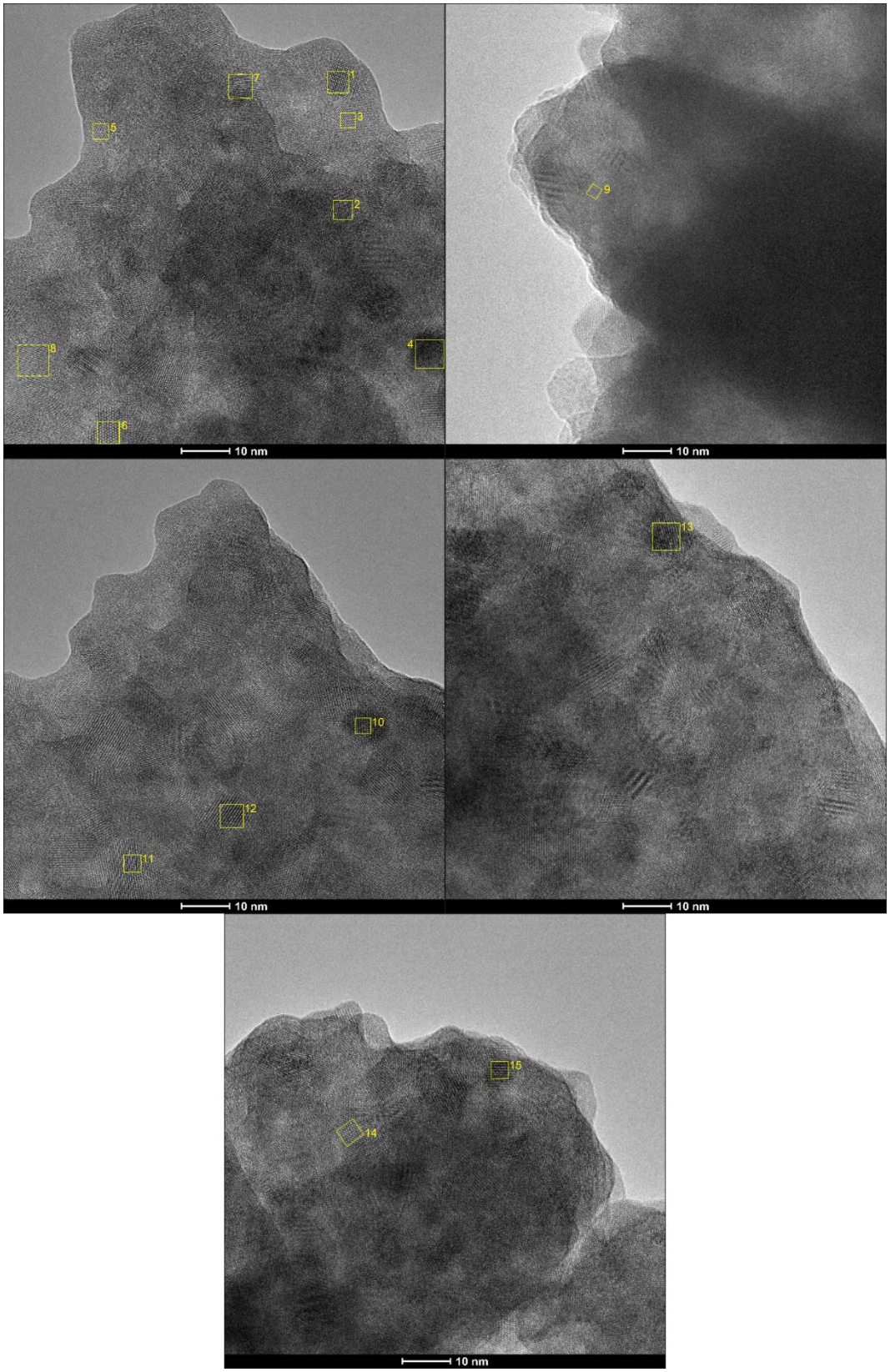

Figure I.1 TEM images of the sample from the phytate + phytase treatment showing areas used for the FFT generation of diffractograms.

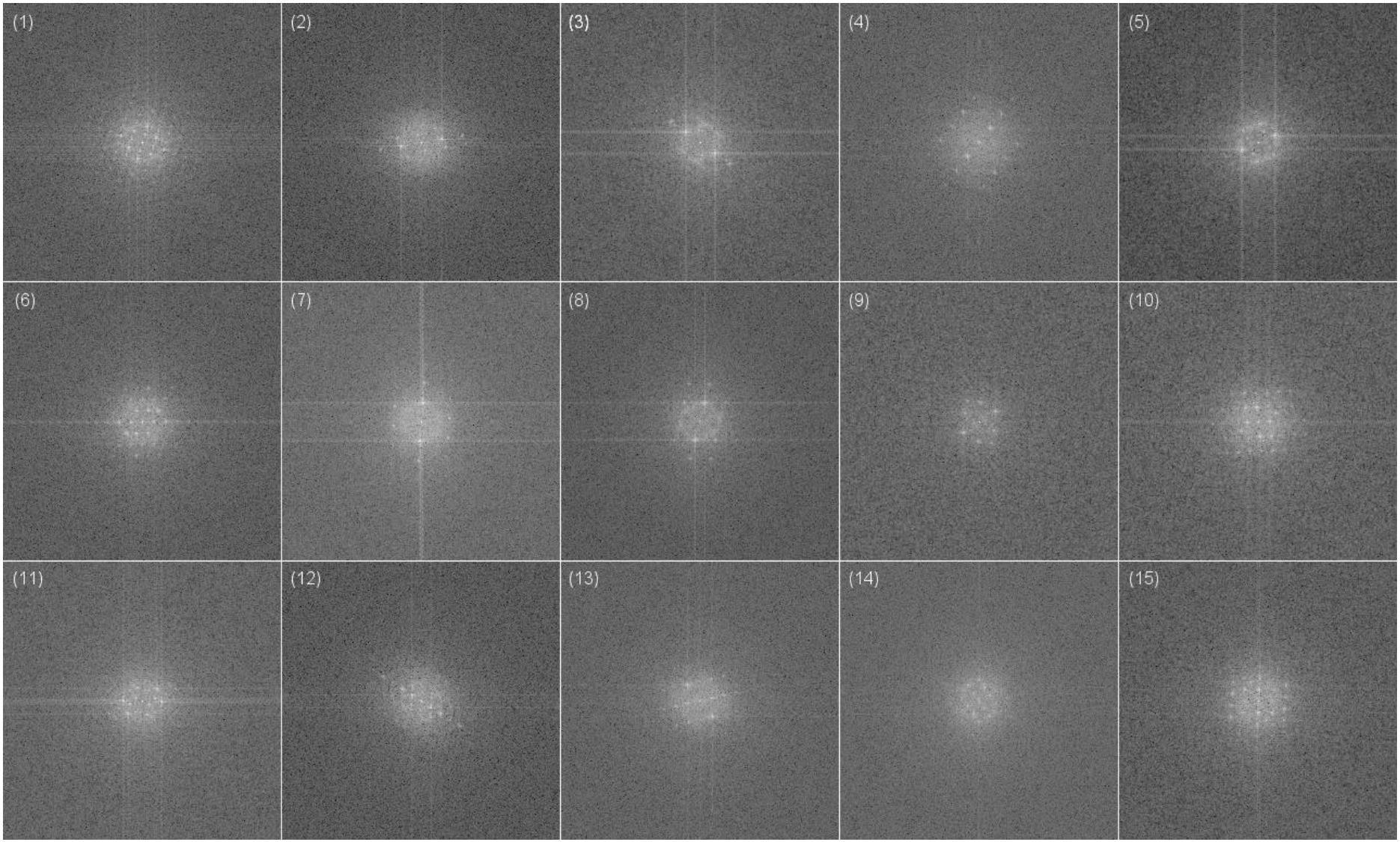

Figure I.2 FFT-generated diffractograms, corresponding to the areas indicated in figure I.1.

Figure I.1 shows the areas of the TEM images of the phytate + phytase treatment sample selected for the generation of the diffractograms shown in figure I.2. The d-spacings measured in each diffractogram were collated into a single list of d-spacings for the material shown in table I.2.

Table I.2 Measured d-spacings for the samples and reported d-spacings for possible phases in the ICSD. D-spacings larger than 1 nm or smaller than 0.25 nm are not listed.

Phytate-only	**Phytate + Phytase**	Rhabdophane-La ($LaPO_4.0.667H_2O$)	Lanthanite ($La(CO_3)_3.8H_2O$)	Hydroxylbastnäsite ($Ce(CO_3)(OH)$)	Tengerite ($Y_2(CO_3)_3.2–3H_2O$)
	ICSD code	194481	22224	238537	72940
d-spacing (nm)					
			0.85		
	0.82				
					0.76
				0.73	
0.72	**0.72**				
		0.71			
0.69		0.69			
0.68					
	0.67				
			0.66		
		0.65			
	0.64		0.64		
			0.62	0.62	
	0.61	0.62	0.61		
0.58	**0.58**				
		0.56			0.56
		0.55			
0.54				0.54	
	0.53			0.53	
0.52			0.52		
	0.51				
	0.5			0.50	
	0.49				
0.48		0.48	0.48		0.48
	0.47			0.47	
		0.46			0.46
	0.45	0.45	0.45	0.45	
	0.44				
	0.43	0.43			
0.42	**0.42**	0.42	0.42		
	0.41	0.41	0.41	0.41	
			0.40		
			0.39	0.39	0.39
			0.38	0.38	0.38
		0.37	0.37	0.37	
	0.36	0.36	0.36	0.36	0.36
0.35	**0.35**	0.35			
0.34	**0.34**	0.34	0.34	0.34	
	0.33	0.33	0.33	0.33	
0.32	**0.32**	0.32	0.32	0.32	
0.31	**0.31**	0.31	0.31	0.31	
0.3	**0.30**	0.30	0.30	0.30	0.30
0.29	**0.29**	0.29	0.29	0.29	0.29
0.28		0.28	0.28	0.28	0.28
0.27		0.27	0.27	0.27	0.27
0.26	**0.26**	0.26	0.26	0.26	0.26
0.25	**0.25**	0.25	0.25	0.25	0.25

The error margins of d-spacings measured from small areas may be as much as ~ 10% (32,33). Considering this, every measured d-spacing was within 10% of a d-spacing associated with rhabdophane except for the d-spacing at 0.82 nm, which was a better match for either lanthanite or tengerite (table I.2). The 0.82 nm d-spacing was only present in one diffractogram (from area 11) which may indicate it was associated with an impurity, such as one of the carbonate phases.

The phytate-only sample was mostly amorphous, but some crystalline regions were present. Diffractograms generated from these regions indicated that these regions together had a similar set of d-spacings to the phytate + phytase sample (table I.2) suggesting that the crystalline phase present in both samples was the same.

Table I.3 Best fits between simulated electron diffraction patterns and measured diffractograms for possible phases calculated using the auto-index feature of the SingleCrystal® 4 software. Σs^2 is a parameter describing how well the simulated electron diffraction pattern matches a grid overlaying the measured diffractogram (a smaller number corresponds to a better fit).

Phase \ Area	**1**		
	Viewing direction	Σs^2	Visual assessment
Rhabdophane	[1 3 1]	0.6267	Reasonable
Lanthanite	[-4 -2 1]	0.2046	Bad
Hydroxylbastnäsite	[-5 4 1 1]	0.4948	Bad
Tengerite	[1 -1 0]	1.374	Bad
Phase \ Area	**2**		
	Viewing direction	Σs^2	Visual assessment
Rhabdophane	[-1 1 3]	0.0555	Reasonable
Lanthanite	[6 -2 3]	0.2112	Reasonable
Hydroxylbastnäsite	[-3 3 0 7]	0.1115	Reasonable
Tengerite	[1 -2 0]	1.164	Bad
Phase \ Area	**3**		
	Viewing direction	Σs^2	Visual assessment
Rhabdophane	[-3 7 2]	0.2111	Reasonable
Lanthanite	[7 1 2]	0.8888	Bad
Hydroxylbastnäsite	[-4 -1 5 6]	0.7433	Reasonable
Tengerite	[-3 4 1]	1.9265	Bad
Phase \ Area	**4**		
	Viewing direction	Σs^2	Visual assessment
Rhabdophane	[-4 -2 7]	0.0797	Reasonable
Lanthanite	[7 8 9]	4.4849	Bad
Hydroxylbastnäsite	[-23 22 1 9]	1.9194	Bad
Tengerite	[-8 3 2]	0.8516	Reasonable
Phase \ Area	**5**		
	Viewing direction	Σs^2	Visual assessment
Rhabdophane	[1 1 1]	0.1313	Bad
Lanthanite	[-1 1 2]	0.0323	Bad
Hydroxylbastnäsite	[-3 0 3 2]	0.4202	Bad
Tengerite	[-1 0 1]	1.4283	Bad
Phase \ Area	**6**		
	Viewing direction	Σs^2	Visual assessment
Rhabdophane	[-1 3 1]	0.3335	Reasonable
Lanthanite	[3 1 2]	0.9765	Bad
Hydroxylbastnäsite	[2 5 -7 2]	0.2096	Reasonable
Tengerite	[1 2 1]	1.7259	Bad

Table I.3 (continued).

Phase \ Area	**7**		
	Viewing direction	Σs^2	Visual assessment
Rhabdophane	[-4 -1 6]	0.2761	Reasonable
Lanthanite	[8 5 9]	4.7252	Bad
Hydroxylbastnäsite	[-25 26 -1 5]	0.5919	Reasonable
Tengerite	[-5 -8 7]	0.9643	Reasonable
Phase \ Area	**8**		
	Viewing direction	Σs^2	Visual assessment
Rhabdophane	[-2 7 6]	0.091	Reasonable
Lanthanite	[-4 3 9]	0.15	Bad
Hydroxylbastnäsite	[-20 19 1 4]	0.0389	Reasonable
Tengerite	[-3 -6 5]	0.9095	Reasonable
Phase \ Area	**9**		
	Viewing direction	Σs^2	Visual assessment
Rhabdophane	[1 8 3]	0.8139	Reasonable
Lanthanite	[-2 -5 4]	0.1652	Bad
Hydroxylbastnäsite	[-11 7 4 3]	0.3682	Reasonable
Tengerite	[3 -1 1]	0.7252	Reasonable
Phase \ Area	**10**		
	Viewing direction	Σs^2	Visual assessment
Rhabdophane	[3 -9 2]	0.2629	Reasonable
Lanthanite	[5 1 3]	0.0242	Bad
Hydroxylbastnäsite	[6 -9 3 3]	0.328	Reasonable
Tengerite	[1 1 1]	0.8282	Reasonable
Phase \ Area	**11**		
	Viewing direction	Σs^2	Visual assessment
Rhabdophane	[3 4 4]	0.1446	Bad
Lanthanite	[-1 2 6]	0.2469	Bad
Hydroxylbastnäsite	[-8 -2 10 7]	0.2324	Bad
Tengerite	[-5 1 1]	2.4287	Bad
Phase \ Area	**12**		
	Viewing direction	Σs^2	Visual assessment
Rhabdophane	[1 -2 1]	0.3055	Reasonable
Lanthanite	[-2 -3 1]	0.658	Bad
Hydroxylbastnäsite	[-3 3 0 3]	0.0578	Reasonable
Tengerite	[0 1 0]	0.8334	Reasonable
Phase \ Area	**13**		
	Viewing direction	Σs^2	Visual assessment
Rhabdophane	[-1 2 5]	0.2856	Reasonable
Lanthanite	[9 1 3]	0.1317	Bad
Hydroxylbastnäsite	[-3 -9 12 4]	0.0381	Reasonable
Tengerite	[-5 -2 3]	0.4409	Bad
Phase \ Area	**14**		
	Viewing direction	Σs^2	Visual assessment
Rhabdophane	[-1 -5 4]	0.0057	Reasonable
Lanthanite	[-4 -1 2]	0.1145	Bad
Hydroxylbastnäsite	[0 3 -3 4]	0.737	Bad
Tengerite	[-3 -2 1]	0.5242	Bad
Phase \ Area	**15**		
	Viewing direction	Σs^2	Visual assessment
Rhabdophane	[2 4 3]	0.7946	Reasonable
Lanthanite	[5 -1 3]	0.322	Reasonable
Hydroxylbastnäsite	[7 4 -11 2]	0.1196	Reasonable
Tengerite	[-3 4 1]	0.9681	Bad

To investigate further whether the measured diffractograms could be matched to any of the possible phases, the auto-index feature of SingleCrystal® 4 was used to calculate a best fit between simulated electron diffraction patterns and the diffractograms. To compare the fits for different phases, the Σs^2 parameter calculated by the software (smaller number = better

fit) and visual assessments were compared. Rhabdophane could be considered a reasonable match for every area examined apart from areas 5 and 11, which no satisfactory match could be found for. In contrast, hydroxylbastnäsite was a reasonable match for 10 areas, lanthanite was reasonable match for 2 areas, and tengerite was a reasonable match for 6.

The fact that rhabdophane matched with more of the generated diffractograms than the other phases investigated indicate that it is the best match for the material present in the phytate + phytase treatment. This, combined with what is known about the sample (a solid consisting predominantly of lanthanum and phosphate), along with the pre-existing knowledge of lanthanum phosphate crystal chemistry (that rhabdophane is the most likely mineral to form under ambient conditions), FTIR and ^{31}P NMR analyses (showing similarity to previous reports of rhabdophane) it is highly likely that rhabdophane was the phase formed in this work. Further work would be required to confirm this unambiguously, and it would be of interest to make comparisons with well defined reference materials and to study the influence of phytate on the electron diffraction patterns of rhabdophane. Additionally, a further factor to consider would be the potential influence of electron beam damage on the samples. Research into amorphous REE carbonates has shown that crystalline transformation products can be formed after a few seconds of exposure to the electron beam during TEM analysis (34). Hypothetically, a similar process could have occurred in this work if the electron beam induced the degradation of the organic phytate molecule. This may be visible in figure I.3, where two TEM images of the same area of the phytate-only treatment sample appear to show an increased amount of crystalline material (indicated by arrows) in figure I.3b which was recorded subsequent to figure I.3a. As these images were recorded at different zoom levels, the effect may be an artifact of recording the images under slightly different conditions, but figure I.3 does indicate that electron beam damage is a factor that should be controlled for in future work imaging this system.

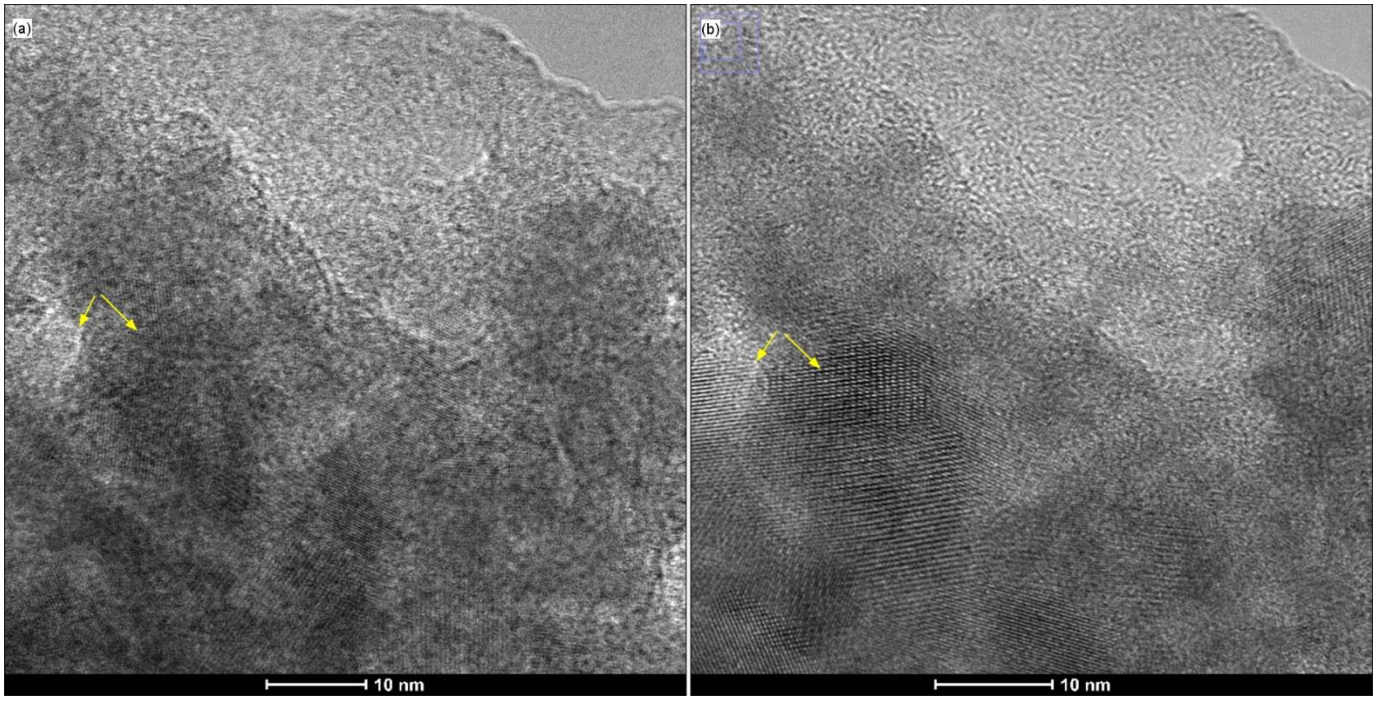

Figure I.3 Two TEM images of the same region of the phytate-only sample. Image (a) was recorded first, followed by image (b).

Appendix I References

1. Schindelin J, Arganda-Carreras I, Frise E, Kaynig V, Longair M, Pietzsch T, et al. Fiji: an open-source platform for biological-image analysis. Nature Methods. 2012 Jul;9(7):676–82.

2. Rueden CT, Schindelin J, Hiner MC, DeZonia BE, Walter AE, Arena ET, et al. ImageJ2: ImageJ for the next generation of scientific image data. BMC Bioinformatics [Internet]. 2017 Dec [cited 2019 May 27];18(1). Available from: https://bmcbioinformatics.biomedcentral.com/articles/10.1186/s12859-017-1934-z

3. Palmer DC. SingleCrystal 4: real-time multi-phase diffraction simulation. J Appl Cryst. 2020 Jun 1;53(3):860–860.

4. Inorganic Crystal Structure Database (ICSD) | Physical Sciences Data science Service [Internet]. [cited 2019 Nov 22]. Available from: https://www.psds.ac.uk/icsd

5. Mesbah A, Clavier N, Elkaim E, Gausse C, Kacem IB, Szenknect S, et al. Monoclinic Form of the Rhabdophane Compounds: $REEPO_4 \cdot 0.667H_2O$. Crystal Growth & Design. 2014 Oct;14(10):5090–8.

6. Momma K, Izumi F. *VESTA 3* for three-dimensional visualization of crystal, volumetric and morphology data. J Appl Crystallogr. 2011 Dec 1;44(6):1272–6.

7. Lucas S, Champion E, Bregiroux D, Bernache-Assollant D, Audubert F. Rare earth phosphate powders RePO4·nH2O (Re=La, Ce or Y)—Part I. Synthesis and characterization. Journal of Solid State Chemistry. 2004 Apr;177(4–5):1302–11.

8. Roncal-Herrero T, Rodríguez-Blanco JD, Oelkers EH, Benning LG. The direct precipitation of rhabdophane (REEPO4·nH2O) nano-rods from acidic aqueous solutions at 5–100 °C. Journal of Nanoparticle Research. 2011 Sep;13(9):4049–62.

9. Ochiai A, Utsunomiya S. Crystal Chemistry and Stability of Hydrated Rare-Earth Phosphates Formed at Room Temperature. Minerals. 2017 May;7(5):84.

10. Hikichi Y, Hukuo K, Shiokawa J. Syntheses of Rare Earth Orthophosphates. BCSJ. 1978 Dec 1;51(12):3645–6.

11. Akers WT, Grove M, Harrison TM, Ryerson FJ. The instability of rhabdophane and its unimportance in monazite paragenesis. Chemical Geology. 1993 Nov;110(1–3):169–76.

12. Boatner LA. Synthesis, Structure, and Properties of Monazite, Pretulite, and Xenotime. Reviews in Mineralogy and Geochemistry. 2002 Jan 1;48(1):87–121.

13. Glorieux B, Matecki M, Fayon F, Coutures JP, Palau S, Douy A, et al. Study of lanthanum orthophosphates polymorphism, in view of actinide conditioning. Journal of Nuclear Materials. 2004 Mar 15;326(2):156–62.

14. Mesbah A, Clavier N, Elkaim E, Szenknect S, Dacheux N. In pursuit of the rhabdophane crystal structure: from the hydrated monoclinic LnPO 4 .0.667H 2 O to the hexagonal LnPO 4 (Ln = Nd, Sm, Gd, Eu and Dy). Journal of Solid State Chemistry. 2017 May;249:221–7.

15. Ni Y, Hughes JM, Mariano AN. Crystal chemistry of the monazite and xenotime structures. American Mineralogist. 1995 Jan 1;80(1–2):21–6.

16. Farmer JM, Boatner LA, Chakoumakos BC, Rawn CJ, Richardson J. Structural and crystal chemical properties of alkali rare-earth double phosphates. Journal of Alloys and Compounds. 2016 Jan 15;655:253–65.

17. Jerbi H, Hidouri M, Glorieux B, Darriet J, Garcia A, Jubera V, et al. Synthesis, crystal structure and optical investigation of the new phosphates: Na7Mg13Ln(PO4)12 (Ln=La, Eu). Journal of Solid State Chemistry. 2010 Aug 1;183(8):1752–60.

18. Li P, Wang Z, Yang Z, Guo Q. Energy Transfer between Activators at Different Crystallographic Sites in Sr3La(PO4)3. J Electrochem Soc. 2012 Jan 12;159(3):H307.

19. Ivanovskikh K, Meijerink A, Ronda C, Piccinelli F, Speghini A, Bettinelli M. Fast UV luminescence in Pr3+-doped eulytite double phosphates. Optical Materials. 2011 Dec 1;34(2):419–23.

20. El Khouri A, Elaatmani M, Della Ventura G, Sodo A, Rizzi R, Rossi M, et al. Synthesis, structure refinement and vibrational spectroscopy of new rare-earth tricalcium phosphates Ca9RE(PO4)7 (RE = La, Pr, Nd, Eu, Gd, Dy, Tm, Yb). Ceramics International. 2017 Dec;43(17):15645–53.

21. Pelczarska A, Watras A, Godlewska P, Radomińska E, Macalik L, Szczygieł I, et al. Structural, Raman, FT-IR and optical properties of Rb3Y2(PO4)3 and Rb3La(PO4)2 doped with Eu3+ ions. New J Chem. 2015 Oct 29;39(11):8474–83.

22. Piotrowska D, Matraszek A, Szulia S, Kosmowska M, Szczygieł I. Thermal and dielectric properties of K3Nd(PO4)2 prepared by Pechini and solid state method. Journal of Alloys and Compounds. 2014 Feb 5;585:337–44.

23. Férid M, Horchani-Naifer K. Synthesis, crystal structure and vibrational spectra of a new form of diphosphate NaLaP2O7. Materials Research Bulletin. 2004 Dec;39(14–15):2209–17.

24. Ben Moussa S, Ventemillas S, Cabeza A, Gutierrez-Puebla E, Sanz J. Structure of trihydrated rare-earth acid diphosphates LnHP2O7·3H2O (Ln=La, Er). Journal of Solid State Chemistry. 2004 Jun 1;177(6):2129–37.

25. Belam W, Mechergui J. Synthesis, X-ray diffraction study and physico-chemical characterizations of KLaP4O12. Materials Research Bulletin. 2008 Aug 4;43(8):2308–17.

26. Shan P, Sun T, Chen H, Liu H, Chen S, Liu X, et al. Crystal growth and optical characteristics of beryllium-free polyphosphate, KLa(PO3)4, a possible deep-ultraviolet nonlinear optical crystal. Scientific Reports [Internet]. 2016 Jul [cited 2020 Jul 21];6(1). Available from: http://www.nature.com/articles/srep25201

27. Kang X, Csetenyi L, Gadd GM. Biotransformation of lanthanum by Aspergillus niger. Applied Microbiology and Biotechnology. 2019 Jan 1;103(2):981–93.

28. Hatada N, Nagai T, Nose Y, Uda T. Reinvestigation of the Phase Equilibria in the La2O3-P2O5 System. J Phase Equilib Diffus. 2013 Jun 1;34(3):196–201.

29. Amezawa K, Tomii Y, Yamamoto N. High-temperature protonic conduction in La7P3O18. Solid State Ionics. 2004 Nov 30;175(1):569–73.

30. Parkhurst DL, Appelo CAJ. Description of input and examples for PHREEQC version 3—A computer program for speciation, batch-reaction, one-dimensional transport, and inverse geochemical calculations. In: US Geological Survey Techniques and Methods, book 6, chap A43 [Internet]. 2013. p. 497. Available from: https://pubs.usgs.gov/tm/06/a43/

31. National Oceanic and Atmospheric Administration. Global Monitoring Laboratory - Carbon Cycle Greenhouse Gases [Internet]. [cited 2020 Jul 30]. Available from: https://www.esrl.noaa.gov/gmd/ccgg/trends/

32. Malm J-O, O'Keefe MA. Deceptive "lattice spacings" in high-resolution micrographs of metal nanoparticles. Ultramicroscopy. 1997 May 30;68(1):13–23.

33. Tsen S-CY, Crozier PA, Liu J. Lattice measurement and alloy compositions in metal and bimetallic nanoparticles. Ultramicroscopy. 2003 Dec 1;98(1):63–72.

34. Vallina B, Rodriguez-Blanco JD, Brown AP, Blanco JA, Benning LG. The role of amorphous precursors in the crystallization of La and Nd carbonates. Nanoscale. 2015;7(28):12166–79.